N O T I C E

THIS DOCUMENT HAS BEEN REPRODUCED FROM MICROFICHE. ALTHOUGH IT IS RECOGNIZED THAT CERTAIN PORTIONS ARE ILLEGIBLE, IT IS BEING RELEASED IN THE INTEREST OF MAKING AVAILABLE AS MUCH INFORMATION AS POSSIBLE

DOE/NASA/0161-10
NASA CR-165193

(NASA-CR-165193) CELL MODULE AND FUEL CONDITIONER DEVELOPMENT Final Report, Oct. 1979 - Jan. 1982 (Westinghouse Research and) 393 p HC A17/MF A01 CSCL 10A

N82-30712

Unclas
G3/44 28733

CELL MODULE AND FUEL CONDITIONER DEVELOPMENT

FINAL REPORT: OCTOBER, 1979 - JANUARY, 1982

D.Q. Hoover, Jr.
Westinghouse R&D Center
Westinghouse Electric Corporation
Pittsburgh, PA. 15235

February, 1982

Prepared for
NATIONAL AERONAUTICS AND SPACE ADMINISTRATION
Lewis Research Center
Under Contract DEN 3-161

for
U.S. DEPARTMENT OF ENERGY
Energy Technology
Division of Fossil Fuel Utilization
Under Interagency Agreement DE-AI-01-80ET17088

S-50-23

DOE/NASA/0161-10
NASA CR-165193

CELL MODULE & FUEL CONDITIONER DEVELOPMENT

FINAL REPORT: OCTOBER, 1979 - JANUARY, 1982

D.Q. Hoover, Jr.
Westinghouse R&D Center
Westinghouse Electric Corporation

February, 1982

Prepared for
NATIONAL AERONAUTICS AND SPACE ADMINISTRATION
Lewis Research Center
Under Contract DEN 3-161

for
U.S. DEPARTMENT OF ENERGY
Energy Technology
Division of Fossil Fuel Utilization

TABLE OF CONTENTS

TABLE OF CONTENTS (Cont.)

TABLE OF CONTENTS (Cont.)

1. Introduction

The work described in this report constituted the second phase of a planned program to develop phosphoric acid fuel cell driven on-site integrated energy systems (PAFC-OS/IES). The first phase (contract DE-AC03-78ET11300) and the second phase (DEN3-161) were funded by DOE and administered and managed by the NASA - Lewis Research Center. Both contracts were carried out by a team comprised primarily of personnel from the Westinghouse R&D Center and the Energy Research Corporation (a subsidiary of St. Joe Minerals Corporation). The accomplishments of the first phase are described in the report "Cell and Stack Design Alternatives" available from NTIS as DOE/ET/11300-1.

The major technical objectives of the second phase were:

1. Develop a suitable PAFC stack technology for the OS/IES application.

2. Develop a conceptual design for a fuel conditioning system to process pipeline gas (natural gas) into a suitable fuel for a PAFC.

The second phase effort on stack technology focused on further development of gas cooling concepts that evolved during the first phase. The second phase stacks also incorporated improvements in cell technology as they became available. Some of these were developed under parallel - technology programs (EC-77-03-1404 and DEN3-205) which were carried out by ERC as part of a comprehensive DOE/NASA PAFC development program. Others were developed by ERC under company sponsored efforts. The stack development effort culminated in the design, fabrication and testing of an advanced air cooled 80 cell (8 kW) PAFC stack.

The second phase effort on fuel conditioning focused on developing a conceptual design of a reformer and acquiring the technical data base needed to design a subsystem suitable for a PAFC-OS/IES.

The work carried out during the first phase revealed the need for a compact, efficient, highly integrated system and the lack of adequate information to design such a system. During the second phase the needed data were acquired and a conceptual design for a suitable fuel conditioning subsystem was developed.

When this effort began, it was the second phase of a six phase effort to commercialize the PAFC in OS/IES. As a result of continuing evaluation, the DOE/NASA emphasis for PAFC commercialization switched from OS/IES to larger power plants (i.e., dispersed generation for electric utilities and cogeneration). Therefore, current plans do not include completion of the OS/IES program. However, the cell and stack technology development provided the basis for a program to develop the larger power plants. As part of this change in emphasis and in recognition of the progress made, the responsibility for pursuing commercialization of PAFC technology was transferred from the Westinghouse R&D (W-R&D) Center to the Westinghouse Advanced Energy Systems Division (W-AESD).

Subsequent to the transfer of contract responsibility to W-AESD, the OS/IES work was continued to an appropriate conclusion under a partial transfer of responsibility and funds (POT) to W-R&D. This report describes the work carried out under the prime contract prior to the transfer and under the POT subsequent to the transfer.

2. Summary

The work described in this report was a continuation of the phosphoric acid fuel cell (PAFC) stack and fuel conditioning system (FCS) development effort started under contract DE-AC03-78ET11300 (Phase I). The results of Phase I indicated the need to focus on these two subsystems, provided guidance in terms of application requirements and provided a technical base on which to build. The present work (Phase II) resulted in the development of PAFC stacks and a conceptual design of a FCS which have acceptable performance characteristics for the OS/IES application. Both the PAFC and FCS development efforts involved a combination of analysis (theory) and corroborating tests.

2.1 Fuel Cell Stack Development

The PAFC stack development culminated in the successful operation of a subscale (nominally 8 kW) air cooled stack incorporating two stack design advances conceived during Phase I and improved cell components developed separately. The performance of this stack at atmospheric pressure was 600 mV/cell at 150 mA/cm^2 and 175°C with simulated reformed fuel composition and flow rates of process and coolant air compatible with the system design. The advanced design features of this stack provided excellent cell temperature uniformity and separation of the process and cooling air streams and retained the inherent simplicity, reliability, and economy of air cooling.

The uniform cell temperatures were primarily due to the cooling plate design shown in Figure 2.1. The primary feature of this design is the increase in heat transfer area (A) provided by branching the cooling channels in the direction of cooling air flow. The increased area reduces the temperature differential between the cells and the cooling air (ΔT) as the air temperature rises. With appropriate channel branching, cell temperature variations can be reduced to less than 1/10 of the temperature

ORIGINAL PAGE IS
OF POOR QUALITY

Dwg. 4250862

Fig. 2.1–Variable area air cooling

rise of the cooling air stream. The cooling plates are made with the same materials and processes as the cell bipolar plates. We have applied for a patent on this design on behalf of DOE.

The concept of separating the cooling air (or other gas) from the process air stream was patented (U.S. Pat. No. 4276355) and the specific embodiment reduced to practice under this contract is illustrated in Figure 2.2. This embodiment provides for the flow of three separate gas streams with rectangular cells so that the electrodes and matrices are identical to those of comparable conventional stacks. To ensure that the bipolar plates would be producible, the versions used in this work had thickness, web, groove and rib dimensions typical of ERC practice and were made using standard ERC processes. A secondary (but important) feature of this design as shown in Figure 2.2 is that the process streams flow in a close approximation to counterflow. This results in a more uniform current density and contributes to the excellent temperature uniformity achieved. This embodiment also provides for equal lengths of all process flow channels.

The stack development effort also included the design, fabrication and testing of 2-23 cell (2 kW) and 2-5 cell stacks incorporating the advanced cooling and process gas flow design and 2-23 cell (2 kW) DIGAS stacks.

2.2 Fuel Conditioning System Development

The fuel conditioning system development effort culminated in a conceptual design for a prototype OS/IES operating on pipeline natural gas. The required flow rates and conditions of all streams were determined for a system incorporating an advanced reformer design, preliminary design and cost information on all major components was obtained, a 10 kW reformer was designed built and tested, and tests were made to verify burner operation and packed bed heat transfer data.

The system analysis of Phase I indicated that counterflow of the reforming stream with both the primary heat source (combustion gases) and the effluent reformed stream was necessary to achieve the overall efficiency

ORIGINAL PAGE IS
OF POOR QUALITY

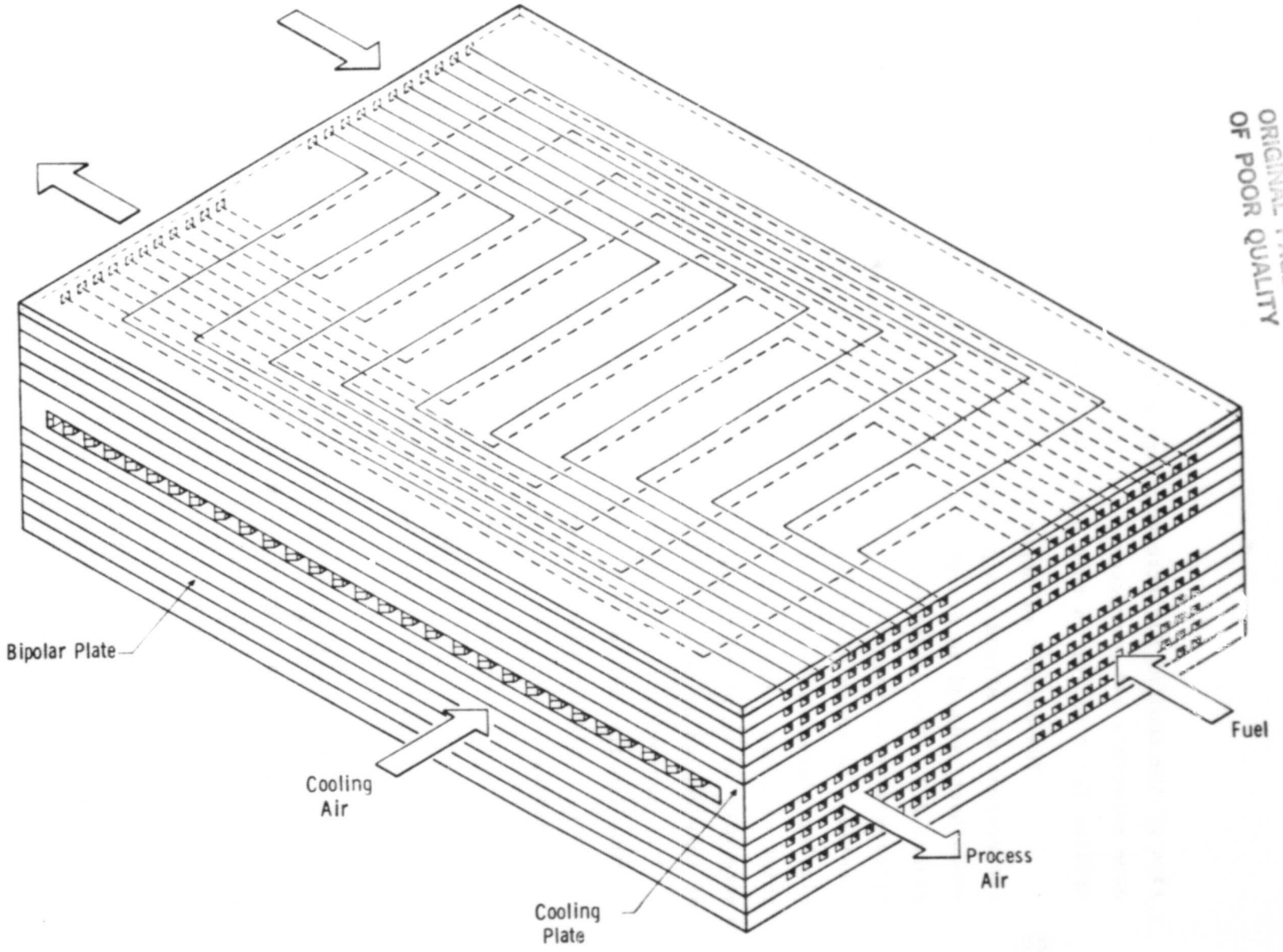

Fig. 2.2 – Separated process gas concept

goals of the OS/IES. The concept shown in Figure 2.3 provides this in a package (suitable for atmospheric pressure) that will be economical to manufacture and readily maintainable. An application for a patent of this design was filed on behalf of DOE. A 10 kW tubular reformer with double counterflow was built and tested to verify the concept and provide data to confirm the heat transfer and kinetic analysis.

The system analysis of Phase I also verified the need to use the PAFC spent fuel stream as the heat source for the reformer. A burner designed to operate on this vitiated fuel stream was designed and tested to verify its stable and efficient operation over conditions that encompassed all possible OS/IES operating points.

ORIGINAL PAGE IS
OF POOR QUALITY

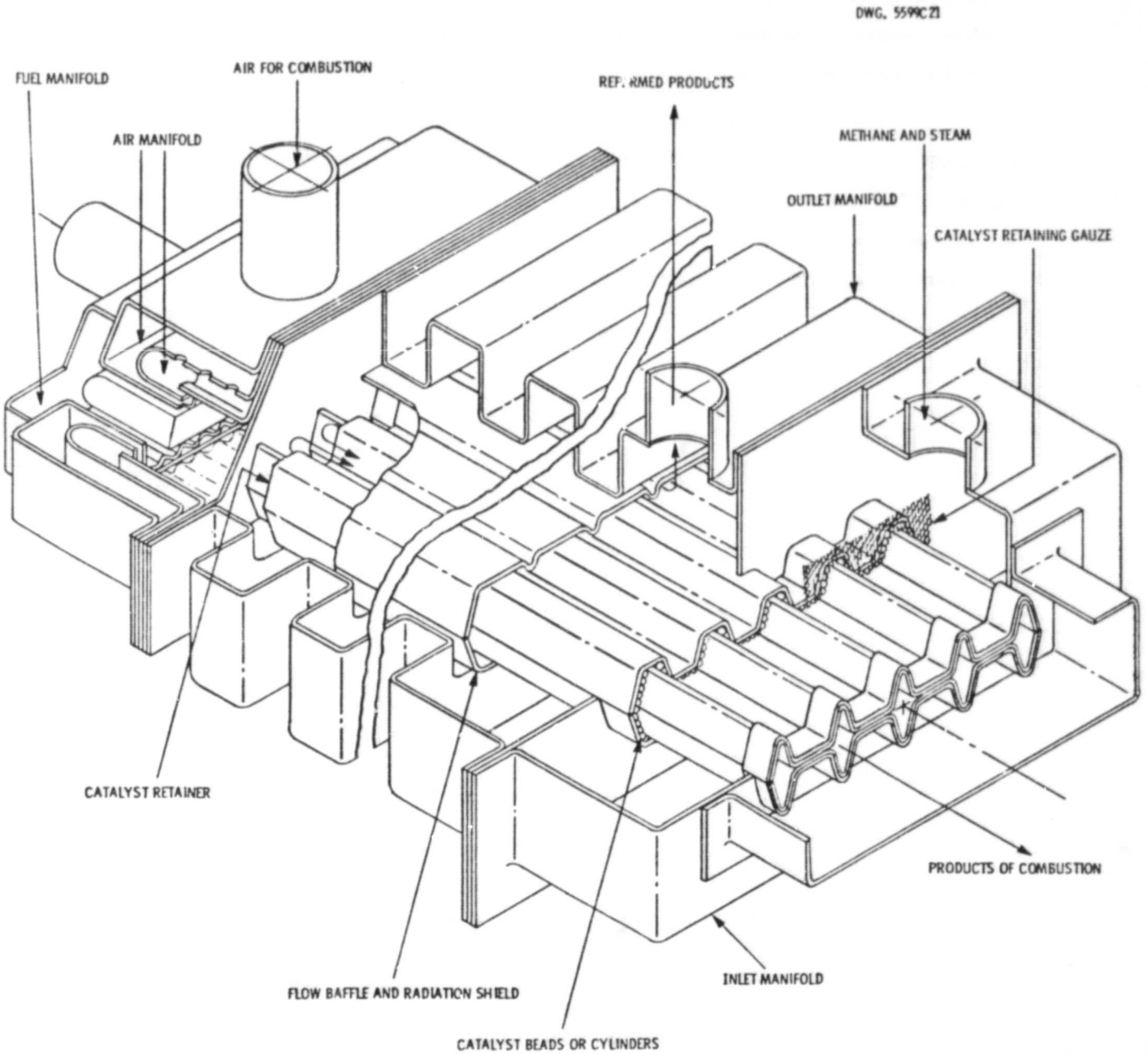

Fig. 2.3 – Double counterflow reformer design

3. Task 1: Design of Large Cell Stacks

The overall objective of this task was the conceptual design of a PAFC module for the OS/IES which would be detail designed, built and tested in succeeding phases of the program. This task was part of a fuel cell development effort that included Tasks 2 and 3 (fabrication and testing of stacks incorporating the evolving design features) and was closely coordinated with them.

The effort on this task comprised continued development of the detailed analytic model started in Phase I, design of test stacks and test stack components, conceptual design of a module, and cost studies and preliminary manufacturability analyses of the module.

Based on the results of Phase I and continuing evaluations, the stack designs considered were air cooled and incorporated the branched channel cooling concept* shown in Figure 2.1 to achieve uniform cell temperatures. The DIGAS† concept (referred to as MK-1 in the contract) provided the basis for the initiation of this program and was described in the Phase I final report and elsewhere in the literature. Separation of the cooling and process air streams (referred to as MK-2 in the contract) as shown in Fig. 2.2** provides a higher oxygen partial pressure to the cathode than DIGAS (and therefore increases performance) while retaining the advantages of air cooling. The design shown in Figure 2.2 was conceived during Phase I but not described because the patent application was not filed. Based on its ability to provide increased performance and other advantages (e.g., elimination of phosphoric acid in the largest heat exchangers of the system) with no significant cost penalty, separated cooling was selected for the module conceptual design.

*An application for a U.S. Patent (Case No. 144090) of this concept was filed.

†U.S. Patent 4,192,906

**U.S. Patent 4,276,355

ORIGINAL PAGE IS
OF POOR QUALITY

Dwg. 4252B47

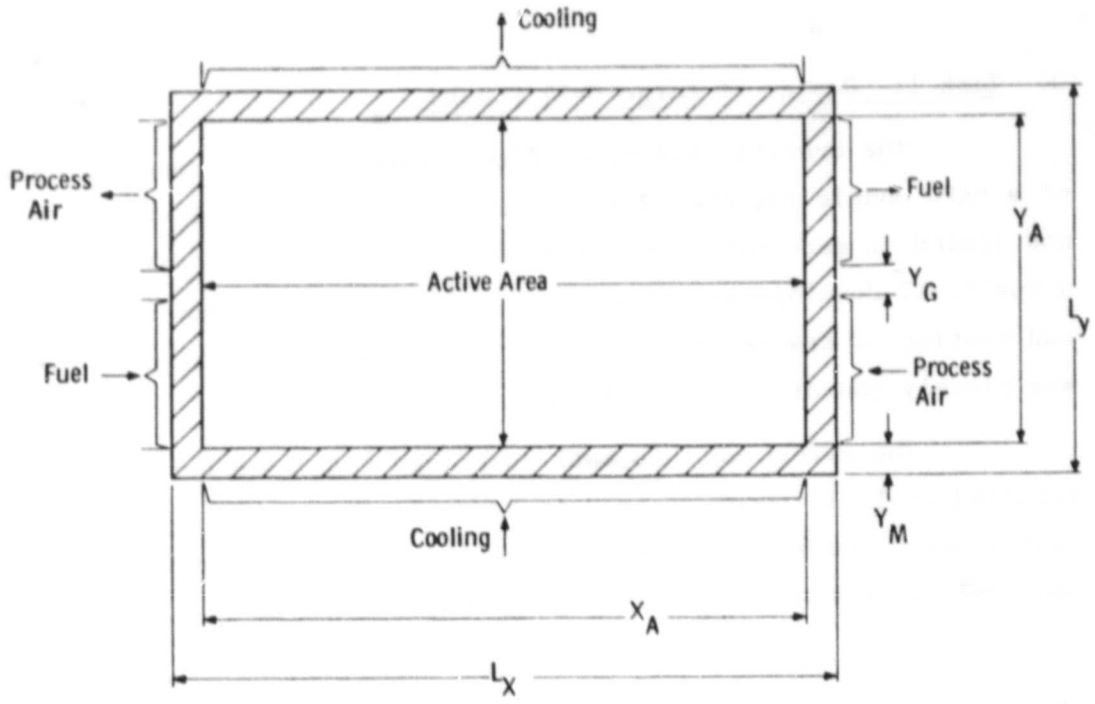

Fig. 3.1.1 – Nomenclature of Z pattern cell

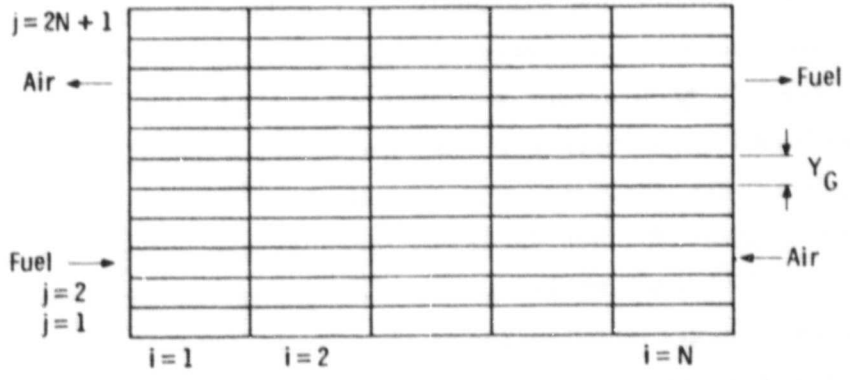

Fig. 3.1.2 – Active area grid for N = 5

Significant results of this task were a conceptual module design which was described in a patent disclosure submitted separately to NASA* for which a patent application (Govt. Case No. S-54116) will be filed, preliminary consideration of the manufacturability of the stack components and assembly of stacks in production quantities and generalization of the detailed analytical model to include all anticipated cell and cooling plate geometries. Work on the module design and manufacturability analysis was curtailed when it became apparent that future work would be directed at larger applications for which pressurized operation would be appropriate.

The results of the work carried out under this task are described at the subtask level in the following sections.

3.1 Detailed Analytical Model

The detailed analytical model developed in phase I was modified to analyze the MK-2 or Z pattern stack design. The computer code named ZCELL calculates the distribution of current density and temperature within a group of cells between pairs of cooling plates from the geometry and operating parameters of the stack. The primary objective of the analysis is to determine the distribution of cooling channels and the location of cooling channel branches which produces the most uniform temperature distribution over the active area.

The nomenclature used is shown in Figure 3.1.1. The overall cell dimensions are L_x and L_y, and the active area dimensions are X_A by Y_A. The locations of process air, fuel and cooling inlets and outlets are indicated. The dimension Y_G is the gasket area separating fuel and process air manifolds. The active area is divided into $N \cdot (2N + 1)$ rectangular finite elements (as indicated for N=5 in Figure 3.1.2) when the fuel and process air flows are each divided into N streams.

*"Fuel Cell Assembly and Design" Westinghouse Disclosure No. RES 80-301.

ORIGINAL PAGE IS
OF POOR QUALITY

Dwg. 4252B46

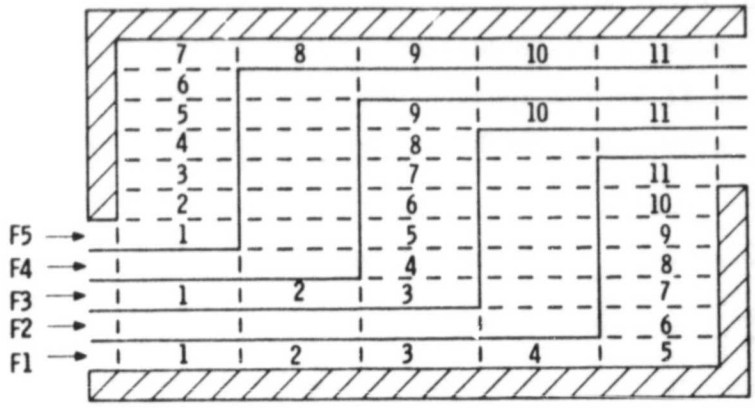

Fig. 3.1.3 – Z pattern fuel flow paths (N = 5)

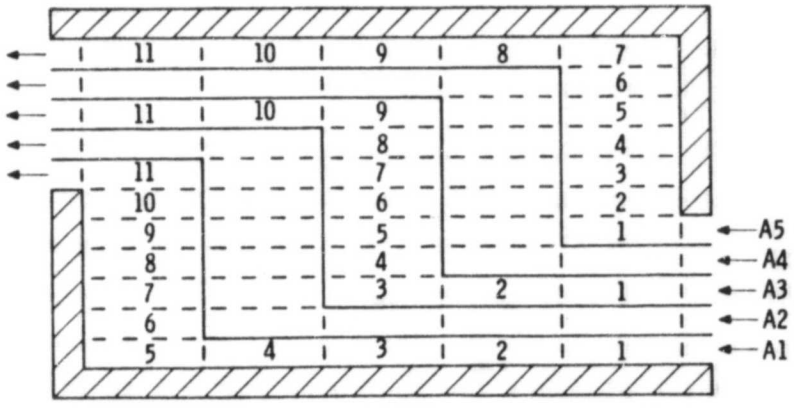

Fig. 3.1.4 – Z pattern process air flow paths (N = 5)

3.1.1 Current Density Distribution

The paths of the fuel streams through the active area grid are shown in Figure 3.1.3 for N=5. Fuel stream F_n enters element k along its path with composition Y_f (n, k) where Y_f describes the mole fraction of each of the fuel stream component gases. For example, fuel stream F_1 flows through 4 elements in the x direction then turns in element 5 and flows in the y direction through elements 6 to 10, then turns in the x direction and exits from element 11. The paths of the process air streams follow a similar pattern as shown in Figure 3.1.4. Air stream A_m enters element ℓ along its path with composition Y_a (m, ℓ) and exits with composition Y_a (m, ℓ+1). The code sets up a map such that given n, k for the fuel stream, the map identifies the element i,j of the active grid and the values of m, ℓ for the air stream. One can thus follow the path of a fuel stream through the elements of the cell and compute current density from the local composition of reactants. For each element i, j a value of local current density $I_{i,j}$ is assumed. The molar flow rates of H_2 into and out of the element i, j are related by

$$\dot{N}_{H_2} (n, k+1) = \dot{N}_{H_2} (n, k) - \frac{A_{i,j} \cdot I_{i,j}}{2F} .$$

Also, the molar flow rates of all non-reacting components of the fuel stream are related by

$$\dot{N}_{nr} (n, k+1) = \dot{N}_{nr} (n, k)$$

where $\dot{N}_{nr}$ in turn represents the CO_2, CO, CH_4 and H_2O present in the fuel stream.

The corresponding relations for the process air stream are

$$\dot{N}_{O_2} (m, \ell+1) = \dot{N}_{O_2} (m, \ell) - \frac{A_{i,j} \cdot I_{i,j}}{4F} ,$$

ORIGINAL PAGE IS
OF POOR QUALITY

$$\dot{N}_{H_2O}\ (m,\ \ell+1) = \dot{N}_{H_2O}\ (m,\ \ell) + \frac{A_{i,j} \cdot I_{i,j}}{2F},$$

and

$$\dot{N}_{N_2}\ (m,\ \ell+1) = \dot{N}_{N_2}\ (m,\ \ell).$$

The assumed value of $I_{i,j}$ is used to calculate the flows and composition out of the element and the mean concentrations within the element. The mean concentrations are then used in the voltage-current density relation to obtain a new value of $I_{i,j}$. This step is repeated until $I_{i,j}$ converges to within 0.1 percent of the previous value.

3.1.2 Voltage Current Characteristics

The fuel cell model adopted to predict the current-voltage curve as a function of temperature and gas compositions is basically the same as that developed during Phase I. The model was fitted to cell performance data by making cell resistance and catalyst utilization functions of temperature as described below.

The voltage equation is

$$V = E - \eta$$

where

V = cell voltage

E = Nernst potential (reversible open circuit E.M.F.)

η = overpotential

The reversible cell potential, E, is given by the Nernst equation

$$E = E_o\ (T) + \frac{RT}{ZF} \ln \left(\frac{Y_{H_2} \sqrt{P_T Y_{O_2}}}{Y_{H_2O}} \right)$$

with

$$E_o\ (T) = 1.261 - 0.00025T$$

where

P_T = total pressure, atm

$E_o(T)$ = standard E.M.F. of the cell at temp. T, volts

R = gas constant, 8.314 joules/(g mole - K)

F = Faradays Constant, 96500 coulombs/g-equivalent

Z = number of electrons transferred per g-equivalent of hydrogen

T = temperature, °K

Y_{H_2} = mean mole fraction of hydrogen at anode

Y_{O_2} = mean mole fraction of oxygen at cathode

Y_{H_2O} = mean mole fraction of water vapor at cathode

The polarization term η consists of four components,

$$\eta = \eta_a + \eta_r + \eta_d + \eta_{CO}$$

where

η_a = activation polarization at cathode, volts

η_r = resistance polarization, volts

η_d = diffusion polarization, volts

η_{CO} = activation polarization at anode due to CO, volts

The cathode activation polarization is given by the Tafel equation

$$\eta_a = \frac{RT}{\alpha_o ZF} \ln \frac{i}{i_o\ (SA)\ (CL)\ (CU)}$$

where

α_o = transfer coefficient, assumed to be 0.5

i = current density, mA/cm^2

i_o = exchange current density of cathode, mA/cm^2

SA = specific catalyst surface area, cm^2/g ($SA = 5 \times 10^5$ cm^2/g)

CL = catalyst loading on cathode, g/cm^2

CU = catalyst utilization factor.

The exchange current is a function of acid concentration, temperature, and partial pressure of oxygen. The acid concentration is a function of water vapor partial pressure which permits correlation of i_o as a function of Y_{O_2}, Y_{H_2O}, and T.

An empirical fit

$$i_o = 232.7 \left(P_T Y_{O_2} \right)^{0.8} \left(P_T Y_{H_2O} \right)^{0.4377} \exp\ (-6652/T)$$

gives i_o within 5 percent in the range of interest.

The resistance polarization is

$$\eta_r = ir$$

where r = specific cell resistance, kohm - cm^2. Test data indicated that for heat treated plates with Mat-1 matrices specific cell resistance is related to temperature by

$$r = r_o + \alpha_r\ (450-T)$$

where

r_o = specific resistance at T=450°K (kohm-cm^2)

α_r = change in specific resistance per degree change in temperature.

The values of r_o and α_r were approximately 0.0005 kohm-cm^2 and 3.5×10^{-6} kohm-cm^2/K respectively for stacks 562 and 564.

ORIGINAL PAGE IS
OF POOR QUALITY

The diffusion polarization was neglected. The effect of diffusion was estimated to effectively lower Y_{O_2} by about 0.004 at $i = 150$ mA/cm^2. The potential change due to this concentration gradient is negligible.

Test data from stacks 561 and 562 showed that η_{co} is proportional to the current density and to the inlet mole fraction of CO in the fuel at a given temperature. By using the temperature dependence (doubling every 15°K) described by Kunz*, the value of η_{co} can be expressed as

$$\eta_{co} = C_o Y_{co} i \, (2)^{\left(\frac{450-T}{15}\right)}$$

where

i = current density (mA/cm^2)

Y_{co} = inlet mole fraction of CO in the fuel

C_o = voltage loss constant for the effect of CO at 450°K (mV·cm^2/mA).

The value of C_o is approximately 2.9 V·cm^2/A for stack 562.

3.1.3 Heat Transfer Analysis

The treed cooling geometry is shown schematically in Figure 3.1.5 and the thermal element grid is shown in Figure 3.1.6. Note that the thermal grid includes the inactive margin around the active cell area which has the same grid as is used in the current density analysis. Either process or cooling flows pass through all of the edge elements except the four corners and the two gasket elements which are shaded in Figure 3.1.6. The cooling flow is in the y direction from j=0 to j=2N+2. There are n_{ci} (not necessarily integer) uniformly spaced cooling channels in element i. The channels have uniform rectangular cross

*Kunz, H. R., "The State of the Art of Hydrogen-Air Phosphoric Acid Electrolyte Fuel Cells", Electrochemical Society Proceedings, Vol. 77-6, 1977.

ORIGINAL PAGE IS
OF POOR QUALITY

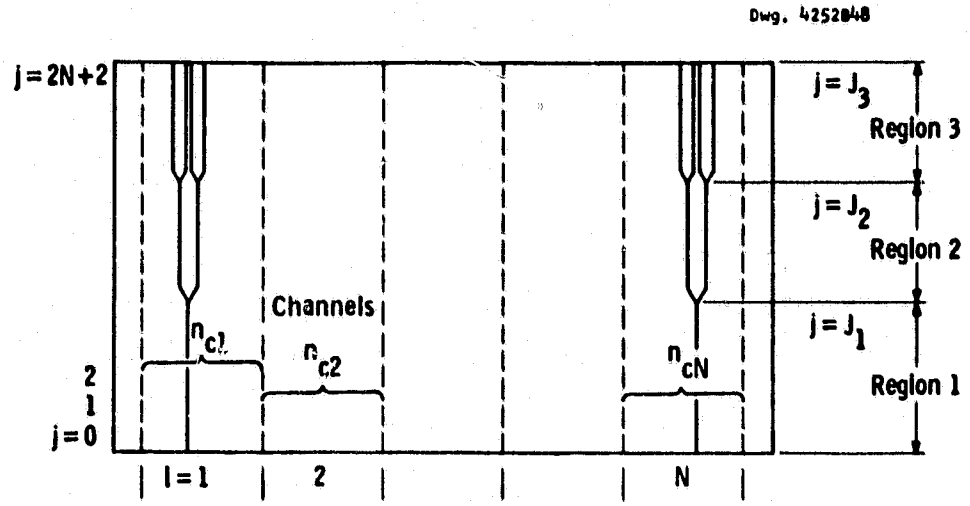

Fig. 3.1.5 – Cooling channel pattern (N = 5)

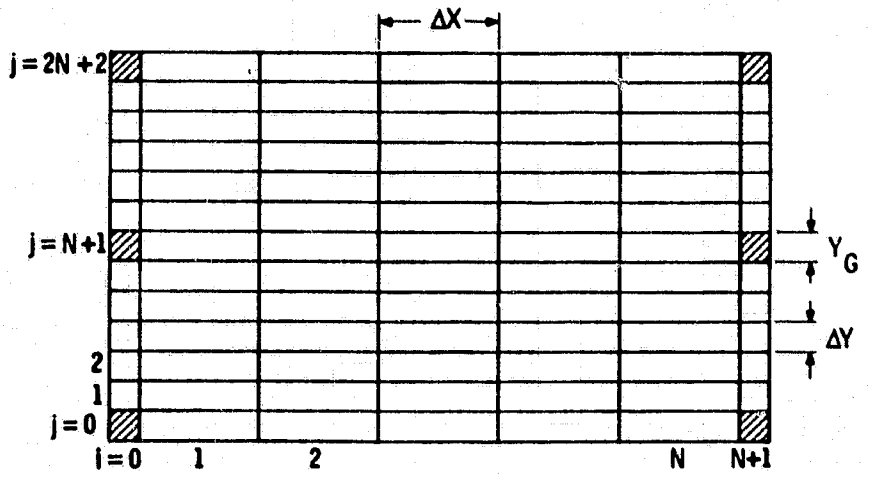

Fig. 3.1.6 – Heat transfer grid (N = 5)

ORIGINAL PAGE IS
OF POOR QUALITY

section within each of the three regions. The geometry shown is typical in that each passage in region 1 ($n_{b_1} = 1$), divides into two branches in region 2 ($n_{b_2} = 2$), which subdivides again into four branches in region 3 ($n_{b_3} = 4$).[2] The j element at the end of each region is identified as J_r for the r region. The dimensions of a channel in region r are a_r by b_r, where the convention $a_r \leq b_r$ is adapted in equations for heat transfer coefficients and pressure drop. The perimeter of subchannel r is

$$S_r = 2\ (a_r + b_r)$$

and the total cooling channel surface area in element i, j is

$$A_{c_{i,j}} = n_{c_i}\ n_{b_r}\ \Delta y_j\ S_r.$$

3.1.4 Heat Transfer Coefficients

The Nusselt number for fully developed laminar flow in rectangular channels for various aspect ratios α, is given by*;

$$Nu_{fd} = 3.61 + 4.63\ (1 - \alpha)^{3.2}$$

Near the inlet of a channel, the heat transfer coefficient is larger than the fully developed value due to development of the laminar boundary layer. If R is the ratio of average Nusselt number for the region 0 to x to the fully developed Nusselt number, then†:

$$R = 1 + \frac{0.0183\ Gz}{1 + 0.04\ Gz^{2/3}}$$

where

Gz = Graetz number

$$= Re\ Pr\ \frac{D}{x}$$

*Rosenhow, W. M. and Hartnett, J. P., "Handbook of Heat Transfer," McGraw-Hill, 1973.

†Eckhert, E.R.G. and Drake, R.M., "Heat and Mass Transfer," 2nd Edition, McGraw-Hill, 1959.

ORIGINAL PAGE IS
OF POOR QUALITY

Re = Reynolds number based on D

Pr = Prandtl number of gas

D = Hydraulic diameter.

At high current densities, or at low values of the cooling gas temperature rise, flow may become turbulent. The fully developed Nusselt number for turbulent flow given is†:

$$N_{u_{fdt}} = 0.116\ [Re^{2/3} - 125]\ Pr^{1/3}$$

and the ratio R for the average Nusselt number from 0 to x to the fully developed Nusselt number is

$$R = 1 + \left(\frac{D}{x}\right)^{2/3}.$$

The average value of R for the interval Δx_j between x_j and x_{j+1} is

$$\overline{R}_j = \frac{x_{j+1}\ R\ (x_{j+1}) - x_j\ \ R(x_j)}{x_{j+1} - x_j},$$

The local average Nusselt number for element j is $\overline{R}_j$ times the appropriate fully developed Nusselt number. The distance x_j refers to the distance from inlet or the distance from the last upstream branch since flow is assumed to redevelop at each branch of the channel.

The group of N_p cells located between a pair of cooling plates has a total thickness

$$t = N_p \cdot t_b + t_c - t_b$$

---

†Eckhert, E.R.G. and Drake, R.M., "Heat and Mass Transfer," 2nd Edition, McGraw-Hill, 1959.

ORIGINAL PAGE IS
OF POOR QUALITY

where

N_p = number of cells per cooling plate

t_b = thickness of a bipolar plate cell

t_c = thickness of a cooling plate cell.

The average temperature of element i,j is $T_{i,j}$ where the element dimensions are Δx_i by Δy_i. The element consists of the N_p cells and plates from the middle of one cooling plate to the middle of the next. The rate of heat conduction to element (i,j) from element (i, j+1) in the plane of the plates is

$$Q_1 = \frac{2k_b \; t \; \Delta x_i \; (T_{i,\, j+1} - T_{i,j})}{\Delta y_j + \Delta y_{j+1}}$$

where

k_b is the thermal conductivity in the plane of the cells.

Similarly, the rate of heat conduction from (i, j-1) to (i, j) is

$$Q_2 = \frac{2k_b \; t \; \Delta x_i \; (T_{i,j-1} - T_{i,j})}{\Delta y_i + \Delta y_{j-1}}$$

Heat conduction rate from (i+1, j) to (i, j) and from (i-1,j) to (i,j) are respectively

$$Q_3 = \frac{2k_b \; t \; \Delta y_j \; (T_{i+1,j} - T_{i,j})}{\Delta x_i + \Delta x_{i+1}}$$

and

$$Q_4 = \frac{2k_b \; t \; \Delta y_j \; (T_{i-1,j} - T_{i,j})}{\Delta x_i + \Delta x_{i-1}}$$

ORIGINAL PAGE IS
OF POOR QUALITY

The rate of heat generation in the element is

$$Q_g = N_p \Delta x_i \Delta y_j q''_{i,j}$$

where $q''_{i,j}$ is the heat generation rate per unit area of a cell. The value of $q''_{i,j}$ is

$$q''_{i,j} = \left(\frac{\Delta H_r}{2F} - V \right) I_{i,j}$$

where

V = cell voltage

F = Faraday's constant

ΔH_r = Heat of reaction per mole of H_2.

The value of $\Delta H_2/(2F)$ is 1.2615 volts at 200C. The cooling gas flow removes heat from element i, j at the rate

$$Q_c = C_{p_c} \dot{M}_c \cdot n_{c_i} \cdot (T_{c_{i,j}} - T_{c_{i,j-1}})$$

where

$\dot{M}_c$ = cooling gas flow rate per cooling channel

$T_{c_{i,j}}$ = cooling gas temperature out of element i,j

C_{p_c} = specific heat of the cooling gas.

ORIGINAL PAGE IS
OF POOR QUALITY

The process air flow removes heat from element i,j at the rate

$$Q_a = C_{p_a} \dot{M}_{am} (T_{am\ out} - T_{am\ in})_{i,j}$$

The subsript m identifies the process air stream which flows through i,j and is determined by the mapping between i,j and m,1 referred to in the current density section.

The fuel flow removes heat at the rate

$$Q_f = c_{p_f} \dot{M}_{fn} (T_{fm\ out} - T_{fm\ in})_{i,j}$$

where the subscript n identifies the fuel stream which flows through element i,j.

The energy balance for each element i,j can then be written as

$$Q_1 + Q_2 + Q_3 + Q_4 + Q_g = Q_a + Q_f + Q_c$$

where the expressions for the various Q's are given above in terms of temperatures of the elements and of the gas streams. For boundary elements, the appropriate Q terms are omitted and the temperature of the applicable gas stream into the element is the inlet temperature to the stack for elements along an inlet edge. Three additional conditions are required for each element, namely the relation between inlet and outlet stream temperature and the heat transfer rate. For process streams, it is assumed that the stream exits at the temperature of the element. Thus

$$(T_{am\ out})_{i,j} = (T_{fn\ out})_{i,j} = T_{i,j}.$$

For the cooling streams, the log mean temperature difference between the element and the cooling gas is used to obtain the heat transferred. The cooling exit temperature for each element with a cooling stream is then given by

OF POOR QUALITY

$$T_{c_{i,j}} = T_{c_{i,j-1}} + (T_{i,j} - T_{c_{i,j-1}})\ (1-e^{-\phi})$$

where

$$\phi = \frac{U_{i,j}\ Ac_{i,j}}{M_c c_{pc} N_{ci}}.$$

$U_{i,j}$ = overall heat transfer coefficient between the element and the cooling gas. The value of $U_{i,j}$ is

$$U_{i,j} = \frac{1}{A_{c_{i,j}}\ R_{cond} + \frac{1}{h_{i,j}}}$$

where R_{cond} is the conduction resistance from the mean temperature of the element to the cooling channel surface. By assuming a parabolic temperature distribution in the stacking direction of an element, the conduction resistance is

$$R_{cond} = \frac{k_t\ t}{12A_{i,j}}.$$

The energy balances for each element and the energy balance for each element of each cooling stream provide a system of linear equations for the unknown temperatures which are solved by a simultaneous equation routine. Each resulting temperature distribution is used to recalculate the current density distribution until convergence.

3.1.5 Results and Discussion

When process air and fuel are preheated close to the average stack temperature, the only significant temperature variation is in the cooling flow direction. The predicted temperature profiles are in good agreement with test results presented in Section 5. For these cases a contour plot of the temperature distribution consists of nearly straight

ORIGINAL PAGE IS
OF POOR QUALITY

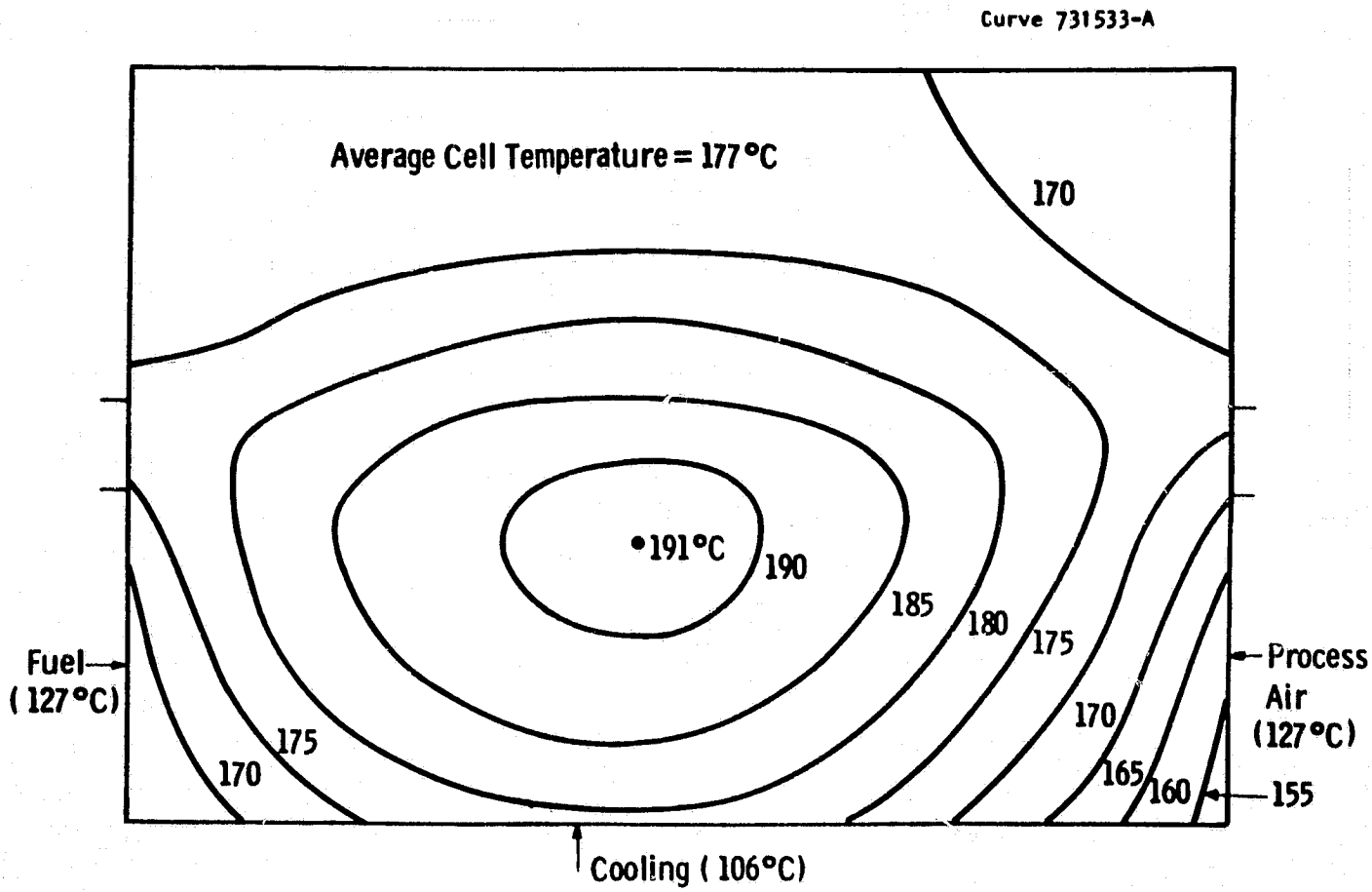

Fig. 3.1.7 – Calculated temperature distribution for active area of active area of Stack 562 with low process inlet temperatures at 200 mA/cm^2

ORIGINAL PAGE IS
OF POOR QUALITY

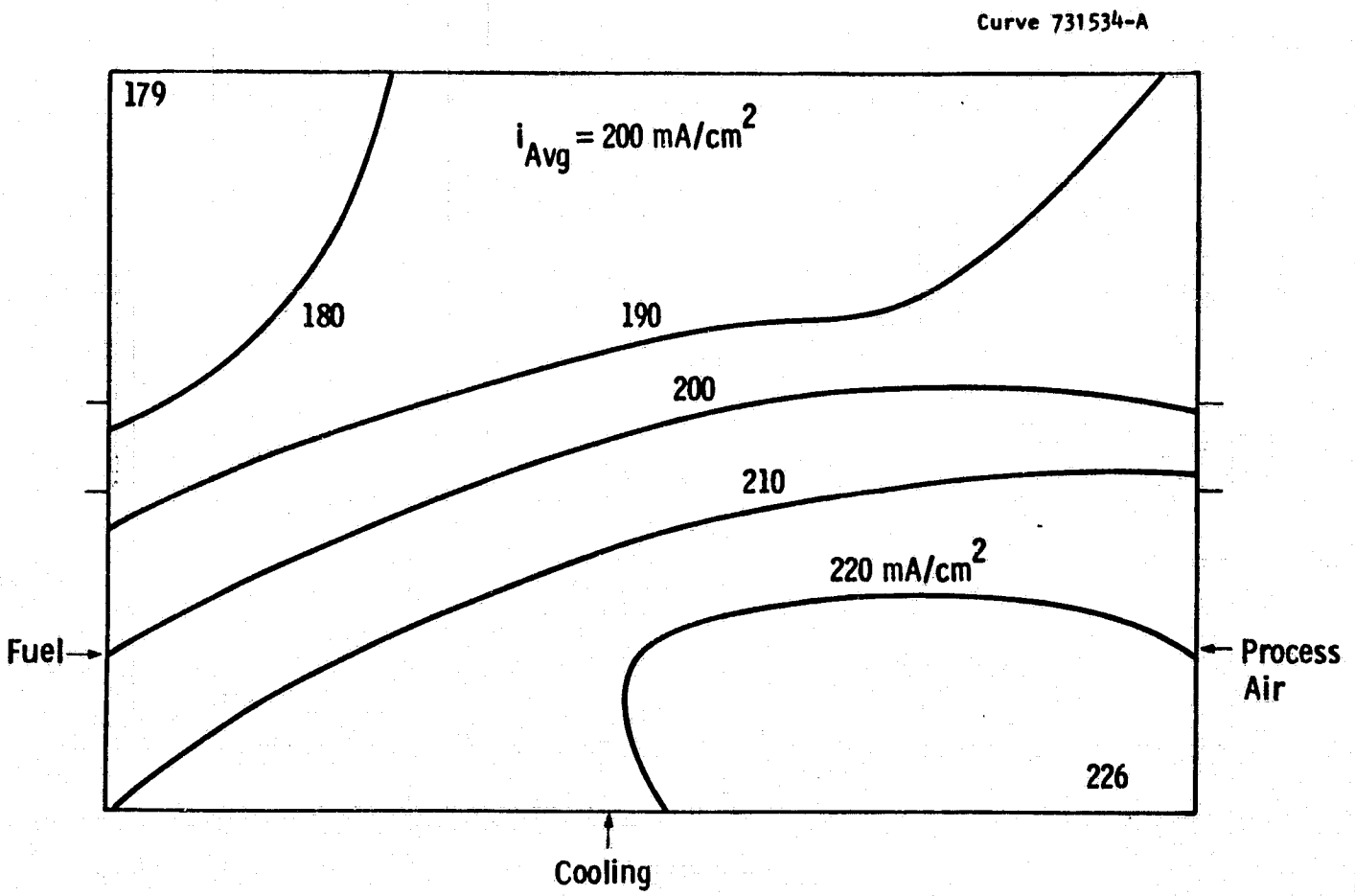

Fig. 3.1.8 – Current density distribution for isothermal cell.

lines of constant temperature normal to the cooling flow direction. When fuel and process air enter the stack significantly below the average cell temperature, a more interesting thermal pattern results. An example for an average current density of 200 mA/cm^2 is shown in Figure 3.1.7 for fuel and process air entering 50°C below the average cell temperature. Other conditions are 70 per cent fuel utilization, 2 stoich process air and 50°C cooling air rise. The cooling channel design is that of Stack 562 with cooling channels uniformly spaced on a 1.27cm pitch. The calculated peak to average gradient is 14°C under these conditions. Relatively small areas near the fuel and process air inlet are cooled below 170°C. The extra cooling at the process air inlet also produces a cooler area near the fuel exit. The results of other calculations show that the colder region near the fuel inlet can be eliminated by omitting one cooling channel per 50°C reduction in fuel inlet temperature below average cell temperature. Likewise the colder region near the process air inlet is eliminated by omitting 1 cooling channel per 40°C reduction in process air inlet temperature. Thus if system considerations dictate lower process inlet temperatures, the cooling design can be customized to maintain temperature uniformity by omitting an appropriate number of channels.

The calculated current density distribution for an isothermal cell is shown in Figure 3.1.8 for the same fuel and process air conditions as above. The maximum current density occurs at the process air corner of the cell and is 13 per cent above the average current density. The minimum current density occurs at the process air exit corner of the cell and is 11 per cent below the average. Figure 3.1.9 presents the current density distribution corresponding to the temperature profile of Figure 3.1.7. The maximum current density is shifted slightly and current densities are reduced along the cooling inlet edge of the cell due to lower than average temperature.

Since there is no satisfactory experimental method of measuring the local current density, confirmation of the predicted current density

ORIGINAL PAGE IS
OF POOR QUALITY

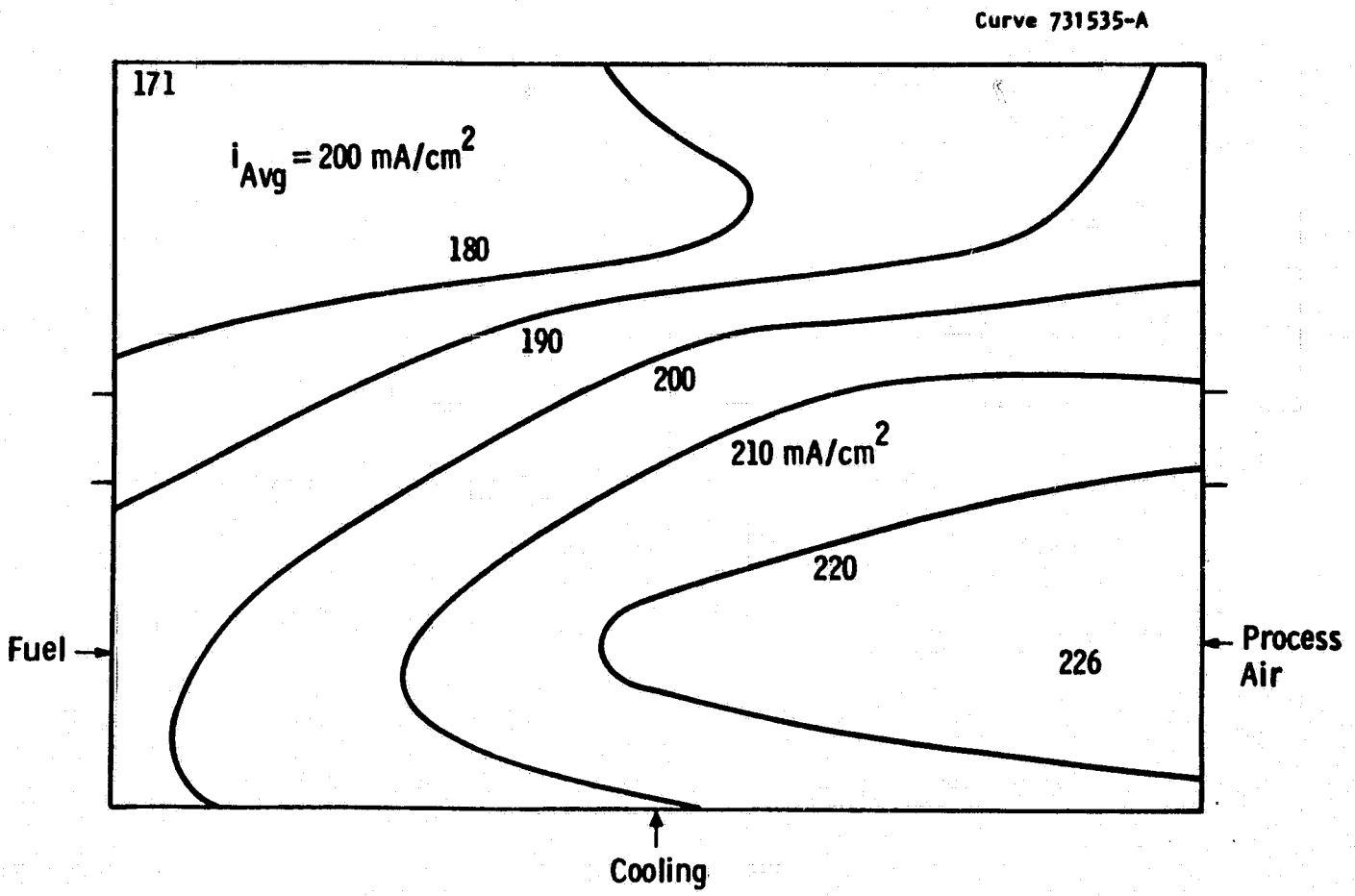

Fig. 3.1.9 – Current density distribution corresponding to temperature distribution of Fig. 3.1.7.

must be inferred from temperature measurement. When process flows enter at the average cell temperature, they produce negligible cooling effects. Under these conditions comparison of measured temperatures at various corresponding locations along cooling channels permits deduction of corresponding current densities. Figures 3.1.8 and 3.1.9 show that predicted current density is slightly greater for a strip near the air inlet than for a strip near the fuel inlet at 70 per cent fuel utilization and 2 stoich air. At 80 per cent fuel utilization, the current densities become approximately equal at the two edges. The temperature profiles for Stacks 562 and 564 confirmed that higher fuel utilization does increase the temperature and the current near the fuel inlet relative to the temperature near the process air inlet. The overall agreement between the model and experiment is considered to be very good. This agreement implies that variations due to matrix and electrode properties and due to compression do not produce significantly different local performance over the area of the cells.

3.2 Stack Design

The purpose of this subtask was to design a series of test stacks which, when fabricated and tested, would provide the technical base for the design of full scale modules for the prototype OS/IES. Based on the Phase I results, two stack concepts were evaluated during Phase II. The first, Mk-1, was the DIGAS concept developed by ERC prior to the start of Phase I. The second, Mk-2, was the separated gas cooling concept conceived during Phase I and shown in Figure 2.2. Improved cell components which were developed in parallel ERC and NASA programs were incorporated into the stacks as appropriate.

A total of nine stacks culminating in an 80 cell stack were designed during Phase II. The design features of these are summarized in Table 3.2.1. As indicated, with the exception of Stack C, all stacks incorporated full size (30 x 43 cm) cells.

The progression from left to right in Table 3.2.1 is basically chronological and indicates the evolution of stack design and cell

TABLE 3.2.1 SUMMARY OF PHASE II STACK DESIGN AND FABRICATION DETAILS

STACK I.D. NUMBER	C	557	558	559	560	561	562	564	800
Plate Size, cm	13 x 38	30 x 43	30 x 43	30 x 43	30 x 43	30 x 43	30 x 43	30 x 43	30 x 43
Number of Cells	3	5	5	23	5	23	23	23	80
Type of Cooling	Process	Process	Process	Digas	Process	Digas	Separate	Separate	Separate
Bipolar Plate Design	Mk-1	Mk-2	Mk-2	Mk-1	Mk-2	Mk-1	Mk-2	Mk-2	Mk-2
Electrodes	One piece	One piece	One piece	One piece	One piece	One piece	One piece	One piece	One piece
Compression Loading	Hand Torquing	Hand Torquing	Hydraulic	Hydraulic	Hydraulic	Hydraulic	Hydraulic	Hydraulic	Hydraulic
Assembly	Dry	Dry	Wet	Wet	Wet	Wet	Wet	Wet	Wet
Current Collection	Spot Welded	Spot Welded	Spot Welded	Compression Fit	Compression Fit	Compression Fit	Compression Fit	Compression Fit	Compression Fit
Electrolyte Flow	Vertical	Vertical	Vertical	Continuous Horizontal	Continuous Horizontal	Continuous Horizontal	Continuous Horizontal	Continuous Horizontal	Continuous Horizontal
End Plate Seal	2 sided	2 sided	2 sided	5 sided	5 sided	5 sided	5 sided	5 sided	5 sided
Matrix	Kynol	Kynol	Kynol	Mat-1	Mat-1	Mat-1	Mat-1	Mat-1	Mat-1
Shims	Kynol	Kynol	Kynol	TFE	TFE	TFE	TFE	TFE	TFE
Cooling Plate Assembly	--	--	--	Epoxy/ Graphite	--	Epoxy/ Graphite	Epoxy/ Graphite	Epoxy/ Graphite	Epoxy/ Graphite
Bipolar Plate Thickness	Standard	Standard	Standard	Standard	Thin	Standard	Thin	Thin	Thin
Heat-Treatment	No	No	No	No	Yes	Yes	Yes	Yes	Yes
Fill Tube	2 piece	2 piece	2 piece	2 piece	One piece	One piece	One piece	One piece	One piece
End Plate Thickness	Standard	Standard	Standard	Standard	Thick	Thick	Thick	Thick	Thick
Tie Bars	Parallel	Parallel	Parallel	Parallel	Parallel	Cross	Cross	Cross	Cross
Matrix Support	No	No	No	Yes	Yes	No	No	Yes	Yes
Resin	Colloid	Colloid	Colloid	Colloid	Colloid	Colloid	Colloid	Varcum	Varcum
Manifolds	Standard	Standard	Standard	Standard	Standard	Standard	Standard	Standard	Floating
Belleville Washers	No	No	No	No	No	No	No	No	Yes

ORIGINAL PAGE IS OF POOR QUALITY

ORIGINAL PAGE IS
OF POOR QUALITY

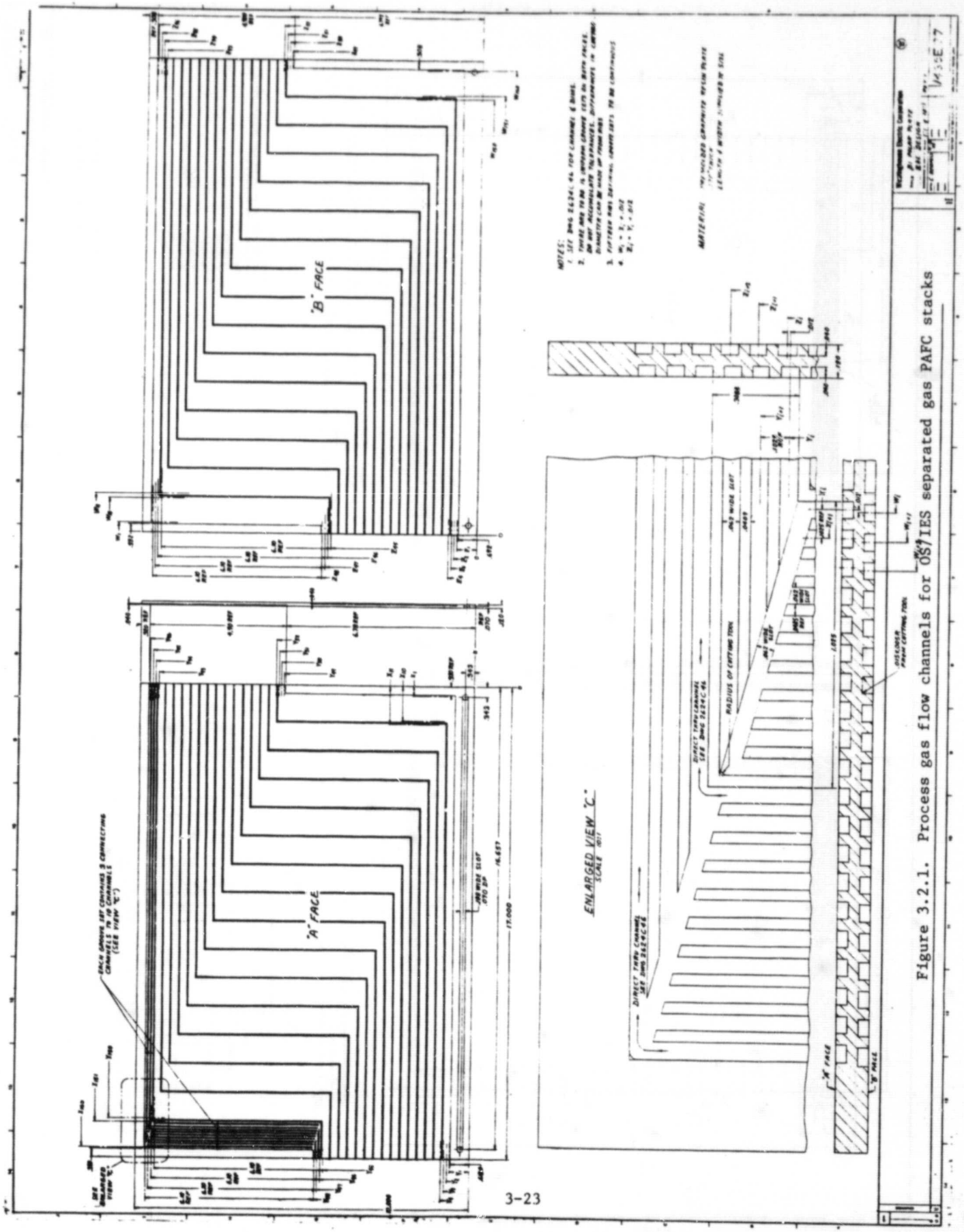

Figure 3.2.1. Process gas flow channels for OSTIES separated gas PAFC stacks

ORIGINAL PAGE IS
OF POOR QUALITY

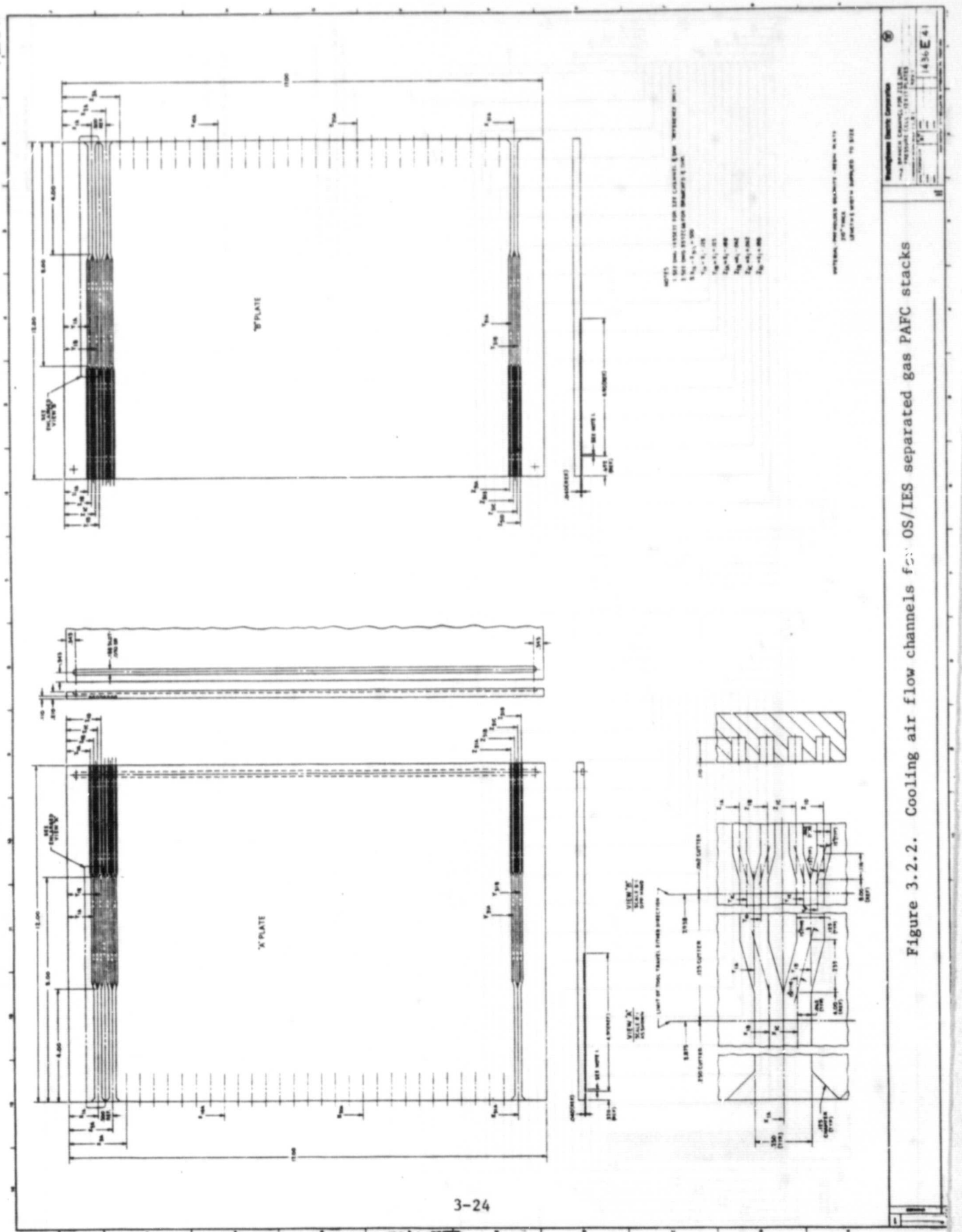

Figure 3.2.2. Cooling air flow channels for OS/IES separated gas PAFC stacks

technology during Phase II. The state-of-the-art at the end of Phase II is represented by Stack 800 and comprises:

- Separated process and cooling air (Mk-2)
- Variable area (branched) cooling passages
- Heat-treated bipolar plates
- Continuous rolled electrodes with nominal platinum loadings of 0.3 and 0.5 mg/cm^2 on the anode and cathode, respectively
- Mat-1* matrices which have smaller more uniform pores and higher temperature capability than Kynol
- Crossed compression (tie) bars which provide better access to the manifolds
- Belleville washers and floating manifolds to accomodate differential thermal expansions (contractions) and mechanical deformation of cell components.

The design features (and fabrication procedures) of all stacks and cells are described in detail in separate documents provided to the NASA Project Manager. The major stack design features developed under this contract are described below.

3.2.1 Mk-2 Plates

The patterns of process air and fuel gas flow channels for state-of-the-art separated cooling (Mk-2) stacks are shown in Figure 3.2.1. The coolers for the stacks were made by cementing plates with the matching faces shown in Figure 3.2.2 together to form the "branched" cooling passages. As indicated in Figure 2.1 and 2.2, each cooler plate had one of the process flow patterns shown in Figure 3.2.1 machined on the adverse face to distribute the appropriate process stream to the anode or cathode of the adjoining cells. Between each cooler plate were four bipolar plates with the patterns shown in Figure 3.2.1 on their two sides to distribute the appropriate gases to the adjoining anodes and cathodes.

*U. S. Patent 4,276,356

ORIGINAL PAGE IS
OF POOR QUALITY

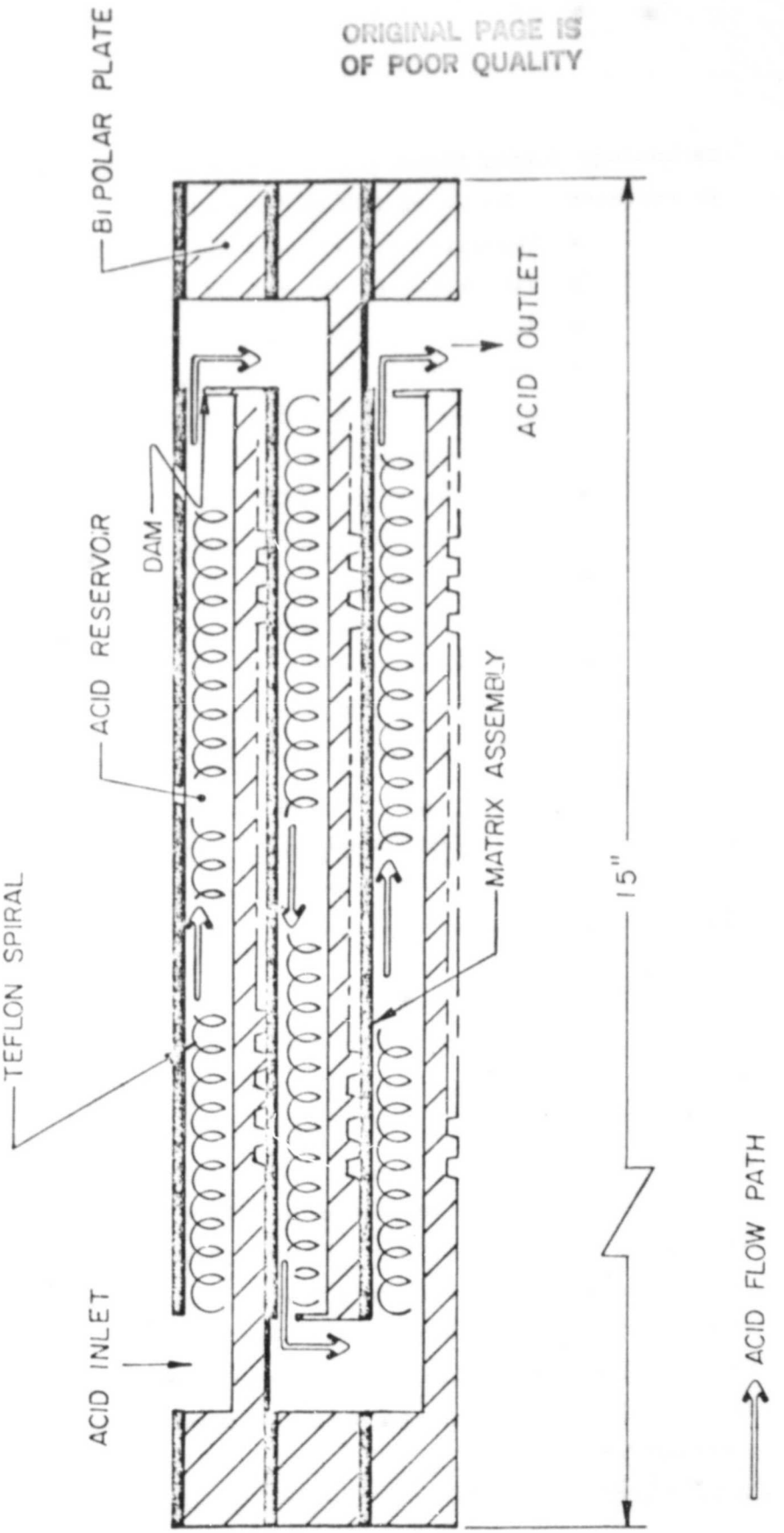

Figure 3.2.3. Schematic of system for acid addition.

The pattern shown in Figure 3.2.1 provides equal flow path lengths for all process streams. The widths and depths of the grooves were based on ERC's experience with conventional (cross-flow) stacks.

The branched cooling channel pattern shown in Figure 3.2.2 was evolved by a coordinated analytic effort using the detailed analytic model described in Section 3.1 and the results of stack tests. The design objective was to achieve uniform cell temperatures to maximize cell performance for fixed cell technology and operating conditions.

3.2.2 Electrolyte Replenishment

The state-of-the-art stacks incorporate a simple and reliable technique for initial filling as well as the replenishment of the electrolyte should this be needed. Figure 3.2.3 is a section of a multi-cell stack through the electrolyte flow channels that are on one face of each plate. This design permits the electrolyte fed on one end of a channel to flow along the channel and through a hole to the channel in a lower cell in a series manner. This design maintains an electrolyte reserve for the matrices with minimal or zero hydrostatic head. Since the electrolyte flows in a series manner, the electrolyte comes into contact with each cell. The electrolyte may be fed at predetermined intervals and/or continuously at predetermined rates. Since the matrix tends to swell as it is filled with electrolyte, a Teflon support coil (or bridge) supports the matrix permitting an unobstructed flow of acid in the channel.

3.2.3 Stack Compression

An analysis was made (Table 3.2.2) of the loss of compressive load on a 2 kW fuel cell stack due to permanent deformation of cell components over time. The permanent deformation of Stack 562 (2 kW, 23-cell) was about 0.008 cm/cell over four months. Since Stack 562 had no load-maintaining device this deformation corresponded to about 20% loss of compressive load on the stack (from 345 to 276 kPa) based on the load versus deflection curve shown in Figure 3.2.4.

While experience with Stack 562 and other 2 kW stacks indicated that this loss of compression had no effect on performance, deformation is proportional to the number of cells. Hence, for an 80 cell stack, the loss of compression would be approximately 117 kPa or 66% of an initial load of 345 kPa. Stack 800 included Belleville springs to maintain the desired compression on the stack. Figure 3.2.5 shows the method of installing Belleville springs on a fuel cell stack and the inset on Figure 3.2.4 shows the spring arrangement used on Stack 800 and the corresponding load/deformation curve.

TABLE 3.2.2
FINAL COMPRESSIVE LOAD ON STACKS
(Initial Load: 345 kPa)

STACK SIZE	TOTAL PROJECTED DEFORMATION, cm	FINAL COMPRESSION, kPa	
		TIE BARS ONLY	TIE BARS PLUS
2 kW (23 cells)	0.175	287	-
8 kW (80 cells)	0.610	117	255

3.2.4 Improved Current Collection Terminal and Terminal Bolt

An improved terminal/current collector design was incorporated in the test stacks, beginning with Stack 559. In earlier stacks, the copper terminal bolt was spot-welded to a current collector as shown in Figure 3.2.6a. The welds tended to break if the terminal bolt was twisted during tightening of the nut to connect the load. The improved design shown in Figure 3.2.6b presses the current collector into the depression in the Haysite as the load nut is tightened so that contact between the terminal and the collector is increased.

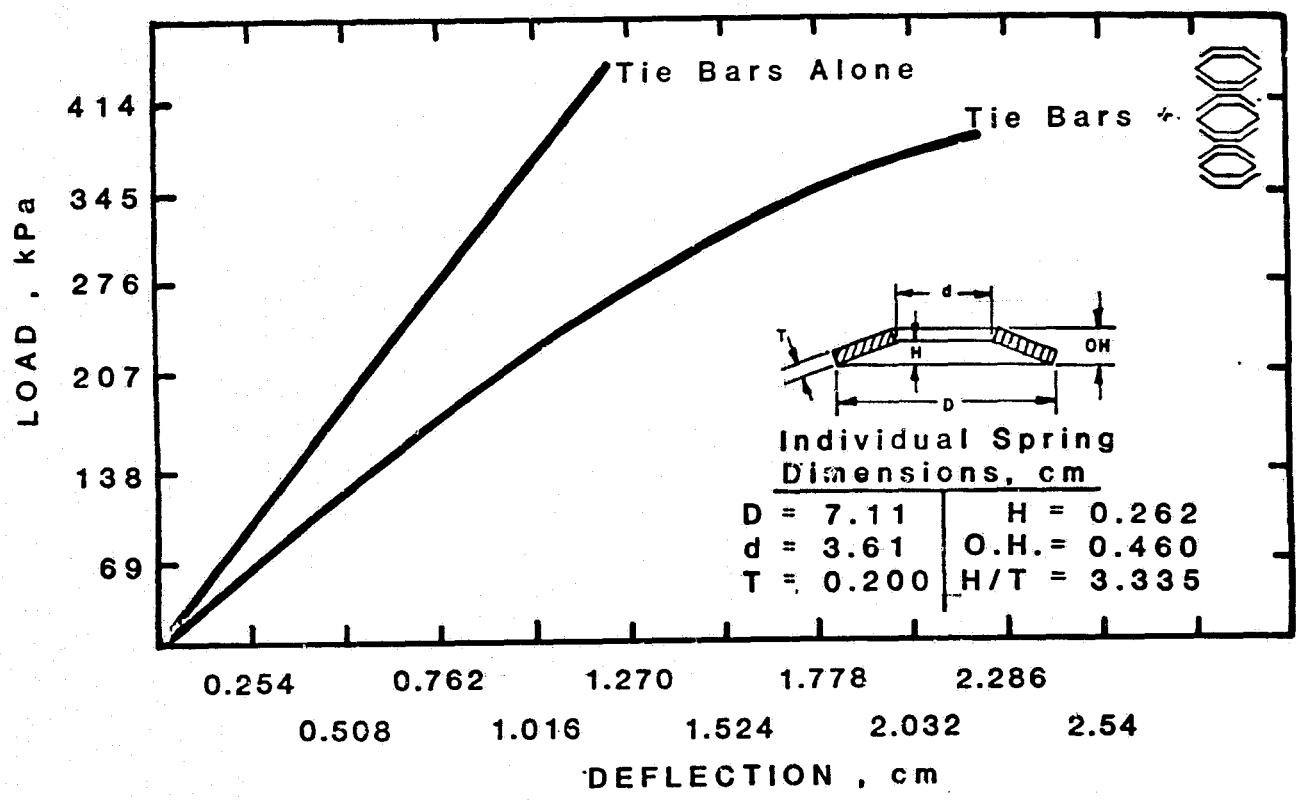

FIGURE 3.2.4 LOAD AGAINST DEFLECTION CHARACTERISTICS OF TIE BARS AND BELLEVILLE WASHERS

ORIGINAL PAGE IS
OF POOR QUALITY

ORIGINAL PAGE IS
OF POOR QUALITY

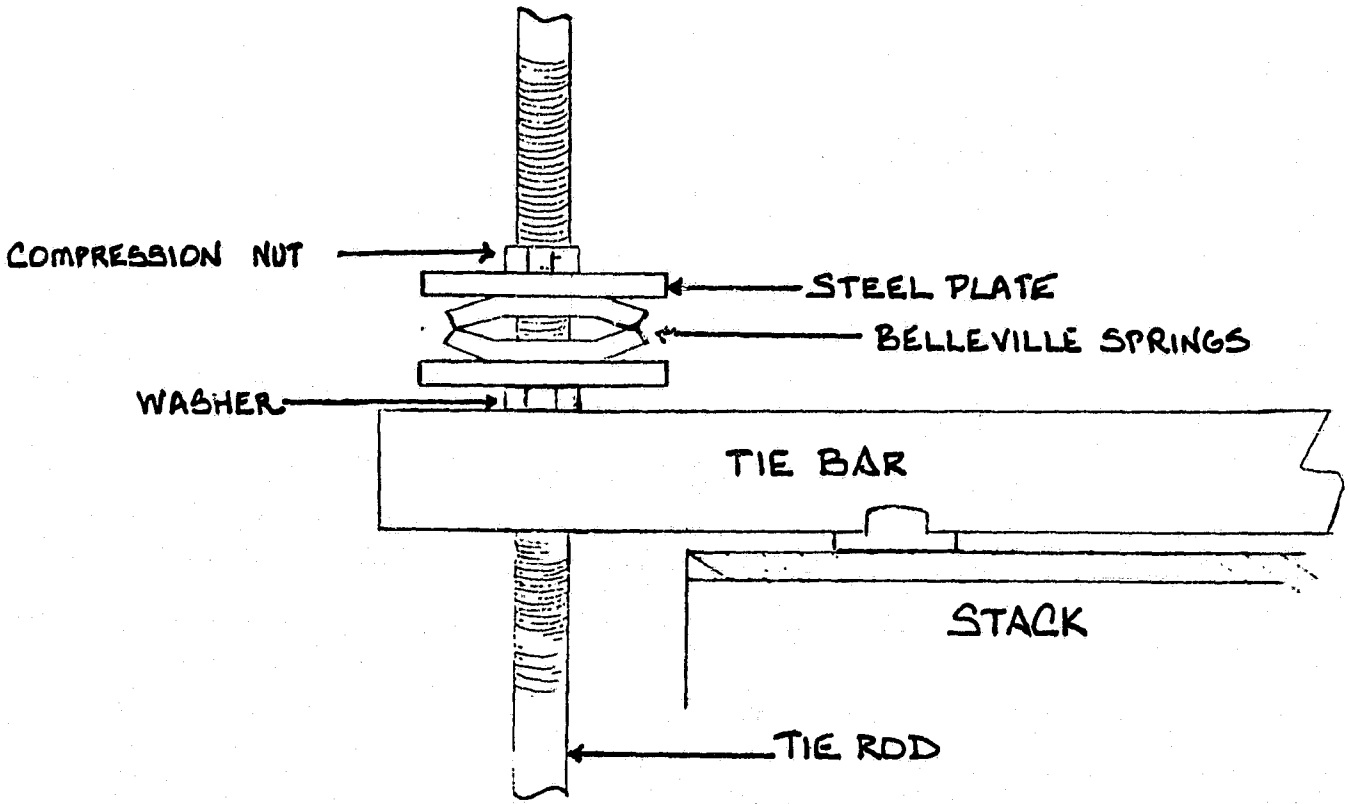

Figure 3.2.5.

TYPICAL BELLEVILLE SPRING APPLICATION

ORIGINAL PAGE IS
OF POOR QUALITY

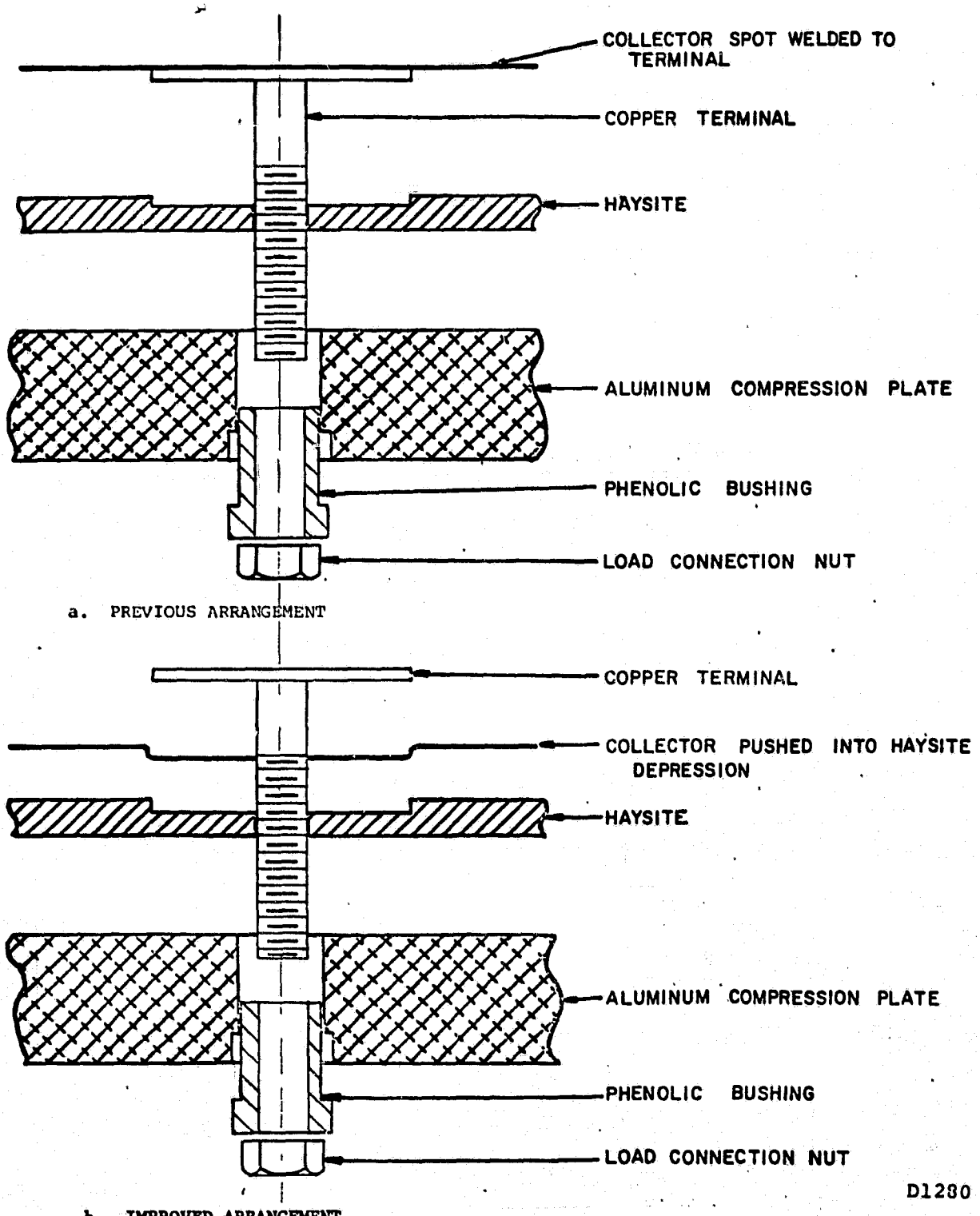

FIGURE 3.2.6. IMPROVED DESIGN OF CURRENT COLLECTOR TERMINALS

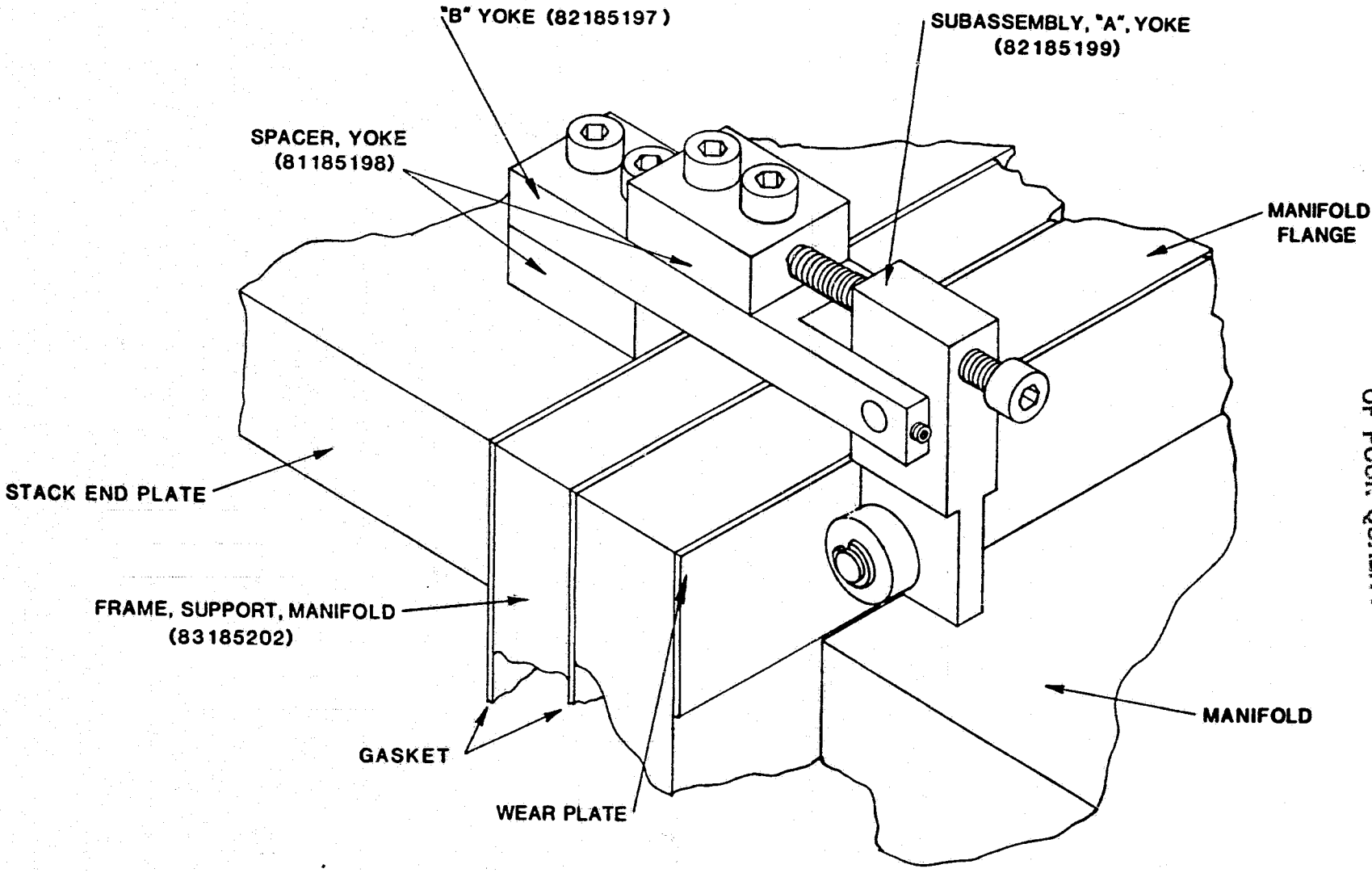

FIGURE 3.2.7. FLOATING MANIFOLD MECHANISM

D1695

3.2.5 Floating Manifold

Changes in stack height due to deformation of cell members and differential thermal expansion between manifolds and the stack are both proportional to the number of cells in a stack. Thus "floating" manifolds are necessary to accommodate the dimensional mismatch which is expected to be as large as 350 mils (240 mils of cell deformation and 80 mils of manifold thermal expansion) in an 80-cell stack. The floating manifold design shown in Figure 3.2.7 was developed and used for Stack 800.

To enhance gas tightness and accomodate the dimensional mismatch, thicker end plates were used to provide a wider sealing area between the stack and the manifold. A special five sided seal was also designed to prevent air leakage between the end plate and the insulator plate.

3.3 Full Scale Fuel Cell Module Designs

The objective of this subtask was the preparation of a conceptual design of a full scale fuel cell which would be detail designed, fabricated and tested in succeeding phases of the program. The effort comprised:

1. Analyses of the processes currently used to manufacture the repeating (cell and cooling plate) components and preliminary designs of equipment and labor required for high production rates.
2. Preliminary design of the stack enclosure components including manifolds, stack compression hardware and seals.
3. Estimates of the equipment, floor space, labor and materials required to manufacture the benchmark modules described below.
4. Estimates of the cost of the manufactured modules using the NASA developed Interim Price Guide Line (IPEG) model.

To provide a basis for the module design a benchmark stack was specified. The benchmark stack comprised 300 full size cells (31 x 43 cm) using the then available ERC technology which included the MAT-1 matrix, rolled anodes and cathodes with nominal platinum loadings of 0.3 and 0.5 mg/cm^2, respectively, and compression molded bipolar plates and cooling plates which were not heat treated. Based on cost-performance studies, the MK-2 design (conceived during Phase I) incorporating separated cooling and process streams, and variable area cooling was selected for the benchmark stack. The stack enclosure for the benchmark module was conceived as part of the design effort and was described in Westinghouse Patent Disclosure No. RES 80-301, "Fuel Cell Assembly and Design" and is the subject of Government Case No. S-54116.

In addition to the conceptual design of the module, the result of this task was an estimated cost of manufacturing of ~$10,000 per module or $330/kW based on the nominal rating of 30 kW per module. Nearly 90% of this is material cost, a major portion of which is the cost of the platinum catalyst, which should be recoverable at the end of the useful life of the module.

The early efforts to design the module enclosure and seals revealed a need for more information on the mechanical behavior of the cell components under compression at the stack operating temperature. Tests to obtain this information were made and these are described in section 5.7.

The details of the design and cost estimation work carried out as part of this Subtask are described below.

3.3.1 Manufacturing Methods and Costs for Repeating Components

A cost estimate for the repeating stack components of the benchmark design based on manufacturing 16,700 fuel cell stacks per year was made. The equipment and processes used in estimating these costs reflect large scale production and do not include laboratory equipment. NASA's (Jet Propulsion Lab. California) Interim Price Guide Line (IPEG) model (which is a subset of NASA's Solar Array Manufacturing Industry Costing Standards - SAMICS) was used for this study.

The word "costing" requires additional explanation. The IPEG model automatically provides for a 20% return on assets. Thus the "costs" shown in this study include this profit plus other standard factors which are a part of the IPEG cost model. The IPEG cost model was selected for this cost estimate because it includes standardized overhead factors eliminating the use of all contractor specific factors. The assumptions used for developing overhead costs and coefficients of the IPEG model are shown in Appendix A of the Third Quarterly Report of this contract.

TABLE 3.3.1

PHOSPHORIC ACID FUEL CELL REPEATING COMPONENTS

JPL IPEG COST MODEL

COST ITEM	IPEG FACTOR	ESTIMATE OF COST ITEM	IPEC COST (MILLION $/YR)	$/KW
Equipment	.489	$5,064,000	2,480	4.96
Floor Space	96.9	22,125 Sq. Ft.	2,140	4.28
Direct Labor	2.133	$4,700,000/Yr.	9.97	19.94
Direct Material	1.255	$111,400,000/Yr.	139.3	278.60
Utilities	1.25	$300,000/Yr.	.4	.80
TOTALS			154.29	308.6

The costs for the repeating components (i.e., cells and cooling plates) of the benchmark module broken down to the five major cost categories of the IPEG costing model are given in Table 3.3.1. It is obvious that material is the dominant cost component (∿ 90%) and the major portion of this component is the platinum catalyst. The platinum and equipment costs used for this study were those prevailing on March 26, 1980. The producer price of platinum at that time was $440.12 per troy ounce. The equipment cost and labor hour inputs for the IPEG calculation were based on preliminary designs of manufacturing facilities. Where practical, modern, continuous high production processes were used as a basis for the cost estimates. The following paragraphs describe the processes in detail.

The equipment and labor estimates were prepared for a benchmark module which contains 300 30 x 43 cm cells of the MK-2 design (separated coolant and process streams, and variable area cooling plates) with the ERC developed electrochemical components.

The flow diagram for the benchmark repeating component manufacturing processes shown in Figure 3.3.1 is based on manufacturing procedures presently in use by ERC. Estimated labor and equipment requirements for a 16,700 module per year facility are summarized in Table 3.3.2 and are based on the processes shown in Figure 3.3.1 In order to improve the cost effectiveness several process steps were modified for high production rates as described below. The preliminary calculations indicate that 139 workers are required to manufacture the repetitive components for 16,700 30 kW stacks per year. This does not include maintenance and other supporting personnel.

The bipolar plate preform currently used was identified as a labor intensive repetitive component. An egg crate type structure is set into the die cavity. The egg crate compartments are each filled with measured amounts of graphite-resin powder. Next, the egg crate is removed leaving different size heaps of powder in the die cavity.

ORIGINAL PAGE IS
OF POOR QUALITY

FIG. 3.3.1. PHOSPHORIC ACID FUEL CELL MANUFACTURE

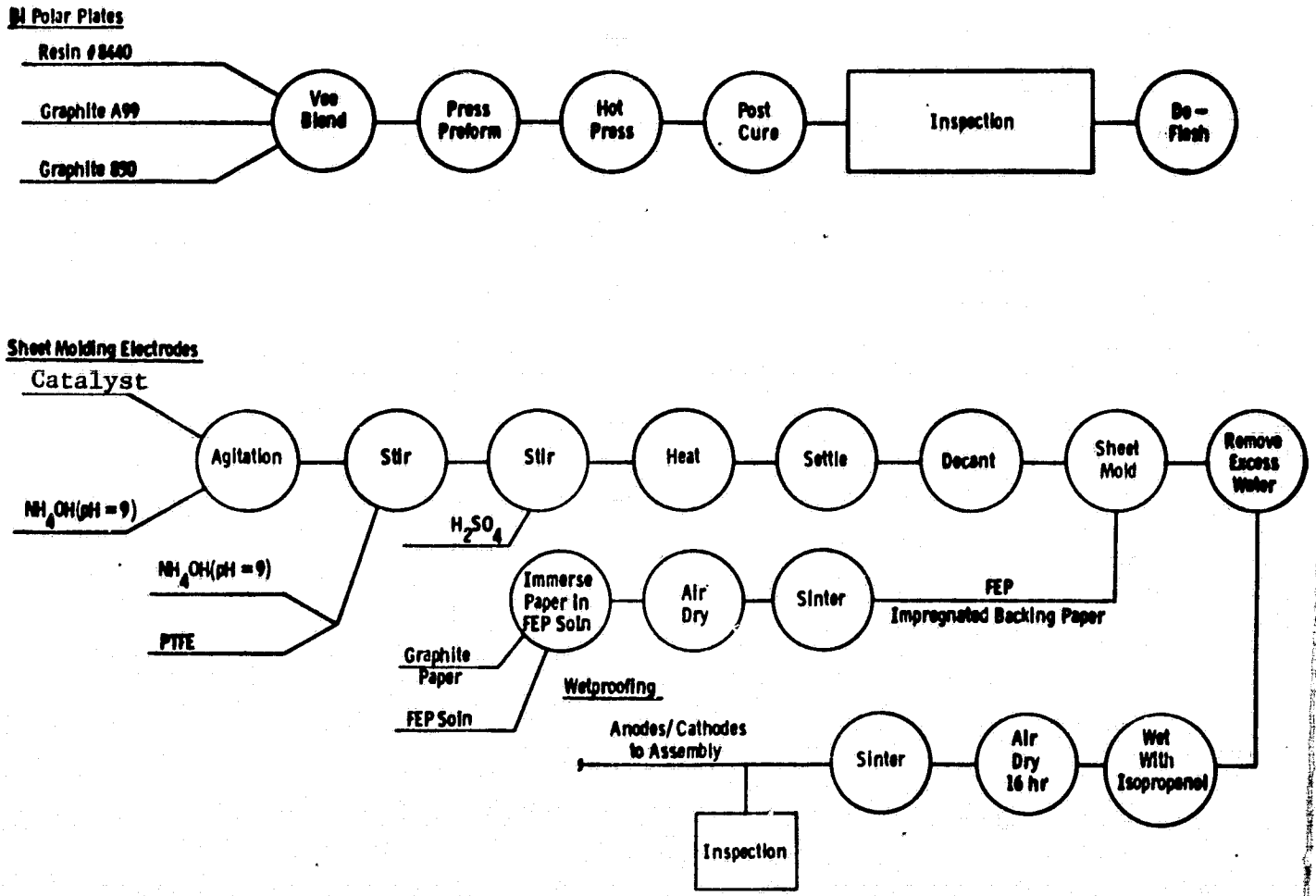

The Flow Diagram for the Matrix is an ERC Proprietary Process

ORIGINAL PAGE IS
OF POOR QUALITY

TABLE 3.3.2

PHOSPHORIC ACID FUEL CELL LABOR & EQUIPMENT ESTIMATES
FOR A 16,667 STACK/YR. MANUFACTURING ABILITY

OPERATION	EQUIPMENT	QTY.	TOTAL COST	OPERATORS
Bi-Polar Plates				
1. Blend	1. Vee Blender 5 Ton Capacity	1	$ 40,000	3
2. Press Preforms	2. 50 Ton Press	7	350,000	24
3. Hot Press	3. 500 Ton Press	12	1,600,000	42
4. Post Cure	4. 5' x 5' x 12' Ovens	10	300,000	6
5. Inspect	5. Thickness Gauge	1	10,000	3
	Leak Tester	1		
6. DeFlash	6. Sandblaster	1	10,000	6
7. Bulk Ram Mat's System		1	250,000	
8. Conveyor System		1	25,000	
			2,585,000	84
Sheet Molding Elect.				
1. Mix Ingredients	1. Agitator-Cooker	2	12,000	2
2. Vacuum Filter	2. Filter Press	24	240,000	36
3. Dewater & Air Dry	3. Roll Press & Oven	24	150,000	36
4. Sinter	4. Belt Oven	24	600,000	
5. Wet Proof Graphite Paper	5. Immersion Tank	6	60,000	9
	Belt Oven, Etc.	6	150,000	9
6. Wash Cathodes	6. Spray Tunnel	3	30,000	9
	Drying Rack	3		
7. Clean SiC & Mix With Other Ingredients	7. Ultrasonic Cleaner	1	4,000	3
	Drying Oven	1	20,000	
	Mixing Tank	1	4,000	
8. Coat Cathodes with SiC	8. Coating Mach.	12	240,000	36
9. Air Dry	9. Drying Oven	12	144,000	--

ORIGINAL PAGE IS
OF POOR QUALITY

TABLE 3.3.2 (Con't.)

OPERATION	EQUIPMENT	QTY.	TOTAL COST	OPERATOR
10. Sinter	10. Belt Ovens	12	300,000	18
11. Inspect	11. Thickness Gauge Porosity Tester	1 1	10,000	3
TOTALS			1,964,000	164

MATRIX

Process is ERC proprietary information. Eight basic steps are involved and require a total of 33 workers and $525,000 worth of equipment.

The punch of the press descends, compacting the powder into a preform of non-uniform density. Currently, the measurements of different powder quantities, handling of the egg crate structure and preform are performed manually. The sequential phases of an automated approach to achieve the same end product are shown in Figures 3.3.2 and 3.3.3. A bottomless box containing the powder pushes the completed preform to a collection device or belt conveyor (not shown). The die cavity is then lowered to a predetermined level. Special compaction punches located in the die cavity are adjustable to accommodate desired volumes. The bottomless box moves to the left, leaving behind a die cavity filled level to the top. The punch descends a fixed level to compact the powder. A lower ram is raised and in turn raises the special compaction punches. Finally, the punch of the press is retracted, the die cavity raised and the completed preform is pushed away. The process repeats. In actual practice, the upper punch and the lower ram may be actuated simultaneously rather than sequentially as described.

The final hot pressing of the preform to produce a bipolar plate is currently done one-at-a-time with a 500 ton press - a costly machine. Use of a press with five individually heated platens (as shown in Figure 3.3.4) will reduce equipment costs. Time studies indicate that five 5-plate presses will produce the required 20,000 plates per day.

The manufacturing concept for continuously assembling fuel cells is depicted in Figure 3.3.5. This is a wet assembly where the phosphoric acid is roller-coated onto the matrix. Since the cutter operates intermittently, it is necessary to separate the coating and cutting operation by a loop pit which allows the coating process to proceed continually. Thus no bead is formed along the coating roller as would be the case in an intermittent operation. A stacking table at the end of the line is indexed downward with each fuel cell. An operator (not shown) manually feeds bipolar plates on to the stacking table prior to the descent of the cutter.

ORIGINAL PAGE IS
OF POOR QUALITY

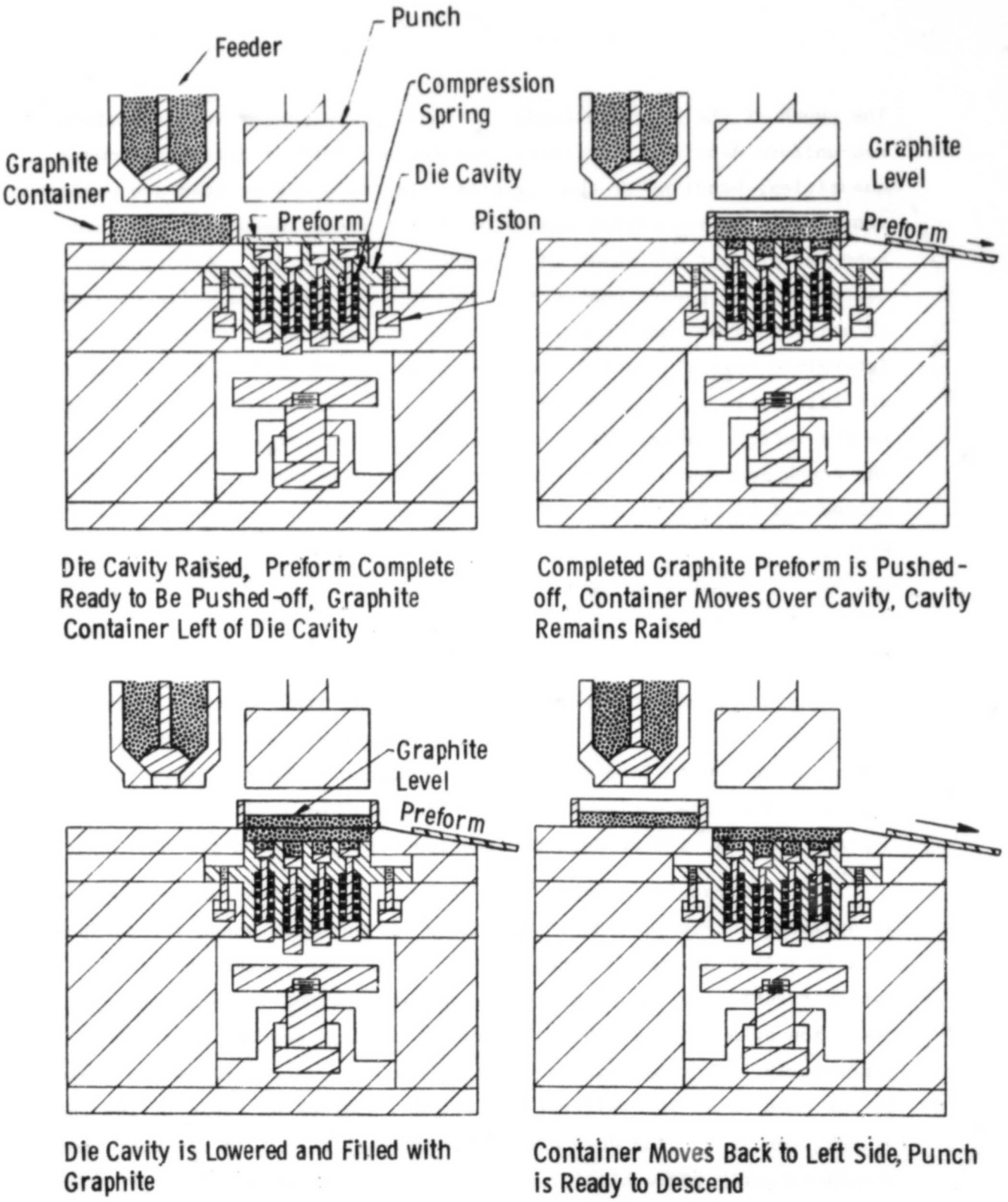

Die Cavity Raised, Preform Complete Ready to Be Pushed-off, Graphite Container Left of Die Cavity

Completed Graphite Preform is Pushed-off, Container Moves Over Cavity, Cavity Remains Raised

Die Cavity is Lowered and Filled with Graphite

Container Moves Back to Left Side, Punch is Ready to Descend

FIGURE 3.3.2 SEQUENTIAL STEPS IN AUTOMATED PLATE PREFORM PRODUCTION

ORIGINAL PAGE IS
OF POOR QUALITY

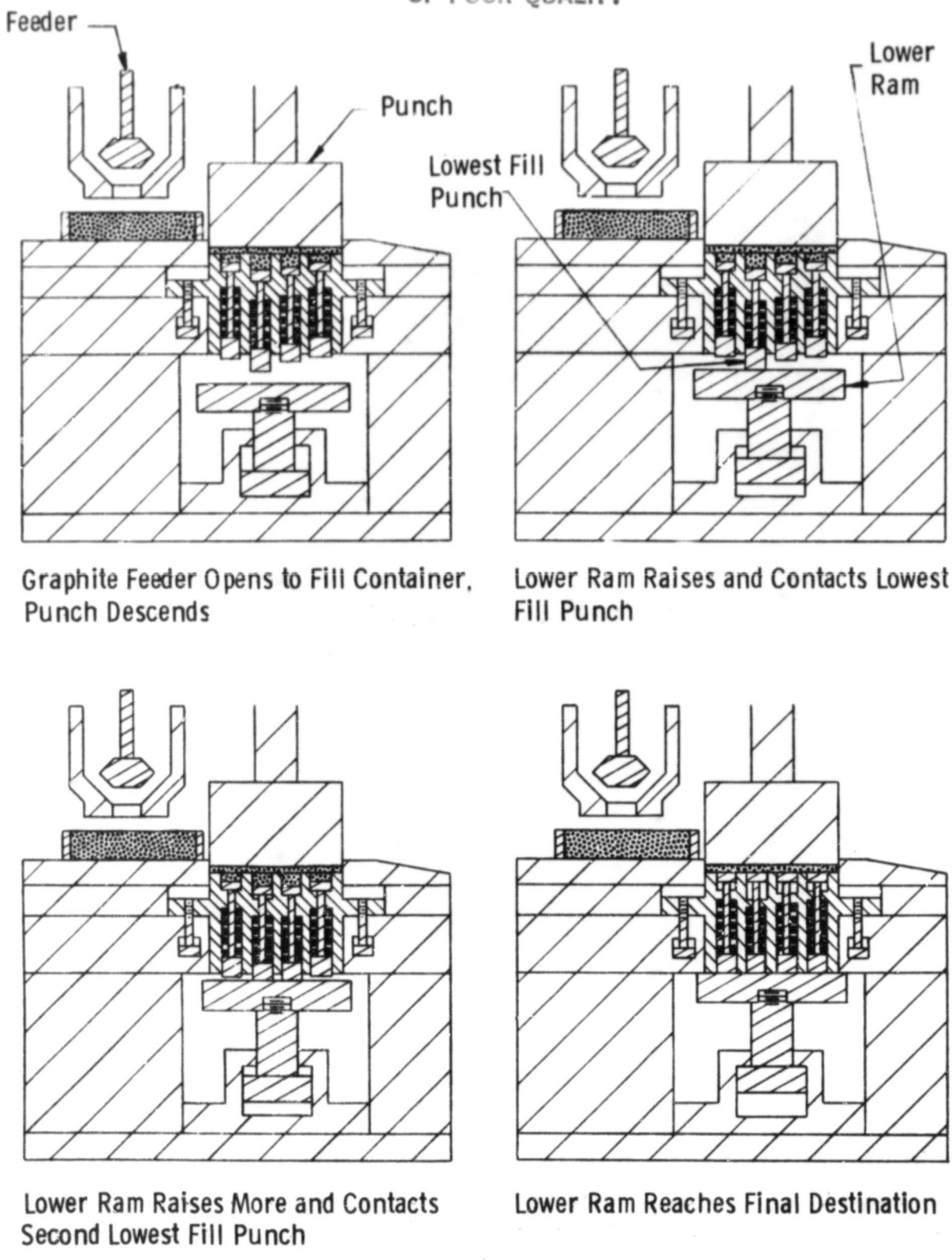

FIGURE 3.3.3 SEQUENTIAL STEPS IN AUTOMATED PLATE PREFORM PRODUCTION

ORIGINAL PAGE IS
OF POOR QUALITY

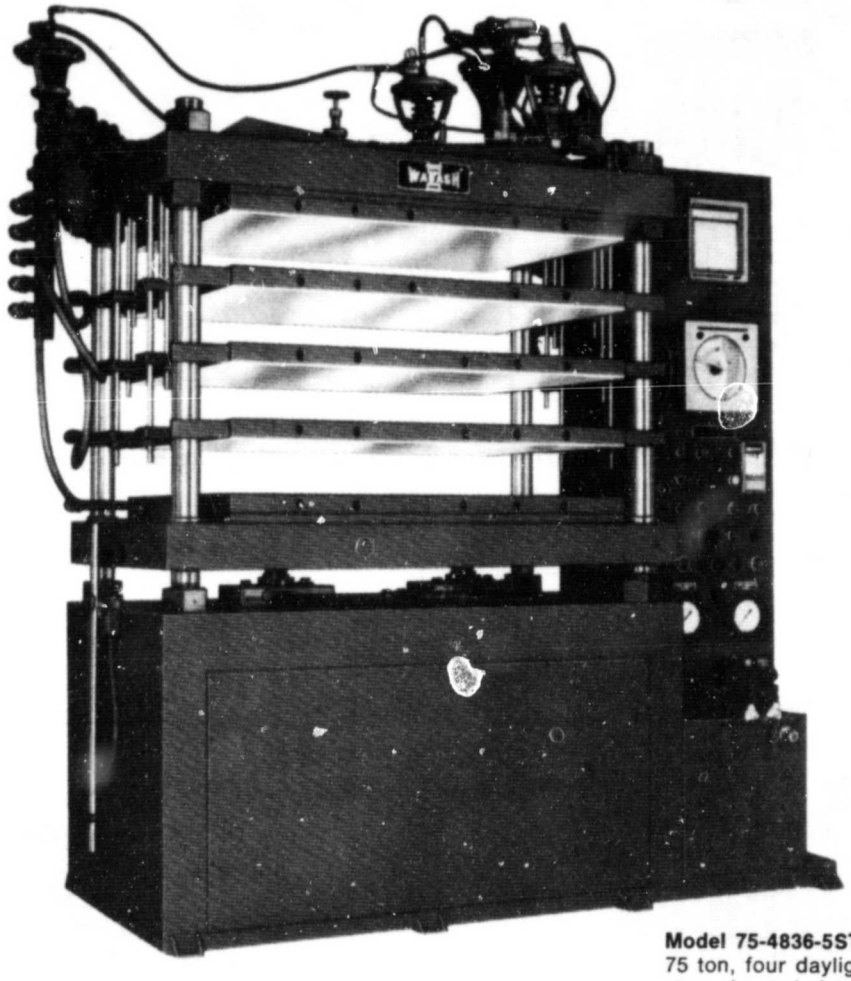

Model 75-4836-5STMAC—
75 ton, four daylights with five steam heated platens, steam valves and temperature controllers.

Figure 3.3.4. 5-platen hydraulic press

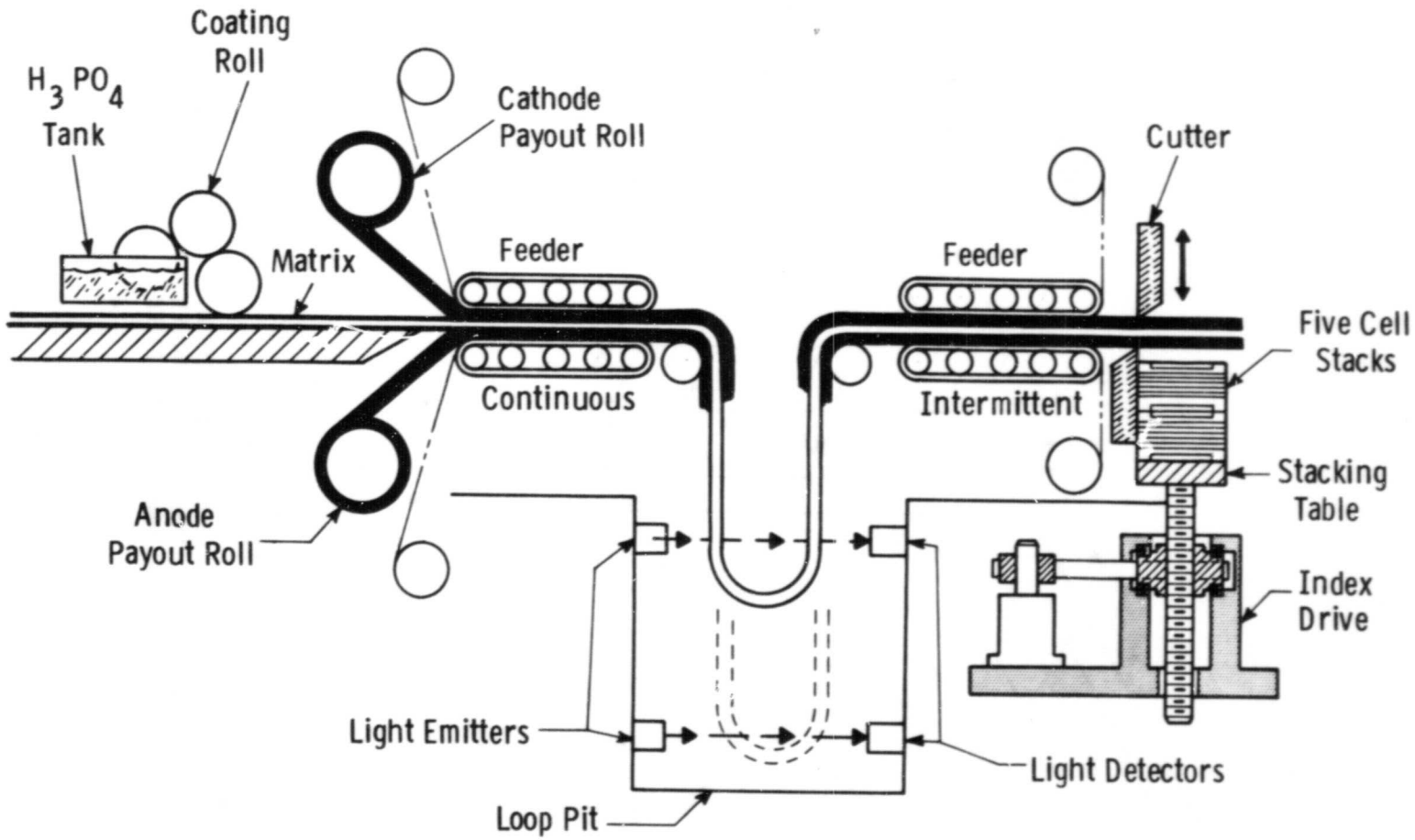

FIGURE 3.3.5. AUTOMATED ASSEMBLY OF PAFC REPEATING COMPONENTS

ORIGINAL PAGE IS
OF POOR QUALITY

ORIGINAL PAGE IS
OF POOR QUALITY

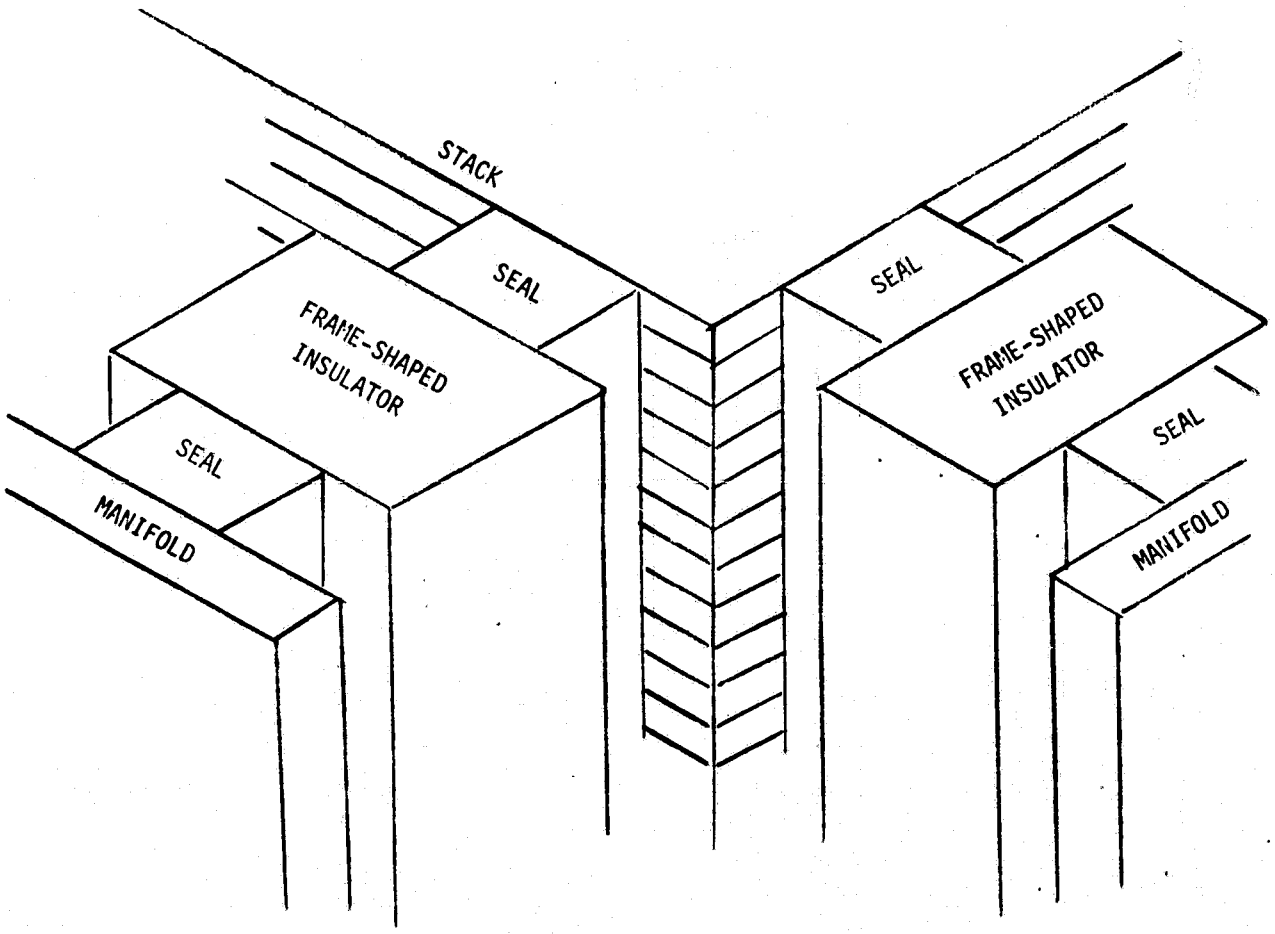

FIGURE 3.3.6

MANIFOLD DESIGN CONCEPT WITH A
FRAME-SHAPED INSULATOR INTERPOSED
BETWEEN METAL MANIFOLDS AND STACK

3.3.2 Manifold Design and Materials

The manifold's major function is to distribute the gas flow evenly over the height of the fuel cell stack. At first glance, it appears that this is not very difficult. There are, however, several factors to be considered. First, the manifold must withstand a 200°C temperature continuously. Second, it has to be corrosion resistant because of its exposure to a phosphoric acid environment. Third, it should reasonably match the thermal expansion characteristics of the fuel cell stack in order to minimize the shear forces on the stack-to-manifold seal once the cell material properties have stabilized. Finally, its surface should be an electric insulator to prevent electric arcing or shorting of the stack. For a short stack (small number of cells) the arcing problem is minor since the total voltage is low. As the number of cells (per stack) increases, the voltage increases proportionally and arcing or electric shorting can become a major problem. Various manifold design concepts and materials to satisfy these requirements were investigated and preliminary estimates of their economic viability were made.

A design concept that interposes a frame-shaped insulator between a metal manifold and the stack to prevent electrical shorting is shown in Figure 3.3.6. The addition of the separate insulator increases the cost of the fuel cell stack by 2 to 3 $/kW because of the cost of the insulator and additional seal between the insulator and the manifold. Moreover, the reliability is diminished since the number of seals is doubled and the probability of failure increased accordingly.

Insulating Materials

The electrical isolation could be provided by coating the metal manifold with an insulating material or by constructing the manifold completely from an insulating material. To be successful the materials must resist corrosion, not deteriorate with age, and be reasonably inexpensive.

ORIGINAL PAGE IS
OF POOR QUALITY

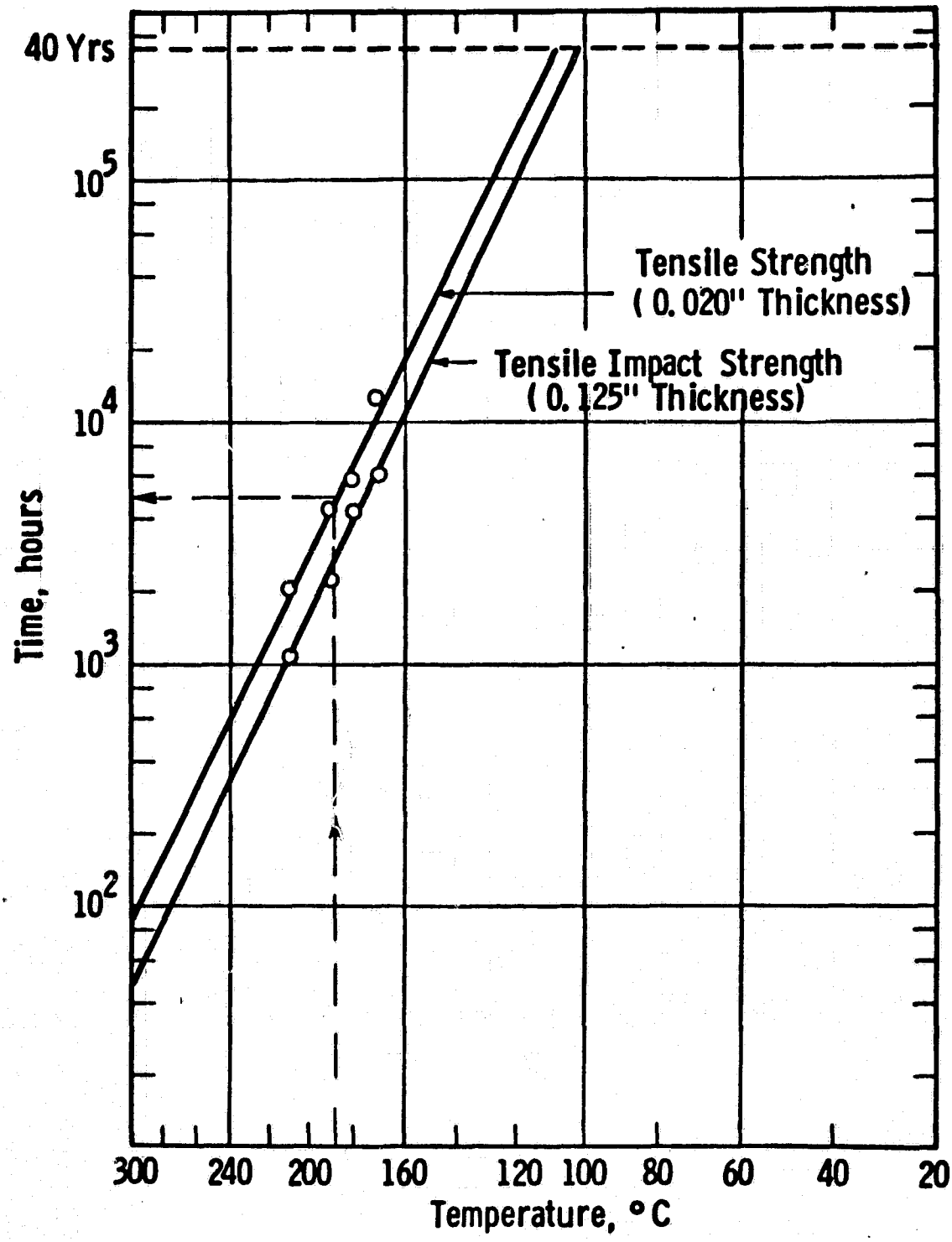

Fig. 3.3.7 – Arrhenius plots at 50% retention of properties for Bakelite Polysulfone P-1700

An initial selection of candidate electrical insulating materials was made by a Westinghouse material selection computer program based on temperature, pressure,and other environmental conditions. We then examined the aging properties of these materials using information generated under another on-going Westinghouse program discussed below. The factors which may accelerate aging in the fuel cell are temperature, voltage, corrosion,and humidity. Ideally, normal operation testing for a long time would provide the desired aging data. However, this is impractical with a large number of candidate materials and the length of time required for such testing. The objective of the on-going Westinghouse materials program is to provide a manual,cataloging and interpreting the available information on the effects of thermal and radiation aging on non-metallic materials. The thermal-aging guide used in this program is an Arrhenius plot relating the logarithm of life to the reciprocal of the absolute temperature. The useful life is defined as the length of time a material can continuously tolerate a given temperature and retain 50% of its mechanical strength. A typical plot is shown in Figure 3.3.7. The dashed lines indicate the useful life for this material is only 5,000 hours at a continuous use temperature of 190°C.

For the materials which emerged as candidates from the aging screening, cost is the major determinant of whether the manifolds should be fabricated completely from the selected materials or from metal coated with these materials. Figure 3.3.8 depicts the material cost relationships of these candidates for complete manifolds (0.32 cm) material and coated on metals (0.08 cm). As might be expected, the lower cost items on the graph are those least likely to be acceptable. The degree of acceptability is discussed in the next sections in which each method of fabricating manifolds is presented.

COST ESTIMATES FOR FUEL CELL MANIFOLDS
FUEL/O_2 AND COOLING AIR
300 CELL UNIT

FIGURE 3.3.8

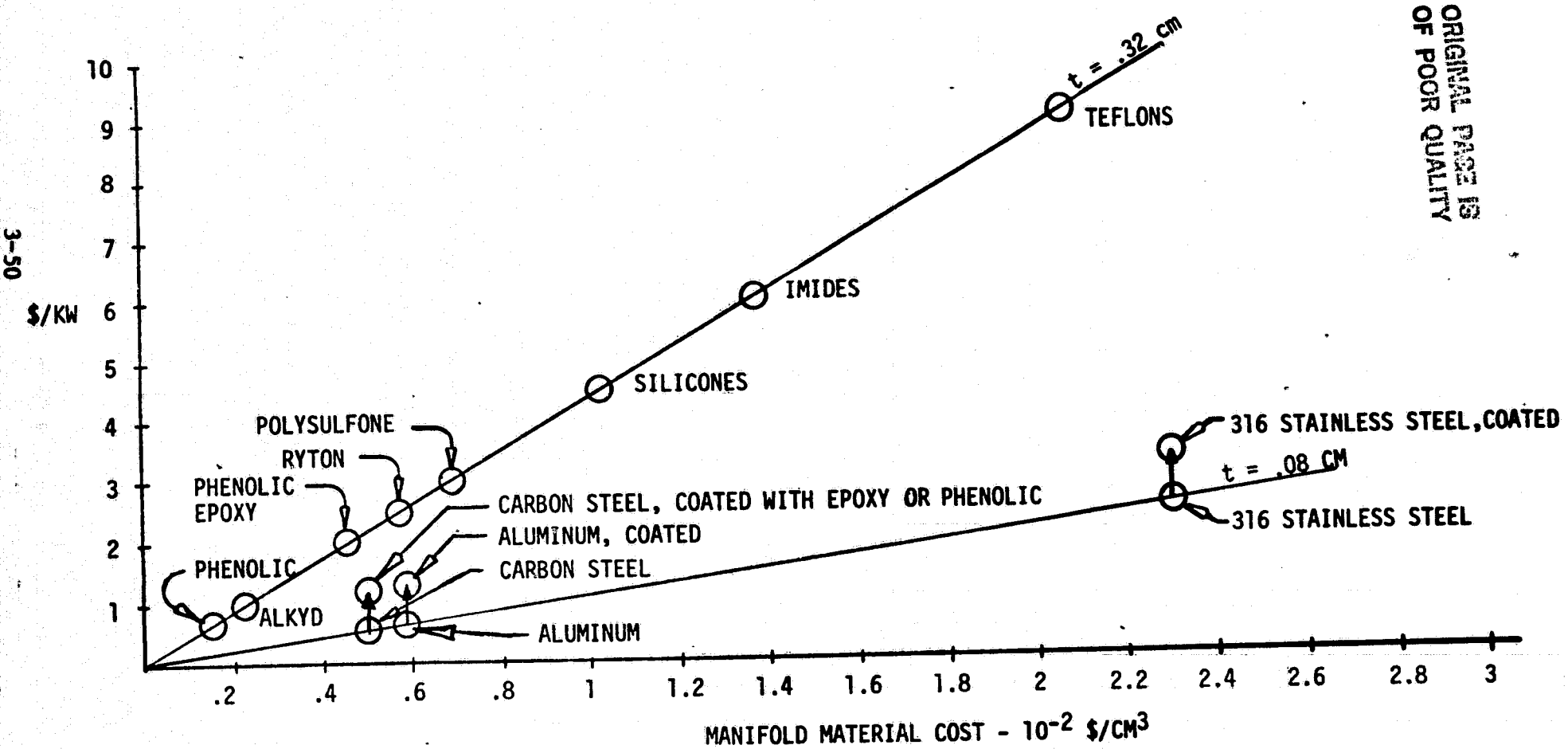

ORIGINAL PAGE IS
OF POOR QUALITY

Manifolds Fabricated Completely From Insulating Materials

Primarily because the electrical insulation problem would be completely nonexistent, the most attractive fabrication method is molding the manifold completely from an insulating material. However, this presents the most difficult material selection problem. Several materials considered are listed in Table 3.3.3 which tabulates estimated cost, life at required operating temperature and manufacturability. The materials which appear most likely to have satisfactory lives in this environment are Teflon, silicones and Ryton. Teflon is too expensive and difficult to mold. The silicones are also difficult to mold and may not have adequate acid resistance. Ryton, whose generic name is polyphenylene sulfide and is made by Phillips Petroleum, is a strong possibility. It has high mechanical strength and rigidity at elevated temperatures and has excellent chemical and solvent resistance. According to the manufacturer, it is U.L. approved for continuous use at 200°C and should present no problems for injection molding into large manifold shapes. Several molders of this material were contacted and, although none had experience with molding large shapes, they had such good success in molding small articles that they anticipated no problems with larger parts. Injection molding is a very low cost fabrication method and since Ryton is the least costly of the conditionally acceptable insulating materials, its use in molded form should be one of the least costly manifold options.

Other insulating materials shown in Figure 3.3.8 are the imides. They have better thermal resistance properties than Ryton but are more than twice as expensive and more difficult to mold. Another possible candidate not shown is polyether sulfone,which suffers from the same cost problem,but is relatively easy to mold.

Metal Manifolds with Protective Coatings

The thermal aging properties of protective coatings are similar to those of the solid molded material,but the mechanical strength requirements are less severe. Figure 3.3.9 illustrates the

Table 3.3.3. Comparison of Plastic Materials

Material Description	Cost $/KW	Average Life at 190°C in Years	Operating Temperature for 5 Yr. Avg. Life in °C	Manufacturability
Glass Reinforced Phenolic Molding Mixture	.75 to 2.00	.5	145	Compression or transfer molding. Difficult to mold large shapes, because material cannot be preformed into sheet molding compounds.
Glass fiber reinforced polyester	1.3	.1	120	Compression or transfer molding. Availability in sheet molding compounds. Makes possible molding of large shapes. Hand Layup possible for prototypes.
Epoxy	2.00 to 7.00	.5	150	Compression or transfer molding. Availability in sheet molding compounds. Makes possible molding of large shapes. Hand Layup possible for prototypes.
Silicones	4.5	>1	200	Compression or transfer molding. Difficulty of molding large shapes unknown at this time.
Fiberglass Reinforced Alkyd	1.0	.1	120	Not investigated at this time.
Polysulfone	3.0	.6	145	Injection or blow molding. Large shapes possible but cost of molds probably very high for injection molding. Vacuum forming possible for prototypes.
Ryton	2.5	>1.0	200	Injection molding. Difficulty of molding large shapes unknown at this time.
Teflon	9.0	>1.0	200	Injection molding. Very difficult to mold because of high melting temperature.

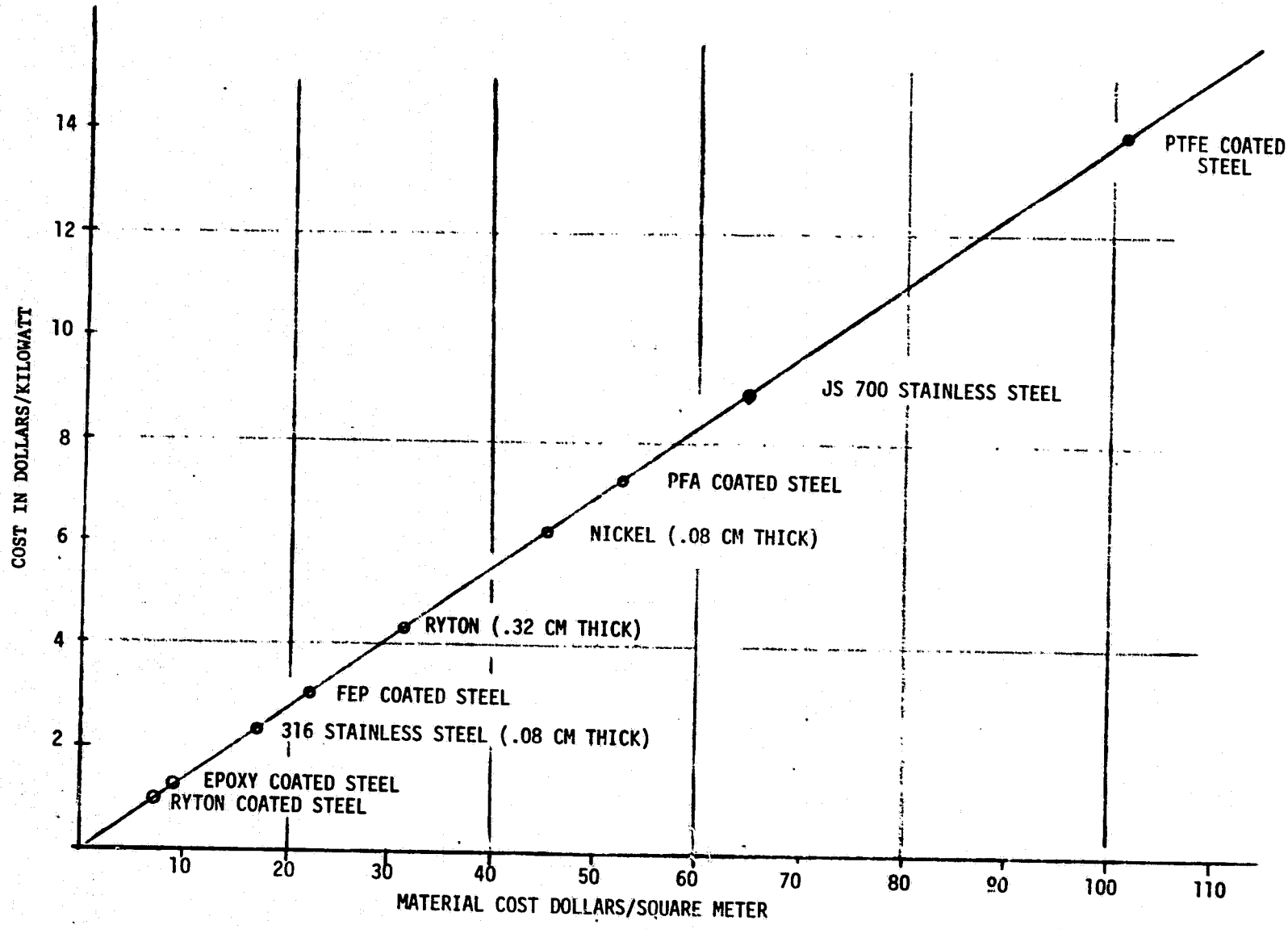

FIGURE 3.3.9. - COST ESTIMATES FOR FUEL CELL MANIFOLDS
FUEL, OXYGEN AND COOLING AIR
300 CELL UNIT

ORIGINAL PAGE IS
OF POOR QUALITY

ORIGINAL PAGE IS
OF POOR QUALITY

relative material costs for several 0.8 mm (0.032 inch) thick sheet metals with protective coatings. For reference purposes, uncoated 316 stainless steel ($1.50/pound), nickel, and 0.32 mm (0.125 inch) thick Ryton (Polyphenylene-sulfide) have been shown. Of the Teflon coatings. FEP (Tetrafluoroethylene-hexafluoropropylene) coated carbon steel has the lowest cost and this corresponds to approximately three dollars per kilowatt for the OS/IH stacks. This is for a 0.25 mm (0.010 inch) thick coat on 0.8 mm (0.032 inch) thick carbon steel. One potential problem with Teflon coatings is their lack of long term adherence to metals. Because of their high cost, PFA and PTFE coated steels are not acceptable. Although not as temperature resistant, Ryton and phenolic coatings deserve strong consideration because of their low cost.

Another possibility is porcelainized steel. Its temperature and chemical resistance is excellent and the cost is comparable to phenolic coated steel. Capital cost for porcelainizing equipment is extremely high.

Uncoated Metal Manifolds

If the electrical insulation problem is considered to be acceptably solved by the insulating frame discussed earlier, uncoated metal manifolds may be a satisfactory choice. Plain carbon steel or aluminum do not appear to be satisfactory choices due to their lack of resistance to phosphoric acid corrosion. Although the actual degree of manifold exposure to this acid is unknown, it is present to some extent in the exit gases. Carbon steel has another problem; water vapor in the exit reactant streams will corrode it.

Conventional 316 stainless steel is relatively low cost and is commonly used for chemical processing equipment. It will corrode upon exposure to 70% phosphoric acid at the rate of 9 mm per year at a temperature of 140°C, which is much more severe than the exposure it will see as a manifold material. Specialty stainless steels are available

such as JS 200 (made by Jessup Steel Company), which under the same conditions corrodes at only 0.3 mm per year. Its cost, however, is more than twice as much as 316, $3.72 per pound versus $1.50 per pound. Nickel 200 is less costly than this and is a good candidate for corrosion resistance. Therefore, as is the case with insulating materials, there are several possibilities and the correct choice can only be made on the basis of successful performance under actual or simulated operating conditions.

3.3.3 Stack Enclosure and Assembly Costs

The stack enclosure is defined as those components of the module that are not repeating components i.e. manifolds, frame members, top and bottom plates, etc. This section presents estimates of the cost of procuring and assembling the parts required for the full scale module described in Westinghouse Patent Disclosure RES 80-301. The summary presented in Table 3.3.3 shows a total cost of $692 or $23 per kW. To obtain costs of procuring the parts, conceptual drawings were sent to several vendors for quotations. The most realistic quotation received was for $820 per stack based on production runs of 10 to 1,000. If, to this, a learning curve is applied, production rates of 16,000 per year should result in costs close to $500 per stack. This compares favorably with information from one of the Westinghouse Divisions which makes products similar to the enclosures required here. The Westinghouse Division's average costing rate including labor and overlead is $.61 per pound of material used. This enclosure design will weigh 803 pounds, so it would cost $490 at $.61 per pound. These costs include fabricating the manifolds out of .32 cm thick sheet steel with a protective coating of 0.5 mm thick polyphenylenesulphide (Ryton) applied on the inside and outside. The investigations discussed in section 3.3.2 indicated that Ryton is a good choice for cost and performance reasons. From a corrosion standpoint only the inside requires coating, but coating both sides should allow the use of only one gasket instead of two with an insulator, thus reducing cost and complication.

TABLE 3.3.3

COST ESTIMATE OF PROPOSED 30 KILOWATT FUEL STACK ENCLOSURE AND ASSEMBLY

1.	Enclosure Components (Outside Vendor)		
	Material (Cold Finished Steel)	$313	
	Hardware (Bolts, Studs, Nuts)	90	
	Labor	97	
	TOTAL		$500
2.	Protective Coating for Manifolds		
	Material (0.5 mm Ryton both sides)	$ 44	
	$5 Direct Labor x 2.133 IPEG factor	11	
	TOTAL		$ 55
3.	Gasket (Purchased)		
	0.54 cm Dia. Extruded Viton		$ 47
4.	Cell Assembly into 5 Cell Short Stacks		
	$28 Direct Labor x 2.133 1 PEG Factor		$ 60
5.	Stack Enclosure Assembly		
	$14 Direct Labor x 2.133 IPEG Factor		$ 30
			$692

$692 at 30 KW = $23/KW

ORIGINAL PAGE IS
OF POOR QUALITY

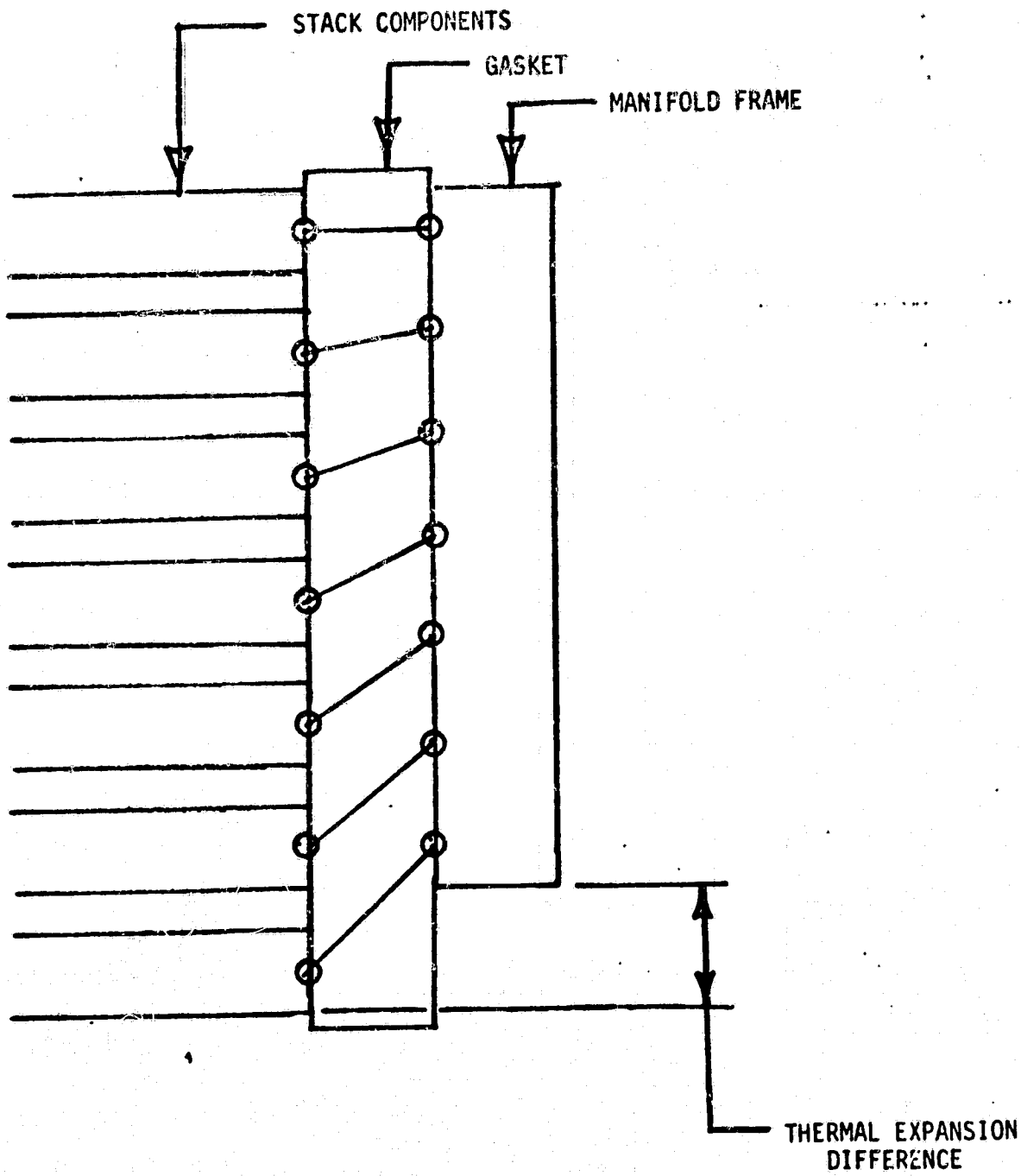

FIGURE 3.3.10. MODEL FOR TRANSMISSION OF FORCES THROUGH GASKET

ORIGINAL PAGE IS
OF POOR QUALITY

Figure 3.3.11. MANIFOLDS RIGIDLY FASTENED TO ENDPLATES, STACK EXPANSION CONSTRAINED BY MANIFOLDS

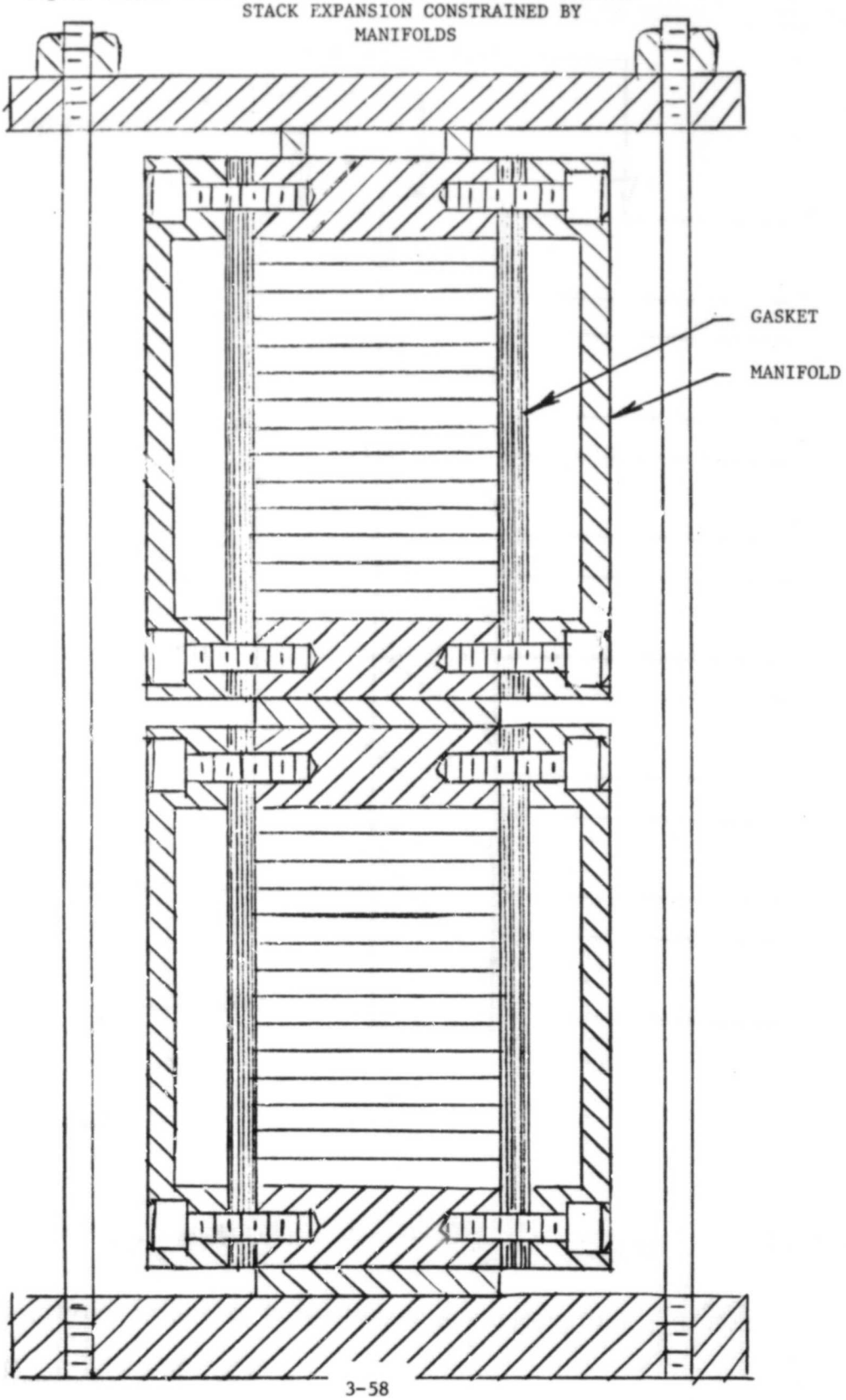

The gasket is a purchased item and is expensive because of the expensive flurolastomer (Viton) required as the material. Cell and enclosure assembly are labor items which are estimated at the values shown in the table.

3.3.4 Seal Design and Materials

As part of the stack design effort, the transmission of forces from the manifold to the stack were analyzed. Figure 3.3.10 illustrates that these forces result from differential expansion of the manifold and stack and are transmitted through a shearing of the gasket. The magnitude of the force depends on the material properties (hence the interest in measuring the thermal expansion coefficients of simulated stacks), temperature, methods of attaching manifolds to stacks, height of stacks, etc.

Preliminary analyses of the restraining effect and the seal stresses were made for two manifold designs shown in Figures 3.3.11 and 3.3.12. As shown, in both cases the 300 cell stack was assumed to be manifolded in 150 cell modules.

The design shown in Figure 3.3.11 is similar to that used in current experimental stacks in that each end of the manifold is bolted into end plates. In this case there will be very little shear stress on the seal because the manifold and stack are forced to expand the same amount by the attachment bolts at each end. Stress caused by this will be absorbed by the stack and manifold and will not be transmitted to or through the seal.

The manifold design shown in Figure 3.3.12 is not fastened to the end plates and does not significantly restrain the stack. The calculated difference in expansion between a steel manifold and each 150 cell stack is 0.8 mm for a temperature rise from 25 to 190°C. This difference must be accomodated by the shear of the gasket material as indicated in Figure 3.3.10. The analysis indicated that the stack compression will increase by about 24 kPa (~6% of nominal value) at

ORIGINAL PAGE IS
OF POOR QUALITY

FLOATING MANIFOLD, STACK EXPANSION UNCONSTRAINED.
GASKETS DEFORM TO ACCOMMODATE
STACK EXPANSION

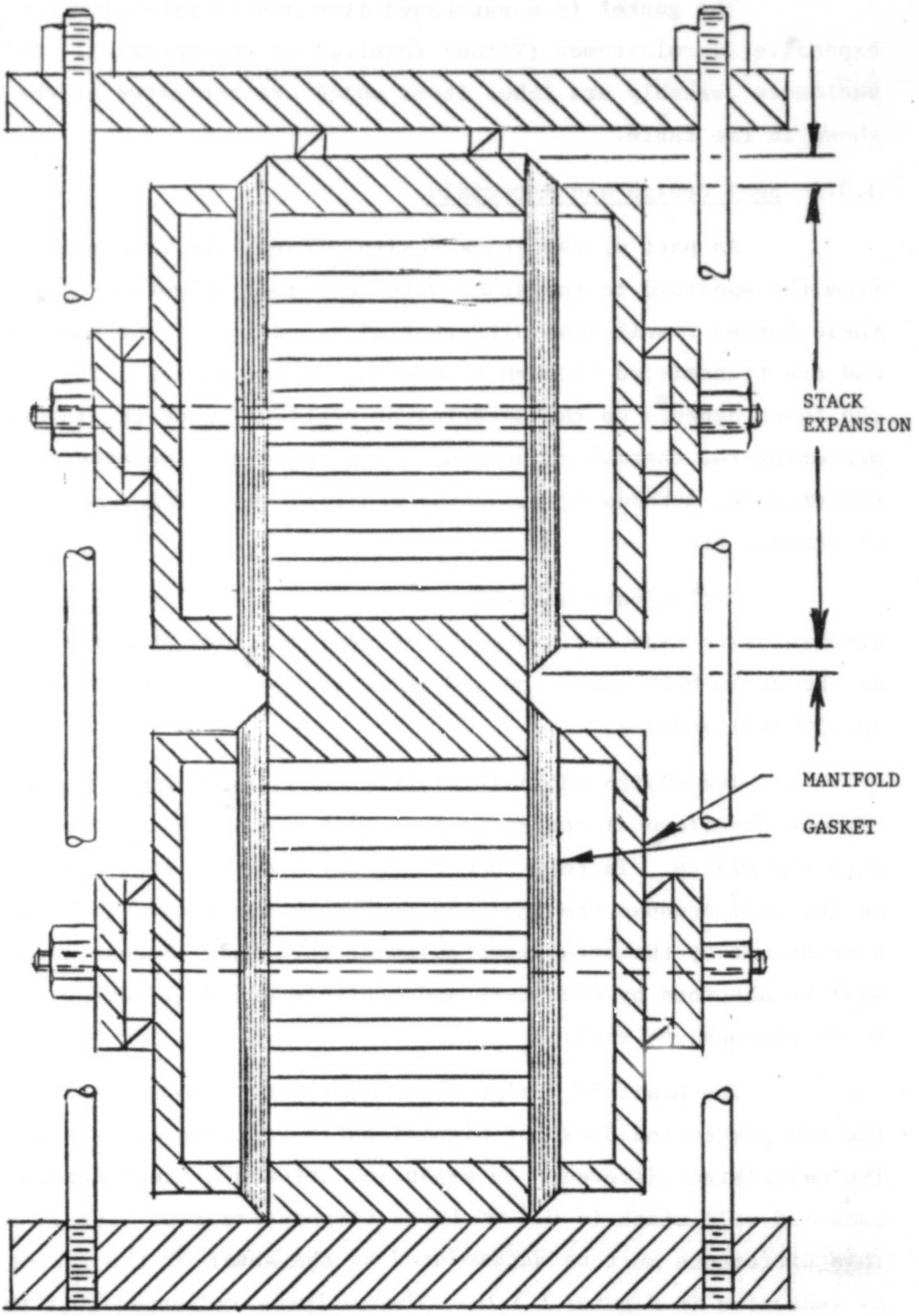

FIGURE 3.3.12

ORIGINAL PAGE IS
OF POOR QUALITY

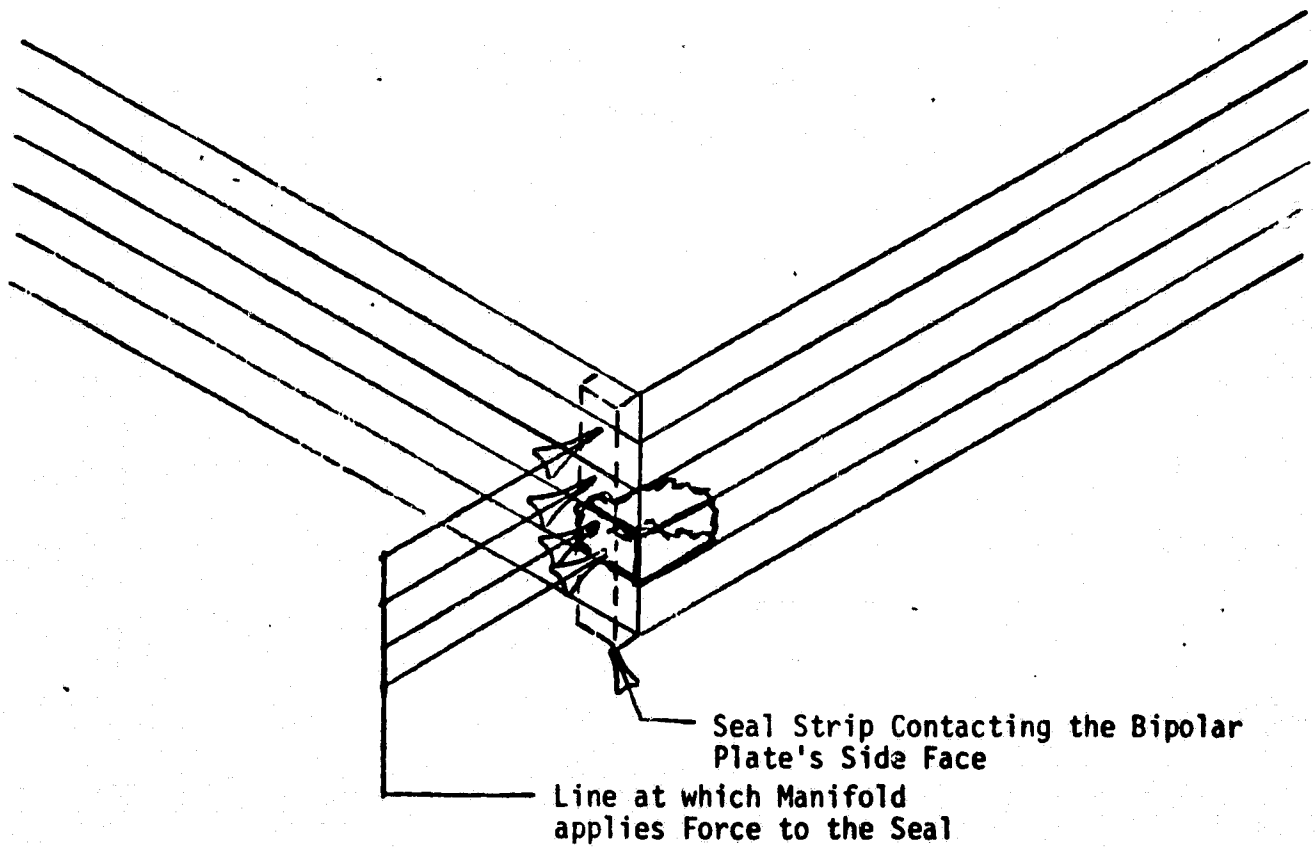

Figure 3.3.13.Manifold Seal Load on Bipolar Plate Corners

Figure 3.3.14. CONCEPTUAL DESIGN OF GROOVE FOR RETAINING GASKET IN MANIFOLD

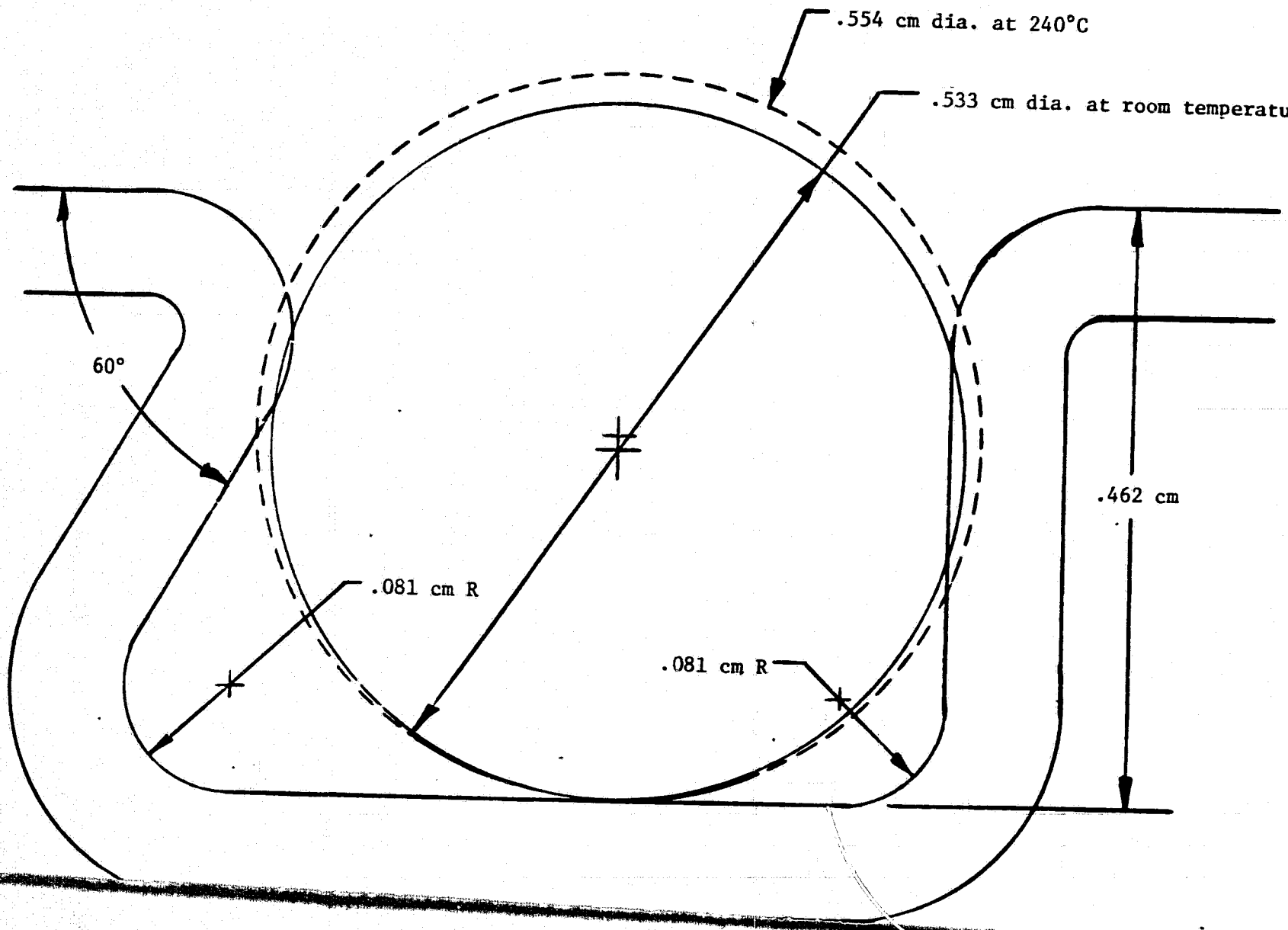

ORIGINAL PAGE IS
OF POOR QUALITY

190°C if steel manifolds and a 5.5 mm diameter fluoroelastomer (Viton) gasket is used. The calculated shear stress in the gasket material is 340 kPa which is about 5% of the published limit for this material. Thus, shear on the seal should present no problem since steel has the greatest thermal expansion mismatch compared to the stack of all materials being considered for the manifold.

An analysis of the compression and shear stresses acting at the corners of the bipolar plate as the manifold seal is forced against the bipolar plate's side face (Figure 3.3.13) was also made. If the seal is placed too close to the bipolar plate corners, there is a danger of fracture. The analysis indicated a maximum shear stress of 230 kPa for a uniform load applied 7.6mm away from the bipolar plate corners. The mechanical strength of the bipolar plates appear to be sufficient to accommodate this stress.

Material, fabrication and cost investigation of seal materials and shapes was performed. Only fluoroelastomers possessed the heat resistance required. Because of the high material cost, closed-cell foam gaskets were considered, but they tend to take more compression set than their solid counter parts. To minimize compression set, the gasket manufacturers made two recommendations. Confine the gasket by locating it in an appropriate groove and limit the gasket's deflection to 10% of its uncompressed height. A groove design which retains the gaskets and can be stamped in a manifold made of sheet metal was conceived and is shown in Figure 3.3.14.

Cost data were developed for solid 0.54 cm and 0.70 cm diameter (circular cross section) fluoroelastomer (Viton or Fluorex) gaskets. In large quantities (over 16 km), the cost of extruded 0.54 cm material is $1.67 per meter or 44 percent of the molded version which has been quoted at $3.80 per meter. As the diameter increases to 0.70 cm, the cost of the molded gasket increases to $5.10 per meter and the extruded version to 2.24 per meter. Provided the extruded gasket can be inexpensively joined, it is the preferable material and would reduce the gasket cost to $1.56 per kilowatt in the .54 cm diameter size.

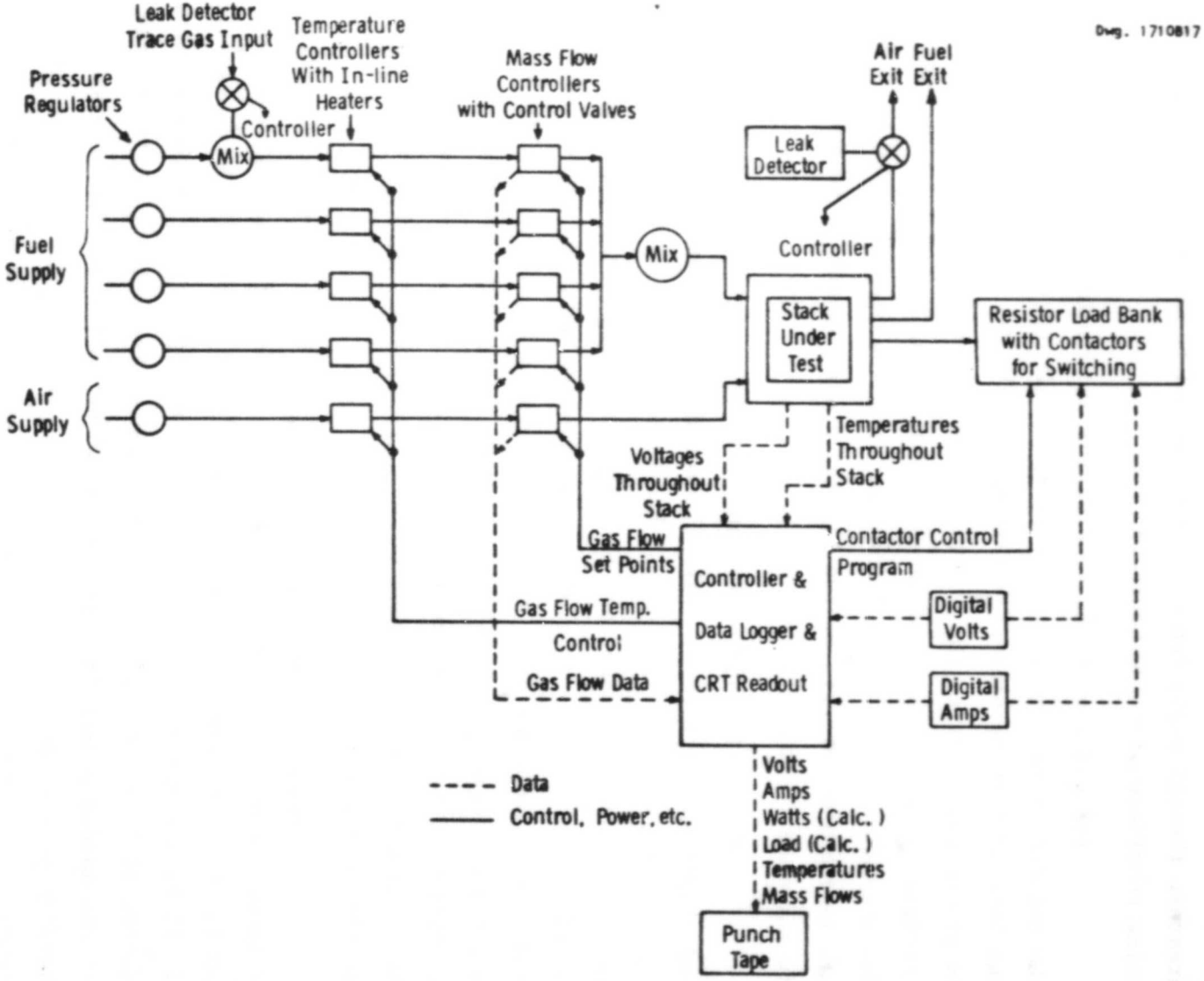

Figure 3.3.15. Conceptual test system for assembled fuel cell stack

ORIGINAL PAGE IS
OF POOR QUALITY

3.3.5 Quality Assurance

As is the case for any manufactured product some method of assuring the quality of the finished product must be utilized. One method is 100% testing of finished product. The costs of giving every module a "stabilization" run of 240 hours and test is prohibitive as established by the analysis that follows.

Figure 3.3.15 represents a conceptual stack test station. The estimated costs are:

Temp. Controllers	$ 200 x 5 =	$1,000
Mass Flow Controllers	1500 x 5 =	7,500
Resistor Bank, Contactors & Control	=	7,000
Digital Voltmeter	=	100
Digital Ammeter	=	200
Controller Punch Tape & Hard Copy	=	30,000
Labor + 10% of Programming Cost	=	12,000
Ductwork, etc.	=	12,000
Miscellaneous	=	3,200
		$73,000

If it takes 240 hours to stabilize the performance of and test each unit and the production rate is 67 units per day (16,700 per year), 670 units will be on test at any one time requiring 670 test stations. At $73,000 each the total capital cost will be $49,000,000. With cost estimates for labor, material, floor space and utilities, the IPEG model was used for estimating total testing costs.

Direct labor will be mainly that required for connection, disconnecting and moving stacks since the test equipment will be equipped with controllers and data loggers. Four persons per shift on a three shift basis should be adequate. At an estimated labor cost of $7.00 per hour, labor costs will be $175,000 per year. Floor space for testing was estimated to be 150 sq. ft. per station for a total of ∿100,000 sq. ft. The major material cost is the 1.73 million liters per hour of hydrogen

ORIGINAL PAGE IS
OF POOR QUALITY

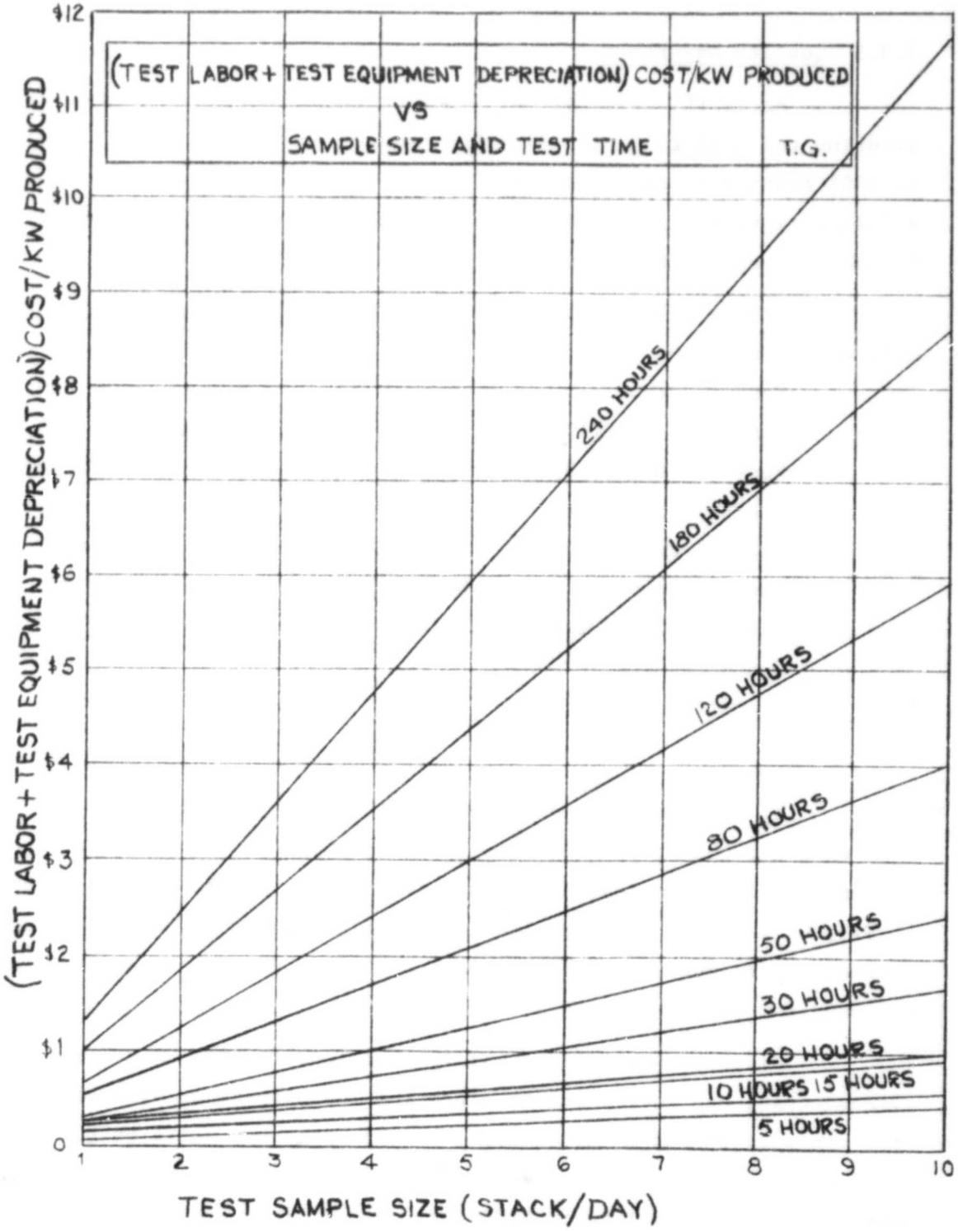

Figure 3.3.16

consumed by the 670 stacks undergoing test. At an estimated large volume cost of hydrogen of $.0002 per liter, the yearly cost will be $2,125,000. Utilities should be an income item instead of a cost item since the stacks on test will produce 20 megawatts of electricity. Since a profitable method of disposing of this can probably be found, no cost for this item was included. The IPEG calculations are shown in Table 3.3.4. The resulting cost for testing of $66.30/kW is unacceptable high. Significant reduction in the "stabilization" time is required in order for 100% testing of finished modules to be viable.

If stabilization cannot be significantly reduced, sample testing of stacks must be considered. Figure 3.3.16 shows the effect on cost of reducing sample size and testing time. Testing a 10% sample, 7 per day instead of 67, for the full 240 hours would reduce the testing cost per kW to $8.50. If the "stabilization" time could also be cut in half the cost would drop further to $4.25/kW, which should be acceptable.

TABLE 3.3.4

PHOSPHORIC ACID FUEL CELL REPEATING COMPONENTS

JPL IPEG COST MODEL

COST ITEM	IPEG FACTOR	ESTIMATE OF COST ITEM	IPEG COST $/YR	$/kW
Equipment	.489	$49,000,000	20,400,000	40.80
Floor Space	96.9	100,000 ft^2	370,000	.75
Direct Labor	2.133	175,000/yr.	9,690,000	19.40
Direct Material	1.255	2,125,000/yr.	2,670,000	5.35
Utilities	1.25			
TOTALS			33,130,000	$66.30

4. Task 2: Stack Fabrication

The purpose of this task was to fabricate components for and assemble stacks for testing. This task along with Task 1 and 2 (stack design and testing) comprised the effort to develop fuel cell modules for the OS/IES application. Primary emphasis was placed on the development of stacks and cooling plates that would achieve maximum performance from the electrochemical components under the operating conditions required by the OS/IES application. The three tasks were integrated and closely coordinated with feedback provided by meetings and participation by key personnel of all three tasks.

The culmination of this task was the successful assembly of a stack of 80 full size (30 X 43 cm) cells incorporating separation of the cooling and process air streams, MAT-1* matrices, heat treated bipolar and variable area cooling plates, and manifold/sealing and compression systems that accommodated the deformation and differential thermal expansion of the stack. The stack design features and assembly procedures used on this stack were developed by fabricating and testing the stacks listed in Table 3.2.1, and critical experiments on methods approaches carried out as part of this task.

In parallel with this program, ERC was developing improved cell components under internally funded projects and parallel technology development contracts (DEN3-205 and EC-77-03-1404) funded by DOE and managed by NASA-LeRC. Close coordination was maintained with these parallel programs and the improved components were incorporated into the stacks fabricated under this task when appropriate and approved by the NASA Project Manager.

---

*U.S. Patent 4,276,356

4.1 Methods and Approaches

The work carried out under this Subtask comprised simple but important experiments which were used to evolve or verify fabrication techniques and design features before incorporating them into 23 cell or larger stacks. Some examples of these are described below.

4.1.1 Stack C

Stack C was a 3-cell, 13 cm x 38 cm stack built to test the innovative acid replenishment/filling scheme described in Section 3.2.2 and the new compression method described below. As shown in Table 3.2.1, the stack was assembled with dry Kynol matrices and nonheat-treated bipolar plates. The stack was satisfactorily wicked in 20 hours at an acid flow rate of 4.5 cm^3/hr and took about 51 cm^3 of acid. The initial acid inventory in the stack was augmented during the first 400 hours of operation; only small acid additions were made after this time. Stack C was tested under load and accumulated a total of ~2000 hours of operation at a stable performance level of 0.57 V/cell at 100 mA/cm^2 as shown in Figure 4.1.1. The dip in on-load performance that occurred around the 58th day was caused by a reduction of air supply due to a cracked air inlet manifold. After the manifold was repaired, performance at the previous level was re-established.

The successful operation of Stack C demonstrated that the new methods of compression and electrolyte filling were suitable for stack assembly.

4.1.2 Stack Compression Method and Techniques

A simple and effective technique was developed to ensure uniform stack compression. The tie bar deflection method previously used was quite cumbersome and time consuming.

The new method illustrated in Figure 4.1.2 used a stack compression jig and four through-hole hydraulic rams (one for each stack tie rod). The rams were connected to a common pressure source so

ORIGINAL PAGE IS
OF POOR QUALITY

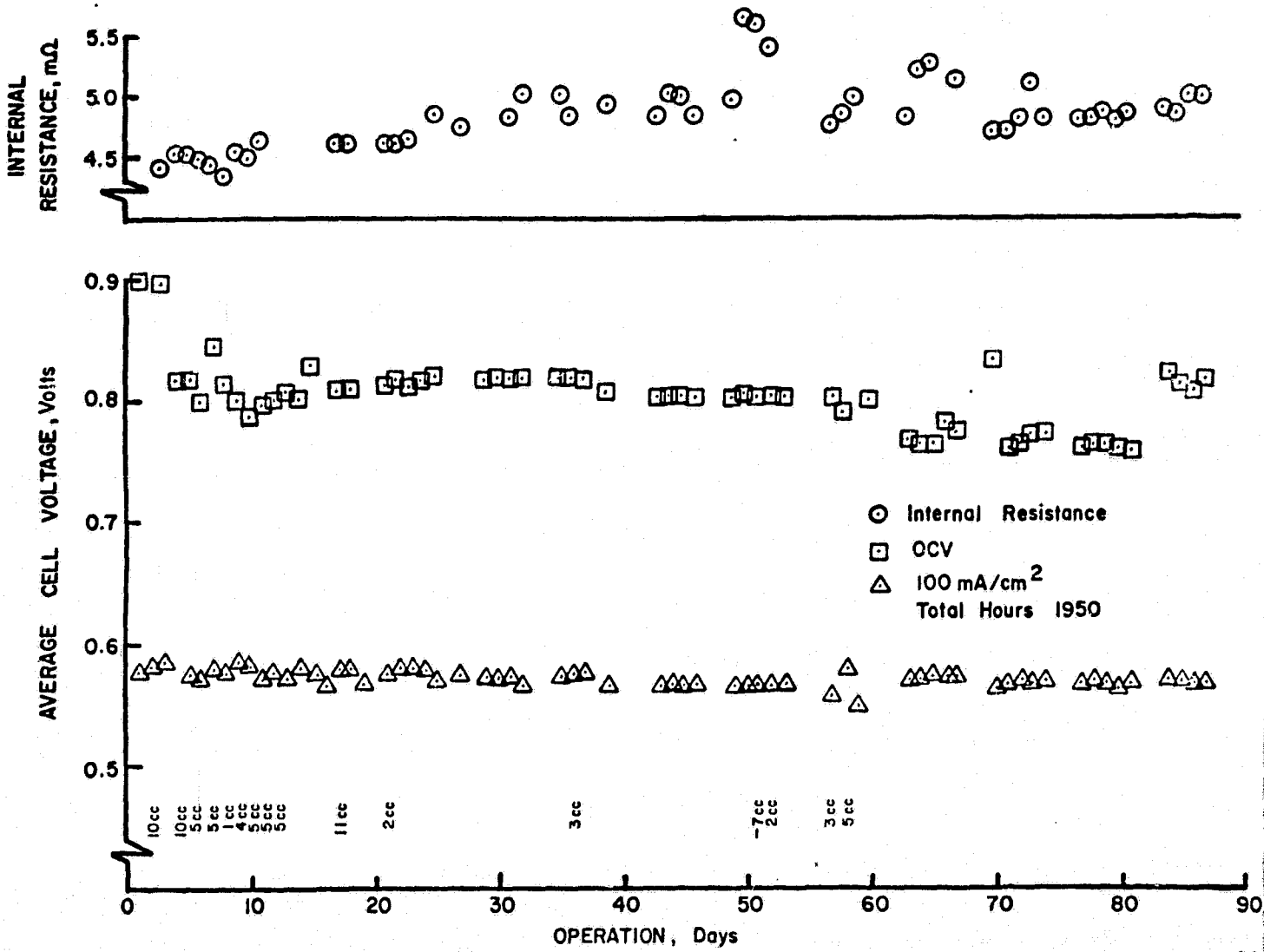

FIGURE 4.1.1. LIFEGRAPH OF STACK C

ORIGINAL PAGE IS
OF POOR QUALITY

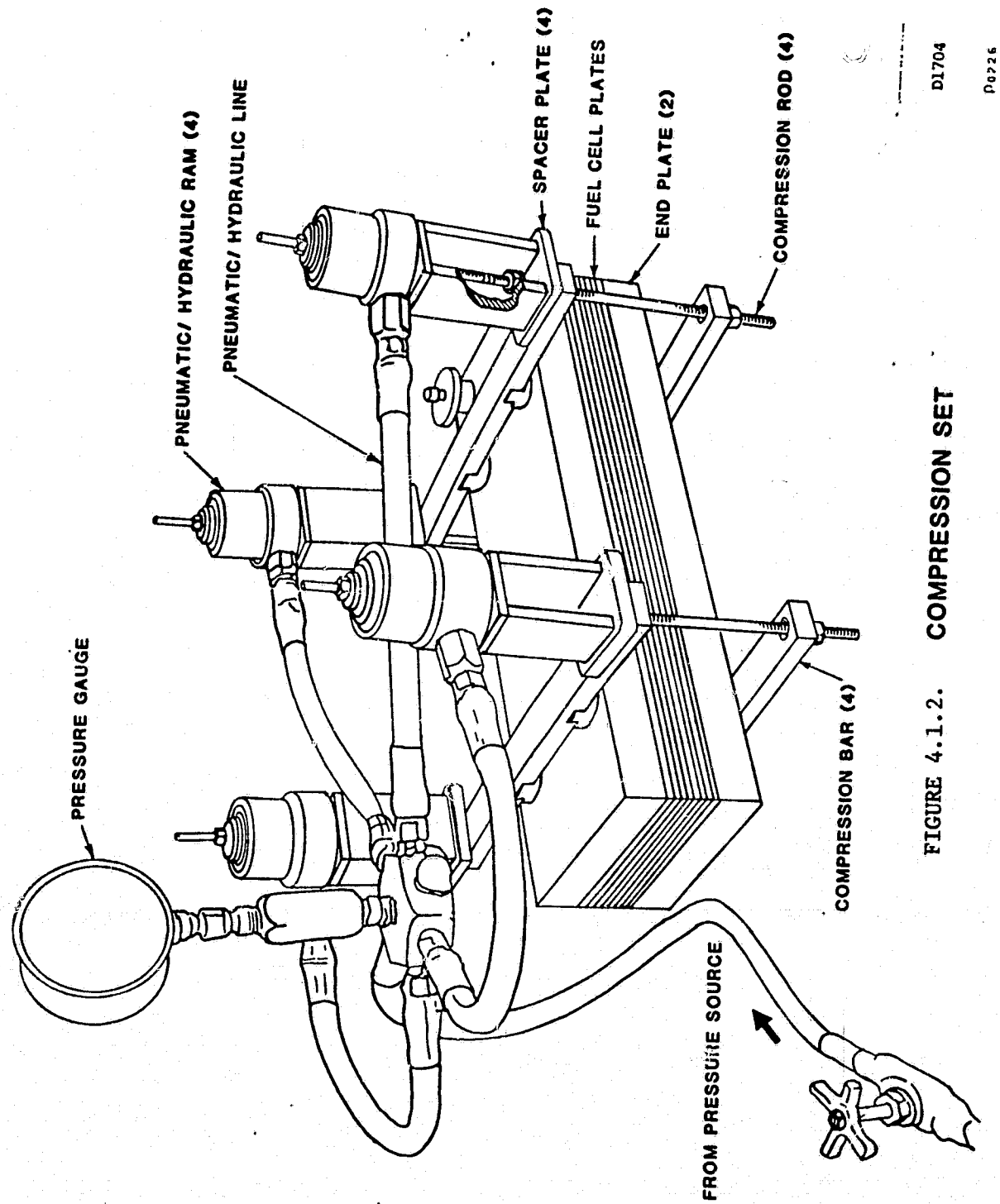

FIGURE 4.1.2. COMPRESSION SET

D1704

an equal pressure was exerted on each tie bar. Each tie bar had two foot pads located at strategic points to distribute the compressive force uniformly over the cell area. When the desired compression was obtained, the ram assemblies (including spacer) were disconnected at the coupling. This method simplified the loading procedure greatly and ensured an accurate and uniform compressive load on the stack.

4.1.3 Highly Conductive Cooler Assembly

The cooler plate design concept requires that two cooler halves be joined together. In Phase I graphite paper was used to reduce the interfacial resistance between the two cooler halves, but this resulted in an increased heat transfer area which reduced the ability of the variable area to achieve a uniform cell temperature. A new method was developed which lowered the contact resistance between the two cooler halves, provided a better seal to prevent reactant crossover, and eliminated the paper in the cooling channels.

The state-of-the-art assembly procedure uses the same conductive graphite-resin as the plate material dissolved in a solvent for easy application. This solution is applied to the ribs of the cooling channels and a high-strength epoxy adhesive is applied on the margins or peripheral area. The plate halves are then aligned, compressed under a predetermined load, and heat treated.

The finished plates have the following advantages:

- Reduced resistance by 10 to 50 fold.
- Materials are compatible with the reaction in the cell (no poisoning).
- Highly acid resistant.
- Permanent bonding for ease of handling, storage and stack assembly.
- Margins are sealed from other process streams.

4.1.4 Stack Dimensional Changes

During operation the stack dimensions change due to a combination of thermal expansion (and contraction) and a combination of permanent and elastic deformations of the components. The magnitude (and direction) of this change is a complex function of the details of stack construction (which affect the distribution of the load among the active and marginal areas of the stack), the temperature level of and its distribution in the stack, properties of the stack materials, the compressive load on the stack (which in turn is affected by the dimensional changes), and the design of the stack compression system. Although the changes are too small to be measured in 5 or 23 cell stacks, simple calculations indicated that they would be significant in an 80 cell stack.

In order to obtain an estimate of the changes which would need to be accommodated by the manifold and compression systems of Stack 800 as well as in the full scale module design, measurements of the dimensional changes of an existing 80 cell stack (built under an ERC in-house project) were made. The results are summarized in Table 4.1.1.

As indicated in Table 4.4.1, the stack height (measured from end plate to end plate) decreased during the acid filling (line 2) and then decreased further during 11 normal startup and shutdown cycles. This was due to a deformation of cell components which creep at elevated temperatures. This decrease in stack height was also indicated by the reduced tie bar deflection in line 3, which resulted in a reduction in cell compression.

For the twelfth cycle, the stack was heated to 178°C with the manifolds removed and the tie rods exposed to room temperature (line 4 in Table 4.1.1). The stack height increased by ∿0.07 cm from its height at room temperature (line 3) but was still ∿0.096 cm shorter than its initial height although the compression as indicated by the deflection of tie bars was coincidentally the same. When cooled to room temperature, the stack height was less than its previous value (line 3) indicating that permanent setting of some material in the stack was still occurring

TABLE 4.1.1

DIMENSIONAL CHANGE IN A 13 cm x 38 cm, 80-CELL, MAT-1 STACK

CONDITION OF THE STACK	TEMP., °C	HEIGHT OF STACK END PLATE TO END PLATE, in. (cm)	HEIGHT DECREASE, in. (cm)	CUMULATIVE HEIGHT DECREASE, in. (cm)	DEFLECTION OF TIE BAR, in. (cm)
1. Stack assembled and compressed	RT	20.856 (52.975)	----	----	1/8 (0.32)
2. Stack heated for acid addition	74	20.828 (52.903)	0.028 (0.072)	0.028 (0.072)	----
3. After eleven cycles	RT	20.785 (52.795)	0.043 (0.109)	0.071 (0.180)	5/64 (0.20)
4. Heated	178	20.818 (52.879)	-0.028 (-0.072)	0.038 (0.096)	~1/8 (~0.32)
5. Cooled	RT	20.774 (52.767)	0.044 (0.112)	0.082 (0.208)	Less than 5/64 (<0.20)
6. Compressed	RT	20.699 (52.575)	0.075 (0.191)	0.157 (0.400)	1.8 (0.32)

ENERGY RESEARCH CORPORATION

ORIGINAL PAGE IS OF POOR QUALITY

after 12 cycles. When the tie bar deflection was adjusted to obtain the original compression of the cells, the measured cumulative permanent set was 0.4 cm (line 6) or 0.005 cm/cell. This data provided the basis for the design of Stack 800 and the full scale module design (∿300-cell stacks) and suggested further work on this subject which is described in Section 5.8.

4.2 General Fabrication Procedures

Details of the materials and fabrication processes followed in the manufacture of components and subassemblies, and the assembly of simulated (5 cell), short stacks (23 cells) and subscale (80 cells) stacks are described in the Procedures Documents supplied to the NASA Project Manager. A general description of these components and of the stacks which were assembled follows, and stack specific procedures are outlined in the following subsections.

4.2.1 Plates

All bipolar, bipolar/cooler, and end-plates in the stack were compression molded from a mixture of graphite-resin powders producing plates of 30.5 cm (12 in.) x 43.2 cm (17 in.) x 0.33cm to 0.56cm (0.13 to 0.22 in). Plates for the Mk-1 design had process gas flow channels molded in the plate while the plates for the Mk-2 design were molded with flat surfaces. The bipolar-cooler plates were formed from two plates with the outer surface containing the process gas flow channels and the cooler channels in the center as shown in Figure 4.2.1. The process gas flow channels of the Mk-2 design, developed in Phase II of this program, and the treed pattern for bipolar/cooler plates, developed in Phase I of this program, were produced by numerically controlled machining. Some of the stacks assembled in this program contained plates which were subjected to a carefully programmed heat-treating schedule which modified the chemistry and structure of the resin, producing thereby a plate having a significantly higher electrical conductivity and improved corrosion resistance. The bipolar/cooler plates were formed by cementing two halves after heat-treatment, except as noted.

ORIGINAL PAGE IS
OF POOR QUALITY

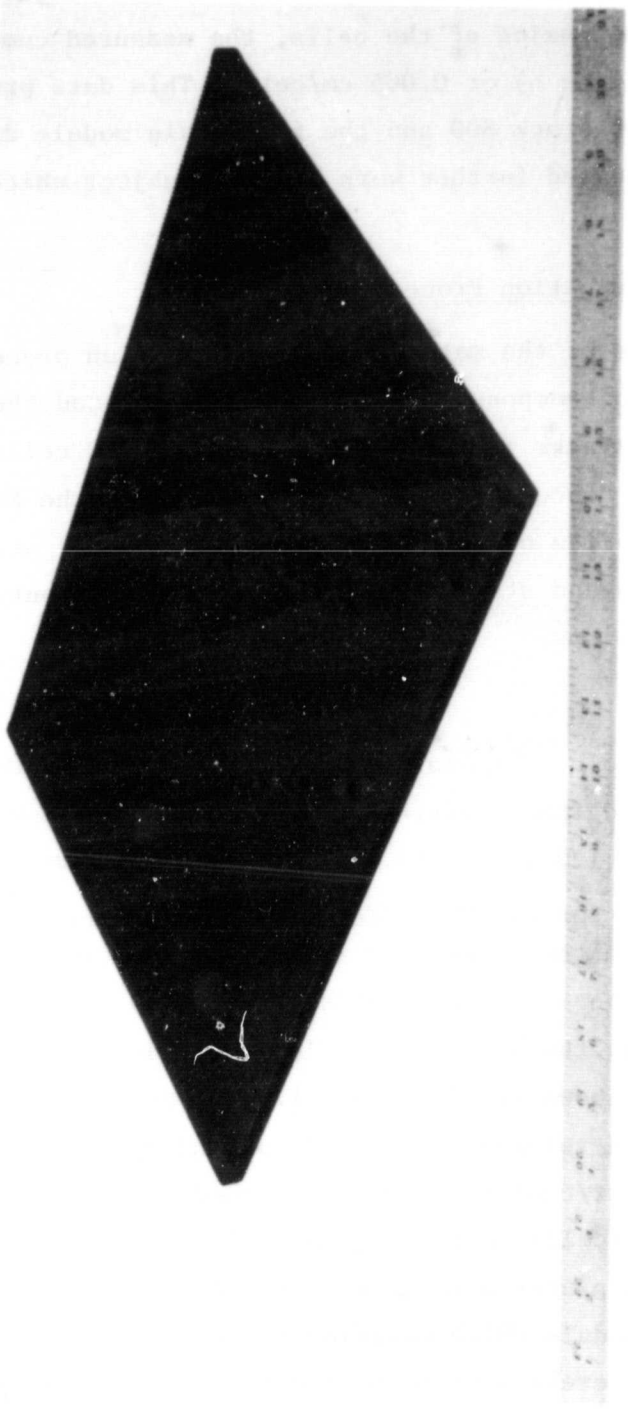

Figure 4.2.1 Assembled graphite-resin cooler

4.2.2 Electrodes

The anodes or cathodes in these cells were constructed with a catalyst layer supported on a porous graphite substrate. The platinum catalyst loadings for the anodes were 0.3 mg/cm^2 and cathodes were 0.5 mg/cm^2.

4.2.3 Matrix

The electrolyte containing matrices for these cells were produced from either a phenolic fiber (Kynol) structure or an ERC patented structure referred to as MAT-1. The latter matrix has a finer pore structure and higher bubble pressure than the Kynol, and is also capable of operating at higher temperature.

Subassemblies of electrodes and plates were produced by cementing electrodes to the appropriate side of each plate. Each plate contained an acid reservoir channel and one or two feed holes so that acid could be supplied to the matrix. The acid reservoir channel was machined into the anode side of Mk-1 plates, or on either the anode or cathode side of the Mk-2 plates depending on the stack being built.

Assembly of the subassemblies into a 5, 23 or 80 cell stack was performed in a dry room in which the humidity was maintained at less than 10% (RH). Acid (100% phosphoric) was supplied to the matrices by either a wicking or wet assembly procedure. Additional acid was supplied to the stack by wicking in a vertical (non-operating) position or by either of two schemes developed in this program for feeding acid to the stack while it was operating in a horizontal position.

The stacks which were planned and assembled are summarized in Table 3.2.1.

4.3 Simulated Stack Fabrication

Three simulated (5-cell, 30 cm x 43 cm) stacks (557, 558 and 560) were fabricated in Phase II. These simulated stacks were used primarily to corroborate and demonstrate the basic component design,

ORIGINAL PAGE IS
OF POOR QUALITY

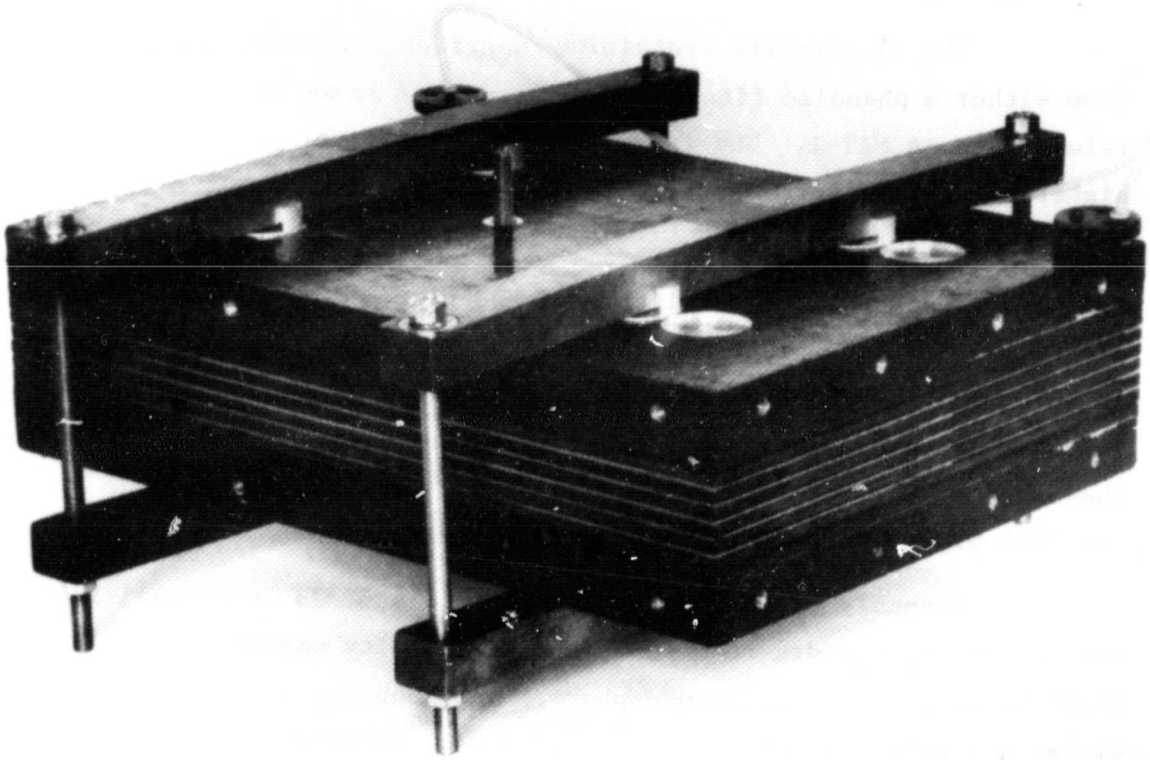

FIGURE 4.3.1. ASSEMBLY OF STACK 557 (The First MK-2 Simulated Stack)

assembly techniques and for endurance testing. These important points were well demonstrated with Stack 560. The key points of each stack fabrication are described below and the design features of each are listed in Table 3.2.1.

4.3.1 Stack 557

Stack 557, the first Mk-2 simulated stack (shown in Figure 4.3.1) was assembled with nonheat-treated bipolar plates and dry Kynol matrices.

The blanks for the bipolar plates were molded oversize so that they might be surface machined flat and parallel before the process gas flow channels were machined. Several different surface machining procedures were attempted, but all were unsuccessful in that the plates tended to overheat and distort while the machining process was in progress. The additional 0.13 cm (0.050 in) in thickness provided for this surface machining was deemed to have an insignificant effect on the performance of the stack and no further attempts at machining were made.

Subassemblies of the plates were assembled dry and compressed to a nominal pressure of 410 kPa (60 psi) using parallel compression bars and tie rods in a four point loading on compression plates at the ends of the stack. The stack was then supported so that the cells were in a vertical position and acid was fed into the cells through the feed holes at each end of the acid reservoir channel located at the bottom of each plate. The matrix of each cell covered the filled reservoir and acid was to fill the fine pore matrix (Kynol) by capillary action. The progress of the acid into the matrix and the electrodes was followed by measurements of electrical impedance.

The addition of acid to this stack was found to proceed at a rate considerably slower than that previously experienced by ERC. Tests of this stack showed a poorer performance which was attributed to insufficient acid in the matrix. Cross-leak indications were also noted.

In post-test examination of these cells it was noted that the matrix-electrode configuration exhibited differing degrees of wetting.

The plate rib pattern impressed into the electrode backing member varied in each cell indicating a difference in compression across the cell. Excessive pinching in some areas by these ribs was considered to be the major reason for the very slow capillary action of the acid in the matrix.

4.3.2 Stack 558

The plates from Stack 557 were stripped of the electrodes and new subassemblies were constructed. The subassemblies were assembled into a stack with acid added to each Kynol matrix as it was added to the stack. The stack was compressed to 410 KPa (60 psi). One day was required for wet assembly and compression. Additional acid was added to the matrices through the fill tube at the top of the stack in the normal horizontal operating position. Acid fed down the stack through the fill hole at the end of the acid reservoir channel in each plate and thus onto each matrix which partially blocked the feed hole. The test results of this stack were encouraging as its performance was significantly better than that of Stack 557. Acid additions were made on several occasions while the stack was operating and an improvement in performance was noted in those cells where an acid deficiency had been indicated by the diagnostic tests. Post-test examination of this stack revealed that a number of process gas channels were filled with electrolyte. All of the electrodes were damp and since no cross-leaks in testing were noted it was apparent that the wet assembly procedure achieved its goal. The flooded process channels were attributed to insufficient wet-proofing in the electrodes, excessive compression in some areas of the cell or both.

4.3.3 Stack 560

This stack included thinner bipolar plates (0.30 vs. 0.43 cm) and thicker end plates (0.56 vs. 0.43 cm) than Stack 558. The molded and machined plates for this stack were given a high temperature heat treatment to improve their electrical and thermal conductivity and corrosion resistance. Each MAT-1 matrix was wet with 48 cm^3 of phosphoric acid and an additional 0.5 cm^3 was added to the reservoir

ORIGINAL PAGE
BLACK AND WHITE PHOTOGRAPH

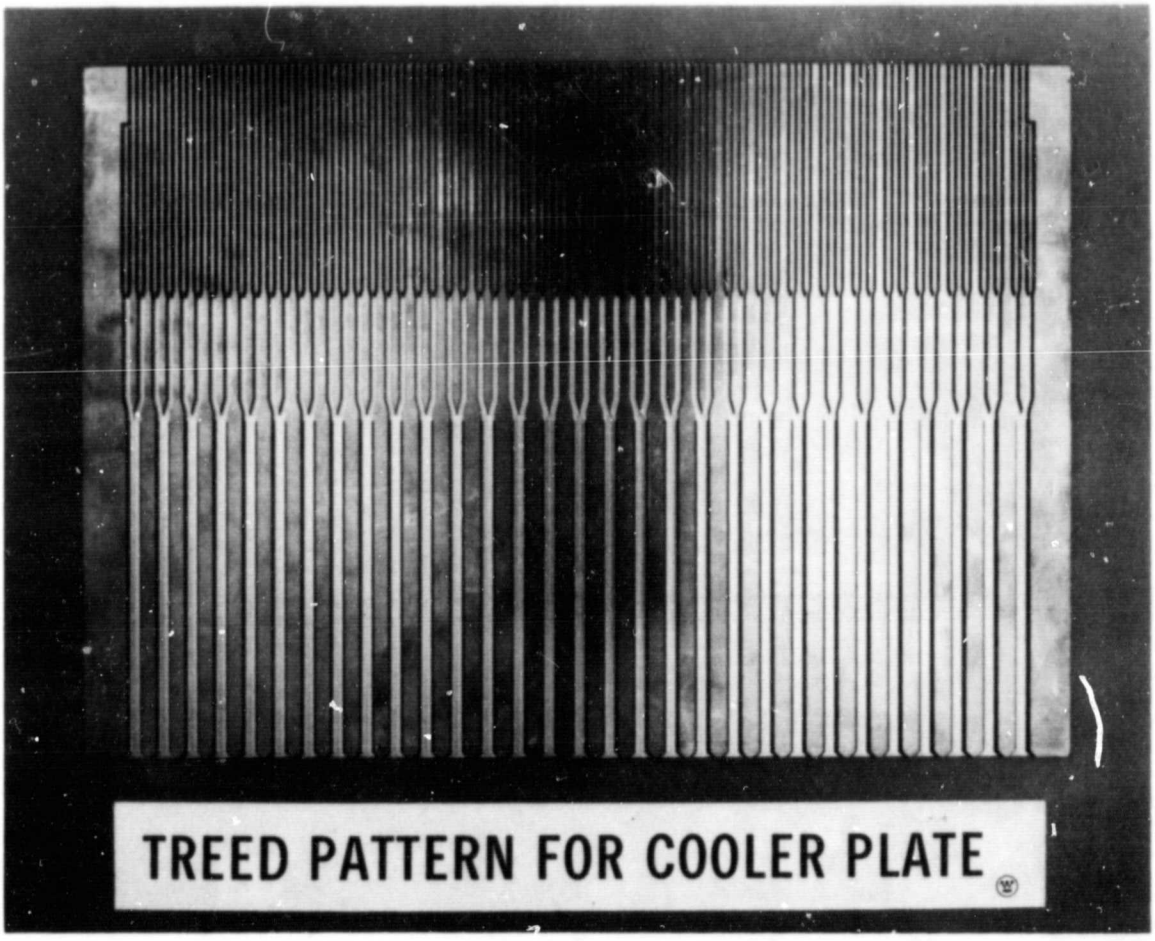

Figure 4.4.1. Photograph of treed cooler plate half for Stack 559

ORIGINAL PAGE
BLACK AND WHITE PHOTOGRAPH

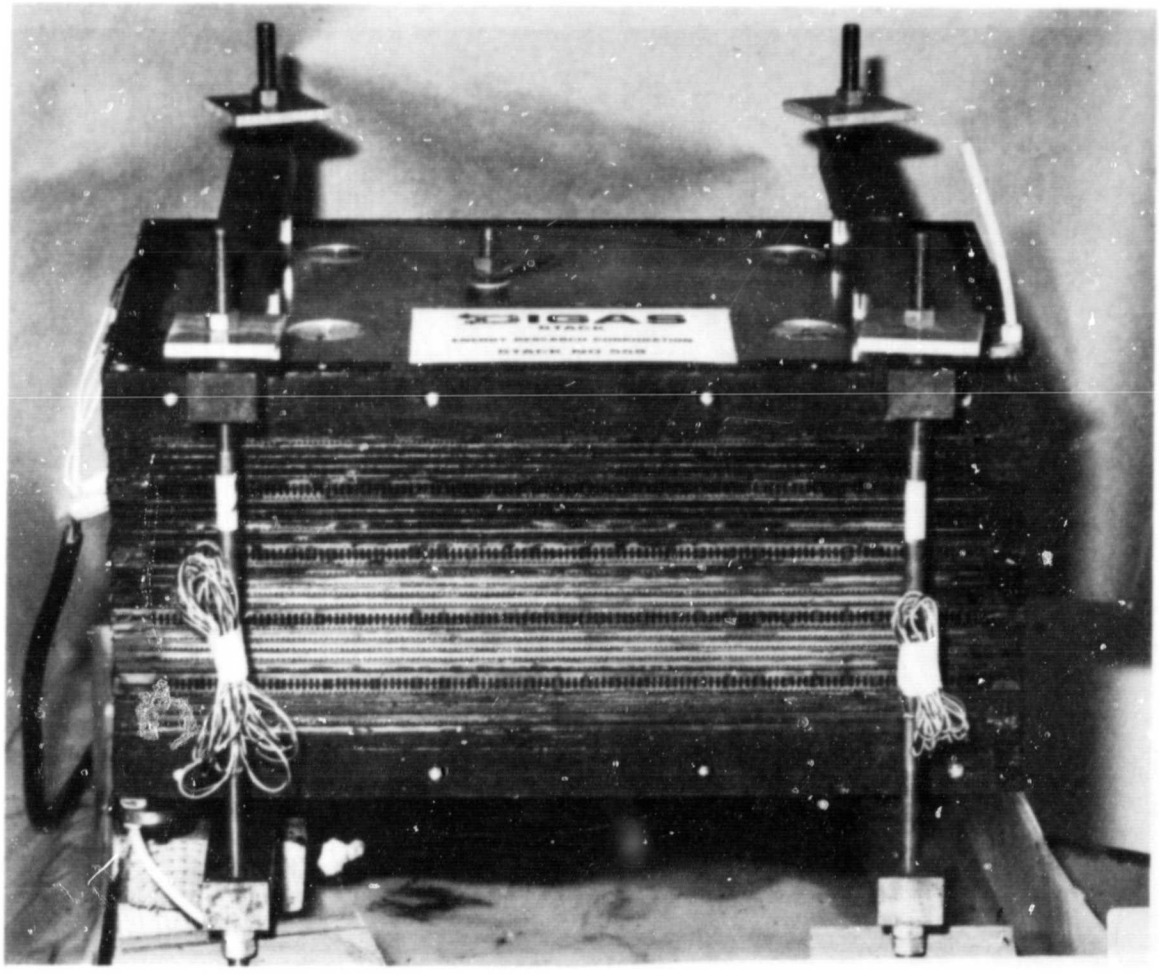

FIGURE 4.4.2. PHOTOGRAPH OF STACK 559

in each cell during the stacking of subassemblies. After holding the heated stack at 83°C for approximately 20 hours, it was compressed to 170 kPa (25 psi) but, because of the degree of acid weeping from the cells, final compression to 340 KPa (50 psi) was not completed until the following day. The electrical impedance of the stack was monitored during the assembly-compression procedure and a stack impedance of 5 mΩ at 97°C was reached at approximately 240 kPa (35 psi). An additional change of less than 10% was recorded in compressing the stack to its final value.

Acid addition of 4 cm^3 per cell was made to the stack through the filler tube at the top of the stack prior to testing. The acid flowed through the stack in a series progression through all of the acid reservoir channels in the cathode side of the plates. The matrix in this assembly is beneath the channel and acid flowing through the stack runs over the matrix.

This stack was operating continously for over 8000 hours as described in Section 5.

4.4 Short Stack Fabrication

Four short (23-cell, 30 cm x 43 cm) stacks (559, 561, 562 and 564) were fabricated in Phase II. These were used for verification of stack design parameters such as temperature distribution, flow distribution, pressure drop, manifold and seal design, and basic cooling concepts. The key points of each fabrication are discussed below and the design features of each are listed in Table 3.2.1.

4.4.1 Stack 559

The Treed cooler pattern for this Mk-1 stack was modified as shown in Figure 4.4.1 to provide for a smooth transition in air flow from the large inlet channels into the smaller channels. This design contained 30 channels with a depth of 0.56 cm (.22 in.) and a pitch between channels which increased towards the fuel exit end of the plate. The cooler flow direction was reversed (from Stack 556) so that cooler

air would exit at the acid reservoir edge. The plates for this stack were not heat treated.

This stack contained the new MAT-1 matrix and the wet assembly procedure developed on Stack 558 was used. The assembled stack stood overnight before compression was started. As in earlier assemblies, the stack was compressed to 170 kPa (25 psi) the first day and heated to ∿90°C overnight before compression was completed (340 kPa (50 psi)). As shown in Figure 4.4.2, the compression bars were parallel and strain gauges were installed on the tie rods to monitor compression changes during operation.

Many of the cooler plates originally molded for this stack were bowed and cracked when machining of the Treed pattern was attempted. These cracks were attributed to residual stresses in the plates resulting from the compression molding process. Bowed plates were found in anode and cathode halves and the direction of the bow was not the same for all plates. The molding procedure was modified for new cooler plates and this solved the warpage problem.

Acid additions to the stack were made to the fill tube at the top of the stack while it was in a horizontal operating position. Flow proceeded down through each of the cells in the acid reservoir channels in a series path.

Acid flow through the stack was quite low (∿1cc/hr) and additional feed tubes inserted into the cooler plates at the acid feed holes did not reveal any specific blocked region in the stack. However, post-test examination of the cells showed extensive blockage of the reservoir channels by the compressed and/or expanded matrix,which runs over the channel (in the anode section of the plate). A major restriction to acid flow was noted in the drain tube, which was partially blocked with the fluorelastomer used as a gasket on the end plate.

4.4.2 Stack 561

This Mark I stack contained the same plate design (DIGAS and Tread Pattern) as Stack 559 but the plates were given a high temperature heat-treatment (developed under the parallel technology program and ERC sponsored projects) after the machining operation to improve their electrical conductivity and corrosion resistance. The bipolar/cooler plate halves were cemented together before heat-treatment and it was noted after heat-treatment that the disparity in linear dimensions between cooler plates and the bipolar plates was as large as 0.25 cm (0.10 in). The linear shrinkage of these plates decreased with increasing thickness (4.2 to 3.8%). Subsequent heat treatment of cooler plates was restricted to half plates to minimize differences in shrinkage between them and the thinner bipolar plates.

The subassemblies of this stack were assembled with the MAT-1 matrix using the wet assembly and compression procedure employed in the assembly of Stack 559. Acid additions to the assembled and compressed stack were made through the top of the stack using series flow through the cells. An acid feed rate of less than 2cc/hr through the stack was similar to that experienced with Stack 559. In post-test examination of the stack it was noted that acid flow might have been impeded by constriction of the acid reservoir channels by the matrix being compressed and/or expanded into the channels.

During the compression of the stack it was noted that one of the center plates (anode of cell 18) cracked (audible & visual) at approximately 170 kPa (25 psi). After compression to 340 kPa (50 psi), there was some suspicion of additional hairline cracks in other plates, but this was proven to be unfounded. During initial testing of this stack, there was no noticeable effect on performance, due to the fine crack. The crack in the plate was approximately 3 cm in from the right end and started at the edge containing the acid reservoir channel (there was no acid fill hole at this end of the plate). After some test time and several thermal cycles of the stack (room to test temperature), this crack progressed into the process flow channels and cross-leaks were detected.

C-2

On post-test examination it was found that the crack had progressed to the fourteenth channel (~5cm). No cracks were found in other plates during the post-test examination. The process grooves of the plates of this stack were relatively free of acid with only an occasional area indicating any potential restrictions to gas flow. The anode or cathode backing papers exhibited varying degrees of acid mist.

The metal manifold of this stack was attached with a plastic (phenolic) frame interposed between it and the stack. To prevent gas leaks between the flat surfaces of the frame and manifold, a flexible high surface temperature gasket material was used. The irregular surface presented by the plates was sealed by several thicknesses (greater than the disparity between adjoining plates) of an uncured fluorelastomer sheet using the frame to form a gasket under pressure at an elevated temperature (80-100°C). This practice was employed in assembling previous stacks but these did not have plate dimensions which varied as much. Gas leaks were not detected in testing this stack. In post-test examination, separation of the in-situ cured gasket material from the heat treated graphite-resin plates required considerably more effort than the precured gaskets used for the manifold frame/manifold seals.

4.4.3 Stack 562

The plates for this Mk-2 stack were given a heat-treatment after machining the process gas flow channels and the Treed cooler channels. In stacking the subassemblies, a MAT-1 matrix was inserted in each cell using the wet assembly procedure. The end heaters, located in the compression plates at either end of the stack were turned on after assembly. Compression of the stack to 340 kPa (50 psi) was completed over a two day period to allow the electrolyte to slowly fill the very fine pores of the matrix and to wet the electrodes.

Post test examination of this stack revealed that the phenolic manifold frame had been overheated to the extent that it was severely charred and embrittled in some sections. The process gas channels of the plates were generally dry and the electrode backing papers had areas in which very fine drops of acid were on the surface,but no completely flooded areas were noted. The matrices were compressed or expanded into the acid reservoir channels but no complete blockage of the channels of the acid fill holes was noted.

4.4.4 Stack 563

This stack was to be built to verify the results obtained in the Stack 561 and to include small changes in the Treed cooler design. However, a decision was made to concentrate on the Mk-2 design and fabrication of this stack was discontinued.

4.4.5 Stack 564

This stack was a duplicate of Stack 562 with a minor modification in the Treed cooling pattern. The first branch was initiated at 10.2 cm (4 in.) instead of 15.2 cm (6 in.) as was the case for all of the earlier Treed patterns.

This stack contained a spiral of Teflon in the acid reservoir channel,which was to support the matrix (MAT-1) and prevent it from impeding acid flow. A wet assembly procedure was followed in stacking these subassemblies with the MAT-1 matrix. The heater in the bottom compression plate was turned on at the start of assembly and the improvement in acid fluidity was apparent shortly after the 5th subassembly was stacked. As with previous stacks, compression was initiated the following day but only to 170 kPa (25 psi). Final compression to 340 kPa (50 psi) was accomplished on the second day.

Figure 4.4.3 is a photograph of Stack 564 with all manifolds installed. It shows the ease of access to the manifolds provided by the crossed arrangement of the cross bars. Although this stack was removed from the test loop so the loop could be modified for testing of Stack 800, further tests were planned so no post-test examination was made.

ORIGINAL PAGE
BLACK AND WHITE PHOTOGRAPH

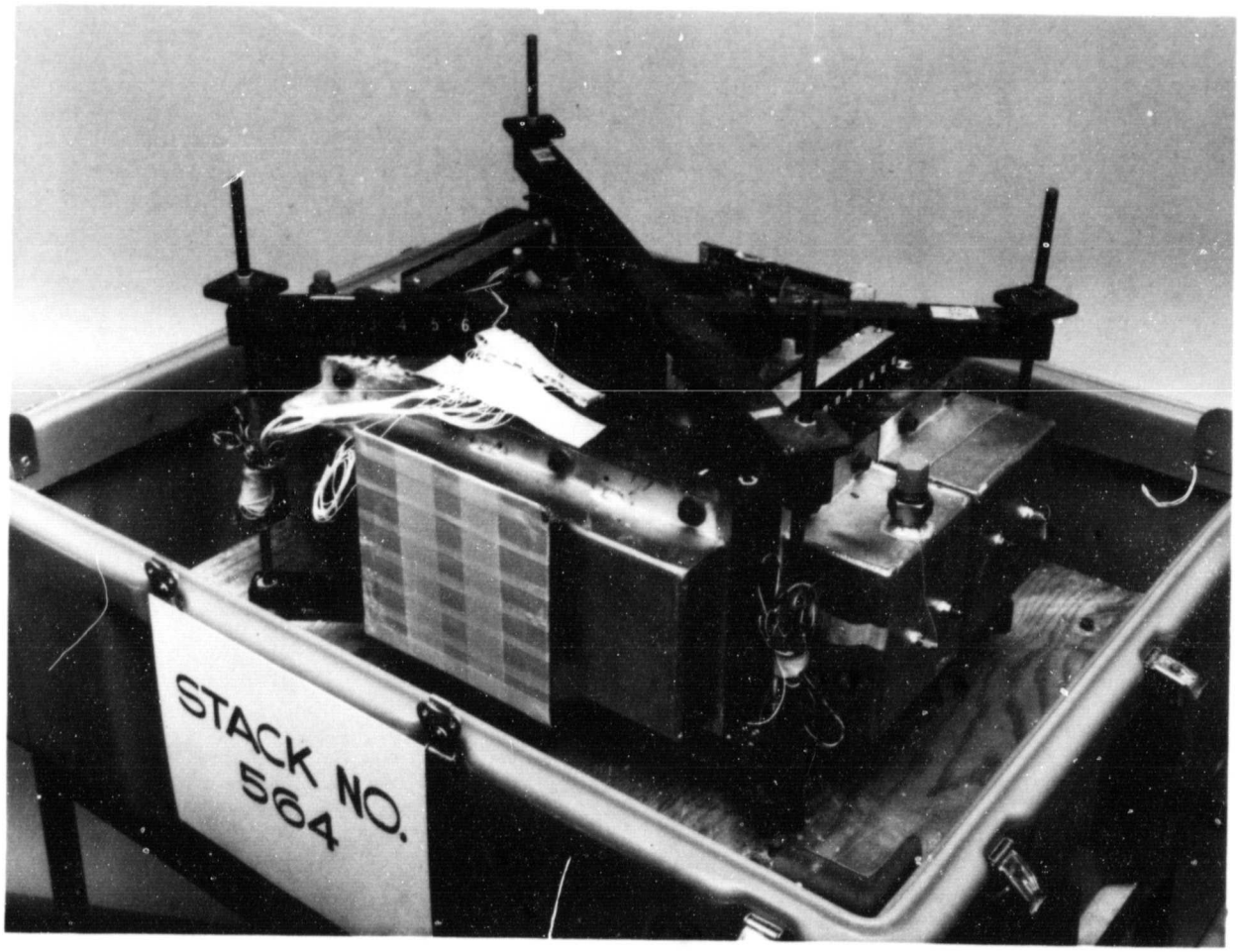

Figure 4.4.3. Photograph of Stack 564

4.5 Subscale Stack (80 cells)

This stack was basically an 80 cell scale-up of Stack 564. The end plates of this stack were coolers in which every other flow passage was closed. The manifold frame was made of steel rather than of a laminated phenolic because of the overheating noted in the short stacks. The metal manifold frames were coated with an insulating layer of a fluorelastomer and separated from the stack by a fluorelastomeric gasket and a thin sheet of Teflon. Because of anticipated creep of the seal components based on measurements described in Subsection 4.1.4 the manifold and compression systems described in Subsections 3.2.3 and 3.2.5 were used to allow for expansion between the stack and the manifold.

The subassemblies of this stack were wet assembled as in Stack 564. Only forty cells were assembled the first day so acid could penetrate the very fine pore structure of the matrix before any significant compression was applied to the lower cells. Compression of the stack to 340 kPa (50 psi) was again divided into a two day procedure. As shown in Figure 4.5.1, this stack was mounted on a stand which was its permanent base in the test loops.

The acid reservoir channels in this stack were provided with Teflon spirals to support the matrix. Attempts were made to add acid to the stack after testing had been in progress about 50 hours. Initially, the acid fill rate was recorded at 10cc/hr. Out of a total of 230cc, approximately 150cc were recovered from the drain tube. Shortly thereafter further attempts were made to supply acid to those cells indicating a need (OCV transients) but, for some reason, the maximum achievable feed rate was less than 2cc per hour. Three of the cooler plates had been provided with auxiliary fill tubes and none of these showed any signs of a blockage in the stack.

Further tests were planned at the time this report was written so post-test examination of the cell electrochemical components or the acid reservoir channels were not performed.

ORIGINAL PAGE
BLACK AND WHITE PHOTOGRAPH

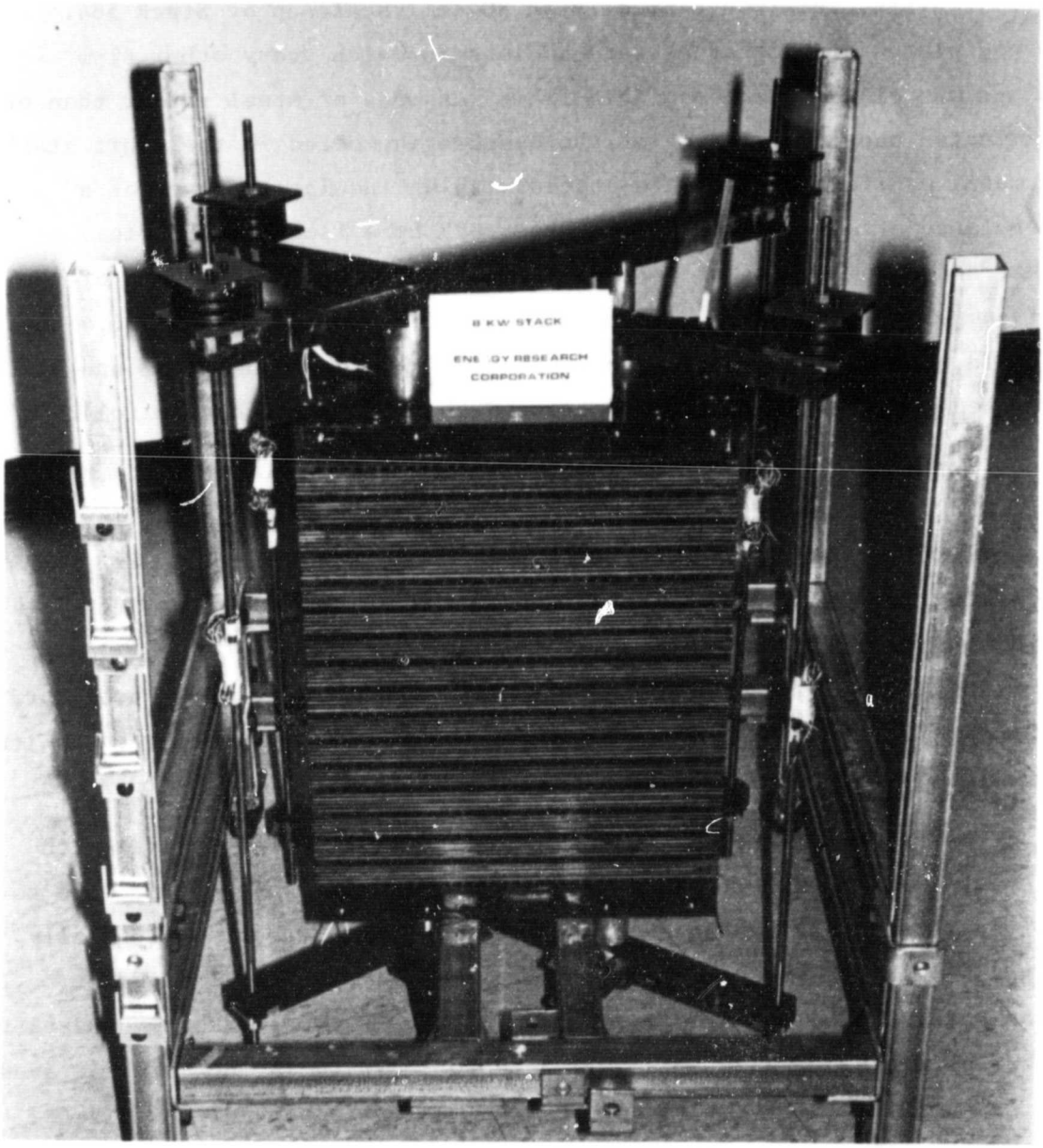

FIGURE 4.5.1. STACK 800 (MK-2, 80 Cell)

5. Task 3: Stack Testing

As a part of the overall effort to develop a PAFC module design appropriate for the OS/IES, the purpose of this task was to verify the performance of the stacks designed under Task 1 and fabricated under Task 2,and provide feedback to those tasks on the effect of various design features and assembly procedures. Close coordination with those tasks was maintained by participation of key personnel on all three tasks, by formal meetings which included members of the NASA management team,and many informal meetings and discussions.

Since the stacks were fabricated at the ERC facility in Danbury, CT, and, the loop built during Phase I to provide for stack operation over the wide range of conditions possible in various OS/IES designs and applications was located at the Westinghouse R&D Center in Pittsburgh,Pa; testing of each 23 cell (short) stack and the 80 cell (subscale) stack comprised a pretest and performance test. The pretests were carried out at ERC to verify the integrity of the assembled stack. The performance tests were carried out at Westinghouse and included measurement of stack performance (polarization) and stack temperature profiles over ranges of fuel composition and utilization (flow rate), process air flow rate, cooling air flow rate, load, and temperatures. The data from these tests provided feedback which was used in evolving the stack design.

The performance of all stacks is summarized in Table 5.1 and the test results are described in the following subsections. A more complete list of stack design features is given in Table 3.2.1 and the design and fabrication of the stacks are described in Sections 3 and 4 respectively.

TABLE 5.1 SUMMARY OF STACK TESTING

STACK I.D. NUMBER	C	557	558	559	560	561	562	564	800
Stack size, kW	0.075	0.5	0.5	2	0.5	2	2	2	8
Hardware size, cm	13 x 38	30 x 43	30 x 43	30 x 43	30 x 43	30 x 43	30 x 43	30 x 43	30 x 43
Number of cells	3	5	5	23	5	23	23	23	75
Design	Mk-1	Mk-2	Mk-2	Mk-1	Mk-2	Mk-1	Mk-2	Mk-2	Mk-2
Cooling mode	Process	Process	Process	Digas	Process	Digas	Separate	Separate	Separate
Heat-treatment	no	no	no	no	yes	yes	yes	yes	yes
Peak cell performance, mV	590†	530†	578†	572†	624* 615**	630* 620**	632* 621**	631* 620**	621**
Time Avg. Cell performance, mV	575†	505†	524†	562†	601*	N/A	N/A	N/A	N/A
Test location	ERC	ERC	ERC	ERC/W	ERC	ERC/W	ERC/W	ERC/W	ERC/W
Run time hours, at ERC at Westinghouse	2000 -	43 -	227 -	62 60	8,338 -	25 90	26 210	22 120	16 50
Total Run time, hours	2000	43	227	122	8,338	115	236	142	66

Utilization

Fuel: 75∿80%
Air: 2∿3 stoich

Temperature: ∿178°C
Pressure: 1 atm.

Current Density

†: 100 mA/cm^2
*: 150 mA/cm^2 with H_2 only
**: 150 mA/cm^2 with 75% H_2 and 25% CO_2

N/A: Not applicable due to short run time at ERC.

ENERGY RESEARCH CORPORATION
ORIGINAL PAGE IS
OF POOR QUALITY

In anticipation of continuation of this program a 2 kW and an 8 kW test loop with capabilities comparable to those of the OS/IES simulation loop were built at ERC as part of this task. These loops were used to pretest the last 23 cell stack (Stack 564) and the 80 cell stack (Stack 800). Also, as part of this task, the W-R&D loop was modified to provide for unattended operation and to test the 80 cell (8 kW) stack.

The 3 and 5 cell (simulated) stacks, which were used to investigate acid management schemes and shim and edge sealing configurations, were tested at ERC. One of these (Stack 560) accumulated over 8 00 hours of operation.

In support of the module design effort, tests on thermal expansion and compressibility of cell materials were made.

The work carried out and test results are described by subtask in the following sections.

5.1 Modify OS/IES Simulation Loop

The objective of this subtask was to modify the OS/IES Simulation loop built during Phase I (and described in the Phase I Final Report) to carry out the Phase II stack performance testing. As Phase II evolved the primary requirements were:

1. Test 2 kW stacks with separated cooling (MK-2) as well as DIGAS (MK-1) cooling.
2. Test MK-2 stacks with a nominal capacity of 8 kW.
3. Provide for unattended operation of the loop for round-the-clock testing.

These requirements were met through a series of changes.

The loop as it now exists, with Stack 800 installed, is shown in Figure 5.1.1. It has the flexibility to test separated air or DIGAS cooled stacks with nominal ratings between 2 and 8 kW at atmospheric pressure over the required range of operating conditions, and it can maintain a set operating condition and record test data without attention.

ORIGINAL PAGE
BLACK AND WHITE PHOTOGRAPH

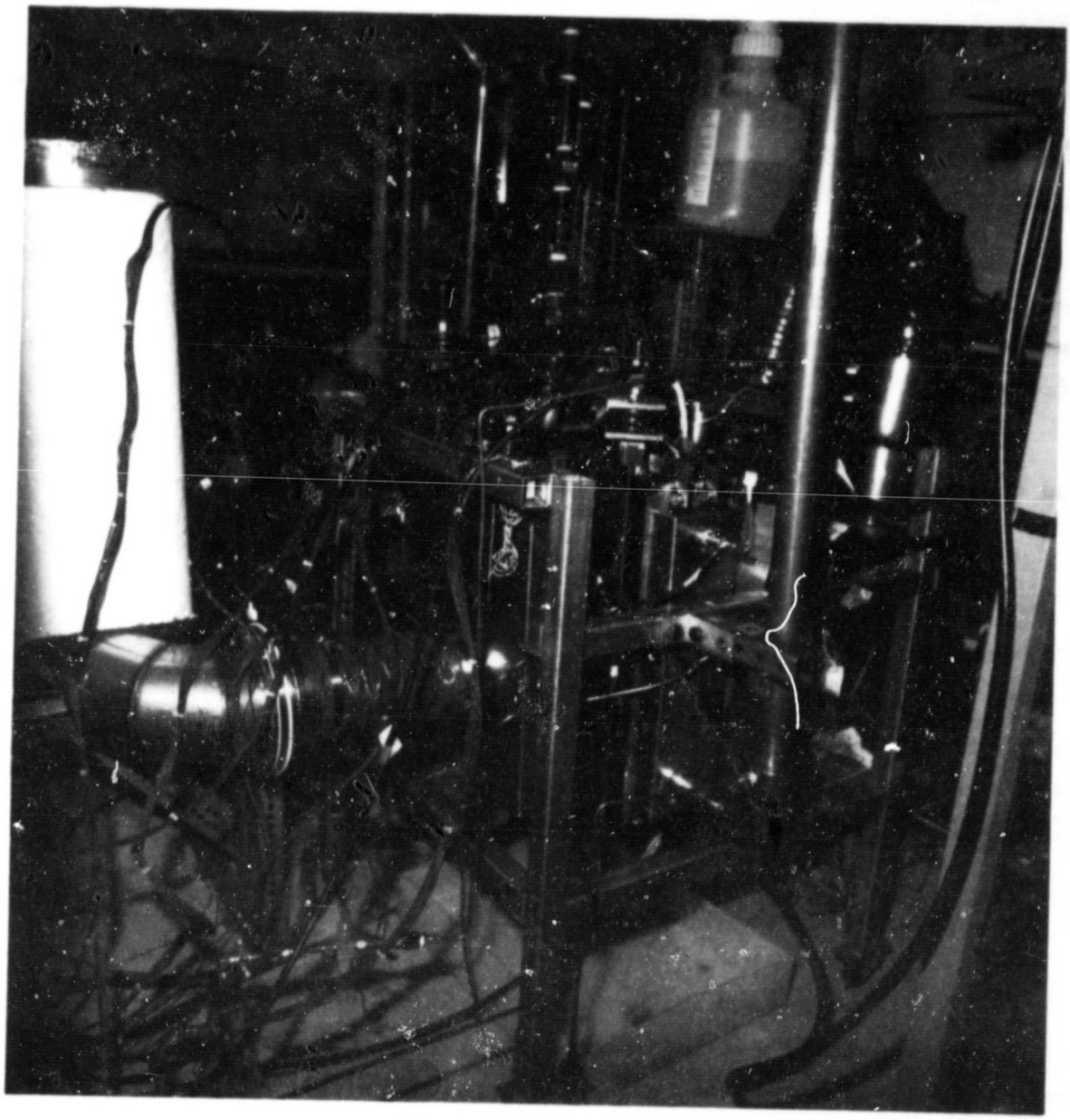

Figure 5.1.1. Stack 800 installed in OS/IES simulation loop

The following sections describe the existing loop by subsystem.

5.1.1 Fuel

The fuel system controls, humidifies and preheats a mixture of H_2, CO_2 and CO at various flow rates and proportions to simulate OS/IES stack operating conditions.

To obtain the desired accuracy over the wide ranges required by the test conditions, two separate systems are used to control and measure the H_2, CO_2 and CO flow rates.

The system described in the Phase I Final Report was retained for testing of 2 kW stacks.

A Waugh Controls Corp. Digital In-Line Blending System was procured and installed for testing 8 kW stacks. This system automatically proportions the H_2, CO_2 and CO streams with an accuracy of $\pm$1% of full scale readings. The system consists of a panel and electronic control module and a module containing manifolding and three pneumatically controlled vales. The orifices currently installed in these valves are suitable for operation at up to 12 kW of fuel cell stack power.

The mixed $H_2/CO_2/CO$ stream is humidified in a bubbler at room temperature. For unattended operation, the level of water in the bubbler is controlled by a solenoid valve that is actuated by a capacitive level indicator installed in the bubbler.

Prior to entering the stack, the humidified fuel is heated by resistance heaters.

5.1.2 Cooling and Process Air

To obtain the larger flow rates of cooling air required by the 8 kW stacks, an Aerovent model PB10A blower with an impeller designed for operation with gas temperatures up to 315°C was installed in the cooling air circulating duct. The inlet of the compressor was connected to the loop by a flange and the discharge by a flexible silicone hose.

For the separated cooled stacks, the rejection of heat from the system was accomplished by venting hot air (after exiting the stack) from the loop and supplying room temperature air via the blower. The proportions of makeup and recirculating air were adjusted to obtain the desired cooling air temperature at the stack inlet. For DIGAS stacks, where it is necessary to independently control makeup (process) air flow heat rejection, the cooling air temperature is controlled by a water cooled heat exchanger and resistance heaters as in Phase I. The resistance heaters are also used to heat the stack for startup and during holding periods. Measurement and control of cooling and makeup air flow rates are as described for Phase I.

The laboratory "house" air compressor supplied the separate process air for the MK-2 stacks. The flow rate is controlled by a manually set valve and measured by a Brooks precision rotameter. Once set, the valve maintained a constant flow rate for unattended operation. The rotameter measured the process air flow to within $\pm$1% of its reading. The process air is heated by a Type GCH Chromalox heater controlled by an Omega model 49 proportioning temperature controller. As for the DIGAS stacks, a Hagan oxygen monitor measures the oxygen content of the exhaust stream to verify air flow rate and the absence of leaks.

5.1.3 Unattended Operation

A Fluke 2240 B data logger with extended chassis was installed to provide data recording and safety monitoring during unattended operation. The chassis extender permits automatic recording of 120 separate temperature and voltage measurements on programmable schedules.

The unit also provides 30 alarm channels which provide for an orderly shutdown should it be necessary during unattended operation. As currently operated, the 30 alarm channels are used to monitor:

1. Lower limits on cell voltages.
2. Upper and lower limits on current.

3. Upper limits on several cell thermocouples.
4. Upper and lower limits on the temperatures of the air and fuel supplies to the fuel cell stack.

When any of these limits are exceeded, the following automatic shutdown sequence is implemented:

1. The constant current power supply is shut down by a relay in its 440 VAC line.
2. A contactor opens, removing load from the stack.
3. The fuel supply is shut off and a nitrogen purge of the fuel loop is turned on by a 3-way solenoid valve.
4. Power to the loop air heater is shut-off.
5. An alarm in the security station is activated.

Recovery from this sequence requires manual reset by operating personnel.

Additional safety is provided by a Bacharach combustible gas sensing system, which continuously monitors hydrogen concentration in the hood enclosing the loop, in the hood ventilation duct, and in the test room. This system also activates the alarm in the security station if any hydrogen is detected. If the detected hydrogen levels approach a second (higher) selected level, the automatic shut down sequence described above is implemented.

A backup safety system is provided by a comparative digital voltmeter which monitors the stack voltage and initiates the shutdown sequence if the high or low set points are exceeded. This protects against a wide range of system failures such as loss of fuel or process air, loss of load, failure of the loop heaters, etc., which will cause the stack voltage to exceed the selected limits.

5.1.4 Load Control

The dissipation of the electrical power produced by the fuel cell stacks is primarily achieved in a bank of air cooled metal wound industrial resistors manufactured by a Westinghouse division. As in Phase I, the resistor bank includes knife switches which vary the

resistance of the bank in discrete steps by changing the series/parallel pattern. A power supply installed between the fuel cell stack and the load bank during Phase II provides continuous selection and automatic regulation of specified currents over the range of 50 to 250 amps required to test stacks of ∿1200 cm^2 cells at atmospheric pressure. The power supply is an Electronic Measurements Inc. SCR model rated to provide 250 amps at up to 40 VDC from a 440 VAC supply.

5.2 Simulated Stack Testing

The following were achieved under this subtask:

- Two 5-cell stack test stations were designed and constructed These stations include all instrumentation necessary for endurance testing;
- The three Mk-2 design simulated stacks (557, 558 and 560) were tested;
- Stack 560 was endurance tested.

5.2.1 Stack 557 (Mk-2, 5-cell)

The main objective of this first Mk-2 simulated stack was to establish the performance of cells with the bipolar plate reactant flow configuration designed for separated cooling stacks. The performance was to be compared with Mk-1 (straight-through) reactant flow channels. The criteria for measuring the success of the Mk-2 design were established as:

- OCV exceeding 0.80 V/cell,
- Average voltage at 100 mA/cm^2 exceeding 0.56 V/cell.

Once these levels were achieved, additional tests on polarization, the effect of reactant gas concentrations on performance, the evaluation of long-term acid management and pressure versus flow measurements were to be made. However, as described in Subsection 4.3.1, Stack 557 required 25 days for initial acid wicking, which was three times the normal wicking time.

Testing of Stack 557 began when wicking appeared to be adequate as indicated by internal resistance (IR) and open circuit voltage (OCV) measurements. Initially, and at a load of 100 mA/cm^2, the performance of the cell averaged 0.53V/cell (OCV = 0.90 V/cell at 177°C). After a few hours and at the same load and temperature, the performance dropped to 0.50V/cell and OCV to 0.80V/cell. Polarization data taken during this period showed an oxygen gain of 98 mV/cell at 100 mA/cm^2. The stack performance dropped to 0.49 V/cell at termination. The falling OCV and increasing IR (from 3.7 to 5.2 mΩ) indicated the possibility of a cross-leak and an inadequate amount of acid which was corroborated by a leak-test.

To correct the apparent wicking problem, it was decided (based on work carried out by ERC on parallel programs) that the next Mk-2 simulated stack (558) would be built with pre-wet matrices to assure adequate electrolyte in the cells.

5.2.2 Stack 558 (Mk-2, 5-cell)

Since Stack 557 did not meet the success criteria established prior to its assembly, the objectives of Stack 557 were shifted to Stack 558, along with additional goals:

- to test wet assembly procedures with the Mk-2 design;
- to test an acid management (i.e., replenishment) scheme with the stack in a horizontal position.

Pretesting of Stack 558 followed the plan shown in Figure 5.2.1. The plan included the measurement of the stack internal resistance and OCV as well as leak tests. At ∿100°C, the stack internal resistance stabilized at ∿1.76 mΩ/cell for several days and the OCV was ∿0.75 V/cell. However, the H_2 on/air off OCV was unstable and declined rapidly.

ORIGINAL PAGE IS
OF POOR QUALITY

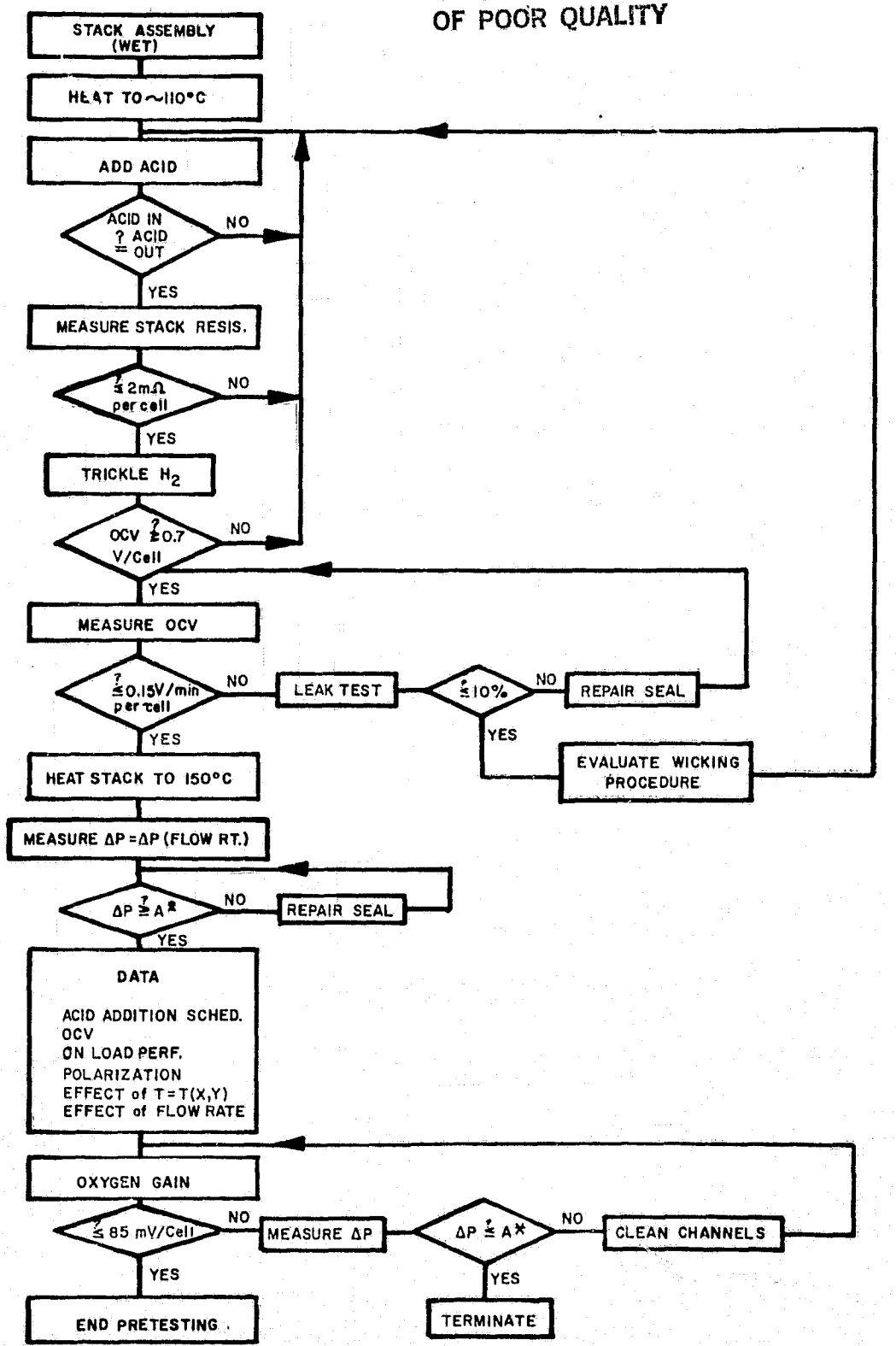

A* = 2ΔP estimated theoretically for a given cell geometry and at a given flow rate.

D1274

FIGURE 5.2.1 FLOW CHART OF PRETEST PROCEDURES

A manifold leak test indicated negligible external leakage. Acid addition was resumed and measurements showed a higher OCV (∿0.82 V/cell) and the H_2 on/air off OCV was more stable.

The testing of this stack proceeded according to the approved test plan, summarized as follows:

- Establish baseline performance at 100 mA/cm^2 and 177°C;
- Obtain polarization data for the stack;
- Determine the effect on stack performance of air flow rates from 2 to 5 stoichs and hydrogen utilizations from 50 to 80%.

The performance history of Stack 558 is shown in Figure 5.2.2. Initially, the average cell voltage was ∿0.57V at 100 mA/cm^2 and 0.88V at open circuit but the OCV and on-load performance dropped. Subsequent acid additions improved the stack OCV but caused only a slight improvement in on-load performance. However, there was a substantial improvement in the on-load performance over that of Stack 557 as shown in Figure 5.2.3. The data were taken on the third day of testing each stack. A performance increase of ∿75 mV/cell at 100 mA/cm^2 and ∿80 mV/cell at 150 mA/cm^2 was achieved by Stack 558 over Stack 557. This gain in performance indicated the advantage of wet assembly versus dry for this Mk-2 design.

The effect of varying air and H_2 flow rates on the on-load performance of Stack 558 is shown in Table 5.2.1. The results indicate that the stack's performance was practically insensitive to H_2 utilization below 75% and air flow rate above 2.3 stoichs. The OS/IES design conditions are 75% H_2 utilization and 2 stoichs air.

Post-test analysis of Stack 558 showed that the matrices and electrodes were drier than in typical cells although 12.2 cm^3 of acid/cell was added to the stack which, when added to the initial 38 cm^3, was a total of 50.2 cm^3/cell. Cell 5 was the driest (in terms of matrix and electrodes) and also had the worst on-load performance of any cell throughout

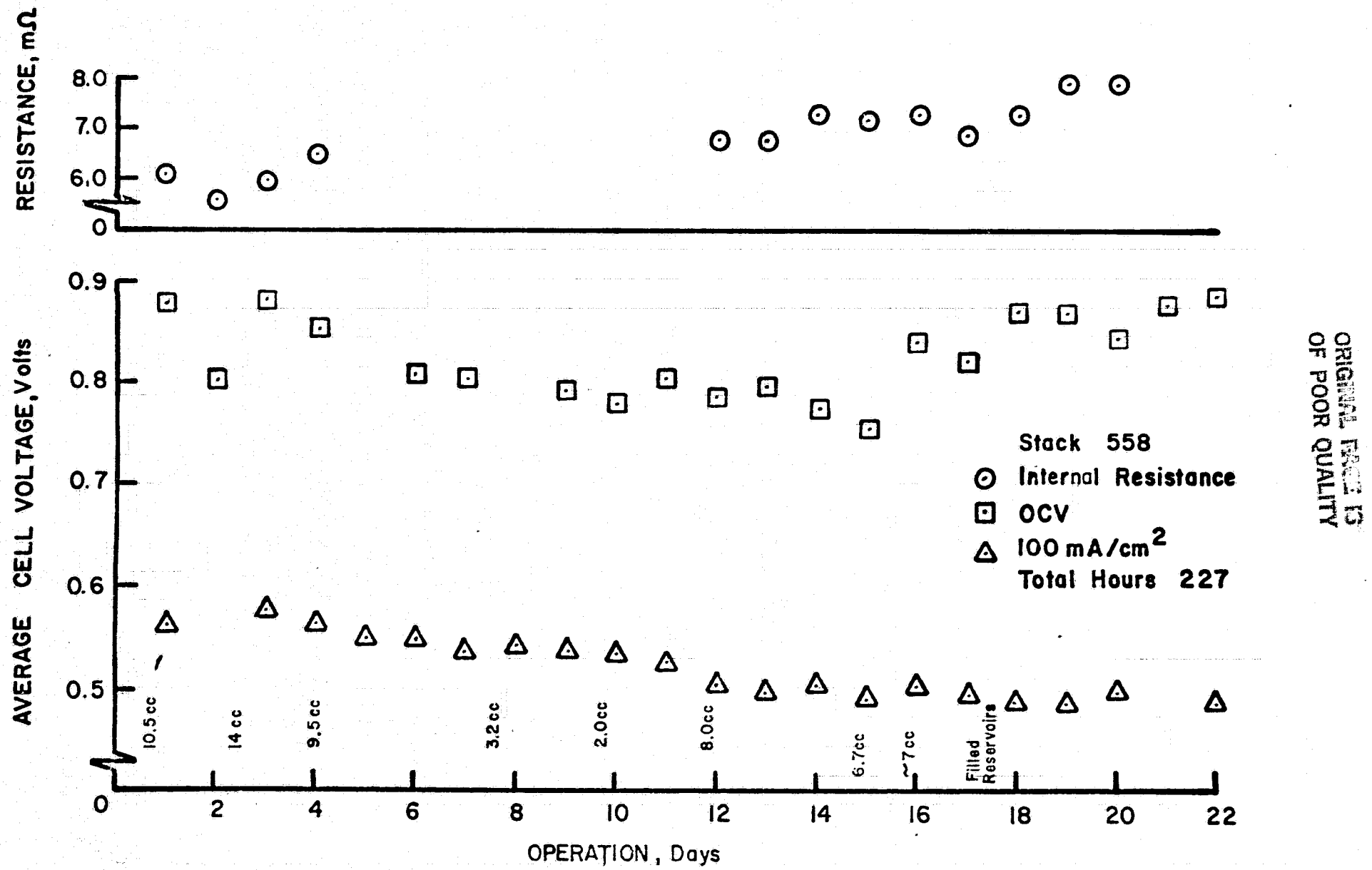

FIGURE 5.2.2 PERFORMANCE HISTORY OF STACK 558

D1279

ORIGINAL PAGE IS OF POOR QUALITY

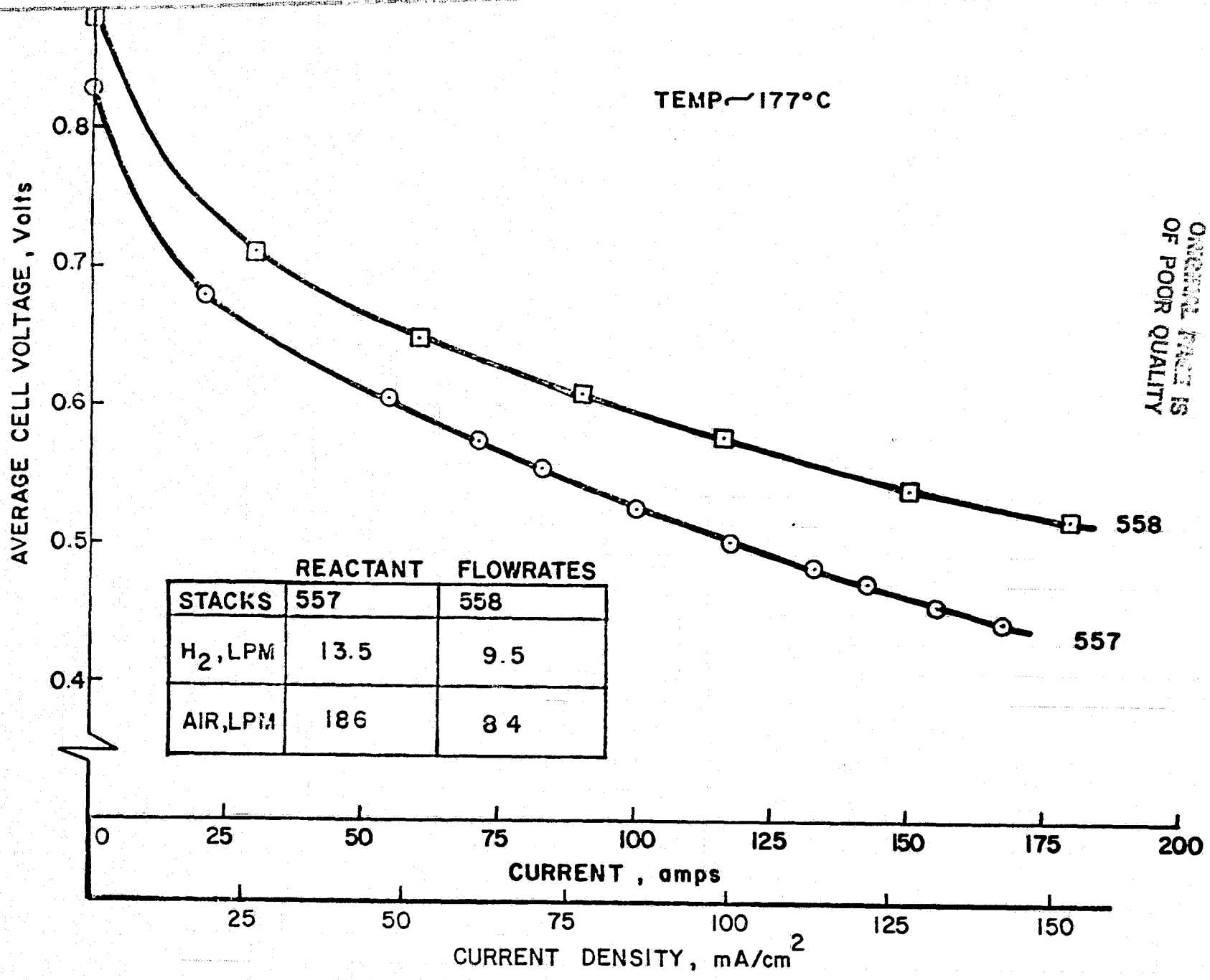

FIGURE 5.2.3 POLARIZATION OF STACKS 557 and 558

ORIGINAL PAGE IS OF POOR QUALITY

ORIGINAL PAGE IS
OF POOR QUALITY

TABLE 5.2.1. EFFECT OF AIR FLOW RATE AND H_2 UTILIZATION ON THE PERFORMANCE OF STACK 558

STOICH AIR	H_2 UTILIZATION, %	AVG. CELL VOLTAGE, V at 100 mA/cm^2
2.3	74	0.538
3.9	74	0.540
6.3	74	0.544
6.0	80	0.528
6.0	50	0.538

the life of the stack. In contrast, Cell 3 was the wettest and exhibited the best on-load performance.

Post-test analysis revealed that the matrices had swelled and caused some obstruction to flow in the acid channels. Thus a matrix support was incorporated in Stacks 559, 560, 564 and 800.

It was apparent that the inability to supply acid to the matrices of Stack 558 after assembly was responsible for its low performance. ERC's experience indicated that it was best to fill matrices with the full amount of acid at the time of assembly. Therefore, all subsequent stacks were wet assembled as described in Section 4.

5.2.3 Stack 560 (Mk-2, 5-cell)

Stack 560 was the first simulated stack fabricated with heat-treated plates. This stack was used to verify design improvements and demonstrate component capabilities preparatory to their incorporation in short stacks. The primary objectives of Stack 560 were to establish the performance of the Mk-2 design with heat-treated plates and Mat-1 matrices over a long time period.

In accordance with the approved test plan, the following tests were carried out:

Pretesting

- Stable and transient OCV tests;
- Pressure drop versus flow for anode and cathode;
- Effect of anode and cathode flows on stack performance;
- Effects of varying anode gas compositions;
- Polarization with varying anode and cathode gas composition.

Endurance test

- Performance at the OS/IES design load of 150 mA/cm^2;
- OCV test;
- Stack internal resistance measurements.

ORIGINAL PAGE IS
OF POOR QUALITY

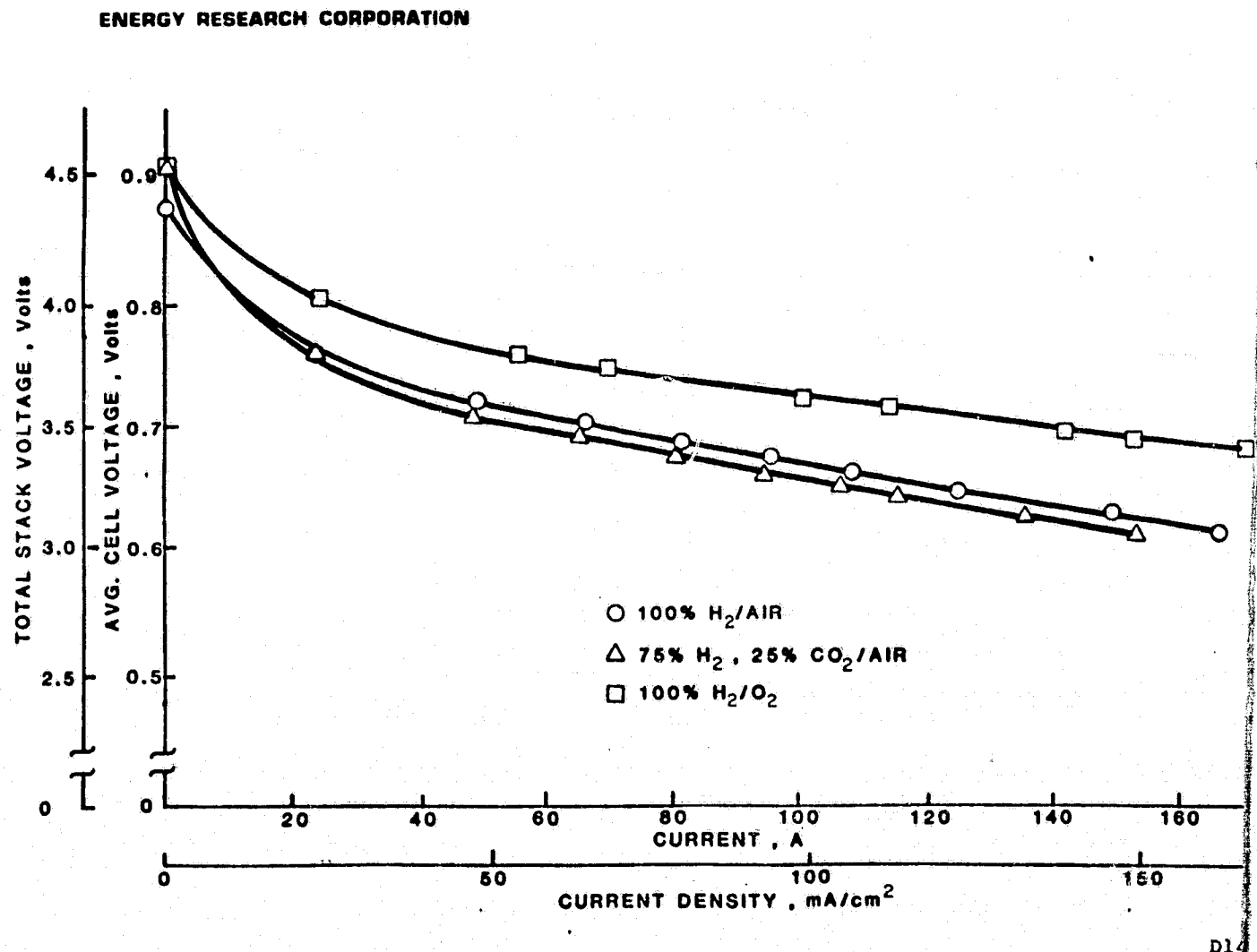

FIGURE 5.2.4. POLARIZATION OF STACK 560

Pretesting

The polarization characteristics of the stack are shown in Figure 5.2.4 and the performance is summarized in Table 5.2.2. Cell by cell baseline data appear in Table 5.2.3. Table 5.2.4 details the open circuit voltages for Stack 560.

The air side pressure drop of Stack 560 was significantly higher than that of Stack 558 as shown in Table 5.2.5. This was due to the reduction in flow area associated with shrinkage during heat-treatment. The pressure drop vs. flow characteristics of Stack 560 are given in Figures 5.2.5 and 5.2.6.

TABLE 5.2.2. PERFORMANCE CHARACTERISTICS OF STACK 560 AT DIFFERENT REACTANT COMPOSITIONS

CONDITIONS	PERFORMANCE, V/cell		
	H_2/O_2	H_2/Air	75% H_2, 25% CO_2/Air
OCV	0.91	0.87	0.91
100 mA/cm^2 (102A)	0.72	0.66	0.65
150 mA/cm^2 (153A)	0.69	0.62	0.61

TABLE 5.2.3. BASELINE PERFORMANCE OF STACK 560 (at 177°C)*

CELL NO.	PARAMETERS	PERFORMANCE, V/Cell					
		OCV	150 mA/cm²				100 mA/cm²
			100% H_2		75% H_2, 25% CO_2		100% H_2
	Length of Operation, hrs	7	40	400	12	400	41.
	Air Flow, Stoich	-	4.7	2.0	4.8	2.0	2.9
1		0.883	0.628	0.629	0.613	0.610	0.661
2		0.954	0.623	0.604	0.611	0.602	0.653
3		0.928	0.629	0.615	0.619	0.612	0.659
4		0.933	0.633	0.634	0.621	0.620	0.667
5		0.923	0.627	0.627	0.616	0.613	0.662
	Avg. Cell Voltage, V	0.924	0.628	0.622	0.616	0.611	0.660
	H_2 Util., %	-	82	82	82	81	80
	Load, A	0	153	152	152	150	100

* *ΔT, stack: 10 to 20°C*

OF POOR QUALITY

ORIGINAL PAGE IS
OF POOR QUALITY

TABLE 5.2.4. INITIAL OCV TEST (STABLE & TRANSIENT) FOR STACK 560

CELL NO.	AIR ON H_2 ON	AIR OFF H_2 ON	AIR OFF H_2 ON (1 MINUTE)	AIR ON H_2 OFF	AIR ON H_2 OFF (1 MINUTE)	AIR OFF H_2 OFF	AIR OFF H_2 OFF (1 MINUTE)
1	0.895	0.867	0.840	0.864	0.854	0.854	0.833
2	0.940	0.919	0.914	0.912	0.898	0.898	0.909
3	0.928	0.901	0.895	0.897	0.885	0.885	0.888
4	0.928	0.907	0.899	0.902	0.884	0.884	0.894
5	0.915	0.892	0.883	0.885	0.874	0.874	0.876
AVG.	0.921	0.897	0.886	0.892	0.879	0.879	0.880

TABLE 5.2.5. PRESSURE DROP COMPARISON

PARAMETERS	STACK 558	STACK 560
Flow, lpm	57 (4 stoich)	57 (4 stoich)
Δp, cm H_2O	9.4	14.7

The effect of cathode gas flow rate on performance is shown in Figure 5.2.7. The performance was stable above 40 lpm (2.9 stoich) air flow. As shown in Figure 5.2.8, the performance was insensitive to fuel utilization below 82% for 100% H_2, and below 66% for fuel diluted with 25% CO_2.

The effect of varying fuel composition is shown in Table 5.2.6. The loss in performance with 25 vol% CO_2 was ~15 mV which is close to the theoretical prediction of 12 mV.

ORIGINAL PAGE IS
OF POOR QUALITY

ORIGINAL PAGE IS
OF POOR QUALITY

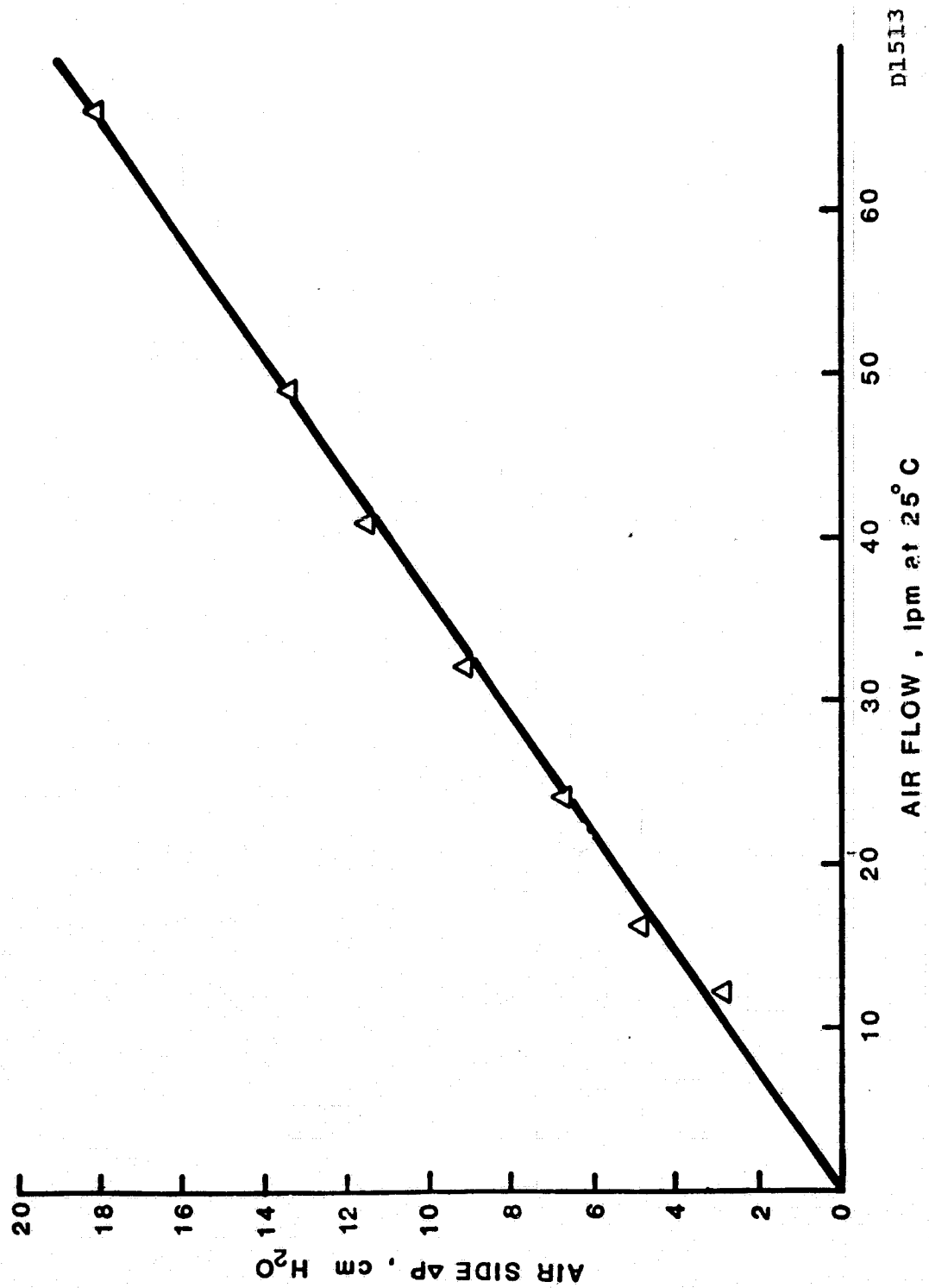

FIGURE 5.2.6. PRESSURE DROP VS. FLOW RATE OF AIR, STACK 560

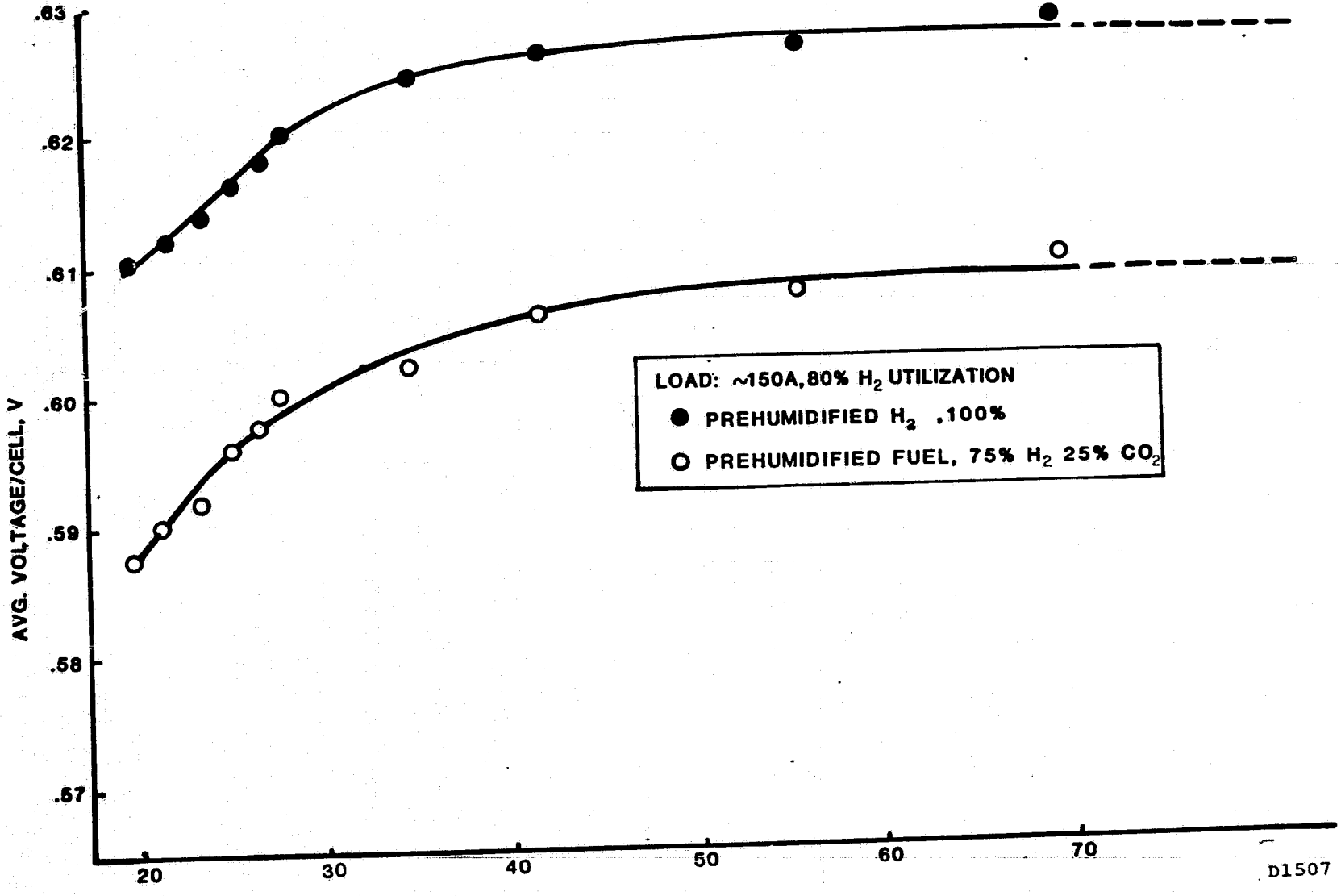

FIGURE 5.2.7. EFFECT OF NO. AIR FLOW ON PERFORMANCE OF STACK 560

ORIGINAL PAGE IS
OF POOR QUALITY

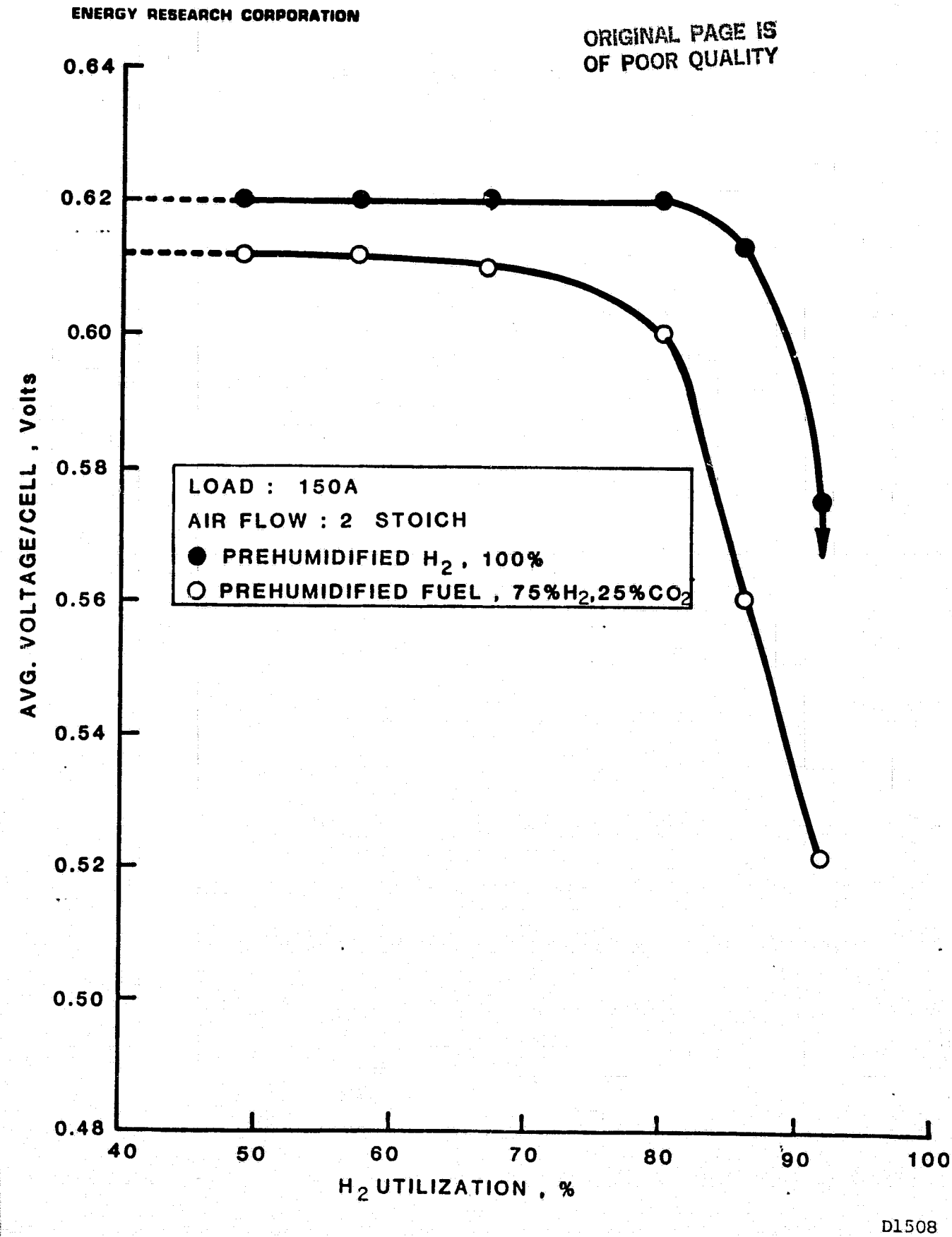

FIGURE 5.2.8. EFFECT OF H_2 UTILIZATION ON STACK PERFORMANCE, STACK 560

ORIGINAL PAGE IS
OF POOR QUALITY

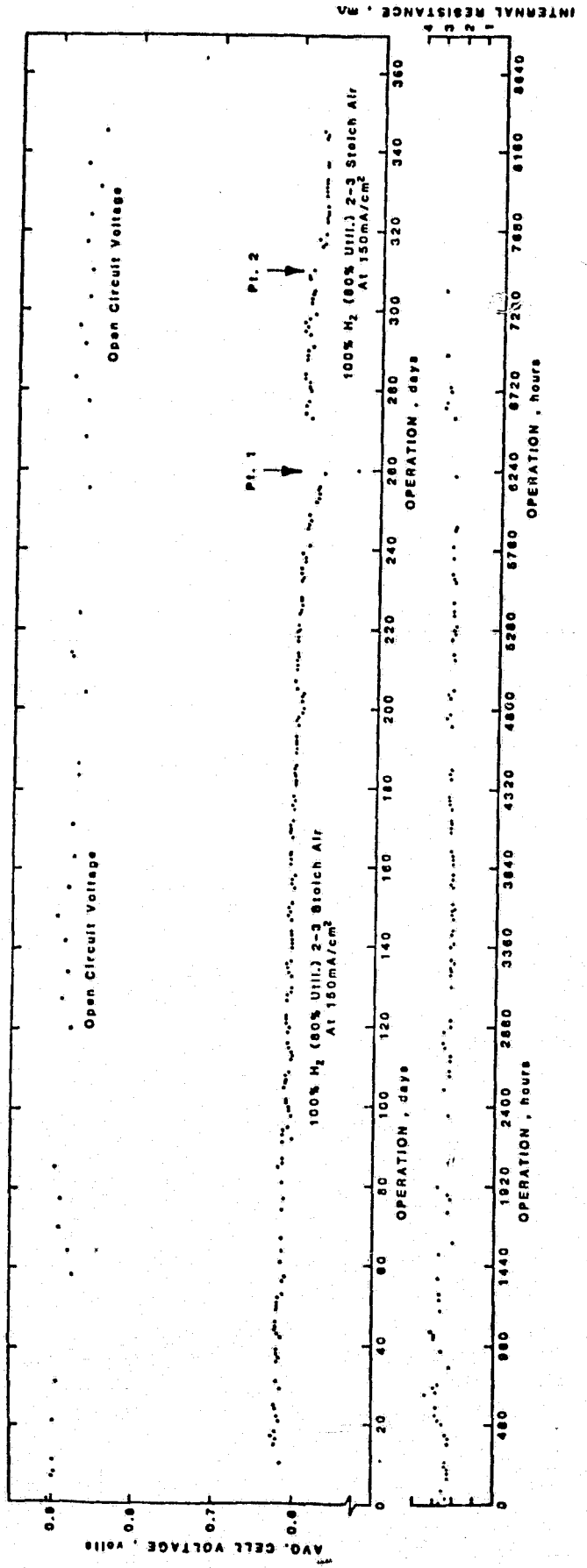

D1774

FIGURE 5.2.9. LIFEGRAPH OF STACK 560

TABLE 5.2.6. THE EFFECT ON PERFORMANCE OF VARYING ANODE GAS COMPOSITIONS
(No. of hrs. in OPERATION: 500)

ANODE GAS COMPOSITION, Vol%			PERFORMANCE* Volts	
H_2	CO_2	CO	at ∿4.8 ST AIR	at ∿2.0 ST AIR
100	0	0	0.622	0.618
75	25	0	0.608	0.602
75	24	1	0.596	0.594
75	22	3	0.588	0.584

*150 mA/cm^2

Endurance Testing

After the pretesting was completed, Stack 560 was endurance tested at 150 mA/cm^2 with hydrogen and air. Figure 5.2.9 shows its stable load performance, OCV and internal resistance. This stack was tested for ∿8300 hours till the end of Phase II. During the first eight months (∿240 days), the performance of the stack was very steady and the time averaged performance was ∿610 mV/cell at 150 mA/cm^2. After this period, the stack underwent air and fuel starvation indicated as points 1 and 2 in the figure. On day 260, a crack was found in the phenolic air inlet manifold. This leak apparently started around day 240 and became progressively worse as the crack became larger. This caused air starvation of the stack and performance failure at point 1. Subsequent to manifold repair, the stack performance almost recovered to its original level. Then, on day 310, the hydrogen supply ran out over the unattended Thanksgiving holidays. The fuel failure (point 2 in Figure 5.2.9) resulted in another drop in performance of 15 mV/cell. After each mishap the stack regained a stable performance which verified ERC's new cell component capabilities and cell/stack design.

ORIGINAL PAGE IS
OF POOR QUALITY

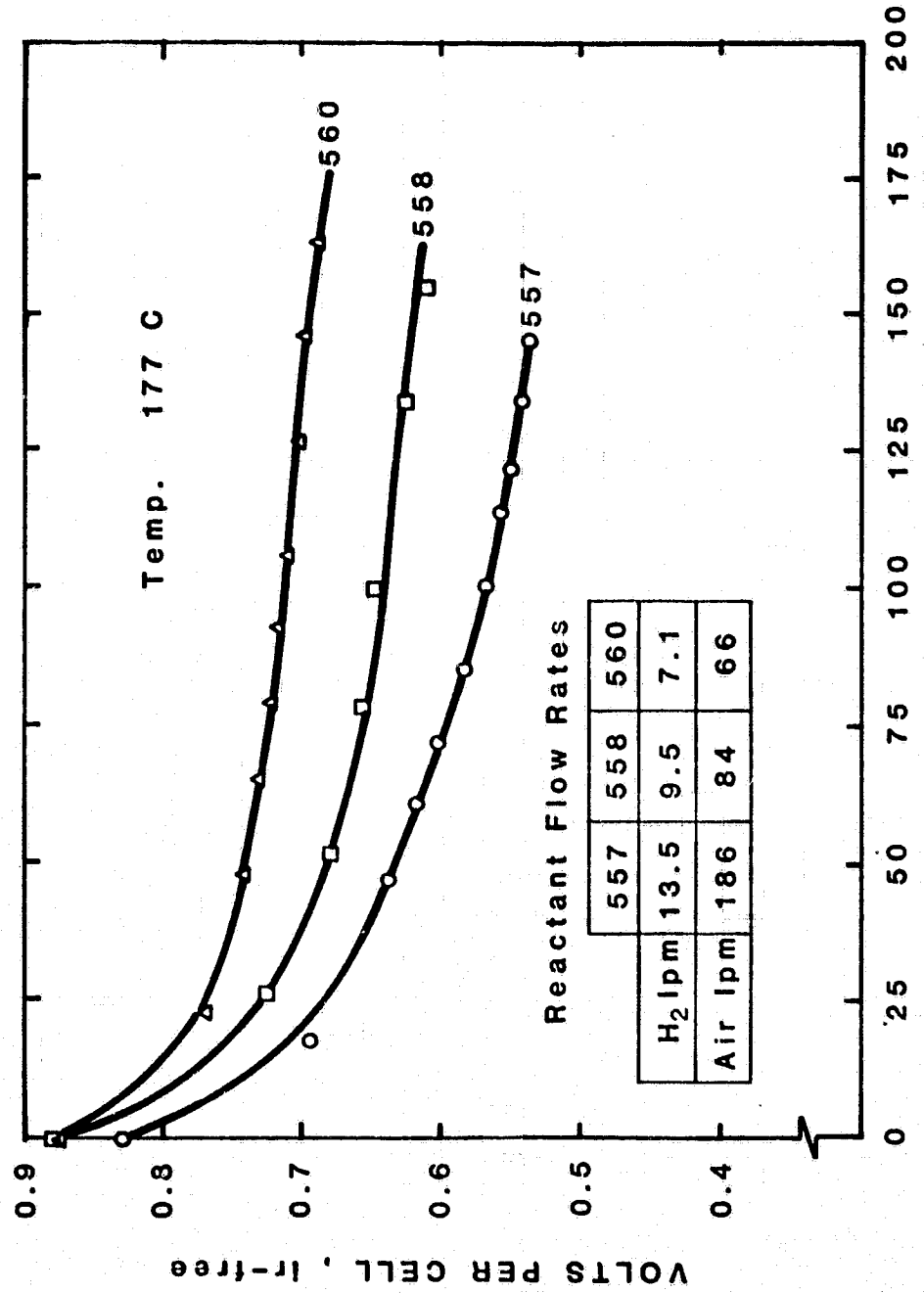

FIGURE 5.2.10. AIR POLARIZATION, STACKS 557, 558, and 560

The performance improvement of this stack with heat-treated bipolar plates and Mat-1 matrices is shown in Figure 5.2.10 which compares the IR corrected performance of the three Mk-2 simulated stacks built in Phase II. Stack 560 shows ∿75 mV gain per cell over the nonheat-treated Stack 558 at 150 mA/cm^2. Other design improvements that led to these gains were discussed in Subsections 3.2 and 4.2, summarized in Table 3.2.1 and described in detail in the procedures document submitted separately to the NASA Project Manager.

In addition, the successful acid additions throughout the life of Stack 560 demonstrated the usefulness of acid addition.

5.3 Short Stack Testing

Short stacks which incorporate a number of coolers were tested to verify the component design and the production and assembly techniques as well as the design parameters such as temperature distribution, flow distribution, pressure drop etc. The experience and knowledge gained in this subtask were utilized in the fabrication and testing of the subscale (80 cell) stack.

Four short stacks were fabricated during Phase II. Each was pretested at ERC to verify its performance, then shipped to Westinghouse for further testing.

5.3.1 Temperature Measurements

A major objective of the stack development on this contract was to achieve uniform temperature profiles with air cooling. The placement of the thermocouples in the short stacks and data interpretation are described in this subsection.

Stacks 559, 561, 562 and 564 were 23 cell stacks with cooling/bipolar plates located after cells 4, 9, 14 and 19. Thermal instrumentation was essentially the same for these stacks and consisted of 4 rows of 5 or 6 thermocouples. Three of the rows were located adjacent (placed in the process gas channels of the bipolar plate) to cells 11, 12 and 13

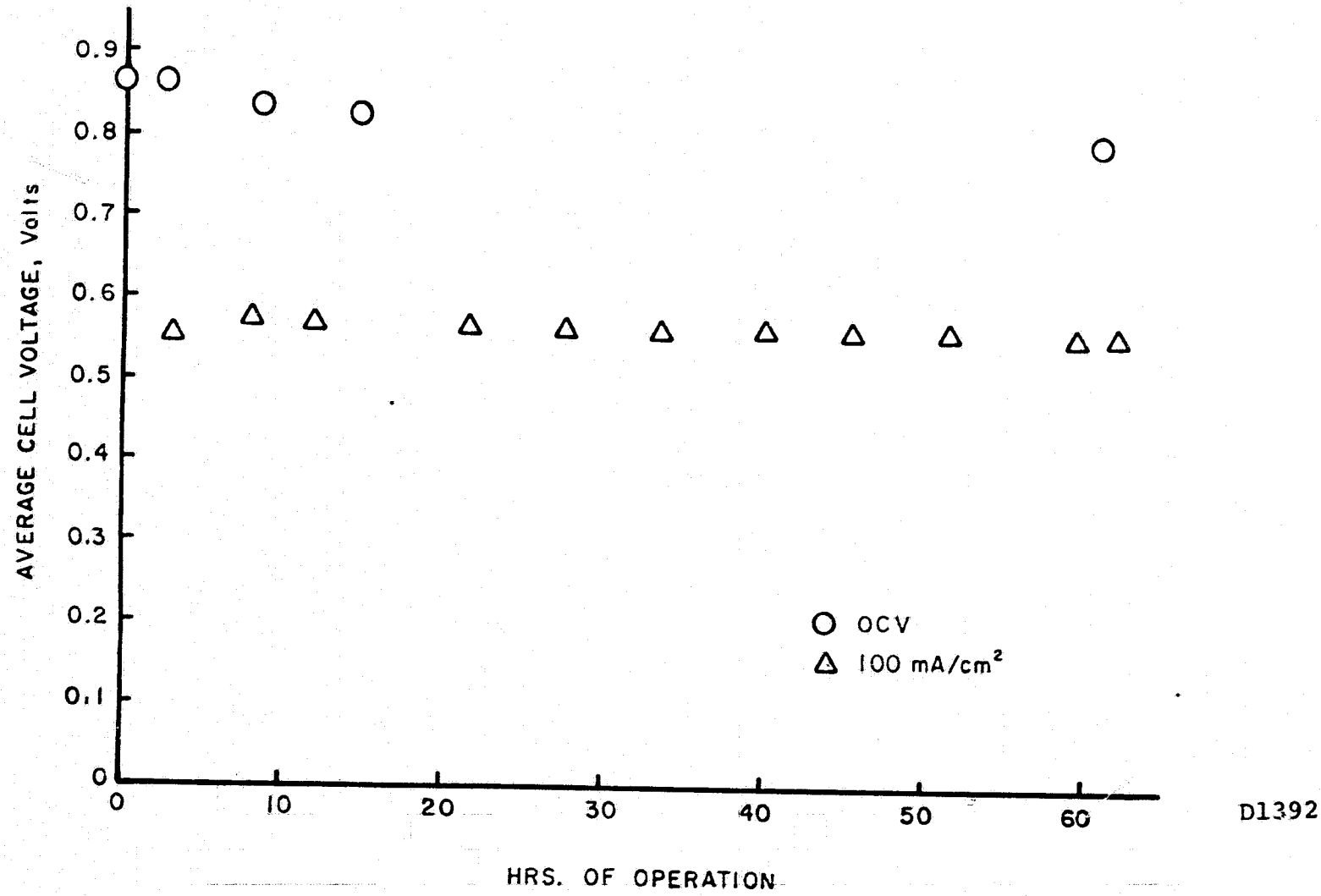

ORIGINAL PAGE IS
OF POOR QUALITY

TOTAL HRS: 62

FIGURE 5-7.1 STACK 559 PERFORMANCE HISTORY

and the fourth row was adjacent to cell 17. The rows for cells 12 and 17 were located along the centerline of the stack in the cooling flow direction. Rows in cells 11 and 13 were 5.1 cm (2 inches) from the hydrogen inlet and outlet edges of the stack. The average temperature of each row was determined using the trapezoidal rule. The mean stack temperature was determined as the average of the three rows between the middle pair of cooling plates.

The primary indication of temperature uniformity adopted for discussing test results is the peak to average temperature gradient. This gradient is defined as the maximum measured temperature minus the mean or average stack temperature. This is the most meaningful gradient since material life is limited by the maximum temperature and cell performance is determined by the average temperature.

5.3.2 Stack 559 (Mk-1, 23-cell)

5.3.2.1 Pretesting

Stack 559 was a DIGAS stack and the only short stack built in Phase II with nonheat-treated plates.

This stack was compressed to 410 kPa and wet-assembled with 45 cm^3/cell of 100% phosphoric acid. Since this quantity was slightly less than the estimated full amount of acid ($\sim$50 cm^3) that a matrix could absorb, additional acid was supplied by the new acid filling scheme during pretesting. The stack took $\sim$5 cm^3 of acid/cell so that the total acid per cell prior to testing was $\sim$50 cm^3, which was in good agreement with the estimated capacity. This acid amount was verified with Stack 560.

This stack was pretested at $\sim$100 mA/cm^2 for 62 hours. Its performance history is shown in Figure 5.3.1. The time averaged performance was $\sim$0.57V/cell which was reasonable for a nonheat-treated stack. After $\sim$60 hours of testing, $\sim$1 cm^3/cell of acid was added to the stack to augment the initial distribution of acid prior to performance testing.

ORIGINAL PAGE IS
OF POOR QUALITY

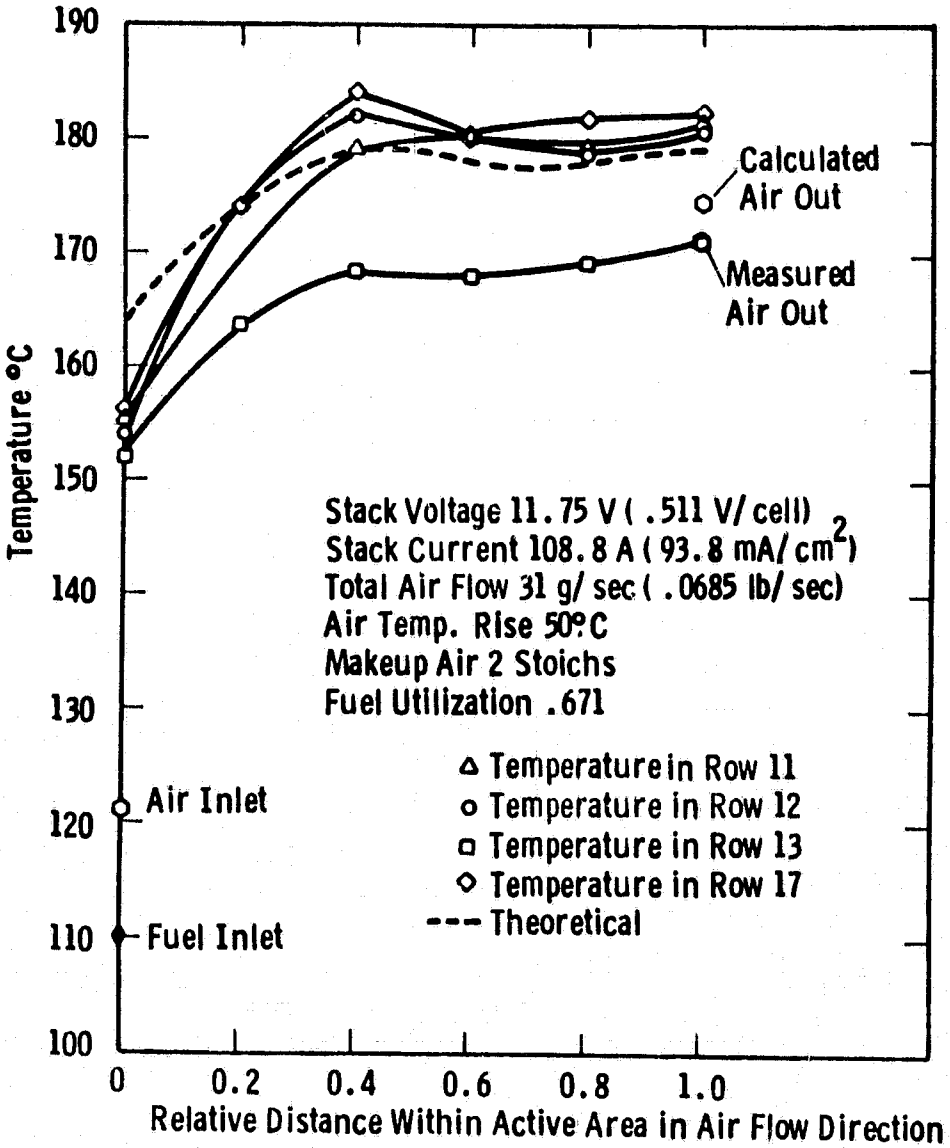

Fig. 5.3.2 — Typical temperature distribution for Stack 559

5.3.2.2 Performance Testing

Conditions for the first test matched those of a pretest made five days earlier and verified that the performance test procedures duplicated the pretest and that the stack was not damaged during shipment.

Following the duplicate test, a series of tests were made to study:

- Temperature uniformity of the stack to assess the effectiveness of the cooling plate design.
- Stack performance at current densities of 50, 100 and 150 mA/cm^2.
- The effect of makeup air flow on stack performance.
- The influence of average cell temperature on stack performance.
- The effect of total stack air flow (recirculating and makeup) on temperature uniformity and stack performance.
- The effect of blocking two cooling channels near the hydrogen exit edge of each cooling plate on temperature distribution.

Detailed results for 12 steady state tests were given in Quarterly Report No. 5 and are summarized and discussed below. The fuel mixture for the tests was nominally 75 percent H_2 with the remainder CO_2. Cell performance was lower than results achieved with subsequent stacks with heat treated plates.

Temperature Distribution

Excellent temperature uniformity was achieved in all tests. For current densities between 90 and 100 mA/cm^2, the peak to average temperature gradient was less than 20% of the air temperature rise. A plot of the temperature distribution for a typical test is shown in Figure 5.3.2. The average temperature in rows 11 and 12 are virtually equal and are approximately 10°C higher than in row 13. The temperature

distribution predicted by the detailed analytical model is shown in Figure 5.3.2 as a dashed curve. The higher slope measured at the air inlet was caused by localized cooling due to the process air and by limited conduction to the inactive area. The test results indicate a higher air flow through the process channels or a lower thermal conductivity than used in the theory. The air flow channels were designed for an air flow split of 16% process and 84% cooling flow. No measurements of the actual split were made.

The overall temperature uniformity can be broken into two components: 1) the peak to average ΔT along a row in the coolant (air) flow direction and 2) the difference between the average temperature of a given row and the average of all rows (fuel flow direction). The spacing of cooling channels was designed to produce equal average temperatures in each row and throughout the stack. This required more closely spaced channels near the hydrogen inlet edge of the stack than at the exit edge. The test results showed a strong tendency for the hydrogen inlet edge (row 11) to overheat as fuel utilization was increased. Before it was discovered that the closer spaced cooling channels were actually located at the hydrogen exit, an experiment was conducted with two cooling channels near the fuel exit edge of each cooling plate plugged. This changed the cooling distribution to the design ratio and produced an excellent balance between the three rows 11, 12 and 13 with reduced coolant flow. However, stack performance had deteriorated too much from initial tests to permit accurate evaluation. Row 11 was undercooled and row 13 was overcooled relative to the intended design in all other tests.

At 2 stoich makeup, the peak to average ΔT's for the stack were 6.6, 9.8 and 15.4°C for respective current densities of 53, 94 and 146 mA/cm^2. The peak to average ΔT's for row 12 were 3.4, 5.1 and 8.0 for the respective tests. Predicted values of these latter ΔT's for 50, 100 and 150 mA/cm^2 are 5, 3 and 7°C, respectively.

Effect of Total Stack Air Flow

Nominal test conditions include an air flow rate corresponding to a temperature rise of 50°C. One test with 26.7°C air rise (approximately double the normal flow) reduced the peak to average ΔT from 10.4 to 8.0°C and the performance improved 7 mV/cell due largely to the increased process flow at the same inlet oxygen concentration. Doubling air flow theoretically increases performance by 5 mV/cell with the 2 stoich makeup used in this test. The increased flow was not expected to make a significant change in temperature uniformity.

The Effect of Current Density and Makeup Air

Polarization curves from steady state tests with 2 and 4.3 stoich makeup air are shown in Figure 5.3.3. by circles and squares, respectively. The data shown by open symbols are for stack average temperatures between 171 and 178°C. The difference due to oxygen concentration for 2 and 4.3 stoich makeup is very close to the expected 25 mV/cell. The darkened circles are for two tests at 2 stoich makeup with mean stack temperatures of 160°C. The difference of 3 mV/°C is higher than the expected effect of 1.2 mV/°C but the tests at low temperature were performed later in the test sequence. Thus, part of the temperature sensitivity observed is due to the decay in performance which occurred during the test period. The extent of the decay in performance is illustrated by the hexagonal points in the figure, which were the second and twelfth tests and were run at 10 stoichs makeup air. Although not at identical conditions, correlations for fuel composition and utilization and temperature level should approximately balance. The results indicate a net decay of about 50 mV/cell over the test period.

5.3.3 Stack 561 (Mk-1, 23-cell)

5.3.3.1 Pretesting

The polarization characteristics obtained during the pretest of this 23-cell DIGAS stack with heat treated plates are shown in Figure 5.3.4. Table 5.3.1 summarizes some important pretest results. As shown

ORIGINAL PAGE IS
OF POOR QUALITY

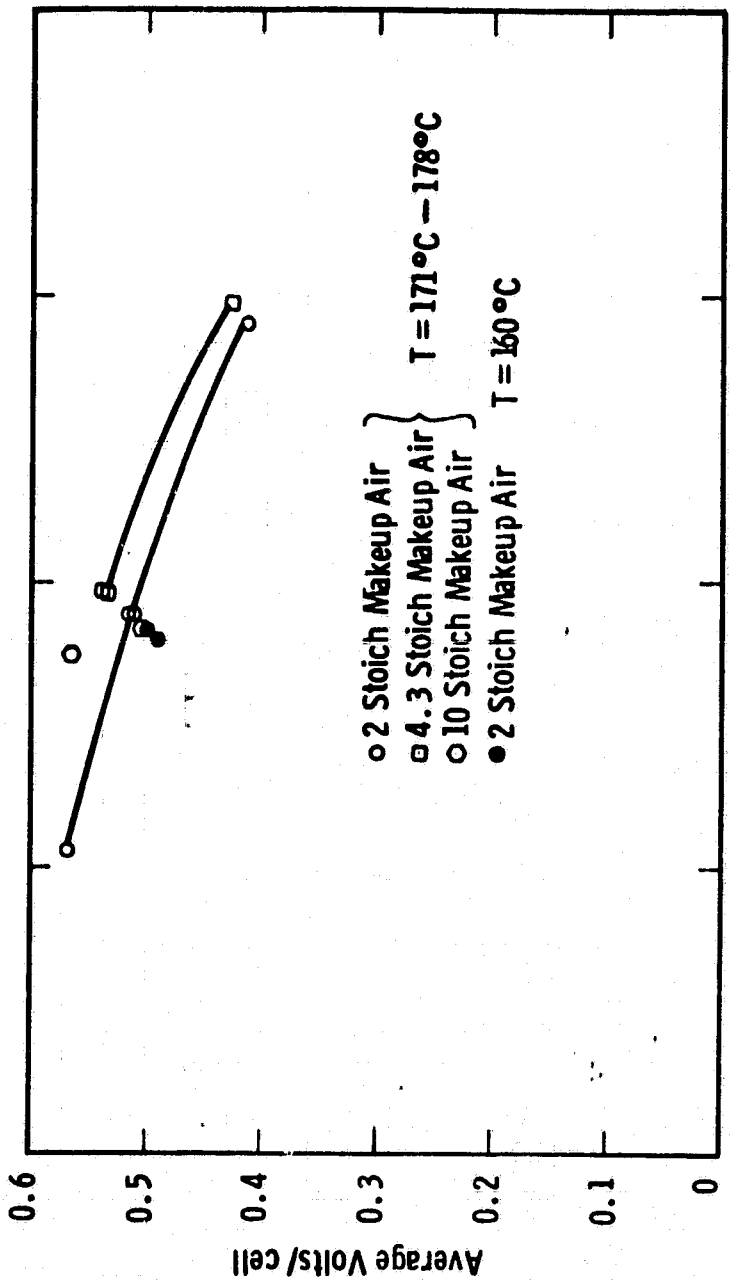

Fig. 5.3.3 – Steady state polarization data for Stack 559

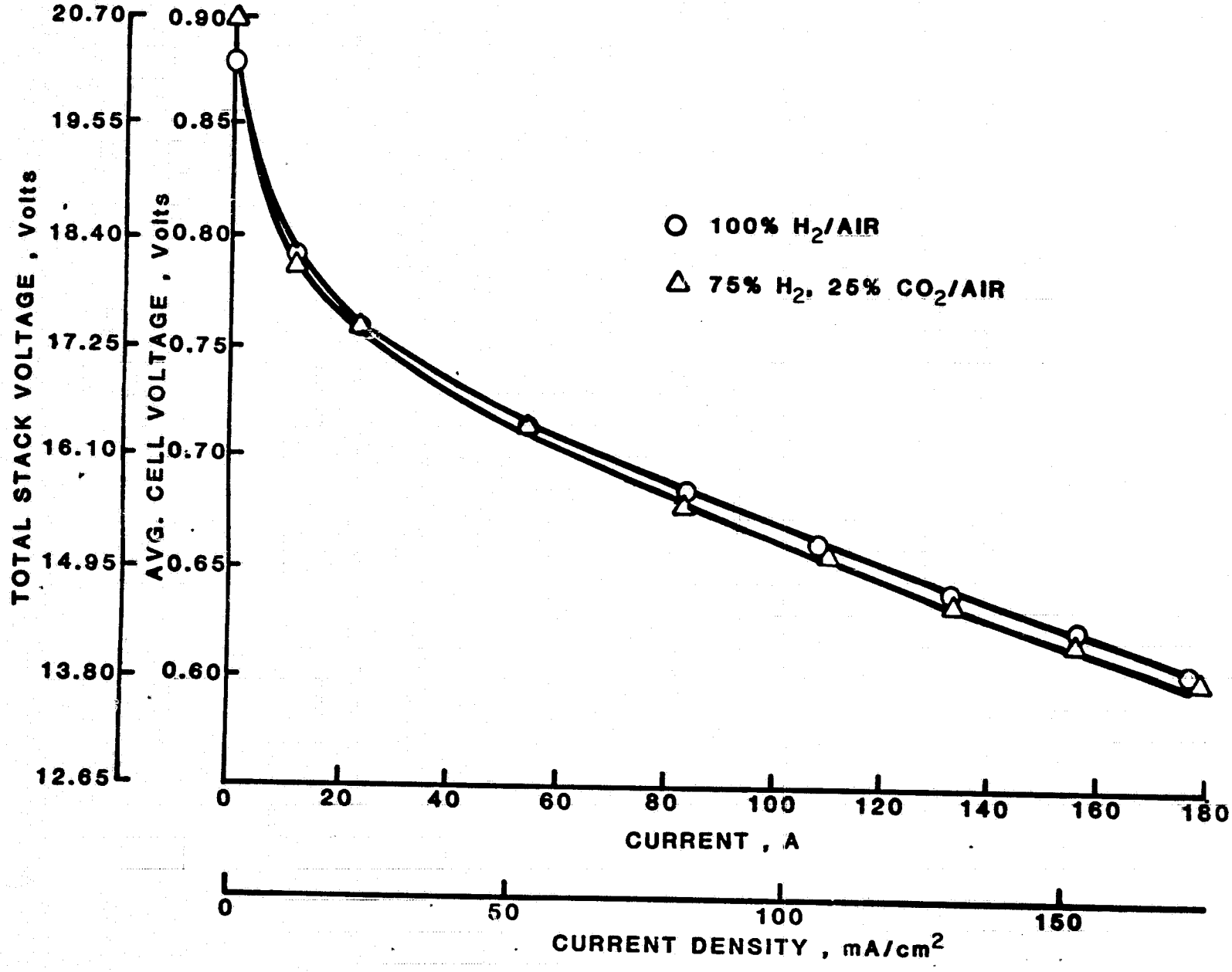

ORIGINAL PAGE IS
OF POOR QUALITY

FIGURE 5.3.4. POLARIZATION OF STACK 561

D1464

ORIGINAL PAGE IS
OF POOR QUALITY

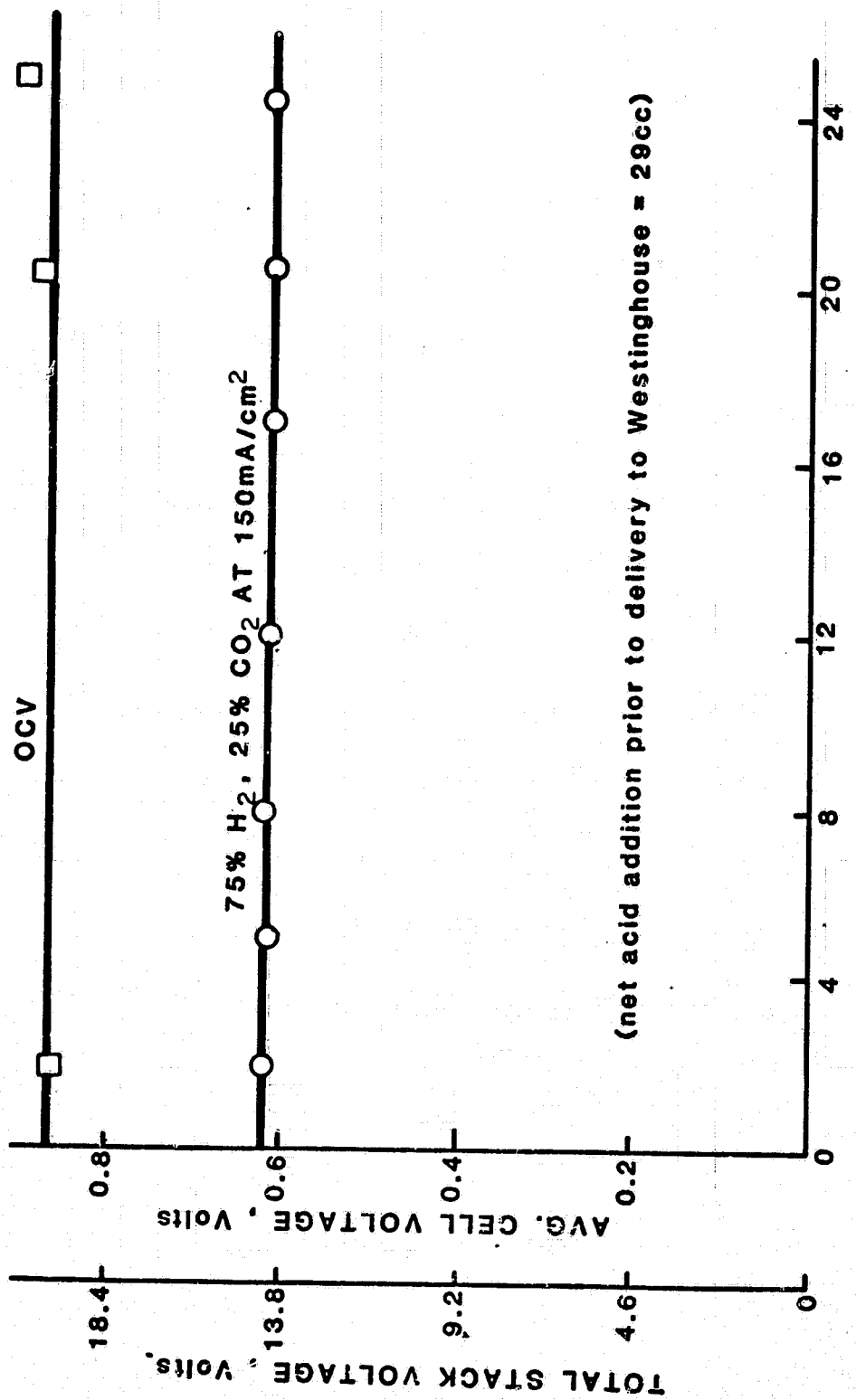

FIGURE 5.3.5. LIFEGRAPH OF STACK 561

ORIGINAL PAGE IS
OF POOR QUALITY

TABLE 5.3.1
PERFORMANCE CHARACTERISTICS OF STACK 561 AT TWO
REACTANT COMPOSITIONS AFTER 20 HOURS

CONDITIONS	PERFORMANCE, V/Cell	
	H_2/Air	75% H_2, 25 CO_2/Air
OCV	0.88	0.90
100 mA/cm^2 (102A)	0.67	0.66
150 mA/cm^2 (153A)	0.63	0.62

in Figure 5.3.1 the initial performance of Stack 559 was ~570 mV/cell at 100 mA/cm^2. The 100 mV/cell improvement is attributable to the use of heat treated plates in Stack 561.

Figure 5.3.5 shows that the average cell voltage at 150 mA/cm^2 with 75% H_2, 25% CO^2 was steady at 0.62 V/cell during the 25 hour pretest period. The H_2 gain of the stack was approximately 12 mV/cell, which agrees closely with theory. Net acid addition during pretest was 29 cm^3 (~1 cm^3/cell).

The sensitivity of Stack 561 to utilization of humidified hydrogen was very low as shown in Figure 5.3.6. This indicated that the stack was gas tight and that the fuel was uniformly distributed among and within the cells. Gas tightness and matrix integrity were confirmed by very small changes in transient OCV (gas or air supply interrupted).

ORIGINAL PAGE IS
OF POOR QUALITY

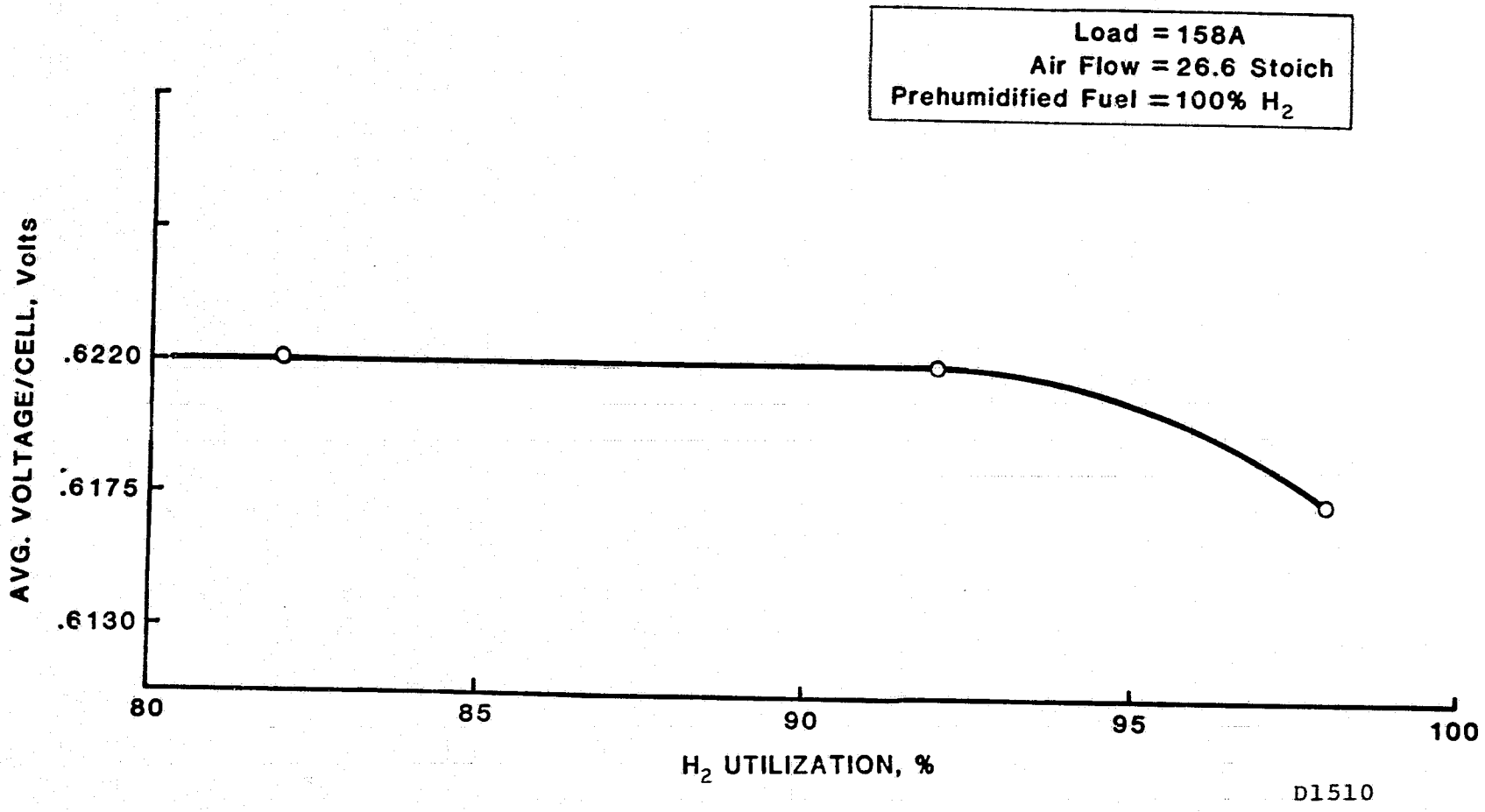

FIGURE 5.3.6. EFFECT OF H_2 UTILIZATION ON STACK PERFORMANCE, STACK 561

5.3.3.2 Performance Testing

Stack 561 was tested at a total of 62 steady state conditions. The performance remained stable with no apparent decay during the test period. Excellent temperature uniformity was obtained for current densities of 58 to 192 mA/cm^2. Test results and test conditions, including results of one pretest as No. 1, are summarized in Table 5.3.2 and discussed in detail below.

Test Conditions

The data in Table 5.3.2 includes inlet temperatures of fuel and air streams, fuel utilization, makeup air flow rate in stoichs, total air flow rate through the stack, air side pressure drop, and dry fuel composition. In all tests, the fuel mixture was humidified by bubbling through room temperature water before heating to the indicated inlet temperature.

The first performance tests (2 to 5) were conducted without insulation on the stack for comparison with pretest data and to observe the cell sensitivity to fuel utilization. These early tests were run by increasing hydrogen flow until a sharp drop in voltage of the stack (or a cell) was observed. They indicated a hydrogen sensitivity at low flows but, after test No. 29, a leak in the fuel supply line downstream of the metering devices was discovered and repaired. Thus the actual fuel flow to the stack for tests 2 through 29 was less and hydrogen utilization greater than indicated.

Test 6 and all subsequent tests were performed with the stack insulated. Temperature distributions of tests 7, 8, 9, 10 and 18, which are representative operating conditions, showed that the average temperature at the hydrogen inlet edge of the stack (row 11) was 10°C higher than that of the exit edge (row 13). Two cooling channels near the hydrogen exit of each cooling plate (2 and 6 from the exit edge) were blocked to improve temperature uniformity. All remaining tests (numbers higher than 29) were made with this modified cooling plate configuration.

ORIGINAL PAGE IS
OF POOR QUALITY

TABLE 5.3.2 –SUMMARY OF TEST CONDITIONS AND TEST RESULTS FOR STACK 561

Test	Current Density, mA/cm^2	Average Volts/Cell, V	Average Temperature, °C	Peak to Average Temperature Difference, °C	Fuel Utilization	H_2 Inlet Mole Fraction (Dry)	CO_2 Inlet Mole Fraction (Dry)	CO Inlet Mole Fraction (Dry)	Fuel Inlet Temperature, °C	Makeup Air, Stoichs	Loop Flow Rate (Makeup + Recirculation), g/sec	Inlet Air Temperature, °C	Air Temperature Rise, °C	Air Pressure Drop, in.H_2O
1	152	.613	177	9.4	.82	.75	.25	0	103	13.3		128	41	
2	158	.586	182	11.9	.72	.75	.25	0	75	8.2	30.0	123	46	1.46
3	101	.647	175	5.6	.46	.75	.25	0	110	9.0	34.0	151	13	1.61
4	98	.630	175	7.8	.75	.75	.25	0	114	9.3	35.0	150	12	1.61
5	100	.647	175	5.4	.46	.75	.25	0	112	9.1		150	13	1.61
6	107	.591	181	9.3	.49	.75	.25	0	71	4.0	25.0	124	46	1.17
7	107	.620	179	8.2	.66	.75	.25	0	120	5.9	22.0	123	49	.89
8	107	.619	186	8.6	.66	.75	.25	0	122	6.0	20.0	122	56	.76
9	156	.588	175	10.7	.64	.83	.17	0	115	6.2	36.0	113	53	1.69
10	156	.578	175	10.5	.64	.83	.17	0	114	3.9	37.0	113	52	1.75
11	194	.566	175	11.8	.59	.89	.11	0	108	4.1	47.8	113	52	3.08
12	107	.635	176	7.7	.51	.80	.20	0	120	6.0	79.0	117	54	.72
13	107	.628	178	7.5	.50	.80	.20	0	120	4.0	19.0	116	56	.73
14	107	.588	181	6.1	.51	.80	.20	0	119	2.0	19.0	115	58	.73
15	156	.570	161	9.5	.55	.85	.15	0	113	3.8	36.0	99	54	1.60
16	194	.544	159	12.3	.58	.93	.07	0	109	4.1	48.5	96	54	2.44
17	107	.609	161	5.8	.51	.80	.20	0	116	4.0	19.0	96	58	.72
18	107	.621	181	9.1	.64	.76	.24	0	121	5.9	21.0	123	53	.81
19	155	.589	177	9.1	.64	.83	.17	0	115	10.9	36.0	115	54	1.71
20	155	.590	179	8.9	.64	.83	.17	0	116	7.2	36.0	116	54	1.72
21	155	.537	182	6.5	.64	.83	.17	0	118	2.1	35.0	113	58	1.71
22	155	.531	166	9.3	.64	.83	.17	0	119	2.1	52.2	114	43	2.82
23	156	.582	178	10.0	.63	.83	.17	0	113	6.1	36.0	116	54	1.70
24	156	.575	179	9.6	.63	.83	.17	0	113	4.0	36.0	116	55	1.69
25	194	.552	178	11.7	.61	.86	.14	0	107	4.1	47.8	114	54	2.58
26	107	.578	176	6.3				0	119		24.0	119	50	1.01
27	194	.496	179	10.4				0	111		50.0	112	55	2.74
28	107	.619	179	9.8				0	116			114	60	.76
29	200	.556	175	14.1				0	102			115	50	2.99
30	107	.621	181	7.3	.77	.76	.24	0	124	5.9	23.0	122	57	.94
31	156	.585	180	9.3	.74	.76	.24	0	113	6.1	37.0	118	57	1.75
32	194	.540	178	12.4	.74	.75	.25	0	104	3.9	50.4	114	56	2.71
33	156	.563	178	9.0	.72	.76	.24	0	111	3.1	37.0	115	56	1.76
34	156	.532	180	7.9	.72	.76	.24	0	112	2.1	37.0	113	60	1.74
35	107	.614	178	6.5	.74	.77	.23	0	124	4.0	24.0	120	56	.98
36	107	.576	174	5.2	.74	.77	.23	0	124	1.9	28.0	120	51	1.19
37	107	.585	151	6.8	.73	.77	.23	0	122	4.1	26.0	95	54	1.20
38	107	.536	155	6.5	.73	.77	.23	0	122	1.6	27.0	97	54	1.13
39	156	.509	163	12.1	.68	.77	.23	0	110	2.1	36.0	97	62	1.70
40	156	.541	154	9.4	.70	.75	.25	0	77	4.0	38.1	89	57	1.76
41	156	.552	162	9.8	.70	.75	.25	0	73	4.0	38.1	99	55	1.77
42	156	.563	170	9.8	.70	.75	.25	0	87	4.0	38.1	108	54	1.80
43	156	.572	178	9.6	.70	.75	.25	0	90	4.0	38.1	117	53	1.82
44	156	.565	171	10.5	.70	.75	.25	0	95	4.0	38.1	107	56	1.81
45	195	.499	156	13.9	.70	.75	.25	0	33	3.9	48.5	86	59	2.51
46	195	.513	164	13.4	.70	.75	.25	0	35	3.9	48.5	95	59	2.54
47	195	.524	172	13.2	.70	.75	.25	0	41	3.9	48.1	104	57	2.56
48	195	.535	180	13.0	.70	.75	.25	0	41	3.9	47.7	114	56	2.59
49	195	.525	172	13.1	.70	.75	.25	0	41	3.9	48.1	103	58	2.56
50	195	.507	173	14.6	.71	.74	.24	.016	100	3.9	48.1	103	60	2.56
51	195	.501	173	15.2	.70	.73	.25	.024	100	3.9	48.1	103	61	2.56
52	195	.483	175	16.3	.70	.72	.24	.040	100	3.9	48.1	103	63	2.56
53	108	.580	151	7.3	.69	.75	.25	0	107	4.4	26.0	92	55	1.02
54	108	.589	158	7.4	.69	.75	.25	0	115	4.3	26.0	102	52	1.04
55	107	.599	166	7.2	.68	.75	.25	0	120	4.4	26.0	112	50	1.07
56	107	.609	178	7.3	.68	.75	.25	0	107	3.9	24.0	122	52	.99
57	107	.604	172	7.4	.68	.75	.25	0	108	3.9	24.0	112	56	.98
58	59	.635	150	6.1	.70	.75	.25	0	120	4.0	15.0	97	52	.42
59	59	.638	152	5.5	.70	.75	.25	0	120	4.0	15.0	105	45	.47
60	59	.643	158	5.2	.70	.75	.25	0	120	4.0	15.0	115	40	.47
61	59	.655	170	5.2	.70	.75	.25	0	120	4.0	15.0	130	36	.48
62	59	.663	180	5.2	.70	.75	.25	0	120	4.0	15.0	142	34	.49

In tests 6 through 29, stack performance was measured as a function of makeup air flow for a series of current densities. The series at 2 stoich makeup was not completed because cells 12 and 14 produced low voltages (high oxygen sensitivity).

After repairing the fuel leak mentioned above, tests 30 to 36 were run to measure the effect of air makeup on performance with a known fuel flow. Comparison of test 31 with test 9 indicates that approximately 14% ((.74-.64)/.74) of the fuel had been leaking. Tests 37 to 39 were run to determine the effect of makeup air flow on performance at lower average temperature.

The remaining tests (40 through 62) were made to determine the effect of average temperature on performance. Seventy percent fuel utilization and 4.0 stoich makeup air were used for these tests. The procedure was to start with low inlet air temperature at a fixed current until steady state operation with an average stack temperature near 150°C was achieved. The air inlet temperature was then raised in steps to obtain steady state performance for stack temperatures between 150 and 180°C. A final point for each current was obtained by lowering air inlet temperature to duplicate data and show that the performance was independent of whether the point was reached by raising or lowering the temperature. This series also included the effect of CO from 0 to 4 percent at 195 mA/cm^2 in tests 49 through 52.

Temperature Distribution

The effects on temperature distribution of blocking 2 cooling channels in each cooling plate is shown by Figures 5.3.7 and 5.3.8 and the effect on performance for the two tests (10 and 43) are given in Table 5.3.2. With the blocked channels the average temperature near the exit edge (row 13) was 8.1°C higher than that of the inlet edge while it was 11.4°C lower with all channels open. The difference between rows 11 and 13 was $\leq$5°C in more than three fourths of the tests with 28 cooling channels (2 channels blocked) per plate. The peak to average gradient was reduced from 10.5°C to 9.6°C by the modification.

ORIGINAL PAGE IS
OF POOR QUALITY

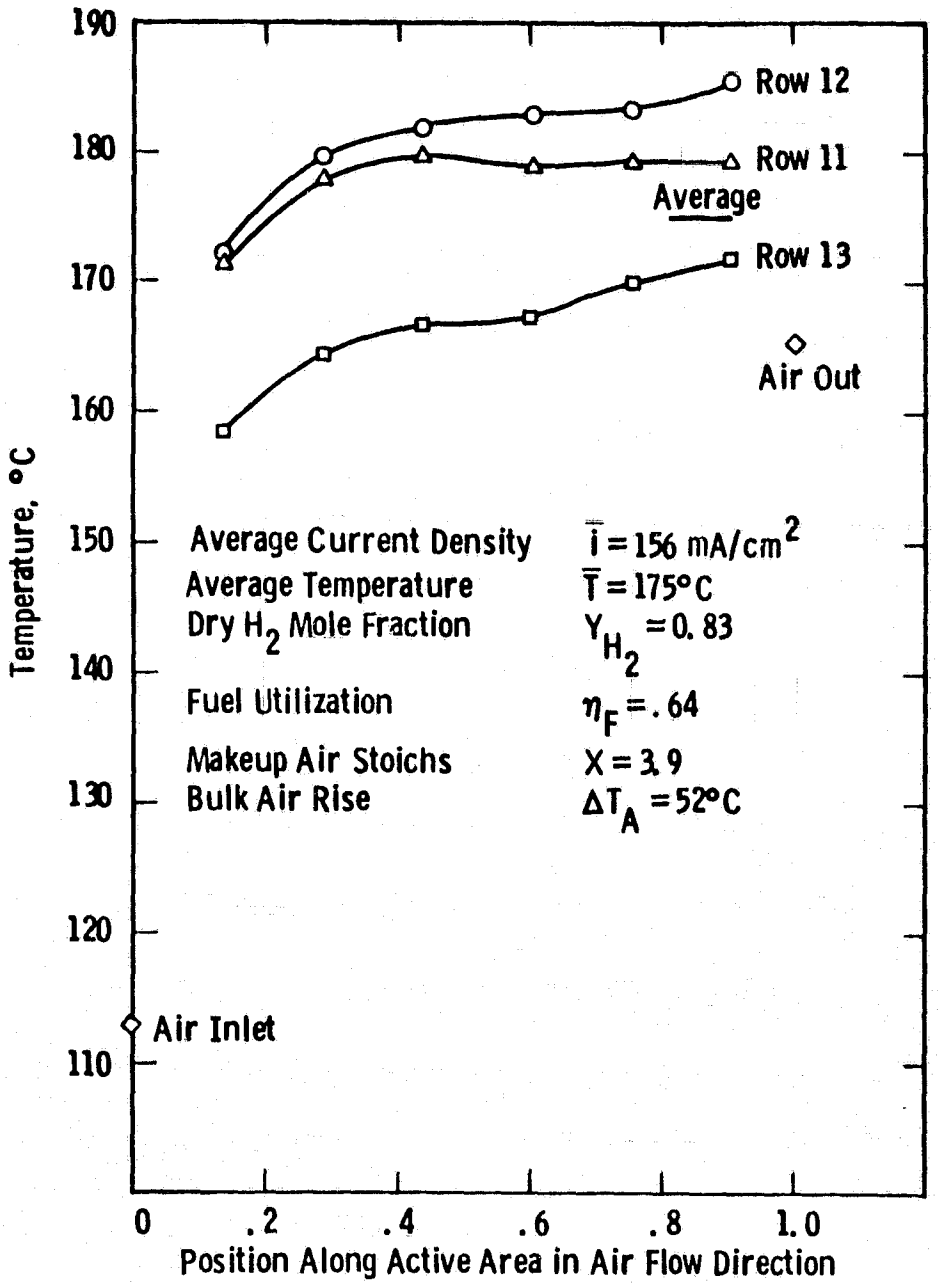

Fig. 5.3.7 – Temperature distribution for stack 561 with all cooling channels open - Test 10

ORIGINAL PAGE IS
OF POOR QUALITY

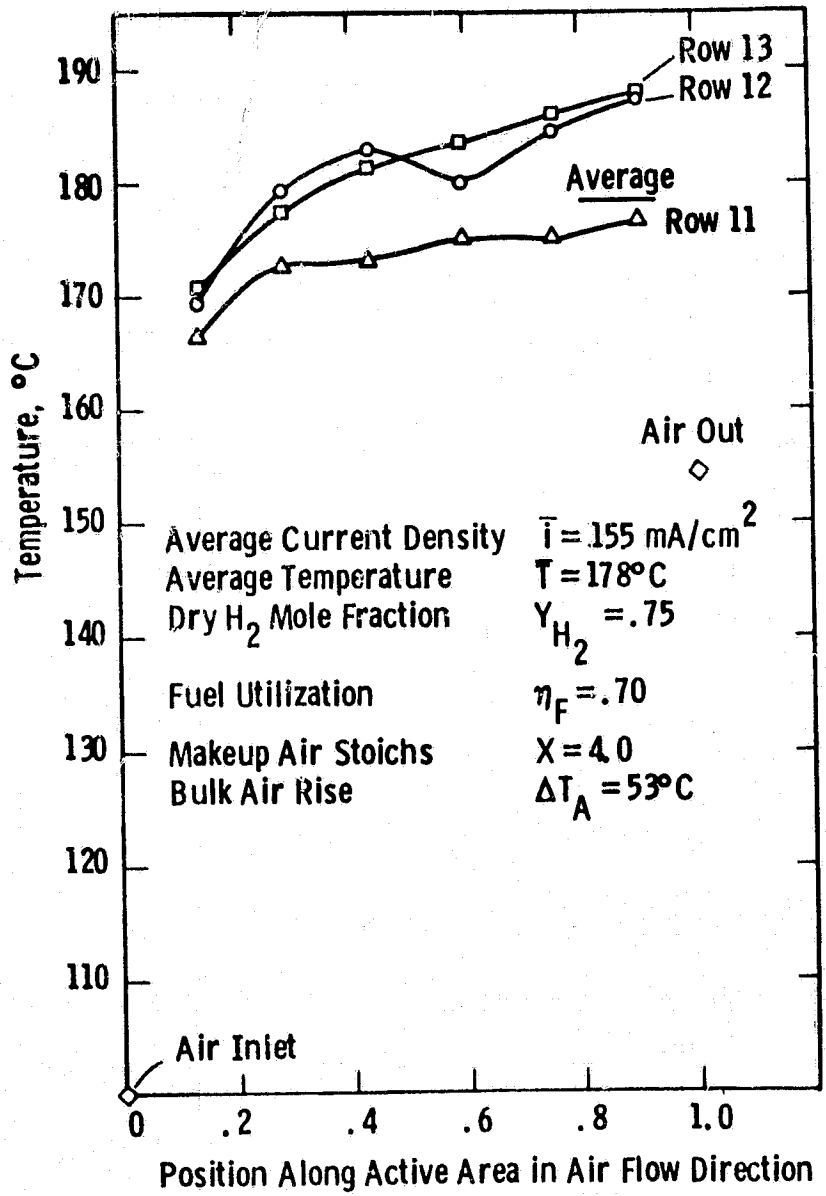

Fig. 5.3.8—Temperature distribution for stack 561 with modified cooling plate Geometry - Test 43

OF POOR QUALITY.

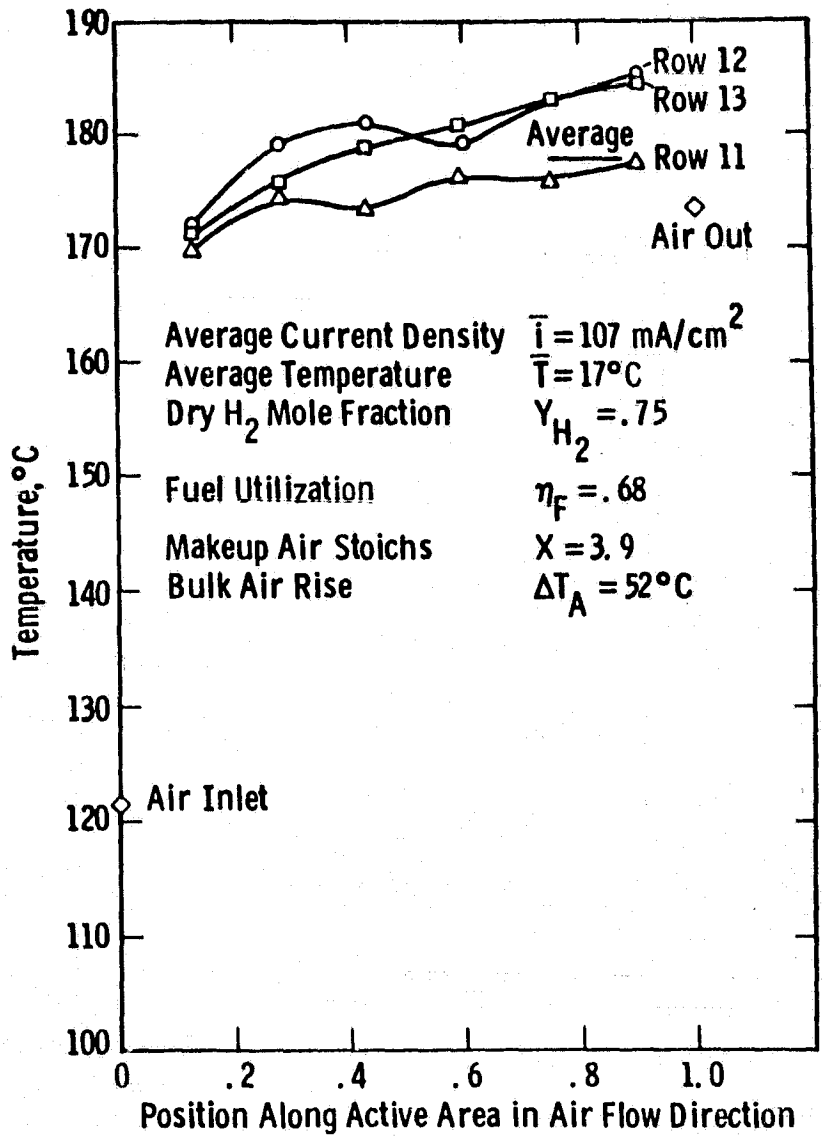

Fig. 5.3.9 —Temperature distribution for stack 561 with all cooling channels open - Test 56

Figures 5.3.9 and 5.3.10 show temperature distributions at 107 and 195 mA/cm^2 for 4 stoich makeup and 70 percent fuel utilization. The distributions are remarkably similar for the two current densities.

Figure 5.3.11 shows the effect of 4% CO on the temperature distribution. For 4% CO, row 13 was 22.7°C below row 11 but the peak to average gradient was still only 16.3°C at a measured average air rise of 62.9°C. At 1.6% CO, row 13 was 5°C below row 11.

Based on these results, we concluded that a design with 28 cooling channels spaced to approximate the plugged configuration would give satisfactory temperature distribution over the range of current densities up to 200 mA/cm^2 for fuels with up to 4% CO for DIGAS (Mk-1) stacks. Although no tests were made with CO in the fuel with 30 cooling channels it is clear that the additional cooling at the hydrogen exit edge would result in low current densities there and a much greater spread in the temperature distribution.

Figure 5.3.12 is a comparison of the measured temperature distribution with those predicted by the detailed analytical model for the test conditions. Numbers on the left of the figure enclosed in parenthesis are calculated temperatures in °C including air in and out. Numbers on the right are the temperatures measured in test 31. The theory predicts a slightly higher temperature at the air leading edge and underpredicts the maximum temperature by about 5°C. The average cell temperature is 180°C for both test and calculation. The test configuration has higher cooling channel density near the hydrogen inlet and lower density near the outlet(variable spacing) than the uniform distribution used for the calculation. Considering the complex interaction among temperature levels, reaction rates, reactant depletions, current densities, heat generation rates and reactant distributions and that only temperatures can be measured directly; the agreement between calculated and measured temperatures is very good.

ORIGINAL PAGE IS
OF POOR QUALITY

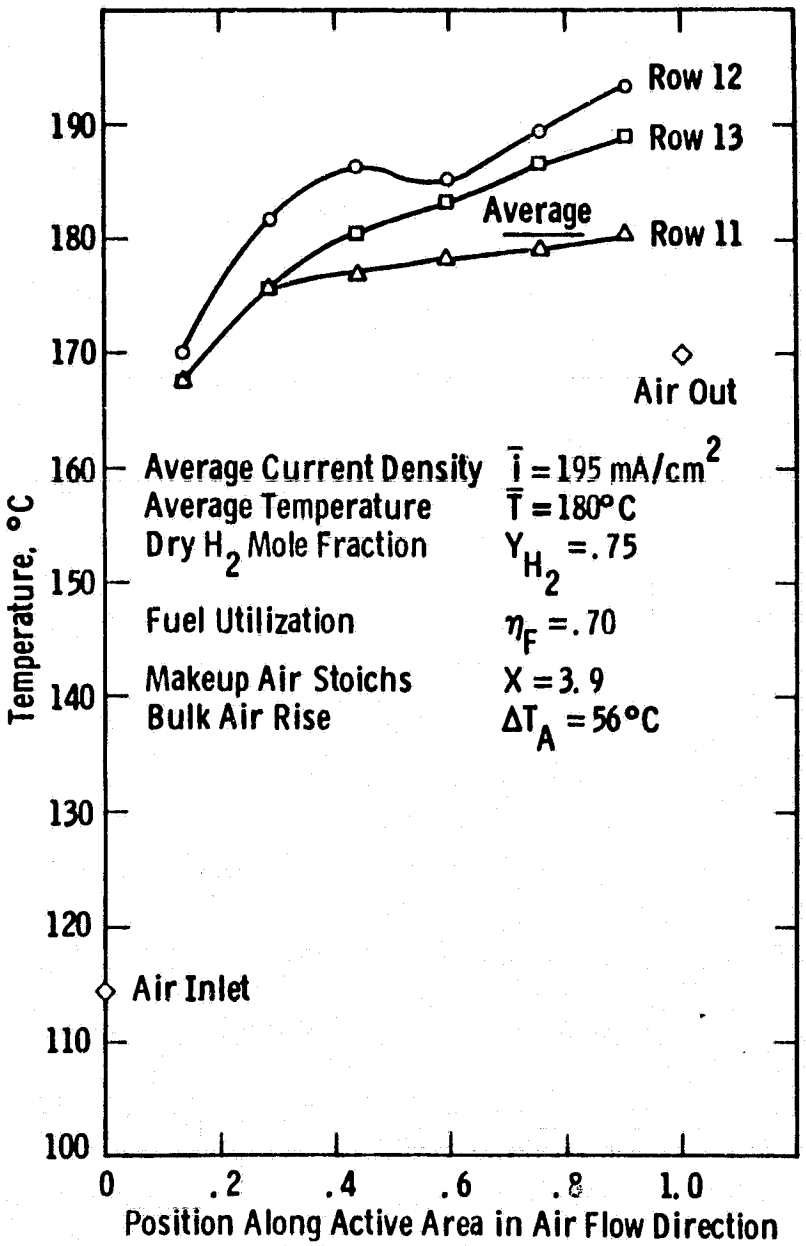

Fig. 5.3.10-Temperature distribution for stack 561 with all cooling channels open - Test 48

ORIGINAL PAGE IS
OF POOR QUALITY

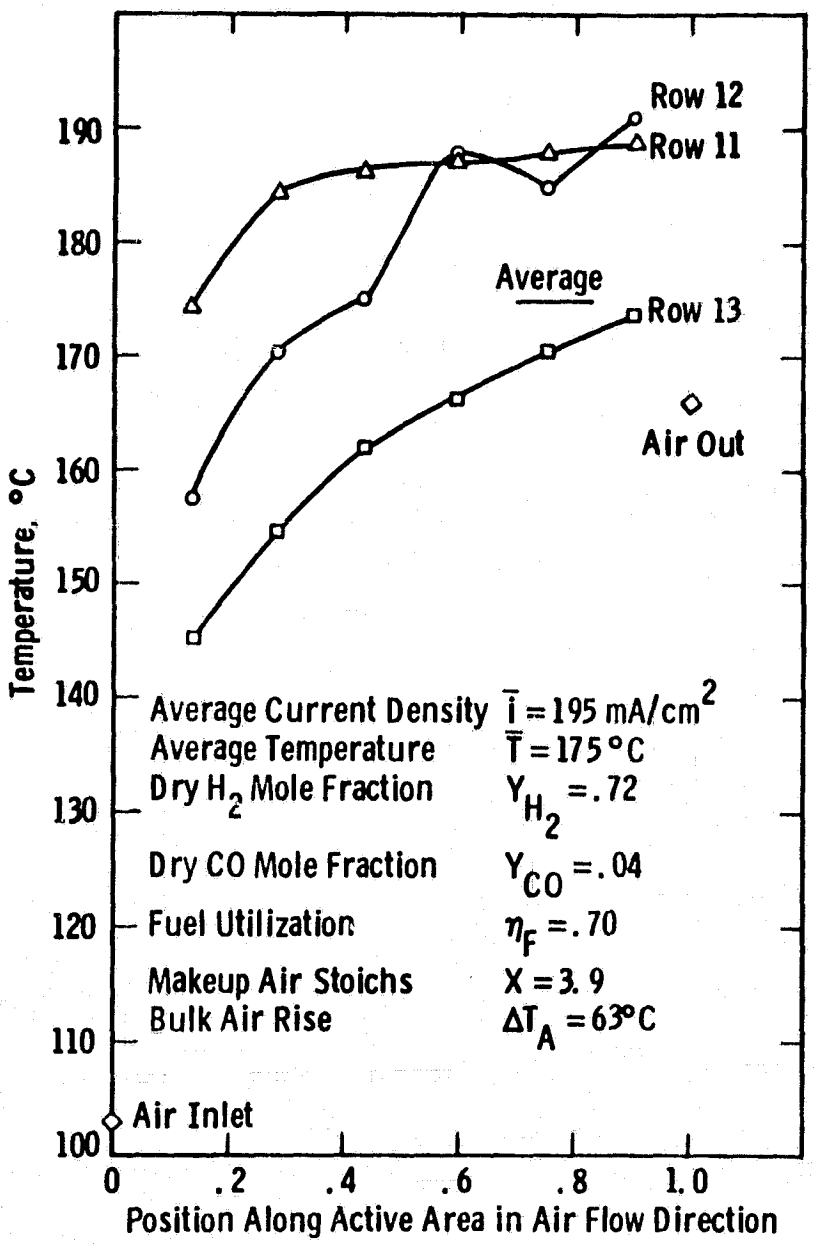

Fig. 5.3.11.—Temperature distribution of stack 561 with modified cooling plate geometry and 4 % CO in fuel-Test 52

ORIGINAL PAGE IS
OF POOR QUALITY

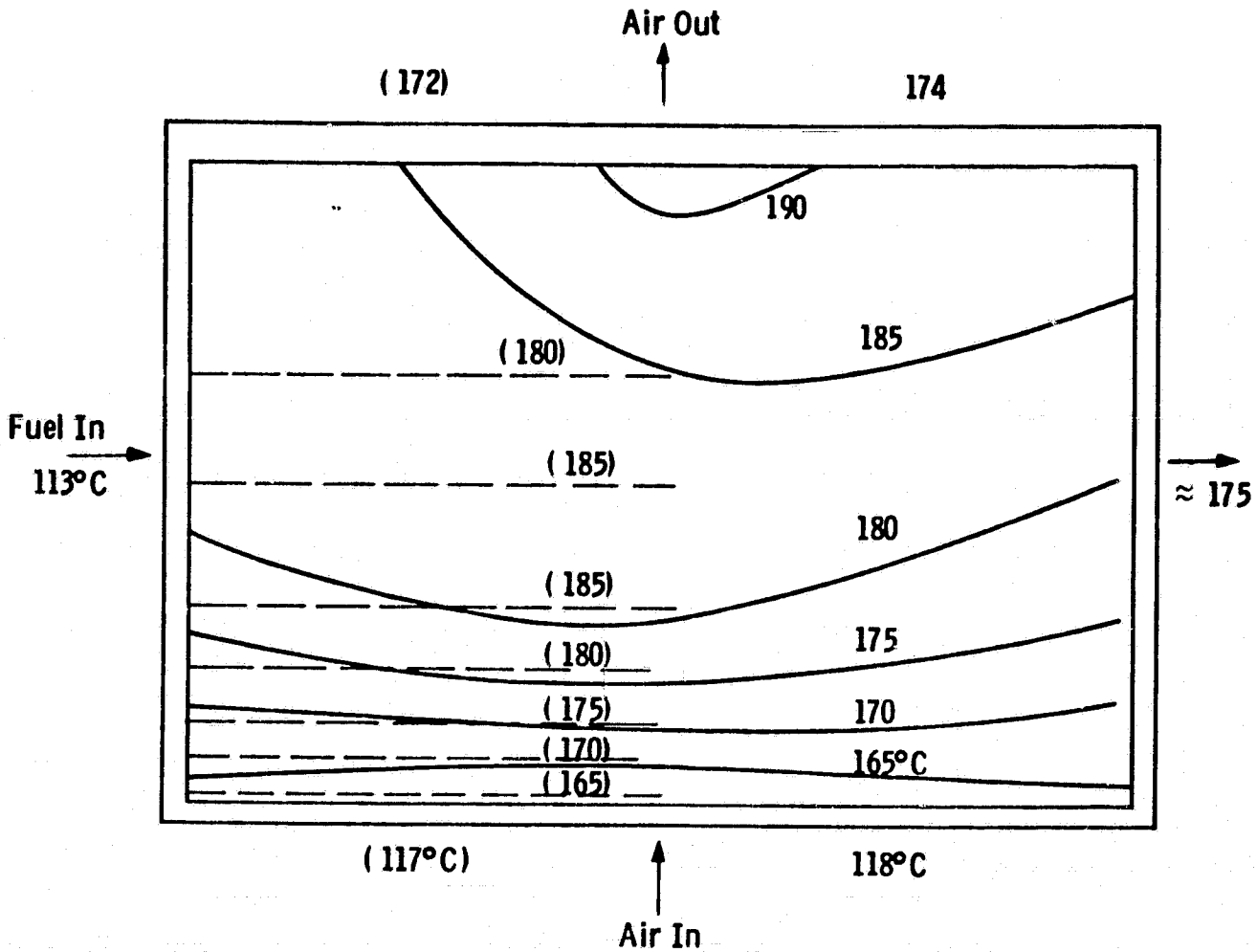

Fig. 5.3.12—Temperature distribution in stack 561-Test 31 compared to predicted values from analytical model in parenthesis

Figure 5.3.13 shows the calculated current density corresponding to the calculated temperature distribution in Figure 5.3.12. The current density is a maximum for any fuel stream at the inlet and decays with distance along the channel. Current density first increases along an air stream due to increased temperature and then decreases as the effect of O_2 depletion becomes significant. The measured temperature distribution indicates that current density varies more sharply in the fuel flow direction than predicted by the present analysis. It is believed that this is due to the fact that water vapor is transferred to the fuel stream. This is consistent with the high observed dewpoint of the anode exhaust stream. The analysis assumed that all water produced is removed by the process air stream.

Effect of Makeup Air Flow

The makeup air flow rate (stoichs) is an important system parameter since it determines the oxygen and water mole fractions in the recirculated and exhaust streams. Low makeup and vent flows reduce blower power and make it easier to recover water and heat from the vent stream but reduce output voltage (or cell efficiency). Figure 5.3.14 shows polarization curves for 2, 3, 4 and 6 stoich makeup for similar temperatures and fuel utilizations. The measured change between 6 and 4 stoichs is about 10 mV compared to a calculated 6 mV. The measured change between 4 and 2 stoichs is about 40 mV compared to a calculated 25 mV. Thus Stack 561 is about 1.6 times more sensitive to makeup flow than predicted by theory. This increased sensitivity would be predicted if the process flow is actually lower than the predicted flow split for the channel design. Pressure drop data suggests this possibility but the evidence is not conclusive.

The Effect of Temperature on Performance

Figure 5.3.15 presents the average cell voltage as a function of average stack temperature for 4 current densities. The flow rates for fuel and air were held constant for each current and the stack temperature was varied by changing the inlet air temperature. Fuel utilization, fuel composition, and makeup stoichs were held constant for all current densities.

ORIGINAL PAGE IS
OF POOR QUALITY

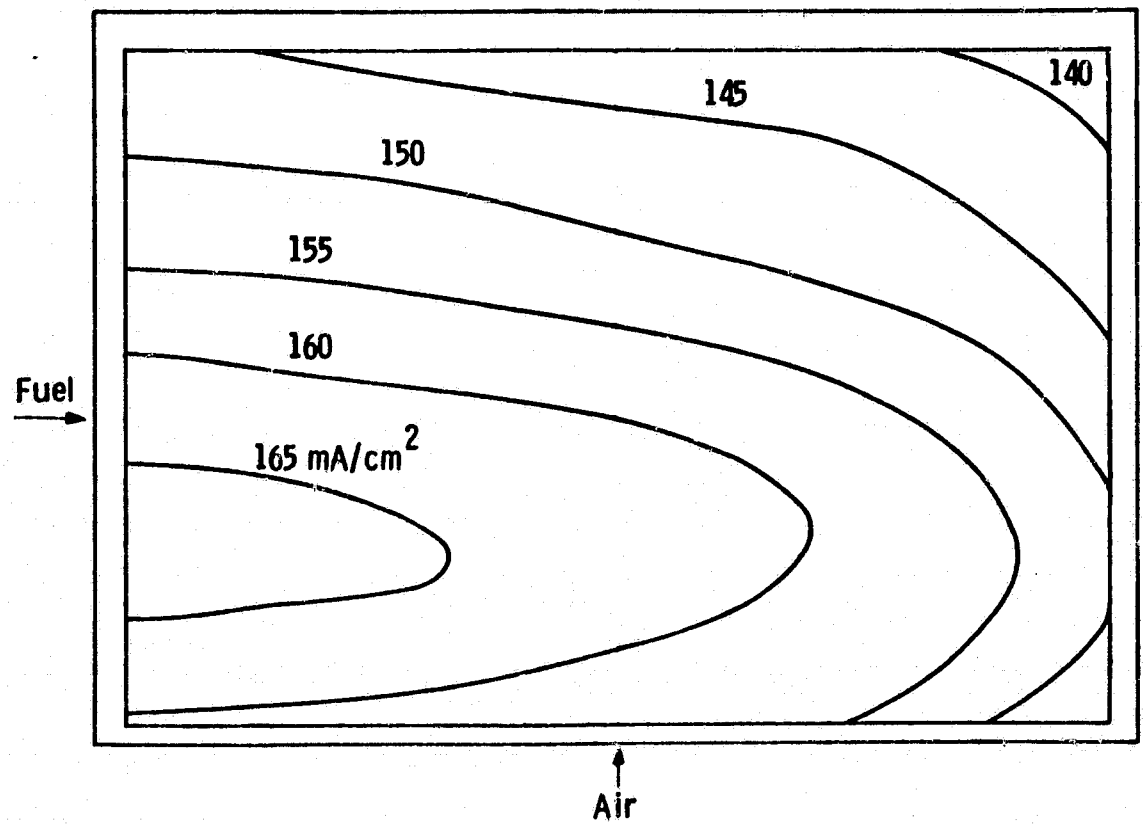

Fig. 5.3.13 – Current density calculated for stack 561 with conditions of Test 31

ORIGINAL PAGE IS
OF POOR QUALITY

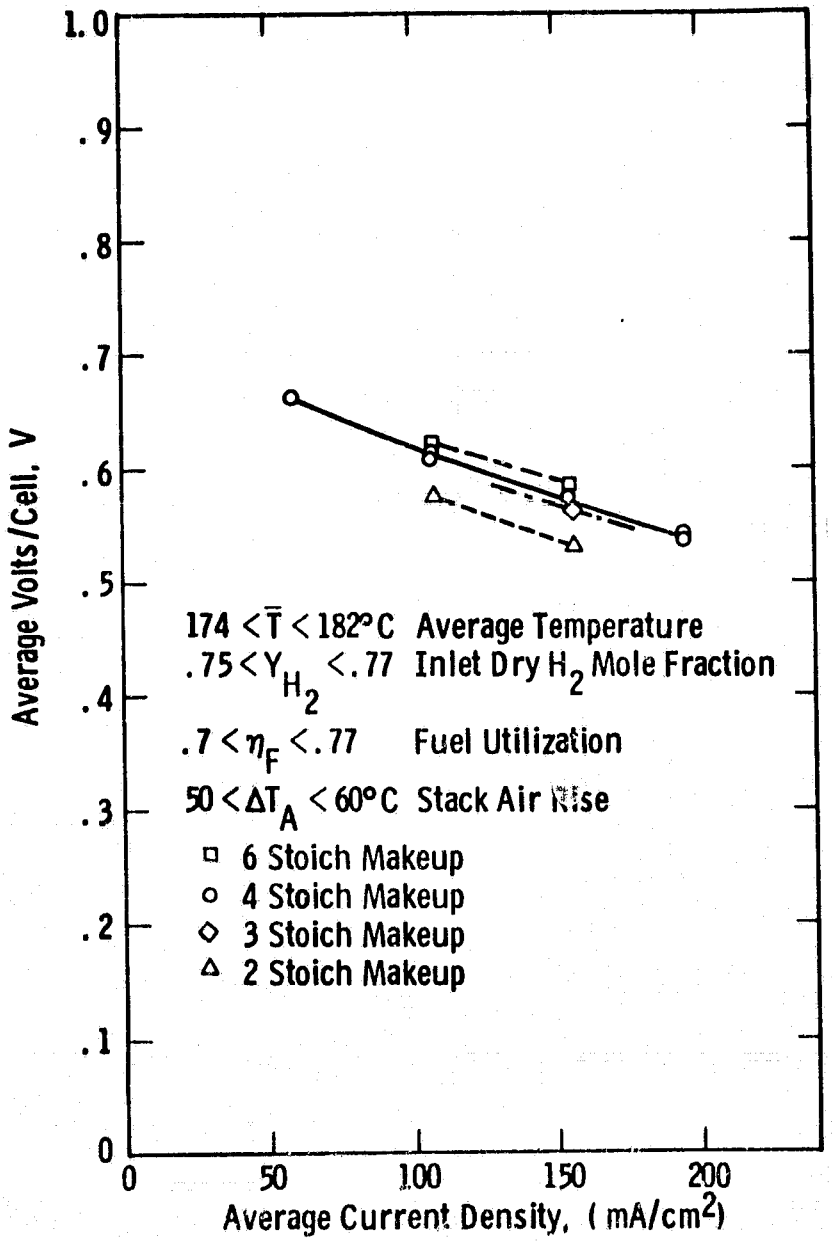

Fig. 5.3.14--Polarization data for stack 561 at various makeup air flow rates

ORIGINAL PAGE IS
OF POOR QUALITY

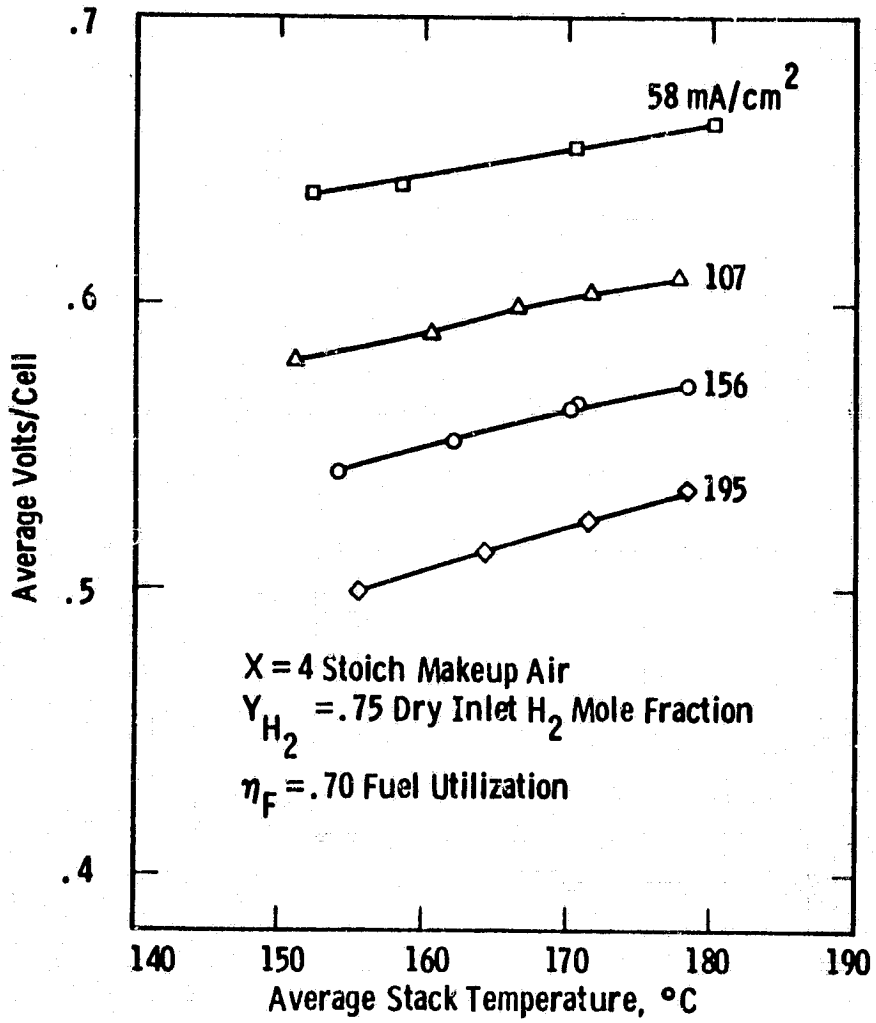

Fig. 5.3.15 – Performance of stack 561 as a function of temperature

The values of 4 stoich makeup and 70% fuel utilization were chosen to avoid the sensitivities observed at lower makeup or higher utilization. The temperature sensitivity under these conditions ranged from 0.94 mV/°C at 58 mA/cm^2 to 1.47 mV/°C at 194 mA/cm^2. The "Handbook of Fuel Cell Performance"* states that this sensitivity is 1.15 mV/°C for phosphoric acid fuel cells. The sensitivity at 107 and 155 mA/cm^2 was within 0.05 mV/°C of this value. The data in Figure 5.3.15 was used to plot the polarization curves in Figure 5.3.16 as a function of average stack temperature by cross plotting.

Effect on CO on Performance

The effect of CO in the fuel on cell voltage with 28 cooling channels per plate was obtained at two current densities. The tests at 107 mA/cm^2 with an average temperature of 179°C showed a voltage loss of approximately 1.74 mV/cell per percent CO for CO concentrations up to 5.5% of the dry fuel. The tests at 195 mA/cm^2 with an average temperature of 174°C showed a voltage loss of 12.6 mV/cell per percent CO for up to 4% CO. These results indicate higher sensitivity of the CO effect to current density and/or temperature than previous data. The "Handbook of Fuel Cell Performance"* lists sensitivity to CO as 6.14 mV per percent CO at 177°C but with a higher anode catalyst loading (0.35 vs. 0.3 mg/cm^2).

5.3.4 Stack 562 (Mk-2, 23-cell)

5.3.4.1 Pretesting

Stack 562 was the first Mk-2 stack incorporating cooling plates. It was pre-tested for 27 hours over a 5-day period with steady and reproducible performance. The following tests were performed:

- Stable and transient OCV tests
- polarization characteristics with varying anode gas composition

*Handbook of Fuel Cell Performance, T. G. Benjamin, Prepared for USDOE by IGT, May 1980.

ORIGINAL PAGE IS
OF POOR QUALITY

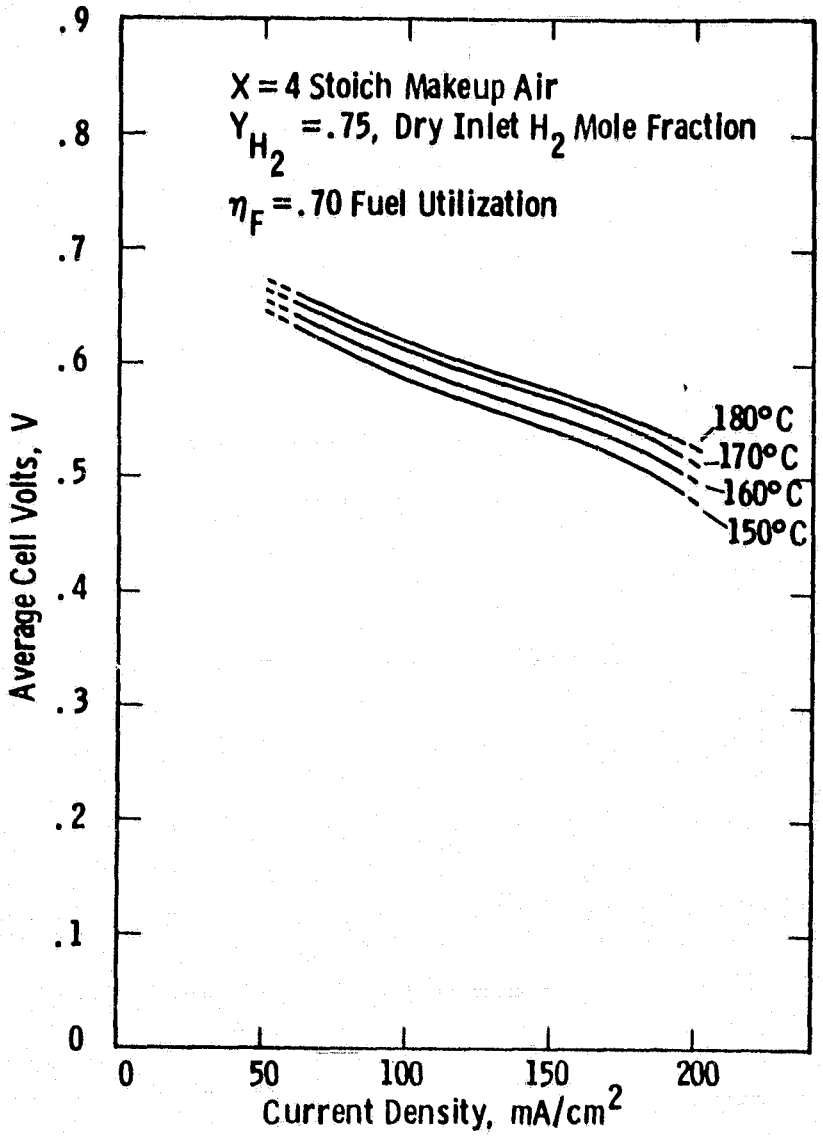

Fig. 5.3.16 – Polarization curves for stack 561 at various temperatures.

- fuel flow rate vs. pressure drop
- process air flow rate vs. pressure drop
- effect of hydrogen flow rate on performance
- effect of air flow rate on performance.

The individual cell performances for two current densities and two fuel compositions are given in Table 5.3.3.

The initial steady state and transient open circuit voltages for the cells indicated that the matrices and electrodes were sufficiently wetted with acid prior to the start of pre-testing and that all cells were functioning properly. The transient voltage drops for all cells were 23 mV or less after one minute. The value specified in the test plan was 150 mV. The OCV and performance at 150 mA/cm^2 on two fuels were constant through the 27 hour test period as shown in Figure 5.3.17.

The polarization data for humidified H_2 and 75% H_2 and 25% CO_2 are plotted in Figure 5.3.18. The performance on H_2/CO_2 showed a drop of ~12 mV/cell at 150 mA/cm^2 compared to the performance on H_2 which agreed exactly with the theoretical prediction.

The process air and fuel pressure drop-flow rate characteristics of Stack 562 are plotted in Figures 5.3.19 and 5.3.20 respectively. The pressure drops for a given flow rate are higher than for Stack 561 due to the reduced flow area of the Z bipolar plates. This is a minor effect on the fuel side and the air side flow rate for a given operating condition is much smaller for the Z plates since only the process gas flows through the passages.

The effects of hydrogen and air flow on stack performance for the two fuels are plotted in Figures 5.3.21 and 5.3.22 respectively. The flow rates are given in terms of utilization of fuel and stoichs of air as well as volume and these provide a means of correlating the pressure drops with stack operation.

ORIGINAL PAGE IS
OF POOR QUALITY

TABLE 5.3.3. PRETEST PERFORMANCE OF STACK 562

Cell No.	~100 mA/cm^2		~150 mA/cm^2	
	100% H_2	75% H_2 25% CO_2	100% H_2	75% H_2 25% CO_2
1	0.666	0.652	0.636	0.624
2	0.667	0.657	0.639	0.626
3	0.661	0.650	0.630	0.618
4	0.670	0.662	0.641	0.632
5	0.654	0.640	0.620	0.611
6	0.669	0.660	0.639	0.630
7	0.665	0.656	0.635	0.626
8	0.670	0.660	0.640	0.630
9	0.669	0.656	0.636	0.625
10	0.661	0.637	0.678	0.610
11	0.670	0.640	0.640	0.618
12	0.647	0.622	0.607	0.589
13	0.664	0.649	0.631	0.618
14	0.659	0.647	0.624	0.612
15	0.661	0.648	0.624	0.618
16	0.667	0.656	0.638	0.629
17	0.663	0.653	0.631	0.621
18	0.670	0.660	0.639	0.630
19	0.666	0.657	0.634	0.626
20	0.668	0.660	0.639	0.632
21	0.669	0.660	0.641	0.632
22	0.658	0.648	0.630	0.620
23	0.666	0.653	0.635	0.625
Average Cell Voltage, V	0.664	0.651	0.633	0.621
Load, A	100	98	151	148
% H_2 Util.	78.5	77.0	79.1	77.5
No. Stoich Process Air	2.5	2.6	2.3	2.5
No. Stoich Cooling Air	31.7	32.3	25.9	26.4
Date	3/16/81	3/16/81	3/17/81	3/17/81
Time	3:39	4:00	11:03	11:43
No. Hours Operation	23.5	23.75	25.75	26.5

ORIGINAL PAGE IS
OF POOR QUALITY

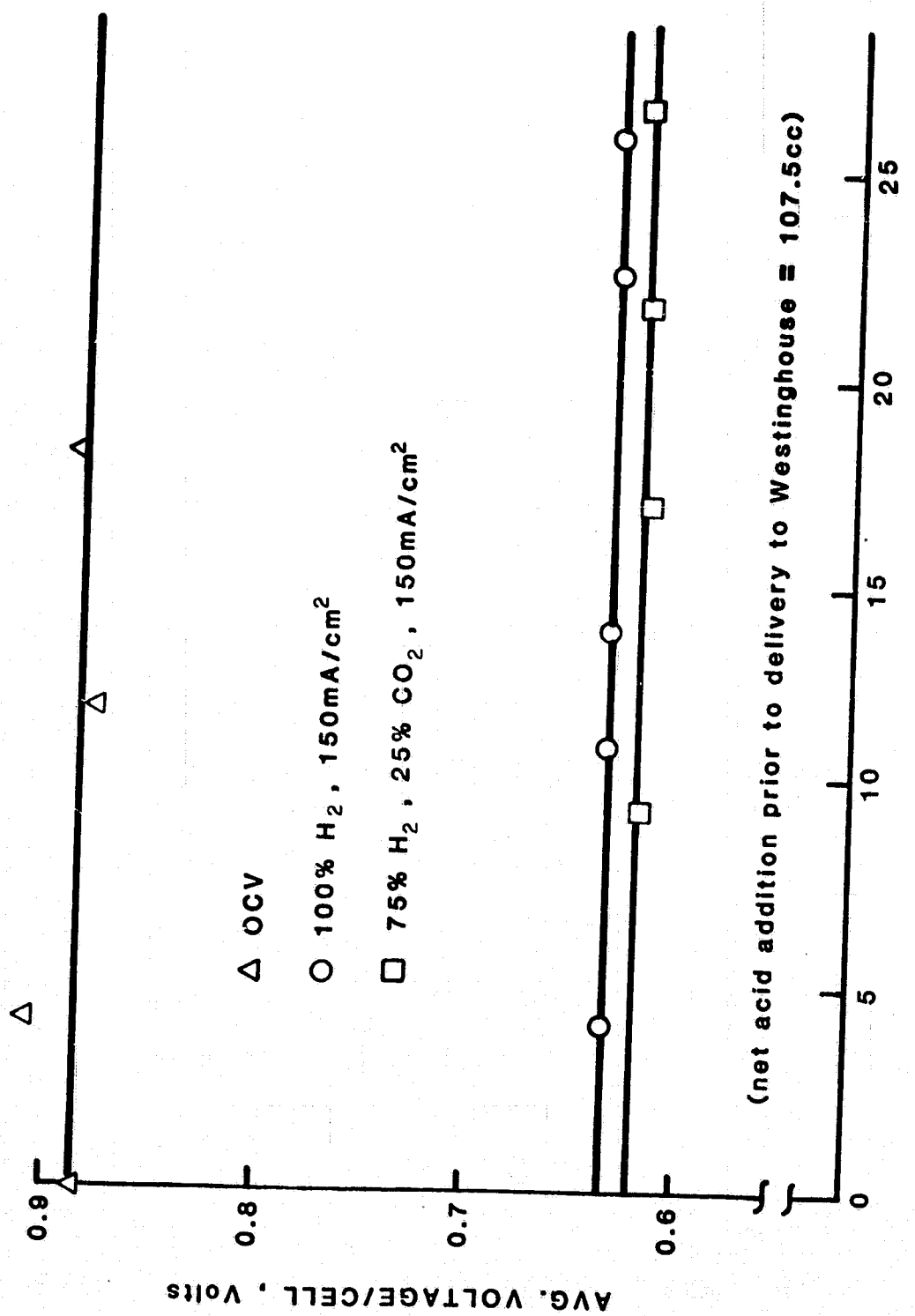

FIGURE 5.3.17. LIFEGRAPH OF STACK 562

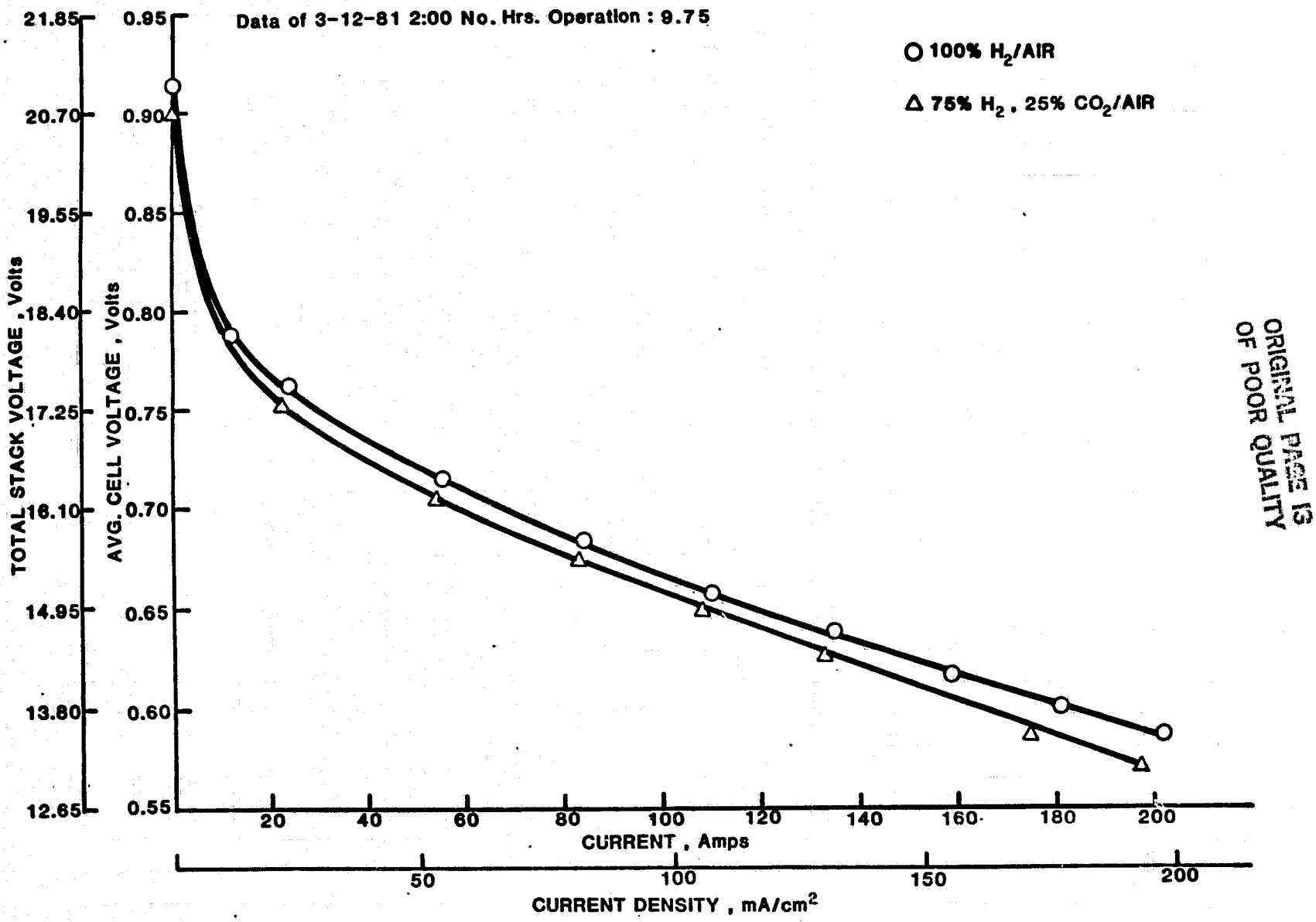

FIGURE 5.3.18. STACK 562 POLARIZATION CHARACTERISTICS

D1529

ORIGINAL PAGE IS
OF POOR QUALITY

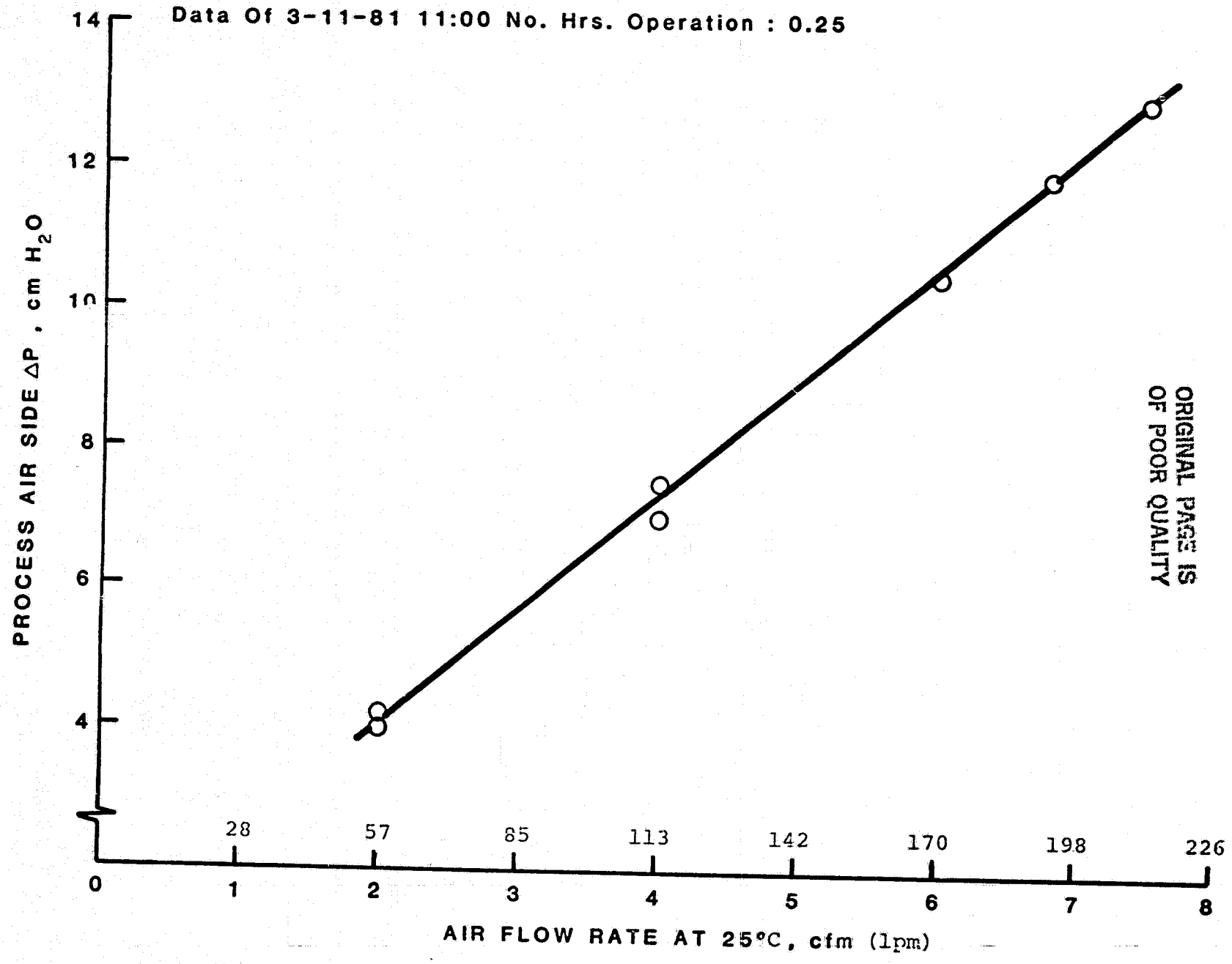

FIGURE 5.3.19. PROCESS AIR FLOW RATE vs PRESSURE DROP, STACK 562

ORIGINAL PAGE IS
OF POOR QUALITY

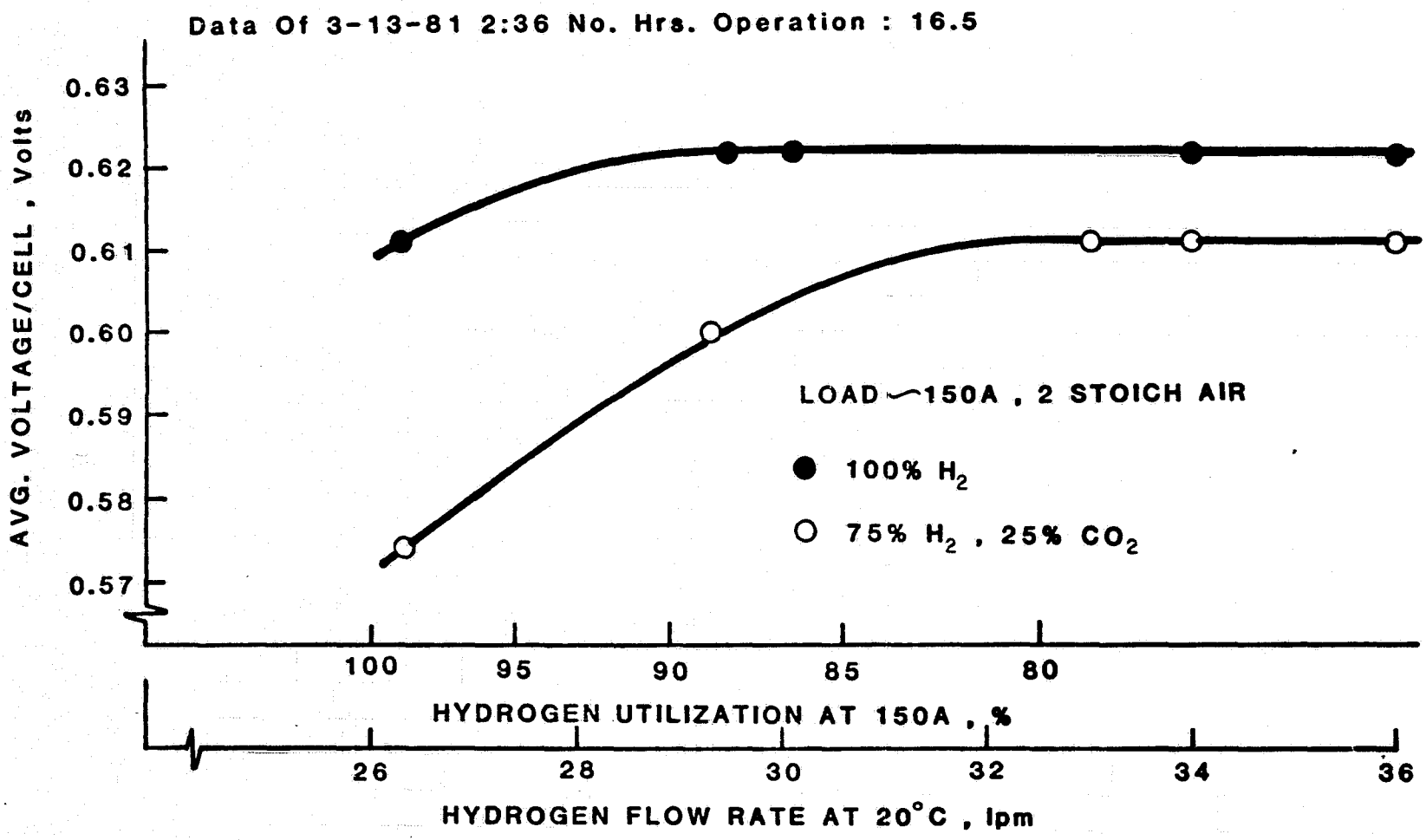

FIGURE 5.3.21. EFFECT OF HYDROGEN FLOW RATE ON STACK PERFORMANCE, STACK 562

ORIGINAL PAGE IS
OF POOR QUALITY

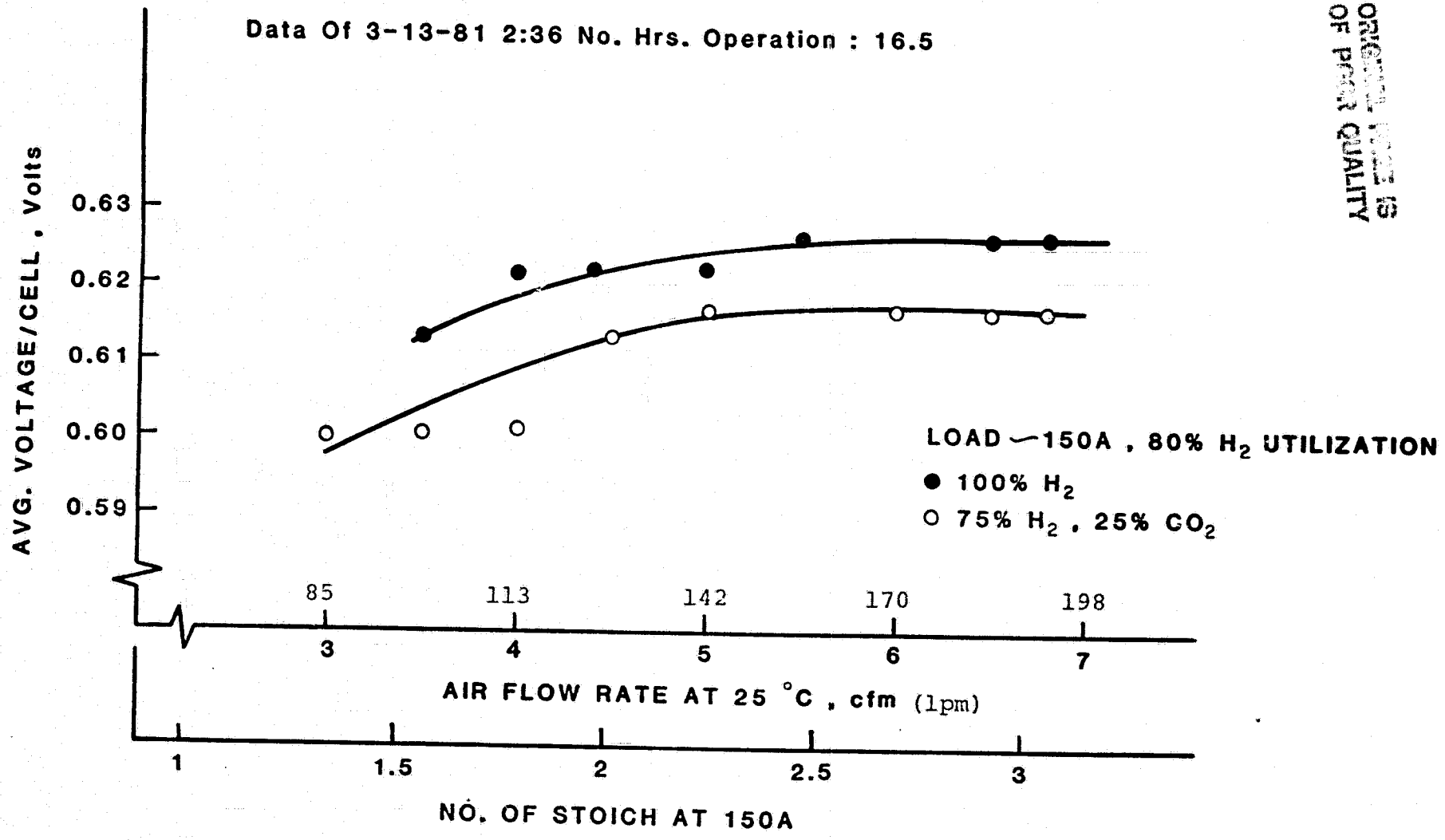

ORIGINAL PAGE IS
OF POOR QUALITY

5.3.4.2 Performance Testing

The test objectives for Stack 562 were to:

- Verify the expected improvement in cell performance for the Mk-2 (Z pattern) design as compared to the DIGAS design.
- Verify the ability of the treed cooling channels to achieve cell temperature differentials substantially smaller than the cooling gas temperature rise over a wide range of operating conditions.
- Acquire data on the effects of various operating parameters (e.g., fuel utilization, temperature level, fuel CO content) on cell performance, temperature distribution and pressure drops for verification and/or modification of the equations used in the lumped parameter and detailed analytical model computer programs.

In accordance with the above objectives, Stack 562 was operated at 131 steady state conditions which are described, along with the results and discussion, below.

The Z channel design in Stack 562 provides separate cooling gas and process air flows. The stack included heat treated bipolar and cooling plates and Mat-1 matrices. The active area after heat treatment was approximately 1030 cm^2. Each cooling plate had 31 equally spaced treed channels. Cooling air enters and exits perpendicularly to the 43.2 cm face of the stack. The 30.5 cm faces are manifolded in two equal sections with opposite faces each containing a process air and fuel inlet/outlet manifold. For the "normal flow" direction tests, the process air and fuel inlets are near the cooling air inlet edge of the stack. For the reverse flow direction, they are near the cooling air exit edge of the stack.

Table 5.3.4 presents a summary of test results and conditions for Stack 562. Test 1 is a pretest, and tests 2, 3 and 4 were made in

ORIGINAL PAGE IS
OF POOR QUALITY

TABLE 5.3.4 – SUMMARY OF TEST CONDITIONS AND TEST RESULTS FOR STACK 562

Test	Current Density, mA/cm^2	Volts/Cell, V	Average Temperature, °C	Peak to Average Gradient, °C	Fuel Utilization	Dry H_2 Inlet Mole Fraction	Fuel Inlet Temperature, °C	Process Air, Stoichs	Process Air Inlet Temperature, °C	Cooling Air Flow g/sec	Cooling Air Inlet Temperature, °C	Cooling Air Temperature Rise, °C	Process Air Pressure Drop, in.H_2O	Cooling Air Pressure Drop, in.H_2O
1	144	.613	173	11.3	.77	.76	114	2.1	123	25.0	122	38	3.70	1.73
2	146	.612	168	15.1	.60	.75	124	3.7	124	48.1	125	36	–	–
3	146	.614	171	13.1	.60	.75	125	3.7	155	34.0	124	39	–	–
4	146	.610	170	10.2	.60	.75	125	3.7	162	34.0	123	36	–	–
5	150	.585	170	18.4	.82	.75	126	2.0	160	37.0	109	52	–	2.25
6	150	.586	173	15.4	.82	.75	133	2.0	183	37.0	109	54	–	2.25
7	150	.586	173	15.4	.82	.75	133	2.0	187	37.0	109	54	–	2.25
8	150	.599	174	8.1	.72	.75	136	2.0	192	37.0	108	54	–	2.26
9	150	.601	173	9.7	.61	.75	139	2.0	175	38.6	108	54	3.35	2.29
10	150	.596	171	7.0	.71	.75	138	2.0	150	39.0	109	53	3.35	2.30
11	150	.607	172	8.4	.71	.75	135	3.0	150	39.0	114	50	4.74	2.30
12	150	.609	171	9.5	.71	75	137	4.0	151	39.0	114	49	6.44	2.30
13	150	.601	175	7.1	.71	.75	135	2.2	148	39.0	114	51	3.20	2.30
14	150	.589	151	11.0	.70	.75	143	4.0	128	38.6	92	50	6.05	2.23
15	150	.598	156	11.5	.70	.75	141	4.0	128	38.1	98	49	6.10	2.24
16	150	.603	163	10.0	.70	.75	142	4.0	140	37.6	105	50	6.16	2.24
17	150	.610	175	9.4	.70	.75	147	4.0	154	37.6	118	49	6.26	2.26
18	100	.628	153	6.9	.71	.75	134	3.9	142	24.0	98	51	3.86	1.11
19	100	.632	158	7.1	.71	.75	134	3.9	148	24.0	105	50	3.89	1.12
20	100	.641	169	7.1	.71	.75	136	4.0	159	24.0	117	48	3.99	1.14
21	100	.648	179	7.6	.71	.75	137	3.9	166	24.0	128	47	4.10	1.17
22	200	.560	160	8.8	.71	.75	148	4.0	156	53.3	87	55	8.20	3.44
23	200	.568	166	10.1	.71	.75	151	3.9	156	52.9	96	54	8.20	3.44
24	200	.575	174	10.0	.71	.75	151	3.9	163	52.9	105	54	8.32	3.44
25	200	.547	151	11.3	.71	.75	149	3.9	139	56.1	78	56	7.97	3.59
26	50	.674	151	6.8	.71	.75	116	4.0	140	11.0	103	48	1.84	.40
27	50	.681	161	7.0	.71	.75	132	4.0	146	10.0	118	42	1.91	.39
28	50	.688	170	7.1	.71	.75	134	4.0	154	11.0	130	39	1.95	.40
29	50	.694	179	6.8	.71	.75	136	3.9	162	11.0	141	36	1.99	.41

TABLE 5.3.4 – SUMMARY OF TEST CONDITIONS AND TEST RESULTS FOR STACK 562. (CONTINUED)

Test	Current Density, mA/cm^2	Average Volts/Cell	Average Temperature, °C	Peak to Average Gradient, °C	Fuel Utilization	Dry H_2 Inlet Mole Fraction	Dry CO Inlet Mole Fraction	Fuel Inlet Temperature, °C	Process Air, Stoichs	Process Air Inlet Temperature, °C	Cooling Air Flow, g/sec	Cooling Air Inlet Temperature, °C	Cooling Air Temperature Rise, °C	Process Air Pressure Drop, in H_2O	Cooling Air Pressure Drop, in H_2O	Mole Fraction of H_2O in Fuel Exhaust	Fraction of Produced Water Transferred To Fuel
30	150	.576	155	6.8	.71	.75	0	140	2.0	139	39.5	89	54	3.01	2.26		
31	150	.586	164	6.9	.71	.75	0	142	2.0	147	39.5	99	53	2.99	2.27		
32	150	.601	181	8.0	.71	.75	0	143	2.0	156	38.6	119	52	3.18	2.28		
33	150	.595	174	6.8	.71	.75	0	145	2.0	154	38.6	110	54	3.12	2.27		
34	100	.616	155	4.0	.71	.75	0	132	2.0	143	23.1	96	54	1.96	1.06		
35	100	.625	163	4.8	.71	.75	0	132	2.0	148	23.6	107	52	1.98	1.08		
36	100	.630	172	4.9	.71	.75	0	133	2.0	152	24.0	114	53	2.02	1.09		
37	100	.637	181	5.2	.71	.75	0	134	2.0	162	24.9	124	52	2.11	1.12		
38	200	.534	153	8.5	.71	.75	0	150	2.0	136	54.9	78	56	3.93	3.58		
39	200	.545	161	8.6	.71	.75	0	151	2.0	147	53.5	87	50	3.99	3.58		
40	200	.555	171	9.0	.71	.75	0	153	2.0	154	53.1	97	54	4.14	3.58		
41	200	.563	180	8.9	.71	.75	0	154	2.0	164	53.1	108	50	4.31	3.58		
42	50	.663	153	5.0	.71	.75	0	110	2.0	132	9.5	103	50	0.96	0.40		
43	50	.671	163	3.6	.71	.75	0	124	2.0	148	9.5	119	52	0.98	0.41		
44	50	.677	171	4.1	.71	.75	0	124	2.0	150	9.5	129	49	1.01	0.42		
45	50	.682	179	4.5	.71	.75	0	126	2.0	153	9.5	139	37	1.03	0.43		
46	150	.603	173	8.7	.71	.75	0	148	3.9	153	38.1	116	49	6.13	2.35	.082	.037
47	150	.598	174	9.8	.71	.74	.015	147	3.9	153	38.1	116	49	6.13	2.35		
48	150	.594	174	10.0	.71	.73	.024	148	3.9	153	38.1	115	49	6.13	2.35		
49	150	.592	174	11.1	.71	.72	.034	148	3.9	153	38.1	116	49	6.13	2.35		
50	150	.590	175	12.3	.71	.72	.044	148	3.9	153	39.5	115	49	6.14	2.35		
51	150	.604	175	9.2	.71	.75	0	150	3.9	153	39.0	116	49	6.14	2.35		
52	150	.597	178	5.5	.71	.75	0	149	2.0	152	39.0	116	51	3.09	2.34	.118	.007
53	150	.593	178	7.3	.71	.74	.015	148	2.0	151	39.0	116	51	3.09	2.34		
54	150	.590	179	6.9	.71	.73	.025	148	2.0	151	39.0	116	51	3.09	2.34		
55	150	.589	178	7.7	.71	.73	.034	147	2.0	151	39.0	116	51	3.09	2.34		
56	150	.587	178	8.1	.71	.72	.044	147	2.0	151	39.0	116	51	3.09	2.34		
57	150	.597	178	7.3	.71	.75	0	150	2.0	151	39.0	116	50	3.10	2.35		
58	201	.567	175	9.9	.72	.75	0	155	3.8	163	51.3	105	54	8.20	3.47		
59	201	.561	176	11.2	.72	.74	.012	155	3.8	163	51.3	105	56	8.20	3.47		
60	201	.557	176	11.8	.72	.74	.019	155	3.8	163	51.3	105	56	8.20	3.47		
61	201	.554	176	13.5	.72	.73	.027	154	3.8	163	51.3	105	55	8.20	3.47	.114	.069
62	200	.569	175	9.4	.72	.75	0	156	3.8	163	51.3	105	57	8.20	3.47	.077	.024

ORIGINAL PAGE IS
OF POOR QUALITY

ORIGINAL PAGE IS
OF POOR QUALITY

TABLE 5.3.4 – SUMMARY OF TEST CONDITIONS AND TEST RESULTS FOR STACK 562. (CONTINUED)

Test	Current Density, mA/cm^2	Average Volts/Cell	Average Temperature, °C	Peak to Average Gradient, °C	Fuel Utilization	Dry H_2 Inlet Mole Fraction	Dry CO Inlet Mole Fraction	Fuel Inlet Temperature, °C	Process Air, Stoichs	Process Air Inlet Temperature, °C	Cooling Air Flow, g/sec	Cooling Air Inlet Temperature, °C	Cooling Air Temperature Rise, °C	Process Air Pressure Drop, in H_2O	Cooling Air Pressure Drop, in H_2O	Mole Fraction of H_2O in Fuel Exhaust	Fraction of Produced Water Transferred To Fuel
63	200	.559	177	9.6	.72	.75	0	156	2.0	148	51.3	105	57	4.12	3.47	.114	.063
64	200	.553	177	11.0	.72	.74	.012	155	2.0	147	51.3	105	56	4.12	3.47		
65	200	.550	178	10.9	.71	.74	.019	154	2.0	146	51.3	105	56	4.12	3.47		
66	200	.547	177	13.4	.72	.73	.027	154	2.0	146	51.3	105	56	4.12	3.47		
67	200	.561	177	9.4	.71	.75	0	155	2.0	147	51.3	105	51	4.12	3.47		
68	100	.647	183	10.9	.71	.75	0	143	4.0	159	27.7	129	52	4.30	0.99	.076	.033
69	100	.644	184	11.7	.71	.74	.021	144	4.0	159	27.7	129	52	4.30	0.99	.124	.085
70	100	.644	184	11.7	.71	.73	.028	145	4.0	154	27.7	129	52	4.30	0.99		
71	100	.643	184	12.0	.71	.73	.035	145	4.0	160	27.7	129	53	4.30	0.99		
72	100	.648	185	11.4	.71	.75	0	144	4.0	156	27.7	128	47	4.30	0.99		
73	100	.636	181	5.0	.71	.75	0	142	2.0	161	27.7	128	47	2.09	1.31		
74	100	.632	180	5.0	.71	.74	.020	143	2.0	160	27.7	128	47	2.09	1.31		
75	100	.631	180	5.0	.71	.73	.028	143	2.0	159	27.7	128	47	2.09	1.31		
76	100	.630	180	5.2	.71	.72	.035	144	2.0	159	27.7	128	47	2.09	1.31		
77	100	.635	180	5.2	.71	.75	0	143	2.0	159	27.7	128	47	2.10	1.32		
78	50	.694	182	9.5	.71	.75	0	134	4.0	163	10.0	142	39	2.20	0.40	.065	.025
79	50	.692	182	10.0	.71	.73	.035	135	4.0	161	10.0	141	40	2.20	0.40		
80	50	.691	182	10.3	.71	.72	.048	134	4.0	162	10.0	141	41	2.20	0.40		
81	50	.691	182	10.2	.71	.71	.056	135	4.0	161	10.0	141	42	2.20	0.40		
82	50	.695	183	10.0	.71	.75	0	135	4.0	163	10.0	142	40	2.20	0.40		
83	50	.689	185	6.2	.71	.75	0	133	2.0	162	10.0	142	42	1.05	0.40	.120	.084
84	50	.686	186	6.1	.71	.72	.040	135	2.0	161	10.0	142	42	1.05	0.40		
85	50	.689	173	10.0	.71	.75	0	133	4.0	157	9.5	126	48	2.20	0.39		
86	50	.685	173	10.4	.71	.72	.041	134	4.0	155	9.5	126	47	2.30	0.38		
87	101	.639	170	7.8	.70	.75	0	147	4.0	156	23.6	114	53	4.33	1.03		
88	101	.633	171	9.3	.71	.72	.040	146	4.0	157	23.6	113	54	4.33	1.03		
89	155	.599	168	6.2	.71	.75	0	131	4.0	153	39.9	102	50	6.42	2.29		
90	155	.585	167	9.7	.71	.72	.039	131	4.0	153	39.9	102	50	6.42	2.29		
91	200	.563	165	9.3	.71	.75	0	145	4.0	150	50.8	94	56	8.25	3.31		
92	200	.539	168	21.5	.71	.72	.040	143	4.0	152	50.8	94	56	8.25	3.31		
93	100	.616	156	9.7	.50	.75	0	139	2.0	134	24.0	98	55	2.17	1.12		
94	100	.629	169	6.2	.51	.75	0	143	2.0	132	24.9	116	51	2.27	1.14		
95	100	.629	164	4.6	.64	.75	0	148	4.0	133	21.8	108	53	4.05	0.99	.065	.039

the OS/IES loop without insulation for comparison with pretest results. Tests 5 to 10 were run to determine sensitivity to fuel utilization and the effect of process air inlet temperature on the temperature distribution. Tests 11 to 13 were made to determine the effect of process air stoichs on cell voltage. Tests 14 through 29 were conducted to obtain a performance map for current densities from 50 to 200 mA/cm^2 with average temperatures from 150 to 180°C with fuel utilization of 70% and process air flow of 4 stoichs for comparison with a similar map made for 561. Tests 30 through 45 were made to obtain a performance map as a function of average cell temperature (150 to 180°C) and current density (50 to 200 mA/cm^2). Tests 46 through 92 were made to determine the effect of CO on performance. Tests 93 through 102 were made to determine the effect of reversed process flow directions on performance and temperature distribution. Tests 103 through 127 included various combinations of fuel and process air inlet temperatures as well as different cooling temperature rises to obtain the effects of these variables on the temperature distribution. Test 128 was run at the maximum current capability (253 mA/cm^2) of the test loop. Test 129 was made at the same conditions as test 110 to verify that stack performance was unchanged. Tests 105 through 131 were made without CO_2 added to the fuel to maintain acceptable performance of cells 1 through 12, which were more sensitive to hydrogen flow and concentration than the other cells. Tests 130 and 131 had the same test conditions as 129 (and 110) and were made following efforts to clear the process flow channels, but the data indicated that no improvement was made.

Performance of Stack 562 was stable during the first 90 tests with a loss of less than 10 mV per cell. Cell No. 12 showed weak performance, about 50 mV below average at 150 mA/cm^2, during the entire test period. With the reversed flow directions (test 95), cell No. 1 was weaker than cell 12 and remained the poorest cell for the rest of the tests.

ORIGINAL PAGE IS
OF POOR QUALITY

TABLE 5.3.4 – SUMMARY OF TEST CONDITIONS AND TEST RESULTS FOR STACK 562. (CONTINUED)

Test	Current Density, mA/cm^2	Average Volts/Cell	Average Temperature, °C	Peak to Average Gradient, °C	Fuel Utilization	Dry H_2 Inlet Mole Fraction	Dry CO Inlet Mole Fraction	Fuel Inlet Temperature, °C	Process Air, Stoichs	Process Air Inlet Temperature, °C	Cooling Air Flow, g/sec	Cooling Air Inlet Temperature, °C	Cooling Air Temperature Rise, °C	Process Air Pressure Drop, in H_2O	Cooling Air Pressure Drop, in H_2O	Mole Fraction of H_2O in Fuel Exhaust	Fraction of Produced Water Transferred To Fuel
96	100	.621	167	8.9	.64	.75	0	150	2.0	133	21.8	108	58	2.27	1.00	.125	.113
97	150	.596	170	6.6	.62	.75	0	144	4.0	142	39.5	109	51	6.38	2.23	.070	.039
98	150	.585	171	6.7	.62	.75	0	145	2.0	145	39.0	109	54	3.36	2.24	.131	.125
99	200	.539	162	11.1	.59	.75	0	165	2.0	145	56.0	91	57	4.41	3.64	.098	.087
100	50	.668	148	5.1	.56	.75	0	130	4.0	137	9.5	101	49	2.00	0.41	.065	.052
101	50	.674	156	4.4	.56	.75	0	131	4.0	137	9.5	112	63	2.02	0.42	.061	.046
102	50	.685	168	4.7	.56	.75	0	135	4.0	139	10.0	113	36	2.03	0.43		
103	150	.597	172	9.3	.71	.75	0	152	4.0	154	39.0	111	51	6.72	2.26		.054
104	150	.582	162	6.6	.71	.75	0	149	4.0	153	54.9	111	39	6.55	3.67		.019
105	150	.607	167	5.5	.71	1.00	0	160	4.0	151	54.0	121	36	6.63	3.68	.207	.073
106	150	.607	168	5.7	.71	1.00	0	159	4.0	152	54.4	121	37	6.49	3.78	.124	.058
107	150	.608	169	5.2	.71	1.00	0	160	4.0	152	38.6	110	49	6.52	2.32	.137	.031
108	150	.592	167	9.7	.71	1.00	0	167	2.0	90	39.9	111	47	3.38	2.30	.248	.100
109	150	.594	170	7.7	.71	1.00	0	169	2.0	115	39.5	110	49	3.42	2.31	.171	.049
110	150	.597	172	6.0	.71	1.00	0	167	2.0	141	39.5	110	51	3.43	2.29	.149	.036
111	150	.599	175	9.8	.71	1.00	0	169	2.0	166	39.5	110	53	3.47	2.30	.175	.052
112	150	.587	167	13.0	.82	1.00	0	163	2.0	91	39.5	110	49	3.54	2.28	.136	.005
113	150	.590	170	10.7	.82	1.00	0	153	2.0	116	39.5	111	50	3.60	2.28	.167	.014
114	150	.593	174	8.5	.82	1.00	0	105	2.0	165	39.0	111	53	3.54	2.28	.148	.008
115	150	.603	180	5.8	.71	1.00	0	167	2.0	149	29.0	103	68	3.61	1.53	.163	.049
116	150	.612	190	6.4	.71	1.00	0	170	2.0	150	23.1	105	80	3.62	1.16	.157	.045
117	150	.573	157	10.2	.71	1.00	0	167	2.0	147	55.8	103	40	3.53	3.77	.181	.060
118	150	.588	168	5.1	.71	1.00	0	168	2.0	147	39.5	103	53	3.56	2.29	.145	.038
119	150	.587	165	10.0	.71	1.00	0	77	2.0	143	39.9	104	51	3.59	2.30	.134	.030
120	150	.589	166	9.4	.71	1.00	0	105	2.0	143	39.5	104	51	3.50	2.30	.130	.028
121	150	.590	167	8.3	.71	1.00	0	148	2.0	143	39.5	104	52	3.47	2.30	.125	.025
122	150	.591	169	6.1	.71	1.00	0	167	2.0	143	39.5	105	52	3.54	2.30	.141	.034
123	150	.592	170	8.2	.71	1.00	0	167	2.0	148	24.5	78	82	3.50	1.19	.125	.018
124	150	.588	166	7.4	.71	1.00	0	168	2.0	147	56.2	116	38	3.53	3.85	.179	.049
125	150	.588	167	8.2	.71	1.00	0	168	2.0	148	39.9	102	52	3.49	2.35	.175	.046
126	150	.589	169	7.4	.71	1.00	0	167	2.0	148	39.0	103	54	3.48	2.23		
127	149	.598	164	6.2	.71	1.00	0	168	4.0	145	39.5	102	51	6.57	2.29		
128	253	.533	166	9.1	.66	1.00	0	164	4.5	149	70.8	94	52	12.33	5.80		
129	150	.599	175	6.6	.71	1.00	0	168	2.0	139	39.0	114	51	3.26	2.23		
130	150	.597	175	6.5	.71	1.00	0	167	2.0	144	39.5	112	52	3.25	2.31		
131	150	.596	174	6.6	.71	1.00	0	167	2.0	145	39.5	111	51	3.26	2.31		

Temperature Distribution in Stack 562

Tests 5, 6 and 7 were run at 150 mA/cm^2, 82 percent fuel utilization and 2 stoich process air. The fuel exit edge of the stack (row 13) remained considerably lower in temperature than the center (row 12) or the fuel inlet edge (row 11) even when the process air temperature was increased to 14°C above the average stack temperature in test 7 as shown in Figure 5.3.23. Since it was suspected that fuel utilization was above the sensitivity point, the fuel flow was increased to reduce fuel utilization to 0.72 in test 8. The improved temperature distribution is shown in Figure 5.3.24. The peak to average differential decreased from 15.4°C to 8.1°C and the terminal voltage increased by 13 mV per cell. Test 9 had slightly reduced process air inlet temperature and fuel utilization of 0.61. The terminal voltage increased an additional 2 mV/cell. Test 10 with fuel utilization of 0.71 and process air inlet temperature of 150°C showed excellent balance between rows 11, 12 and 13 and a peak to average temperature differential of only 7°C with a 53°C measured cooling air rise (Figure 5.3.25). Performance of test 10 was 3 mV below test 8, largely due to a 3°C lower average temperature. Figures 5.3.26 and 5.3.27 show the temperature distributions for 150 and 200 mA/cm^2 at 70 percent fuel utilization with 4 stoich process air. The higher process air flow in these tests resulted in a slightly larger peak to average temperature differential (10°C) and an apparent increase in current density near the hydrogen inlet edge of the stack as compared to 2 stoich air flow.

The effects of varying fuel inlet temperature from 77-169°C and process air inlet temperature from 90-166°C were measured for the baseline current density (150 mA/cm^2), cooling air inlet temperature (110°C), and cooling air temperature rise (55°C). With one exception, the peak to average cell temperature differences were between 5 and 11°C which are 9 to 20 percent of the cooling air temperature rise. With a very low process air temperature (91°C) and a very high fuel temperature (163°C) the difference was 13°C or 24% of the cooling air rise.

ORIGINAL PAGE IS
OF POOR QUALITY.

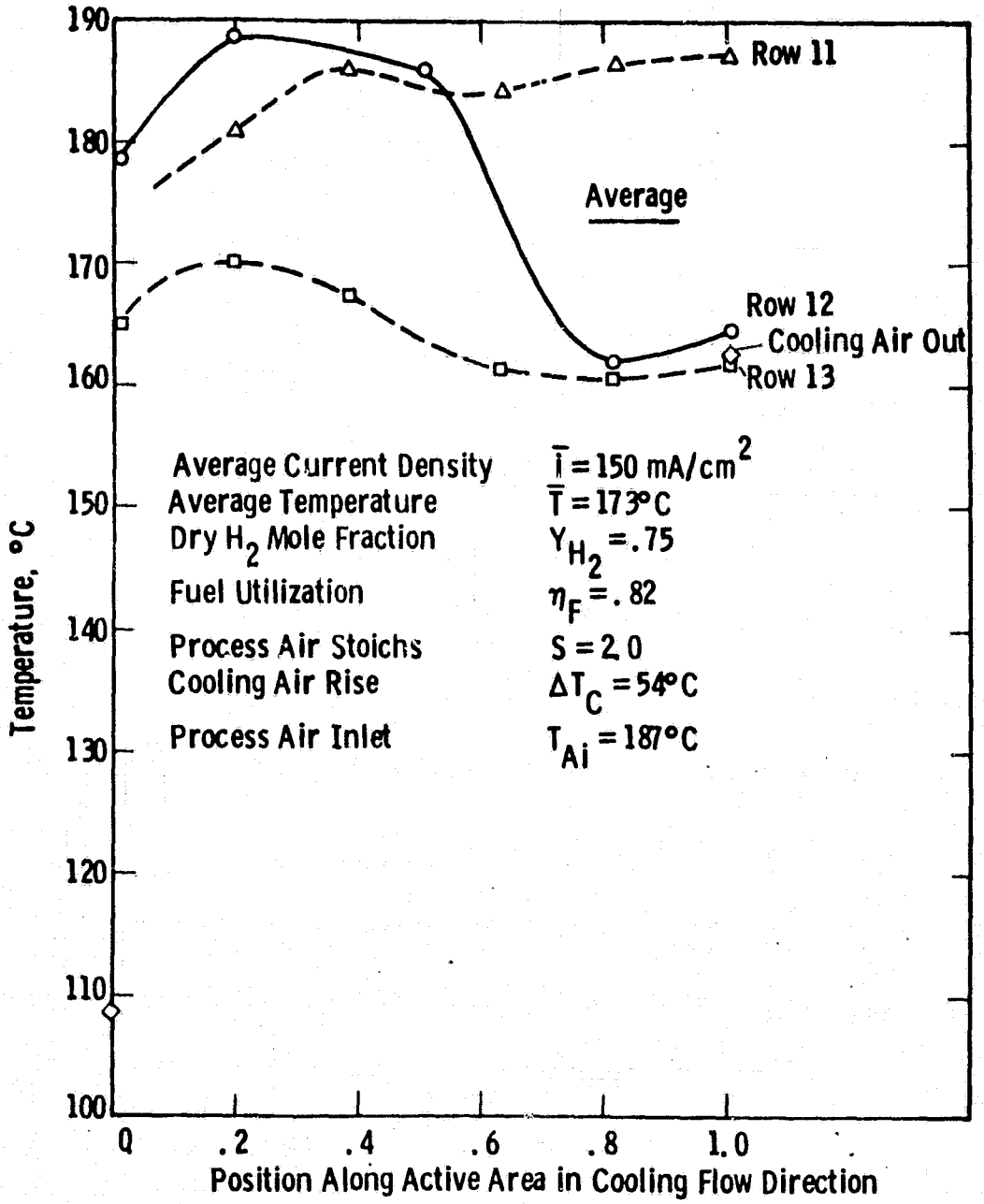

Fig. 5.3.23-Temperature distribution in stack 562-Test 7.

ORIGINAL PAGE IS
OF POOR QUALITY

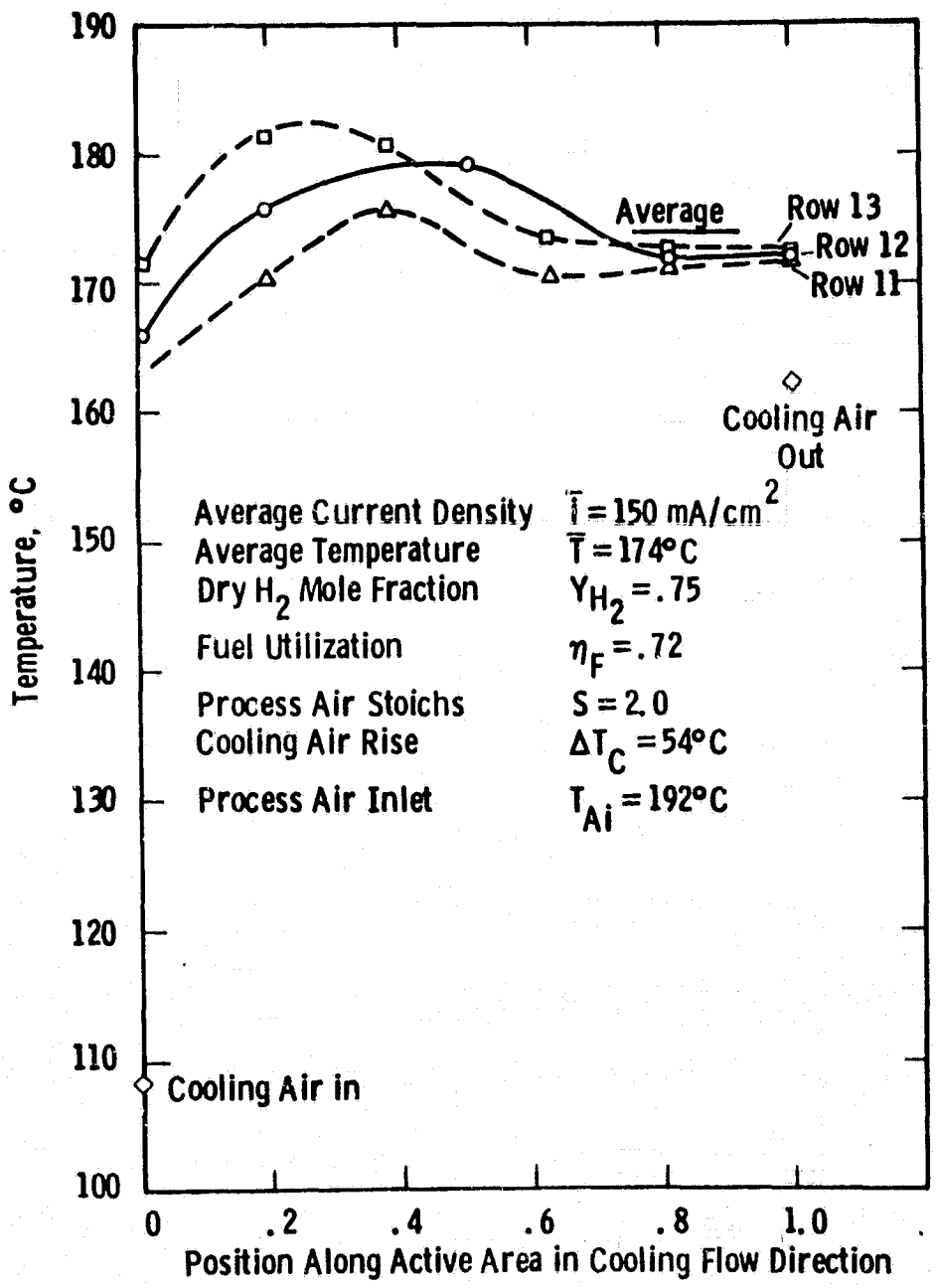

Fig. 5.3.24 – Temperature distribution in stack 562 - Test 8

ORIGINAL PAGE IS
OF POOR QUALITY

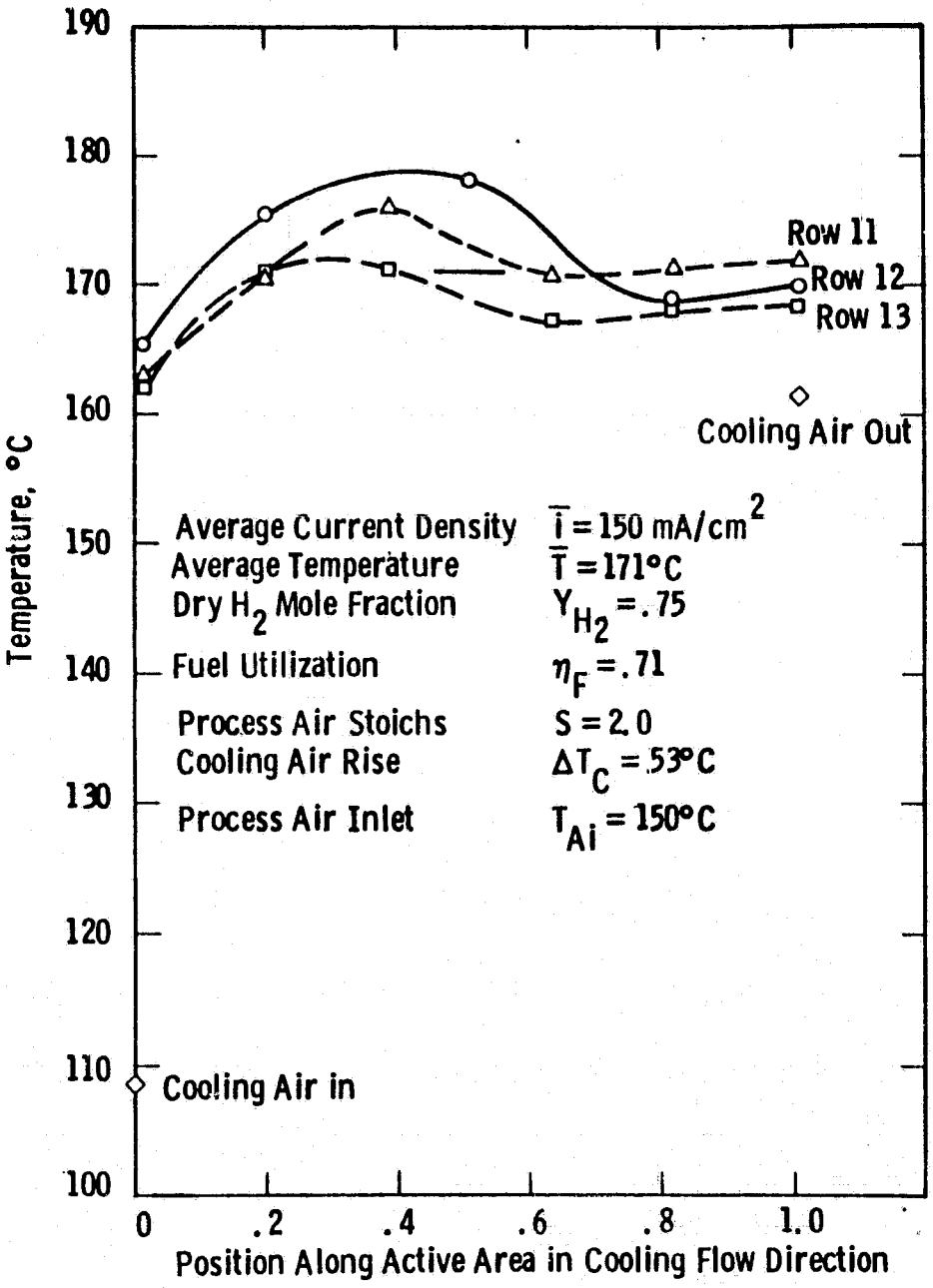

Fig. 5.3.25– Temperature distribution in stack 562 - Test 10

ORIGINAL PAGE IS
OF POOR QUALITY

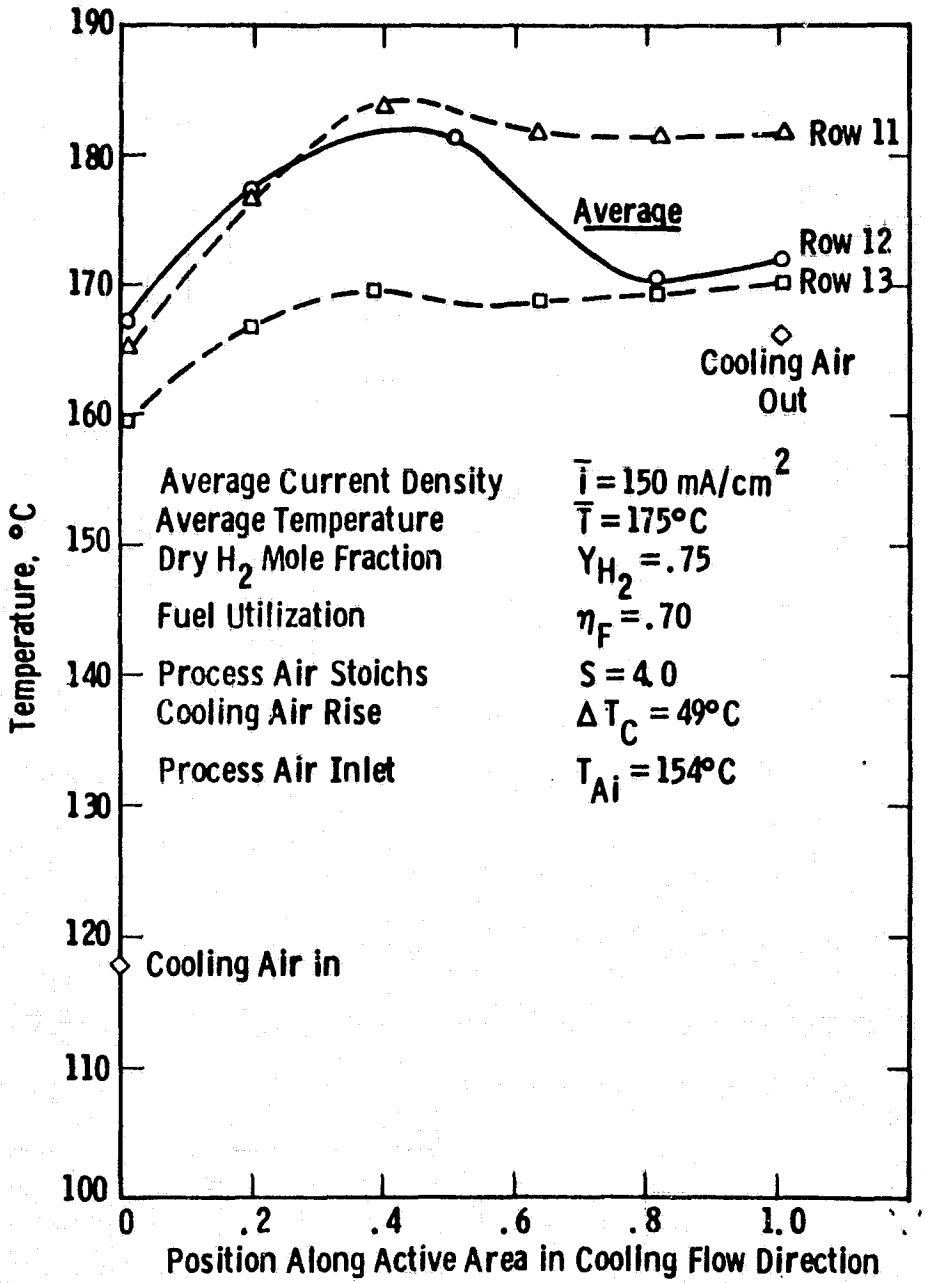

Fig. 5.3.26– Temperature distribution in stack 562 - Test 17

ORIGINAL PAGE IS
OF POOR QUALITY

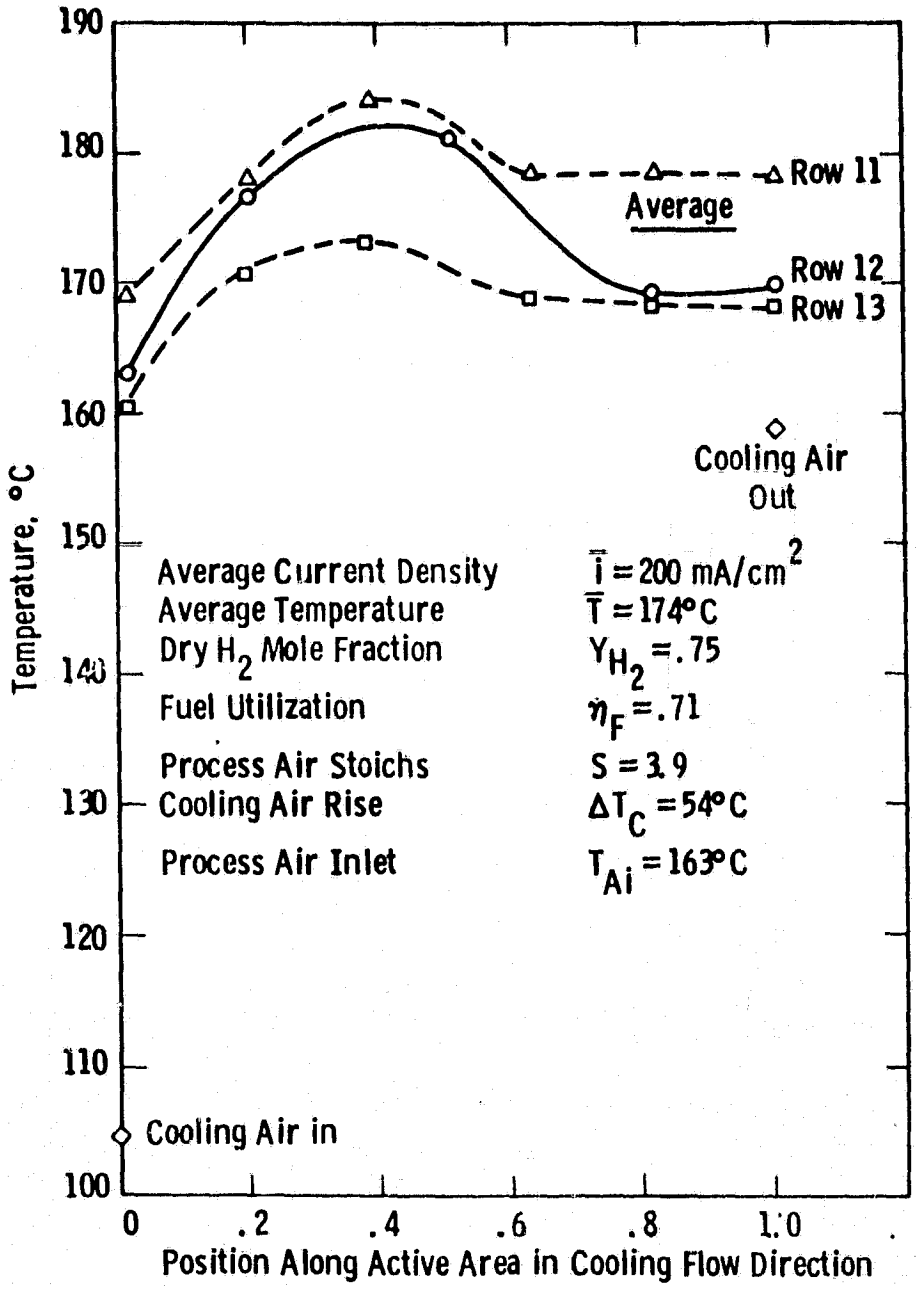

Fig. 5.3.27– Temperature distribution in stack 562 - Test 24

For a current density of 253 mA/cm^2, the peak to average difference was 9.1°C or 18% of the cooling air temperature rise of 52°C.

The cooling air temperature rise (which is inversely proportional to cooling air flow rate) was varied from 36°C to 82°C for a current density of 150 mA/cm^2 with an average cell temperature of about 170°C. The peak to average differences varied between 5.5 and 10.2°C but, due to the complexity of the pattern changes and small changes in other operating parameters, these do correlate easily with cooling air rise.

The temperature distributions showed that little improvement could be expected by varying cooling channel spacing for 2 stoich process air on Mk-2 stacks. A redistribution of cooling channels toward the hydrogen inlet edge could improve uniformity at higher process air flows and/or at higher fuel utilization. The fact that the maximum temperature occurred nearer the cooling inlet than to the exit indicated that the cooling channels should branch nearer to the cooling inlet. Results from the detailed analytical model also predicted that more uniform temperatures would be obtained by earlier branching in the Mk-2 stacks.

Effect of Temperature on Performance

Figure 5.3.28 shows the performance of Stack 562 for 2 and 4 stoichs of process air as a function of average temperature. Performance at 2 stoichs was 10 to 16 mV lower than for 4 stoich. The temperature sensitivity ranges from .67 mV/°C at 50 mA/cm^2 to 1.09 mV/°C at 200 mA/cm^2.

Spent Fuel Dew Point

Measurements of spent fuel dew points to determine the portion of the generated water vapor that is carried out by this stream were made for 39 tests and the results are given as mole fraction of the stream and portion transferred in Table 5.3.4. For 15 tests (most with reversed flow) with 2 stoichs process air and 71% utilization of a fuel stream consisting of room temperature humidified hydrogen, an average 4.4% of the generated water vapor was carried out in the spent fuel stream. For 3 tests with normal flow and ∿62% utilization of humidified 75% H_2 -

ORIGINAL PAGE IS
OF POOR QUALITY

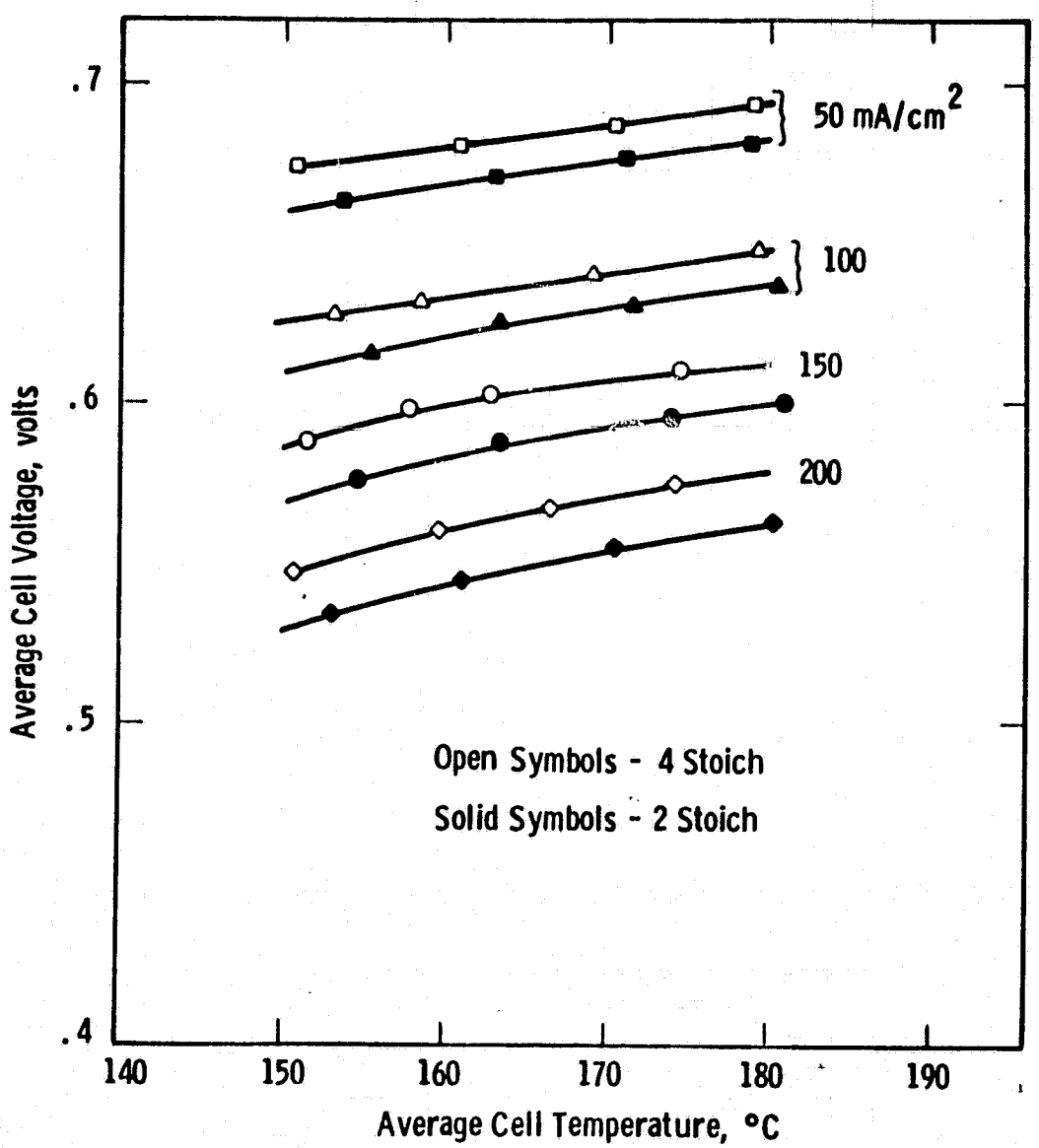

Fig. 5.3.28—Performance of Stack 562 as a function of temperature for 2 and 4 Stoich process air

25% CO_2 fuel and 2 stoichs process air this increased to approximately 11%.

The results indicate that:

1. Increasing makeup flow decreases the water vapor transfer as one would expect since the driving force (partial pressure on the air side) is reduced.
2. The addition of CO to the fuel increases the amount of water vapor transferred (e.g., tests 61 and 62 and 68 and 69).

Effect of CO on Performance

Forty-nine quasi-steady tests were run to determine the effect of CO on performance. These tests are termed quasi-steady since only 20 minutes was allowed for equilibration at each CO level. Dry CO mole fractions in the fuel ranged from 0 to 0.048. The voltage loss was proportional to inlet mole fraction of CO at each test condition. According to the theoretical model the CO effect doubles from every 15°C drop in temperature. Thus,

$$\Delta V\ (T) = \Delta V(177) \times 2^{\left(\frac{177-T}{15}\right)}$$

can be used to correct CO effect measured at T to a reference of 177°C. This relation appeared to be satisfied reasonably well and was used to correct data to a reference temperature of 177°C. Table 5.3.5 gives the CO effect at 177°C expressed in mV/(percent CO in the inlet fuel). The CO effect increases approximately linearly with current density up to 150 mA/cm^2 but the value at 200 mA/cm^2 is about 35 percent higher than predicted by a linear fit of the lower current density data.

ORIGINAL PAGE IS
OF POOR QUALITY

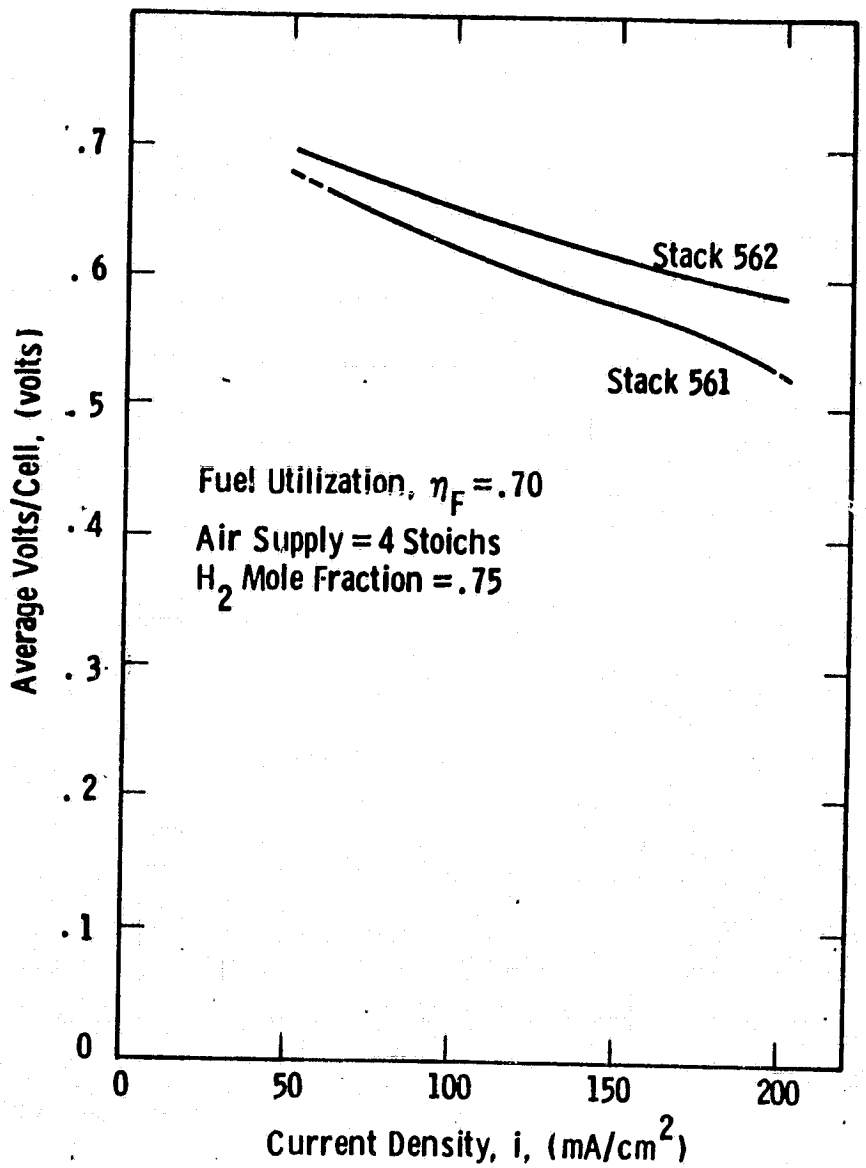

Fig. 5.3.29 – Polarization curves for stacks 561 and 562 at average temperature of 180°C

TABLE 5.3.5
EFFECT OF CO ON VOLTAGE AT
TEST CURRENT DENSITIES

Current Density mA/cm^2	CO effect at 177°C mV/(%CO)
50	.9
100	2.1
150	2.8
200	5.3

5.3.4.3 Comparison of Stacks 561 and 562

The polarization curves for Stacks 561 and 562 are plotted in Figure 5.3.29 for an average temperature of 180°C for direct comparison. The difference in average cell voltage ranges from 19 mV at 50 mA/cm^2 to 52 mV at 200 mA/cm^2. The theoretical O_2 gain of Stack 562 over 561 due to separation of cooling with 4 stoichs process (makeup) air is 12 mV per cell. The additional gain observed must then be due to reduced polarization (e.g., lower resistance or higher catalyst utilization), an H_2 gain associated with the observed reduction in water vapor in the anode exhaust of 562 or a statistical variation in cell performance between the two stacks.

The data analysis technique developed in Phase I was applied to the data of Figures 5.3.15 and 5.3.28 to obtain catalyst utilization and specific cell resistance for the two stacks assuming no H_2 gain. The results are compared in Figure 5.3.30. The catalyst utilizations determined this way are virtually identical for the two stacks. The specific resistance, however, is about 33 percent lower for Stack 562 than for Stack 561. This difference in resistance accounts for 38 mV at 200 mA/cm^2. Data on previous stacks indicated a significant effect on resistance due to O_2 partial pressure or mole fraction, but 38 mV appears too large to be due to a 4.6 percent difference in mean O_2 concentration (17.7 for 562 vs. 13.1 for 561).

ORIGINAL PAGE IS
OF POOR QUALITY

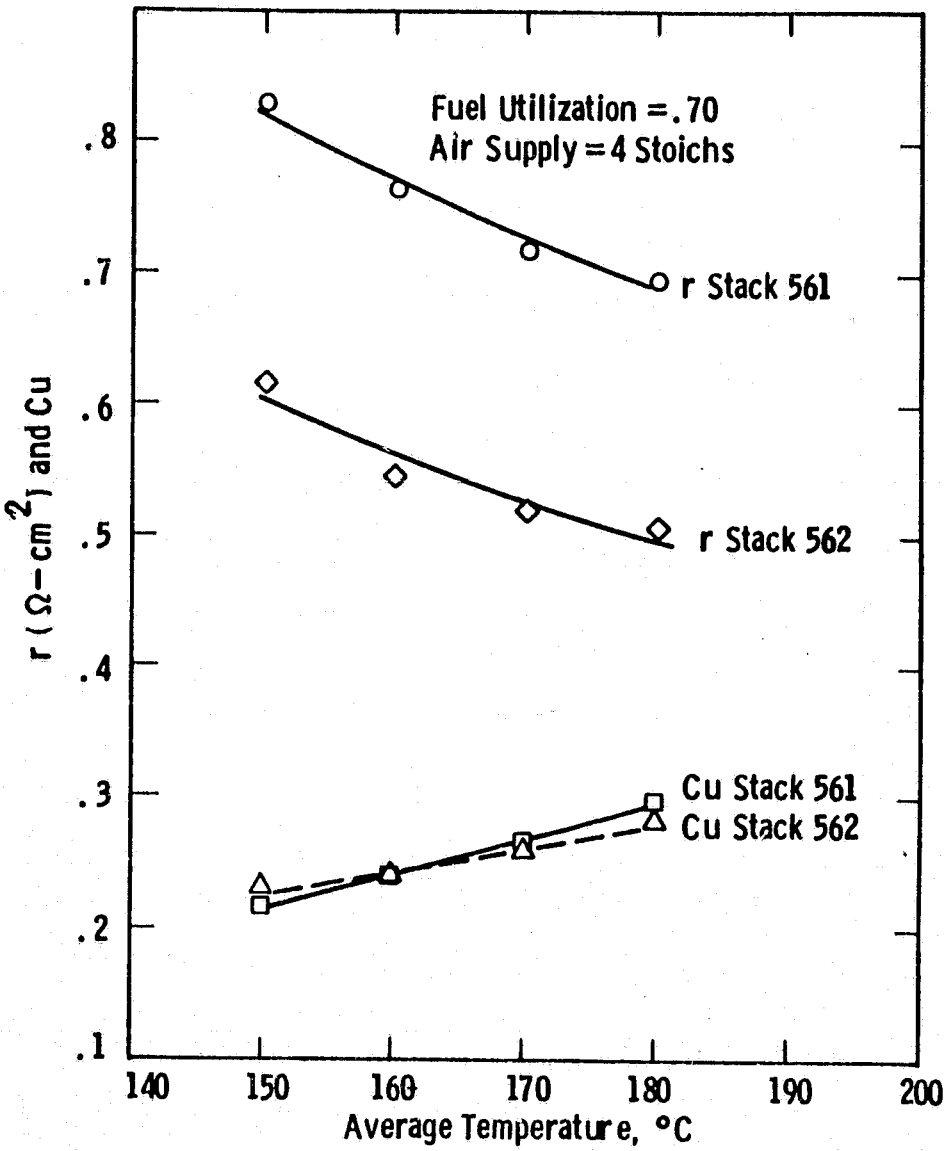

Fig. 5.3.30 – Specific cell resistance and catalyst utilization for stacks 561 and 562 vs temperature

The cell to cell data for 561 showed five to seven cells significantly below the average cell voltage, while 562 showed only one cell having significantly lower than average performance. Comparison of the average of the best 18 cells in each stack showed a difference of about 25 mV per cell between 562 and 561 at 200 mA/cm^2. Thus, statistical variations in cell performance between the two stacks may account for a significant part of the performance difference, but this may, in turn, be due to some unaccounted for effect of the design, such as reduced moisture in the fuel stream reducing H_2 sensitivity of cells.

The temperature uniformity of Stacks 561 and 562 was essentially the same when compared on the basis of peak to average temperature differential. Both stacks showed better uniformity at 2 stoichs than at 4. The profiles along the cooling direction are similar except 562 had peak temperatures nearer the cooling inlet. This was expected since the cooling effect of the process air is less in the Mk-2 configuration and occurs in a different area. The data indicate that the Mk-2 design shows a performance gain greater than the theoretical 0_2 gain of 28 mV/cell when both are operated with 2 stoichs of process/makeup air.

The power outputs of Stacks 561 and 562 for similar operating conditions are plotted against stack terminal voltage and stack current in Figures 5.3.31 and 5.3.32. These are the formats which would be of most use to designers who must interface other equipment with the fuel cell or for systems analysts attempting to make tradeoff studies

The curves in Figures 5.3.31 compare the stack power outputs for the same efficiency (voltage). They indicate a significantly greater output for Stack 562 than for 561 for any terminal voltage. The percentage difference is highest at high efficiency (∿51% at 15.5V) but is significant at the lower values (∿38% at 13.5) corresponding to high power. This advantage would be more pronounced with lower makeup air flows than the four stoich conditions at which the data were taken. At the same power outputs, Stack 562 has a higher efficiency than 561. For example, at the nominal rated power of 2 kW the 562's terminal voltage is 7.5% greater than 561's (14.3 vs. 13.3V) corresponding to a 7.5% greater efficiency.

ORIGINAL PAGE IS
OF POOR QUALITY

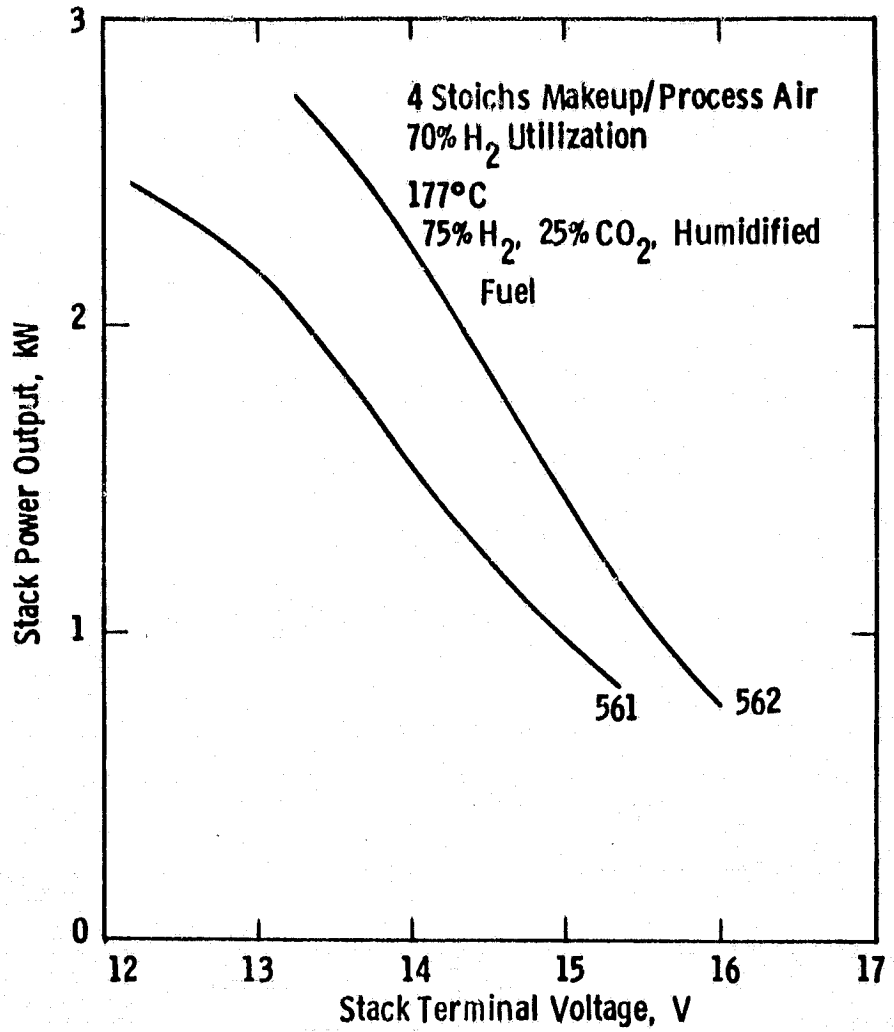

Fig. 5.3.31 – Comparison of power outputs vs terminal voltage for stacks 561 and 562

ORIGINAL PAGE IS
OF POOR QUALITY

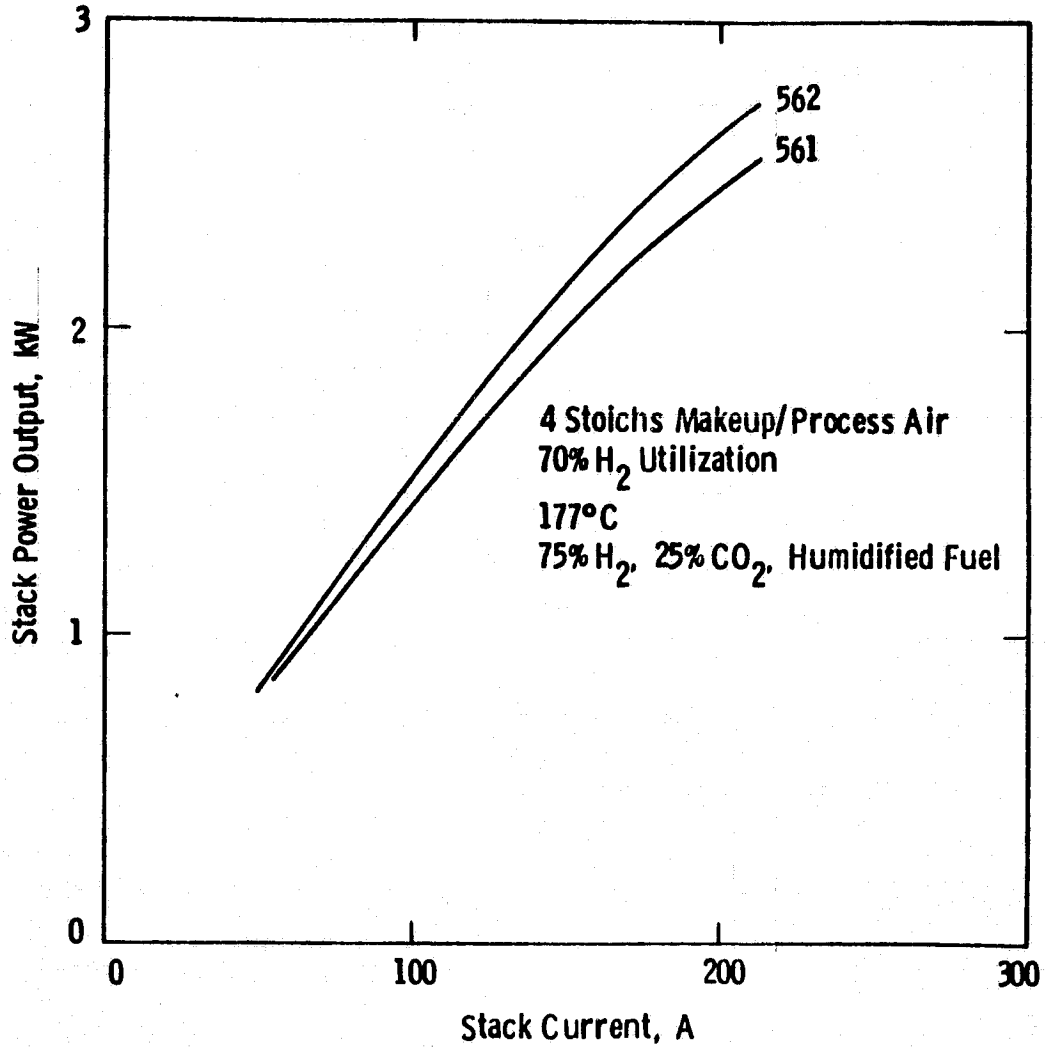

Fig. 5.3.32 – Comparison of power output vs current for stacks 561 and 562

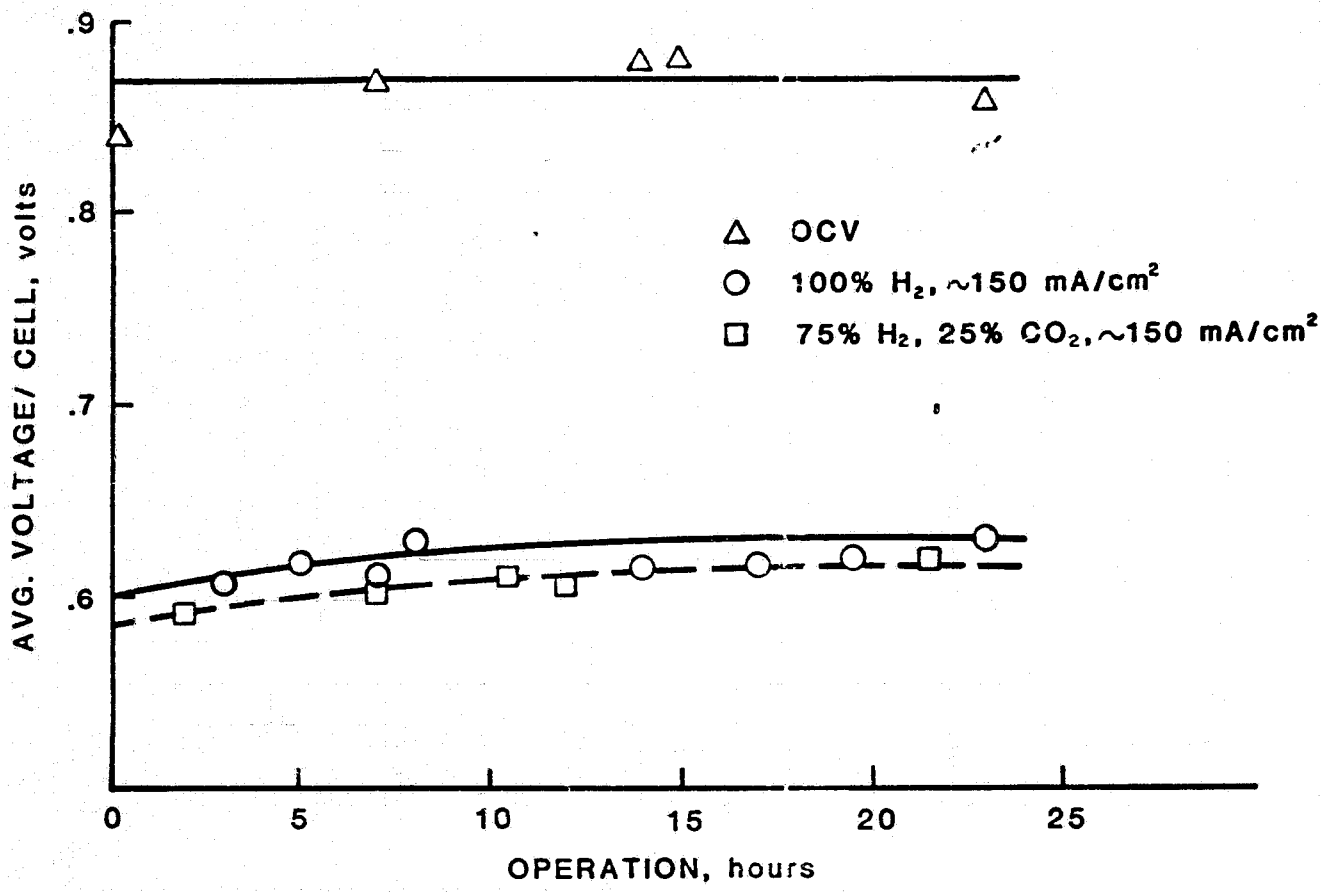

FIGURE 5.3.33 PRETEST PERFORMANCE OF STACK 564

OF POOR QUALITY

Since, unlike voltage, there is no direct relationship between current and efficiency, the greatest significance of Figure 5.3.32 may be the fact that the power output of these stacks is apparently well below their maximum value when operating at 200 mA/cm^2 at atmospheric pressure. Although no one can deny the importance of operating at high efficiency, the potential for reducing capital costs by operating at maximum power output should be carefully considered in cost/performance tradeoff studies.

5.3.5 Stack 564 (Mk-2, 23-cell)

Stack 564 was the second Mk-2 design 2 kW stack and was essentially a duplicate of Stack 562. Changes in design and fabrication were based on experience gained and are described in the appropriate sections of this report.

5.3.5.1 Pretesting

Pretesting included measurement of:

- Steady and transient OCV's,
- performance at 150 mA/cm^2,
- polarization,
- effect of fuel gas composition,
- process air pressure drop,
- effect of hydrogen utilization,
- effect of process air utilization.

The initial OCV data for individual cells indicated that the electrochemical components were sufficiently wet with acid to proceed with on-load testing and that the manifold and shim seals of the stack were gas-tight. The baseline (150 mA/cm^2 on hydrogen and air) performance of this stack during the 23 hour pretest period was ∿625 mV/cell as shown in Figure 5.3.33. Small variations in voltage are due to small differences in cell temperatures and stack current. The polarization characteristics of Stack 564 in Figure 5.3.34 were comparable to those of Stack 562.

There was a 10 mV drop per cell with 25% CO_2 in the fuel feed and an additional 6 mV drop with 1% CO. These agree with theoretical

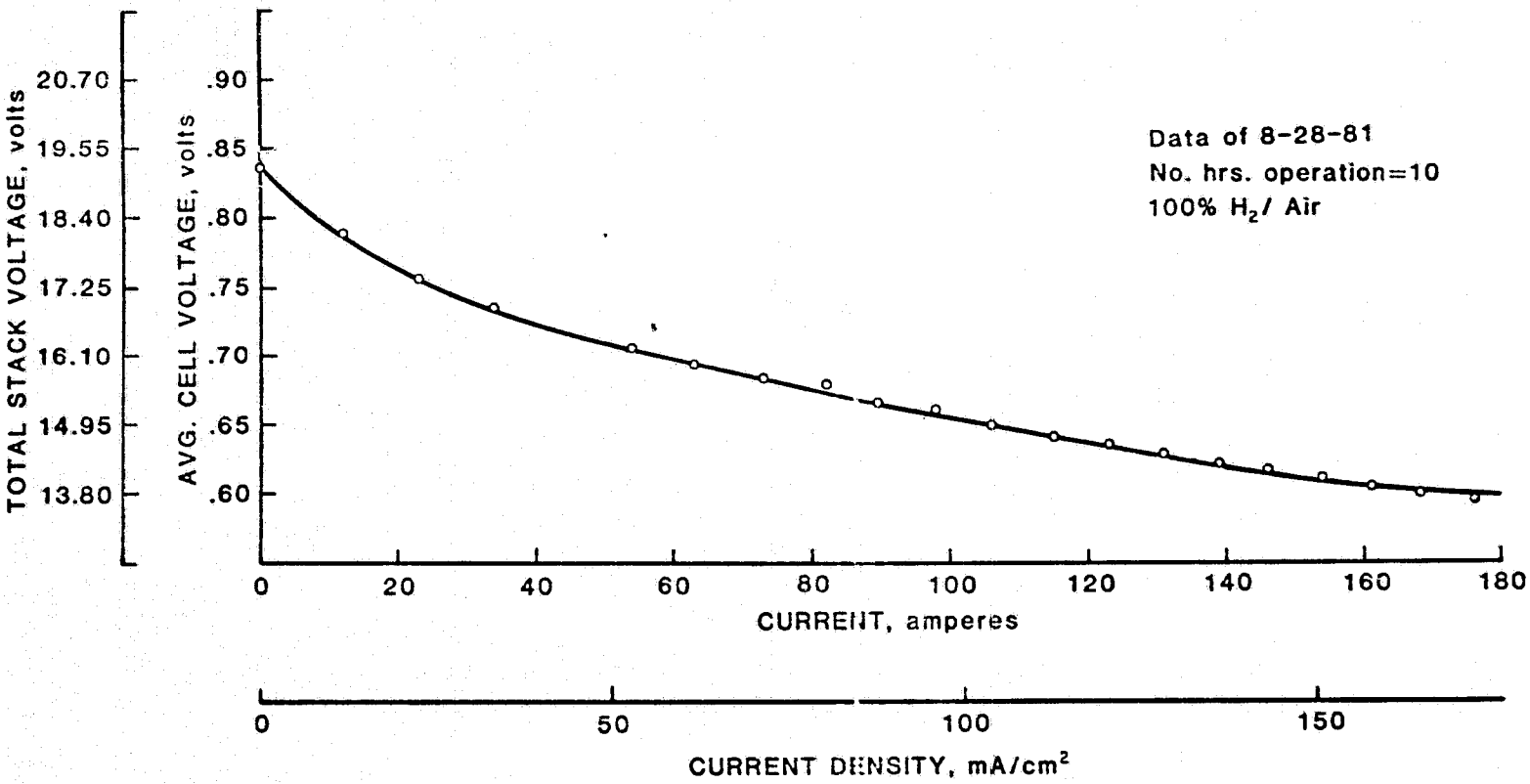

FIGURE 5.3.34. POLARISATION, STACK 564

predictions. The measured process air pressure drops were about 20% higher than those of Stack 562. Tests with varying hydrogen and air utilization indicated that the cells were capable of running with 5 mV loss (from peak performance) at 150 mA/cm^2 with 1.5 stoich air and 90% hydrogen utilization.

5.3.5.2 Performance Testing

The objectives of Stack 564 performance tests were to:

1. Verify the improvement in temperature distribution (compared with Stack 562) with the modified tree cooling pattern.
2. Acquire data on the effects of various operating parameters (e.g., fuel utilization, temperature, fuel CO content) on cell performance.

Accordingly, Stack 564 was tested at 59* steady state conditions which are described, along with the results and discussion, below.

Table 5.3.6 presents a summary of tests and conditions for the 59 tests. The first 4 tests were run without insulation. Tests 5 and 6 compared performance at 70 and 80 percent fuel utilization. Tests 7 thru 29 were made to obtain performance maps at 150 and 200 mA/cm^2 for temperatures between 150 and 180°C with 2 and 3 stoichs of process air. Tests 30 through 33 obtained the effect of fuel utilization on performance and temperature distribution for utilizations from 70 to 85 percent. Tests 34 through 38 obtained the effect of fuel and process air inlet temperatures on the temperature distribution. Tests 39 through 58 obtained the effect of CO on cell performance from 50 to 200 mA/cm^2. Tests 59 and 60 were run at high and low cooling air flow rates to obtain effect of cooling gas temperature rise on temperature uniformity.

*Although the last test is numbered 60, 18 was excluded from the number sequence so there are 59 tests.

ORIGINAL PAGE IS
OF POOR QUALITY

TABLE 5.3.6 – SUMMARY OF TEST CONDITIONS AND TEST RESULTS FOR STACK 564

Test	Current Density mA/cm^2	Volts/Cell V	Average Temperature °C	Peak to Average Gradient °C	Fuel Utilization	Dry H_2 Inlet Fraction	Dry CO Inlet Mole Fraction	Fuel Inlet Temperature °C	Process Air Stoichs	Process Air Inlet Temperature °C	Cooling Air Flow g/sec	Cooling Air Inlet Temperature °C	Cooling Air Temperature Rise, °C	Process Air Pressure Drop cm H_2O	Cooling Air Pressure Drop cm H_2O	Mole Fraction of H_2O In Fuel Exhaust	Fraction of Produced Water Transferred to Fuel
1*	150	0.611	172	9.5	0.70	1.00	0.0	166	2.0	168	–	115	47	13.4	4.19	–	–
2*	99	0.634	173	7.3	0.62	0.75	0.0	158	2.0	156	35.4	108	15	5.94	4.69	–	–
3*	156	0.599	179	8.5	0.69	0.75	0.0	163	2.7	167	39.5	139	34	12.4	5.75	–	–
4*	156	0.598	176	7.2	0.66	0.77	0.0	171	2.7	175	40.1	127	38	12.4	5.83	–	–
5	100	0.633	171	7.5	0.70	0.75	0.0	163	2.0	169	29.1	113	57	5.89	2.73	–	–
6	100	0.629	172	4.5	0.80	0.75	0.0	158	2.0	169	29.1	114	56	5.89	2.73	–	–
7	150	0.597	177	6.0	0.80	0.75	0.0	175	2.0	174	36.7	113	57	9.19	5.22	–	–
8	150	0.572	190	4.8	0.80	0.75	0.0	141	2.0	148	39.5	99	53	8.46	5.47	–	–
9	150	0.588	161	4.5	0.80	0.75	0.0	143	2.0	149	39.2	108	58	8.87	5.49	–	–
10	150	0.591	170	5.2	0.80	0.75	0.0	144	2.0	154	39.1	116	53	9.12	5.55	0.132	0.057
11	150	0.597	180	5.0	0.80	0.75	0.0	145	2.0	159	39.0	120	50	9.27	5.59	0.119	0.045
12	150	0.602	178	8.0	0.80	0.75	0.0	147	3.0	156	39.0	120	51	14.1	5.59	–	–
13	200	0.530	147	4.5	0.80	0.75	0.0	150	2.0	141	58.3	88	52	11.1	9.68	0.125	0.092
14	200	0.543	156	5.2	0.80	0.75	0.0	152	2.0	141	57.6	98	52	11.4	9.65	0.126	0.094
15	200	0.550	165	5.4	0.80	0.75	0.0	153	2.0	152	56.0	99	53	11.7	9.64	0.120	0.090
16	200	0.559	176	6.0	0.80	0.75	0.0	154	2.0	160	55.3	110	53	12.2	9.58	0.120	0.089
17	200	0.563	173	10.1	0.80	0.75	0.0	153	3.0	151	55.3	110	51	–	–	–	–
19	150	0.584	161	4.9	0.80	0.75	0.0	144	2.0	149	39.9	100	53	8.53	5.43	0.135	0.076
20	150	0.590	159	8.2	0.80	0.75	0.0	144	3.0	146	39.9	100	52	13.0	5.41	0.092	0.021
21	150	0.581	150	9.0	0.80	0.75	0.0	146	3.0	136	39.9	90	53	12.7	5.41	0.087	0.017
22	150	0.603	178	8.9	0.80	0.75	0.0	146	3.0	165	39.9	120	51	13.9	5.49	0.093	0.021
23	150	0.606	178	7.5	0.70	0.75	0.0	150	3.0	163	38.1	121	51	–	–	–	–
24	[illegible]	[illegible]	[illegible]	[illegible]	[illegible]	[illegible]	[illegible]	[illegible]	[illegible]	[illegible]	[illegible]	[illegible]	[illegible]	[illegible]	[illegible]	[illegible]	[illegible]
25	200	0.556	158	8.8	0.80	0.75	0.0	153	3.0	146	54.9	93	53	17.5	9.95	0.089	0.023
26	200	0.580	176	8.6	0.80	0.75	0.0	154	3.0	161	53.1	112	52	18.4	8.95	0.091	0.024
27	200	0.562	169	10.0	0.80	0.75	0.0	152	3.0	151	53.1	104	54	18.1	8.57	0.081	0.016
28	200	0.568	179	9.9	0.80	0.75	0.0	153	3.0	162	51.3	114	54	18.5	8.56	0.092	0.017
29	200	0.545	153	10.5	0.80	0.75	0.0	151	3.0	135	53.5	86	56	16.9	8.49	–	–
30	150	0.591	173	6.6	0.80	0.75	0.0	145	2.0	144	34.9	112	55	8.81	4.96	0.115	0.060
31	150	0.575	175	13.9	0.85	0.75	0.0	145	2.0	143	34.7	112	57	8.94	4.94	0.115	0.059
32	150	0.593	173	5.7	0.75	0.75	0.0	148	2.0	144	34.8	111	56	8.99	4.94	0.119	0.054
33	150	0.594	174	5.0	0.70	0.75	0.0	149	2.0	144	34.8	112	56	9.03	4.94	0.109	0.057
34	150	0.592	174	5.8	0.80	0.75	0.0	152	2.0	155	35.8	112	55	9.02	4.96	0.125	0.053
35	150	0.592	174	7.8	0.80	0.75	0.0	149	2.0	145	35.8	112	56	9.08	4.97	0.124	0.052
36	150	0.591	173	8.2	0.80	0.75	0.0	135	2.0	134	35.7	112	55	9.00	4.93	0.123	0.051
37	150	0.590	172	9.7	0.80	0.75	0.0	127	2.0	125	35.7	112	55	9.03	4.94	0.121	0.049
38	150	0.588	171	10.3	0.80	0.75	0.0	118	2.0	115	35.6	112	56	8.96	3.91	0.122	0.050
39	150	0.591	172	5.7	0.80	0.75	0.0	146	2.0	153	36.3	110	55	8.99	4.91	0.127	0.048
40	150	0.582	173	7.7	0.80	0.739	0.0145	148	2.0	154	36.3	110	57	9.04	4.93	–	–
41	150	0.576	174	9.3	0.80	0.729	0.0278	146	2.0	153	36.3	110	57	9.12	4.94	0.115	0.043
42	150	0.573	175	10.6	0.80	0.721	0.0389	146	2.0	153	36.3	110	58	9.14	4.95	0.112	0.042
43	150	0.570	176	11.4	0.80	0.713	0.0500	147	2.0	152	36.2	109	58	9.02	4.94	0.111	0.042
44	150	0.592	173	6.6	0.80	0.75	0.0	150	2.0	153	36.3	110	57	9.02	4.94	–	–
45	50	0.672	169	6.4	0.80	0.76	0.0	130	2.0	141	13.6	132	35	3.10	0.97	0.115	0.031
46	50	0.671	175	6.9	0.80	0.728	0.0391	135	2.0	144	15.9	134	40	3.12	0.99	–	–
47	50	0.670	176	7.7	0.80	0.712	0.0600	136	2.0	145	15.9	133	43	3.19	1.00	0.113	0.060
48	50	0.678	177	7.8	0.80	0.76	0.0	134	2.0	146	13.6	134	44	3.18	0.99	0.115	0.031
49	100	0.620	166	6.1	0.80	0.75	0.0	149	2.0	149	23.1	109	56	6.31	2.66	0.113	0.037
50	100	0.612	167	7.4	0.80	0.733	0.0208	149	2.0	149	23.6	109	56	5.92	2.64	0.171	0.097
51	100	0.609	167	8.7	0.80	0.726	0.0320	149	2.0	149	23.6	110	56	6.35	2.69	0.163	0.091
52	100	0.607	168	9.3	0.80	0.726	0.0397	149	2.0	149	22.7	110	57	6.43	2.62	0.148	0.078
53	100	0.622	167	6.3	0.80	0.75	0.0	150	2.0	149	22.7	110	56	6.38	2.62	0.116	0.059
54	200	0.557	176	6.4	0.80	0.75	0.0	156	2.0	158	50.8	110	55	12.4	8.28	0.136	0.051
55	200	0.569	178	6.3	0.80	0.742	0.0114	156	2.0	158	50.8	109	57	12.9	8.29	0.130	0.048
56	200	0.563	179	8.3	0.80	0.734	0.0218	157	2.0	159	50.3	110	58	12.1	8.27	0.126	0.046
57	200	0.562	179	8.9	0.80	0.728	0.0305	156	2.0	159	50.3	109	58	13.3	8.27	0.119	0.041
58	200	0.558	178	5.8	0.80	0.75	0.0	159	2.0	159	50.3	109	58	13.7	8.29	0.122	0.039
59	150	0.587	172	6.4	0.80	0.75	0.0	149	2.0	159	53.1	124	39	9.18	8.79	–	–
60	150	0.594	179	8.8	0.80	0.75	0.0	150	2.0	160	28.1	105	78	9.47	3.66	–	–

*Uninsulated Tests

ORIGINAL PAGE IS
OF POOR QUALITY

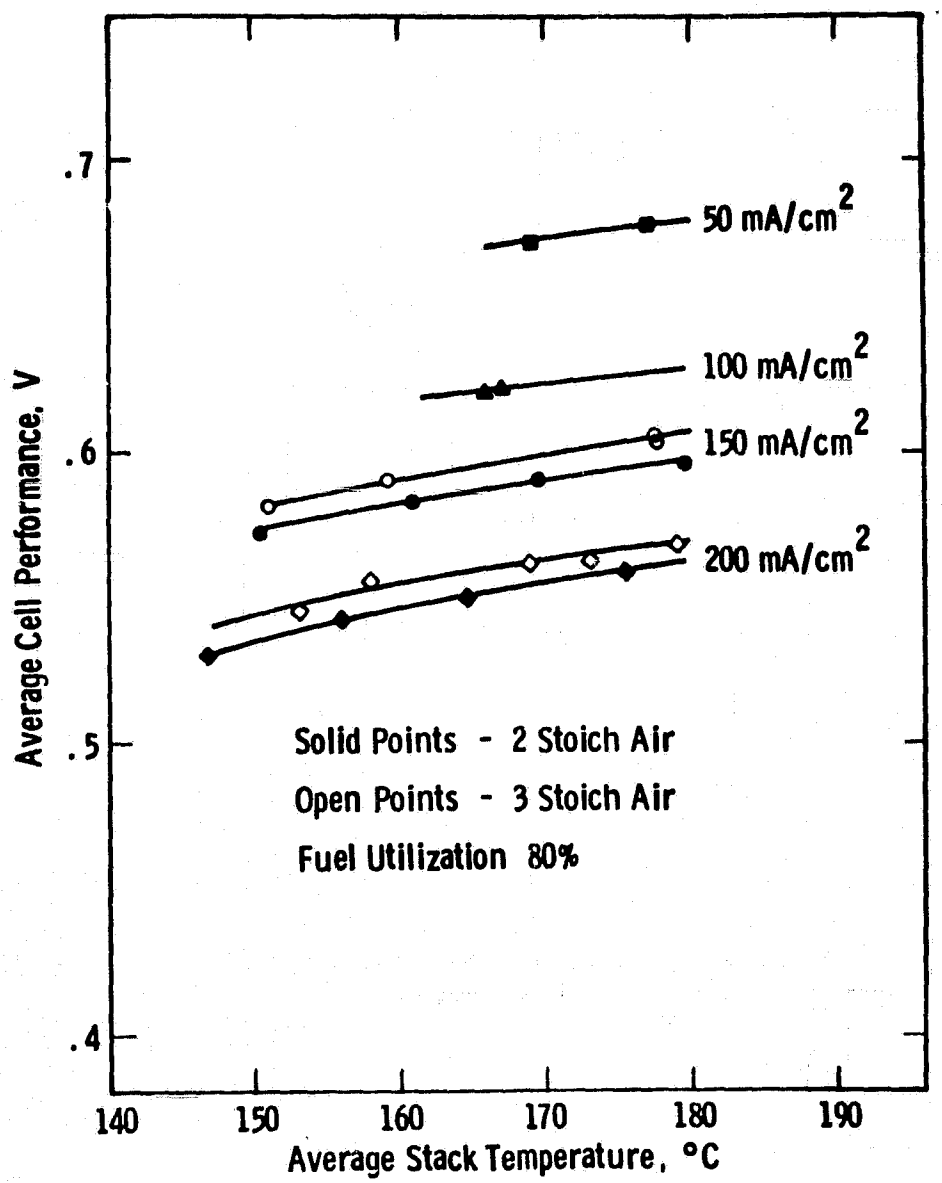

Fig. 5.3.35—Performance of stack 564 as a function of temperature and current density

ORIGINAL PAGE IS
OF POOR QUALITY

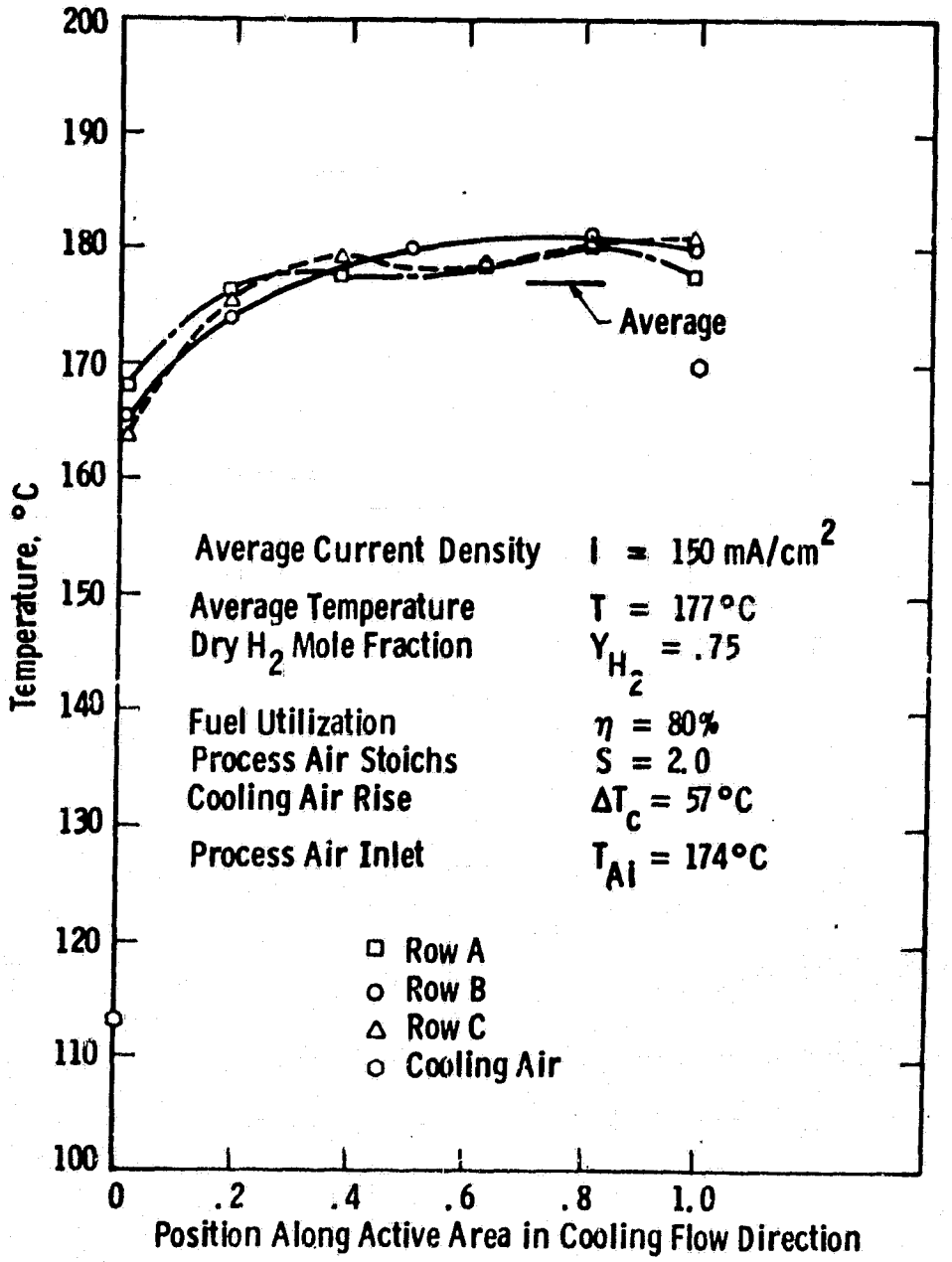

Fig. 5.3.36 —Temperature distribution in stack 564 - test 7

For all tests except Test 1 (for which the fuel was H_2) the volume ratio of H_2 to CO_2 was maintained at 3:1. The fuel was humidified at room temperature for all tests.

The average cell performance, based on terminal voltage, is shown in Figure 5.3.35 for 2 and 3 stoich process air and 80 percent fuel utilization. The two stoich performance at 150 and 200 mA/cm^2 was virtually identical to Stack 562 performance at 70 percent utilization.

The effect of temperature on cell voltage at 150 and 200 mA/cm^2 ranged from .78 mV/°C to .97 mV/°C with a mean value of .86 mV/°C which is slightly lower than for Stack 562.

Temperature Uniformity

The temperature uniformity of Stack 564 was excellent. The peak to average gradient for 50 to 58°C cooling gas rise ranged from 4.0 to 6.6°C for tests at 2 stoich process air and 80 percent fuel utilization (no CO) when process and fuel inlet temperature were within 15°C of the average stack temperature. The peak to average gradient exceeded 10°C for only 5 tests; one at 85 percent utilization, one at 5 percent CO, two at low process air inlet temperatures, and one at 3 stoich process air. Figures 5.3.36 through 5.3.41 show temperature distributions at various conditions. The first two are for 2 stoich process air at 150 and 200 mA/cm^2. Figure 5.3.38 is at 150 mA/cm^2 with approximately equal fuel, process and cooling inlet temperatures. Cold process air lowers the average temperature of row A by about 12°C while the cold fuel has little effect on row C.

Figure 5.3.39 shows that the addition of 5 percent CO at 150 mA/cm^2 increases the temperature at the fuel inlet edge (row C) and reduces it at the fuel exit edge (row A). Theoretically, the effect on current density distribution is similar. Figures 5.3.40 and 5.3.41 show the effect on temperature distribution of cooling air temperature changes of 39 and 70°C respectively with other conditions similar to those for the 57°C case shown in Figure 5.3.36. The results with a 39°C rise are very similar to those with a 57°C rise, but with a 70°C rise, there is a tendency toward

ORIGINAL PAGE IS
OF POOR QUALITY

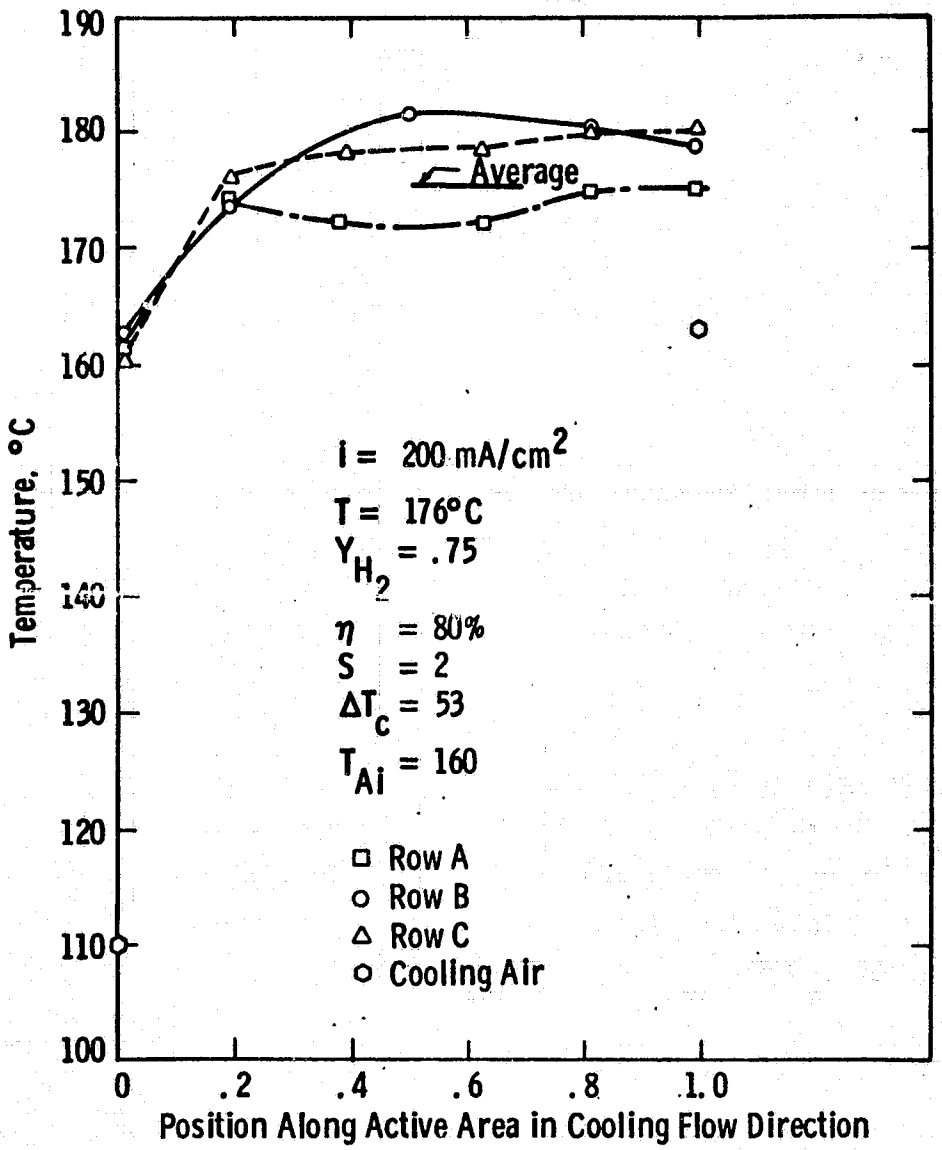

Fig. 5.3.37 –Temperature distribution in stack 564 - test 16

C-3

ORIGINAL PAGE IS
OF POOR QUALITY

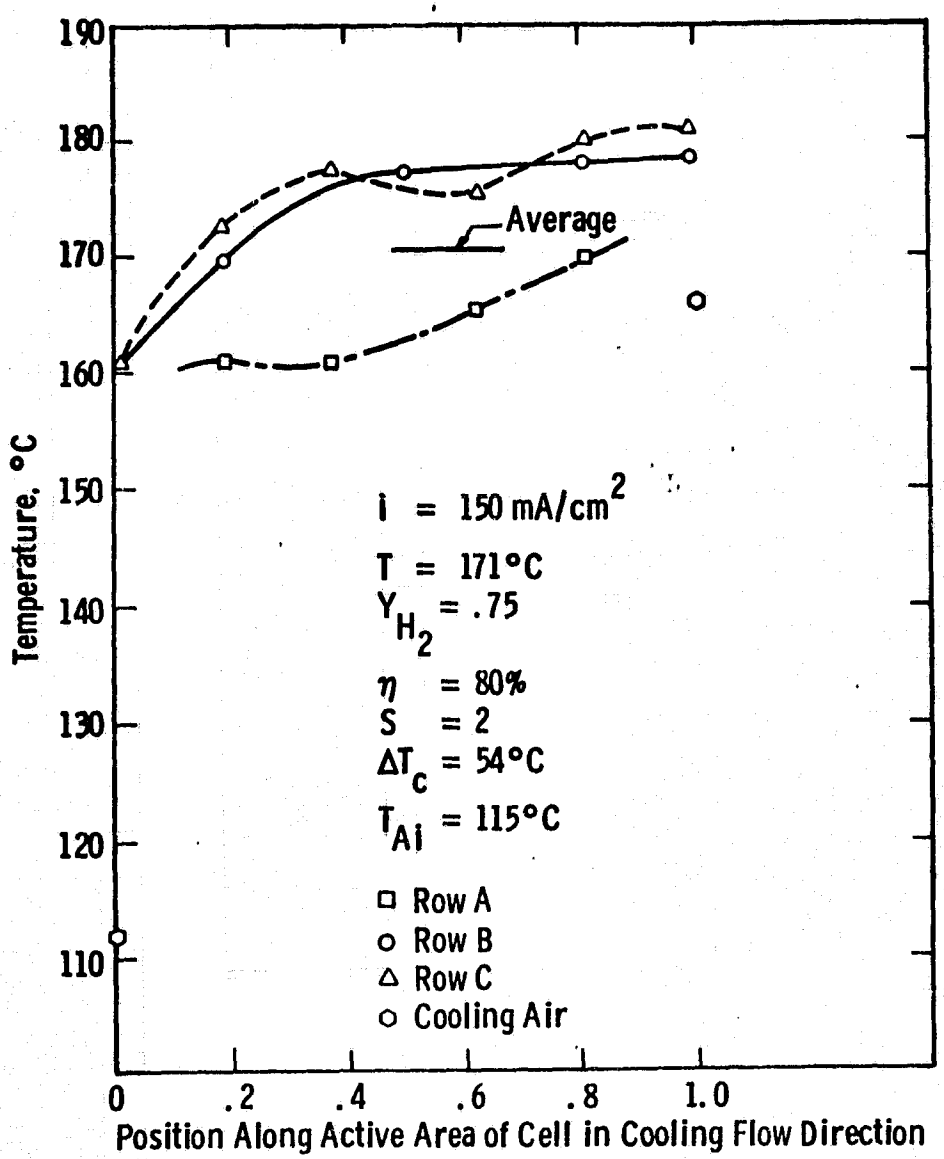

Fig. 5.3.38—Temperature distribution in stack 564 - test 38

ORIGINAL PAGE IS
OF POOR QUALITY

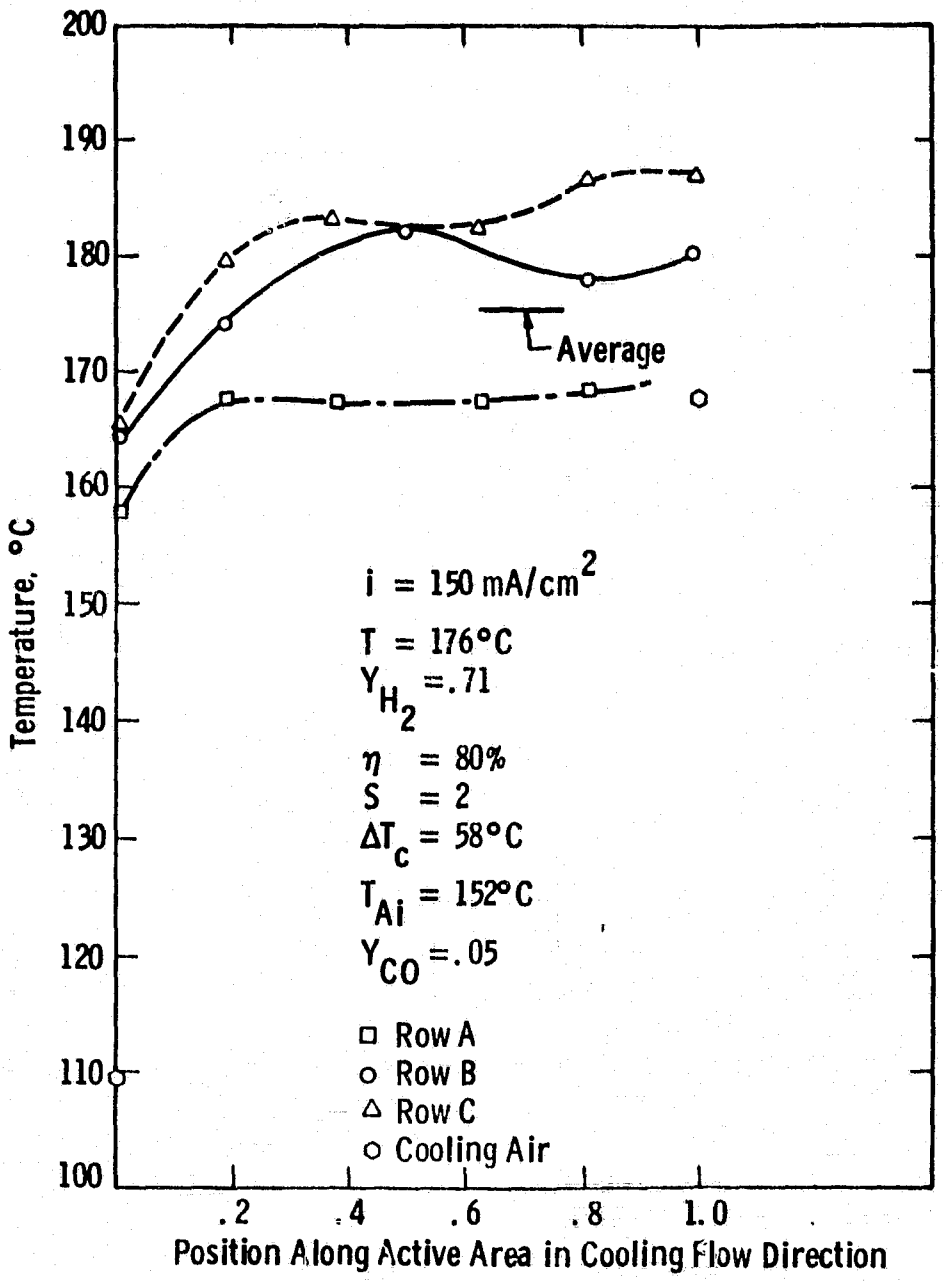

Fig. 5.3.39 —Temperature distribution in stack 564-test 43

ORIGINAL PAGE IS
OF POOR QUALITY

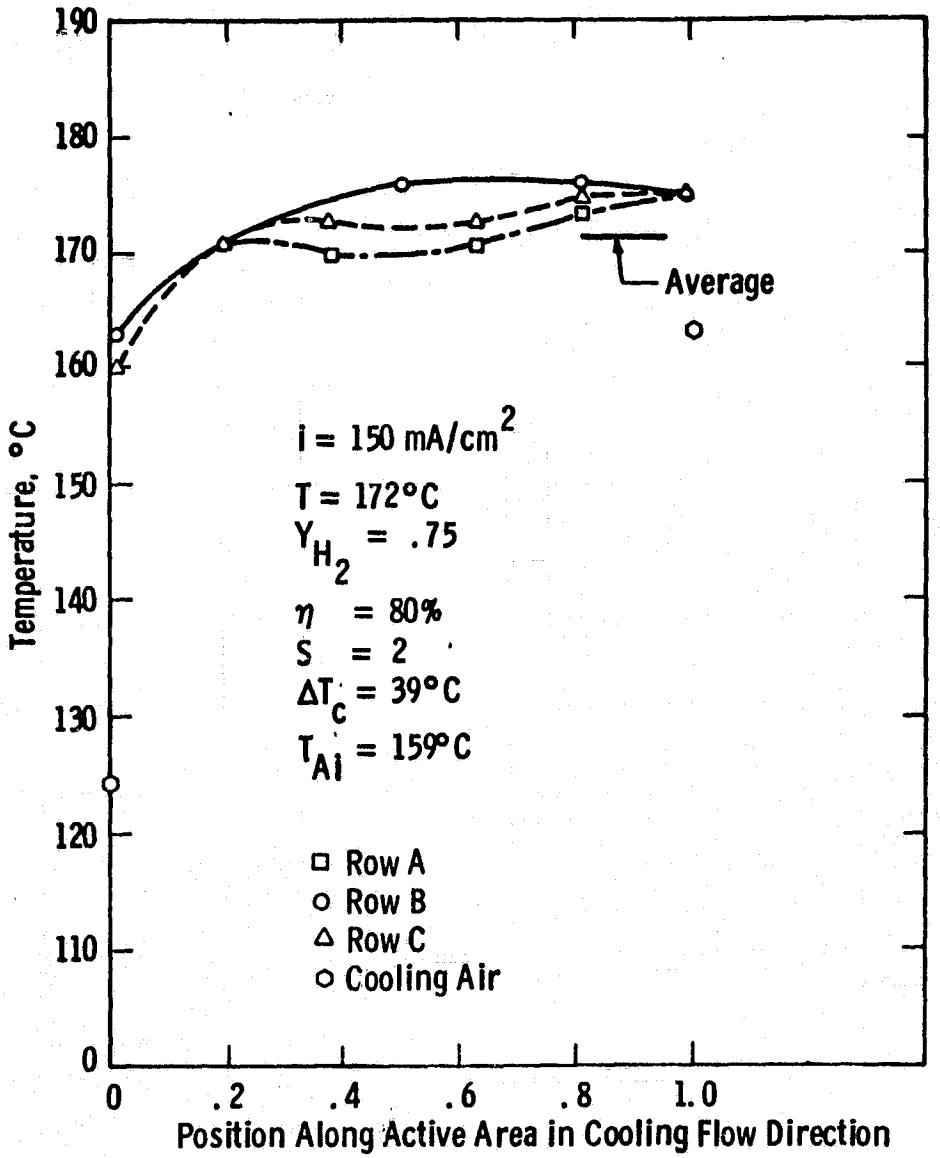

Fig. 5.3.40 –Temperature distribution in stack 564 - test 59

ORIGINAL PAGE IS
OF POOR QUALITY

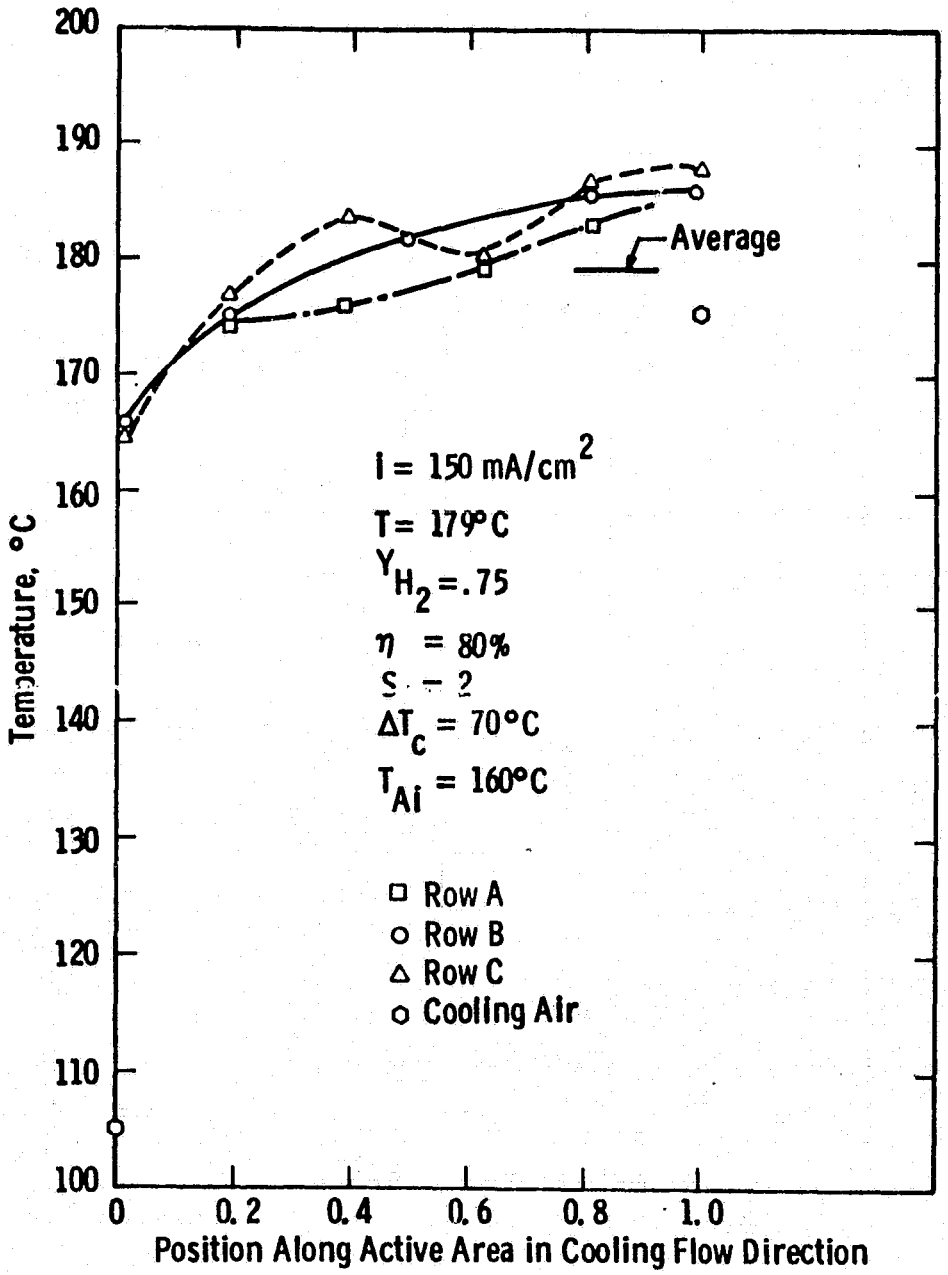

Fig. 5.3.41 –Temperature distribution on stack 564 - test 60

ORIGINAL PAGE IS
OF POOR QUALITY

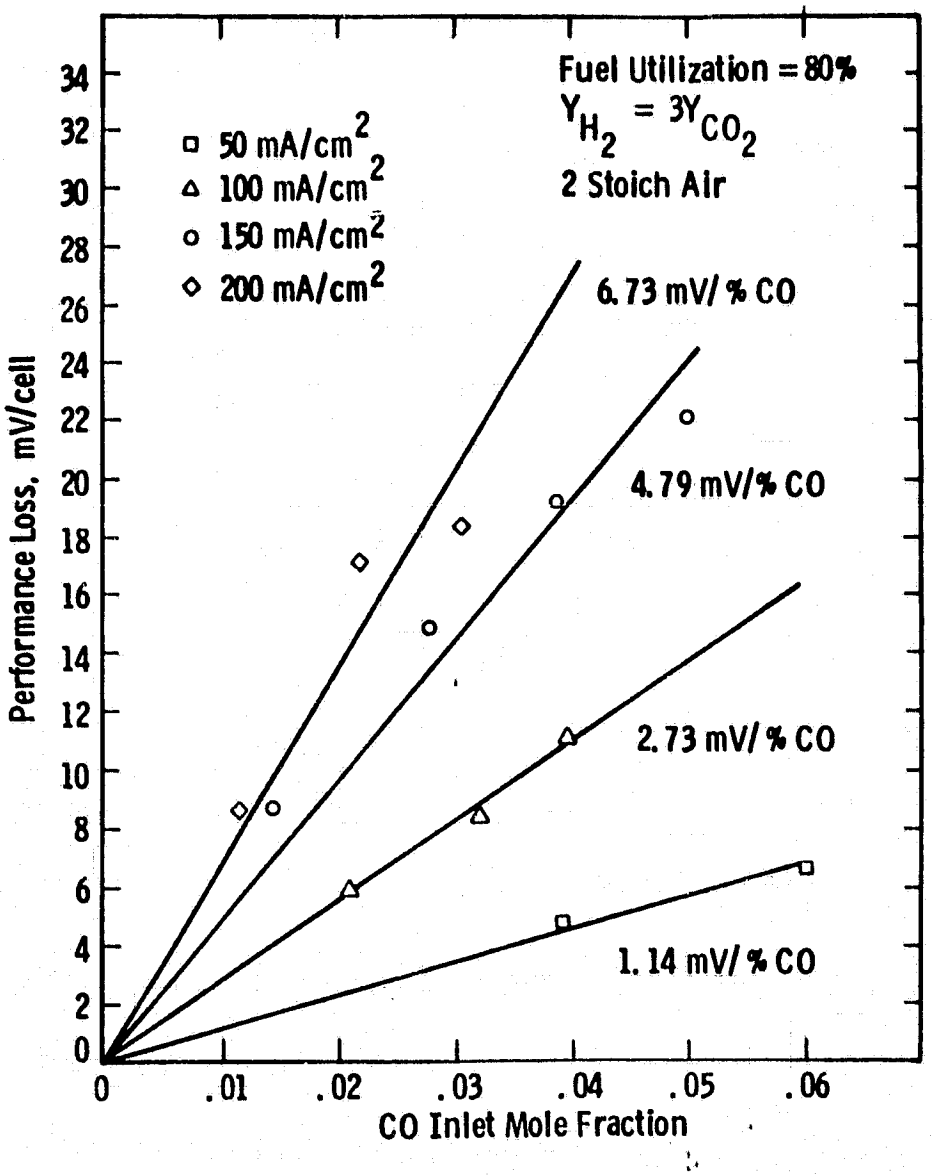

Fig. 5.3.42 – Performance loss due to carbon monoxide corrected to 177°C

ORIGINAL PAGE IS
OF POOR QUALITY

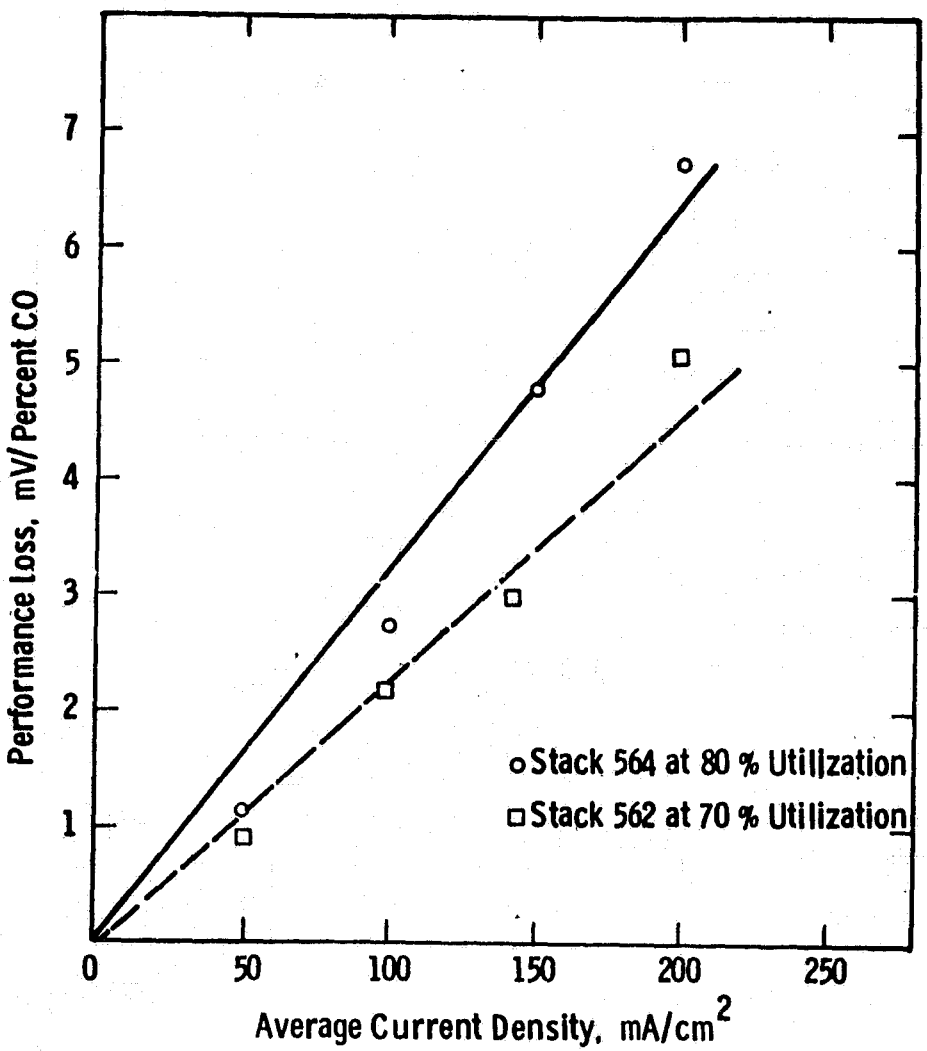

Fig. 5.3.A3—Rate of performance loss due to carbon monoxide at 177 °C as a function of current density

higher temperatures at the cooling air exit edge. However, even with the 70°C rise, the peak to average difference is only 8.8°C or 12.6 percent of the cooling air rise.

Effect of CO on Performance

According to the theoretical model, the CO effect doubles for every 15°C drop in temperature. Thus

$$\Delta V(T) = \Delta V(177) \times 2^{\left(\frac{177-T}{15}\right)}$$

can be used to correct the CO effect measured at T to a reference of 177°C. The corrected results for CO tests of Stack 564 are shown in Figure 5.3.42 as a function of CO inlet mole fraction. The straight lines are least squares fits of the data at current densities of 50, 100, 150 and 200 mA/cm^2. The fit indicates that the CO effect is approximately linear with inlet mole fraction at each current density. The slopes at various current densities plotted in Figure 5.3.43 shows the CO effect was approximately linear with current density for Stack 564. Figure 5.3.43 also indicates a smaller CO effect for Stack 562 but this was due to the need to operate Stack 562 at lower H_2 utilization as discussed in Subsection 5.3.42.

Water in Fuel Exit Stream

The dew point of the fuel exit stream was measured for 41 of the tests and used to compute the exit water mole fraction and the fraction of produced water transferred to the fuel stream. Correction was made for the water in the humidified inlet fuel stream based on the mean water use rate during each test day. For 33 tests at 2 stoich air, the water mole fraction in the exit fuel averaged 0.118 which corresponds to 5.1 percent of produced water being transferred to the fuel stream. For the 8 tests at 3 stoich air the water mole fraction averaged 0.091 with 2.1 percent of produced water transferred to the fuel. The corresponding average mole fraction of water in the exit process air stream was 0.91 at 2 stoich and 0.133 at 3 stoich air. The mole fraction of water in the fuel exit thus averages about 65 percent of the mole fraction of water in the exit air.

ORIGINAL PAGE
BLACK AND WHITE PHOTOGRAPH

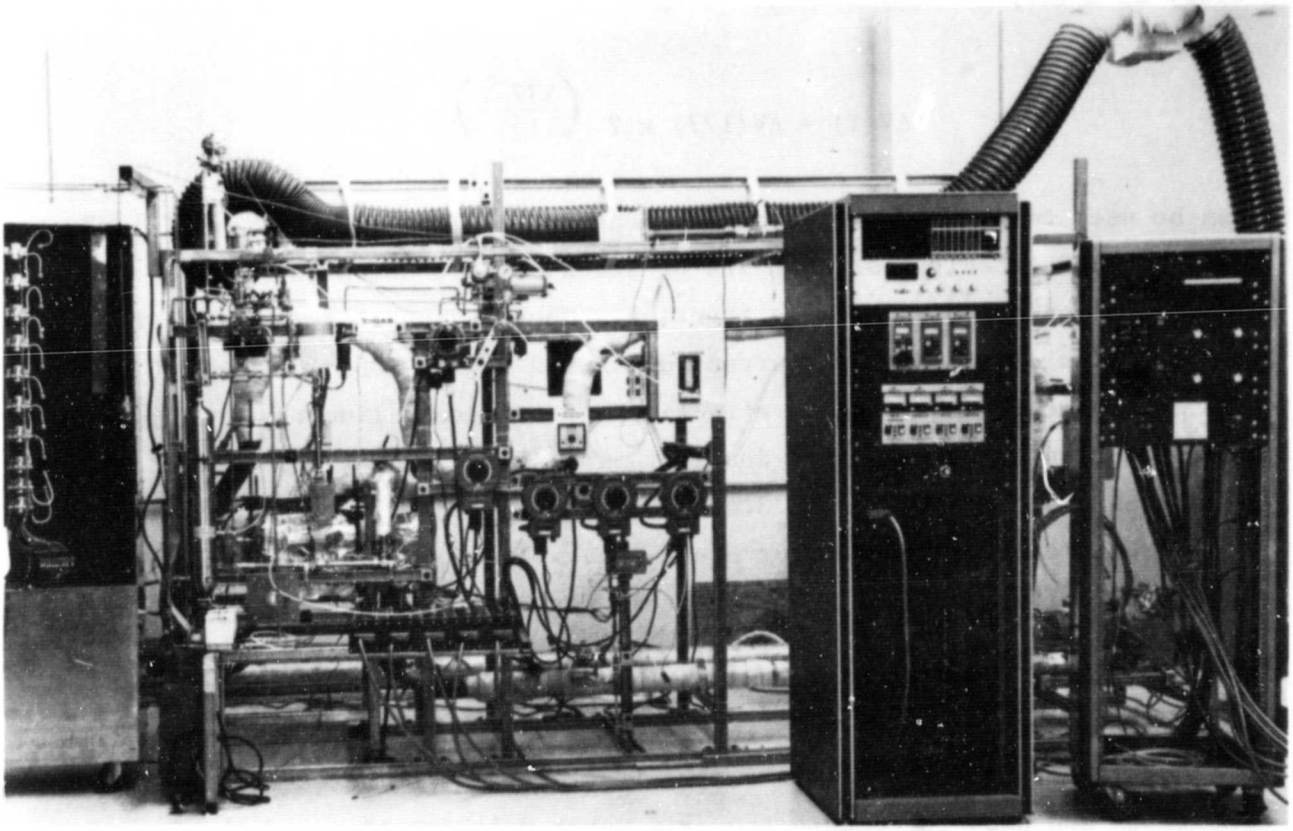

FIGURE 5.4.1. ERC 2 kW TEST FACILITY

Continuous Testing

Stack 564 was placed on continuous test for a 25 day period at 99 mA/cm^2 with 2 stoich air and 80 percent fuel utilization. After 8, 13 and 25 days, the current was increased to 150 mA/cm^2 to compare performance with previous tests. Performance remained stable during the test period. A total test time of 719 hours of operation was accumulated prior to removal from the loop to prepare for testing of Stack 800.

5.4 Test Facility Construction

The objective of this subtask was the design and construction of facilities to test stacks under OS/IES operating conditions. One 2 kW and one 8 kW test facility were constructed at ERC. The design of these test stands was similar to that built at Westinghouse during Phase I and modified as described in Section 5.1.

5.4.1 2 kW Test Facility

A photograph of the completed 2 kW test facility is shown in Figure 5.4.1. The salient features of this facility are:

Dual Flow Configuration

- DIGAS (Distributed Gas i.e., Mk-1 design) stacks
- separate gas cooling (i.e., Mk-2) stacks

Automatic Control

- of fuel composition and flow rates
- of stack exit air temperature

Safety and Stack Protection Features

- stack overheating protection
- ΔP monitor across cell/stack to prevent damaging the cells
- H_2 level monitor in air stream and in room
- electric power failure protection
- blower failure protection
- automatic operation shutdown

Operation

- data scanning and recording by an automatic data acquisition system
- round-the-clock unsupervised operation

Flow Ranges

This test station is capable of operation over the following flow ranges:

	Flow Ranges SLPM (SCFM)		
	Nom.	Max.	Min.
Hydrogen	42 (1.5)	56 (2)	11 (0.4)
Carbon Dioxide	10 (0.35)	14 (0.5)	3 (0.1)
Carbon Monoxide	-	2 (0.07)	-
Air Makeup (Mk-1)	140 (5)	1680 (60)	85 (3)
Loop Air	1700 (60)	2240)80)	425 (15)
Process Air (Mk-2)	113 (4)	280 (10)	56 (2)

Controlled Operating Parameters

- current (load)
- temperatures (air, fuel, cell and stack average)
- reactant compositions
- air and fuel flow rates
- humidity of fuel supply

Performance Measurements

- cell voltage
- temperatures - stack distribution
- pressure in all streams (also monitor ΔP across stack)
- water content in air streams and in room (also used as portable H_2 detector)
- oxygen concentration in air streams.

All of the above measured parameters and operational parameters are logged by an automatic data acquisition system.

Figure 5.4.2 is a schematic of the DIGAS configuration of the 2 kW test facility. The fuel (H_2, CO_2 and CO) is supplied from individual cylinders through the valves (V3 through V5) of the fuel mass flow controller which blends the gas streams in preset proportions. The blended fuel passes through the anode humidifier (AH) and the fuel preheater, which controls the fuel mixture temperature.

Room air is drawn through a filter and supplied to the stack by the blower. The makeup flow rate is measured by a turbine flowmeter (F1) and controlled by the manual valve, V1. The air preheater is used mainly for startup. Sufficient gas is vented from the stack to maintain the desired recirculation rate. The temperature of the recycled stream is controlled by valve V6 which controls the ratio of flows through heat exchanger and bypass lines. The makeup airflow is controlled by valve V8. The makeup air and recycle gas flow rates are individually measured by flowmeters F2 and F6. The facility was designed for total cathode gas flows as high as 40 stoichs for a 2 kW stack.

Since the determination of the effects of temperature level on stack performance is a major objective of testing in this program, instrumentation and controls must provide for control and measurement of this parameter. In this loop, controller C1 adjusts the recycle flow through the heat exchanger to maintain a specified stack outlet air temperature, T2, independent of recirculation or makeup air flow rates. If the outlet air temperature changes, the GFT* in the exit air manifold sends a signal to controller C1 which will adjust V6 to pass more or less air through the heat exchanger to lower or raise the recycle stream temperature until the air outlet temperature is back to the desired set point.

An automatic (DAS) data acquisition system processed and printed out all pertinent data and provided alarms. This system was shared with the 8 kW Test Facility and is described in Subsection 5.4.3.

*GFT is a gas-filled thermometer which acts directly on the pneumatic controller, C1. The thermocouple, T2, is used for data logging and on/off control.

ORIGINAL PAGE IS
OF POOR QUALITY

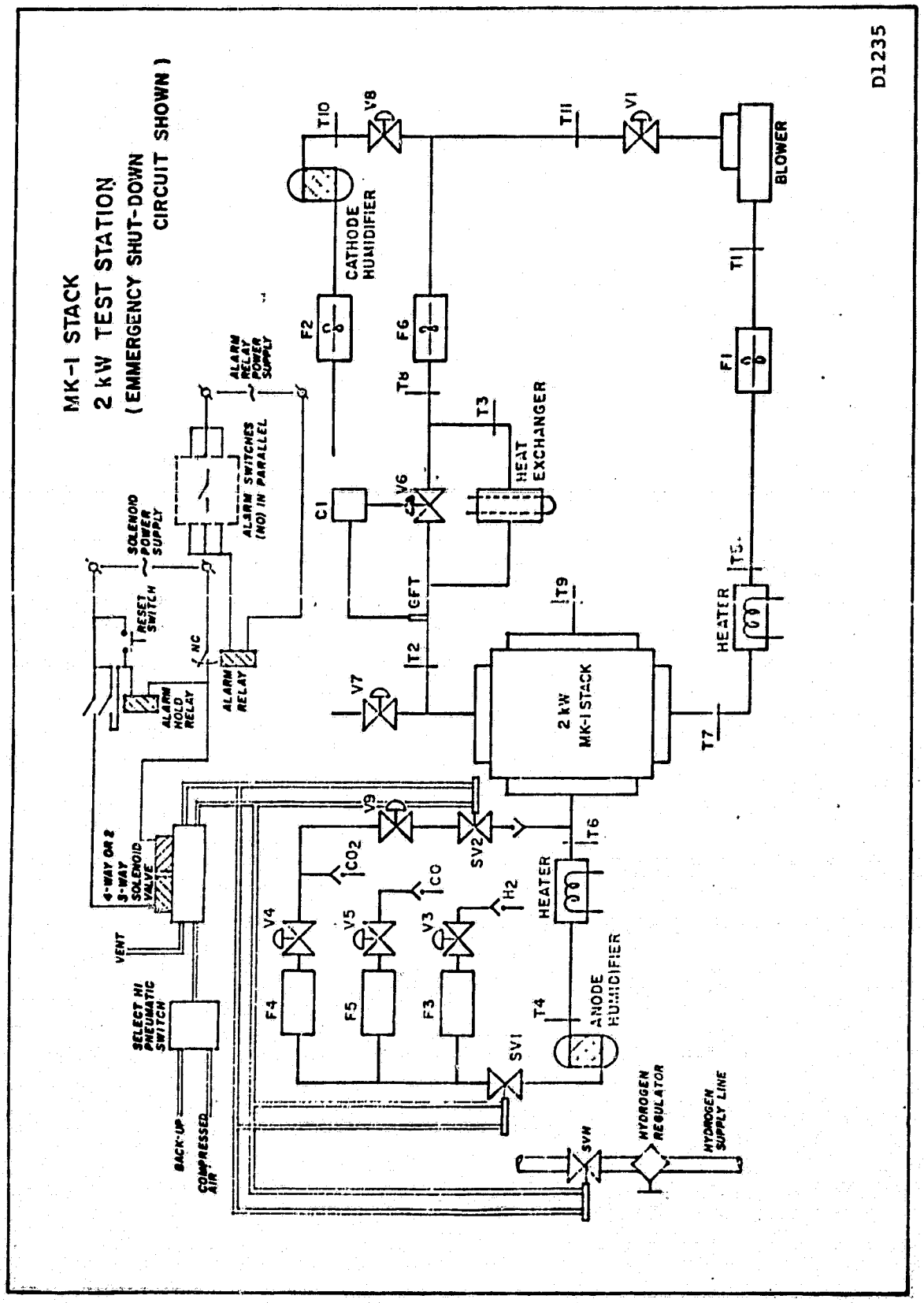

Figure 5.4.2. 2 kW Test station for MK-1 stacks, (emergency shut-down circuit shown)

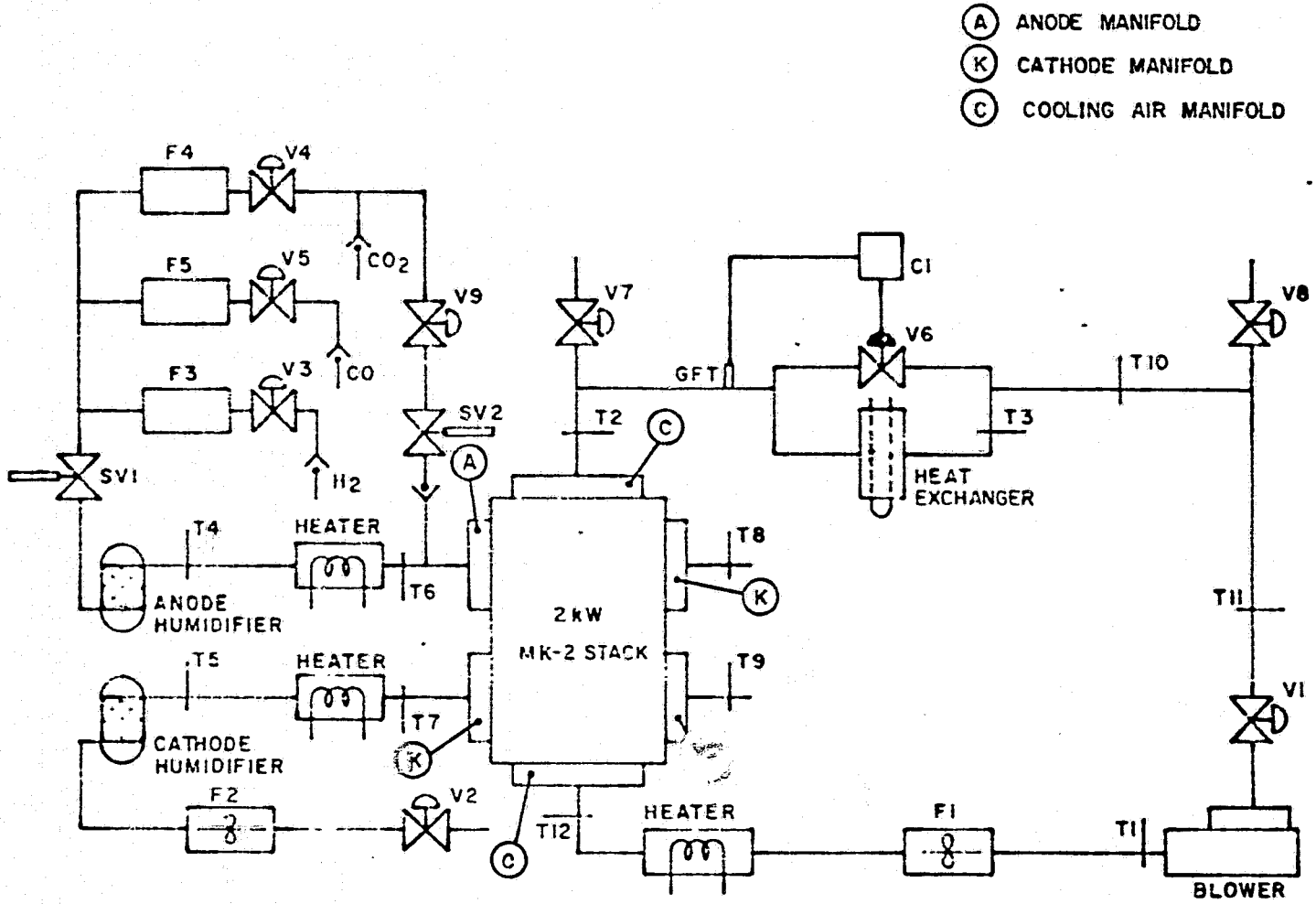

D1101

ORIGINAL PAGE IS OF POOR QUALITY

FIGURE 5.4.3. MK-2 STACK 2 KW TEST STATION

ORIGINAL PAGE IS
OF POOR QUALITY

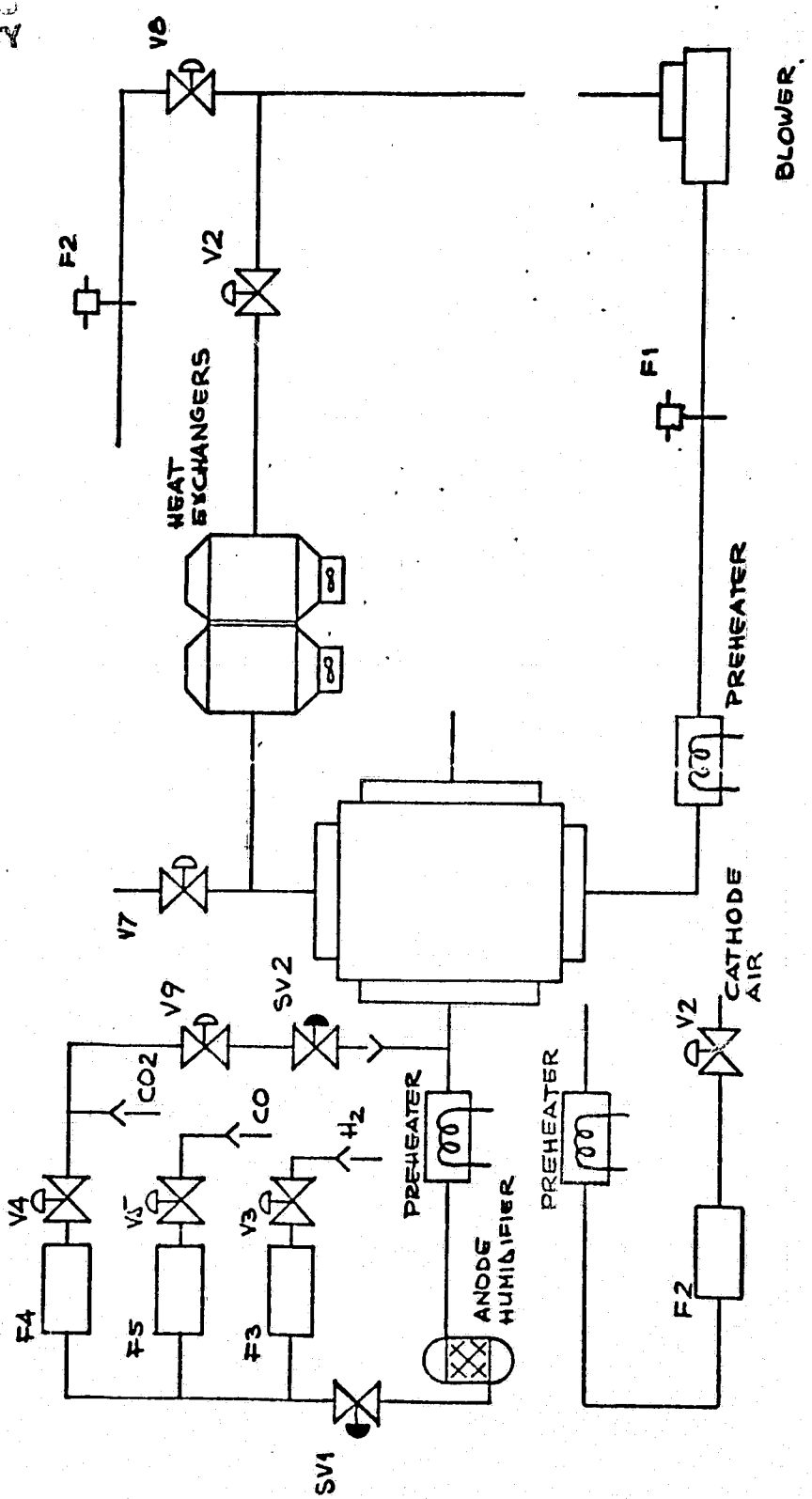

FIGURE 5.4.4. 8 kW TEST STATION

Figure 5.4.3 is a schematic of the 2 kW flow loop configured for stacks with separated air cooling. The makeup (or process air) is fed directly to the separate cathode inlet manifold and all cathode products are vented from the stack. Valves V7 and V8 are retained to vent air from the recycle line during warmup and to provide makeup for any air leakage respectively.

5.4.2 8 kW Test Facility

As shown by the schematic diagram in Figure 5.4.4, the 8 kW test facility has the same salient features as the separated gas cooling configuration of the 2 kW test station. Minor modifications and improvements made for this station were:

- The air blower motor solid state speed control increased the blower turn-down ratio resulting in better control of the recirculating flow.
- Air-to-air heat exchangers were used to cool the recirculating stream instead of the combination of the air-to-water heat exchanger, its controller and the bypass loop to increase controlability and eliminate the possibility of water leaking into the air stream.

The 8 kW test station is capable of operating over the following flow ranges.

	Flow Ranges SLPM (SCFM)		
	Nom.	Max.	Min.
Hydrogen	113 (4)	340 (12)	14 (0.5)
Carbon Dioxide	28 (1)	113 (4)	14 (0.5)
Carbon Monoxide	-	14 (0.5)	0
Air Makeup (Mk-1)	566 (20)	11,300 (400)	425 (15)
Loop Air	7080 (250)	15,600 (550)	1700 (60)
Process Air (Mk-2)	453 (16)	850 (30)	28 (1)

ORIGINAL PAGE IS
OF POOR QUALITY

TABLE 5.4.1 DAS PRINTOUT FOR STACK 800

#800 DATE 11:19 TIME 16:43

CURRENT OUTPUT Amps	190.33	OXYGEN IN,%	21.00
STACK VOLTAGE Volts	43.99	OXYGEN OUT,%	10.50
POWER OUTPUT Wats	8373.00	CATHODE WATER OUT,%vol	.43
ANODE TOTAL FLOW,SCFM	7.1	COOLING FLOW,SCFM	169.5
HYDROGEN %	80.7	MAKE-UP %	0.0
CARBON DIOXIDE %	19.3	RECYCLE %	100.0
CARBON MONOXIDE %	.0	PROCESS FLOW,SCFM	17.4
UTILIZATION %	70.8	UTILIZATION %	55.6

CELL VOLTAGES

CC	-.043						
01	.573			41	.602	61	.603
02	.584			42	.576	62	.569
03	.571			43	.593	63	.586
04	.572			44	.586	64	.602
05	.579			45	.575	65	.588
CP01	.003	CP05	-.003	CP09	.004	CP13	-.004
06	.546	26	.613	46	.568	66	.585
07	.588	27	.593	47	.573	67	.584
08	.607	28	.600	48	.585	68	.597
09	.582	29	.600	49	.583	69	.591
10	.584	30	.604	50	.585	70	.580
CP02	-.004	CP06	-.004	CP10	-.010	CP14	-.006
11	.592	31	.594	51	.599	71	.601
12	.584	32	.605	52	.582	72	.597
13	.671	33	.596	53	.595	73	.582
14	.496	34	.601	54	.594	74	.580
15	.603	35	.593	55	.593	75	.581
CP03	-.004	CP07	-.004	CP11	-.004	CP15	-.009
16	.586	36	.583	56	.600	76	.576
17	.583	37	.592	57	.587	77	.586
18	.597	38	.607	58	.597	78	.576
19	.602	39	.599	59	.593	79	.580
20	.599	40	.597	60	.602	80	.569
CP04	-.004	CP08	-.004	CP12	-.007	CP	
						CC	-.212

STACK TEMPERATURES

140	132.2	155	197.7	170	160.3	185	171.0
141	147.7	156	174.1	171	177.4	186	173.5
142	165.4	157	173.7	172	186.2	187	128.9
143	167.0	158	191.8	173	190.7	188	151.8
144	173.9	159	131.1	174	178.7	189*	.9
145	137.3	160*	.9	175	194.4	190	166.8
146	152.7	161	163.2	176	188.2	191	179.9
147	161.3	162	162.2	177	143.5	192*	.9
148	169.6	163	182.3	178*	.9	193	177.7
149	147.9	164*	.9	179	182.3	194	129.7
150	179.3	165	175.7	180	183.4	195	163.0
151	176.1	166	192.7	181	195.3	196	77.2
152	191.7	167	191.2	182	131.4	197	164.4
153	187.8	168	123.9	183	151.5	198	136.5
154	152.4	169	157.0	184	170.6	199	119.7

*Broken thermocouples

5.4.3 Automatic Data Acquisition and Control

A computerized system for acquiring, processing, and displaying operational data was developed for and shared by the 2 kW and 8 kW test loops. The system also provided automatic control of the test conditions, and alarms and automatic shutdown procedures in case some malfunction produced an out-of-limits operating condition. The operating parameters which were controlled and recorded and the measurements which were recorded are listed in Subsection 5.4.1.

Table 5.4.1 is a sample printout of stack and individual cell performance for Stack 800 operating at 8373 watts at a utilization of 70.8% on a fuel containing 19.3% CO_2. Table 5.4.2 is a printout of individual cell steady state and transient OCV's for Stack 800.

The alarm and control features of the computerized system were used to provide the safety and stack protection features listed in Subsection 5.4.1.

5.5 Pretest of Subscale Stack

The objective of this task was to verify the performance of and correct any problems of the subscale stack (Stack 800) prior to its performance tests. Stack 800 was an 80 cell stack of the Mk-2 design and was the culmination of the stack development of Phase II of the OS/IES program.

The initial OCV tests indicated that all cells except 24 were performing well. Two alternative courses of action to correct the Cell 24 problem were evaluated. The first was to replace the defective cell and the second was to bypass it by means of a low-resistance external short. The second route was chosen since it was an opportunity to develop a method of repair that could later be applied in the field. The 5-cell pack containing Cell 24 was shorted out by taking advantage of the structure of the cooling plates. Teflon-insulated copper jumper cables were inserted in the channels of the cooling plates bounding the pack. This, in effect, converted the stack to a 75-cell stack. Pretesting was resumed following

ORIGINAL PAGE IS
OF POOR QUALITY.

Table 5.4.2. OCV Printout for stack 800.

OCV #800 DATE 11:20 TIME 09:03

	AIR ON FUEL ON	AIR OFF FUEL ON (1 min*)		AIR ON FUEL OFF (1 min*)		AIR OFF FUEL OFF (1min*	
01	.000	.000	.000	.000	.000	.000	.000
02	.913	.911	.903 6	.909	.891	.905	.892
03	.900	.897	.887 10	.893	.874	.890	.871
04	.915	.913	.903 10	.910	.889	.906	.887
05	.904	.901	.889 12	.894	.873	.887	.867
06	.919	.916	.906 10	.912	.893	.907	.889
07	-.000	-.000	-.000	-.000	0.000	-.000	-.000
08	.922	.921	.918 3	.919	.896	.912	.895
09	.896	.893	.878 15	.890	.876	.886	.869
10	.921	.918	.909 9	.914	.899	.909	.895
11	.893	.891	.873 16	.887	.868	.885	.859
12	.911	.909	.898 11	.905	.894	.901	.889
13	.000	.000	.000	.000	.000	.000	.000
14	.915	.912	.899 13	.907	.892	.902	.889
15	.915	.913	.904 9	.908	.892	.900	.886
16	.977	.970	.945 25	.955	.961	.944	.935
17	.797	.795	.784 11	.790	.769	.783	.754
18	.916	.913	.902 11	.909	.905	.905	.895
19	-.000	-.000	.000	0.000	-.000	.000	-.000
20	.919	.917	.905 12	.912	.909	.909	.900
21	.889	.886	.869 17	.882	.881	.877	.864
22	.895	.892	.878 14	.887	.884	.882	.869
23	.868	.865	.832 33	.858	.855	.852	.819
24	.881	.881	.877 4	.878	.880	.874	.872
25	-.001	-.000	-.000	-.000	-.000	-.000	.000
26	.022	.012	.003	.019	.028	.014	-.007
27	.020	.019	.005	.008	.011	.011	.011
28	-.009	-.008	-.003	-.003	-.024	-.007	-.010
29	-.030	-.026	-.009	-.015	-.019	-.022	-.004
30	.013	.011	.006	.003	.007	.013	.011
31	-.000	-.000	-.000	.000	-.000	.000	-.000
32	.911	.906	.879 27	.903	.902	.902	.891
33	.920	.917	.898 19	.914	.919	.913	.907
34	.887	.883	.863 20	.877	.874	.872	.858
35	.923	.922	.902 20	.921	.921	.920	.912
36	.909	.906	.889 17	.903	.902	.900	.893
37	-.000	-.000	-.000	-.000	0.000	.000	.000
38	.898	.895	.879 16	.892	.890	.889	.881
39	.929	.926	.907 19	.924	.924	.922	.915
40	.928	.927	.910 17	.927	.926	.926	.919
41	.933	.934	.915 19	.932	.932	.932	.922
42	.915	.914	.896 18	.912	.911	.911	.903
43	-.000	.000	-.000	-.000	.000	0.000	.000
44	.948	.949	.927 22	.942	.942	.935	.922
45	.938	.941	.922 19	.938	.939	.942	.933
46	.923	.916	.875 41	.909	.907	.894	.882
47	.892	.887	.862 25	.883	.887	.872	.869
48	.938	.938	.922 16	.931	.928	.928	.917
49	.000	.000	.000	0.000	0.000	-.000	-.000
50	.905	.903	.886 17	.899	.897	.896	.887
51	.913	.911	.897 14	.903	.902	.899	.893
52	.887	.883	.861 22	.873	.874	.862	.848
53	.900	.897	.876 21	.887	.886	.880	.864

*Data taken 1 min. after one reactant or both reactants were shut off.

5.4.3 Automatic Data Acquisition and Control

A computerized system for acquiring, processing, and displaying operational data was developed for and shared by the 2 kW and 8 kW test loops. The system also provided automatic control of the test conditions, and alarms and automatic shutdown procedures in case some malfunction produced an out-of-limits operating condition. The operating parameters which were controlled and recorded and the measurements which were recorded are listed in Subsection 5.4.1.

Table 5.4.1 is a sample printout of stack and individual cell performance for Stack 800 operating at 8373 watts at a utilization of 70.8% on a fuel containing 19.3% CO_2. Table 5.4.2 is a printout of individual cell steady state and transient OCV's for Stack 800.

The alarm and control features of the computerized system were used to provide the safety and stack protection features listed in Subsection 5.4.1.

5.5 Pretest of Subscale Stack

The objective of this task was to verify the performance of and correct any problems of the subscale stack (Stack 800) prior to its performance tests. Stack 800 was an 80 cell stack of the Mk-2 design and was the culmination of the stack development of Phase II of the OS/IES program.

The initial OCV tests indicated that all cells except 24 were performing well. Two alternative courses of action to correct the Cell 24 problem were evaluated. The first was to replace the defective cell and the second was to bypass it by means of a low-resistance external short. The second route was chosen since it was an opportunity to develop a method of repair that could later be applied in the field. The 5-cell pack containing Cell 24 was shorted out by taking advantage of the structure of the cooling plates. Teflon-insulated copper jumper cables were inserted in the channels of the cooling plates bounding the pack. This, in effect, converted the stack to a 75-cell stack. Pretesting was resumed following

ORIGINAL PAGE IS
OF POOR QUALITY

Table 5.4.2. OCV Printout for stack 800.

OCV #800 DATE 11:20 TIME 09:03

	AIR ON FUEL ON	AIR OFF FUEL ON (1 min*)		AIR ON FUEL OFF (1 min*)		AIR OFF FUEL OFF (1min)	
01	.000	.000	.000	.000	.000	.000	.000
02	.913	.911	.903 8	.909	.891	.905	.892
03	.900	.897	.887 10	.893	.874	.890	.871
04	.915	.913	.903 10	.910	.889	.906	.887
05	.904	.901	.889 12	.894	.873	.887	.867
06	.919	.916	.906 10	.912	.893	.907	.889
07	-.000	-.000	-.000	-.000	0.000	-.000	-.000
08	.922	.921	.918 3	.919	.896	.912	.895
09	.896	.893	.878 15	.890	.876	.886	.869
10	.921	.918	.909 9	.914	.899	.909	.895
11	.893	.891	.873 16	.887	.868	.885	.859
12	.911	.909	.898 11	.905	.894	.901	.889
13	.000	.000	.000	.000	.000	.000	.000
14	.915	.912	.899 13	.907	.892	.902	.889
15	.915	.913	.904 9	.908	.892	.900	.886
16	.977	.970	.945 25	.955	.961	.944	.935
17	.797	.795	.784 11	.790	.769	.783	.754
18	.916	.913	.902 11	.909	.905	.905	.895
19	-.000	-.000	.000	0.000	-.000	.000	-.000
20	.919	.917	.905 12	.912	.909	.909	.900
21	.889	.886	.869 17	.882	.881	.877	.864
22	.895	.892	.876 16	.887	.884	.882	.869
23	.868	.865	.832 33	.858	.855	.852	.819
24	.881	.881	.877 4	.878	.880	.874	.872
25	-.001	-.000	-.000	-.000	-.000	-.000	.000
26	.022	.012	.003	.019	.028	.014	-.007
27	.020	.019	.005	.008	.011	.011	.011
28	-.009	-.008	-.003	-.003	-.024	-.007	-.010
29	-.030	-.026	-.009	-.015	-.019	-.022	-.004
30	.013	.011	.006	.003	.007	.013	.011
31	-.000	-.000	-.000	.000	-.000	.000	-.000
32	.911	.906	.879 27	.903	.902	.902	.891
33	.920	.917	.898 19	.914	.919	.913	.907
34	.887	.883	.863 20	.877	.874	.872	.858
35	.923	.922	.902 20	.921	.921	.920	.912
36	.909	.906	.889 17	.903	.902	.900	.893
37	-.000	-.000	-.000	-.000	0.000	.000	.000
38	.898	.895	.879 16	.892	.890	.889	.881
39	.929	.926	.907 19	.924	.924	.922	.915
40	.928	.927	.910 17	.927	.926	.926	.919
41	.933	.934	.915 19	.932	.932	.932	.922
42	.915	.914	.896 18	.912	.911	.911	.903
43	-.000	.000	-.000	-.000	.000	0.000	.000
44	.948	.949	.927 22	.942	.942	.935	.922
45	.938	.941	.922 19	.938	.939	.942	.933
46	.923	.916	.875 41	.909	.907	.894	.882
47	.892	.887	.862 25	.883	.887	.872	.869
48	.938	.938	.922 16	.931	.928	.928	.917
49	.000	.000	.000	0.000	0.000	-.000	-.000
50	.905	.903	.886 17	.899	.897	.896	.887
51	.913	.911	.897 14	.903	.902	.899	.893
52	.887	.883	.861 22	.873	.874	.862	.848
53	.900	.897	.876 21	.887	.886	.880	.864

*Data taken 1 min. after one reactant or both reactants were shut off.

ORIGINAL PAGE IS
OF POOR QUALITY

TABLE 5.4.2 OCV PRINTOUT FOR STACK 800 (Continued)

54	.904	.901	.883 18	.894	.894	.889	.87
55	-.000	-.000	-.000	-.000	-.000	-.000	-.00
56	.908	.906	.884 22	.900	.900	.895	.87
57	.895	.892	.874 18	.885	.881	.879	.86
58	.902	.897	.868 24	.895	.893	.890	.88
59	.912	.910	.893 17	.896	.890	.881	.86
60	.932	.932	.915 17	.927	.927	.924	.91
61	-.000	0.000	-.000	.000	.000	.000	.00
62	.902	.898	.872 26	.886	.887	.874	.85
63	.931	.931	.917 14	.928	.927	.925	.91
64	.919	.917	.899 18	.912	.912	.910	.90
65	.937	.936	.920 16	.933	.933	.932	.92
66	.941	.942	.929 13	.941	.940	.938	.92
67	.000	.000	.000	.000	.000	.000	.00
68	.937	.937	.922 15	.932	.932	.930	.92
69	.883	.879	.853 26	.869	.869	.858	.83
70	.925	.924	.907 17	.918	.889	.912	.87
71	.924	.922	.901 21	.912	.910	.903	.88
72	.936	.936	.921 15	.932	.933	.931	.92
73	.000	.000	.000	.000	.000	.000	.00
74	.938	.939	.919 20	.936	.938	.937	.92
75	.938	.939	.933 6	.938	.938	.937	.92
76	.891	.888	.870 18	.880	.878	.871	.85
77	.935	.934	.911 23	.930	.932	.928	.91
78	.940	.942	.928 14	.940	.941	.942	.93
79	.000	.000	.000	.000	.000	.000	.00
80	.939	.938	.910 28	.927	.930	.921	.91
81	.946	.947	.924 23	.944	.947	.947	.94
82	.939	.939	.923 16	.931	.928	.921	.90
83	.929	.927	.911 16	.923	.922	.919	.90
84	.922	.919	.899 20	.908	.906	.895	.87
85	-.000	.000	-.000	.000	.000	.000	.00
86	.942	.944	.932 12	.942	.942	.942	.93
87	.927	.927	.912 15	.921	.921	.919	.91
88	.936	.933	.900 33	.929	.934	.934	.92
89	.929	.930	.914 14	.924	.924	.923	.91
90	.934	.933	.920 13	.928	.927	.926	.91
91	.000	.000	.000	.000	.000	.000	.00
92	.925	.923	.915 8	.917	.916	.912	.90
93	.934	.932	.919 13	.925	.925	.922	.91
94	.928	.926	.909 17	.918	.915	.908	.89
95	.932	.932	.922 10	.929	.903	.920	.89
96	.931	.929	.913 16	.922	.923	.920	.91
97	-.000	-.000	-.000	-.000	-.000	-.000	-.00
TOTAL	68.790	68.670	67.370	68.260	67.950	67.950	66.97

OCV #800 DATE 11:20 TIME 09:03

ORIGINAL PAGE IS
OF POOR QUALITY

TABLE 5.5.1 INITIAL OCV TEST (STABLE AND TRANSIENT) FOR STACK 800

Cell No.	AIR ON FUEL ON	AIR OFF FUEL ON	1 MIN*	AIR ON FUEL OFF	1 MIN*	AIR OFF FUEL OFF	1 MIN*
1	0.913	0.911	0.903	0.909	0.891	0.905	0.892
2	0.900	0.897	0.887	0.893	0.874	0.890	0.871
3	0.915	0.913	0.903	0.910	0.889	0.906	0.887
4	0.904	0.901	0.889	0.894	0.873	0.887	0.867
5	0.919	0.916	0.906	0.912	0.893	0.907	0.889
6	0.922	0.921	0.918	0.919	0.896	0.912	0.895
7	0.896	0.893	0.878	0.890	0.876	0.886	0.869
8	0.921	0.918	0.909	0.914	0.899	0.909	0.895
9	0.893	0.891	0.873	0.887	0.868	0.885	0.859
10	0.911	0.909	0.898	0.905	0.894	0.901	0.889
11	0.915	0.912	0.899	0.907	0.892	0.902	0.889
12	0.915	0.913	0.904	0.908	0.892	0.900	0.886
13	0.977	0.970	0.945	0.955	0.961	0.944	0.935
14	0.797	0.795	0.784	0.790	0.769	0.783	0.754
15	0.916	0.913	0.902	0.909	0.905	0.905	0.895
16	0.919	0.917	0.905	0.912	0.909	0.909	0.900
17	0.889	0.886	0.869	0.882	0.881	0.877	0.864
18	0.895	0.892	0.878	0.887	0.884	0.882	0.869
19	0.868	0.865	0.832	0.858	0.855	0.852	0.819
20	0.881	0.881	0.877	0.878	0.880	0.874	0.872
26	0.911	0.906	0.879	0.903	0.902	0.902	0.891
27	0.920	0.917	0.898	0.914	0.919	0.913	0.907
28	0.887	0.883	0.863	0.877	0.874	0.872	0.858
29	0.923	0.922	0.902	0.921	0.921	0.920	0.912
30	0.909	0.906	0.889	0.903	0.902	0.900	0.893
31	0.898	0.895	0.879	0.892	0.890	0.889	0.881
32	0.929	0.926	0.907	0.924	0.924	0.922	0.915
33	0.928	0.927	0.910	0.927	0.926	0.926	0.919
34	0.933	0.934	0.915	0.932	0.932	0.932	0.922
35	0.915	0.914	0.896	0.912	0.911	0.911	0.903
36	0.948	0.949	0.927	0.942	0.942	0.935	0.922
37	0.938	0.941	0.922	0.938	0.939	0.942	0.933
38	0.923	0.916	0.875	0.909	0.907	0.894	0.882
39	0.892	0.887	0.862	0.883	0.887	0.872	0.869
40	0.938	0.938	0.922	0.931	0.928	0.928	0.917
41	0.905	0.903	0.886	0.899	0.897	0.896	0.887
42	0.913	0.911	0.897	0.903	0.902	0.899	0.893
43	0.887	0.883	0.861	0.873	0.874	0.862	0.848
44	0.900	0.897	0.876	0.887	0.886	0.880	0.864
45	0.904	0.901	0.883	0.894	0.894	0.889	0.879
46	0.908	0.906	0.884	0.900	0.900	0.895	0.878
47	0.895	0.892	0.874	0.885	0.881	0.879	0.865
48	0.902	0.897	0.868	0.895	0.893	0.890	0.880
49	0.912	0.910	0.893	0.896	0.890	0.881	0.864
50	0.932	0.932	0.915	0.927	0.927	0.924	0.915
51	0.902	0.898	0.872	0.886	0.887	0.874	0.859
52	0.931	0.931	0.917	0.928	0.927	0.925	0.913

this solution and the stack performance verified the viability of the repair method.

The cell by cell steady and transient OCV's are given in Table 5.5.1 with data from the shorted cells (Nos. 21-25) deleted. The pretest cell by cell performance at 150 mA/cm^2 with 80% H_2, 20% CO_2 and air are given in Table 5.5.2. The stack polarization characteristics are compared to those of Stack 562 (a 23-cell Mk-2 stack) in Figure 5.5.1. The two polarization curves are almost identical, showing that the scaling up to 8 kW was successful and that cell performance reproducibility was achieved. Performance data for the stack at 186 mA/cm^2 (190 A) are given in Table 5.4.1. At this load, the stack gave a power output of 111 W/cell which is well above the Phase II performance goal of 90 W/cell.

5.6 Subscale Stack Performance Testing

The objectives of Stack 800 performance tests were to:

1. Determine performance of cells in a scaled up (larger number of cells) stack under various operating conditions.
2. Verify the ability of the treed cooling channels to achieve cell temperature differentials substantially smaller than the cooling air temperature rise in a scaled up stack.

Stack 800 was installed and testing begun with 75 operating cells since five of the original 80 cells had been shorted and sealed as described in Section 5.5. At the end of the second test listed in Table 5.6, the water level regulator for the fuel humidification chamber malfunctioned causing water to be introduced into the fuel inlet manifold and flooding the bottom group of 5 cells. After the water was drained from the manifolds, attempts to dry and resupply acid to these cells failed to restore performance. The bottom group of 5 cells was then shorted and tests were completed with 70 operating cells. The method used for shorting was similar to that employed during pretesting but,

ORIGINAL PAGE IS
OF POOR QUALITY

TABLE 5.5.1 Continued

Cell No.	AIR ON FUEL ON	AIR OFF FUEL ON	1 MIN *	AIR ON FUEL OFF	1 MIN *	AIR OFF FUEL OFF	1 MIN *
53	0.919	0.917	0.899	0.912	0.912	0.910	0.900
54	0.937	0.936	0.920	0.933	0.933	0.932	0.920
55	0.941	0.942	0.929	0.941	0.940	0.938	0.929
56	0.937	0.937	0.922	0.932	0.932	0.930	0.922
57	0.883	0.879	0.853	0.869	0.869	0.858	0.835
58	0.925	0.924	0.907	0.918	0.889	0.912	0.877
59	0.924	0.922	0.901	0.912	0.910	0.903	0.887
60	0.936	0.936	0.921	0.932	0.933	0.931	0.920
61	0.938	0.939	0.919	0.936	0.938	0.937	0.924
62	0.938	0.939	0.933	0.938	0.938	0.937	0.928
63	0.891	0.888	0.870	0.880	0.878	0.871	0.853
64	0.935	0.934	.911	0.930	0.932	0.928	0.919
65	0.940	0.942	0.928	0.940	0.941	0.942	0.933
66	0.939	0.938	0.910	0.927	0.930	0.921	0.911
67	0.946	0.947	0.924	0.944	0.947	0.947	0.940
68	0.939	0.939	0.923	0.931	0.928	0.921	0.902
69	0.929	0.927	0.911	0.923	0.922	0.919	0.907
70	0.922	0.919	0.899	0.909	0.906	0.895	0.876
71	0.942	0.944	0.932	0.942	0.942	0.942	0.934
72	0.927	0.927	0.912	0.921	0.921	0.919	0.911
73	0.936	0.933	0.900	0.929	0.934	0.934	0.929
74	0.929	0.930	0.914	0.924	0.924	0.923	0.913
75	0.934	0.933	0.920	0.928	0.927	0.926	0.918
76	0.925	0.923	0.915	0.917	0.916	0.912	0.907
77	0.934	0.932	0.919	0.925	0.925	0.922	0.914
78	0.928	0.926	0.909	0.918	0.915	0.908	0.894
79	0.932	0.932	0.922	0.929	0.903	0.920	0.893
80	0.931	0.929	0.913	0.922	0.923	0.920	0.911
TOTAL	68.79	68.67	67.37	68.26	67.95	67.95	66.97

*Data taken the minute after either one reactant or both reactants were shut off.

ORIGINAL PAGE IS
OF POOR QUALITY

TABLE 5.5.2

BASELINE PERFORMANCE OF STACK 800 at ∿150 mA/cm^2

Cell No.	Cell Voltage, V	Cell No.	Cell Voltage, V	Cell No.	Cell Voltage, V
1	0.615	31	0.633	56	0.633
2	0.624	32	0.637	57	0.625
3	0.615	33	0.633	58	0.635
4	0.614	34	0.636	59	0.630
5	0.623	35	0.634	60	0.637
6	0.598	36	0.622	61	0.637
7	0.631	37	0.630	62	0.611
8	0.639	38	0.641	63	0.628
9	0.627	39	0.636	64	0.638
10	0.626	40	0.636	65	0.627
11	0.631	41	0.638	66	0.622
12	0.625	42	0.621	67	0.623
13	0.665	43	0.634	68	0.630
14	0.583	44	0.628	69	0.628
15	0.638	45	0.622	70	0.619
16	0.625	46	0.620	71	0.633
17	0.620	47	0.628	72	0.630
18	0.628	48	0.630	73	0.621
19	0.638	49	0.624	74	0.619
20	0.624	50	0.624	75	0.620
26	0.637	51	0.637	76	0.616
27	0.624	52	0.624	77	0.622
28	0.633	53	0.632	78	0.612
29	0.631	54	0.637	79	0.617
30	0.639	55	0.633	80	0.613

Total Voltage, V	46.93
Avg. Cell Voltage, V	.626
Load, A	149
H_2 Utilization, %	53.2
No. Stoich Process Air	2.48
No. Stoich Cooling Air	27.0

DATE: 11-20-81
TIME: 3:59
HRS. OPERATION: 15

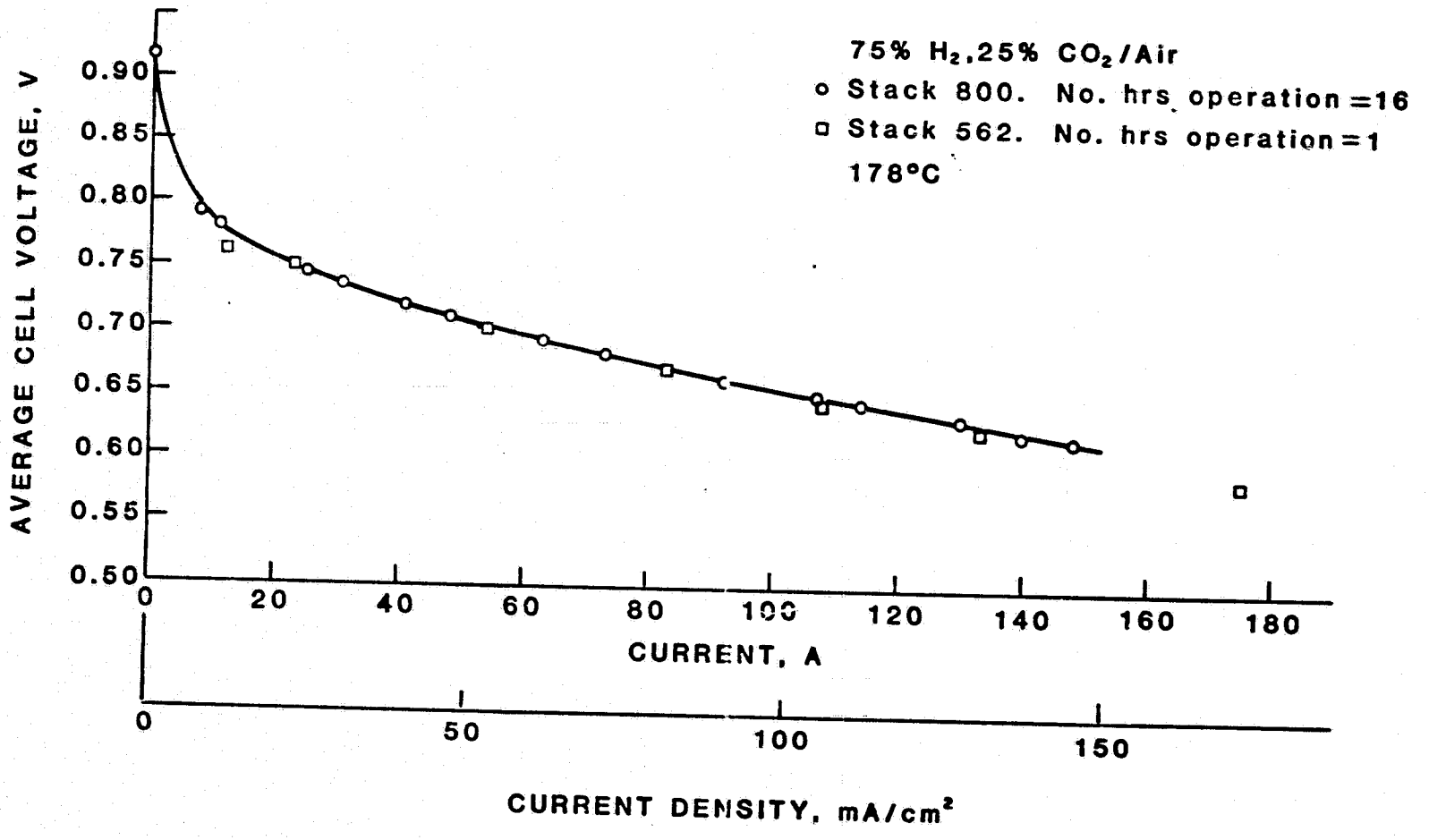

FIGURE 5.5.1 STACK POLARIZATION COMPARISON

ORIGINAL PAGE IS
OF POOR QUALITY

ORIGINAL PAGE IS
OF POOR QUALITY

TABLE 5.6 – SUMMARY OF TEST CONDITIONS AND TEST RESULTS FOR STACK 800

Test	Current Density mA/cm^2	Volts/ Cell V	Average Temperature °C	Peak to Average Gradient °C	Fuel Utilization	Dry H_2 Inlet Fraction	Dry CO Inlet Mole Fraction	Fuel Inlet Temperature °C	Process Air Stoichs	Process Air Inlet Temperature °C	Cooling Air Flow g/sec	Cooling Air Inlet Temperature °C	Cooling Air Temperature Rise, °C	Process Air Pressure Drop cmH_2O	Cooling Air Pressure Drop cmH_2O
1	119	0.629	175	10.4	0.57	0.75	0	121	3.1	143	114.3	133	34	11.1	3.51
2	119	0.583	171	11.7	0.57	0.75	0	127	3.1	139	114.2	120	42	11.2	3.65
3	150	0.595	171	12.2	0.59	0.75	0	161	4.0	154	119.0	116	47	18.3	4.25
4	150	0.595	172	11.2	0.70	0.75	0	162	3.0	163	119.0	116	48	13.9	4.28
5	150	0.587	174	13.0	0.75	0.75	0	163	2.0	158	119.0	116	48	9.02	4.28
6	150	0.591	172	10.6	0.71	0.75	0	155	3.0	151	127.0	112	52	13.7	4.52
7	150	0.592	173	11.0	0.71	0.75	0	156	3.0	141	127.0	113	53	14.0	4.48
8	50	0.686	179	5.7	0.72	0.75	0	145	3.0	148	78.0	156	19	5.03	2.37
9	100	0.631	173	11.7	0.70	0.75	0	150	3.2	145	75.3	119	52	9.53	2.35
10	200	0.559	173	13.6	0.67	0.75	0	154	3.0	142	148.0	99	64	19.3	5.72
11	100	0.605	157	10.2	0.72	0.75	0	150	2.0	149	78.0	98	55	6.10	2.30
12	100	0.617	160	12.1	0.71	0.75	0	150	2.0	148	79.0	110	54	6.27	2.40
13	100	0.626	175	8.9	0.71	0.75	0	150	2.0	145	79.4	120	52	6.35	2.41
14	50	0.684	149	9.7	0.56	0.79	0	147	2.0	149	79.4	122	24	3.35	2.34
15	50	0.643	149	9.1	0.70	0.75	0	146	2.0	145	79.4	122	24	3.35	2.34
16	50	0.[illegible]	159	8.4	0.69	0.75	0	147	2.0	146	79.8	131	24	3.21	2.36
17	50	0.670	156	4.5	0.76	0.75	0	146	3.0	152	79.8	130	23	5.00	2.36
18	50	0.678	166	4.3	0.76	0.75	0	146	3.0	146	77.6	142	20	5.04	2.35
19	150	0.587	149	10.1	0.71	0.75	0	155	3.0	148	129.0	85	56	13.3	4.68
20	150	0.579	156	9.3	0.70	0.75	0	155	3.0	142	128.0	95	54	13.3	4.72
21	150	0.589	164	9.4	0.70	0.75	0	157	3.0	145	128.0	105	53	13.5	4.72
22	150	0.597	173	10.4	0.70	0.75	0	156	3.0	142	127.0	115	52	13.1	4.72
23	200	0.529	150	13.0	0.71	0.75	0	155	3.0	142	156.0	74	63	17.9	6.22
24	200	0.541	158	10.8	0.72	0.75	0	156	3.0	140	156.0	74	62	17.7	6.60
25	200	0.558	165	11.9	0.72	0.75	0	155	3.0	150	156.0	95	60	17.9	6.32
26	200	0.563	164	13.5	0.72	1.00	0	150	3.0	142	156.0	98	59	17.9	6.32
27	200	0.561	175	13.8	0.72	0.75	0	156	3.0	144	151.0	104	61	18.0	6.10
28	100	0.610	150	8.7	0.70	0.75	0	154	3.0	139		93	54	8.53	2.47
29	100	0.619	158	8.9	0.70	0.75	0	154	3.0	148		109	53	8.76	2.58
30	100	0.627	169	10.3	0.70	0.75	0	154	3.0	146		116	51	8.84	2.52

ORIGINAL PAGE IS
OF POOR QUALITY

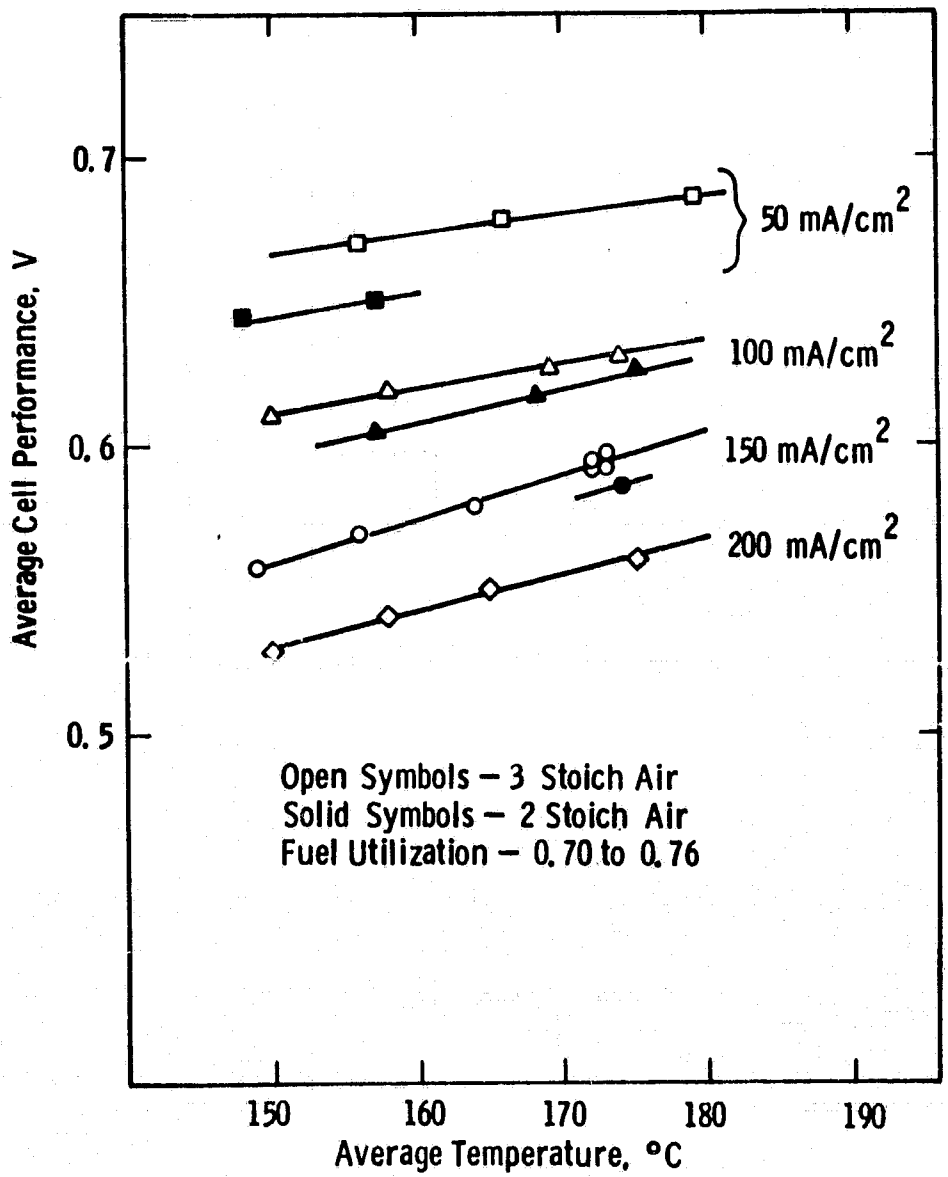

Fig. 5.6.1 – Performance of stack 800 as a function of temperature and current density

since it was done without removing the stack from the loop, validated the methods use as a field repair.

Test results and conditions for the 30 steady state tests are shown in Table 5.6.

5.6.1 Performance

Figure 5.6.1 shows the performance of Stack 800 with 2 and 3 stoichs of process air for current densities from 50 to 200 mA/cm^2. Performance at 2 stoichs was about 10 mV lower than at 3 stoichs. The temperature sensitivity ranges from .68 mV/°C at 50 mA/cm^2 to 1.28 mV/°C at 200 mA/cm^2. The cell performance was nominally 10 mV less than Stacks 562 and 564 under similar conditions.

5.6.2 Temperature Uniformity

Thermal instrumentation of Stack 800 consisted of a total of 56 thermocouples located alternately in eight of the 16 five cell groups between cooling plates. Locations along the cooling flow path and location relative to the fuel inlet edge of the stack were the same as those described in Subsection 5.3.1. A typical temperature distribution is shown in Figure 5.6.2 for 150 mA/cm^2 (Test 22). Locations of the data points are shifted the width of one symbol in the figure to separate symbols for the three distances from the fuel inlet edge of the stack. Temperatures near the fuel inlet were essentially the same as those near the fuel outlet and those along the stack centerline and there was no systematic trend from top to bottom of the stack.

The peak to average temperature gradient ranged from 5 to 14°C for tests with cooling air rise between 47 and 64°C at current densities from 50 to 200 mA/cm^2. These results are similar to those for Stacks 562 and 564.

ORIGINAL PAGE IS
OF POOR QUALITY

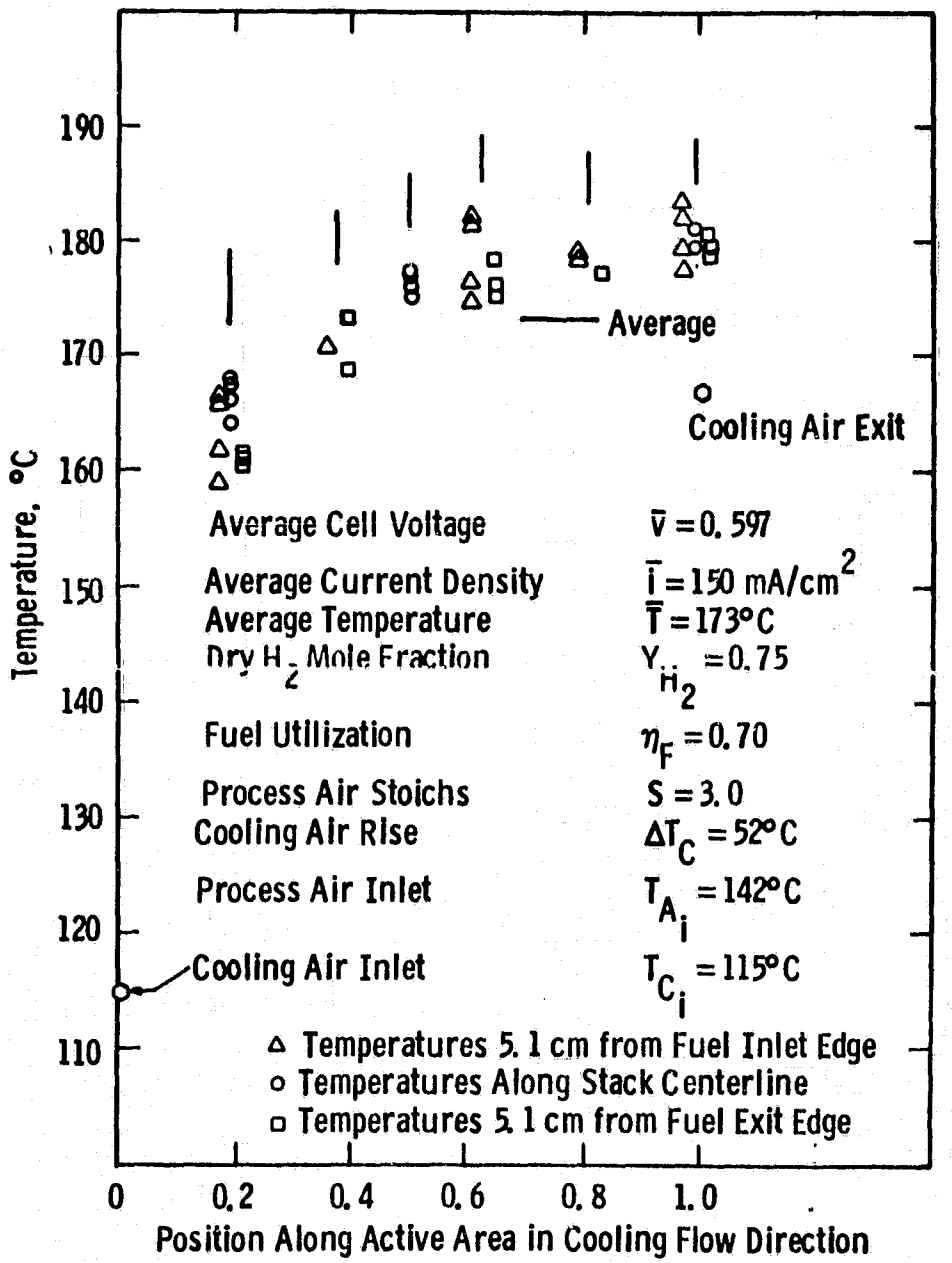

Fig. 5.6.2—Temperature distribution in Stack 800 – Test 22

5.6.3 Conclusions

The results of Stack 800 tests verified successful scaling up (increasing the number of cells) of separated gas cooled stacks. There were no measurable differences in cell temperature uniformity from those obtained in shorter (23 cell) stacks and cell performance was comparable to those obtained in the shorter stacks. In addition, the stack presented two opportunities to use the unique features of the cooling plates to bypass poorly performing cells and continue operation of the stack.

5.7 Full Scale Test Facility Design

The objective of this task was to prepare for the construction of a facility to test full scale OS/IES fuel cell modules during Phase III. As a result of the transfer of the program to AESD and switch in emphasis to power plants, no work was carried out on this subtask. The AESD did design and build facilities to test stacks of up to 30 kW under pressurized conditions.

ORIGINAL PAGE IS
OF POOR QUALITY

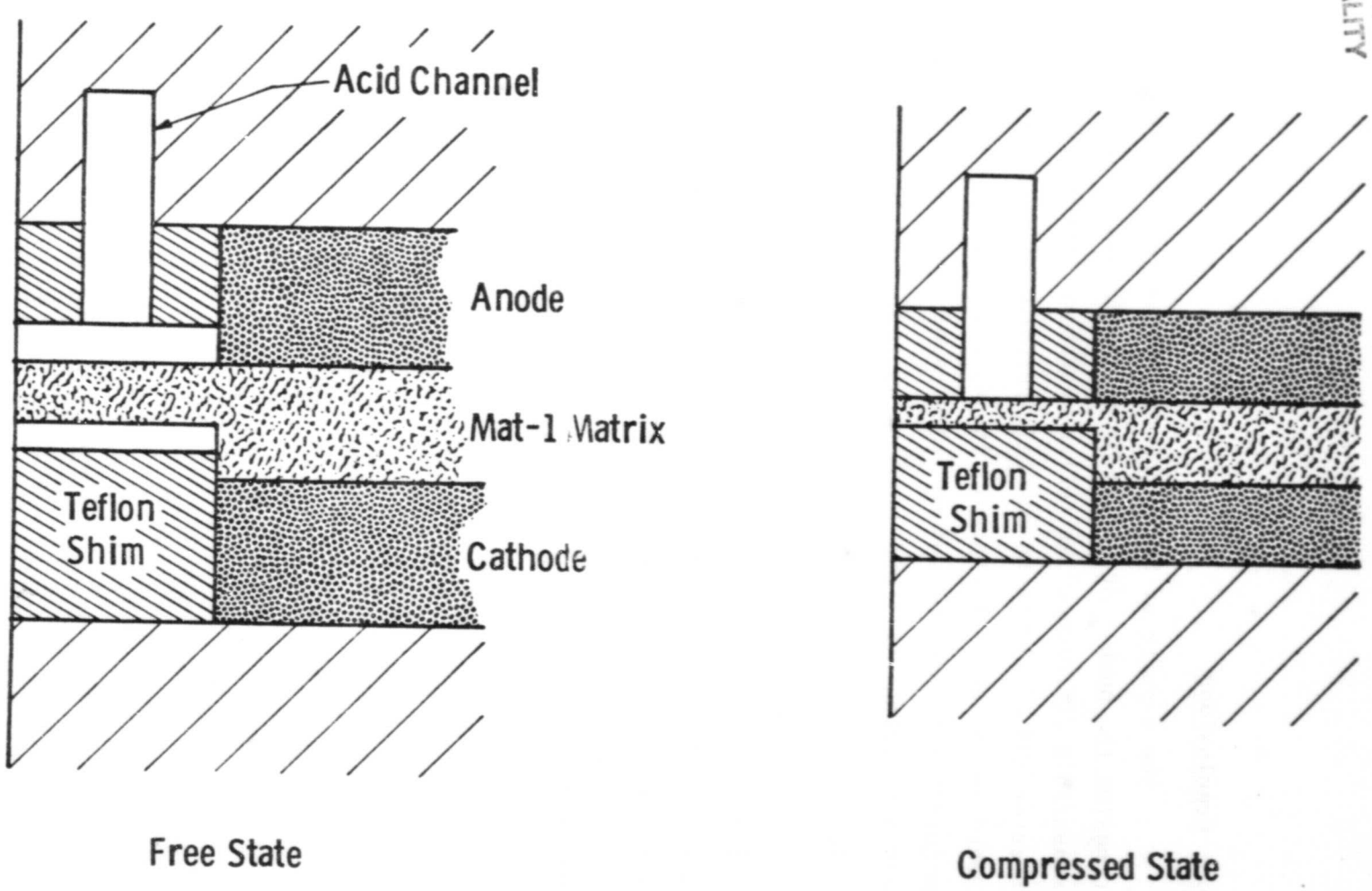

Fig. 5.8.1 —Cross section through a hypothetical phosphoric acid fuel cell before and after applying a compressive load

5.8 Material Characterization of Cell Components

Early in the design effort it became clear that more data on the thermal and mechanical properties of the cell materials was needed to evaluate new ideas, calculate contact forces between components, calculate the differential motion between stack and manifold and the resulting shear forces applied to the stack-to-manifold seal. The need for this data and the inadequacy of height change measurements made on developmental stacks is illustrated by the following example.

A cross-section through a hypothetical cell before and after compression is shown in Figure 5.8.1. The shims shown in this design seal the edges of the fuel cell to prevent intermixing of the reactant gases, act as mechanical stops to limit compression of the anode-matrix-cathode composite into the gas flow channels, and electrically insulate adjacent cells in the inactive area. If the thermal and mechanical properties of the repeating component materials are not available, the distribution of forces and their changes with time cannot be determined analytically and the correct thickness of these shims must be determined by trial and error for each design. During the development phase of a project, it is good engineering practice to design components so they can be readily changed to permit the evaluation of different configurations before committing to costly and long-lead time tooling. Once the development has been completed, it is equally good engineering practice to review and simplify the design (i.e., the functions of several components are combined into one component, or parts are eliminated and product cost is reduced). For example, the developmental design in Figure 5.8.1 may be simplified by increasing the thickness of the bipolar plate in the region occupied by the upper shim and eliminating the shim, reducing the thickness of the lower shim by increasing the thickness of the bipolar plate, and/or it may be eliminated by a coat of insulating material (such as a liquid fluoro-elastomer) on the raised portion of the bipolar plate. The availability of the basic thermal and mechanical properties of the components permits calculating and analyzing the dimensions of the revised bipolar plates and minimizing the experimentation required to evaluate new ideas.

ORIGINAL PAGE IS
OF POOR QUALITY

Dwg. 5600C18

TABLE 5.8.1 – SUMMARY OF LOAD VERSUS DEFORMATION COMPRESSION TEST DATA

Ref. Test #	Description of Test Specimen	Contact Surface Topography	A_N Area of Article Nominal mm^2	A_E Area of Article Effective mm^2	N Number of Specimens Per Test Article or Equivalent	L Height of Test Article mm	P Maximum Applied Load Newtons	$\sigma = \frac{P}{A_E}$ Stress = Load ÷ Effective Area Kilopascals	Number of Test Cycles Performed	Number of Test Cycles Averaged are the Last	ΔL Change in Height of Test Article mm	ΔL Change in Height Determined by Linear Approximation for the Given Load Range mm	Linear* Approximation Used	$\epsilon = \frac{\Delta L}{L}$ Linear Strain mm/mm	$E = \frac{\sigma}{\epsilon}$ Linear Modulus of Elasticity Kilo-Pascals $\times 10^3$	Linear Modulus of Elasticity $Lbs/in^2 \times 10^3$	T Temperature at Which Tests Were Performed °C
1-1	Anode-Matrix-Cathode	Flat	726	Same	14	18.87	360	490	1	1	0.508	0.508	Chord	0.027	18	2.6	25
2-2.1	Anode-Matrix-Cathode	Ribbed	645	103	1	1.40	140	1380	1	1	0.023	N.A.	Chord	N.A.	N.A.		25
2-2.0	Anode-Matrix-Cathode	Ribbed	645	103	1	1.40	70	680	1	1	0.081	0.081	Chord	0.059	12	1.7	25
1-3	Anode-Matrix-Cathode	Flat	726	Same	14	18.87	890	1230	10	1	0.701	0.812	Tangent	0.043	29	4.1	25
1-2	Anode-Matrix-Cathode	Flat	726	Same	14	19.25	360	490	12	3	0.272	0.211	Tangent	0.011	45	6.5	25
2-2.2	Anode-Matrix-Cathode	Ribbed	645	103	1	1.40	890	8610	1	1	0.615	0.467	Tangent	0.340	25	3.7	25
2-13	Anode-Matrix-Cathode	Ribbed	645	103	4	5.58	890	8610	1	1	2.057	1.727	Tangent	0.310	28	4.0	25
1-5	Anode-Matrix-Cathode	Flat	726	Same	14	18.54	360	490	9	3	0.424	0.320	Tangent	0.017	29	4.1	200
1-6	Anode-Matrix-Cathode	Flat	726	Same	14	18.54	890	1230	16	1	1.041	1.260	Tangent	0.067	18	2.7	200
1-16	Anode-Matrix-Cathode	Ribbed	41	6.5	6	8.38	17	2580	1	1	0.965	0.965	Chord	0.115	22	3.3	200
1-8	Mat-1, Matrix	Flat	726	Same	84	18.72	360	490	9	3	0.305	0.264	Tangent	0.014	35	5.0	25
1-9	Mat-1, Matrix	Flat	726	Same	84	18.72	890	1230	10	1	0.991	1.295	Tangent	0.069	18	2.6	25
1-11	Mat-1, Matrix	Flat	726	Same	84	17.60	360	490	15	3	0.305	0.312	Tangent	0.018	27	4.0	200
1-12	Mat-1, Matrix	Flat	726	Same	84	17.60	890	1230	16	1	1.092	1.500	Tangent	0.085	15	2.1	200
2-14	Bipolar Plate	Ribbed	645	103	5	18.82	890	8610	1	1	0.254	0.152	Tangent	0.008	1,000	150	25
1-13	Bipolar Plate	Flat	36	Same	4.77	17.93	2000	56500	6	2	0.048	0.048	Tangent	0.003	21,000	3,000	25
1-14	Bipolar Plate	Flat	36	Same	4.77	17.93	2000	56500	7	2	0.122	0.122	Tangent	0.007	8,000	1,200	200

* The Distinction Between the Chord and Tangent Approximation for Article Deformation is Illustrated in Figure 5.

Initially, the materials tests were intended to measure the thermal expansion characteristics of the materials. However, early results (which were confirmed by measurements of height changes on developmental stacks) revealed that the more significant material characteristic was the apparent creep (and other "permanent" dimensional changes) of the components which occurred, over time, under compression and/or at the stack operating temperature. As a result of this evolution of objective, the materials tests comprised two series performed by different groups using different equipment and flat and ribbed (to simulate actual bipolar plate topography) specimens. The nonlinear and time dependent nature of the stress-strain curves of the materials further complicated direct comparison of the results of the two test series. The following discussion summarizes and rationalizes the materials test results.

5.8.1 Cell Active Area

The first tests (1-1 through 1-3 in Table 5.8.1) measured the effects of repeated cycles on sandwiches of the soft materials of the cell active area (anode-matrix-cathode) at room temperature. The sandwiches were compressed in a fixture with flat faces as shown in Figure 5.8.2. Figure 5.8.3 depicts the sixth through the ninth cycles of a typical test article for comparison with the first test cycle of a similar article given in Figure 5.8.4. The distance between start and end points in the first cycle is much larger than in subsequent test cycles. The congruence of the load vs. deformation plots shown in Figure 5.8.3 indicates that the mechanical property changes have essentially taken place by the sixth cycle for the load range over which these tests were performed. For the tenth compression cycle of another similar article, the applied force range was increased from 360 to 890 newtons (80 to 200 lb.)* and the load vs. deformation plot with a kink depicted in Figure 5.8.5

*The test data was originally obtained in English units and then converted to SI units. The conversion was rounded off to prevent implication of greater precision.

ORIGINAL PAGE IS
OF POOR QUALITY

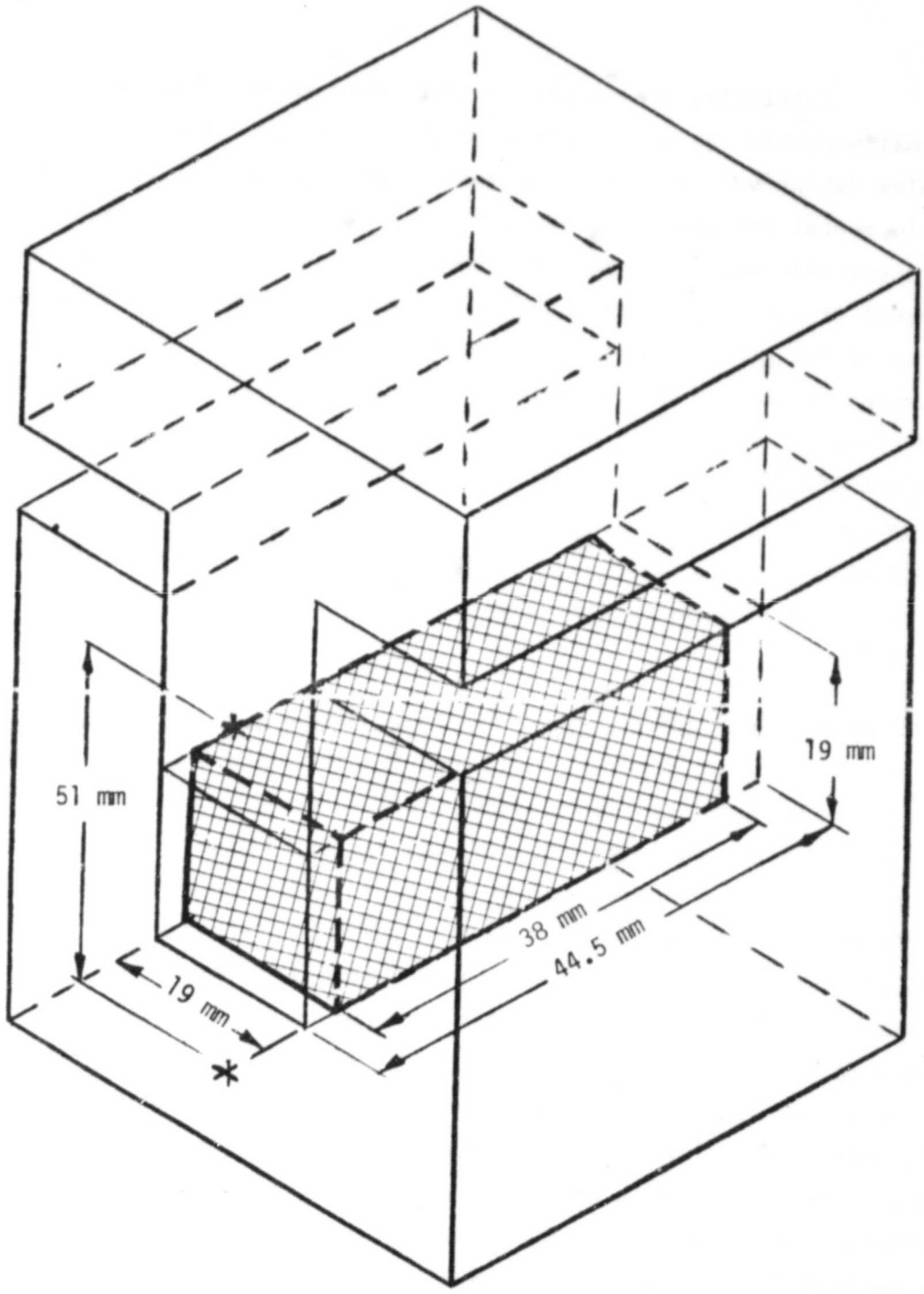

TEST FIXTURE FOR DETERMINING LOAD/DEFORMATION DATA

FIGURE 5.8.2

ORIGINAL PAGE IS
OF POOR QUALITY

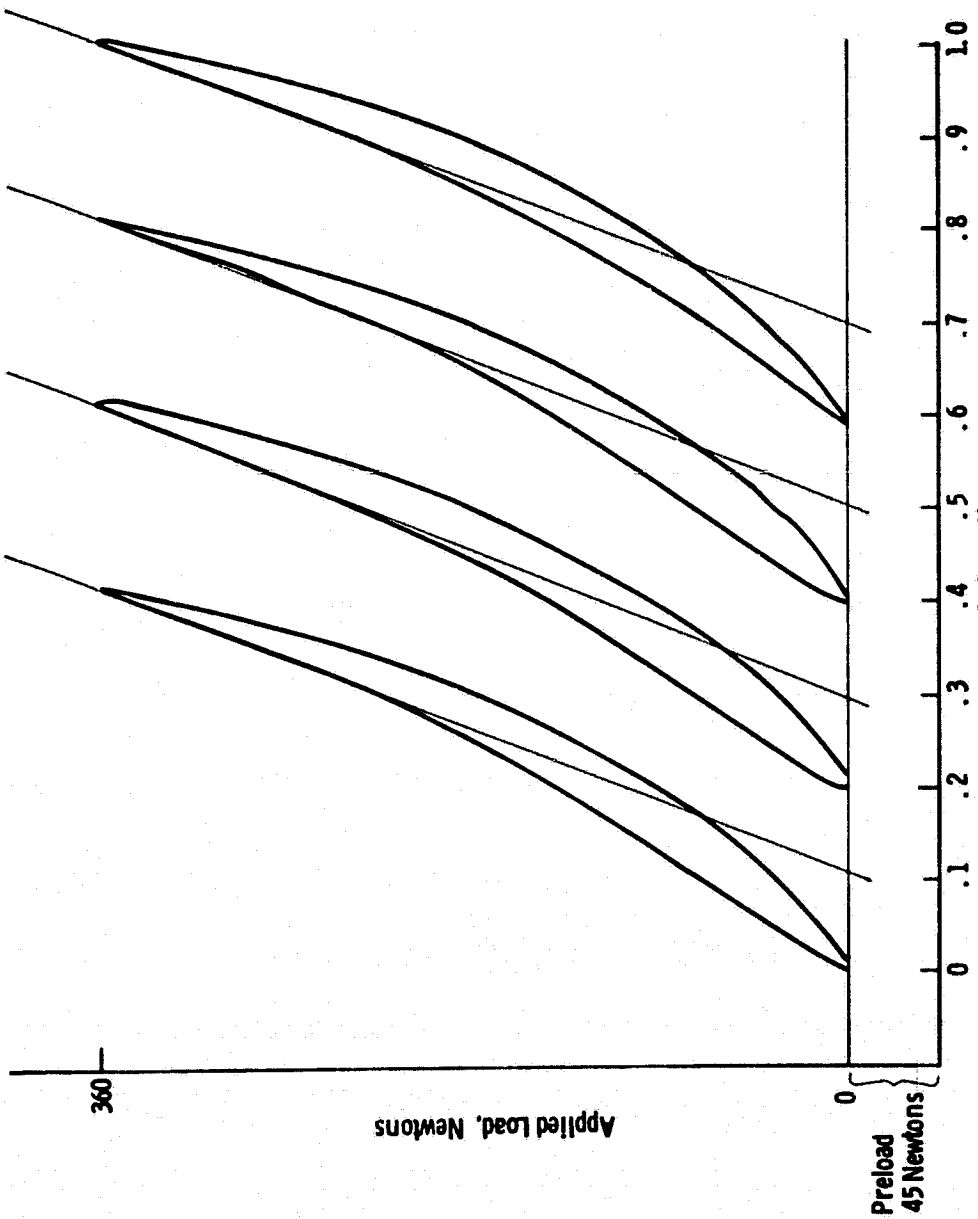

Fig. 5.8.3 – Load versus deformation plot 6th, 7th, 8th and 9th compression cycle, anode-Mat-I matrix-cathode composite. Height of Test Article: 18.54 mm, Temperature: 200°C

ORIGINAL PAGE IS
OF POOR QUALITY

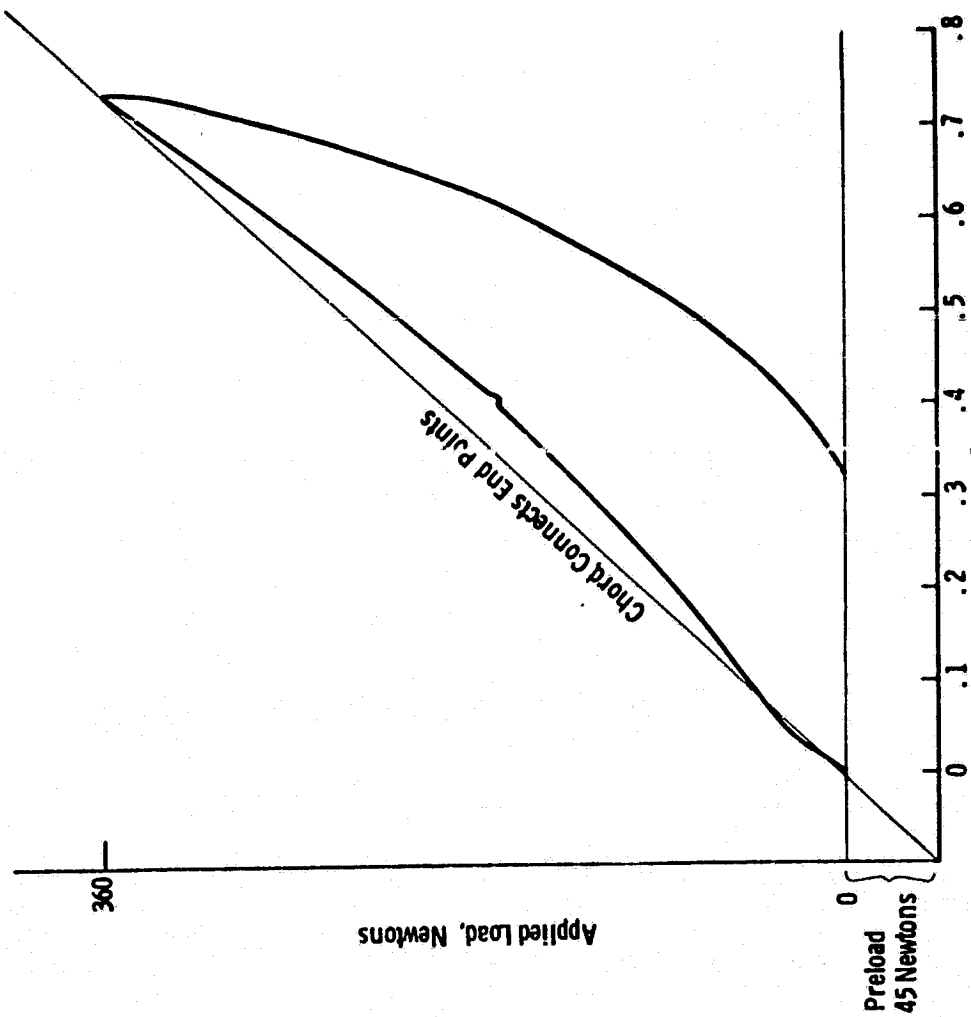

Fig. 5.8.4 – Load versus deformation plot 1st compression cycle, anode-Mat-I matrix-cathode composite. Temperature: 200°C, Height of Test Article: 18.54 mm

was obtained. While the plot over the initial range (0 to 360 newtons (80 lbs.)) is curvilinear, it is almost a straight line for loads exceeding 450 newtons (100 lbs.). The 450 N load corresponds to a stress of 620 kPa (90 psi) on the 726 mm^2 specimen. Thus, it appears that, for stresses over 620 kPa (90 psi), the composite was sufficiently compacted to behave like a solid. As approximated by the tangent to the linear portion of the curve, the modulus of elasticity is 29 MPa (4,100 psi) at room temperature (line 4 in Table 5.8.1).

Compression tests of anode-matrix-cathode sandwiches between two ribbed bipolar plates with the flow channels perpendicular to each other were also made (Tests 2-2.0, 2-2.1, 2-2.2 and 2-18). In these tests the applied force was 900 newtons (200 lb.), but, because of the bipolar plate's flow channels, the contact area was 16% of the nominal area. Consequently, the maximum stress to which the soft composite was subjected was 8.5 MPa (1,250 psi). The modulus of elasticity is ∿28 MPa (4,000 psi) using the tangent approximation.

Additional tests of these configurations were performed at 200°C (the stack's operating temperature). Results for comparable tests (1-5 vs. 1-2 and 1-6 vs. 1-3) indicate that the module of elasticity at 200°C are approximately 2/3 those at room temperature.

As indicated in Figure 5.8.5 straight lines were fitted to the data points of the load versus deformation graph for given load ranges. Usually the line is a tangent. However, in some cases where only the end points are known, the straight line is a chord connecting the maximum and minimum applied-load point. The chord approximation gives a linear function over the entire load range at a sacrifice in accuracy. The tangent gives a linear function over a more limited load range, but tends to be more representative for the given load range. The summary of the data in Table 5.8.1 indicates which method was used for calculating the modulus of elasticity.

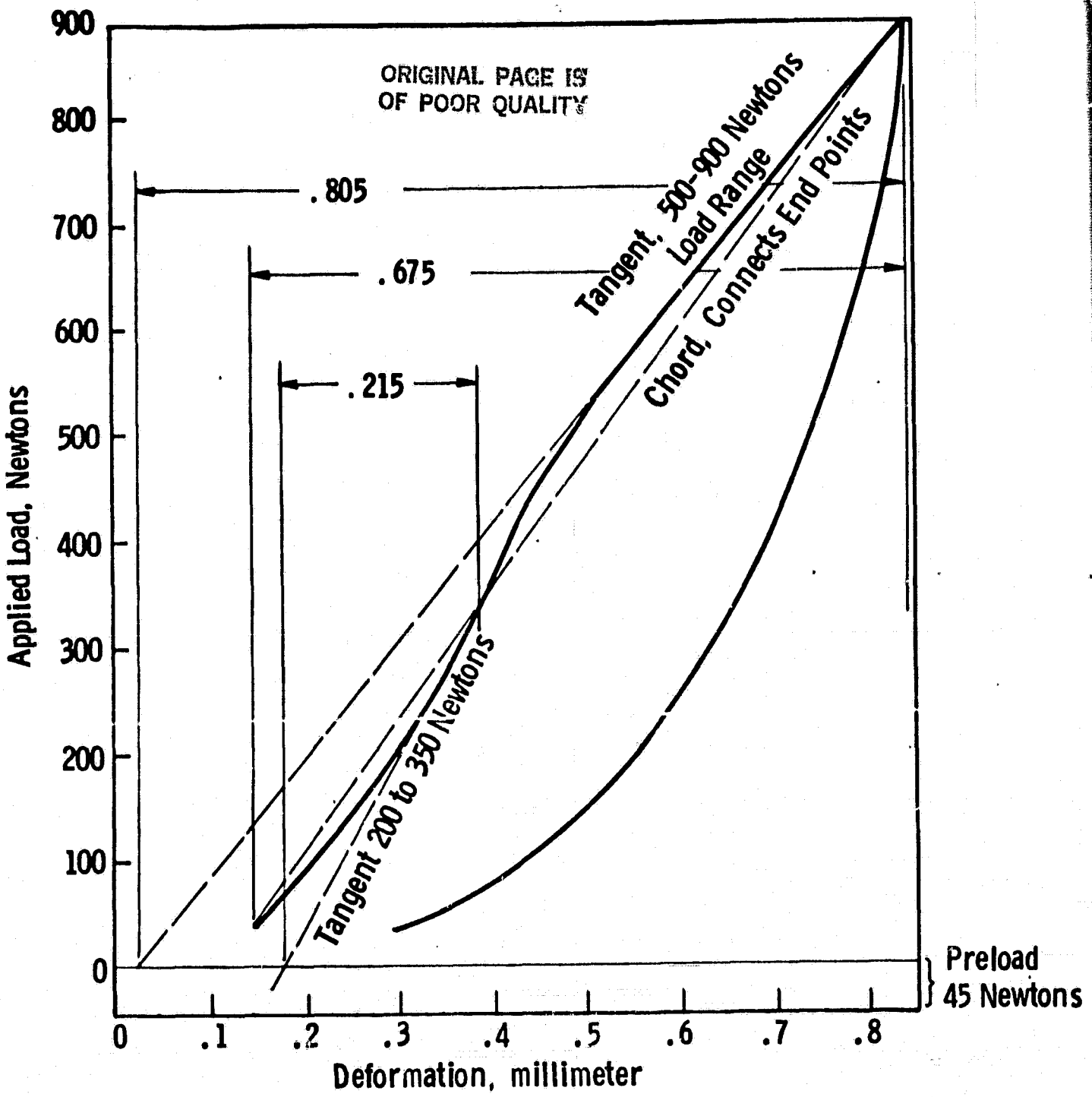

Fig. 5.8.5 —Load versus deformation, test #3
Test article height 18.58 mm
Test performed at room temperature 25°C

As indicated previously, a number of compression cycles (~9) must be performed before reproducible plots are obtained at low loads. For the sake of completeness, the moduli of elasticity "E" for the first compression cycles are shown for tests 1-1 and 2-2.0. When ribbed surfaces were used, the ribs were oriented at right angles to each other so that the contacting surface was approximately 16% of the nominal surface. A stack of 14 sandwiches was used for test 1-1 and one sandwich was used for test 2-2.0. The moduli, 18 and 12 MPa (2600 and 1700 psi), show reasonable agreement, considering the differences in test articles, that the tests were carried out at low loads and that the slopes used were the chords between beginning and end points. As shown for tests 1-3, 2-2.2 and 2-13, when the applied load was increased to 890 newtons (200 lbs.) and the data points were fitted by a tangent, the agreement among the test data was much better (i.e., 29, 25 and 28 MPa (4100, 3700 and 4000 psi)).

We, therefore, conclude that for the anode-matrix-cathode composite, a modulus of elasticity of approximately 26 MPa (3750 psi) is applicable over a wide range of pressures and temperatures. Moreover, the modulus is not too sensitive to differences of the contact surfaces. This is a very desirable result, since new flow channel dimensions or configurations can be readily incorporated without fear of affecting the mechanical properties of the anode-matrix-cathode composite.

5.8.2 Matrix

The mechanical properties of the Mat-1 matrix by itself were measured since the matrix extends over the inactive areas of the bipolar plates, as shown in Figure 5.8.1. While the modulus of elasticity for the Mat-1 matrix does not exhibit a great sensitivity to temperature changes ranging from room temperature to 200°C, it reduces to approximately one half of its value when the pressure is increased from 490 kilopascals (70 psi) to 1230 kilopascals (180 psi) (Table 5.8.1). Since the inactive

area of the bipolar plate is only about 10% of the total nominal area (1300 cm^2 or 204 in^2) and the nominal pressure over the total area is 400 kilopascals (60 psi), there is a great likelihood that the local pressure in the inactive area exceeds 500 kilopascals (80 psi). Thus the lower modulus, applicable over the upper load range, should be used.

5.8.3 Bipolar Plates

The non-heat-treated bipolar plates have a modulus of 1 GPa (150,000 psi) (Test 2-14). After heat treatment, the modulus increased to 21 GPa (3 million psi) at room temperature (Test 1-13). This was reduced to 8 GPa (1.2 million psi) at 200°C (Test 1-14). The large difference between the heat treated and non-heat-treated material can probably be attributed to the reduced resin content of the heat treated material.

5.8.4 Conclusions

Based on these tests, the stack contraction (and, therefore, the relative motion which the stack-to-manifold seals must accommodate) is primarily a function of the compression load. The modulus of elasticity of the active area composite ranges from 18 MPa (2600 psi) to 28 MPa (4100 psi) for an applied stress ranging from 350 to 8500 kPa (50 to 1250 psi) and a temperature ranging from 25 to 200°C. An important caveat is that allowance must be made for the initial deformation which occurs during the first few compression cycles at the lower loads. One way to accommodate this is to subject the stack to an appropriate number of compression cycles at 200°C before attaching the manifold-to-stack seals and manifolds. Most of the permanent deformation will have taken place and the repeating components will have mechanically stabilized greatly, reducing the relative motion that the manifold-to-stack seals must accommodate.

Due to the very high elastic moduli of the bipolar plate materials (particularly the heat treated version), the elastic deformation of the stack occurs in the matrix-shim and anode-matrix-cathode composites. In addition to their elastic deformation, the matrix and the anode-matrix-

cathode composite deform permanently at effective pressures in excess of 700 kPa (100 psi). These materials behave structurally like corrugated cardboard, although not as extreme. When a flat piece of corrugated cardboard is compressed between two flat blocks, it will return to its original thickness as long as the corrugations are not permanently deformed. This is the behavior of the anode-matrix-cathode composite, observed at effective pressures from 400 to 600 kPa (60 to 80 psi). However, if corrugated cardboard is subjected to pressure sufficient to crush the corrugations and eliminate or greatly reduced the air space between the face sheets, the board is permanently deformed and then behaves like solid cardboard - that is, it has changed from a soft to a hard thinner stiffer spring. Since the effective contact area of the bipolar plate is much smaller than its nominal area, the anode-matrix-cathode sandwich in the inactive area is permanently deformed when a nominal load greater than 400 kPa (60 psi) is applied to the stack.

Mathematical models were developed to calculate the pressure distribution over the fuel cell surface and the expected height changes resulting from this pressure distribution. Depending on the effective area, different gas flow channel configurations are expected to result in greater or smaller height changes which must be accommodated by stack-to-manifold seals. We now have the tools to calculate these changes.

6. Task 4: Fuel Conditioner Subsystem Development

The overall objective of this task was the preparation of a conceptual design of a fuel conditioning subsystem for the OS/IES which would be detail designed, built,and tested in succeeding phases of the program. The analysis carried out in Phase I indicated that, to achieve the desired overall system efficiency, this subsystem would have to be highly integrated thermally itself and with the other subsystems of the OS/IES. At the same time, the technology assessment carried out in Phase I indicated that the data base required to design a suitable subsystem was not available.

The effort on this task comprised subsystem and component analyses, component and catalyst tests, vendor contacts,and integration of the resulting information into a conceptual design.

In the original plan, the design of this subsystem was to be coordinated with and guided by a continuing system analysis which was deleted from the contract in order to focus the available resources on development of the fuel cell and fuel conditioning subsystems, which were identified as critical items during Phase I. As a result, the subsystem conceptual design is based primarily on the OS/IES requirements defined during Phase I. Deletion of the system analysis also necessitated a greater effort than originally planned for in this task on analysis and development of the subsystem process flow chart and thermodynamic state points and control system.

Briefly the results of this task are the conceptual design of the prototype subsystem, the conception of a suitable reformer design* (Figure 2.3), catalyst and packed bed heat transfer data, operation of a 10 kW double counterflow reformer, operation of a suitable burner for the OS/IES reformer, a computerized analysis of the reformer,and vendor

*A patent application (Case No. 49733) was filed for this design.

data on ancillary equipment (i.e., heat exchangers, compressors, pumps, etc.). Together, these provide the starting point, data, and tools for the detailed design of a prototype fuel conditioning subsystem.

The results are described by subtask in the following sections.

6.1 Fuel and Water Definitions

The objective of this subtask was to determine appropriate pipeline gas and water composition specifications to provide a basis for designing and specifying equipment for the conceptual design of the prototype system. The criterion of "appropriateness" that evolved during the course of the study was that the resulting system design should be simple (to be reliable and cost effective) and suitable for a large part of the potential OS/IES market. The approach used comprised surveying the available information to determine the range of compositions by market area and then narrowing the specification down by trade-off studies. All decisions were arrived at in consultation with NASA personnel and approved by the NASA Project Manager.

The work and resulting specifications are described in detail in the following sections.

6.1.1 Fuel Definition

The OS/IES fuel conditioning system could be designed to utilize any of the various gases that enter an urban apartment house through the "natural gas" supply pipe. The challenge was to narrow the spectrum of gas compositions to those gases that will permit a simple, cost effective fuel conditioner to serve a large part of the potential OS/IES market. Data was collected, analyzed and discussed with NASA Lewis and Jet Propulsion Laboratory personnel, and the following conclusions were made:

1. Propane/air peak shaving gas would not be processed by the prototype system. This eliminates the need to deal with high (3% to 15%) oxygen content gases and propylene (C_3H_6). The exlusion of propane/air peak shaving gas from the prototype design will not prevent the addition of an oxygen removal reactor with heat exchangers and a propylene hydrogenation reactor with increased hydrogen recycle when and if needed for commercial systems.

2. The prototype system will be designed for the following range of natural gas compositions:

	Composition, Vol %	
	Range	Average
CH_4	72.4 to 95.15	89.4
C_2H_6	2.5 to 11.32	5.1
C_3	0.71 to 5.07	1.9
N_2	0.3 to 17.1	2.9
CO_2	0 to 1.98	0.7
He	0 to 0.34	-
	TOTAL	100.0

These compositions represent over 150 individual natural gas sources in the U.S., and represent nearly all of the actual natural gas compositions that a commercial OS/IES system will be required to operate on.

3. Oxygen content is set at 0.3% maximum to miminize the potential for catalyst sintering.

4. Sulfur compounds in the gas, including odorant materials required by law such as mercaptans, aliphatic sulfides and thiophane will be set at 20 ppm V maximum. This will require removal via a hydrodesulfurization (HDS) reactor and a zinc oxide bed.

5. SNG synthesized from coal will be an acceptable feedstock for the prototype system hardware. Generally such gas is rich in hydrogen and has lower C_3^+ contents than normal natural gas so some adjustment in flows and operation may be necessary.

6. An olefin level of $\leq$0.2 vol % will be specified for the prototype system. This effectively precludes operation on oil derived gas and coke oven gas but, since their use in natural gas supply systems is small and decreasing, such an olefin limit should not significantly restrict the OS/IES market.

7. The pressure levels established for gas lines entering residential units by the various state utility commissions will be the basis for the prototype design. These pressures vary from 500 to 5000 Pa.

8. Water content in pipelines is generally specified as one pound per million standard cubic feet of natural gas and to prevent freezing in the gas meter, the gas dew point must be below minimum ambient temperatures. This very low level of water is negligible for OS/IES design purposes.

The information and analyses that led to these conclusions are described in detail in the 1st and 2nd Quarterly Reports of this contract.

6.1.2 Water Definition

The objective of this subtask was to develop a feedwater specification to provide a basis for designing the water conditioning subsystem and specifying the equipment for it.

Phase I work showed that sufficient water could be recovered (by condensation) from the exhaust streams of the fuel cell to provide the feed for the fuel conditioning system. Using this stream would eliminate the need for a separate supply during normal operation, but the recovered water would contain dissolved gases and phosphate ions. Since a treatment system with its associated capital costs and operating costs would be required to remove these impurities, it was not obvious that the recovery and use of this water would be more cost-effective than the use of a separate (tap water) supply. Therefore, to develop an appropriate water specification, both alternatives were evaluated.

The evaluation comprised the determination of the impurities that would be in the recovered water, a survey of the impurities that would be found in various tap waters and an estimate of the equipment and operating costs required to treat each supply.

The method and assumptions used to determine the impurity levels in the recovered stream are described in detail in the 2nd Quarterly Report and the results are shown in Table 6.1.1. The concentration of phosphate ions is based on a gas content of 0.5 ppmv P_4O_{10} determined experimentally by ERC.

A rather extensive survey of city tap water supplies was undertaken. As reported in the 4th Quarterly of this contract the levels and types of impurities varied greatly among cities and seasonally for some cities. However, less than 1/3 of the large cities had water supplies with lower total dissolved solids (TDS) than the recovered waters. Since the cost studies carried out as part of the Ancillary Subsystem Data Base task showed that water treatment costs were primarily determined by TDS, the costs for treating recovered water would be lower than for tap water in 2/3 of the cities surveyed and only marginally greater in most others.

The use of recovered water has the further advantages of:

1. Eliminating the cost of purchasing water,
2. Reducing the discharges to environment thus reducing disposal costs,
3. Permitting the design of a standardized water treatment plant rather than one tailored for each supply,
4. Eliminating seasonal changes in feedwater quality and the accompanying changes in plant operation, and
5. Eliminating the potential for degradation of the shift catalyst by the fluoride and chloride present in most tap water supplies.

TABLE 6.1.1

ESTIMATED RECOVERED WATER STREAM IMPURITIES

Values in ppm (by wt)

	Combined	Exhaust Air	Exhaust Spent Fuel
PO_4	67.5	77.6	33.5
CO_2	76.7	--	328.0
CO	0.1	--	0.5
H_2	0.1	--	0.5
CH_4	<0.05	--	<0.2
O_2	6.6	3.6	--
N_2	11.3	12.1	--

ORIGINAL PAGE IS
OF POOR QUALITY

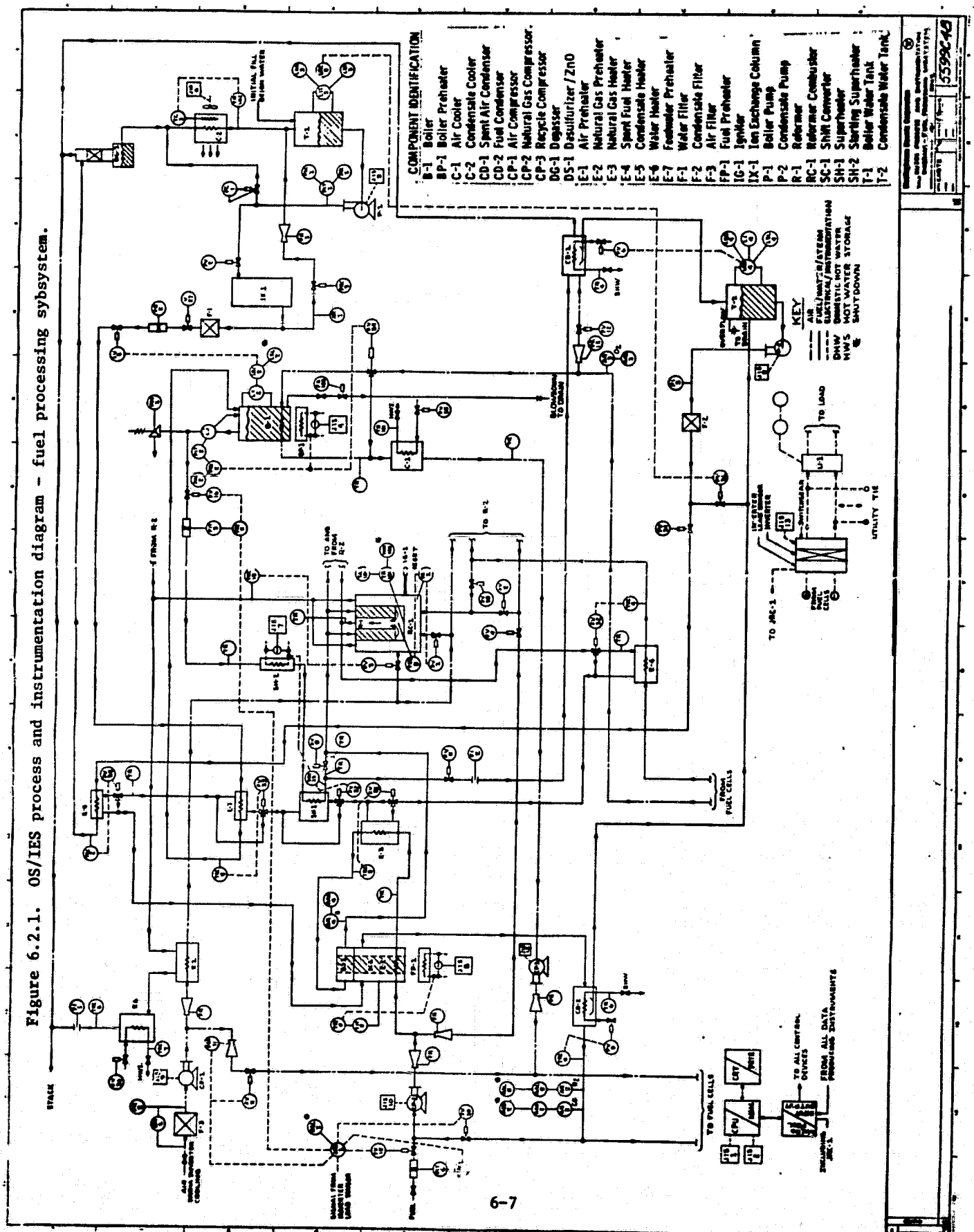

Figure 6.2.1. OS/IES process and instrumentation diagram - fuel processing sybsystem.

Based on these considerations, the water specification given in Table 6.1.1 was selected as the basis for design of the water treatment subsystem for the prototype fuel conditioning system.

6.2 Interface Specifications

The objective of this task was the determination and specification of the interfaces of the fuel conditioning subsystem with the other subsystems (fuel cell modules, apartment and inverters) of the OS/IES and the services available. Due to the highly integrated nature of the system, these could only be determined by developing a process flow diagram for the complete system at full and part (1/3) load. Since no system task was included in this contract, the operational characteristics of the other subsystems were taken to be those determined in Phase I. The fuel conditioning subsystem operational requirements to match these interfaces were then determined for the fuel and water specifications given in Section 6.1 at full and part load.

A state point diagram for the Fuel Conditioning Subsystem had been prepared during Phase I of this Program. This was upgraded during Phase II to a P & ID,which is shown in Figure 6.2.1. The state points for the Fuel Conditioning Subsystem at full load (120 kW DC) are given in Table 6.2.1 and the chemical compositions are shown in Table 6.2.2. Table 6.2.3 shows the state points for the Fuel Conditioning Subsystem at one third load (40 kw DC). Since the chemical compositions at full and one-third power are essentially the same, the compositions for one third power are those shown in Table 6.2.2.

The operating scenario used for calculating the part load state points and stream compositions assumed a fixed utilization of hydrogen in the fuel cells and a fixed composition of spent fuel. The reformer heat requirement will be met by spent fuel,so no supplementary methane is required for steady part load operation. This also implies that the reformer temperature will be reduced at part load to reduce methane conversion. This should contribute to more reliable, longer lived reformer operation. In establishing the configuration shown by the

TABLE 6.2.1

STATE POINTS FOR FUEL CONDITIONING SUBSYSTEM AT FULL LOAD (120 kw DC)

	Equipment Item No.	Hot Side (°C) Inlet	Hot Side (°C) Outlet	Cold Side (°C) Inlet	Cold Side (°C) Outlet	Mass Flow (kG/hr) Hot Side	Mass Flow (kG/hr) Cold Side	Thermal Load (kJ/hr)
Air Preheater	E-1	393	230	60	316	290	214	56200
Natural Gas Preheater	E-2	166	248	21	149	103	33	10300
Natural Gas Heater	E-3	328	312	149	204	103	33	4800
Spent Fuel Heater	E-4	388	328	177	316	103	79	17800
Condensate Heater	E-5	232	166	38	100	103	71	18500
Water Heater	E-6	230	121	27	82	290	154	35500
Feedwater Preheat	E-7	282	232	38	85	103	71	14200
Reformer(Both Modules)	R-1	1200	393	204	388	290	103	313000
Spent Air Condenser	CD-1	177	37	10	63	564	1100*	258000
Fuel Condenser	CD-2	248	54	10	63	103	322*	74100
Boiler	B-1	177	158	85	149	7220	71	170000
Superheater	SH-1	312	282	149	204	103	71	8800
Air Cooler	C-1	158	127	27	82	7230	1130	266000
Condensate Cooler	C-2	100	38	21	32	71	1620	18500

* Supplemented by cooling tower water during low domestic hot water demand periods.

ORIGINAL PAGE IS
OF POOR QUALITY

TABLE 6.2.2

CHEMICAL COMPOSITIONS OF STREAMS FOR FUEL CONDITIONING SUBSYSTEM IN MOLE FRACTIONS

	Cold Side		Hot Side		Cold Side		Hot Side	
	Inlet	**Outlet**	**Inlet**	**Outlet**	**Inlet**	**Outlet**	**Inlet**	**Outlet**
	E-1				E-2			
Air	1.0	1.0						
CH_4					0.639	0.639	0.011	0.011
H_2O			0.204	0.204	0.043	0.043	0.257	0.164
H_2					0.234	0.234	0.561	0.654
N_2			0.574	0.574				
O_2			0.081	0.081				
CO					0.023	0.023	0.103	0.009
CO_2			0.141	0.141	0.061	0.061	0.067	0.161
	E-3				E-4			
CH_4	0.639	0.639	0.011	0.011	0.027	0.027	0.011	0.011
H_2O	0.043	0.043	0.257	0.257	0.259	0.259	0.257	0.257
H_2	0.234	0.234	0.561	0.561	0.310	0.310	0.561	0.561
CO	0.023	0.023	0.103	0.103	0.022	0.022	0.103	0.103
CO_2	0.061	0.061	0.067	0.067	0.382	0.382	0.067	0.067
	E-5				E-6			
CH_4			0.011	0.011				
H_2O	1.0(ℓ)	1.0(ℓ)	0.257	0.257	1.0(ℓ)	1.0(ℓ)	0.204	0.204
H_2			0.561	0.561				
N_2							0.574	0.574
O_2							0.081	0.081
CO			0.103	0.103				
CO_2			0.067	0.067			0.141	0.141

ORIGINAL PAGE IS OF POOR QUALITY

TABLE 6.2.2 (continued)

	Cold Side		Hot Side		Cold Side		Hot Side	
	Inlet	Outlet	Inlet	Outlet	Inlet	Outlet	Inlet	Outlet
	B-1				SH-1			
CH_4							0.011	0.011
H_2O	1.0 (ℓ)	1.0 (g)	0.25	0.25	1.0 (g)	1.0(g)	0.257	0.257
H_2							0.561	0.561
N_2			0.69	0.69				
O_2			0.06	0.06				
CO							0.103	0.103
CO_2							0.067	0.067
	C-1				C-2			
Air					1.0	1.0		
H_2O	1.0(ℓ)	1.0(ℓ)	0.25	0.25			1.0(ℓ)	1.0(ℓ)
N_2			0.69	0.69				
O_2			0.06	0.06				

ORIGINAL PAGE IS
OF POOR QUALITY

TABLE 6.2.2 (continuted)

	Cold Side		Hot Side	
	Inlet	Outlet	Inlet	Outlet
		E-7		
CH_4			0.011	0.011
H_2O	1.0(ℓ)	1.0(ℓ)	0.257	0.257
H_2			0.561	0.561
N_2				
O_2				
CO			0.103	0.103
CO_2			0.067	0.067
		CD-1		
CH_4				
H_2O	1.0 (ℓ)	1.0 (ℓ)	0.25	0.109
H_2				
N_2			0.69	0.819
O_2			0.06	0.072
CO				
CO_2				

	Cold Side		Hot Side	
	Inlet	Outlet	Inlet	Outlet
		R-1&2		
CH_4				
H_2O	0.229	0.011	0.204	0.204
H_2	0.656	0.257		
N_2	0.084	0.561		
O_2				
CO			0.574	0.574
CO_2			0.081	0.081
	0.008	0.103		
	0.022	0.067		
			0.141	0.141
		CD-2		
CH_4				
H_2O	1.0(ℓ)	1.0(ℓ)	0.011	0.012
H_2			0.164	0.115
N_2			0.654	0.692
O_2				
CO				
CO_2			0.009	0.009
			0.161	0.171

ORIGINAL PAGE IS
OF POOR QUALITY

TABLE 6.2.3. STATE POINTS FOR FUEL CONDITIONING SUBSYSTEM AT ONE-THIRD LOAD (40 kw DC)

Apparatus	Hot Side (°C) Inlet	Outlet	Cold Side (°C) Inlet	Outlet	Mass Flow (kG/hr) Hot Side	Cold Side	Nominal Thermal Load (kJ/hr)
Air Preheater (E-1)	393	227	60	321	65	48	12900
Natural Gas Preheater (E-2)	174	247	21	181	23	7.3	2900
Natural Gas Heater (E-3)*	328	321	181	204	23**	7.3	450
Spent Fuel Heater (E-4)*	388	328	177	316	23**	18	4100
Condensate Heater (E-5)*	240	174	38	100	23**	16	4200
Water Heater (E-6)	227	121	27	82	65	34	7900
Feedwater Preheater (E-7)*	290	240	38	85	23**	16	3160
Reformer (R-1) (both modules)	1200	393	204	388	65	23	70,200***
Spent Air Condenser (CD-1)	177	37	10	63	127	247	59,000
Fuel Condenser (CD-2)	247	44	10	63	23	80	17,800
Boiler (B-1)	177	156	85	149	1605	16	38,500
Superheater (SH-1)*	321	290	149	204	23**	16	1900
Air Cooler (C-1)	157	127	27	82	1620	254	58,500
Condensate Cooler (C-2)	100	38	21	38	16	242	4160

* Utilizes bypass control of hot fluid to provide required cold side outlet temperature.

** Combined mass flow through heat exchanger and bypass valve

***Combustion gas

ORIGINAL PAGE IS OF POOR QUALITY

ORIGINAL PAGE
BLACK AND WHITE PHOTOGRAPH

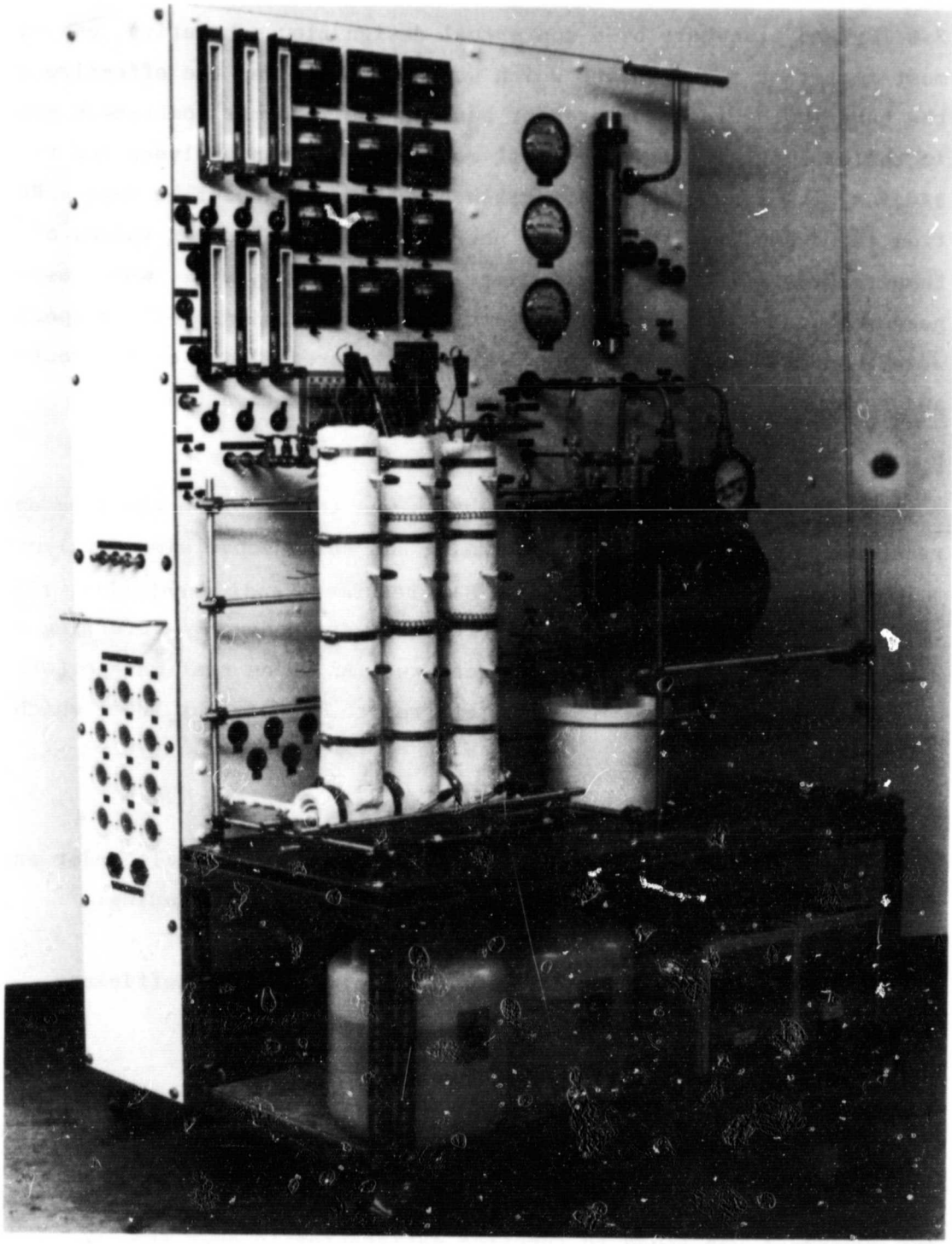

Figure 6.3.1 Test station for kinetic study

F & ID (and elsewhere by a conceptual design flow schematic), one of the most important requirements which was considered was the effective use of the heat in the reformer product gas, in the reformer combustion gas and in the cooling air from fuel cell modules. Various analyses and tradeoff studies were conducted to establish how this could best be done. Results from these studies produced the necessary detailed design values of temperatures, flows, pressure, stream compositions, etc., which were needed to prepare equipment performance specifications. These specifications were then used to contact suppliers for the preliminary costs, configuration and technical design information discussed in Section 6.4.

6.3 Catalyst Data Base

The objective of this subtask was to establish the data base required to select the steam reforming and shift conversion catalysts and provide design data for the 10 kW reformer, and, eventually, the commercial OS/IES. Activity measurements were made on 4 reforming and 2 shift catalysts available from vendors. An aging test was performed on the steam reforming catalyst, referred to as Catalyst 100*, which had a superior activity.

6.3.1 Test Station and Differential Reactor

Figure 6.3.1 is a photo of the test station built under and used in this subtask. The station is capable of accommodating:

- a tubular differential reactor,
- a packed bed reactor capable of producing sufficient hydrogen for a 2 kW fuel cell stack,
- a shift reactor,
- a guard bed reactor.

Shakedown runs of the test station included testing of the vaporizer, water pumps, temperature controllers, and gas sampling analysis system. The equipment was found to function satisfactorily over the expected range of test conditions.

*The designation of this catalyst and of the shift Catalyst 201 are proprietary under the terms of an agreement between ERC and their vendor. The designation has been supplied to the NASA Program Manager.

ORIGINAL PAGE IS
OF POOR QUALITY

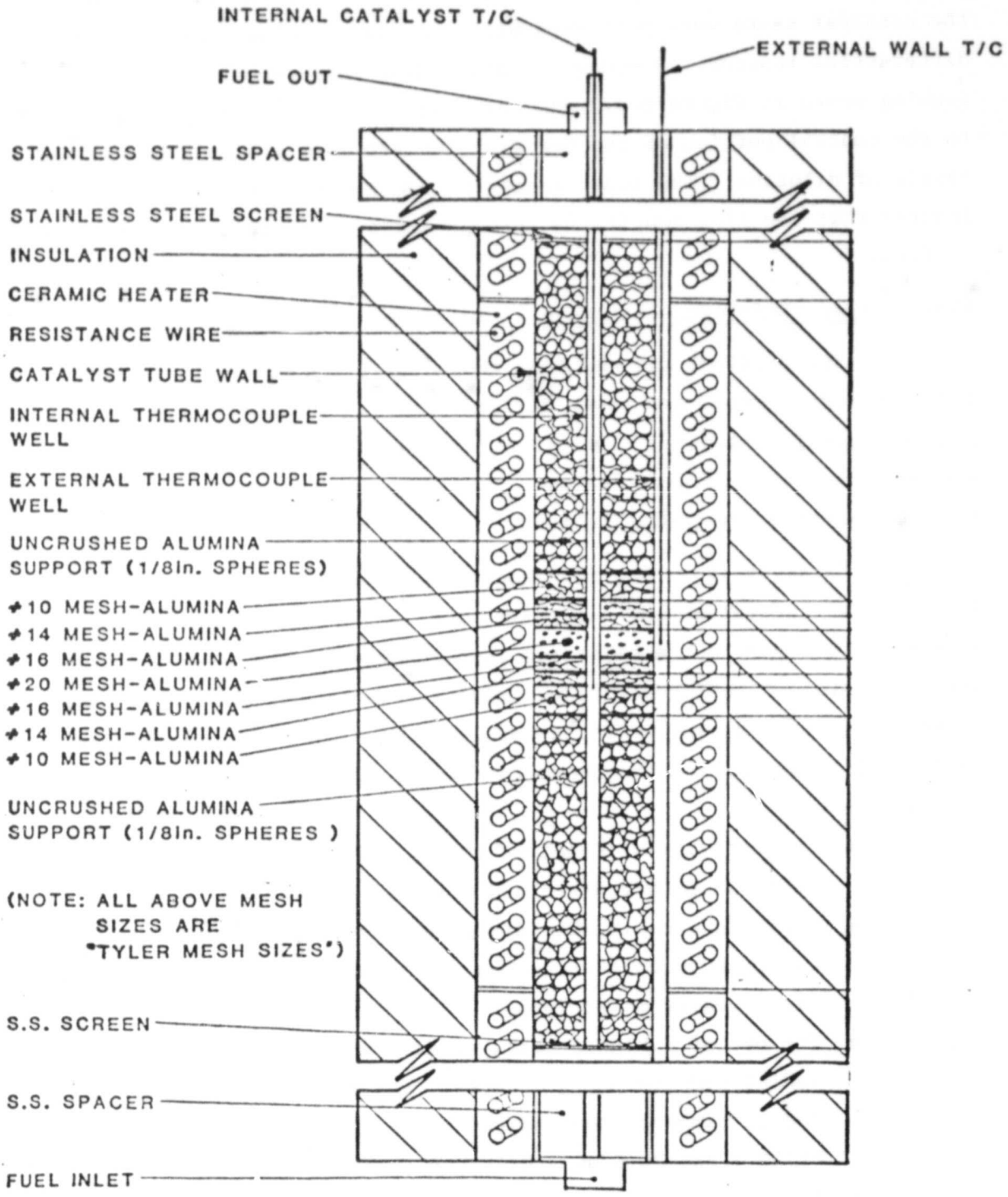

FIGURE 6.3.2. STEAM REFORMER EXPERIMENTAL SET-UP

In order to obtain the desired sensitivity and discrimination the catalyst tests were performed with the test reactor configured as a differential reactor. Based on pressure drop measurements the bed packing shown in Figure 6.3.2 was selected. The test catalyst was added to the central portion of the bed (labeled #20 mesh alumina) to various levels of dilution. The long lengths of inert material and heaters insured that the flow conditions through the test section were known and uniform.

6.3.2 Steam Reforming Catalysts

The physical and chemical characteristics of the four catalysts tested are given in Table 6.3.1. A summary of the test results is given in Table 6.3.2 and details of the results are discussed for each catalyst below. Based on its high activity, Catalyst 100 was selected for the aging test.

Catalyst 100: The methane-steam reforming experiments were initiated with Catalyst 100 using dilution of four parts inert 20 mesh alumina to one part of catalyst and then changed to 25 parts alumina to one part catalyst to further reduce radial temperature gradients. Both crushed (16-20 mesh) and pelleted catalysts were used. The pertinent results of these experiments shown in Figures 6.3.3, 6.3.4 and 6.3.5 indicate that:

- The activity of Catalyst 100 is 150 μg mole/g atm. s at 500°C in both crushed and pelleted form.
- There is a negligible difference in diffusion-free activation energy between the crushed (17.5 kcal/g mole) and the pelleted (16.5 kcal/g mole) forms.
- The use of a higher catalyst dilution ratio provides smaller radial temperature gradients. For example, at 700°C, the radial temperature gradient was 17°C at a dilution ratio of 25:1 and 30°C at a dilution ratio of 4:1.
- The small difference in activity between the crushed and the pelleted catalysts, indicates that the catalyst pore radii are sufficiently large to permit the internal mass diffusion resistance to be neglected.

TABLE 6.3.1

PHYSICAL AND CHEMICAL CHARACTERISTICS OF REFORMING CATALYSTS

Trade name	Catalyst 100*	United Catalyst G-91	United Catalyst C11-9-02	Katalco 23-1
Particle size, mm	4.2(D)x4.2(H)	3(D)x4(H)	16(OD)x6(ID)x8(H)	16(OD)x5.6(ID)x7(H)
Particle type	Pellet	Pellet	Ring	Ring
Bulk density, kg/liter	0.9	0.85	1.29	1.21
Chemical composition	25% Ni/ Al_2O_3+MgO	15% Ni/ Al_2O_3+K_2O	12% Ni/ Al_2O_3	12% Ni/ Al_2O_3
Form	Reduced	Oxidized	Oxidized	Oxidized

*Proprietary information

ENERGY RESEARCH CORPORATION

ORIGINAL PAGE IS OF POOR QUALITY

TABLE 6.3.2 COMPARISON OF DIFFERENT CATALYSTS ON METHANE REFORMING

CATALYST				ACTIVATION ENERGY, kcal/gmole		ΔT, °C	Activity at 500°C
No.	State as Received	Sugg. Operating Temp., °C	Type	Diffusion - Free	Diffusion - Limited	Radial	μgmole/gatm.s
100	Reduced	400-870	Crushed	17.5	6-9	+4	150
			Pelleted	16.5	6-9	+8	150
UC G-91	Oxidized*	400-850	Crushed	22.5	1-9	-4	15
			Pelleted	20.0	2-9	-1	60
UC C-11-9-02	Oxidized*	400-850	Crushed	21.0	4-8	-2	10
			Pelleted	14.8	4-8	-5	30
Katalco 23-1	Oxidized*	400-1040	Crushed	-	-	-	-
			Pelleted	13.2	-	+1	10

$\Delta T = T_{wall} - T_{bed}$

T_{wall} = Reactor wall temperature

T_{bed} = Reactor bed temperature

Crushed particle = 16-20 mesh (0.5mm)

*Oxidized catalysts were reduced prior to testing.

ENERGY RESEARCH CORPORATION

ORIGINAL PAGE IS OF POOR QUALITY

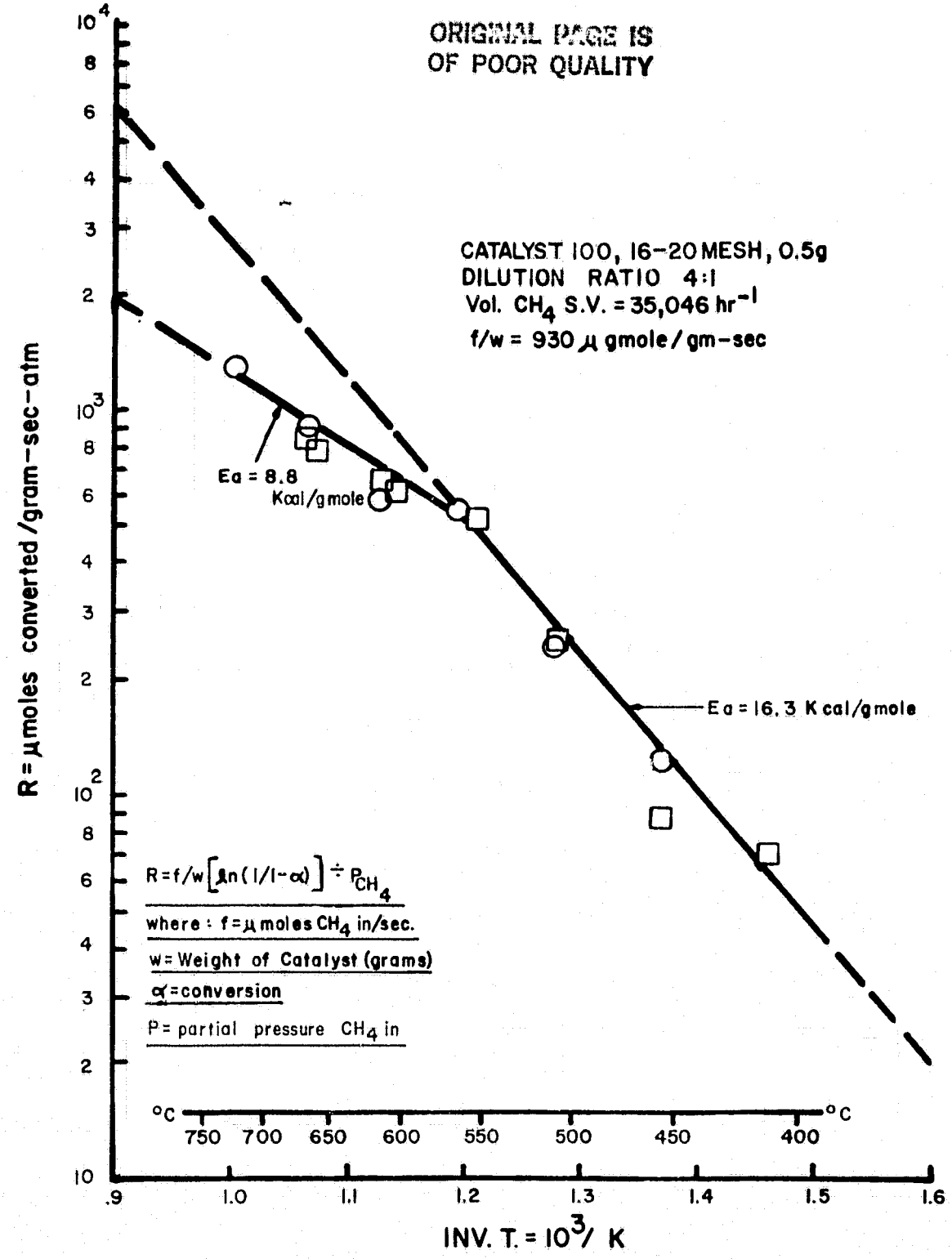

FIGURE 6.3.3 TEMPERATURE DEPENDENCE OF RATE CONSTANT FOR CATALYST 100 (CRUSHED) AT A DILUTION RATIO OF 4:1

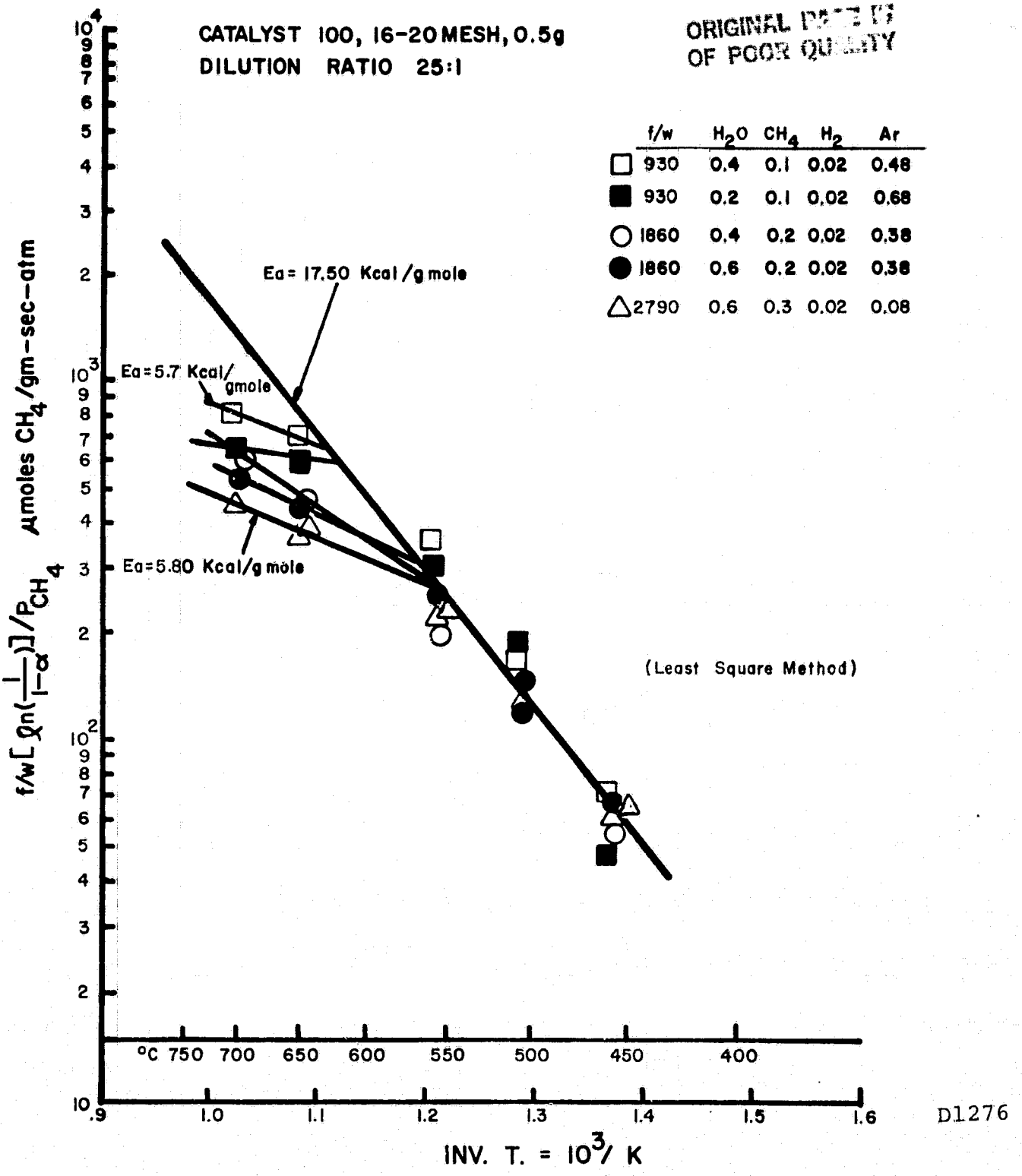

FIGURE 6.3.4 TEMPERATURE DEPENDENCE OF RATE CONSTANT FOR CATALYST 100 (CRUSHED) AT A DILUTION RATIO OF 25:1

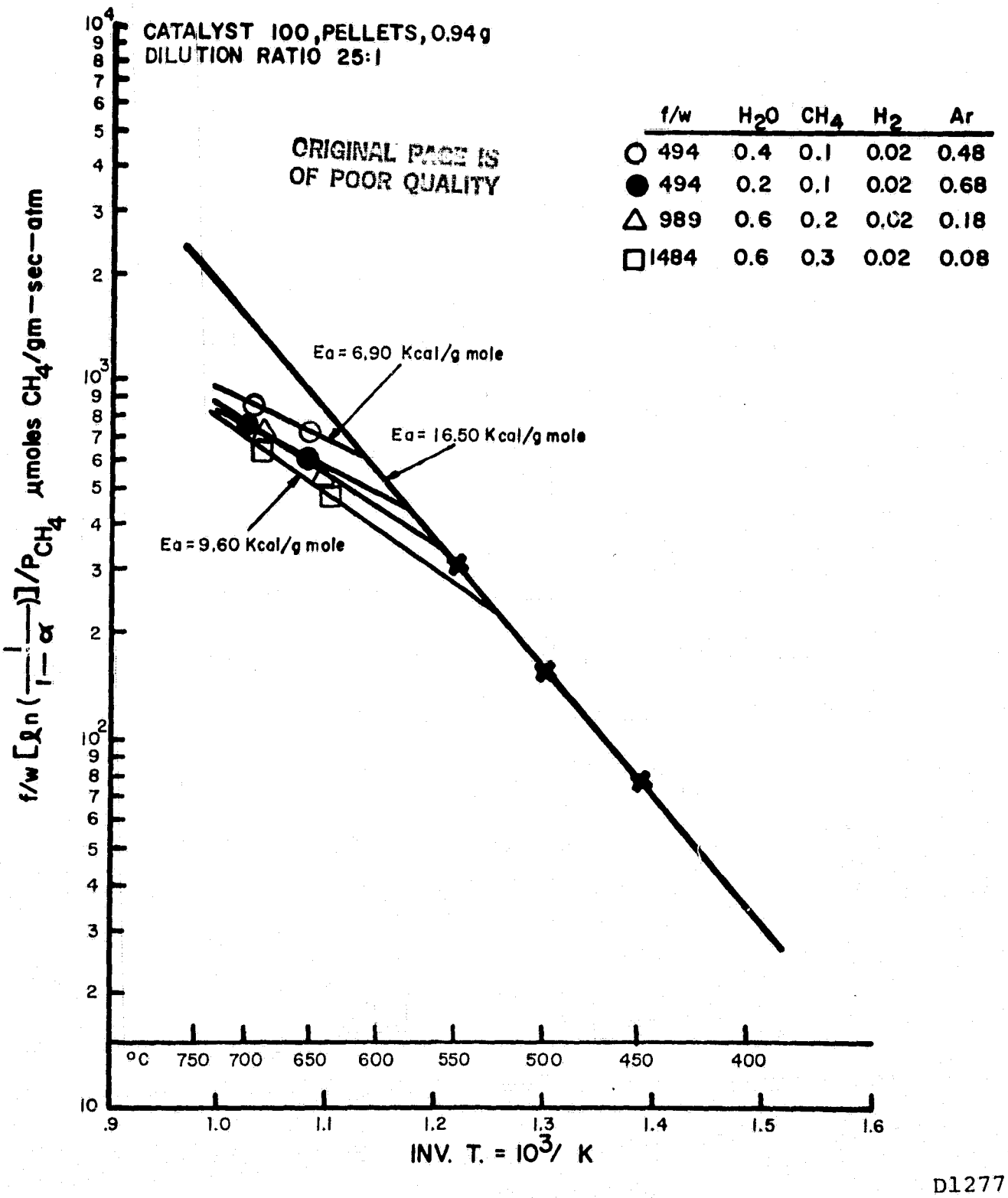

D1277

FIGURE 6.3.5 TEMPERATURE DEPENDENCE OF RATE CONSTANT FOR CATALYST 100 (PELLETS) AT A DILUTION RATIO OF 25:1

ORIGINAL PAGE IS
OF POOR QUALITY

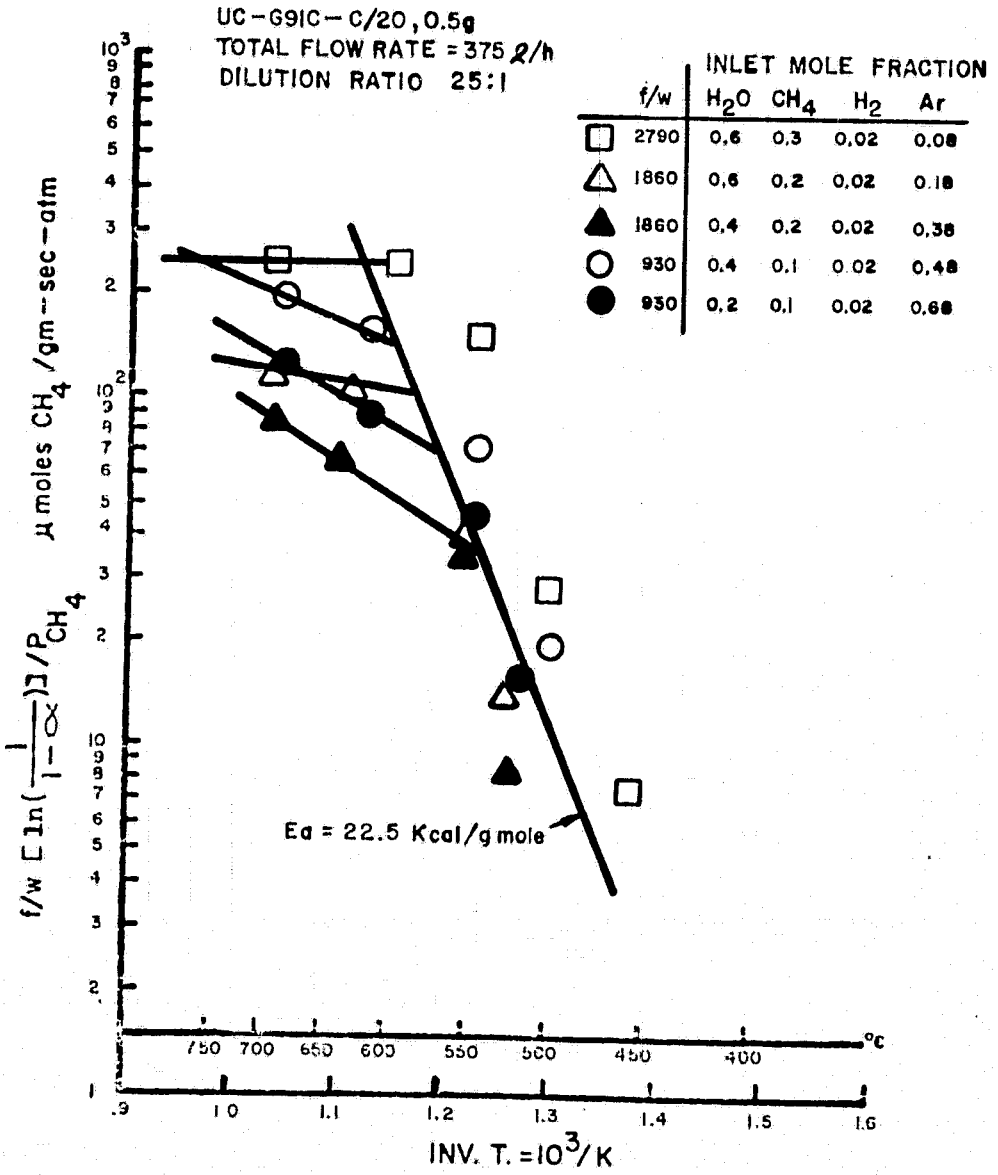

FIGURE 6.3.6 TEMPERATURE DEPENDENCE OF RATE CONSTANT FOR UNITED CATALYST G-91 (CRUSHED)

D1312

- The diffusion-free activation energy is approximately 17 kcal/gmole and the diffusion-limited activation energy is between 6 and 9 kcal/gmole.
- Diffusion became the limiting factor at temperatures between 550 and 620°C, increasing with a decrease in methane space velocity. Because of the complexity of the internal and external mass diffusion effects, more experiments would be needed to determine the influence of temperature on activity under diffusion limited conditions.
- At temperatures below 550°C, the reaction could be expressed as a simple first-order reaction of methane: where,

$$R = k_o \exp(-E/RT) P_{CH_4}$$
$$E = 17.0 \text{ kcal/gmole}$$
$$k_o = 11.0 \text{ gmole } CH_4/\text{g atm.s.}$$

United Catalyst G-91: The tests of United Catalyst G-91 also were performed with crushed (16-20 mesh) and pelleted particles at a catalyst dilution of 25 parts alumina to one part catalyst. The results of these experiments shown in Figures 6.3.6 and 6.3.7 indicate that:

- The diffusion-free activation energy was around 20-22.5 kcal/gmole.
- The pelleted catalyst had a higher activity (60 μgmole/g atm.s at 500°C) than the crushed catalyst (15 μgmole/g atm.s at 500°C). This is surprising because, if the catalyst is homogeneous, it should have a higher surface area and, therefore, higher activity.
- The radial temperature gradient of -4°C for the crushed form indicates that the reactor bed temperature was higher than the wall temperature. This is contrary to expectations for an endothermic reaction. Re-examination of the equipment, repeat of the experiments and contact with manufacturer provide no positive explanation. We now believe that the active component, Ni, was not distributed uniformly in the catalyst and that crushing deactivated this catalyst.

ORIGINAL PAGE IS
OF POOR QUALITY

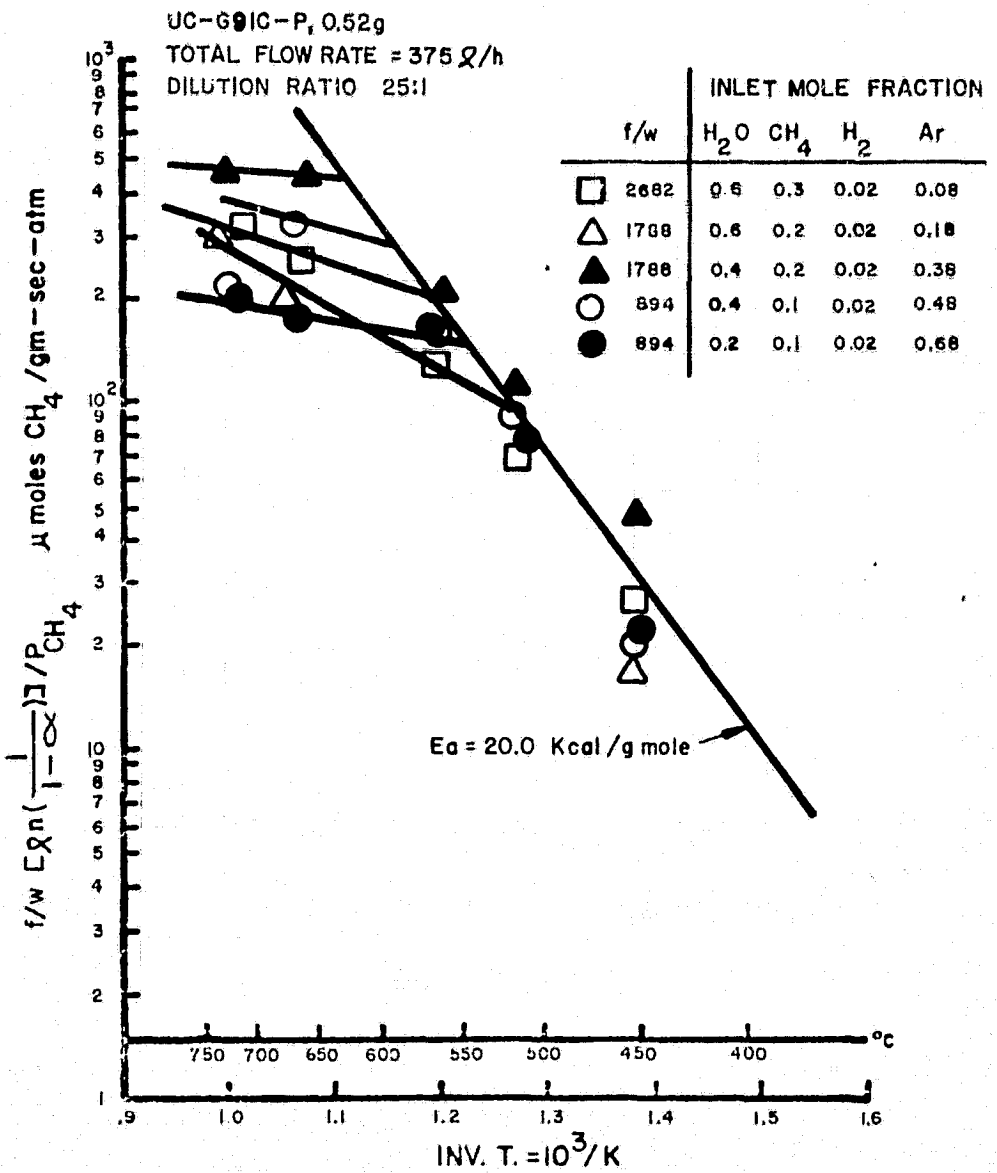

FIGURE 6.3.7. TEMPERATURE DEPENDENCE OF RATE CONSTANT FOR UNITED CATALYST G-91 (PELLETS)

ORIGINAL PAGE IS
OF POOR QUALITY

UC-C-11-9-02/16-20 MESH
0.5 g
Total Flow Rate = 375 ℓ/hr
Dilution Ratio = 25 : 1

	$\frac{f}{w}$	Inlet Mole Fraction CH_4	H_2O	He	H_2	DATE of TEST
○	930	0.1	0.2	0.68	0.02	7/16/80
●	930	0.1	0.4	0.48	0.02	7/17/80
△	1860	0.2	0.4	0.38	0.02	8/4/80
▲	1860	0.2	0.6	0.18	0.02	8/5/80
□	2790	0.3	0.6	0.08	0.02	8/6/80

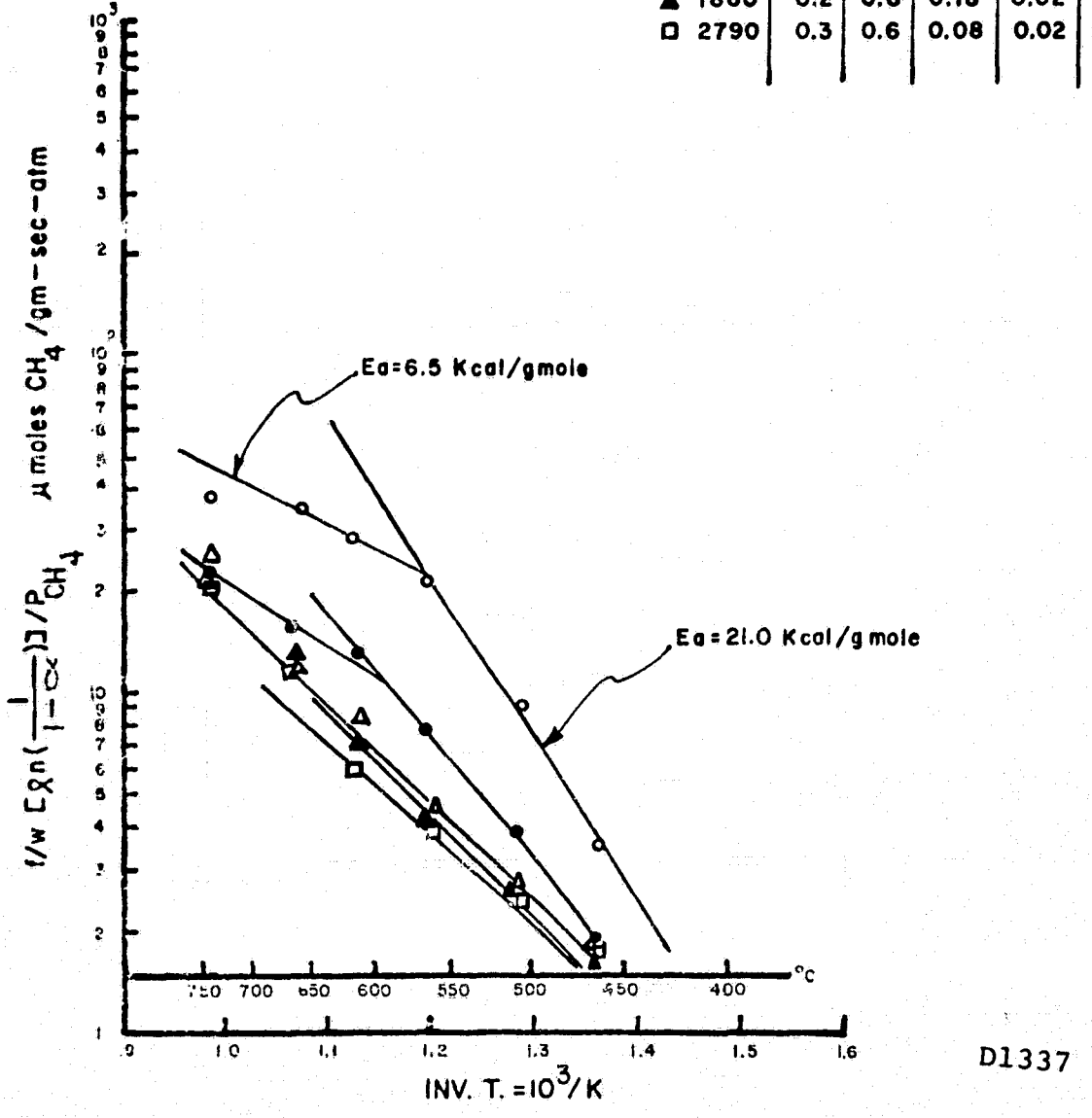

FIGURE 6.3.8. TEMPERATURE DEPENDENCE OF RATE CONSTANT FOR UNITED CATALYST C-11-9-02 (CRUSHED)

ORIGINAL PAGE IS
OF POOR QUALITY

UC-C-11-9-02/P
3.0 g
Total Flow Rate = 375 ℓ/hr
Dilution Ratio = 5:1

	$\frac{f}{W}$	Inlet Mole Fraction CH_4	H_2O	He	H_2	DATE of TEST
□	465	0.3	0.6	0.08	0.02	8/8/80
▲	310	0.2	0.6	0.18	0.02	8/11/80
△	310	0.2	0.4	0.38	0.02	8/12/80
	(Catalyst Regenerated)					
●	155	0.1	0.4	0.48	0.02	8/13/80
○	155	0.1	0.2	0.08	0.02	8/14/80

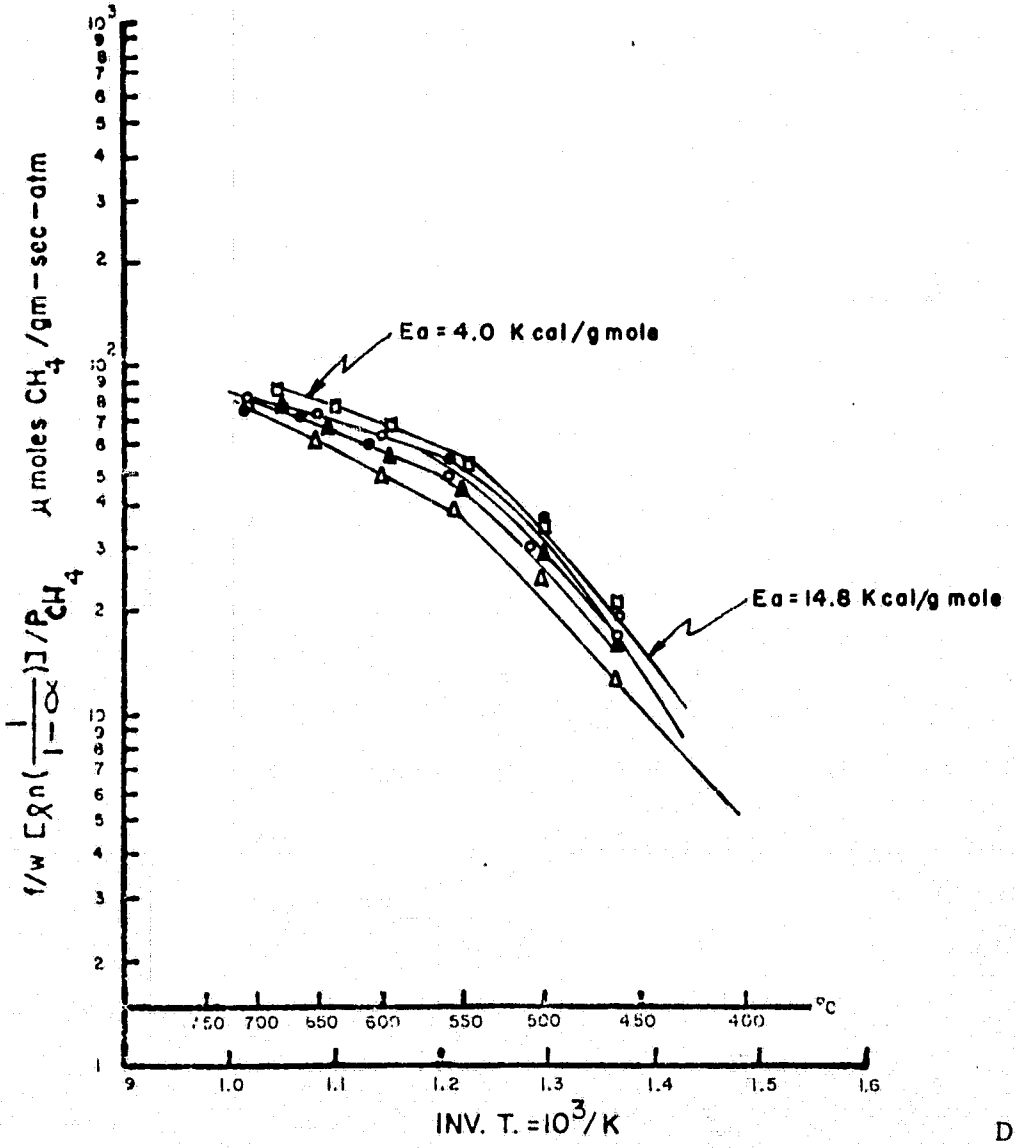

FIGURE 6.3.9 TEMPERATURE DEPENDENCE OF RATE CONSTANT FOR UNITED CATALYST C-11-9-02 (PELLETS)

United Catalyst C-11-9-02: Tests of this catalyst were conducted with crushed (16-20 mesh) catalyst at dilutions of 25 parts alumina to one part catalyst and with pellets at a dilution of five parts alumina to one part of catalyst. The results in Figures 6.3.8 and 6.3.9 show that:

- as with the UC G-91 catalyst, the pelleted catalyst had higher activity than the crushed catalyst and the radial temperature gradient was negative.
- The large difference in the diffusion-free activation energy between the crushed (21 kcal/gmole) and the pelleted (14.8 kcal/gmole) catalyst supports the hypothesis that crushing changes the characteristics of the United Catalysts.
- The activity of the UC C-11-9-02 catalyst (especially for the crushed form) decreased in the short time that elapsed during the activity testing.
- Since the pelleted catalyst UC C-11-9-02 was a ring, the uneven distribution of the catalyst in the reactor would cause some reactant to bypass the catalyst resulting in lower conversion and activity than if it was distributed evenly. Therefore the activity of this pellet catalyst is higher than shown in Figure 6.3.9.

Katalco 23-1: The Katalco 23-1 catalyst was tested with pelleted particles at a dilution ratio of 10:1. The results in Figure 6.3.10 indicate that the pelleted catalyst had an activity of 10 μgmole/g atm.s at 500°C and a diffusion-free activation energy was 13.2 kcal/mole for the pelleted forms. The activity with crushed particles (16-20 mesh) was too low to be measured even with twice the usual catalyst charge.

ORIGINAL PAGE IS
OF POOR QUALITY

Inlet Mole Fraction

f/w	H_2O	CH_4	H_2	He
195	0.4	0.1	0.02	0.48

Katalco 23-1
(Pellet, 2.38g)
Total Flow Rate = 375 ℓ/hr
Dilution Ratio = 10:1

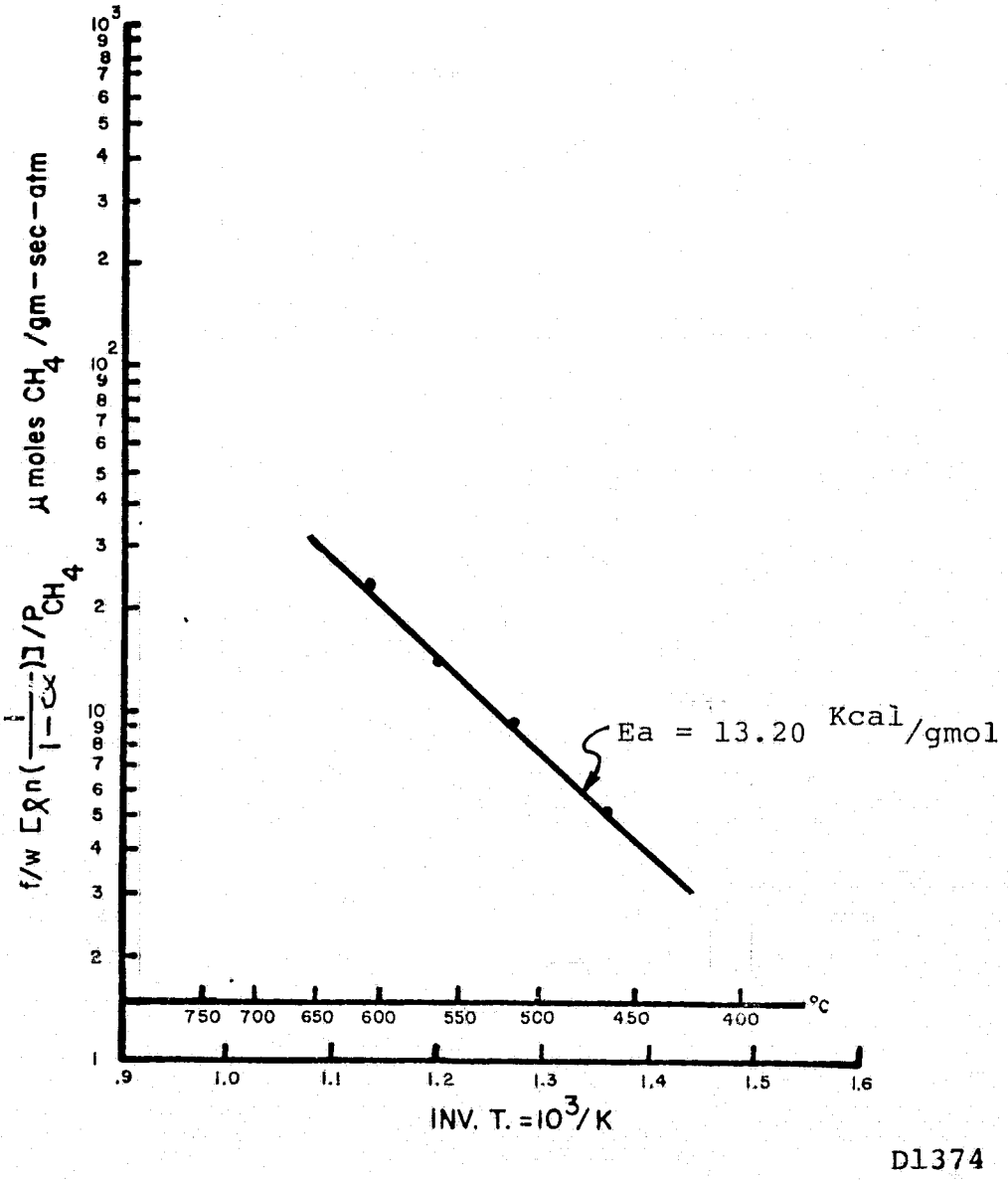

FIGURE 6.3.10. TEMPERATURE DEPENDENCE OF RATE CONSTANT FOR KATALCO 23-1 (PELLETS)

Comparison. A comparison of the four methane-steam reforming catalysts is summarized as follows:

1. Catalyst 100 had a considerably higher activity in both crushed and pelleted particles than the other three catalysts (150 vs. 10 to 60 μgmole/g atm.s at 500°C).
2. There was no significant difference in the catalyst activity of the crushed and pelleted catalysts for Catalyst 100. For the other three, crushing deactivated the catalyst.

6.3.3 Shift Catalyst Testing

The physical and chemical properties of the two shift catalysts, evaluated are presented in Table 6.3.3.

TABLE 6.3.3
PHYSICAL AND CHEMICAL PROPERTIES OF SHIFT CATALYSTS

Trade Name	Catalyst 201	United Catalyst 18HC
Particle size, mm	4.6 (H) x 4.6 (D)	2.4 (H) x 4.8 (D)
Particle type	Pelleted	Pelleted
Bulk density, kg/liter	1.06	1.29
Chemical composition	CuO/ZnO + Cr_2O_3	CuO (42%)/ZnO (47%) + Al_2O_3 (10%)
Form as received	Oxidized	Oxidized

Carbon monoxide shift tests were made using crushed (16-20 mesh) and pelleted particles of Catalyst 201 and UC-18HC.

Since both Catalyst 201 and UC-18HC were in the oxidized form, reduction of the catalysts using the manufacturer's recommendations was necessary before testing. The procedures involved control of the hydrogen concentration to maintain the temperature of the catalyst bed below 260°C and the space velocity of the reducing gas between 500 and 1500 hr^{-1} over a period of eight hours.

ORIGINAL PAGE IS
OF POOR QUALITY

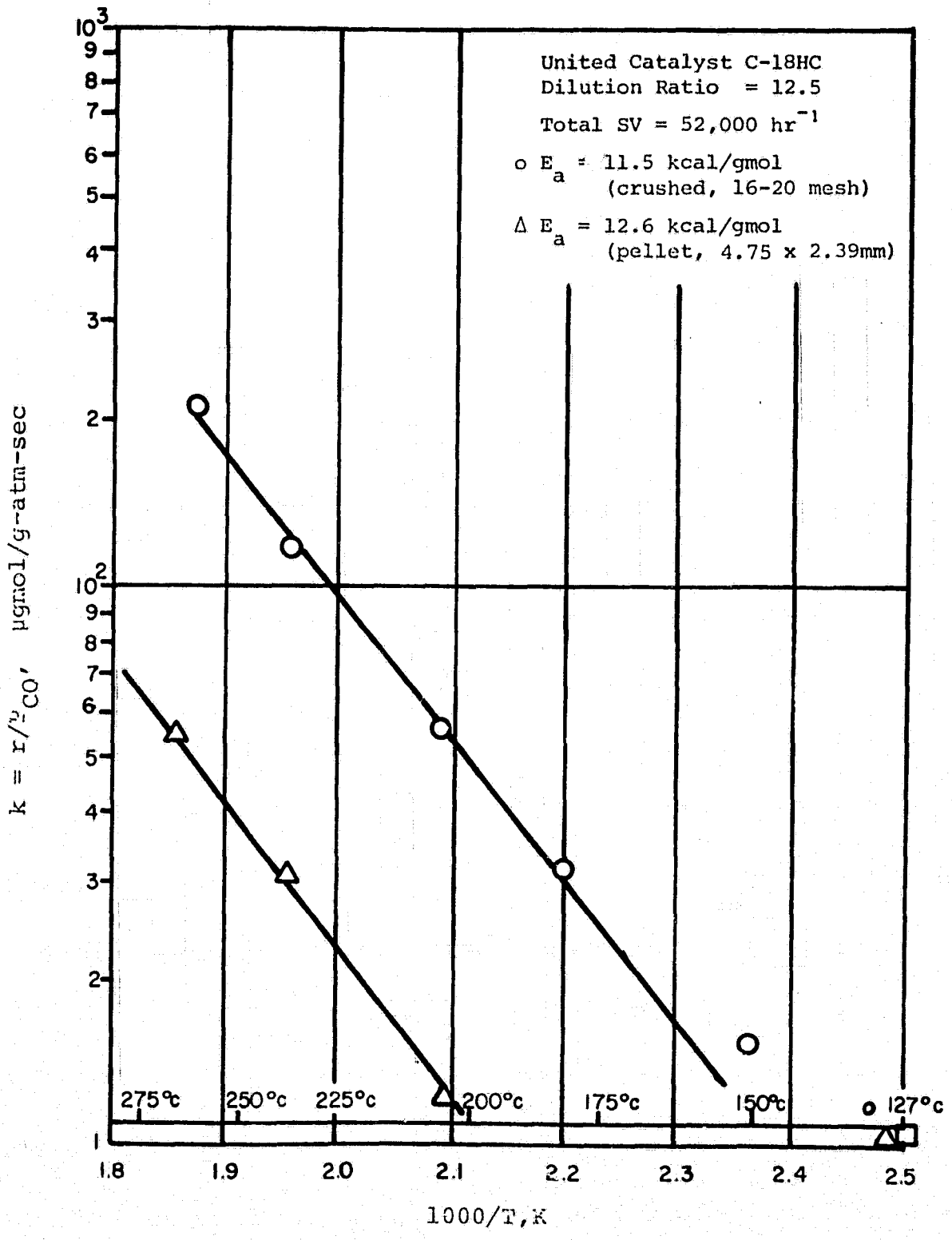

D1423 Ral

FIGURE 6.3.11. ARRHENIUS PLOT FOR SHIFT CATALYST UC C-18HC, CRUSHED

Figures 6.3.11 and 6.3.12 show the test results for UC C-18HC and Catalyst 201 respectively in crushed and pelleted forms. A comparison of the data is given in Table 6.3.4. The results may be summarized as follows:

- For UC C-18HC, the rate of the CO shift reaction was first order with respect to CO and was independent of H_2O concentration (i.e., $r = k P_{CO}$). For Catalyst 201, the reaction rate was first order with respect to both CO and H_2O (i.e., $r = k P_{CO} P_{H_2O}$). The dissimilarity may be due to the catalyst supports which were zinc and aluminum oxides for UC C-18HC and zinc and chromium oxides for Catalyst 201.
- The catalysts had similar activation energies.
- For shift conversion conditions of 0.26 atm. water partial pressure and 204C temperature, the crushed UC C-18HC catalyst had a slightly higher activity than Catalyst 201 (55 vs. 48 μgmole/g atm. s at 204°C).
- The crushed catalyst UC C-18HC had a much higher activity than the pelleted (55 μgmole/g atm.s vs. 13 μgmole/g atm. s at 204°C). The reason for the low activity of the pelleted catalyst is unknown. When the experiments were repeated, the same results were obtained.
- The crushed Catalyst 201 had a higher activity (48 μgmole/g atm. s. vs. 28 μgmole/g atm. s at 204°C) but a similar activation energy (12.0 kcal/gmole vs. 11.0 kcal/gmole) to the pelleted. There was no evidence to indicate a diffusion effect in the testing temperature range (150-300°C).
- Based on these results, Catalyst 201 is recommended for use in the shift reactor of the OS/IES prototype.

ORIGINAL PAGE IS
OF POOR QUALITY

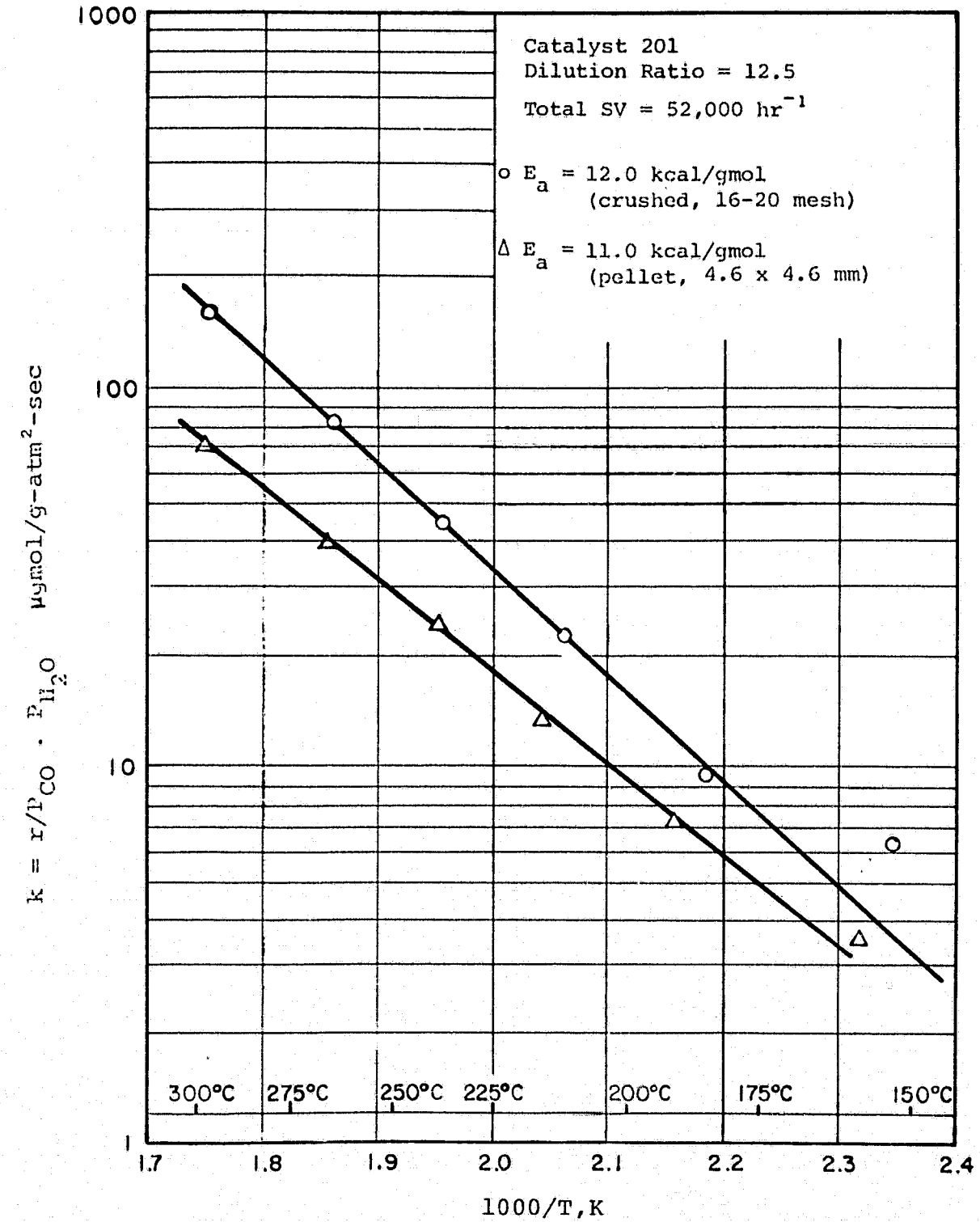

D1445

FIGURE 6.3.12 ARRHENIUS PLOT FOR SHIFT CATALYST 201

ORIGINAL PAGE IS
OF POOR QUALITY

TABLE 6.3.4
COMPARISON OF CO SHIFT CATALYSTS

			AT 204°C (400°F)	
CATALYST	TYPE	ACTIVATION ENERGY kcal/gmole	ΔT radial,* °C	ACTIVITY† μgmole/g atm. s
UC C-18HC	Crushed	11.5	-2	55
UC C-18HC	Pelleted	12.6	-1	13
201	Crushed	12.0	-2	48†
201	Pelleted	11.0	-2	28†

* $\Delta T_{radial} = T_{wall} - T_{bed}$

†Catalyst activity measured at $P_{H_2O} = 0.26$ atm.

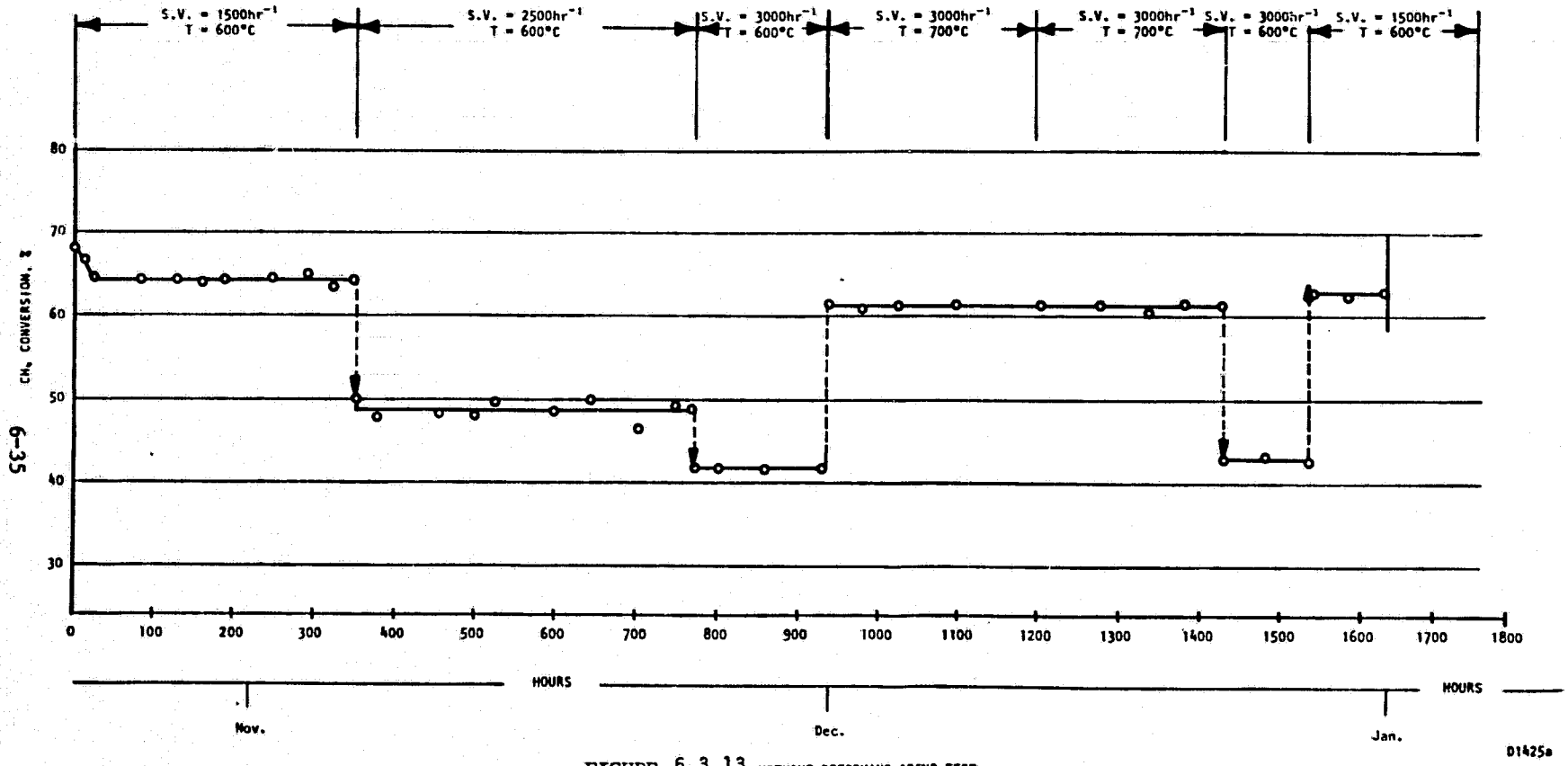

FIGURE 6.3.13 METHANE REFORMING AGING TEST

ORIGINAL PAGE IS
OF POOR QUALITY

6.3.4 Steam Reforming Aging Test

An aging test of 1630 hours was conducted on 27g of Catalyst 100 in pellet form (4.20 mm x 4.20 mm). The experimental results are shown in Figure 6.3.13. Table 6.3.5 is an example of the comparison of experimental data and calculated equilibrium conditions for fresh catalyst.

As shown in Figure 6.3.13, the methane conversion decreased from a fresh catalyst conversion of 68% to a steady value of 64% in a period of 35 hours and no further change occurred up to 350. Since the methane conversion of 64% at 1500 hr^{-1} was too close to the equilibrium conversion to provide the desirable test sensitivity, the space velocity was increased to 2500 hr^{-1} for 440 hours and then to 3000 hr^{-1} for 150 hours. At these conditions, the methane conversion was constant at 49% and 41% respectively. Since the catalyst showed no significant decay at 600°C at space velocities up to 3000 hr^{-1}, the temperature was raised to 700°C at a space velocity of 3000 hr^{-1} to accelerate any decay of catalyst activity. The methane conversion remained constant at 62% for 490 hours. When the temperature was reverted to 600°C, the methane conversion was the same as before at space velocities of 1500 hr^{-1} and 3000 hr^{-1}.

Catalyst 100 had no significant decrease in activity during 1630 hours of testing using high purity (research-grade) methane. Sintering of the catalyst, with subsequent loss of effective surface area, did not appear to occur at temperatures as high as 700°C.

TABLE 6.3.5 STEAM REFORMING AGING TEST

TEST CONDITIONS		
Catalyst	Catalyst 100	
Catalyst weight, g	22.7	
Catalyst volume, cm^3	19.3	
CH_4 Space velocity, hr^{-1}	1500	
Inlet feed:		
CH_4, l/hr	28.962	
H_2O, l/hr	86.886	
H_2, l/hr	2.896	
Reactor Temperature:	Wall, °C	Catalyst Bed, °C
Exit	611	559
Middle of bed	619	549
Inlet (prior to catalyst)	635	604

TEST RESULTS		
	EXPERIMENTAL	EQUILIBRIUM (585°C)
CH_4 conversion, %	67.6	70
Dry gas:	Mole Fraction	
CH_4	0.0896	0.082
H_2	0.7227	0.727
CO	0.0555	0.067
CO_2	0.1322	0.124

ENERGY RESEARCH CORPORATION
ORIGINAL PAGE IS OF POOR QUALITY

6.4 Ancillary Subsystem Data Base

The primary objective of this subtask was to develop information and/or data on the ancillary equipment (e.g., water conditioners, compressors, pumps, heat exchangers) to support the conceptual design of the fuel conditioning subsystem. An initial determination of the ancillary equipment requirements based on the process flow diagram developed during Phase I provided the starting point for this work. These were refined during Phase II as a result of the interface requirements effort described in Section 6.2 and the information acquired through tradeoff studies, vendor feedback analyses, and experimental work carried out as part of this effort.

The approach selected and results obtained for the main items of ancillary equipment are described below.

6.4.1 Water Conditioning Equipment

The objective was to develop a conceptual design and specification for the water treatment equipment required for the fuel conditioning system of the prototype OS/IES.

As part of the effort to determine if water recovered from the fuel cell exhaust was preferable to a separate water supply (tap water), a tradeoff study was carried out. This study was described in detail in the 2nd and 3rd quarterlies of this contract and is summarized below. The main conclusion of this study was that the use of recovered water was clearly more cost effective in over 70% of the potential OS/IES market and only marginally more expensive in others. Since it had the additional advantages listed in Section 6.1.2, recovered water was specified for the prototype design.

Figure 6.4.1 is a schematic diagram of the water treatment system for the prototype design. Detailed specifications for the major equipment items of this system were submitted separately to the NASA Project Manager and some examples are included in Appendix A.

ORIGINAL PAGE IS
OF POOR QUALITY

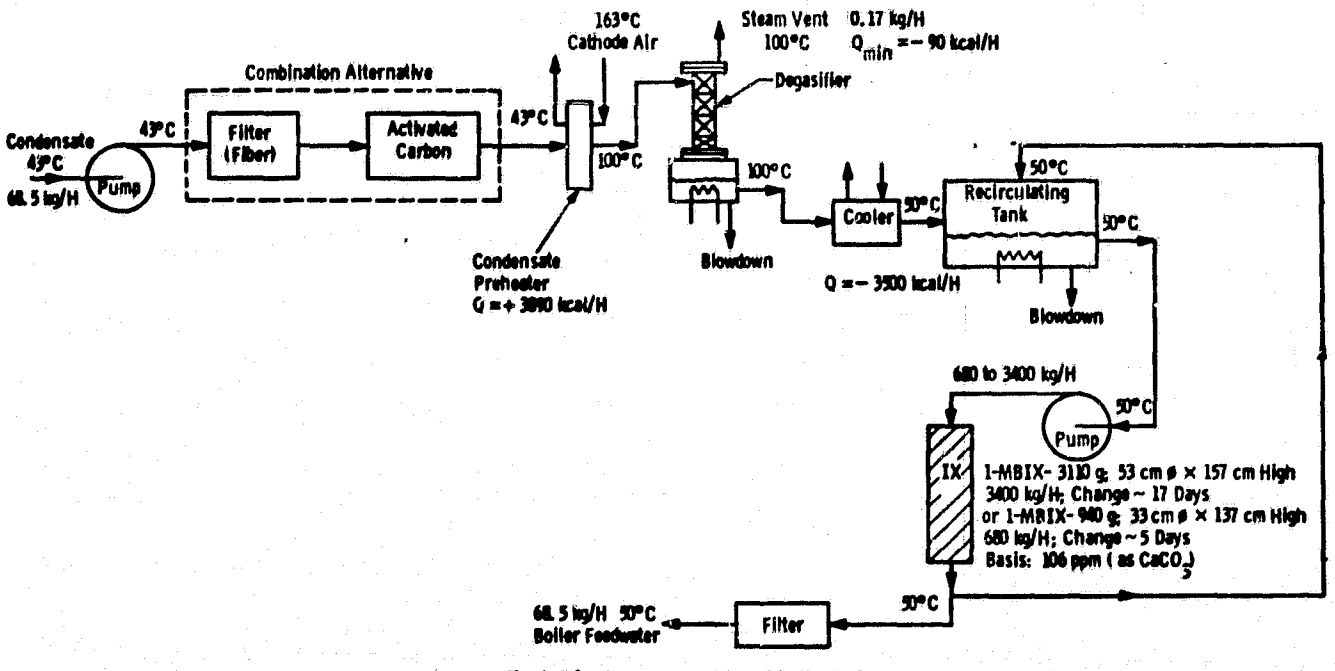

Fig. 6.4.1 – Condensate water purification train

Quality of Treated Water

The recommended specification of the water to be delivered by the conditioning system was established as that specified for the DOE 40 kW power plant and is listed in Table 6.4.1. These were obtained from a set of "Fuel Cell Materials Specifications" provided by the NASA Project Manager.

TABLE 6.4.1

BOILER FEEDWATER SPECIFICATION

	Recommended	(Goal)
Electrical Resistivity at 25°C	>1 M ohm	(>5)
pH at 25°C	6-8	-
Dissolved Oxygen	<0.1 ppm	(<0.005)
Free CO_2	<5 ppm	(<1)
Suspended Solids	<1 ppm	(<0.1)

Our studies comfirmed that these were representative of commercial practice but that the goal specifications listed in the table may be attainable with little change in equipment or cost.

If all of the solids in the recommended feedwater specification were carried over to the reformer, its performance would be degraded as they filled the voids in the bed. An analysis, described in the 5th Quarterly Report, showed that with a boiler blowdown of less than one liter per hour the solids carried over to the reformer during 14000 hours of operation would occupy less than 0.1% of the bed volume. This blowdown rate would also maintain the solids level in the boiler well within the limits of accepted boiler practice.

Conceptual Design of Prototype System

The schematic diagram shown in Figure 6.4.1 and the equipment specifications comprise the conceptual design of the water conditioning system for the prototype OS/IES. The design is capable of producing boiler feedwater of the quality specified above from an input stream with the impurities specified in Table 6.1.1. In addition, the fiber filter and activated carbon filter will remove unspecified particulate matter which may be picked up in the system.

The design shown evolved from tradeoff studies that included calculations and discussions with vendors and these are described in detail in the 2nd and 3rd Quarterly reports.

The primary equipment item is the ion exchange train. Due to the size of OS/IES installations it is not feasible to have skilled personnel dedicated to the servicing of the equipment. Therefore, the use of columns with replaceable cartridges to be regenerated by a vendor was specified. This should also simplify the operation and increase the availability of the prototype system. The lowest vendor estimated cost for supplying this service was less than $\$6.00/m^3$, which corresponds to approximately 2 mils/kWh. Quotes received from two other vendors were greater by a factor of 5. Due to the preponderance of this cost (>90%) and the uncertainty indicated by the range of estimates, a final determination of the total system cost was deferred to the final design stage.

Tap Water

As mentioned above, the major cost of conditioning water is associated with the operation of ion exchange columns. In turn, this cost is largely determined by the quantity of dissolved solids in the water supply. Since the survey of water supplies discussed in Section 6.1.2 indicated that the city water would contain more solids than the recovered water for more than 70% of the potential OS/IES market, the comparison was based on an equal content. For this condition, the major differences in cost of operation is the cost of purchasing tap water. This cost ranges from $\$.06/m^3$ to $\$.30/m^3$ or from 1 to 5% of the lowest cost of ion exchanging. Although the function and operating temperature of the combination filter/activated carbon bed are different for tap water (Fig. 6.4.2), their operating cost is so small ($<\$.07/m^3$) that they will not significantly affect the overall economics.

Since there was no cost or operational advantage associated with operation on tap water in most areas and the use of recovered water has the advantages given in Section 6.1.2, use of recovered water was selected for the prototype design.

6.4.2 Fluid Flow and Heat Transfer Equipment

The objectives of this effort were to determine the availability of and develop specifications and obtain preliminary cost data for the heat exchangers, compressors, etc. required for the prototype fuel conditioning system. A major consideration in this effort was to minimize the need for special designs and/or development in order to minimize the cost and lead time, and maximize the reliability and operating availability of the prototype. This was achieved to the extent possible by soliciting inputs and suggestions from appropriate vendors of commercial equipment and extensive discussions with representatives of the Harrison Radiator Division of GMC. The final prototype system conceptual design and detailed equipment specifications evolved as a result of these discussions.

ORIGINAL PAGE IS
OF POOR QUALITY

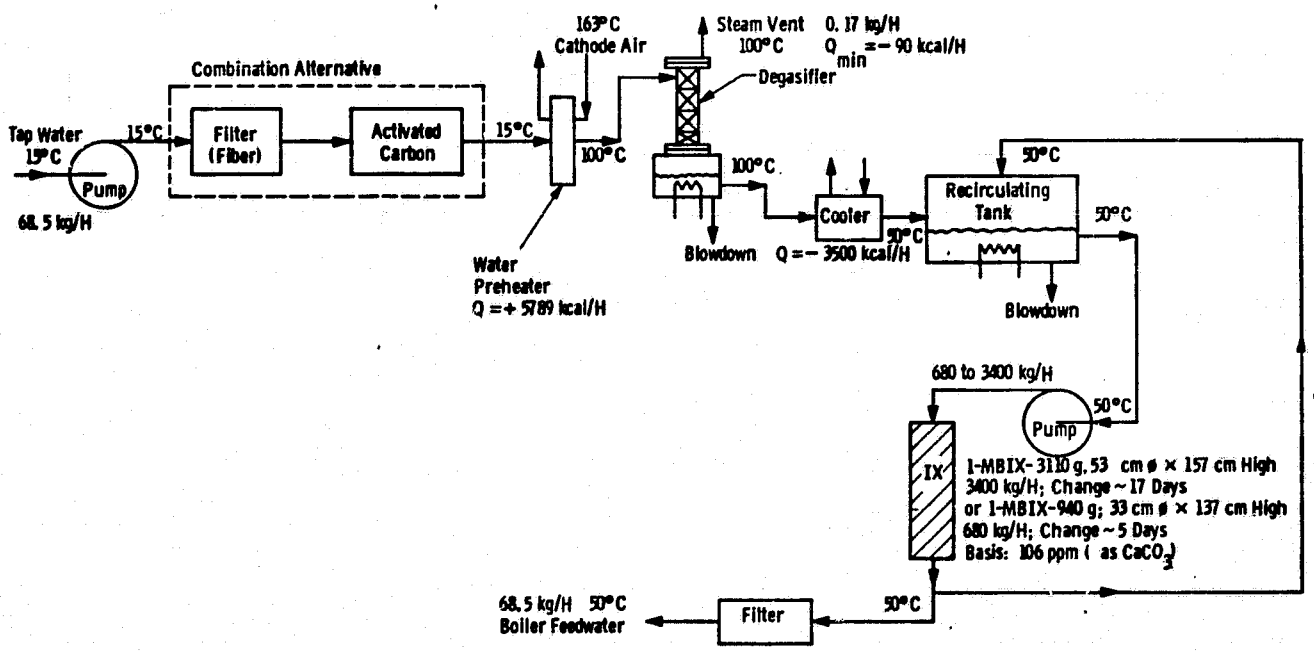

Fig. 6.4.2– Tap water purification train

The full and part load stream compositions, temperatures and flow rates given in Section 6.2.0 provided the design requirements for this equipment. The gas pressures shown in Figure 6.7.1 were determined by calculating the pressure drops around the system using preliminary estimates of pipe diameters (Figure 6.4.3) and lengths and the pressure drops specified for the heat exchangers, reformer, shift converter, etc. The pressures were in turn used in the compressor and pump specifications.

Detailed performance specifications were prepared for each of the equipment items and these were submitted to appropriate vendors in formal written requests for quotation. Copies of these specifications were also transmitted separately to the NASA Project Manager and several examples are included in Appendix A. The results of the formal RFQ are described in detail in the 8th Quarterly Report. The lowest cost estimates obtained for each of the major items of ancillary equipment are summarized in Table 6.4.2.

The "shift converter" shown in Fig. 6.2.1 is a special design. The size and dimensions were obtained by scaling from a 40 kW design provided by the NASA Project Manager and, therefore, no vendor quotes were obtained. It incorporates the fuel desulfurization, deoxygenation and preheating (to absorb the exothermic heat of the shift reaction) as well as the shift conversion into a single vessel. The cost estimate shown in Table 6.4.2 is an engineering estimate based on known costs of fabricating similar vessels and does not include the cost of shift catalyst or ZnO absorbent for desulfurization.

6.4.3 Burner Development and Heat Transfer Tests

The planned objective of this subtask was the development of a burner for a 60 kW flat slab reformer capable of stable, efficient and environmentally benign operation on the fuel cell spent fuel stream over the range of operating conditions anticipated for an OS/IES. The bluff body diffusion burner design shown in Figure 6.4.4 satisfies these

ORIGINAL PAGE IS
OF POOR QUALITY

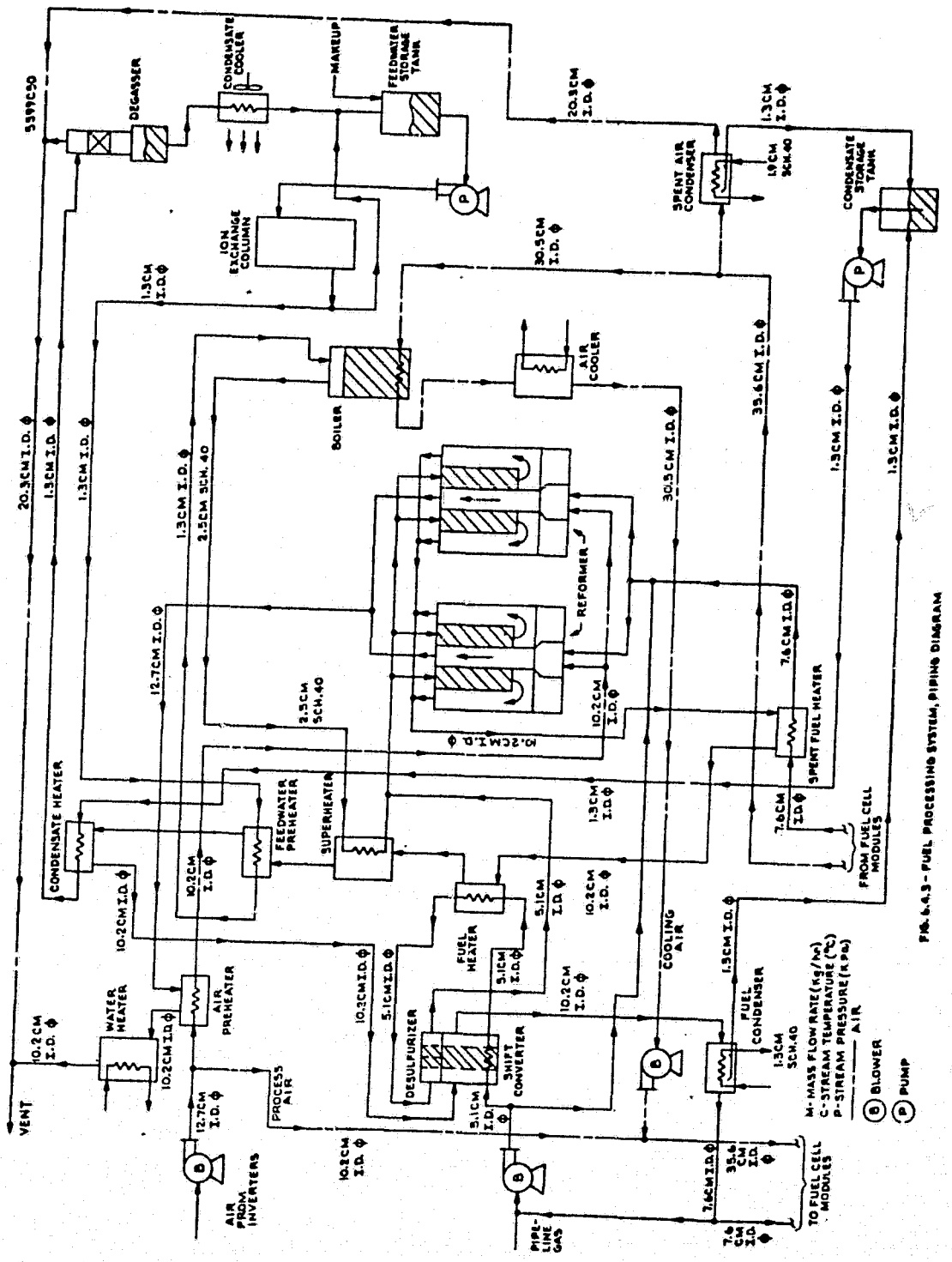

FIG. 6.4.3 - FUEL PROCESSING SYSTEM, PIPING DIAGRAM

TABLE 6.4.2

LOWEST PRELIMINARY COSTS FOR MAJOR ANCILLARY EQUIPMENT ITEMS

Item No.	Name	Lowest Quote Received
Heat Exchangers		
E-1	Air Preheater	$485
E-3	Natural Gas Heater	$185
E-4	Spent Fuel Heater	$650
E-5	Condensate Heater	$200
E-6	Water Heater	$490
E-7	Feedwater Preheater	$200
C-1	Air Cooler	$810
C-2	Condensate Cooler	$100
CD-1	Spent Air Condenser	$2,175
CD-2	Fuel Condenser	$1,995
B-1	Boiler	$2,475
BP-1	Start-Up Boiler (Electric)	$2,389
SH-1	Superheater	$200
SH-2	Start-Up Superheater (Electric)	$1,312
Gas Compressors		
CP-1	Air Compressor	$3,032
CP-2	Natural Gas Compressor	$4,825
CP-3	Recycle Compressor (High Pressure Design)	$6,438 (H.P. Blower)
CP-3A	Recycle Compressor (Low Pressure Design)	$9,231
Pumps		
P-1	Boiler Pump	$160
P-2	Condensate Pump	$~100
SC-1	Shift Converter	$3,000
TOTAL		$40,252

ORIGINAL PAGE
BLACK AND WHITE PHOTOGRAPH

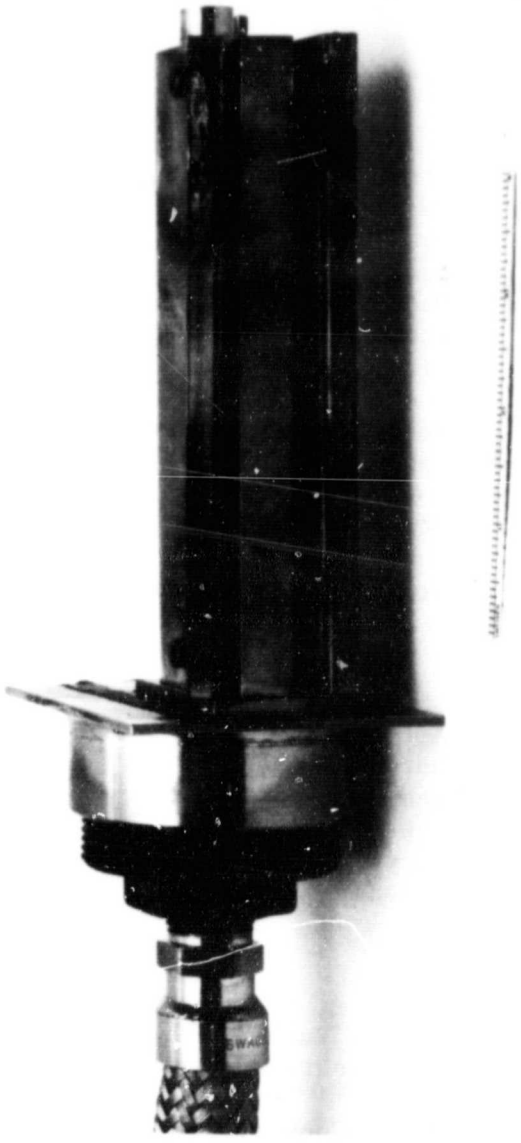

Figure 6.4.4. Bluff body burner - front view

ORIGINAL PAGE
BLACK AND WHITE PHOTOGRAPH

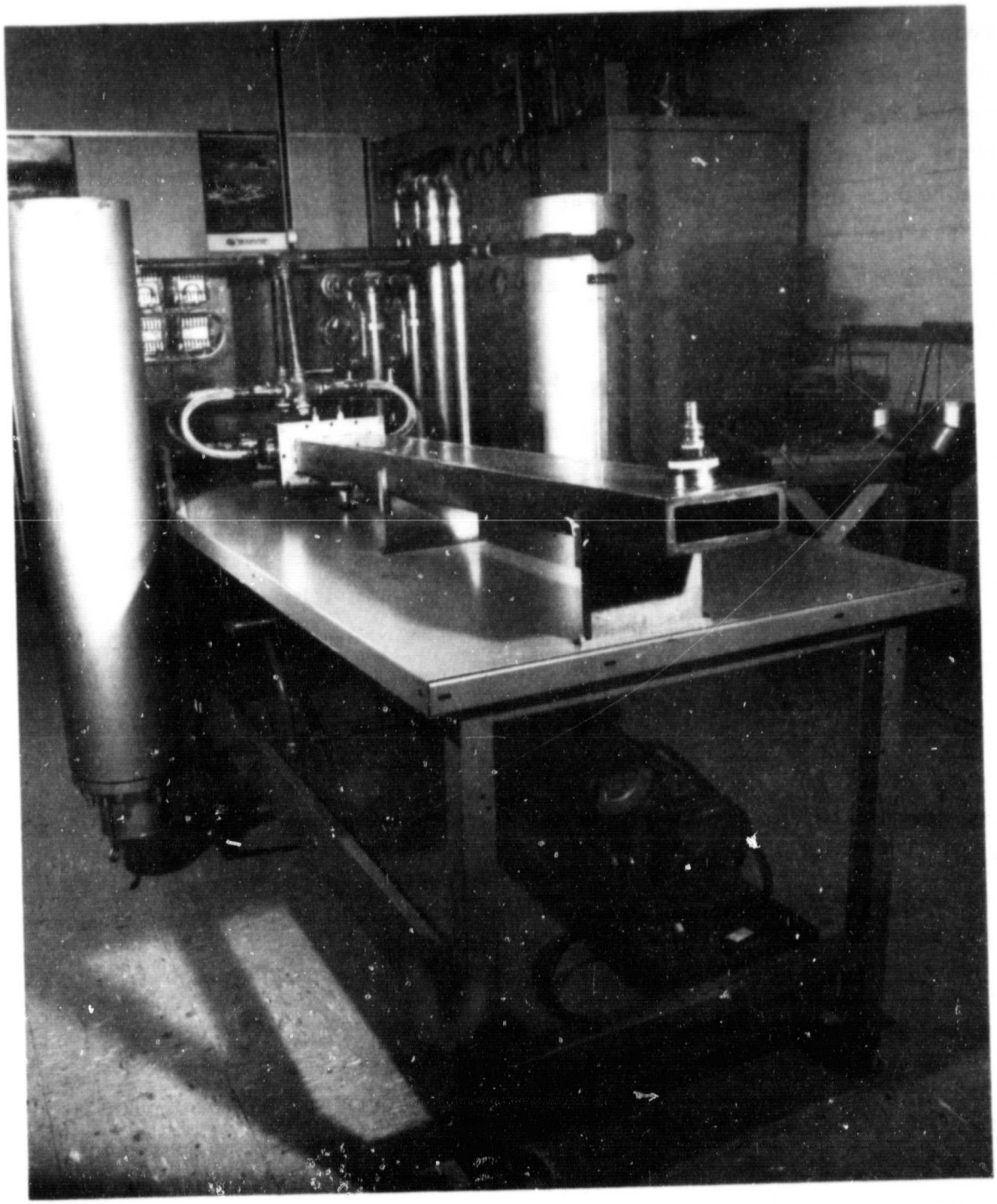

Figure 6.4.5. Reformer burner test rig

requirements as shown by the discussion of burner test results. The burner test rig (shown in Figure 6.4.5) was then used to measure packed bed heat transfer coefficients since it provided appropriate flow rates and compositions of combustion gases in a full scale rectangular duct. The burner and heat transfer test results are described below. The design of the test rig and the operating procedure are described in detail in the 2nd and 4th Quarterly Reports of this contract respectively.

Burner Tests

The burner for the OS/IES reformer must operate on the spent fuel which has a low combustible content and heating value and, depending on system design, may have a water vapor content as high as 25%. With the flat slab design, it must spread the combustion products over a wide area. The objective of these tests was to develop and demonstrate a burner concept that could operate stably over the required load range on these fuels. In the burner design shown in Figures 6.4.4 and 6.4.6 the fuel is introduced through the round tube, flows around the (central) bluff body and mixes with the air which flows around the outer sheet metal wrapper. The initial design did not have angles welded to the wrapper edges and mixing of the fuel and air depended on laminar diffusion. The resultant long, low intensity flames were not stable over the desired range of operating conditions. The addition of the angles provide for a region of turbulent mixing of the two streams. The test results described below refer to this configuration.

Burner Tests

The burner shown in Figures 6.4.4 and 6.4.6 was sized for a 60 kW reformer. Lean flammability limit tests were run on the burner at air flows corresponding to fuel cell outputs of 60 and 30 kW over wide ranges of fuel/air ratios. The composition and heating value of the spent gas that was used for the tests are tabulated in Table 6.4.3 along with a lower moisture content fuel which corresponded to a system with water removal between the fuel cell and the burner. Since the tests were

ORIGINAL PAGE
BLACK AND WHITE PHOTOGRAPH

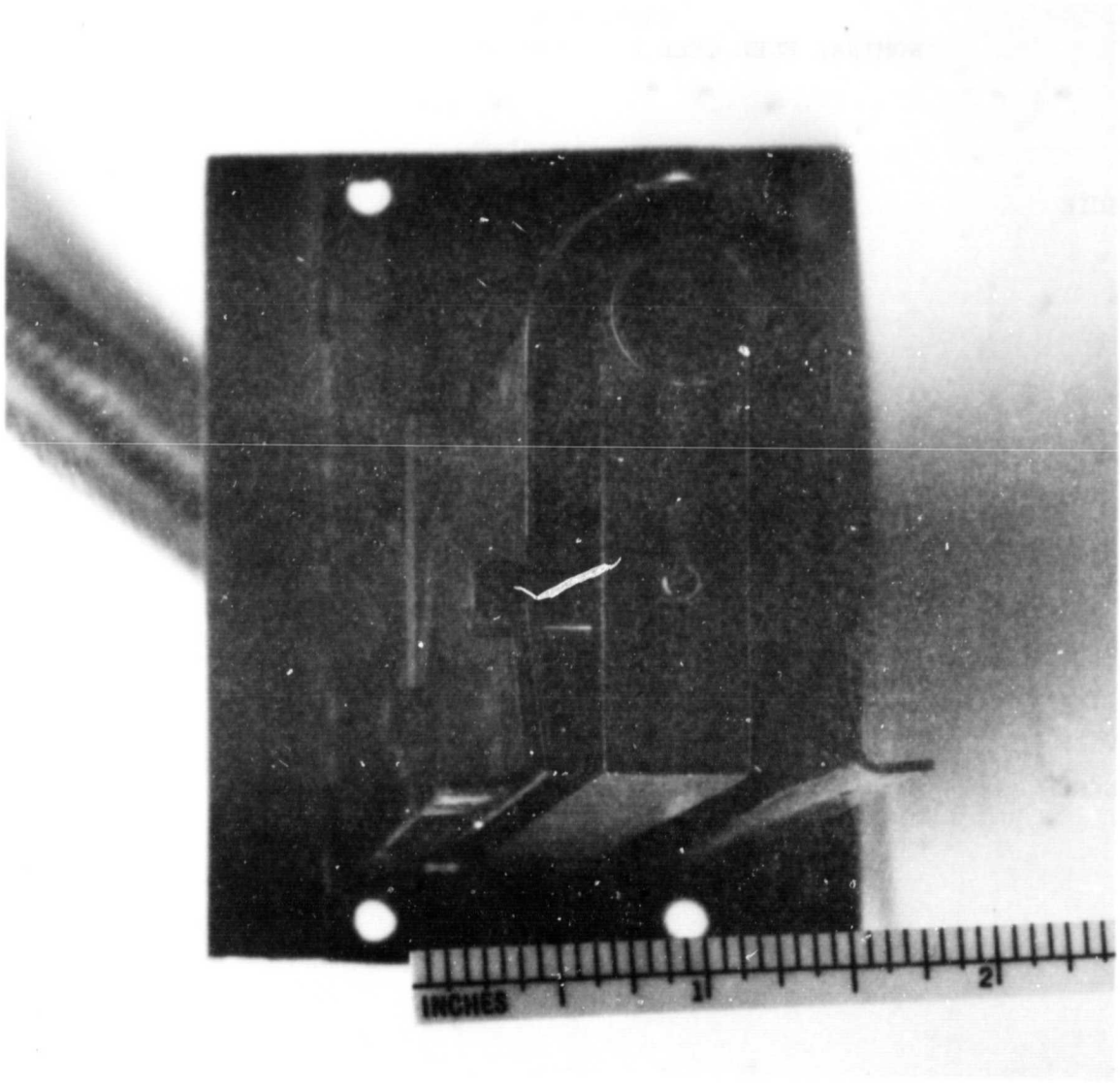

Figure 6.4.6 Bluff body burner - side view

TABLE 6.4.3
NOMINAL FUEL CELL EFFLUENT GAS COMPOSITION

	PER CENT BY VOLUME		
	"WET"		"DRY"
SPECIE	USED	PROPOSED	
CH_4	2.87	3.50	3.78
CO	2.35	2.90	3.10
H_2	32.21	39.30	42.41
CO_2	38.50	47.00	50.71
H_2O	24.07	7.30	0.00
LHV BTU/SCF	122	149	161

successful on the high water vapor content fuel gas, no testing was required to demonstrate effective burner capability on the low water vapor content fuel. The combustion chamber was evaluated for turndown or lean limit blowout range at atmosphereic pressure over the following ranges:

Air flow	0.32 to 0.80 normal* m^3/minute
Fuel Flow	0.008 to 0.08 normal m^3/minute
Air Temp	93 to 315°C
Fuel Temp	115 to 415°C

The method used to determine the lean blowout limit was to establish the air flow rate (nominally 0.32 m^3/min for 30 kW operation and 0.67 m^3/min for 60 kW operation) through the combustion air system and a nitrogen flow rate of approximately 0.13 m^3/min through the fuel system. The heaters were brought on-line and the air and fuel systems were preheated to the test conditions prior to ignition in order to conserve the fuel. When the desired burner inlet conditions were attained, the fuel gas was substituted for the nitrogen and the burner was lit. Fuel flow was rapidly decreased until an air equivalence ratio [actual fuel/air ratio divided by stoichiometric fuel/air ratio] of about 20 was reached, at which time the fuel rate was reduced in 10% increments until blowout occurred.

In Figure 6.4.7 the last combustion points prior to blowout are shown in terms of the correlating variables. The region below the line represents the area of stable combustion. The correlating variables are the air equivalence ratio, volumetric flow rate (Q), and the volumetric weighted temperature of fuel and air (T). The correlation parameter Q/T^2 is based on the Longwell parameter $\dot{M}^2/V \cdot P^2$ (mass flow/reactor volume-pressure^2) with the second order temperature effect included as suggested by Hottel. While the correlation of the limits of flammability with the correlation parameter is very good (correlation coefficient = 0.928), the trend of

*at 0°C and 101.3 kPa, 1 normal m^3 = 37.3 standard ft^3

ORIGINAL PAGE IS
OF POOR QUALITY

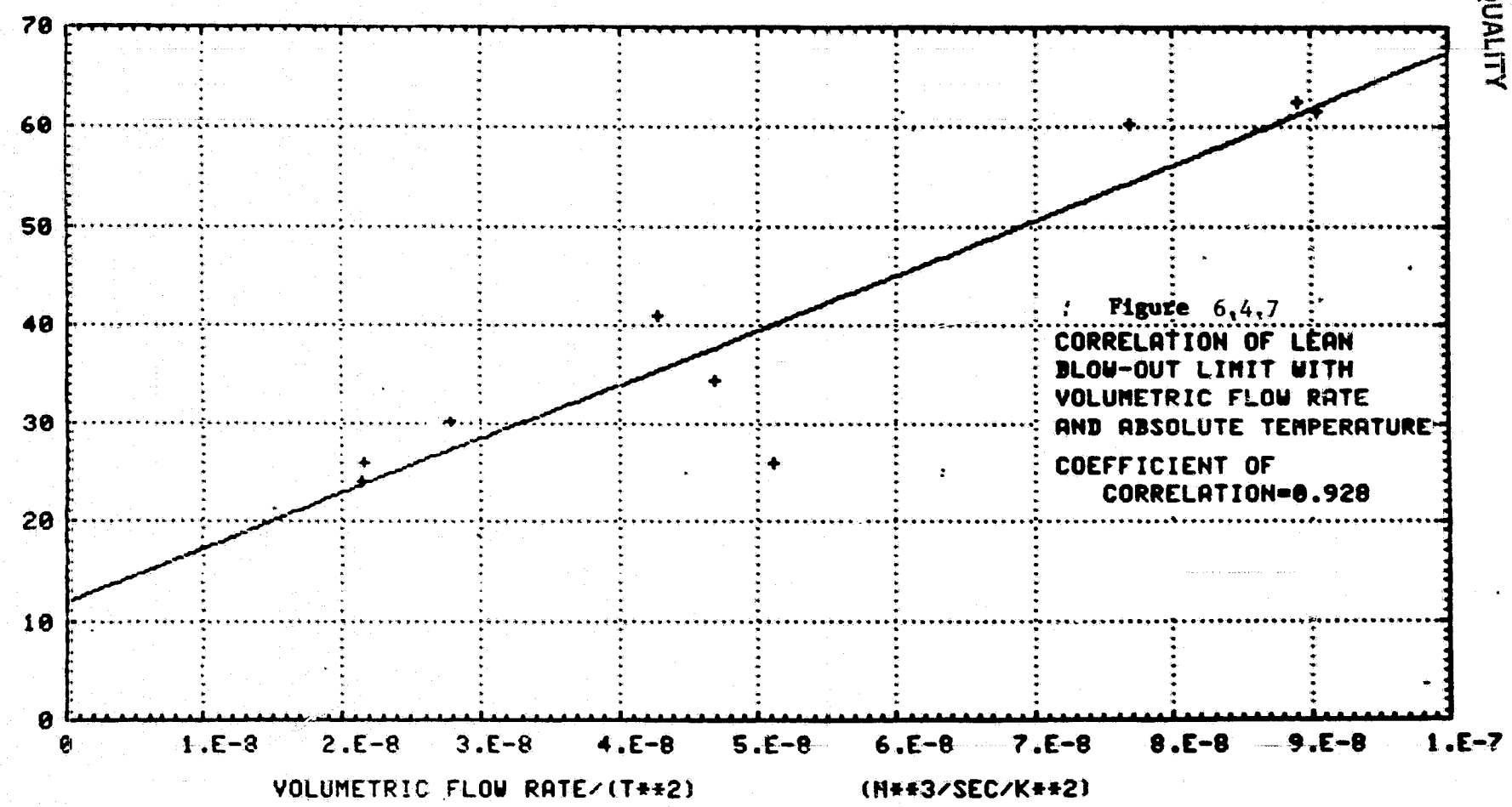

Figure 6.4.7

ORIGINAL PAGE IS
OF POOR QUALITY

increasingly lean blowout as the severity of the conditions increases with higher flows or lower inlet temperature, was contrary to expectations and the general behavior of combustion systems. This may be due to the heat loss of the flame to the environment in the water cooled flame duct. At low flows and high inlet temperatures, the value of Q/T^2 would be the smallest while the heat losses would be the greatest resulting in rapid quenching of the flame and requiring a relatively higher chemical energy release or lower air/fuel ratio than at the higher flows and lower inlet temperatures.

The burner demonstrated excellent performance levels at the high turndown conditions (>20) where flameout occurred. The temperature rise across the burner prior to blowout was as low as 30°C at air equivalence ratios between 30 and 40. NO_x emissions were less than 2 ppm at all conditions due to the low heating value of the fuel and the resulting low flame temperature, but improvements are needed in the CO and unburned hydrocarbon emissions, which approached values of 1400 ppm and 400 ppm respectively, at the 30 kW condition. A minor improvement in air/fuel mixing in the prototype burner could provide satisfactory part load CO and hydrocarbon emissions. The burner in its present configuration can provide a thermal source for evaluating the heat transfer elements of the reformer and serve as a design basis for an integrated burner-reformer unit.

Packed Bed Heat Transfer

To determine the applicability of various published correlations of packed bed heat transfer data, the burner test rig was used. This rig provided the ability to test a full scale packed bed with combustion products at design flow ratios, temperatures and compositions.

As indicated in Figure 6.4.8, a 44 mm by 152 mm rectangular cross section heat exchanger was installed downstream of the reformer burner. This section was packed with 13 mm diameter balls. With a fuel composed of 3.09% CO, 3.79% CH_4, and 50.70% CO_2 by volume, a flame

C-4

ORIGINAL PAGE IS
OF POOR QUALITY

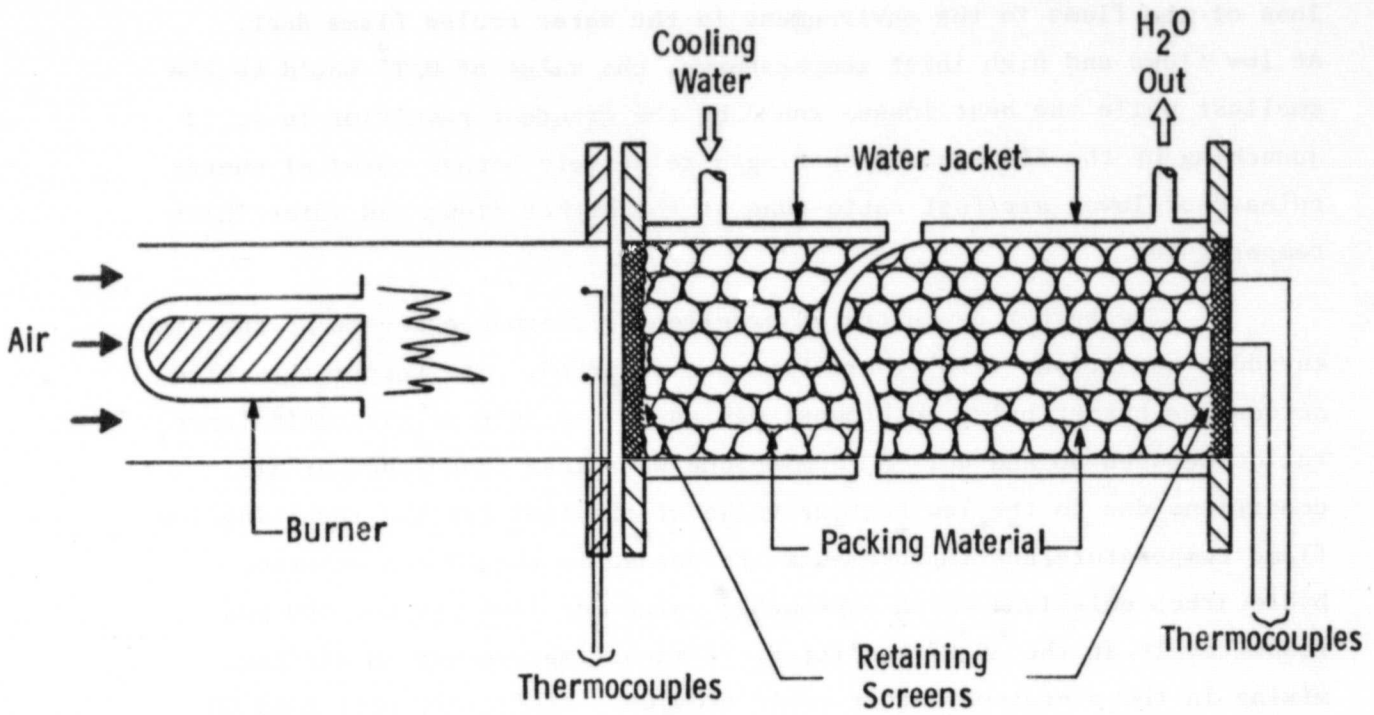

Fig. 6.4. 8– Packed bed heat exchanger test facility

temperature of approximately 870°C (1600°F) was maintained at the inlet to the heat exchanger with about an 800°C drop across the 1.4 m length of the heat exchanger. Tests with stainless steel and high density alumina ceramic balls were run to determine the effect of packing material on heat transfer coefficients. Six millimeter mesh stainless steel screen was welded on the inlet flange to contain the balls. The heat exchanger was packed in the vertical position and the stainless steel screen was clamped over the oulet flange before installation into the test facility. It was estimated that there was a forty percent void fraction in the bed.

A total of nine tests were run. The test conditions and results are summarized in Table 6.4.4. In addition the results are plotted along with standard correlations from the literature in Figure 6.4.9. The agreement between the experiments and the Leva correlation for cooling is excellent. The correlating parameters are the Nusselt number $\left(\frac{h\ D_E}{k}\right)$, where D_E is the duct equivalent diameter, and the Reynolds number $\left(\frac{GD_p}{\mu}\right)$, where D_p is the diameter of the individual balls of packing.

TABLE 6.4.4
PACKED BED HEAT EXCHANGER TEST RESULTS

Test No.	Average Heat Transfer Coefficient ($W/m^2/°C$)	Bed Material	Reynolds Number	Nusselt Number	$h(Btu/h/Ft^2/°F)$
1	64.8	SS	190	68.8	11.4
2	82.4	SS	194	87.8	14.5
3	83.5	SS	212	88.3	14.7
4	77.2	SS	37.8	181.8	13.6
5	140	SS	824	148	24.6
6	66.5	CER	214	70.5	11.7
7	55.7	CER	231	59.1	9.8
8	109	CER	572	116	19.2
9	110	CER	812	117	19.4

ORIGINAL PAGE IS
OF POOR QUALITY

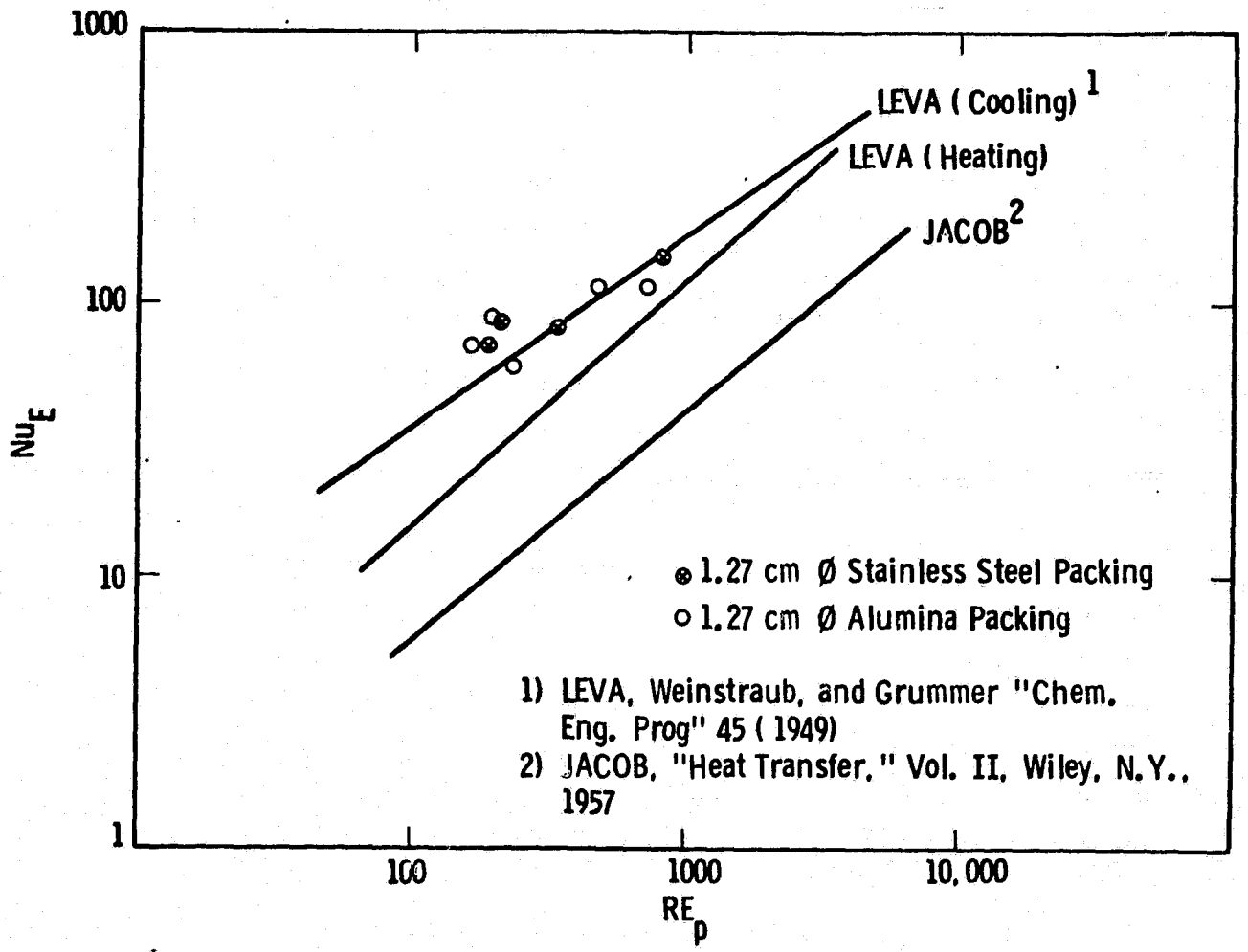

Fig. 6.4.9— Comparison of packed bed test results with standard correlations.

6.4.4 Reformer Design

The conceptual reformer design for the prototype FCS consists of two identical units of the design shown in Fig. 2.3. Each unit is sized to provide sufficient hydrogen for 60 kW-d.c. of fuel cell output. The double counter-current flow configuration provides for excellent utilization of heat and the flat slab is a manufacturable and maintainable embodiment that is appropriate for atmospheric pressure operation. The corrugated walls provide for thermal expansion with rigidity. In this design, hot combustion gases flow from the burner through the inner tubes. The reforming gases flow (in the counterflow direction) through the catalytic bed in the annular space adjacent to the combustion gas tubes. The gases turn 180° on exiting the catalytic bed to flow counter (and transfer heat) to the reforming stream.

The 60 kW reformer dimensions given in Table 6.4.5 for the idealized design and nomenclature of Figure 6.8.5 were calculated based on experimental data obtained in the 10 kw tubular reformer tests (Section 6.6) and parametric studies performed using the BOLTAR computer model (Section 6.8). The idealized design consists of three concentric rectangular ducts. A 1.27 cm thick catalytic bed is sandwiched between a 1.27 cm thick product gas return duct and a central 1.9 cm thick combustion gas duct. Overall dimensions for the reformer module are .684 m wide by 1.25 m high with a thickness of .093 m. This design should provide for an 80-90% methane conversion at the flow rates and temperatures projected in the fuel processing system.

TABLE 6.4:5: 60 KW REFORMER DIMENSIONS

Catalyst volume = .02124 m^3

Catalytic duct cross-sectional area = .017 m^2

ASLAB1 = .610m BSLAB1 = .019m
(Combustion Gas Duct - 1.9 cm thick).

ASLAB2 = .617m BSLAB2 = .027m

ASLAB = .643m BSLAB = .052m
(Catalytic bed - 1.27cm thick)

DELTA = .00381m (Wall thickness)

AASLAB = .676m BBSLAB = .085m
(Product Gas Duct - 1.27 cm thick)

Z = 1.25m (height)

6.4.5 Controls and Instrumentation Subsystem

The objective of this task was to define the control and instrumentation requirements and develop a conceptual design of the CIS for the prototype fuel conditioner subsystem. Further development and the detail design were to be carried out in subsequent phases of the program.

The Phase II effort included:

1. Determination of the functional requirements of the CIS.
2. Determination of the control functions required for stable and efficient part load operation.
3. Development of detailed operating procedures to be carried out by the control system.
4. Determination of equipment availability, including a microprocessor, to perform the necessary functions.

The resulting control system (valves, sensors, by-pass loops, etc.) is shown in the P&ID diagram (Figure 6.2.1) and is described in more detail below and in Appendix B.

Functional Requirements

The purpose of the Control and Instrumentation Subsystem (CIS) of the prototype is to provide control of the components to adapt the process flow configuration to meet the time varying operational requirements and acquire, display, and record data. The control action must achieve the following objectives:

1. Safety of operation is maintained at all times so that there is no hazard to personnel and equipment.
2. The performance is optimized at part load conditions.
3. Startup and shutdown are achieved in orderly fashion within specified operating conditions of all components.

The subsystem is designed mainly for automatic unmanned operation and provisions are included for a portable test unit which can be used for power system diagnostics during maintenance service or for manual operation. The safety related actions are always taken automatically. The following

functions are performed by the CIS:

- Startup and shutdown
- Recording and/or display of various pressures, temperatures, flow rates, currents, voltages and power.
- Partial or total shutdown at the incipience of unsafe conditions.
- Load follow with rapid transient capability supplied by an electrical grid.
- Surplus power delivery to an electrical grid.
- Computation of flow rates, process composition and electrical power.
- Optimization and coordination of the performance of all components within the power unit.
- Transmission of performance data and alarms to either a local or remote point.
- Acceptance of manual control commands from a local or remote terminal.

Description of Prototype CIS

The OS/IES Fuel Processing System comprises five interrelated subsystems, i.e.,

1) Condensate Water Subsystem
2) Fuel Flow Subsystem
3) Spent Fuel Subsystem
4) Water/Steam Subsystem
5) Air Subsystem

The subsystems are controlled independently of each other by a master controller, but a change in any subsystem function could have an effect on the operation of any or several other subsystems. Overiding the master controller are the alarm devices in each of the subsystems which can shut down the whole fuel processing system in the event that a dangerous or damaging condition persists beyond some selected time interval.

The master controller JRC-1 shown in Fig. 6.2.1 receives its signal from the output voltage of the fuel cell(s). This in turn is a function of the load demand. The controller then roughly positions all critical valves to correspond to a change of load (e.g., one third to two thirds load). Trimming is then done as required by power pulses to the various motor drives. The distribution of fuel and air to the individual fuel cells is accomplished by diverter or damper valves which are not part of the fuel processing system. The prototype control is complicated but it will be simplified for commercial units based on results of prototype tests. All instrument readings, monitoring and generating (including data from the fuel cells and inverter) data will be recorded during development. For the prototype unit, the fuel cell is connected to the utility line so that it can feed surplus electrical energy to the grid and is not required to follow the load instantaneously.

The valves shown in Fig. 6.2.1 are for control. Not shown are many manual and isolation valves which would be installed around each major component enabling one to remove the component from service for repair or replacement. Quotations were not solicited for these valves, meters or instruments, however many manufacturers catalogs were obtained and reviewed to establish that these minor components with the required operating characteristics are available.

It should be pointed out that much of the instrumentation shown in Fig. 6.2.1 is actually part of the control and microprocessor system (at least for the prototype), but is shown at the transmitter location in order to avoid the confusion of many dashed instrumentation lines. Similarly some of the shorter lines shown connecting transmitters to controllers and valves directly would be connected through the microprocessor.

The system described above and shown in Fig. 6.2.1 evolved through development of various operating scenarios and incorporated feed back from manufacturers and reviews by control engineers at the Westinghouse R&D Center. Step by step procedures for startup and load changes were

ORIGINAL PAGE
BLACK AND WHITE PHOTOGRAPH

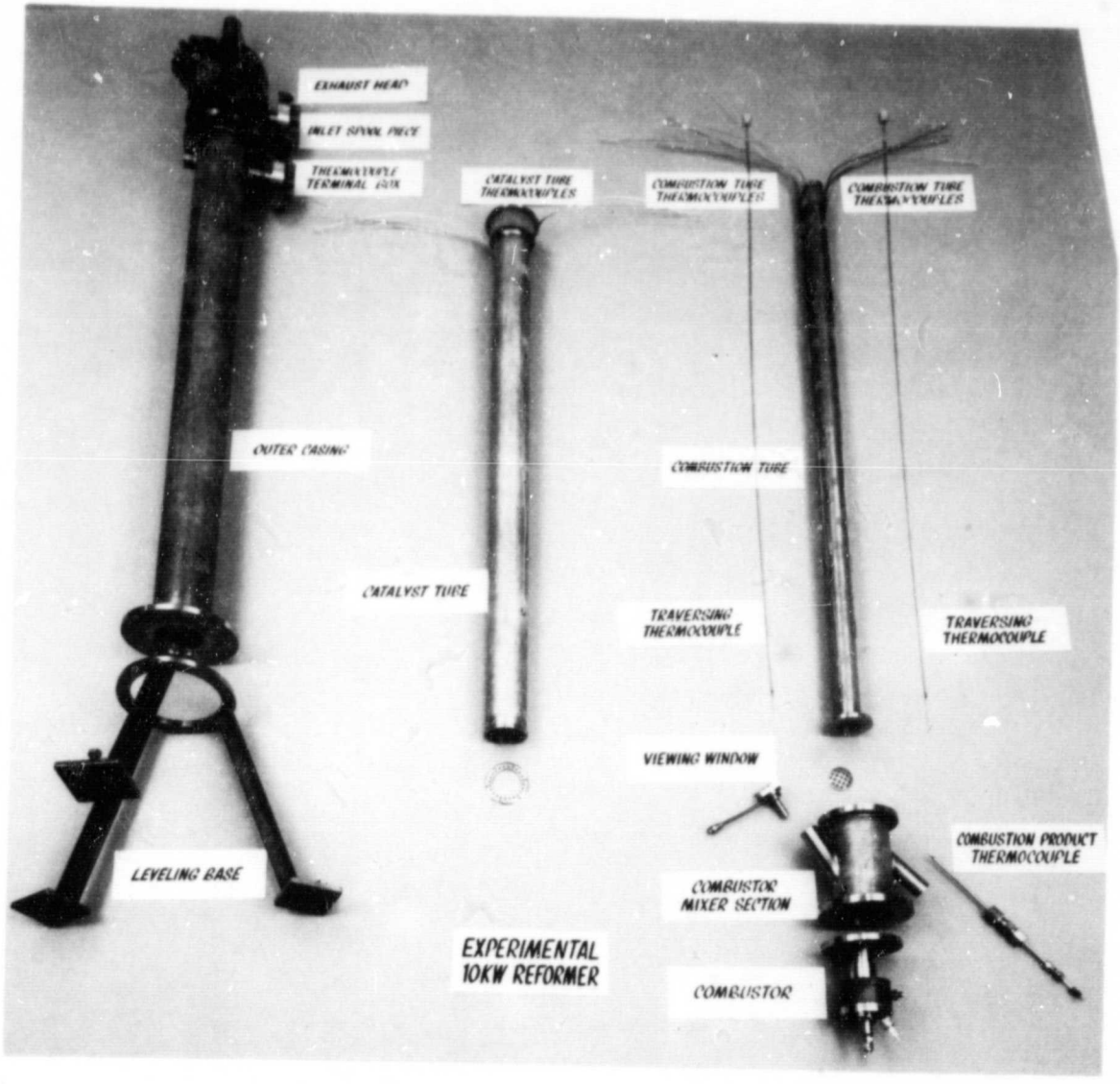

Figure 6.6.1. Dissassembled 10kw reformer

developed to determine the functions required and these are included in Appendix B.

Based on the detailed procedures, the preliminary microprocessor specification included in Appendix B was prepared and sent to six suppliers. The Figures referred to in the preliminary specification were subsequently modified to Figure 6.2.1 through a series of telephone conversations and informal meetings.

It was determined that any of the six suppliers could provide microprocessors to satisfy the CIS requirements. The preliminary quotations ranged from $20,000 for the hardware alone to $48,000 for the hardware and software.

6.5 Critical Systems Parameters

The objective of this subtask was to identify and explore the effects of various OS/IES operating and design parameters on the fuel conditioning subsystem to arrive at an optimum system. Since the system task was deleted from the contract, there was no opportunity to explore these tradeoffs fully. As a result no work was carried out under this subtask. However, with the framework provided by the Phase I OS/IES design, subsystem and component optimizations were made as described in the discussions of the work carried out in other subtasks.

6.6 10 kW Reformer

In order to achieve its potentially high energy utilization, the OS/IES requires a reformer that recovers the endothermic heat of the reforming reaction from the combustion of the spent fuel stream and by recuperation from the exiting reforming stream. At the same time, it must be compact and inexpensive and its capacity is far smaller than those of commercial reformers. The double counterflow flat slab concept shown in Figure 2.3 promises to satisfy these requirements for the atmospheric pressure OS/IES. In order to gain operating experience and obtain performance data under actual operating conditions, the 10 kW reformer shown in Figures 6.6.1 and 6.6.2 was designed, built,and tested.

ORIGINAL PAGE
BLACK AND WHITE PHOTOGRAPH

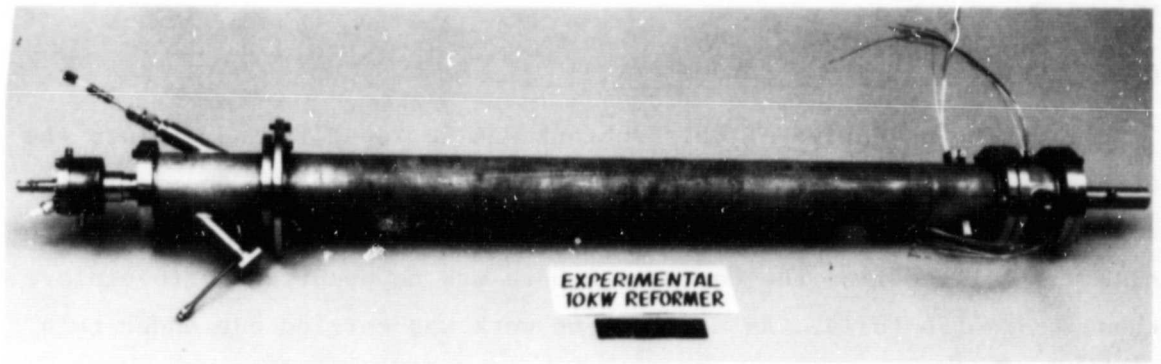

Figure 6.6.2. Assembled 10kw reformer

The experience and data acquired under this subtask provide a firm technical basis for the design and construction of a 60 kW double counterflow reformer for a prototype OS/IES system. The temperature and composition measurements and performance of the reformer verified the BOLTAR program described in Section 6.8 and insure that it is a viable design tool.

6.6.1 Reformer Design and Fabrication

In order to simplify the design and fabrication and provide for operation at elevated pressures, if required, a tubular design (Figure 6.6.3) was selected. The unit was sized to provide 80-90% conversion of a methane flow of 110 g mol /hr (∿10 kW of fuel cell output) with a steam flow of 330 g mol/hr. The computer program described in Section 6.8 was used to perform the heat transfer and reaction rate calculations required to size the unit. The calculation resulted in an active length of 1.2m with the three tubes having diameters of 5, 8 and 10 cm respectively from the inner (combustion tube) to the outer. The spent fuel combustion products flow upward through the inner tube, the reforming stream flows down through the catalyst bed located in the 1.3 cm annulus between the 2 inner tubes and the products of the reformation flow upward in the 0.8 cm annulus between the middle and outer tube.

As shown in Figure 6.6.3, bellows are used in the two inner tubes to accomodate the differences in thermal expansion which will occur due to the differences in temperature among the tubes at operating conditions. The tubes are 316 SS and the flanges are 304 SS. The arched plate shown at the bottom of the combustor tube to support the heat transfer packing is Inconel 600.

The combustor shown in Figure 6.6.3 is a vortex burner that was available from a previous project. It was operated over the complete range of conditions anticipated prior to its use. The ceramic lined mixer between the reformer and the combustor provides for straightening of the flow and completion of combustion between the burner and the active area of the reformer.

ORIGINAL PAGE IS
OF POOR QUALITY

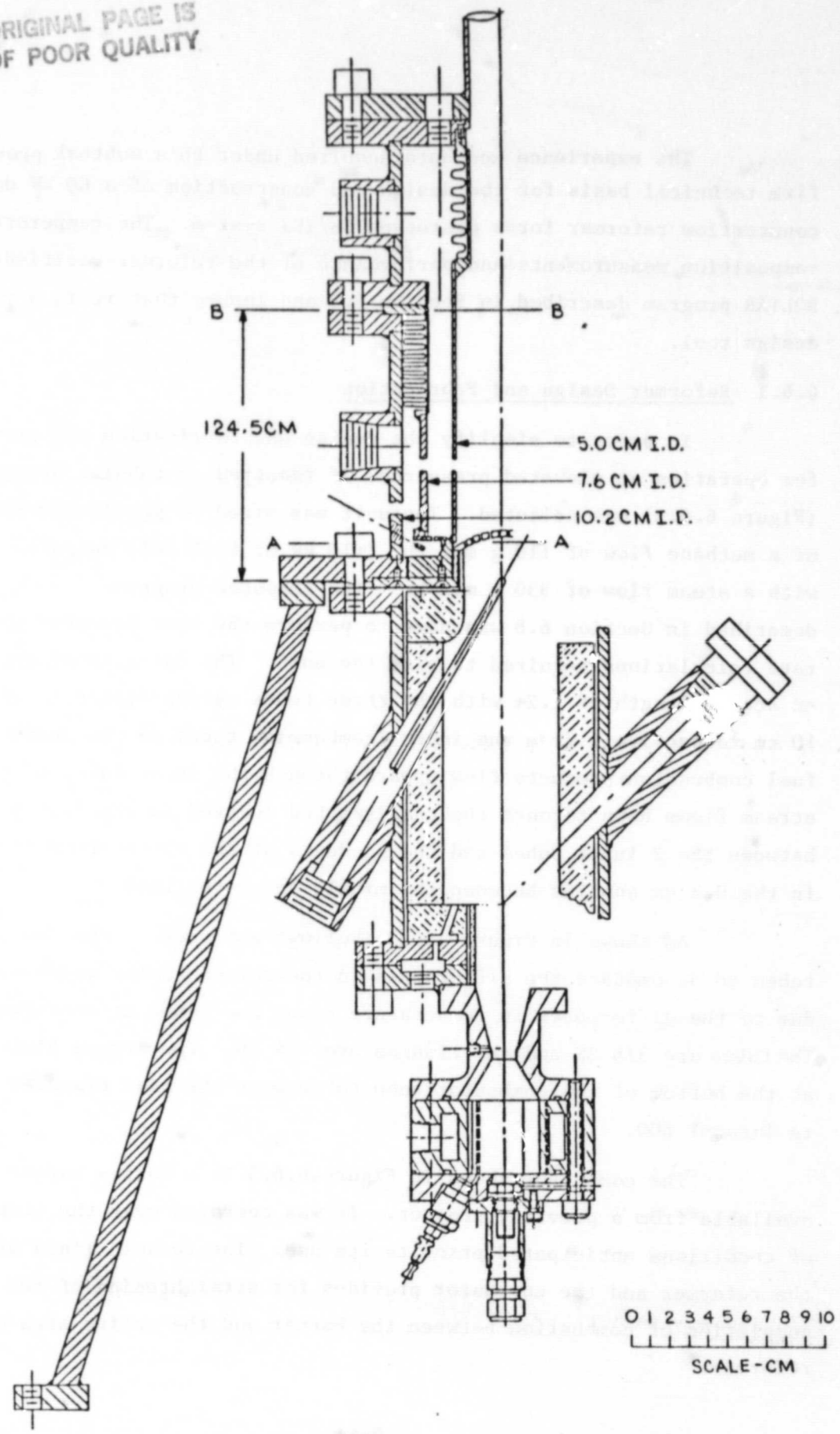

FIG.6.6.3 ASSEMBLY OF 10 KW REFORMER

The 10 kW reformer model was built in the Westinghouse R&D model shop from the assembly drawing shown in Figure 6.6.3. The 124.5 cm dimension i.e., the length of the reformer section was the only dimension given to the machinist. All other dimensions were scaled from the drawing and the various components were machined to fit. The three thermocouple junction boxes, thermocouples, sight port, flexible bellows, and combustor were supplied by the "cognizant engineer."

All temperature measurements in the reformer were made with thermocouples, although sight ports were installed at several locations for the use of optical or radiation pyrometers. With the exception of the combustion gas inlet temperature, which required a platinum rhodium couple, chromel alumel couples were used. The type and location of the thermocouples may be seen with reference to Figure 6.6.4. Two columns of thermocouples (1-3, 21-24) are placed 180° apart on the outer surface of the catalyst reformer tube. Three columns (4-20) are located 120° apart on the outer surface of the combustion tube. One column of reformer and combustion tube thermocouples are on a common radius with one traversing thermocouple(28). Eventually the traversing couples (28 and 29) were displaced a few degrees to reduce interference with the gas flow through the catalyst. The platinum rhodium couple (27) may be seen at the entrance to the combustion tube.

All wall thermocouples were vacuum welded, sealed, and spot welded to the reformer tube and combustion tube walls. Bundles of lead wires were brought out through three junction blocks. The traversing thermocouples are sheated 1/16" diameter chromel alumel and slide inside a 1/8" diameter tube which is fixed at both the upper and lower ends as shown in Figure 6.6.4.

6.6.2 Test Station Design and Construction

Figure 6.6.5 is a flow diagram of the test station designed and built to provide the conditions needed for the double counterflow, 10 kW reformer tests. The system provides a mixture of controlled,

ORIGINAL PAGE IS
OF POOR QUALITY

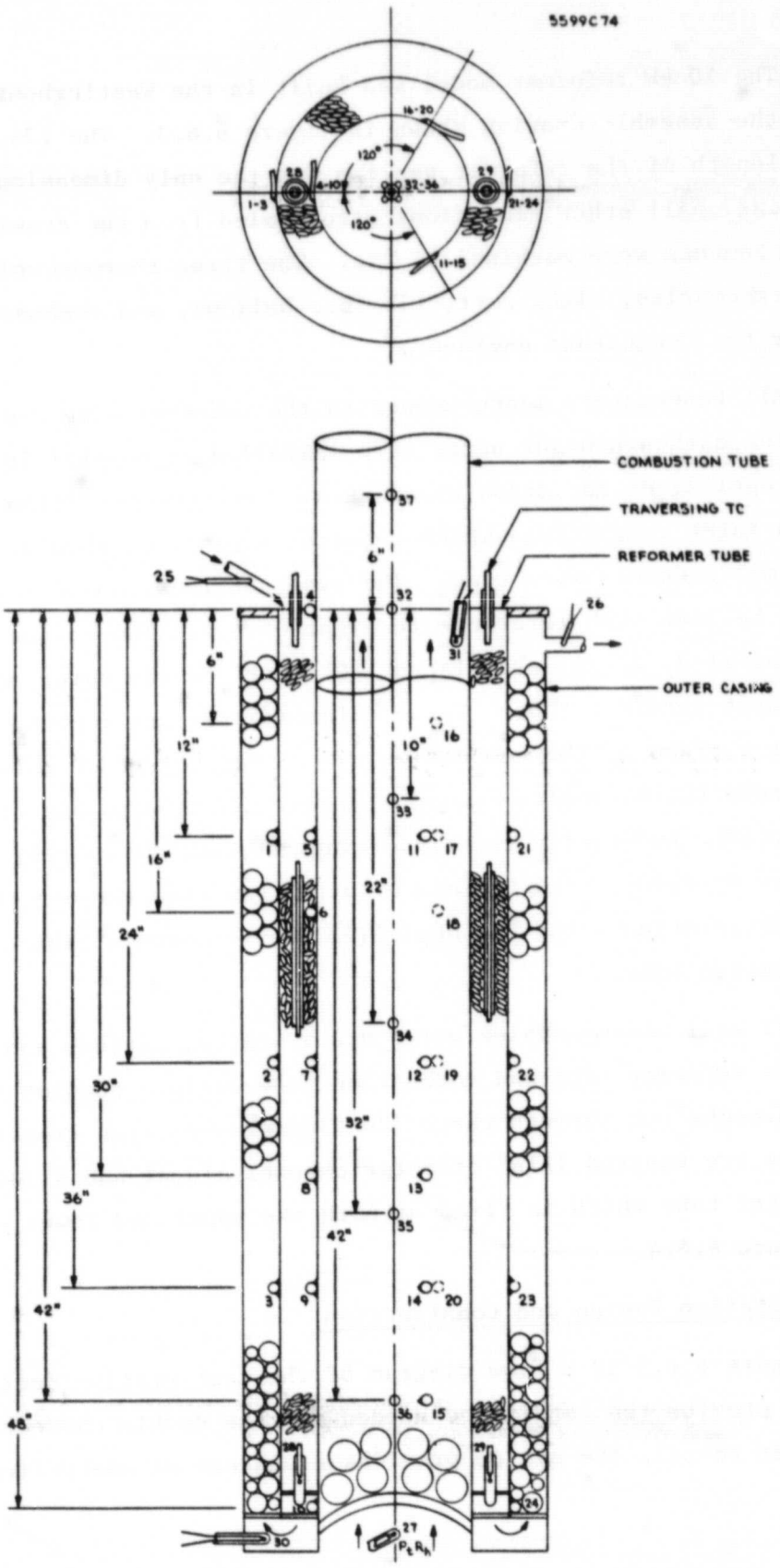

FIG. 6.6.4 10KW EXPERIMENTAL REFORMER THERMOCOUPLE LOCATION

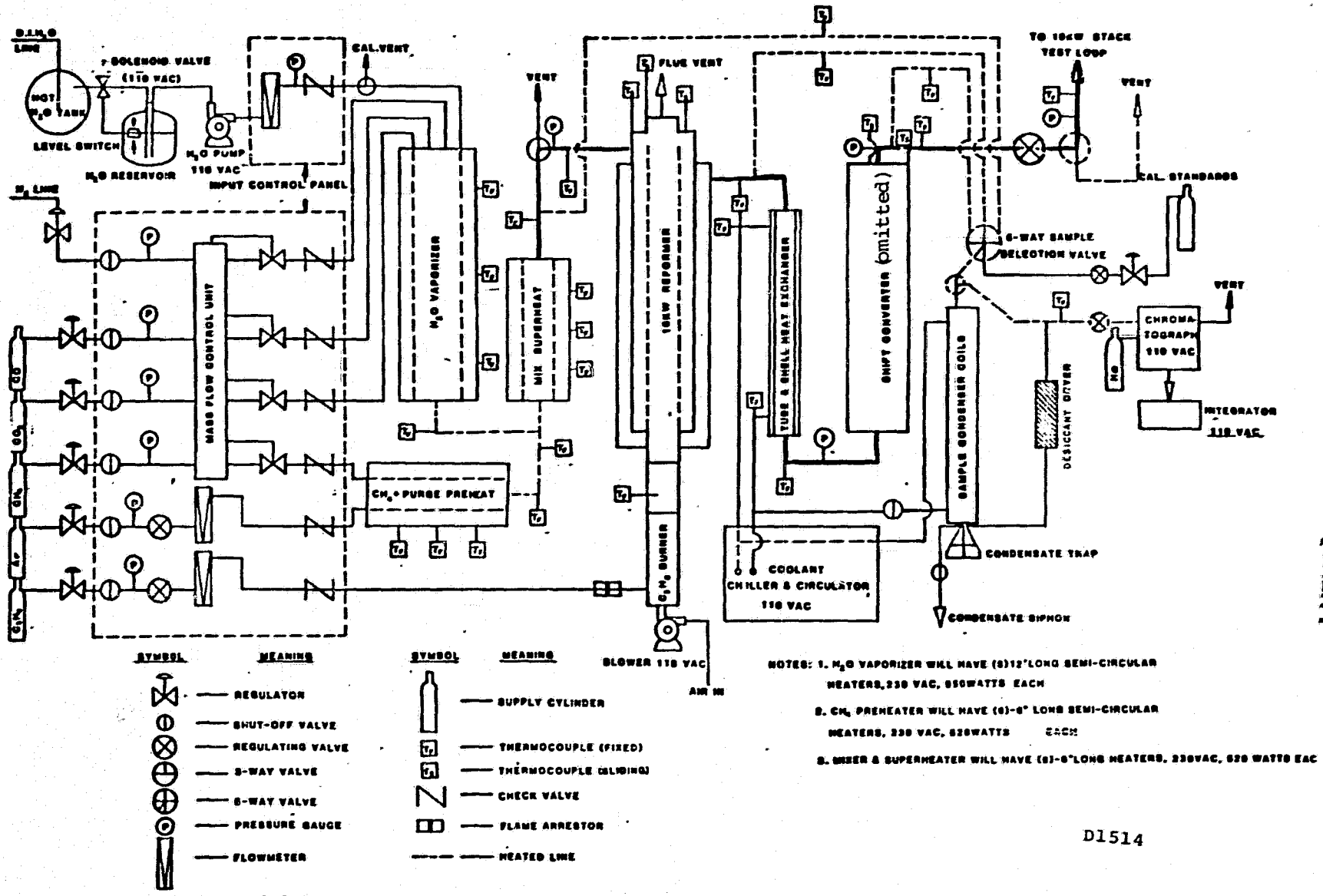

FIGURE 6.6.5. FLOW DIAGRAM FOR 10 kW METHANE/STEAM REFORMER

ORIGINAL PAGE IS OF POOR QUALITY

ORIGINAL PAGE IS
OF POOR QUALITY

TABLE 6.6.1. 10 kW REFORMER TESTS

Reforming Feed	Reformer Gas Flow Rate, kg/hr	Burner Gas Flow Rate, kg/hr	Burner Gas Inlet Temp., °C	Completion
Series 0 Shakedown dry run of the integrated system				✓
Series 1 No catalyst, no packing in combustion gas				
1. $Ar + H_2O$	9.05	26.34	1093	✓
2. $CH_4 + H_2O$	9.05	26.34	1093	✓
Series 2 With catalyst but no packing in combustion gas				
1. $Ar + H_2O$	9.05	26.34	1093	✓
2. $Ar + H_2O$	9.05	26.34	1204	omitted
3. $CH_4 + H_2O$	9.05	26.34	1093	✓
4. $CH_4 + H_2O$	9.05	26.34	1204	✓
Series 3 With catalyst and with packing in combustion gas (No packing in the regenerative, outer annular space)				
1. $Ar + H_2O$				
1a.	9.05	26.34	1000	✓
1b.	9.05	19.76	1000	omitted
1c.	9.05	13.17	1000	omitted
1d.	6.79	19.76	1000	✓
1e.	4.53	26.34	1000	omitted
1f.	4.53	13.17	1000	✓
2. $CH_4 + H_2O$				
2a.	9.05	26.34	1093	✓
2b.	9.05	19.76	1093	✓
2c.	9.05	13.17	1093	✓
2d.	6.79	19.76	1059	✓
2e.	4.53	26.34	1093	✓
2f.	4.53	13.17	1104	✓
Series 4 With catalyst packing in the regenerative, outer annular space and packing with combustion gas				
1. $CH_4 + H_2O$	9.05	26.34	1000	omitted
2. $CH_4 + H_2O$	9.05	26.34	1100	omitted

✓ = completed

metered, and preheated water vapor, carbon dioxide, carbon monoxide, hydrogen, and methane. The reformer products are cooled in a shell and tube heat exchanger prior to venting. The shift converter shown in the figure was intended for use in later phases of the contract in which products were to be used for stack testing. This was not done during this phase.

As shown in the figure, samples of the process gas could be obtained from the reformer inlet or exhaust or downstream of the shell and tube heat exchanger by positioning of the 5-way sample valve. This valve also provided for sending the sample through a dryer loop or directly to the chromatograph and for a calibration standard for the chromatograph.

Figure 6.6.6 is a photograph of the test station with the 10 kW reformer (wrapped in reflective insulation) installed.

6.6.3 10 kW Reformer Testing

Table 6.6.1 summarizes the series of tests planned and conducted for the 10 kW reformer. The Series 0 test was a shakedown dry run on the integrated system; included in it were the reformer, thermocouples, vaporizer, automatic water generating system, temperature controllers, burner, cooling condenser and gas chromatography analyzer. The remaining tests were planned to provide heat transfer data as well as reaction rate data. Series 1 was an empty tube run (i.e., no catalyst or packing in the tubes). For Series 2, the pelleted form of the reforming Catalyst 100 described in Section 6.4.3 was added. For Series 3, 9.5mm diameter alumina spheres were added in the flue gas tube (inner cylinder) to increase heat transfer from the combustion products to the reforming stream.

The purpose of the Series 1 and 2 tests was to provide a base-line to determine the extent in heat transfer (and reaction conversion) improvement obtained with packing in the flue gas and product tubes. The Series 4 tests would have shown the further improvement resulting

ORIGINAL PAGE IS
OF POOR QUALITY

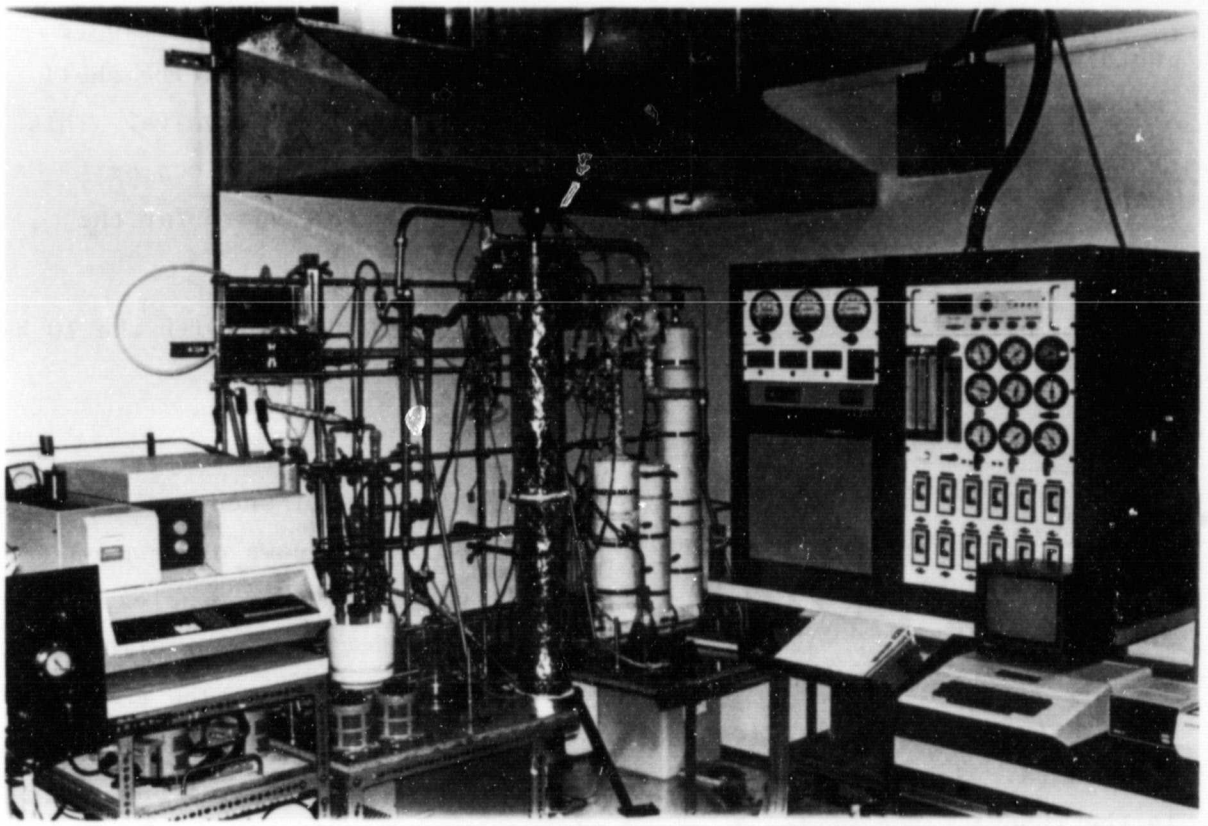

Figure 6.6.6 10 kW double counterflow reformer installed in reformer test station

from packing in the regenerative annular space. The series was not run due to a lack of time and funds.

The improvement in heat transfer with catalyst and packing is shown in Figures 6.6.7 in which the temperature profiles of the inert gases (Argon plus water vapor) under similar sets of flow conditions, i.e., Runs 1.1, 2.1, 3.1a (no reaction runs) are plotted. The packing in the flue clearly improved heat transfer and produced a much more uniform temperature distribution in the reforming bed. The lower final temperature shown for Run 3 was largely due to a lower combustion products temperature as given in Table 6.6.1.

Figure 6.6.8 compares the temperature distributions of the reforming gases when the reactions took place (runs 2.3 and 3.2a). The improvement of 70°C with packing on the flue gas side was accompanied by a substantial increase in CH_4 conversion (from 15% to 80%) and a concomittant ($\sim$57%) increase in heat supplied to the endothermic reforming reaction.

The effect of the endothermic nature of the steam reforming reaction on the thermal profile in the bed is vividly shown in Figure 6.6.9 which compares temperature profile obtained with inert gases with those obtained with reforming gases.

The measured CH_4 conversions and product compositions for Series 2 and 3 are summarized in Table 6.6.2. In most cases the conversions are close to the theoretical equilibrium values for the same exit temperatures and in two cases (2.3 and 3.2a), the methane conversions are higher than the theoretical equilibrium conversions. The reformer output product at the 10 kW reformer design condition (i.e. Run 3.2a) had the following compositions:

Dry Basis	Mole %
Hydrogen	72
CO_2	13
CO	10

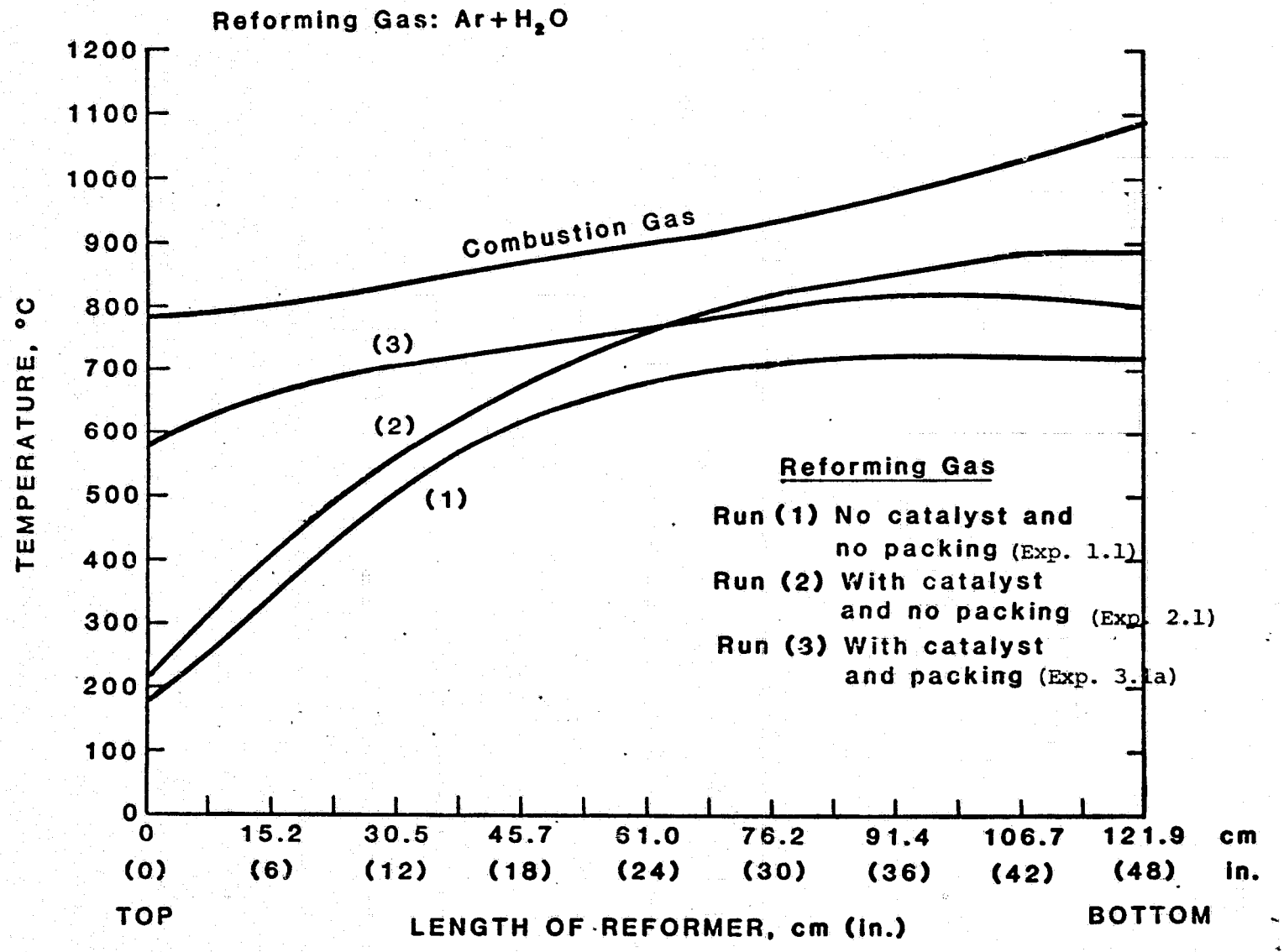

ORIGINAL PAGE IS
OF POOR QUALITY

D1841

FIGURE 6.6.7. EFFECT OF CATALYST AND PACKING ON TEMPERATURE DISTRIBUTION (INERT GASES)

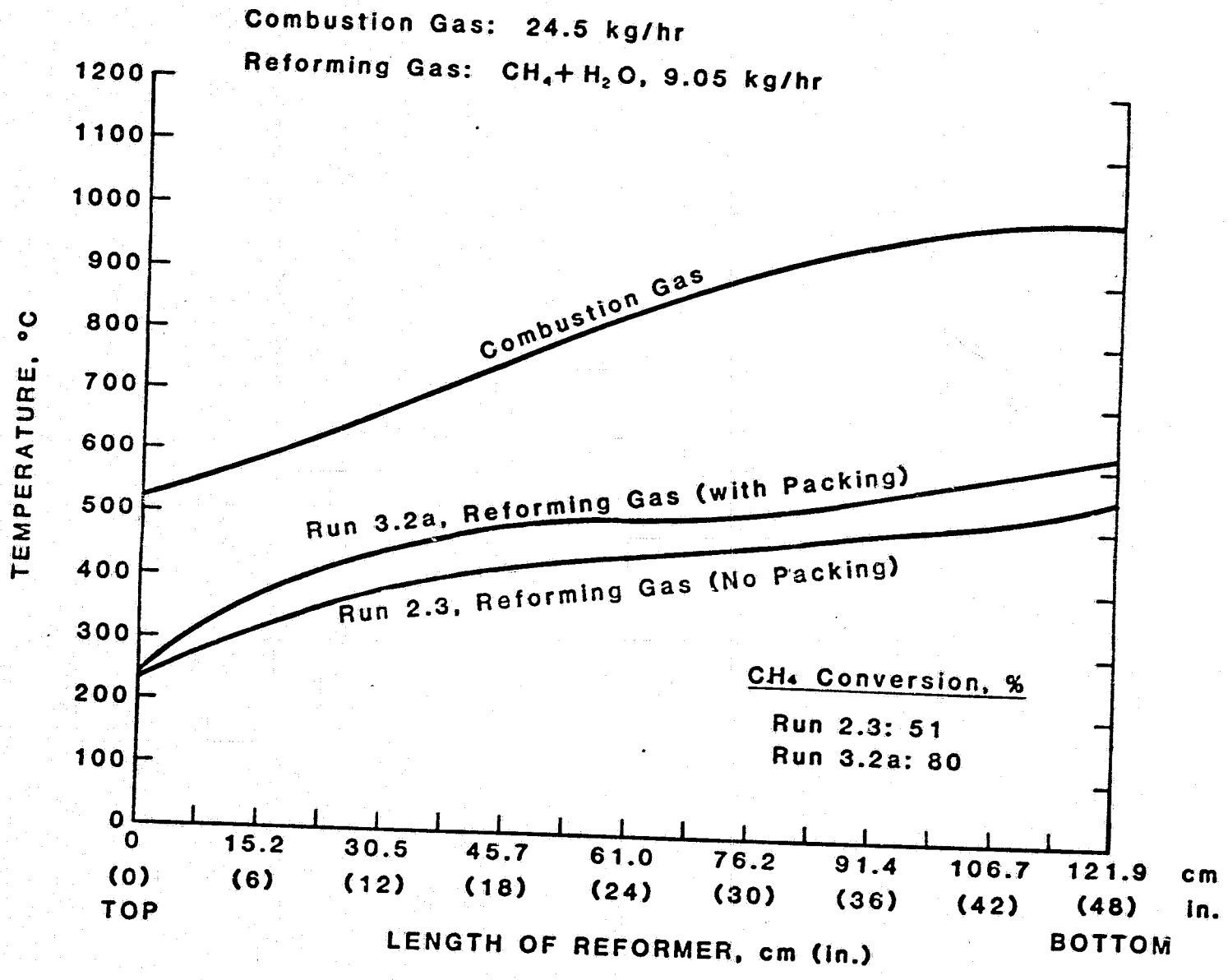

FIGURE 6.6.8. EFFECT OF CATALYST AND PACKING ON TEMPERATURE DISTRIBUTION (REFORMING GASES)

D1842

ORIGINAL PAGE IS
OF POOR QUALITY

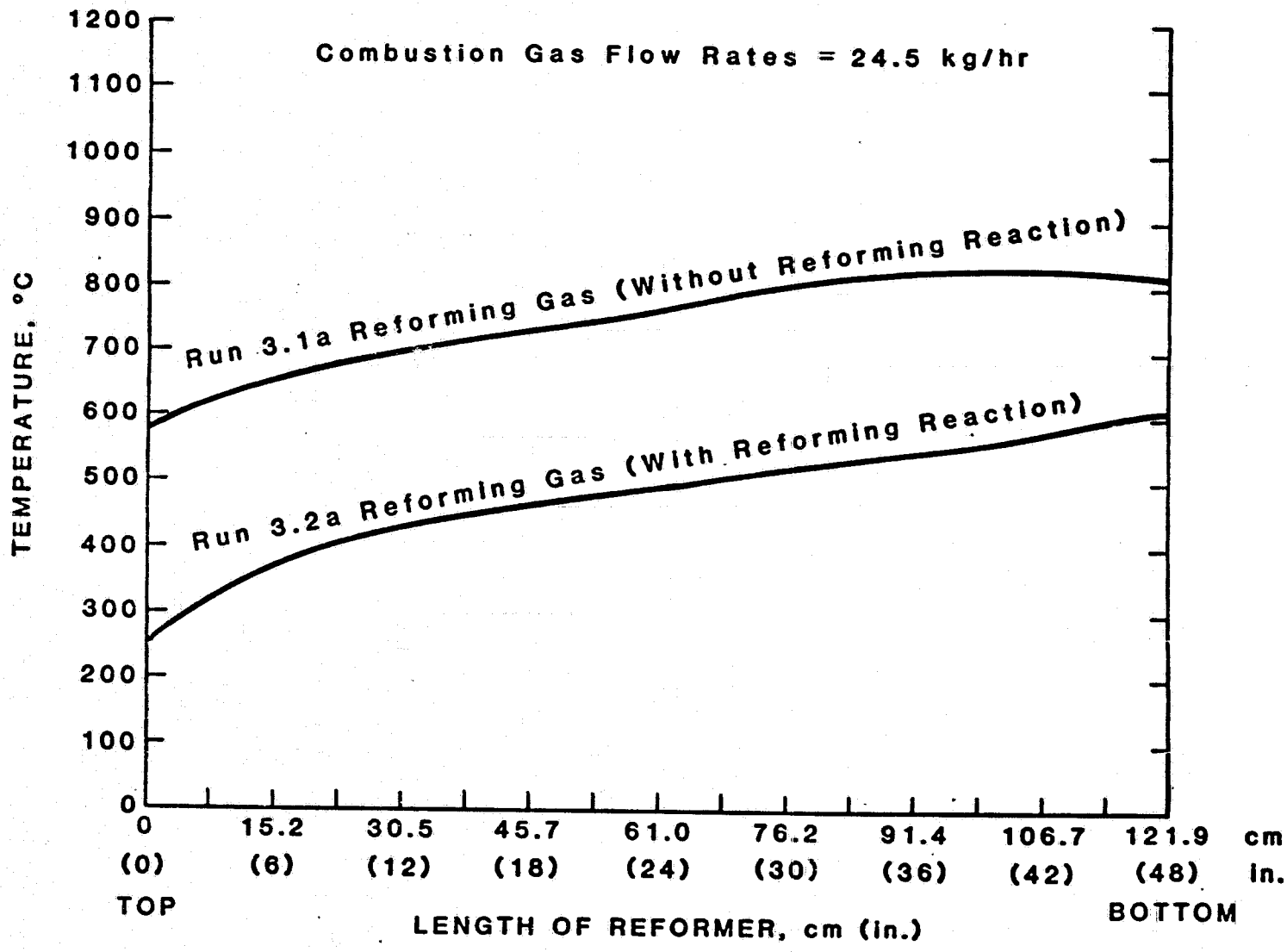

FIGURE 6.6.9. EFFECT OF REACTION ON TEMPERATURE DISTRIBUTION

ORIGINAL PAGE IS
OF POOR QUALITY

TABLE 6.6.2 SUMMARY OF 10 kW TEST RESULTS

RUN NO.	CH_4 S.V., hr^{-1}	FUEL INLET TEMP., °C	COMBUSTION GAS INLET TEMP., °C	COMBUSTION GAS FLOW RATE, kg/hr	CATALYST BED EXIT TEMP., °C	CH_4 CONVERSION, % EXPERIMENTAL	CH_4 CONVERSION, % EQUILIBRIUM	REFORMER PRODUCT, MOLE % H_2	CH_4	CO_2	CO
2.3*	929	197	1079	25.24	570	51.25	50.68	62.7	18.1	13.83	5.2
2.4*	929	210	1211	24.98	605	63.4	64.68	71.7	11.15	10.5	6.5
3.2a	929	173	1015	24.52	619	79.84	73.4	72.13	5.6	12.52	9.74
3.2b	929	190	1093	19.84	614	62.5	67.83	72.45	10.32	14.49	2.74
3.2c	929	207	1093	13.22	570	47.98	50.68	68.44	16.41	14.99	0.16
3.2d	697	201	1059	18.53	694	93.3	93.76	73.99	1.75	10.30	14.06
3.2e	465	254	975	22.17	883	99.61	99.93	74.98	0.13	8.56	16.33
3.2f	465	235	1104	13.08	732	95.32	96.93	75.71	1.12	9.68	13.25

*Series 2 runs (without packing in the combustion gas tube)

ORIGINAL PAGE IS
OF POOR QUALITY

ORIGINAL PAGE IS
OF POOR QUALITY

TABLE 6.6.3

Packed Bed Heat Transfer Data

Point #	Series	Exp	hl	Nu	Re'	Pr
1*	3	2A	23	92	867	.74
2	3	2A (repeat)	22	85.7	774	.74
3	3	Extra run	43	189	770	.73
4	3	2B	21	87.4	690	.73
5	3	2C	16	73.8	501	.73
6	3	2D	18	67.2	575	.74
7	3	2E	17	61.7	651	.75
8	3	2F	14	58.8	445	.73
9	3	Extra run 2	7	35.3	228	.73
10	3	1A (Argon)	18	66.4	732	.74
11	3	1D (Argon)	15	53.7	522	.75
12	3	1F (Argon)	12	43.2	365	.75
13	2	1 (Annulus)	36.4	56.6	115.6	.87
14	3	1D (Annulus)	22	44.4	108.5	.89
15	3	1F (Annulus)	21	32.7	59	.88

*Runs 1-12 represent calculations from the combustion tube.

In a complete system, a shift reactor would reduce CO concentration and improve hydrogen yield.

6.6.4 Data Analysis

The 10 KW reformer tests provided additional heat transfer information which was used to verify and refine the correlations used in the BOLTAR program. Analysis of the raw data comprised a least square cubic fit of the heat transfer using an energy balance to determine the heat transfer rates. For the reformer annulus, only steam/argon experimental data were used to eliminate the confounding effect of the endothermic reformer reaction on the energy balance.

Table 6.6.3 lists the packed bed data, which was used in the analysis. The test conditions are described in Table 6.6.1.

The combustion tube data (points 1-12) was fitted by the dimensionless equation:

$$Nu = .773\ Re^{.7}\ Pr$$

Point 3 was not included in the fit because it was taken under nonsteady operating conditions.

The reformer annulus data (points 13, 14, 15) was fitted by the equation:

$$Nu = 1.95\ Re^{.69}\ Pr.$$

The characteristic dimensions used in the dimensionless equations are the passage equivalent diameter (4x cross section area/wetted perimeter) for the Nusselt number and the diameter of a packing particle for the Reynolds number.

6.7 Prototype Fuel Conditioning System Conceptual Design

The preparation of the conceptual design of the fuel conditioning system comprised the determination of the operating requirements of the system, the development of a process diagram for the system, determination of the process state points at full and part load (1/3) operating conditions and preliminary design of a control system. Since there was no overall OS/IES design or analysis task included in Phase II, the application requirements were primarily based on the OS/IES analysis of Phase I. The state points defined the operating conditions of the various components and subsystems of the fuel conditioning system and these in turn were used in defining the operating ranges and design specifications for the components and subsystems. Thus, the conceptual design provided the system integration function. As in any such effort, the final version of the conceptual design was evolved through a series of iterations as feedback on the effects of various operating requirements and design choices on the complexity and therefore cost and operability became available. All decisions on overall system design requirements were discussed with and approved by the NASA Project Manager and his technical advisors during review meetings.

6.7.1 System Operating Requirements

The basic function of the fuel conditioning system is to convert the primary fuel available to the OS/IES into the hydrogen stream required by the PAFC for the range of OS/IES operating conditions. As a result of the Phase I work and continuing evaluations during Phase II, the following list of specific operational requirements were established:

- Design point operation to provide sufficient hydrogen flow for 120 kW D.C. PAFC at 80% utilization.
- Primary fuel is pipeline gas with the composition given in Section 6.1.1.
- Utility tie line to provide startup energy and response to rapid electrical load changes.

- Concentration of carbon monoxide in PAFC fuel to be 1% or less by volume.
- Thermal integration with overall system to include
  - use of PAFC spent fuel in reformer burner
  - use of PAFC by-product heat to generate steam for reformer feed
  - supply heat from spent fuel condensers to thermal system of OS/IES
  - use of heat produced in inverters to preheat combustion air
- Maximum practical thermal integration in and among components of fuel conditioning subsystem.
- Exhaust emissions to be compatible with appropriate standards.
- Process water for steam reforming to be supplied by condensate from spent fuel and air streams.
- PAFC fuel must be free of trace elements or contaminants that would be harmful to the cells.

Some of the items on the above list were imposed by external considerations (e.g. 1% CO and emission standards), some resulted from supplemental tradeoff studies carried on during Phase II (e.g. water recovery as opposed to purchase of makeup water), some resulted from the Phase I work (e.g. maximum thermal integration is essential to achieve the overall energy utilization goals of the OS/IES) and some were selected to simplify the design and operation of the prototype system (e.g. use of a utility tie line as a backup and elimination of peak shaving gas from the primary fuel composition). In all cases the selection was made in consultation with the NASA project management team and were deemed appropriate for the conceptual and prototypical nature of the design. The considerations and supplemental studies which led to the selections

ORIGINAL PAGE IS
OF POOR QUALITY

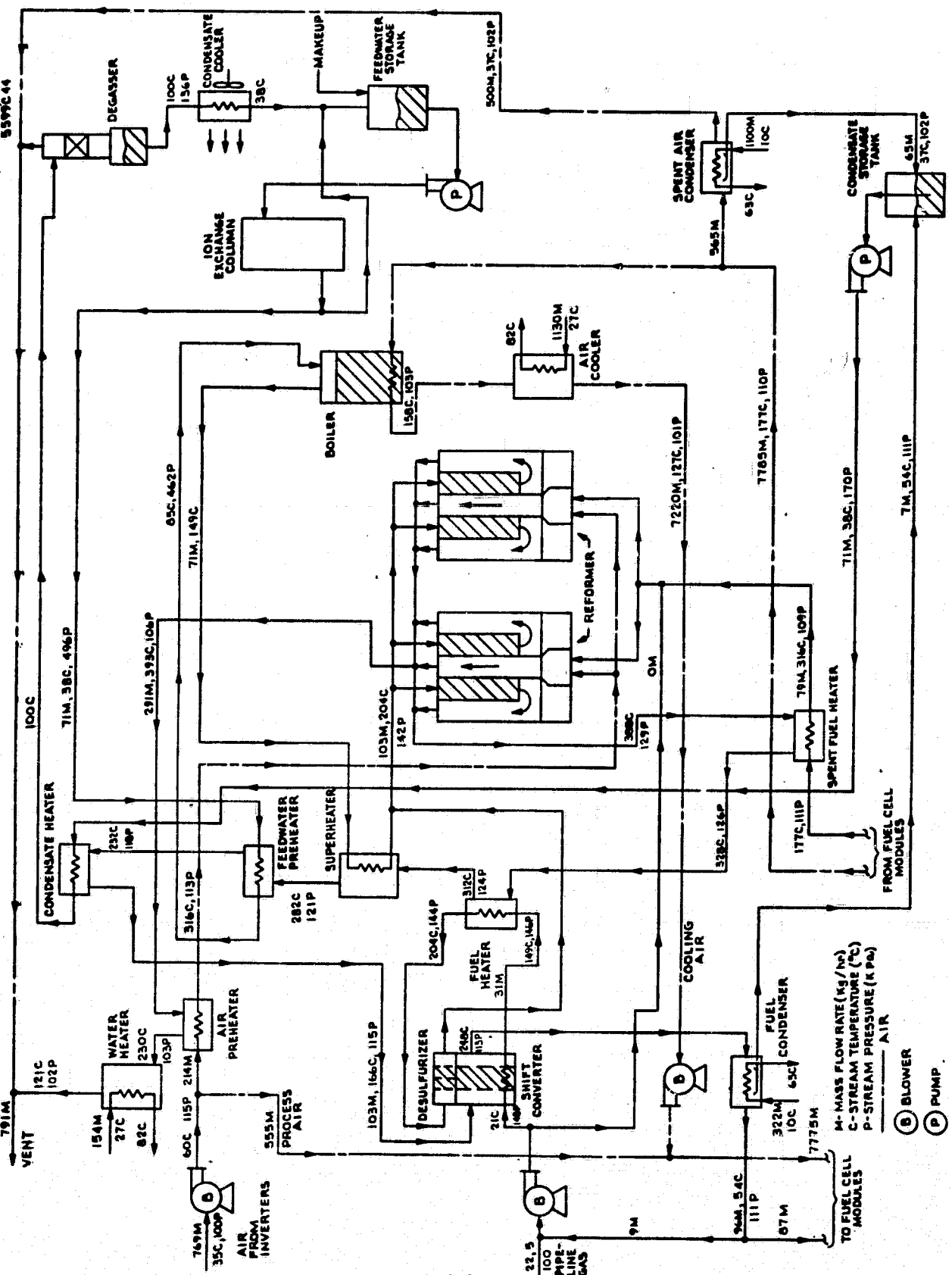

Figure 6.7.1 Fuel Processing System, Major Equipment and Process Flow Diagram for 100% Load (120 kW)

are described in other sections of this report and/or in the Quarterly Reports published during the course of the work.

6.7.2 Process Flow Diagram

Based on the system requirements defined above, the process flow and major equipment diagram shown in Figure 6.7.1 was developed. The design point (120 kW-D.C.) process stream mass flows and temperatures shown are compatible with the PAFC and OS/IES requirements determined by the system analysis of Phase I. The stream compositions based on the pipeline gas composition given in Section 6.1.1 are given in Section 6.2. The aliphatics in the specified fuel were treated as methane formed by reaction with the recycled hydrogen. The inert gases present in the feed stream (nitrogen and CO_2) are not included in the stream compositions since, at the low specified levels, their effect would be insignificant.

In order to complete the ancillary equipment specifications and determine the control requirements of the system, the state points for one part load operating condition were needed. In the absence of a system analysis task, these were obtained for 1/3 load (40 kW) in the following manner. It was assumed that the fuel cells would be operated at a fixed hydrogen utilization and that the composition of the spent fuel returned to the reformer burner would have the same composition as at the design point. These assumptions require that the fuel supplied to the PAFC at part load have the same composition as at the design point. This, in turn, implies that the reformer operating temperature will be reduced at part load to maintain a constant methane conversion efficiency (if both reformer modules are used) which should contribute to longer lived and more reliable reformer operation. This operating scenario also permits the reformer heat requirements to be met by the spent fuel stream at all operating conditions and results in the same process stream compositions as the design point. The resultant flows and temperatures, which were calculated using the system design program developed in Phase I, are given in Figure 6.7.2. Due to the increased efficiency of the PAFC at part load the required flows are considerably lower than 1/3 ($\sim$23%) of

Fig. 6.7.2. Fuel processing system, major equipment and process flow diagram for one third (40 KW)

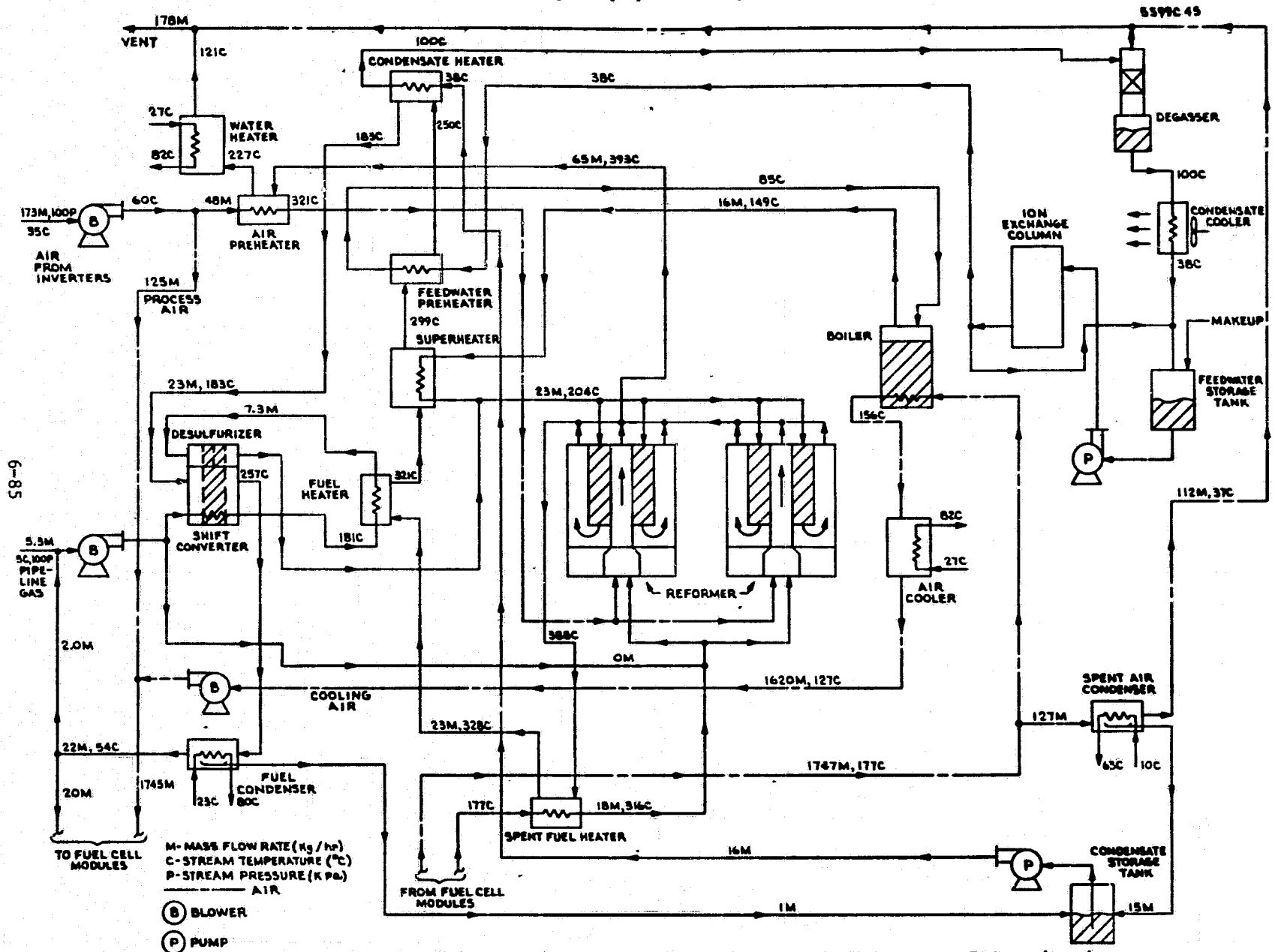

FIG. 6.7.2 - FUEL PROCESSING SYSTEM, MAJOR EQUIPMENT AND PROCESS FLOW DIAGRAM FOR ONE THIRD LOAD (40 KW)

ORIGINAL PAGE IS
OF POOR QUALITY

the full load flows. Also, as indicated in the table and described in the discussion of the control system (Section 6.4), the operating characteristics of some of the heat exchangers require that by-passes be used to achieve the desired heat balances.

The state points given in Figures 6.7.1 and 6.7.2 and the compositions were the basis for the specifications of ancillary equipment which were submitted to vendors. The specifications also included pressure drops for heat exchangers and pressure rises for pumps and compressors. These were based on engineering judgements initially but were modified iteratively as actual values became available from vendors.

6.8 Computer Model

6.8.1 Introduction

The steam/methane reformer is the principal element in the fuel processor system. Consequently, for accurate design and analysis, a model incorporating heat transfer and kinetic effects is required. This was accomplished by the REPENT program, written for a single reformer tube with counter-current flow of the combustion and reforming gases. However, this model was too limited to apply to the variety of proposed designs so the equations were generalized to include different geometries and flow arrangements and several model options were added. This more flexible program was described in detail in several topical reports submitted to the NASA project manager.

The BOLTAR model allows the user to exercise the following options:

- inclusion/deletion of the water gas shift reaction
- flat slab or tubular geometry
- co-current, counter-current, or double counter-current flow arrangement
- choice of several heat transfer correlations
- product gas annulus packing
- CALCOMP plotting option
- heat exchanger approximation for "cooler" areas of the catalytic bed.

Model derivation, use, and results are detailed in the topical reports and copies of the program will be submitted to the NASA Project Manager. This section provides an overview, and discusses:

1. model development
2. model use
3. model predictions and parametric studies
4. model accuracy - comparison with experimental data.

6.8.2 Model Development

The model equations were developed in detail in the topical reports, and are summarized in this section. Table 6.8.1 lists the model assumptions. Figure 6.8.1 shows the tubular double counter-current flow reformer in perspective, as it is considered by the model. Figure 6.8.2 represents an axial cross-section, including a central plug for heat transfer enhancement. Figure 6.8.3 illustrates a variation, where the product and combustion gas flow paths are interchanged. Figure 6.8.4 displays a flat slab geometry, double counter-current flow reformer in perspective, while Figure 6.8.5 shows the dimensional variables used in the model.

Two reactions are assumed to occur within the reformer:

$$CH_4 + 2H_2O = CO_2 + 4H_2 \qquad (1)$$

$$CO + H_2O = CO_2 + H_2 \qquad (2)$$

The demethanation reaction, equation 1, is kinetically controlled, while equation 2, the water gas shift reaction, is assumed to be equilibrium controlled. Carbon deposition is neglected. Using this two reaction scheme, all molar flows within the reformer can be represented in terms of the feed molar flow rates and the two conversions (Table 6.8.2).

A pseudo first-order rate expression is used to describe the demethanation reaction kinetics (equation 3 and 4).

$$-r_{CH_4} = k\Delta P, \quad \frac{g\ mol}{hr\ g_{cat}} \qquad (3)$$

$$= k_o e^{-EA/RT} \left(P_{CH_4} - P_{CH_4,E} \right). \qquad (4)$$

This can be substituted into the reactor design equation to yield the kinetic mass balance.

TABLE 6.8.1

BOLTAR MODEL ASSUMPTIONS

1. Reforming and combustion gases flow with complete radial but no axial mixing (i.e., plug flow).
2. Only axial temperature changes are allowed, and radial temperature profiles are neglected.
3. A uniform temperature exists throughout each catalyst particle, and it is the same as the gas temperature in that section of the catalytic bed.
4. Distributor and manifold entrance effects are negligible.
5. The reaction kinetics are adequately described by a pseudo first-order rate equation.
6. The kinetic expression represents a "global" or overall rate, and, hence includes reactivity differences found within the catalyst particles.
7. All gases behave ideally in all sections of the reformer.
8. Bed pressure drops are neglected.
9. Heat transfer is primarily by forced convection. Specific radiant heat transfer terms for the two stream models are neglected, as are heat losses to the environment.
10. A single reformer tube is analyzed. Thus, all the tubes in the reformer behave independently of one another.
11. Equations 1 and 2 represent the reformer reactions. Reaction 1 is kinetically controlled, while reaction 2 is equilibrium controlled. No carbon deposition is allowed in the reformer.

FOR DOUBLE COUNTER CURRENT FLOW MODELS (THREE STREAMS)

12. No heat transfer occurs between the product and combustion gases.
13. No reactions occur in the product gases.

ORIGINAL PAGE IS
OF POOR QUALITY

Dwg. 7707A78

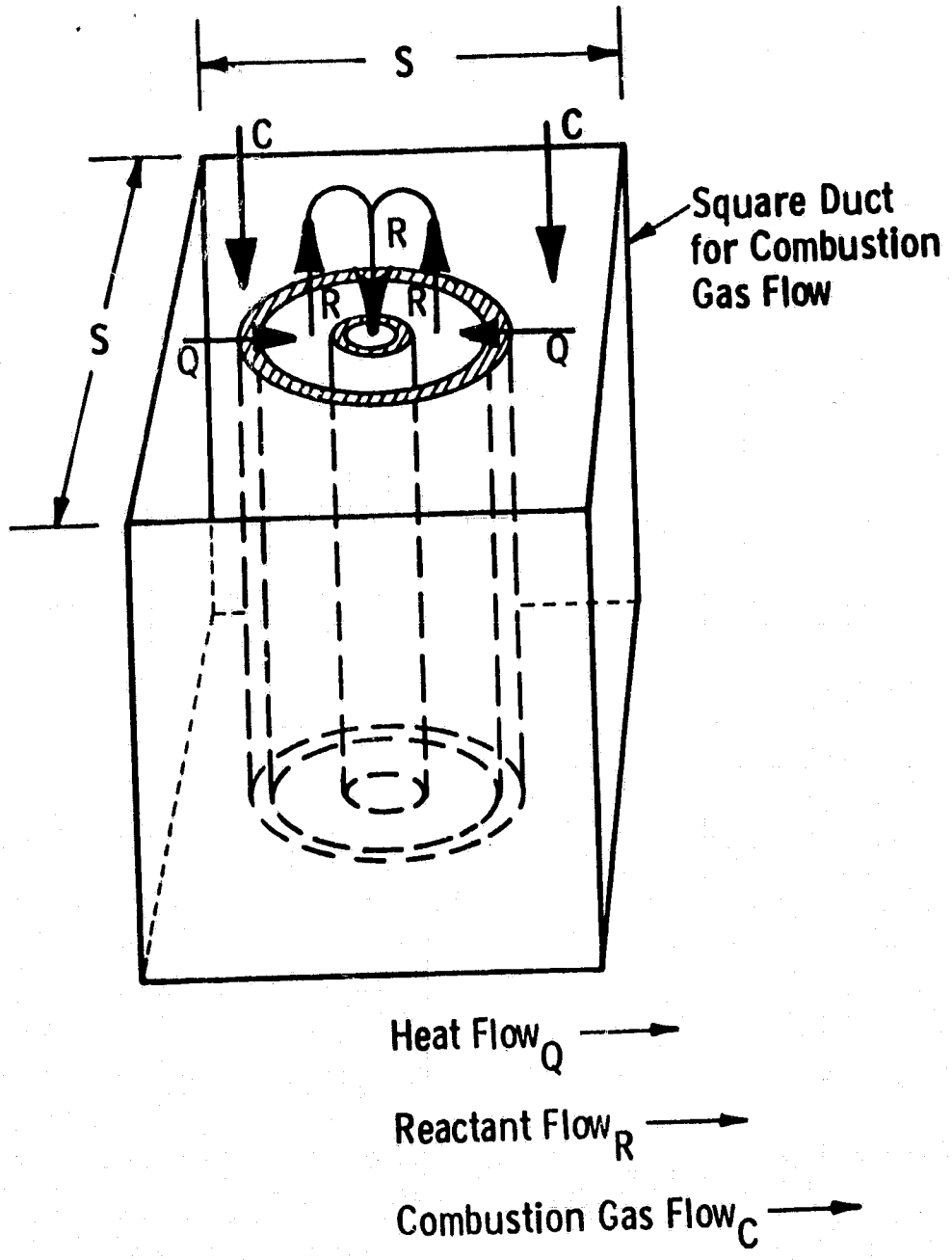

Fig. 6.8.1 – Heat transfer surfaces

ORIGINAL PAGE IS
OF POOR QUALITY

Dwg. 4246B16

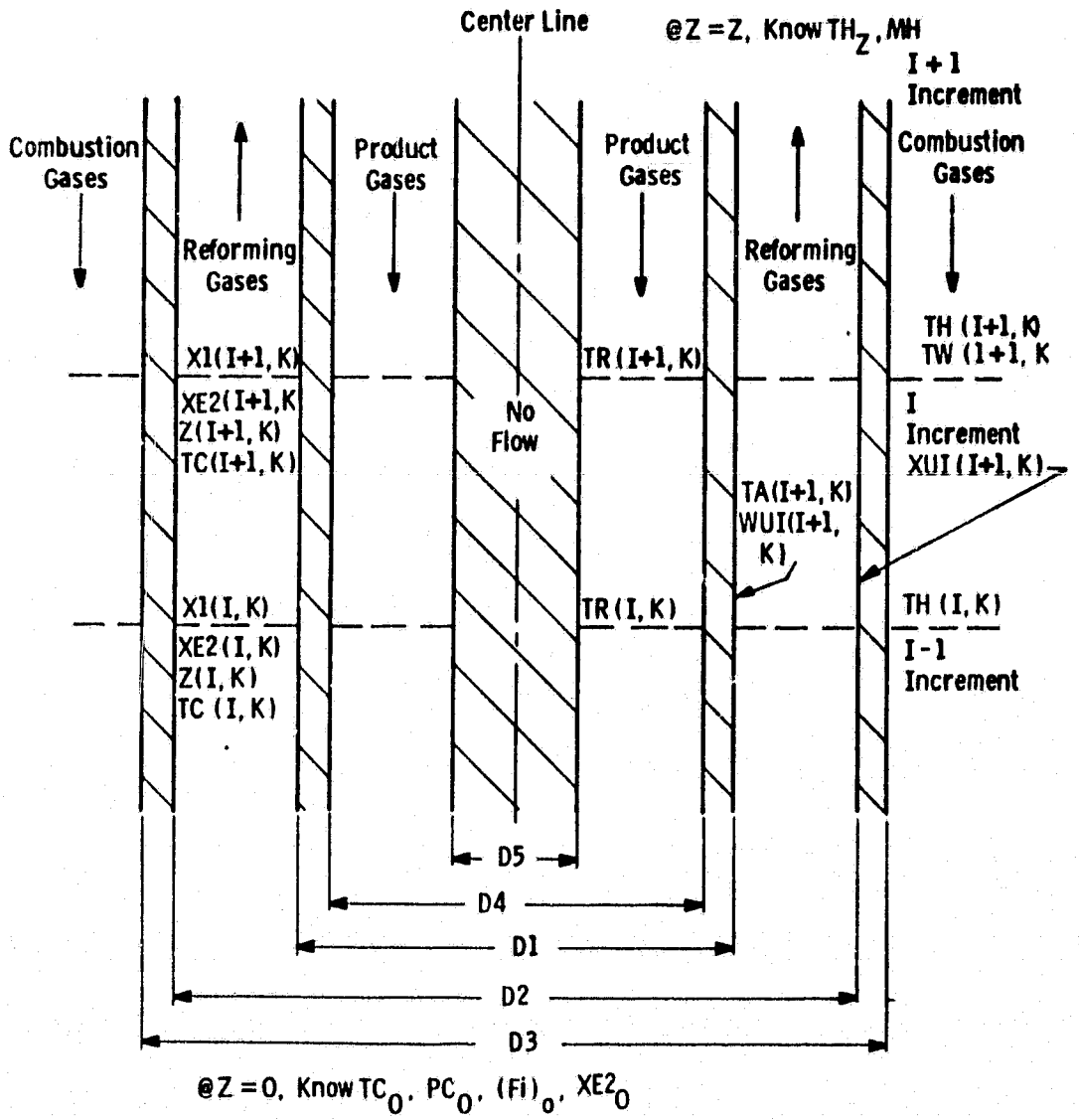

Fig. 6.8.2 – Double counter-current flow, tubular geometry reformer model (regenerative gasses flow on the inside)

ORIGINAL PAGE IS
OF POOR QUALITY

Dwg.424;814

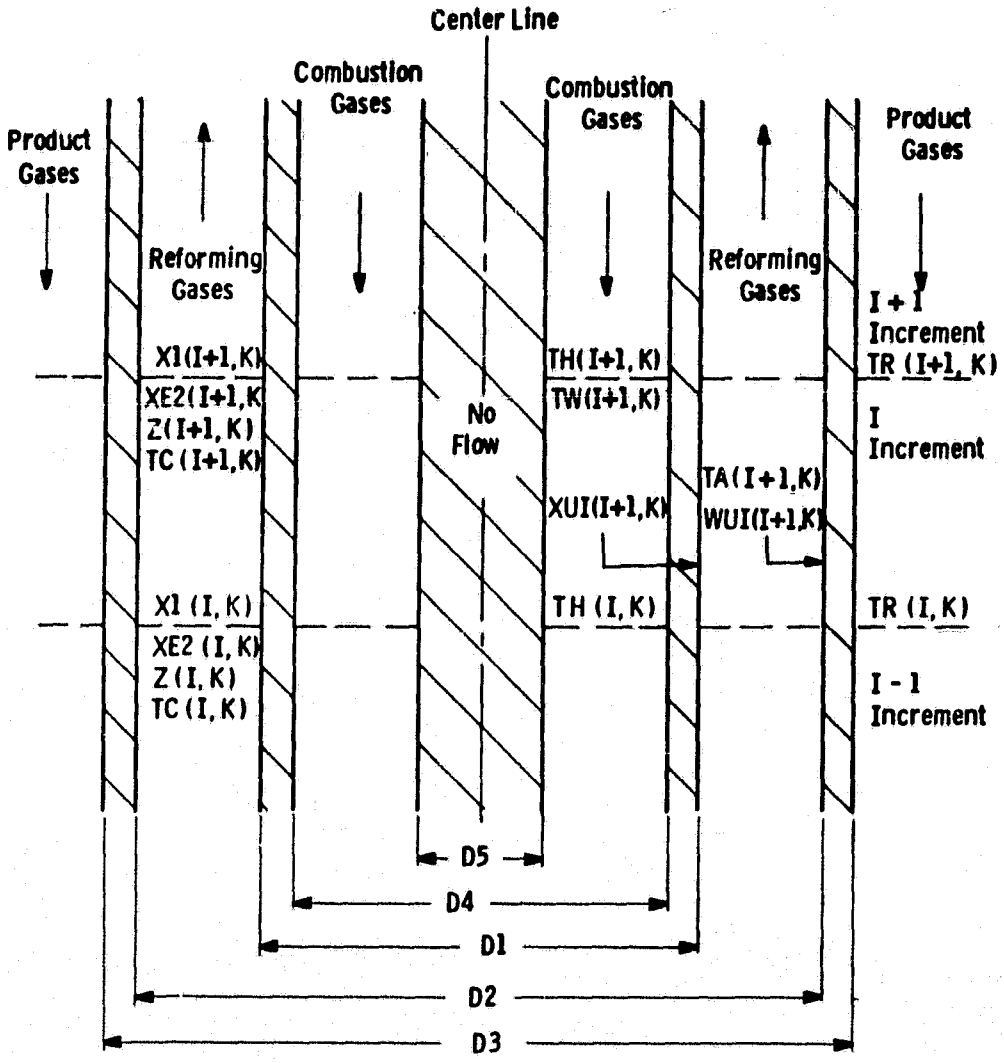

@Z = 0, Know TC_0, PC_0, $(F_i)_0$, $X1_0$, $XE2_0$

Fig. 6.8.3 – Double counter-current flow, tubular geometry reformer model (regenerative gases flow on the outside)

ORIGINAL PAGE IS
OF POOR QUALITY

Dwg. 7756A88

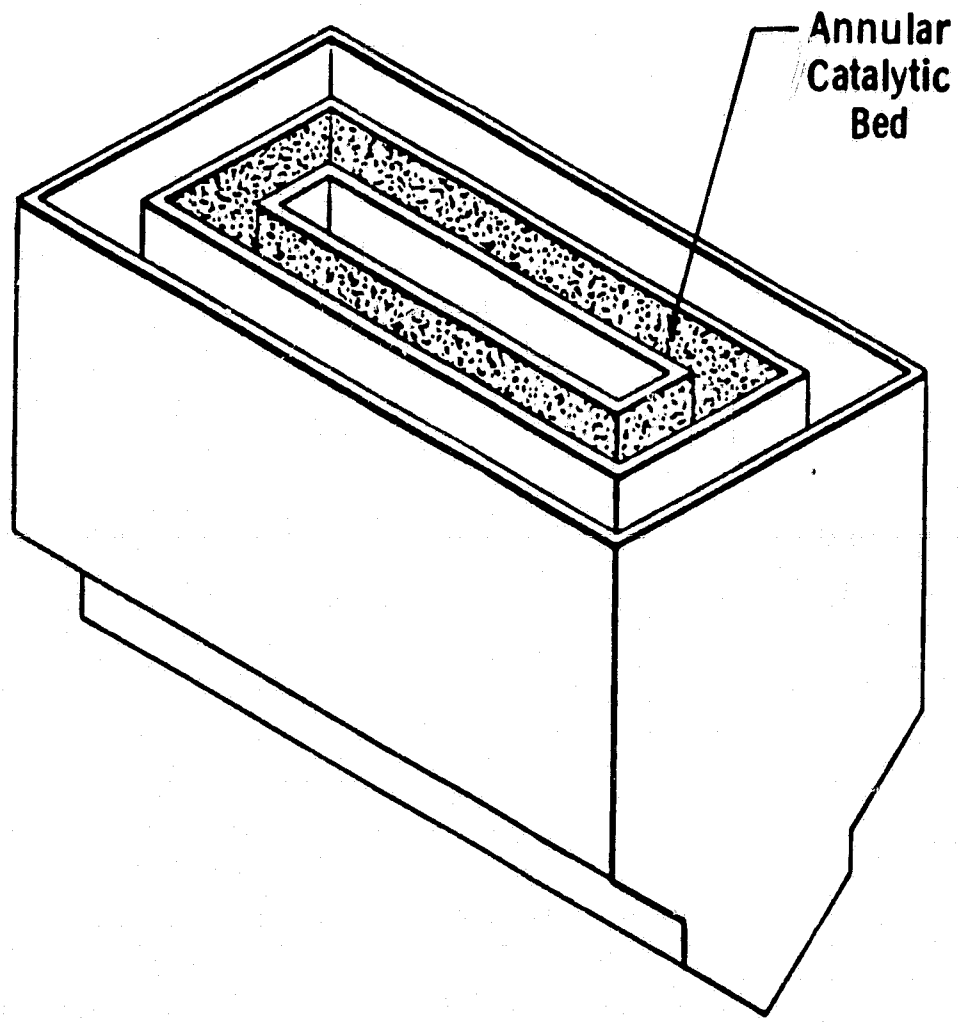

Fig. 6.8.4 – Flat slab geometry, double counter current flow reformer

ORIGINAL PAGE IS
OF POOR QUALITY

Dwg. 4246815

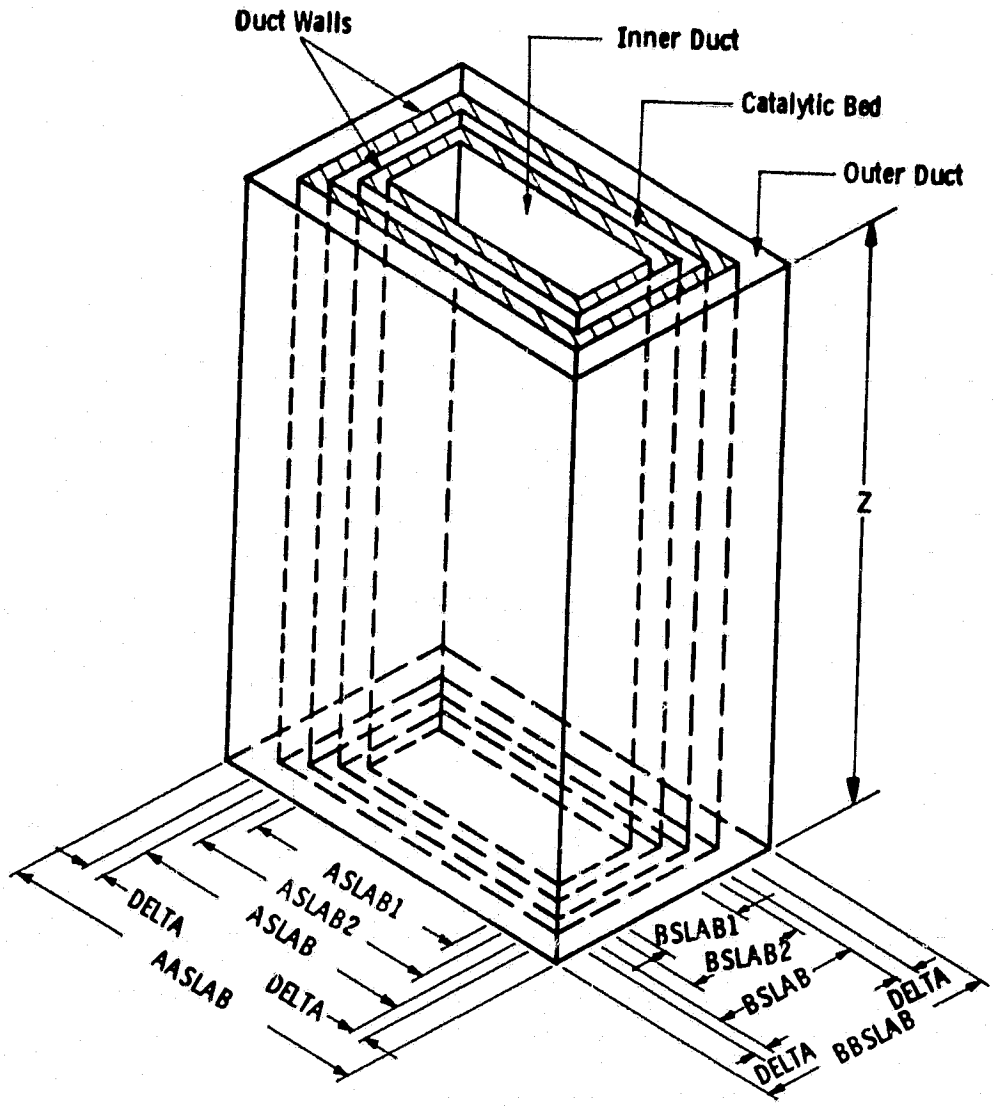

Fig. 6.8.5 – Dimensions and variables for the flat slab geometry, double counter-current flow models

ORIGINAL PAGE IS
OF POOR QUALITY

TABLE 6.8.2

MOLAR FLOW/RATES AS A FUNCTION OF REACTION CONVERSIONS

(Basis: 1 hour flows)

Component	Moles in Feed	Moles Produced by Reaction (5-1)	Moles Produced by Reaction (5-2)	Moles present
CH_4	F1	-X1F1	0	F1 - X1F1
CO	F2	0	-X2 (F3 + X1F1)	F2 - X2 (F3 + X1F1)
CO_2	F3	X1F1	X2 (F3 + X1F1)	F3 + X1F1 + X2 (F3 + X1F1)
H_2O	F4	-2X1F1	-X2 (F3 + X1F1)	F4 - 2X1F1 - X2 (F3 + X1F1)
H_2	F5	4X1F1	X2 (F3 + X1F1)	F5 + 4X1F1 + X2 (F3 + X1F1)
N_2	F6	0	0	F6
Totals	F	2X1F1	0	F + 2X1F1

Equilibrium expressions may be written for the reactions given by equations (1) and (2).

$$K1 = \frac{P_{CO_2} P_{H_2}^4}{P_{CH_4} P_{H_2O}^2} \qquad (5)$$

$$K2 = \frac{P_{CO_2} P_{H_2}}{P_{CO} P_{H_2O}} \qquad (6)$$

These equations can be expressed in terms of the component molar flow rates and conversions.

Energy balances are required for all gas streams in the reformer. For co-current and counter current flow arrangements, two balances can be written, and solved explicitly for the reformer and combustion gas stream temperatures. For a double counter-current flow arrangement, three balances are necessary, and an iterative technique is required for solution. Adjustments also have to be made to the heat transfer area term, depending upon the location of the product gas flow area (compare Figures 6.8.2 and 6.8.3). Substitution of a tube wall temperature profile in place of the combustion gases eliminates that energy balance and simplifies the solution.

The model's principal equations are listed in Table 6.8.3. There are five equations:

1. kinetic mass balance
2. demethanation equilibria
3. water gas shift equilibria
4. reform gas energy balance
5. combustion gas energy balance (or a wall temperature profile).

There are also five variables (kinetic conversion X1, equilibrium

TABLE 6.8.3

BOLTAR MODEL BASIC EQUATIONS

1. Kinetic Mass Balance

$$\frac{dX1}{dZ} = \frac{e_B \, k_o}{u_o \, c_o} \, e^{-EA/RT} \, [\Delta P] \qquad (7)$$

2. Demethanation Reaction Equilibrium

$$K1 = \frac{P_{CO_2} \, P_{H_2}^{\,4}}{P_{CH_4} \, P_{H_2O}^{\,2}} \qquad (8)$$

3. Water Gas Shift Equilibrium

$$K2 = \frac{P_{CO_2} \, P_{H_2}}{P_{CO} \, P_{H_2O}} \qquad (9)$$

4. Reformer Gas Energy Balance

$$(\Sigma FACPA)dTC = UI(TH-TC)_{avg} \, \pi(DZ) \, dZ + \Sigma F(-OH_R)dx \qquad (10)$$

5. Combustion Gas Energy Balance

$$(MH) \; (CH)dTH = UI(TH-TC)_{avg} \, \pi(DZ)dZ \qquad (11)$$

conversion XE, water gas shift conversion XE2, reformer gas temperature TC, and combustion gas temperature TH). Hence, a unique solution is possible. The double counter-current flow arrangement adds one variable (the product gas temperature) and one equation (the product gas energy balance), therefore, a unique solution also exists.

The model solves the system of equations by using a finite difference/incremental approach. All differentials in equations 7-11 are expressed as finite differences over a small height increment ΔZ. Output (i+1) variables are then calculated in terms of input (i) variables and known values. The equations are numerically integrated over the height of the reformer, and converged with respect to the boundary conditions.

6.8.3 Model Requirements and Use

Table 6.8.4 lists the input data required for the calculational routines. There are three types of input variables. Routing variables inform the computer of the model variation being run, the input data format, and which calculational routines are to be used. The design variables involve the catalytic parameters and the reformer dimensions. Operating variables are the feed flow rates, pressure, inlet temperatures, and inlet conversions. From this information, the model calculates the temperature and composition profiles along the reformer tube.

Model use involves keypunching 6-10 data cards, depending upon the model variation. Use also requires the proper control card sequence for the computer system. Detailed input data arrangements are described in several topical reports.

6.8.4 Model Predictions and Parametric Studies

Table 6.8.5 provides a summary of parametric studies and predictions performed utilizing the BOLTAR model. The input and output parameters for the studies are detailed in the topical reports.

The design studies of the 10 kW double counter-current flow reformer described in Section 6.6 are of special interest. Tables 6.8.6 and 6.8.7 list the input data for the wall temperature profile and

TABLE 6.8.4

BOLTAR - Required Program Input Variables - Double Counter-Current Flow Models

Routing Variables

JESUIT - inclusion/deletion of the water gas shift reaction

MARTIN - geometry switch: flab slab or cylindrical tube

CALVIN - flow arrangement: co-current/counter-current/double counter-current

GBURNS - heat transfer options

DENVER - product gas heat transfer options

IDEBUG - intermediate output switch

LORD - selected intermediate output switch

JOHN - CALCOMP plotting selection switch

MARK - heat exchanger approximation switch

JACK - high temperature shift catalyst switch for product gas annulus

Design Variables

A. Catalytic Parameters

k_o = Arrhenius frequency factor

E_A = activation energy

ρ_B = catalyst bed density

ε = void fraction

B. Dimensions

Z = height

Slab geometry: ASLAB, BSLAB, DELTA, AASLAB, BBSLAB, DP (catalyst particle diameter), ASLAB1, ASLAB2, BSLAB1, BSLAB2

Tubular geometry: D1, D2, D3, S, DP, D4, D5

Operating Variables

Flow Rates

A. Reformer gases - FO, F1, F2, F3, F4, F5, F6

B. Combustion gases - MH, CG1, CG2, CG3, CG4, CG5, CG6

C. Wall profile coefficients - ATW, BTW, CTW, DTW

ORIGINAL PAGE IS
OF POOR QUALITY

TABLE 6.8.4 (Con't.)

P = pressure

TCO = inlet reformer gas temperature

THZ, (THO) } inlet combustion gas temperature

X1 (1,1), XE2 (1,1) } inlet conversions

*Underlined variables are deleted when one uses the double counter-current flow models.

TABLE 6.8.5
PARAMETRIC STUDY SUMMARY

Flow Arrangement	Geometry: Tubular	Geometry: Flat Slab
Co-Current	5 kW	20, 60 kW
Counter-Current	5 kW, 10 kW 2 kW (ERC)*	20, 60 kW
Double Counter-Current	10 kW (UTC), 10 kW (Section 6.6)	60, 120, 500, 1000 kW

*Actual capacity is considerably less than 2 kW (∿.7 kW). This reformer tube is also electrically heated.

ORIGINAL PAGE IS
OF POOR QUALITY

TABLE 6.8.6

10 kw Experimental Reformer Design

Parametric Studies - Wall Profile Model Input Data

Routing Variables

JESUIT = 0

MARTIN = 1

CALVIN = 3. (double counter-current flow, product gases flow on the outside)

GBURNS = 1.

IDEBUG = 0

LORD = 40

JOHN = 0

MARK = 0 or 1 (as needed)

Flow Rates [kg mol/hr]

Reforming gases: FO = .45, FL = .11, F4 = .34, all others are zero

Exterior Wall Temperature Profiles

"427C Profile" TW_0 = 427C, $TW_{.5}$ = 760C, TW_1 = 830C, TW(Z) = 427. + 201Z + $(-21.9)Z^2$

"593C Profile" TW_o = 593C, $TW_{.5}$ = 871C, TW_1 = 1010C, TW(Z) = 593. + 160 + $(-14.8)Z^2$

Catalyst Information†

k_o = .391 kg mol/(hr),(Pa),(kg cat)
EA = 7.11×10^7 J/kg mole
RHOB = 1150 kg cat/m^3 bed
EPS = .469

TABLE 6.8.6 (Con'd.)

Dimensions [m]

D1 = .0508 D2 = .0792 D3 = .0825 (S = .0959)*

DP^{+} = .0361 D4 = .0475 D5 = 0.

Z = 1.321 (52")

Other Input Data

P = 124 kPa

X1(1,1) = 0.

XE(1,1) = 0.

Temperatures are as indicated in Table (7.4)

*S has no meaning for exterior wall temperature profile runs

+equivalent spherical volume diameter

†D. W. Allen, E. R. Gerhard, and M. R. Likens, Jr., "Kinetics of the Methane - Steam Reaction," Ind. Eng. Chem., Process Design and Development, Vol. 14, No. 3, 1975.

TABLE 6.8.7

10 kW EXPERIMENTAL REFORMER - COMBUSTION GAS MODEL INPUT DATA

Routing Variables

JESUIT = 0

MARTIN = 1

CALVIN = 3.

GBURNS = 2. (annular heat transfer correlation)

IDEBUG = 0

LORD = 40

JOHN = 0

MARK = 0

Flow Rates [kg mol/hr]

Reforming gases: FO = .45, FL = .11, F4 = .34, all others are zero (0.)

Combustion gases:

regular: MH = 1.485, CG3 = .33, CG4 = .286, CG6 = .869, all others are zero (0.).

300% excess:

MH = 3.2624, CG3 = .33, CG4 = .286, CG6 = 2.6464, all others are zero

Catalyst Information

k_o = .391 kg mol/(hr),(Pa),(kg cat)

EA = 7.11×10^7 J/(kg), (mol)

RHOB = 1150 kg cat/(m^3 bed)

EPS = .469

Dimensions [meters]

D1 = .0508 D2 = .0792 D3 = .0825 S = .0959

DP = .0361 D4 = .0475 D5 = 0.

Z = 1.321 (52") (DPHO = .00978 (3/8"))

Other Input Data

P - 124 kPa

X1 (1,1) = 0.

XE2 (1,1) = 0.

combustion gas flow model runs, respectively. Tables 6.8.8 and 6.8.9 list the respective model outputs. Figure 6.8.6 displays the strong catalyst particle size effect upon the modified overall heat transfer coefficient. Figure 6.8.7 shows how the heat transfer effect translates into a conversion catalyst size dependency. This analysis assumes that the catalyst reactivity does not vary with particle size. This assumption was verified experimentally as reported in the 5th Quarterly Report.

The 10kW reformer design studies are summarized as follows:

1. Heat transfer considerations strongly affect the reformer's performance, and catalyst particle size effects figure prominently in the heat transfer calculations.

2. Changing the reformer gas inlet temperature (TCO) over the range 260 - 540 C has a negligible effect upon the exit conversion (<5%).

3. A reformer gas temperature greater than ∿390C is required for the reformer reactions to proceed.

4. The combustion gas temperature profile (heat source) essentially determines the reformer's performance.

5. The predicted conversion and temperature profiles are parabolic. In several cases, the profiles can be adequately represented by a linear fit.

6. Metal wall temperatures predicted by the combustion gas model are 40 - 90 C above wall profile model temperatures for the same conversions and heat transfer conditions. This is probably due to variations and uncertainties in the external heat transfer coefficient.

7. The 10kW reformer is equilibrium limited, that is, the reformer gas exit conversion approaches (within 5%) the equilibrium conversion calculated at the exit conditions.

TABLE 6.8.8

10kW EXPERIMENTAL REFORMER - PARAMETRIC STUDIES (WALL PROFILE MODEL)

Input Data Used						Output			
Run #	Mark	TCO (C) (F)	Wall Profile (C)	TCZ (C)	TWZ (C)	U (W/m^2, °C)	XI	XE	H_2 Produced (kg mol/hr)
1	1	204	427	575	888	56.8 (set)	38.7	43.3	.167
2	1	260	427	577	888	56.8 (set)	39.4	43.8	.170
3	1	316	427	580	888	56.8 (set)	40.3	44.6	.174
4	1	371	427	583	888	56.8 (set)	41.4	45.5	.178
5	1	204	427	619	888	85.2 (set)	53.1	57.0	.223
6	1	260	427	620	888	85.2 (set)	53.6	57.4	.224
7	1	316	427	622	888	85.2 (set)	54.3	58.0	.237
8	1	371	427	625	888	85.2 (set)	55.2	58.8	.241
9	1	204	427	653	888	114 (set)	64.9	68.2	.266
10	1	260	427	655	888	114 (set)	65.3	68.6	.268
11	1	316	427	656	888	114 (set)	65.8	69.0	.269
12	1	371	427	658	888	114 (set)	66.4	69.5	.271
13	1	204	593	617	1018	56.8 (set)	52.5	56.4	.221
14	1	260	593	619	1018	56.8 (set)	53.5	57.2	.224
15	1	371	593	627	1018	56.8 (set)	55.8	59.3	.233
16	0	482	593	635	1018	56.8 (set)	59.0	62.1	.245
17	1	204	593	674	1018	85.2 (set)	71.9	74.7	.290
18	1	260	593	677	1018	85.2 (set)	72.6	75.4	.292
19	1	316	593	679	1018	85.2 (set)	73.4	76.0	.295
20	0	371	593	682	1018	85.2 (set)	74.5	77.0	.298
21	1	371	593	681	1018	85.2 (set)	74.4	76.9	.298
22	0	427	593	685	1018	85.2 (set)	75.6	78.0	.302
23	0	482	593	691	1018	85.2 (set)	76.8	79.1	.307
24	0	538	593	696	1018	85.2 (set)	78.4	80.4	.311
25	1	204	593	736	1018	114 (set)	86.6	88.0	.337
26	1	260	593	739	1018	114 (set)	87.0	88.4	.338
27	1	316	593	746	1018	114 (set)	88.2	89.4	.341
28	0	482	593	758	1018	114 (set)	89.8	90.8	.345
29	1	204	593	814	1018	100-145	94.8	95.2	.360
30	1	260	593	819	1018	108-145	95.1	95.4	.361
31	1	316	593	830	1018	123-146	95.7	95.9	.362
32	0	482	593	844	1018	132-146	96.3	96.5	.363
33	1	204	427	680	888	99.4-143	73.7	76.4	.296
34	1	371	427	684	888	122-143	75.1	77.7	.301

ORIGINAL PAGE IS OF POOR QUALITY

TABLE 6.8.9

10kW REFORMER - COMBUSTION GAS MODEL STUDIES

Run #	Input: Flow Rates	Output: TCO(C)	THZ(C)	TCZ(C)	THO(C)	TWZ(C)	XUI (W/m^2,°C)	WUI (W/m^2,C)	XI	XE	H_2 Produced (kg mol/Hr)
50	Regular	371	1093	617	639	814 (Two=471)	45-58	55-62	51.8	56.6	.217
51	Regular	371	1204	645	673	886 (Two=486)	46-60	56-63	61.7	66.1	.254
52(1)	Regular	371	1316	672	672	959 (Two=499)	47-62	56-64	70.4	74.4	.280
53	300% Excess	371	1093	649	799	828 (Two=541)	48-57	56-63	63.5	66.7	.260
54(2)	300% Excess	371	1204	688	859	904 (Two=569)	49-59	57-64	75.7	78.4	.307
55(3)	300% Excess	371	1316	751	933	1018 (Two=606)	51-62	57-65	88.7	90.1	.337
56(4)	300% Excess	371	1204	691	857	1118 (Two=779)	50-57	57-64	76.7	79.1	.306

(1) Conversion Error Norm = 1.6%
(2) Conversion Error Norm = 10.7%
(3) Conversion Error Norm = 10.5%
(4) Combustion Gas Duct Considered Filled with 3/8" Alumina Spheres, Overall Coefficient Not Doubled, LORD = 30.

ORIGINAL PAGE IS OF POOR QUALITY

ORIGINAL PAGE IS
OF POOR QUALITY

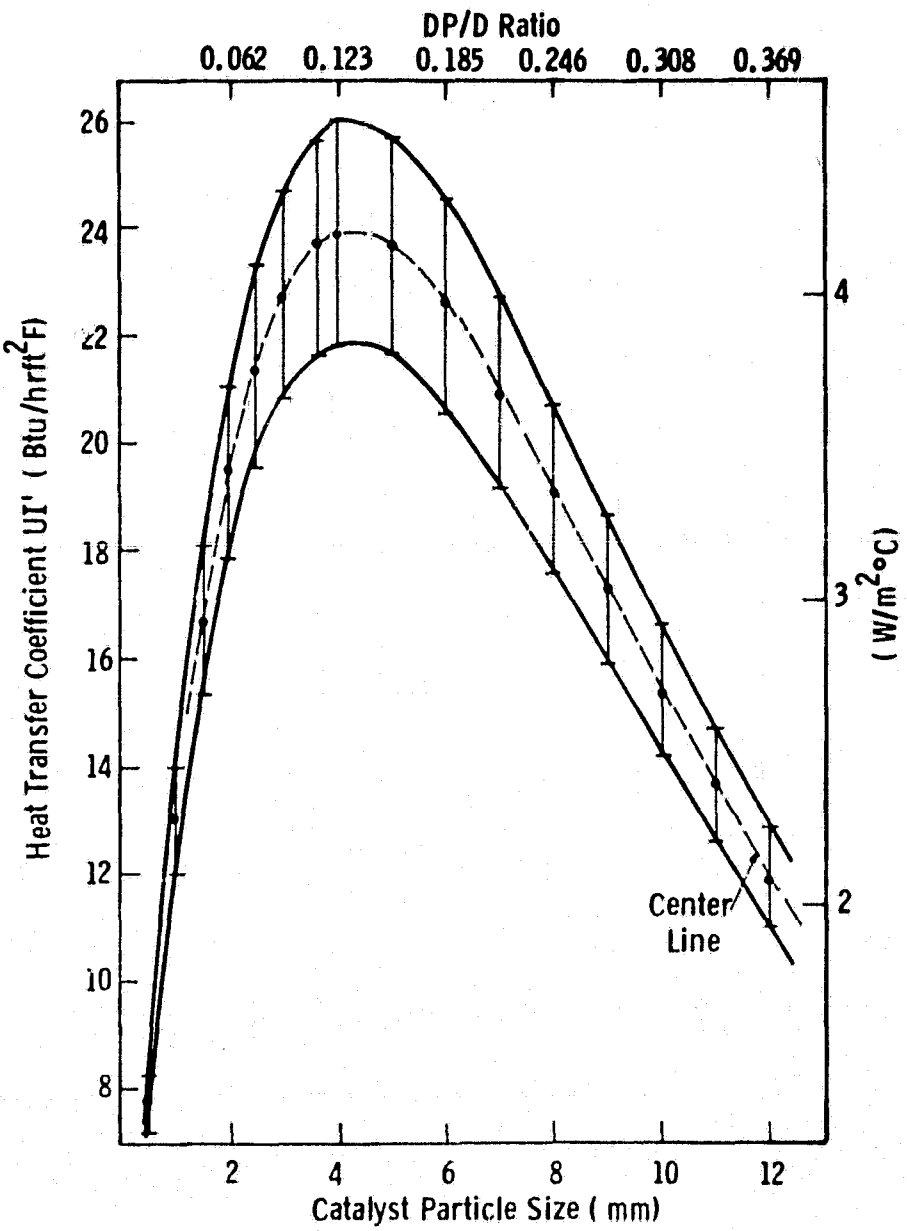

Fig. 6.8.6 – Catalyst particle size effects on heat transfer (10 kW experimental reformer, wall profile model)

ORIGINAL PAGE IS
OF POOR QUALITY

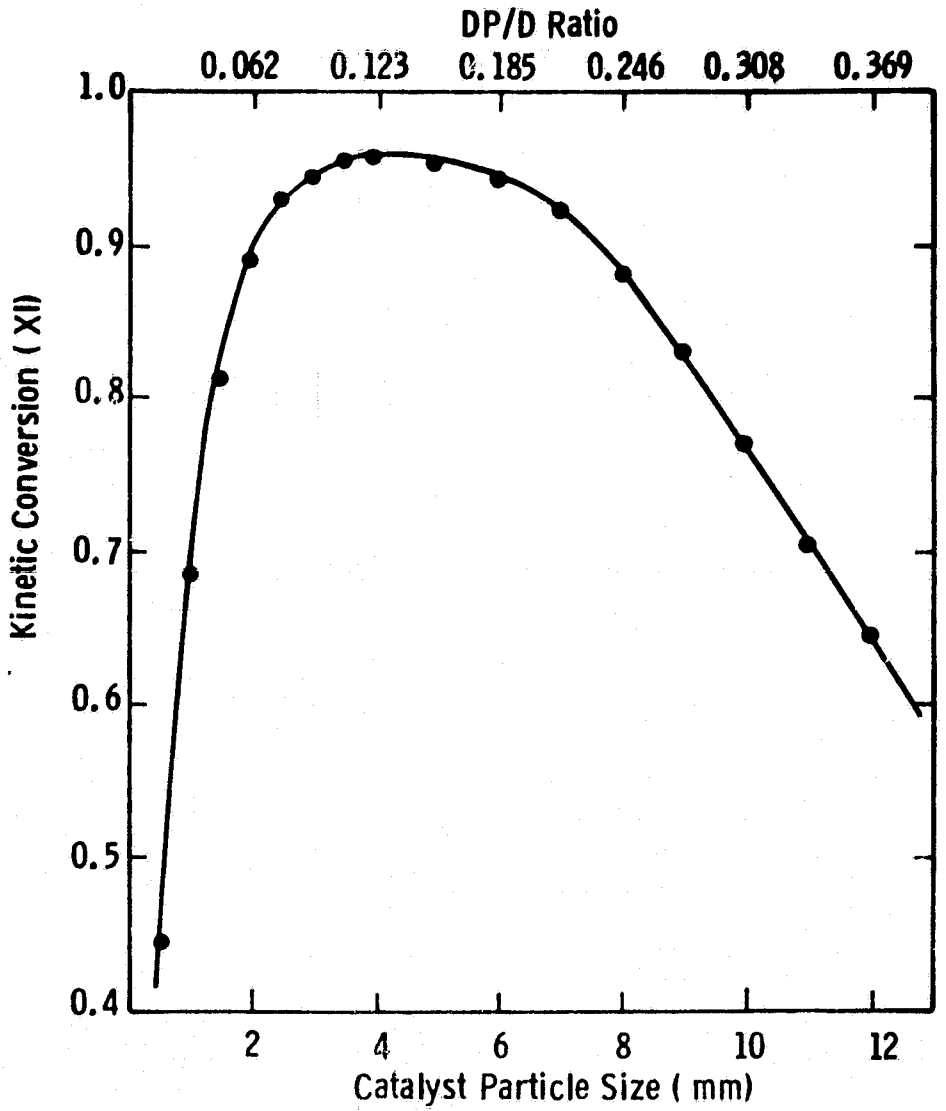

Fig. 6.8.7 – Catalyst particle size effects upon conversion (same activity catalyst – 10 kW experimental reformer, wall profile model)

ORIGINAL PAGE IS
OF POOR QUALITY

TABLE 6.8.10
PHILLIPS PETROLEUM REFORMER DATA*

	Given (from the article)	Used in BOLTAR
Height, m	12.2	Z = 12.2
Tube ID, cm	13	D2 = 13
Tube wall thickness, cm	1.35	use D3 - 15 cm (wall thickness = 1.3 cm
Catalyst particle size, cm	1.59 x 1.59 x .48 rings	1.27 spheres
Mass flow rate, kg/hr m^2 (superficial)	26700	using 7:1 stream; methane ratio, corresponds to FO = 19.1, FL = 2.39, F4 = 16.7 kg mol/hr
Steam/methane ratio	7:1	7:1
Gas mix inlet temperature, C	364	364
Tube wall temperatures, C	TW = 704 + 31Z - $1.20Z^2$ (first m unheated, Z in m)	same, entire tube heated
Inlet pressure, MPa absolute	1.45	P = 13.2 throughout
Outlet pressure, MPa absolute	12.3	
Gas mix outlet temperature, C	799	823 (calculated)
Feed carbon converted, %	91.7	86.1 (calculated)
Tube wall outlet temperature, C	927	904 (calculated)
Inlet Particle Reynolds Number	5000	4270 (calculated)

*Hyman, M. H., "Simulate Methane Reformer Reactions," Hydrocarbon Processing, Vol. 47, No. 7, July 1968.

8. Sufficient hydrogen production can be obtained with the 427C wall temperature profile (runs 33 and 34 in Table 8). Satisfactory hydrogen production is also obtained when the 593C profile is used, along with a single side heat transfer coefficient (UI') greater than 70 kcal/m^2h. Satisfactory hydrogen production is also predicted by the combustion gas model when a 3.2:1 combustion gas/reformer feed gas molar ratio is used.

6.8.5 Model Accuracy

The BOLTAR model has been compared to two sets of reformer data. Table 6.8.10 shows the comparison with open literature data. As the last four lines of the table indicate, the model has duplicated the data very well. This is remarkable given the assumptions in the BOLTAR program and its derivation were for the small fuel cell reformer, not for refinery scale equipment.

Model predictions have also been compared to ERC small reformer tube data (2.5 cm ϕ x 45 cm long, "2 kW", electrically heated). Three choices of input parameters were used due to uncertainties in the heat transfer and catalyst activity values. Predictions were within 7-14% of the temperature profile (calculated using an error norm analysis), within 7-11% of the exit equilibrium conversion, within 6-18% of the exit kinetic conversion. Conversions are estimated low, while the temperature profiles are predicted higher. Therefore, the model provides a conservative design basis, and produces a slightly oversized reformer design.

6.8.6 Summary

The BOLTAR computer model has been developed as a design and analytical tool for fuel cell system reformers. The model is very flexible, and allows the user to exercise various options. Double counter-current flow model variations are also included.

Several parametric studies have been performed using the model. These are described in topical reports submitted separately to the NASA Project Manager. Studies of the 10 kW experimental reformer indicate that it will meet its design specifications. Model predictions have been compared to experimental data, and found to agree within 7-14% of the temperature profile, and within 6-18% of the exit conversions.

7. Management and Documentation

Attainment of the overall objective of this program, the development of commercially viable phosphoric acid fuel cell OS/IES, requires a broad range of technical expertise. This expertise was available in various groups within the two participating corporations, Westinghouse and ERC, and the NASA technical management team. Bringing this expertise to bear on the problem required a free flow of information and close cooperation between personnel and the two corporations, among autonomous groups within each corporation and with members of the NASA technical management team.

A separate management task was deemed appropriate to foster communication and the close cooperation required, to provide for timely and coherent documentation of work done by the various groups and to coordinate the planning of future work. The work breakdown structure of this task comprised three subtasks. The work accomplished under each of these major tasks is discussed below.

Briefly, a close working relationship was maintained among the team members, and technical objectives of the contract were achieved and the documentation required by the contract was provided.

7.1 Management

The objectives of this subtask were:

a) assign the responsibilities for, establish the objectives of, establish schedules for, and allocate resources to the technical tasks

b) establish communications among key contributors to the technical tasks

c) provide overall supervision and coordination of the technical tasks.

The unsolicited proposal submitted to NASA for this work designated the task leaders and major contributors and specified the technical objectives and schedule for each task. The overall cost of

the program was comprised of estimates of the financial and technical resources required for each task. Since the work statement of the contract received from NASA closely followed the proposal on those tasks which were accepted, the requirements of this task were initially met by informal meetings with the task leaders and other key personnel to review the work statement and resolve any questions. In those cases requiring early transfer of information between technical tasks, additional meetings involving appropriate members of each group were arranged.

As work progressed and the subsystem designs evolved, the descriptions of technical tasks were refined, schedules modified, resources reallocated and efforts redirected. In nearly all cases, these changes occurred as a result of presentations and discussions at the review meetings organized under the reporting subtask. The review meetings provided an invaluable forum for intertask communication and coordination of efforts. They were always attended by the NASA Project Manager and the Westinghouse and ERC Project Managers, and generally were attended by other members of the NASA management team, by all task leaders and other Westinghouse and ERC key contributors. Some meetings included other cognizant managers from the three organizations. The meetings were comprised of verbal reports (by task leaders and other key contributors) of ongoing work and the avenues for future work which appeared attractive, followed by discussions open to all those present. The relaxed atmosphere of the meetings facilitated interactive discussions and a free exchange of viewpoints among project contributors with a wide range of technical expertise. Technical approaches were selected and schedules revised and resources reallocated only when a consensus of the group was reached and the decisions were approved by the NASA Project Manager. This approach fostered a sense of involvement and contribution among the participants and undoubtedly contributed greatly to the success of the project.

Since the work of the technical tasks required contributions from a number of disciplines, the management organization was necessarily a matrix. As proposed, an advisory committee comprised of upper level

managers and line managers of each Westinghouse and ERC group contributing technical personnel was established. One formal meeting of this group was convened to review the technical work and several valuable recommendations resulted. More importantly, many informal discussions with the committee members were held concerning both technical questions and the manpower requirements of the contract. It seems clear that the additional interest in the project engendered by their status as committee members was a major factor in their willingness to contribute their time and commit their people to it. As a result, the needed talents were always available to the project when needed. The fact that the manager of the Energy Systems Division of Westinghouse and the President of ERC were committee members was also an ever present indication of the committment of the two organizations to the success of the work.

As a result of the NASA/DOE decision to increase the emphasis on the large power plant application for PAFC, prime responsibility for this contract was transferred to the Westinghouse Advanced Energy System Division (AESD) July 1, 1981. The OS/IES work described in this report was completed under a partial order transfer from AESD to the R&D Center.

7.2 Reporting and Documentation

The specific objectives of this subtask were:

a) prepare agendas for and conduct review meetings
b) prepare Monthly Technical Narratives, Quarterly Technical Progress Reports and the Final Report and the required Financial Management Reports.
c) prepare and submit recommendations for technical approaches to the NASA Project Manager for approval.

Meetings

The review meetings were always scheduled and the agendas drawn up after discussion with and approval of the NASA Project Manager. These meetings were invaluable in facilitating communication among project participants (see the discussion of supervision and coordination above) and much of the technical planning evolved at these meetings.

During the 28 months of work, 6 review and planning meetings were held at the Westinghouse R&D Center, 2 were held at the ERC facilities in Danbury, CT and 2 were held at NASA-LERC. Several of the meetings were integrated with reviews of the separate ERC contracts on PAFC electrochemical technology and planning of the AESD Electric Utility Program to facilitate coordination of the efforts.

In addition to the planned review meetings, many meetings among various groups of project personnel were arranged and held as appropriate. These ranged from meetings of two people to gatherings involving the Westinghouse and ERC project managers, all task leaders, other key contributors to the project and members of the Advisory Committee.

Several presentations were also made to cognizant DOE personnel and their representatives as requested and talks based on work done on this program were given at the National Fuel Cell Seminars of 1980 and 1981.

Reports

The contract required Quarterly Technical Progress Reports and Monthly Technical Narratives. Rather extensive reports describing the work accomplished in considerable detail were submitted each month as well as quarterly. The technical contents of these reports were submitted by the task leaders and other key personnel to the Westinghouse and ERC project managers who edited the contributions and integrated them into cohesive reports. These were then submitted for patent approval to the NASA Project Manager. When appropriate, patent disclosures were submitted with the patent approval copies of reports. Approximately 10 patent disclosures were submitted as a result of work on this contract and patent applications were filed on at least 2 of these on behalf of DOE. Typically, the NASA Project Manager recommended deletion of some material that might adversely affect DOE's patent position and made other useful editorial comments which were incorporated into the reports before final publication. A total of 8 Quarterly Technical Progress Reports and 18 Monthly Technical Narratives were published.

The contract also required Monthly Contractor Financial Management Reports, Monthly Contract Financial Management Performance Analysis Reports and Quarterly Contractor Financial Management Reports. These were prepared on the appropriate NASA forms and submitted by the Westinghouse Project Manager using data provided by the accounting departments of the Westinghouse R&D Center and ERC. These were also distributed to task leaders and cognizant managers of Westinghouse and ERC to keep them informed of the status of their work relative to the plans and available funds. Supplementary reports on total costs by task and contact were supplied (as graphs) to the NASA Project Manager at his request.

In addition to the contract required reports several "topical" reports giving detailed descriptions of analyses and computer programs, copies of computer programs, documents describing in detail the procedures used in fabricating PAFC components and assembling stacks and a detailed plan for Phase III were submitted to the NASA Project Manager.

Weekly and monthly technical highlights were transmitted as requested by the NASA Project Manager.

Recommendations

As discussed above (Section 7.1) most of the decisions on technical approaches and selection of subsystem configurations were arrived at by consensus of the participants in the review meetings. When appropriate, letters summarizing the results of these discussions were written and submitted to the NASA Project Manager for his approval.

7.3 Planning

The objectives of this task were:

a) Develop a detailed plan for Phase III.

b) Make appropriate adjustments in plans for subsequent phases.

With the approval of the NASA Project Manager the detailed plan for Phase III and the modified overall program plan were prepared

by the Westinghouse AESD under an Interworks Requisition and submitted to the NASA Project Manager. In the Westinghouse Corporate structure, the AESD responsibilities include commercialization of new power generation technologies. Since it was agreed by the Westinghouse and NASA management people that responsibility for the OS/IES program would be transferred to AESD prior to or at the start of Phase III, their preparation of the plan was an appropriate transitional step.

APPENDIX A

FUEL PROCESSING SUBSYSTEM
EQUIPMENT SPECIFICATIONS

ORIGINAL PAGE IS
OF POOR QUALITY

STEADY STATE HEAT TRANSFER REQUIREMENTS

FULL POWER NORMAL DUTY SPECIFICATION

NAME/NUMBER: Air Preheater/E-1

SERVICE: Gas to Air(1)

Maximum Heat Duty, kJ/Hr,(BTU/Hr): 56,150 (53,180)

	Hot Side		Cold Side	
Mass Flow Rate, kg/Hr,(lb/Hr)	290(639.3)		214(471.8)	
	Inlet	**Outlet**	**Inlet**	**Outlet**
Composition, mol fraction				
CH_4				
H_2O	0.204	0.204		
H_2				
N_2	0.574	0.574	Air	Air
O_2	0.081	0.081		
CO				
CO_2	0.141	0.141		
Molecular Wt	28.552		28.970	
Fluid Properties				
Density, kg/m^3,(lb/ft^3)				
Therm. Cond., W/m^2 °C,(BTU/Hr ft^2 °F)				
Sp. Heat, kJ/kg°C, (BTU/lb°F)	1.1849(0.2830)		1.0241(0.2446)	
Viscosity, Pa·S, (lb/ft hr)				
Temperature, °C, (°F)	393(739.4)	230(446)	60(140)	316(600.8)
Pressure, kPa, (psia)	106.1(15.39)	103.8(15.06)	17.6(17.05)	115.3(16.72)
ΔP, kPa, (in H_2O)	2.24(9)		2.24(9)	

Notes: (1) Sulfur free products of combustion/Compressed, filtered air.

ORIGINAL PAGE IS
OF POOR QUALITY

STEADY STATE HEAT TRANSFER REQUIREMENTS

ONE-THIRD POWER NORMAL DUTY SPECIFICATION

NAME/NUMBER: Air Preheater/E-1

SERVICE: Gas to Air

Heat Duty, kJ/Hr,(BTU/Hr): 12,850(12,170)

	Hot Side		Cold Side	
Mass Flow Rate, kg/Hr,(lb/Hr)	65(143.3)		48(105.8)	
	Inlet	Outlet	Inlet	Outlet
Composition, mol fraction				
CH_4				
H_2O	0.204	0.204		
H_2				
N_2	0.574	0.574	Air	Air
O_2	0.081	0.081		
CO				
CO_2				
Molecular Wt	28.552		28.970	
Fluid Properties				
Density, kg/m^3,(lb/ft^3)				
Therm. Cond., W/m^2 °C,(BTU/Hr ft^2 °F)				
Sp. Heat, kJ/kg°C, (BTU/lb°F)	1.1844(0.2829)		1.0245(0.2447)	
Viscosity, Pa·S, (lb/ft hr)				
Temperature, °C, (°F)	393(739.4)	227(440.6)	60(140.0)	321(609.8)
Pressure, kPa, (psia)				
ΔP, kPa, (in H_2O)				

GAS COMPRESSOR SPECIFICATION

STEADY STATE NORMAL DUTY OPERATION

COMPRESSOR NAME/NUMBER: Air Compressor/CP-1

FLUID: Air

FLOW RATE: 377 SCFM (1693.2 lb/Hr) - Full Power
85.8 SCFM (385.8 lb/Hr) - 1/3 Power

STATIC DISCHARGE PRESSURE: 70 in H_2O (2.52 psi)

INTAKE PRESSURE: Ambient

DISCHARGE TEMPERATURE: 140°F

INTAKE TEMPERATURE: Ambient

FLUID COMPOSITION: 78.03 v/o N_2
20.99 v/o O_2
0.98 v/o Ar

FLUID MOLECULAR WEIGHT: 28.970

PUMP SPECIFICATION

STEADY STATE NORMAL DUTY OPERATION

PUMP NAME/NUMBER: Recirculation And Boiler Feed Pump/ P-1

FLUID: Deionized Water at ∿1 Megohm Resistivity

FLOW RATE: 180 GPH at all power levels

DISCHARGE PRESSURE: 100 psia

INTAKE PRESSURE: 14.7 psia

ΔP: ∿85 psi

FLUID TEMPERATURE: ∿100°F

DEGASIFIER SPECIFICATION

NAME/NUMBER: Degasser/DG-1

TYPE: Mechanical, packed bed, steam scrubbing, spray, steam vented

WATER FLOW RATE: 160-185 lb/hr. (72.6 - 83.9 kg/hr.)
(AT FULL POWER)

INLET WATER TEMP: ∿212°F (∿100°C)

STEAM AND NONCONDENSIBLE GASES VENT RATE: 10 ft^3/hr., min (0.17 kg/hr.)

TYPICAL INLET WATER QUALITY:
CO_2 - 77 ppm (w)
O_2 - 6.6 ppm (w)
CO - 0.1 ppm (w)
H_2 - 0.1 ppm (w)
CH_4 - <0.05 ppm (w)
N_2 - 11.3 ppm (w)
H_3PO_4 - 69.6 ppm (w)

REQUIRED OUTLET WATER QUALITY:
CO_2 - <5 ppm (w)
O_2 - <0.1 ppm (w)
CO - --
H_2 - --
CH_4 - --
N_2 - --
H_3PO_4 - --

CODE REQUIREMENT: ASME Coding is optional

ION EXCHANGER SPECIFICATION

NAME/NUMBER: Ion Exchanger System/IX-1, F-1

TYPE: Replaceable Cartridges; two bed combination followed by mixed bed.

COMPONENTS: Cation bed; anion bed; mixed-bed
Prefilter and polishing filter
Purity meter
Manifolds, piping and valves

REMOVAL CAPACITY: 28,000 Grains

WATER CIRCULATION RATE: 5 GPM

FILTERS: Prefiller for gross particulate matter
Removal
Postfilter for polishing

PURITY METERS: Following two bed combination and mixed bed.

INLET WATER QUALITY: Recovered condensate containing 70 ppm H_3PO_4 (67.5 ppm PO_4); cations are corrosion products (Fe, Cu, Al). Also particulate corrosion products.

OUTLET WATER QUALITY: 1M ohm-cm; pH 6-8; Suspended solids <1ppm; Dissol. O_2- <0.1 ppm; free CO_2 - <5 ppm.

AIR FILTER SPECIFICATION

NAME/NUMBER: Air Filter/F-3

FLUID: Air

FLOW RATE: 377 SCFM

OPERATING TEMPERATURE: 100°F (Max)

OPERATING PRESSURE: 14.7 psia

NOTES: Filter F-3 may be provided as part of the air compressor package.
Air source identified as coming from inverter cooling.
Allowable pressure drop before replacement of filter element is TBD.

WATER FILTERS SPECIFICATIONS

NAME/NUMBERS: Water filter/F-1; condensate filter/F-2

FLOW RATES: F-1 & F-2 --- 19 GPH

WATER QUALITY-INLET: F-1 Deionized water, 1 Mohm-cm; pH 6-8, Dissol O_2 <0.1 ppm; free CO_2 <5 ppm; particulate resin particles and corrosion products.

F-2 Recovered condensate containing 70 ppm H_3PO4, 76.7 ppm CO_2; 0.1 ppm CO, 0.1 ppm H_2, <0.05 ppm CH_4, 6.6 ppm O_2, 11.3 ppm N_2; particulate corrosion products.

WATER QUALITY-OUTLET: F-1, F-2 Suspended solids <1 ppm; other properties - same as in inlet water.

FILTER TYPE: Removable cartridge type; cellulose fiber or wound filament type.

OPERATING TEMPERATURE: F-1 & F-2 - 105°F

OPERATING PRESSURE: F-1 & F-2 - 100 psig (max)

SIMULTANEOUS CARBON TREATMENT: Simultaneous carbon treatment, for removal of organic impurities, by passing the water thru activated carbon, and filtration should be considered as an option.

NOTE: Filter F-1 may be provided as part of the ion exchange system package.

RECOVERED CONDENSATE WATER STORAGE TANK SPECIFICATION

NAME/NUMBER: Condensate water tank/T-2

CAPACITY: 150 Gallons

ORIENTATION: Horizontal or vertical

HEADS: Dished, ellipsoidal, flat, etc.

OPERATING PRESSURE: Ambient

OPERATING TEMPERATURE: 105°F (Max)

MATERIALS OF CONSTRUCTION: Fiberglass reinforced polyester (FRP)
High density polyethelene
Light gage 300 series S/S

NOZZLES: 2 - 3/4"
3 - 1/2"
1 - 15" Manway

SUPPORTS: Cradles, support legs, others

FLUIDS: Recovered condensate

TYPICAL FLUID QUALITY:

CO_2 - 77 ppm (w)	CO - 0.1
O_2 - 6.6 ppm (w)	H_2 - 0.1
H_3PO_4 - 69.6 ppm (w)	CH_4 - <0.05
N_2 - 11.3 ppm (w)	

CODE REQUIREMENT: ASME coding is optional

BOILER WATER STORAGE TANK SPECIFICATION

NAME/NUMBER: Boiler tank/T-1

CAPACITY: 150 Gallons

ORIENTATION: Horizontal or vertical

HEADS: Dished, ellipsoidal, flat, etc.

OPERATING PRESSURE: 10 psig

OPERATING TEMPERATURE: 105°F (max)

MATERIALS OF CONSTRUCTION: Fiberglass reinforced polyester (FRP)
High density polyethelene
Light gage 300 series S/S

NOZZLES: 2 - 3/4"
3 - 1/2"
1 - 15" Manway

SUPPORTS: Cradles, support legs, others

FLUIDS: Demineralized, degassed water, 1-5 Mohm

TYPICAL FLUID QUALITY:

Elec. Resistivity	- >1 Mohm at 25°C
pH	- 6.8
Dissolved O_2	- <0.1 ppm
Free Co_2	- <5 ppm
Suspended Solids	- <1 ppm

CODE REQUIREMENTS: ASME Coding is optional

APPENDIX B

CONTROL FUNCTIONS AND MICROPROCESSOR SPECIFICATION

Operating Procedure - Startup

"Black" start will be initiated by pushbutton* at which point the computer takes over bringing the system first to one third and subsequently to full load or to whatever the load requirement is at that time. The procedure will consist of first starting up the water/steam system; then the electrical preheaters in proper sequence. The air and fuel systems are then activated, the reformers one at a time, and the critical temperature and fuel quality monitored. In each case the primary control is on fuel and its flow is approximately matched by air (and coolant). With all support systems functioning and the fuel cell stacks reaching design open circuit voltage, the disconnect switch is closed and power is fed to the load and/or to the utility line as required at that time.

The starting sequence follows with reference to Figure 6.2.1.

1. Energize the computer by start-up switch JIS-1 and initiate startup by pushing start button JIS-2. Ensuing sequences are computer actuated.
2. Check recirculation (T-1) tank level. If low by level switch LSH-3 fill** with make up (deionized) water. If adequately high, pump (P-1) starts with switch JIS-3; valve PV-2 is closed, valve PC-1 is open.
3. Build pump pressure PIT-1 to set point of valve PC-1. When PSL-1 indicates adequate pressure recirculating valve PV-2 opens and controls with PRC-3. Valve PV-27 remains closed.
4. Monitor flow with meter FR-1 and water purify with analyzer AR-1. If purity and flow are adequate valve PV-27 opens and water flow is controlled with valve LV-2.

*It is possible that startup could be accomplished manually once the computer has established the proper component timing and sequence.
**This is accomplished manually from an external source.

5. When boiler water level is normal as shown by level indicator LIT-2, activate electric boiler heater BP-1 with switch JIS-4. PRC-2 will control boiler pressure.
6. Open water valve FV-6 to provide cooling water to condenser CD-1.
7. With boiler B-1 at normal pressure as indicated by pressure indicator PIT-2, open flow control valve FV-16 and bypass valve FV-5 providing a flow of wet steam to condenser CD-1. Monitor with TR-24 to check adequate water flow through CD-1, and FI-2 to check adequate steam flow.
8. When level in condensate tank T-2 is normal as shown by level indicator LIT-4, start condensate pump P-2 with switch JIS-5. Build pump pressure by closing bypass valve PV-36.
9. With adequate pump pressure as shown by pressure indicator PIT-3 open circulating valve FV-24 carrying condensate to the degasser DG-1.
10. Start cooler C-2 Fan with switch JIS-6. Monitor condensate temperature with indicator TRC-102.
11. Activate electric superheater SH-2 with switch JIS-7. Control superheat temperature with TRC-23.
12. Preheat shift converter SC-1 and fuel preheater E-2 with electric heater FP-1 via switch JIS-8. Control temperature with TRC-35.
13. Start air compressure CP-1 with switch JIS-9, opening flow control valve FV-1 to reformer combustor RC-1 to purge combustor system at low fire (1/3 load) condition.
14. Open valve FV-26 to provide cooling water to water heater E-6.
15. When temperature indicator TIT-35 on shift converter SC-1 indicates 150°C and purge flow (control not shown) has been established per flow indicator FI-1 for an adequate time, open natural gas block valve and flow control valve FV-15.
16. Start gas compresser CP-2 with switch JIS-10 and open gas valve FV-15 permitting desulfurized fuel to pass through the system, as monitored by AR-4, to the reformer combustor RC-1. Control of this flow is by valve FV-15 at a start-up flow position. Normally fuel flow is controlled by desired system output voltage.

17. Activate ignitor IG-1 with fuel valve FV-28 in low fire position and admitting combustion air through control valve FV-1 as needed for ignition. Control primary chamber temperature with TRC-1. It should not exceed 1000°C until flow is established in the reformer tubes. Control secondary air flow with TRC-15 to limit exit temperature from combustor to 450°C.
18. When TRC-1 indicates that stable combustion is established energize fuel cell start-up electrical heating elements.
19. Start RC-2 with IG-2 according to step 17.

20. Start recycle compressor CP-3 with switch JIS-12 to circulate air through the fuel cells. A portion of the air passes through the condenser CD-1 to the exhaust. Open valve FV-12 to permit air to exit. Fresh air flow is controlled via FV-11 and FRC-11 to provide adequate oxygen to the fuel cells, as indicated by AR-3.
21. When indicator TRC-13 shows adequate superheat, close valve FV-5 to condenser CD-1 and open valve FV-8. admitting superheated steam to reformer RC-1. Secondary air is automatically throttled by TRC-15 to maintain 450°C at combustor outlet. Steam flow is controlled by FRC-5.
22. Air control valve FV-1 maintains combustion temperature TRC-1 at 1000°C. Monitor wall temperature TIT-100 which it should not exceed 1000°C.
23. Increase steam flow with control valve FV-16 as indicated by flow meter FIT-5 to a three to one proportion based on flow through inlet fuel valve FV-15. Meter gas/steam mixture to reformer with ratio control through JRC-1.
24. Monitor AR-2 for CO and AR-5 for H_2 gas samples. When fuel gas is of adequate quality, JRC-1 will open recycle valve FV-10 to provide an appropriate hydrogen flow for the hydrodesulfurizer DS-1. Maintain fuel valve FV-15 via meter FIT-6 in low flow position.

25. When temperature TRC-35 of shift converter SC-1 is maintained by process heat, fuel preheater FP-1 will be programmed to shut off via switch JIS-8.
26. Admit cooling water to fuel condenser CD-2 with valve FV-9. Monitor temperature with indicator TR-6. Admit cooling water to air cooler C-1 with valve FV-25. Monitor temperature with recorder TR-101.
27. Electric boiler heater BP-1 will be programmed to shut down via switch JIS-4 when boiler pressure by controller PRC-2 is maintained by process flow.
28. Air flow to water cooler C-2 will be maintained by TC-1 thermostatic control of water temperature with reference to TRC-102.
29. With adequate fuel quality* as indicated by gas samples AR-2 for CO and AR-5 for H_2 and with fuel cell reaching design open circuit voltage, close disconnect switch JIS-13 feeding power through the inverter to the utility line (and load) as required. Shut off fuel cell startup heaters and superheater SH-2.
30. Allow the system to come to equilibrium at the one third load condition.

Operating Procedure - Load Change

With the system operating normally at a given load, each of the five subsystems, controlled independently must respond to a load change:

(a) Electrical load on the fuel cell increases.

(b) electrical load on the fuel cell decreases.

Their responses are integrated through JRC-1, and are described with reference to Figure 6.2.1 as follows.

*Prior to reaching adequate fuel quality say during startup or sudden load increase the partially reformed fuel from either or both reformers may be returned to the CP-2 (gas compressor) inlet for recycling via control valve FV-10 or to the reformer combustor(s); RC-1, supplementing the raw gas feed via manipulation of flow valves FV-4 and FV-4'.

Subsystem (1) - CONDENSATE WATER RETURN

Object: To maintain normal water levels in T-1 via LRC-3 and in T-2 via LRC-4.

Normal Condition: Pump P-1 is controlled by JIS-3, circulating water through the ion exchange column 1X-1 and supplying make up water to the boiler B-1.
Pump P-2 is controlled by JIS-5 maintaining pressure via PRC-3 and FV-36. FV-36 would be normally closed and FV-34 normally open with water from T-2 pumped to condensate heater E-5 to the Degasser DG-1, the condensate cooler C-2 and back to T-1. Water return to T-2 comes from condenser CD-1 and CD-2, and from superheater SH-1 via FV-5.

Condition (A) - Water level in T-1 rises as noted by LRC-3 and activates high level switch LSH-3.

1) Control by opening FV-36 and partly closing FV-24.
Result: Condensate Heater E-5 must be partly bypassed via FV-30, heating less condensate to DG-1 and hence less condensate through cooler C-2 to T-1. Control of FV-30 is by TRC-2 to bypass some heat around E-5; water level in T-2 rises (LIT-4) and activates LSH-4.

2) Close FV-6 to CD-1, condensing less water and sending water vapor to the stack. Alternately use overflow from T-2, control by LIT-4 via LRC-4.
Note: T-2 can be open to atmosphere because water has not been degassed. T-1 must be sealed from atmosphere, using vacuum, floating head, or accumulator, etc.

3) Subsequent to 2) i.e., bypassing E-5, control (with C-3) fuel gas temperature to SC-1 adjusting louver by TZ-1 via TRC-90 and TIT-90 (Must not exceed 180°C into SC-1 to favor H_2 production) - fan running via JIS-20. Note: This item could be considered part of fuel flow subsystem.

4) An overflow pipe is provided as a back-up.

Condition (B) - Water level drops in T-1 via LRC-3 and low level switch LSL-3.

Note: No low level alarms or system shutdown are provided in either T-1 or T-2. These functions are however, provided with boiler B-1 and will be considered under the water/steam sub-system.

1) additional water could be added through the "initial fill" of T-1 but preferably -

2) Control by increasing flow from T-2 to T-1 by partly closing FV-36 and opening FV- 24.

RESULT: More heat will be required by condensate heater E-5 requiring closing of FV-30 and lowering temperature to SC-1. If louver in C-3 is completely closed, inlet temperature to SC-1 may drop below anticipated 170°C (which still favors the reaction of $CO + H_2O \rightleftharpoons CO_2 + H_2$) but may require additional heat elsewhere in the system, say from natural gas heater E-3.

3) Level of water in T-2 will drop as indicated by LSL-4 requiring FV-6 to open for further cooling and condensing of spent air in CD-1. Note: If excess hot water is produced by CD-1 as indicated by TR-24, it may be necessary to cool it or discard it.

4) Some additional condensate may be obtained from the spent air by opening FV-12 and simultaneously FV-11 for more make up air.

RESULT: Change in quality of spent air may upset the generating process and cooling system as will the functioning (i.e., less steam), of the steam generator B-1. (May require electrical heat via BP-1 and J1S-4).

Subsystem (2) - FUEL FLOW AND PROCESSING

Object: To desulfurize natural gas and react it with steam producing a fuel high in hydrogen and as low as possible in carbon monoxide for the fuel cell as it responds to electrical load requirements of the system.

Normal Condition: The fuel cell is running at a steady state condition supplying the electrical energy required at the time by the load. For a given electrical load on a cell there will be a corresponding voltage and although this voltage drops as the load requirement increases and rises as the load decreases, the resulting AC output from the inverter will be maintained constant by thyristor control. The fuel conditioning subsystem provides the primary control for the OS/IES fuel cell modules and it controls on the basis of fuel cell output voltage.

CONDITION (A) - Electrical load on the fuel cell(s) increases resulting in a reduced voltage signal being sent to master controller JRC-1. JRC-1 increases the natural gas and steam flow to the reformer. The reformer temperature will drop since initially the spent fuel stream will contain less H_2 and the same CO and CH_4 as at the lower load condition. JRC-1 will increase the supply of natural gas to the reformer by opening FV-4.

JAC-1 may also supplement the process heat exchanger with electrical heat via the fuel preheater FP-1, the boiler preheater BP-1 and the starting superheater SH-2.

1) Voltage at the inverter drops with load being picked up by the utility line. Low voltage signal from inverter load sensor goes to JRC-1 Master Controller.

2) Natural gas flow is increased through FV-15 as indicated by FIT-6 and FRC-6. Simultaneously FV-10 opens proportionately, adding hydrogen for desulfurization to the natural gas, and FV-16 opens proportionately, adding steam to maintain the proper steam to carbon ratio indicated by FIT-5 and FRC-5. Some of the increased fuel flow (above that being used in the fuel cell) may be returned to the reformer combustor (to supply additional heat) via FV-4 as indicated by FR-205 with possible additional raw fuel from FV-4'. This transient condition would occur only until the quality of the fuel, i.e., low CO and high H_2 is satisfactory for the fuel cell where upon FV-4 closes.

RESULT: Temperature of natural gas from E-3 (to desulfurizer DS-1 drops requiring adjustment of bypass valve FV-31 as indicated by TRC-3. Quality of steam may degrade requiring adjustment of FV-32 as indicated by TRC-13 (outlet temperature from superheater SH-1. And if control is insufficient, electrical heat must be added to SH-2 via JIS-7. Meanwhile if quality is low, some steam may be bypassed via FV-5 to CD-1.

3) Raw fuel (with added hydrogen) is heated in E-2 with heat supplied from the SC-1 process. Additional heat could be supplied by electrical assist i.e., by FP-1 but preferably by E-3 with temperature maintained by TIT-13 and TRC-13 and controlled with bypass valve FV-31.

4) Heated raw fuel enters desulfrizer DS-1 and is monitored by AR-4 for sulfur level (continued high sulfur level shuts the system down via AAH-4.) Heat for the process is from SC-1. If insufficient heat is available as indicated by TIT-91, additional heat may be supplied from E-3 via TRC-91 to FV-31 and possibly by FP-1 via JIS-8, as monitored by TRC-13.

5) Desulfurized fuel gas mixes with steam and enters reformer(s) reacting and picking up heat in the catalyst bed side.

6) Reformed fuel gas passes through the following heat recovery devices to the shift reactor SC-1:

a) E-4, the spent fuel heater which maintains temperature by TIT-4 and TRC-4 by controlling with bypass valve FV-32.

b) E-3, the natural gas heater which maintains temperature by TIT-13 and TRC-13 by controlling with bypass valve FV-31.

c) SH-1, the steam superheater which maintains temperature by TIT-23 and TRC-23 by controlling with bypass valve FV-32.

d) E-7, the feed water preheater which maintains temperature by TIT-5 and TRC-5 by controlling with bypass valve FV-33.

e) E-5, the condensate heater which maintains temperature by TIT-2 and TRC-2 by controlling with bypass valve FV-30.

f) C-3, the fuel cooler needed to lower the reformed gas temperature to that required by the shift converter SC-1 under those conditions where

much of the heat has been bypassed around E-4, E-3, SH-1, E-7, and/or E-5. It maintains temperatures by TIT-90, and TRC-90, by controlling louvers TZ-1 and fan switch JIS-20.

7) Fuel passes through shift converter SC-1 to the fuel condenser CD-2 returning condensed water to T-2, and producing domestic hot water. Temperature is maintained by TIT-9 and TRC-9 controlling with FV-9.

8) Fuel gas is monitored for CO and H_2 by AIT-2 and AIT-5, ARC-2 and ARC-5. During the transient time of load change some of the fuel gas is bypassed to the reformer as described under 2) above. Continued high CO and low H_2 readings by ASH-2 and ASL-5 shut the system down. When CO and H_2 readings return to normal, FV-4 closes and all of the processed fuel passes to the fuel cell (or is bypassed to the CP-2 inlet via FV-10). If the reformer(s) can maintain temperature FV-4' also closes.

9) It is assumed that the completely processed fuel of 8) is split by diverter balancing valves or dampers between the four fuel cell stacks according to their individual operating load voltages by master controller JRC-1.

CONDITION (B). Electrical load on the fuel cell(s) decreases, resulting in an increasing voltage signal being sent to master controller JRC-1.

RESULT: JRC-1 decreases fuel and steam flow to the reformer. All of valves and controls work in reverse to those of condition (A). Some heat will definitely be thrown away via the fuel cooler C-3, and possibly up the stack as bypassed around E-1, the air preheater, and E-6, a water heater. Additional air will be required to cool the reformer(s) as indicated by TIT-8 and TRC-15 controlling flow valve FV-3.

NOTE: For large changes in load JRC-1 will position the various valves but for minor changes or trimming JRC-1 will pulse the various actuators.

Subsystem (3) - SPENT FUEL USAGE

OBJECT: To recover both thermal and chemical energy from the "spent" fuel anode effluent.

NOTE: The principal use for the spent fuel is for combustion heating of the reformer(s), supplying energy to the reforming process. The combustion product is then used for air preheating and heating water.

It is assumed that the reformers will be started one at a time. Thus unprocessed natural gas is used to heat the first reformer and the partially reformed effluent is returned via FR-205 and FV-4 replace the natural gas heating reformer 1 and/or to start up reformer 2. When both reformers are functioning satisfactorily indicated by ARC-2 and ARC-5 all the processed fuel will flow to the fuel cells(s) with FV-4 closed. Normally the system is now running at part load.

CONDITION (A) - load increases

RESULT: Initially flow through the fuel cell tends to increase because of the increased consumption of H_2. As the pressure level in the system drops, the mass flow will then decrease. The decrease is aggravated by the need to supply more hydrogen to the desulfurizer. Raw natural gas must be supplied to the combustion side of the reformer for catalyst heating as the steam and natural gas feed streams are increased. Eventually an increased flow of reformed fuel reaches the fuel cell, load capability increases, and the heat content of the spent fuel becomes sufficient for the reforming reaction.

1) Spent fuel is heated in E-4 by reformed fuel. Temperature of spent fuel monitored by TIT-4 and controlled by TRC-4 via FV-22 bypass valve in reformed fuel line.

2) Spent fuel enters RC-1, the reformer combustor via flow valve FV-28 (normally open), supplemented by raw or partially reformed fuel via FV-2 during start up and/or load change. Combustion monitored by TIT-1 and controlled by TRC-1 via air flow valve FV-1 in combustion air line.

RESULT: 1) Control valve LV-2 closes. E-7, the feed water preheater overheats.

2) Bypass valve FV-33 passes reformed gas around E-7 as does FV-30 around E-5.

3) Fuel cooler C-3 picks up thermal load with some additional heat taken out at fuel condenser CD-2.

4) Simultaneously with steam rate lowered by JRC-1 via FV-16, FIT-5, and FRC-5, heat is bypassed around SH-1 via FV-32 and around B-1 via FV-34 operating from pressure transmitter PIT-2 and PRC-2.

5) Excess air heat must be removed by C-1, the air cooler.

6) Safety valve PSV-1 protects against high pressure, and high level switch LSH-2 opens blowdown valve FO-100 in the event of excess boiler water.

CONDITION "B" - Water level drops in B-1 with increase in steam requirement for electrical load increase.

RESULT: 1) LSL-2 opens LV-2 admitting more water to E-7.

2) Bypass valve FV-33 shifts to supply more heat to E-7 and there may be insufficient heat temporarily for the condensate heater E-5 and degasser in DG-1.

With increase in electrical load (drop in fuel cell voltage) Master Controller JRC-1 increases steam flow via FIT-5, FRC-5, and FV-16.

1) Bypass valve FV-32 moves to supply more heat to SH-1. If insufficient heat is available electrical heat may be supplied via TRC-23 and JIS-7 to SH-2 until more high temperature reformer fuel reaches SH-1.

2) Simultaneously boiler pressure drops via PRC-2 and PIT-2.

3) Flow valve FV-34 is moved by PRC-2 to supply more heat to B-1.

4) If insufficient heat is available, electrical heat may be required from boiler preheater BP-1 via JIS-4 until more spent hot air becomes available from the fuel cells and component cooling.

5) Simultaneously less hot water will be available for C-1.

3) Combustion gas temperature monitored by TIT-8 in combustion chamber and TIT-15 in exhaust, and controlled by TRC-15 via secondary air valve FV-3.

4) Critical metal temperature monitored by TIT-100 and alarm TAH-100. Shut down by TAHH-100.

NOTE: Similar valves and controls are required for reformer R-2 not shown enabling it to start and function independently from R-1.

5) Combustion product from reformer(s) supplies air preheat via E-1, the air preheater. Air temperature monitored by TIT-41 and controlled by TRC-41 via bypass valve FV-41 in combustion product line.

6) Combustion product heats water, HWS, in water heater E-6. Temperatures monitored by TIT-6 in outlet combustion gas line and TIT-7 in hot water line and controlled by TRC-6 bypassing combustion gas via FV-42 and TRC-7 via water flow valve FV-26 and FV-42.

Subsystem (4) - WATER PREPARATION AND STEAM PRODUCTION

OBJECT: To supply required amounts of water to the steam boiler and superheated steam to the reformer.

NOTE: The water is that condensed and stored in T-2 and T-1. It receives a final polishing before entering the steam boiler. Saturated steam from the boiler is superheated and blended with the desulfurized fuel entering the reformer.

1) It is assumed that pump P-1 is operating normally via JIS-3, circulating water through ion-exchange column 1X-1 with a portion passing isolation valve PV-27, water filter F-1, turbine flowmeter FR-2, control valve LV-2 and hence to the feedwater heater E-7 and to boiler B-1.

2) Steam from boiler is superheated in SH-1 and blended with desulfurized fuel at the reformer.

CONDITION "A" - Load decreases requiring less steam, water level rises in B-1 via LIT-2 and LRC-2.

Subsystem (5) - Air Flow

OBJECT: To supply the required amounts of air to the combustion (reaction) portions of the system and to those components requiring cooling. To recover heat where available from the cooling air and condensed water from the "spent" (reaction) air for recycling.

NOTE: Combustion or reaction air is used in the reformer(s) where it divides into primary (combustion) and secondary (cooling). Similarly, air to the fuel cell(s) divides into reaction air and cooling air and is recombined as "spent" air, shown with a dot/dash line. Since control of the fuel cell(s) is not part of the fuel processing, the division of air between the cells and between reaction and cooling is not shown. However, it could be handled by the master controller, JRC-1 as could the cooling air to the inverter. Finally although the cooling of C-2 and C-3 is by means of air, it is not the process air so is not included in subsytem (5).

With air compressors or blowers (CP-1 and CP-3) operating normally via JIS-9 and JIS-12 inlet air is taken at least partially from the inverter cooling passing through inlet air filter F-3. The air system is shown with dash dot lines.

1) Blower air is supplied to the reformer where it burns spent fuel supplying process heat.

2) Blower air is blended with cooled "spent" air and supplied to the fuel cell(s) for reaction and cooling.

3) Air is supplied to the inverter for cooling purposes and returned to the compressor inlet - this line is not shown.

4) Both cooling and process, i.e., "spent" air from the fuel cell(s) is used to heat the steam boiler with some of this extracted ahead of the boiler and cooled to remove water for recycling.

5) Further cooling of "spent" air after the boiler is accomplished before returning this air to the fuel cell via a recycling blower.

6) Make up air is added beyond the recycling blower, equal in amount to that extracted in 4) i.e., approximately 8%.

CONDITION "A" - Load increases. Fuel and steam to reformer(s) increase initially followed by increased process fuel to the fuel cell(s), requiring more air.

RESULT:

1) Temperature in reformer combustor rises as indicated by TIT-1 and TRC-1 which opens FV-1 admitting more combustion air.

2) If gas temperature is excessive (or insufficient) as indicated by, TIT-15 and TRC-15, the secondary air rate is adjusted via FV-3. Control of the reformed gas temperature is also accomplished with TIT-8 and TRC-15 via FV-3.

3) Beyond this point the various controls operate as described in subsections (2) and (3).

4) Steam pressure drop as indicated by PIT-2 and PRC-2 adjusts damper valve FV-34 (and possibly adds electrical energy).

5) Beyond this point the controls operate as described in subsection (4).

6) With additional fuel now flowing to the fuel cell(s) more air for reaction is supplied by valves and controls not shown becuase they are not part of the fuel processing subsystem.

7) Adjustment of the air extracted and make up air is accomplished with FIT-12 and FRC-12 operating on FV-12 and FIT-11 and JRC-1 operating on FV-11.

8) Beyond this point the controls operate as described in subsection (1).

9) Cooling air (not shown) is increased to the inverter and back to the blower inlet CP-1.

CONDITION "B" - Load decreases, requiring less fuel and steam to the reformer as well as to the fuel cell(s).

RESULT: All controls operate in reverse to the description of Condition "A". Initially there may be a need to bypass some of the heat exchangers with heat lost to the stack via FI-1 and through cooler C-3.

1) Spent fuel to reformer may have a higher heating value and require more air via FV-1 and FV-3.

2) Although less steam will be required, there will also be less "spent" air (initially at lower temperature) entering the boiler. The effects may balance but if not, the "spent" air temperature can be controlled by C-1 as monitored by TIT-25, and controlled by TRC-25 and flow valve FV-25.

EQUIPMENT SPECIFICATION - PRELIMINARY March 27, 1980

FUEL CELL MICROPROCESSOR FACILITY

1. SCOPE

This preliminary specification covers the requirements of a microprocessor to function with a fuel processing/fuel cell combined cycle system. In brief it must monitor, control, and log data for the complete system. The heat recovery portion of the combined cycle is not being considered at this time.

2. DEFINITION OF SYSTEM

The system comprises five major components:

- Desulfurizing
- Reformer
- Shift Converter
- Steam Generator
- Fuel Cell

The first four of these components prepare the fuel for use in the fuel cell. In addition to the major components there are several ancillary components consisting of at least four heat exchangers and five coolers, a gas compressor and blower, gas storage bottles, meters, burners, heaters, many valves and many monitoring points. The electrical system includes a rectifier, an inverter, storage, and more monitoring and controlling instrumentation as well as complex switching. The heat recovery and usage for the system is not within the scope of this specification.

3. SYSTEM OPERATION

The various monitoring and control points may be seen with reference to the flow diagram of Figure 6.2.1. Following through the diagram,

fuel (natural gas) is compressed and passed through a desulfurizer. It is mixed with steam, entering a reformer. From the reformer it passes through a shift converter and then to the fuel cell. Because of the nature of the process at various steps it is necessary to cool or heat the fuel hence the heat exchangers and coolers. Air is added by a blower at two points in the cycle. Cathode gas is discarded but the anode product is returned and burned in the reformer and from there it is used superheat steam. Because of reaction time delays in some of the components, storage supplies and surge vessels are used. Storage in the form of electrical energy i.e., battery is also shown. This becomes essential if a grid supply is unavailable and it can operate in conjunction with the grid either for start up or faster load following. Four fuel cell assemblies with individual monitoring and controls are anticipated.

3. FACILITY OPERATION

The Microprocessor Facility will be required to monitor and control the complete system. To this end it must start and stop the unit and make appropriate changes in the operation of each component keying their functions in an optimum manner with a view to best following the electrical load cycle.

The primary input to the facility will be an indication of electrical load demand. On the strength of this signal the microprocessor supplies process gas from storage to the fuel cell and at the same time activates the fuel processing part of the system to take over supplying process gas and at the same time to restock the storage vessel.

A secondary input will be indications of trouble, a malfunction, over temperature, dangerous gas composition, etc. which may activate an alarm or shut down the system if the alarm is ignored or uncorrectable, or if the malfunction is instantaneously dangerous. This control must be overriding on the process control.

At this time the following items have been identified with the associated function:

	Item	Number	Function
(A)	Alarm Indicators	40	Monitor and Control - Input
(P)	Pressure Indicators	44	Monitor
(T)	Temperature Indicators	50	Monitor
(S)	Gas Samplers	13	Monitor
(E)	Electrical Instruments	16	Monitor and Control - Input
(V)	Valves and Switches	40	Control - Output

Some of these serve a duplicate function as will be noted, for example, alarm monitor and control, but these must be kept separate.

All inputs will be in the form of electrical signals, from thermocouples, pressure transducers, and even gas analyzers (and battery specific gravity). All outputs will also be electrical although they may control either electrically operated or possibly pneunatic valves.

4. FACILITY REQUIREMENT

A microprocessor facility is required which will monitor and record 150 pressures, temperatures, currents, voltages, and gas compositions.

The facility must control the process from startup through a load following function and to shutdown, through the operation of 40 valves and switches.

The facility must also monitor 40 alarm stations, signalling trouble and/or shutting down the system. This function must be overriding.

Load following and the alarm systems must be followed continuously. Speed and frequency of recording data are not important. The recorded

data should be visual as well as on paper and/or magnetic tape compatible with the R&D and Waltz Mill computers.

The facility should be portable -- for use at various sites. It is intended at this point for use on test stands and for evaluation and process development. Eventually its use will lead to a specification for a microprocessor for the OS/IES installation.